CELL SIGNALING AND NEURAL CIRCUITS IN CHRONIC DISEASES OF THE CENTRAL NERVOUS SYSTEM

EDITED BY: Francesco Ferraguti, Sigismund Huck and Joerg Striessnig
PUBLISHED IN: Frontiers in Synaptic Neuroscience

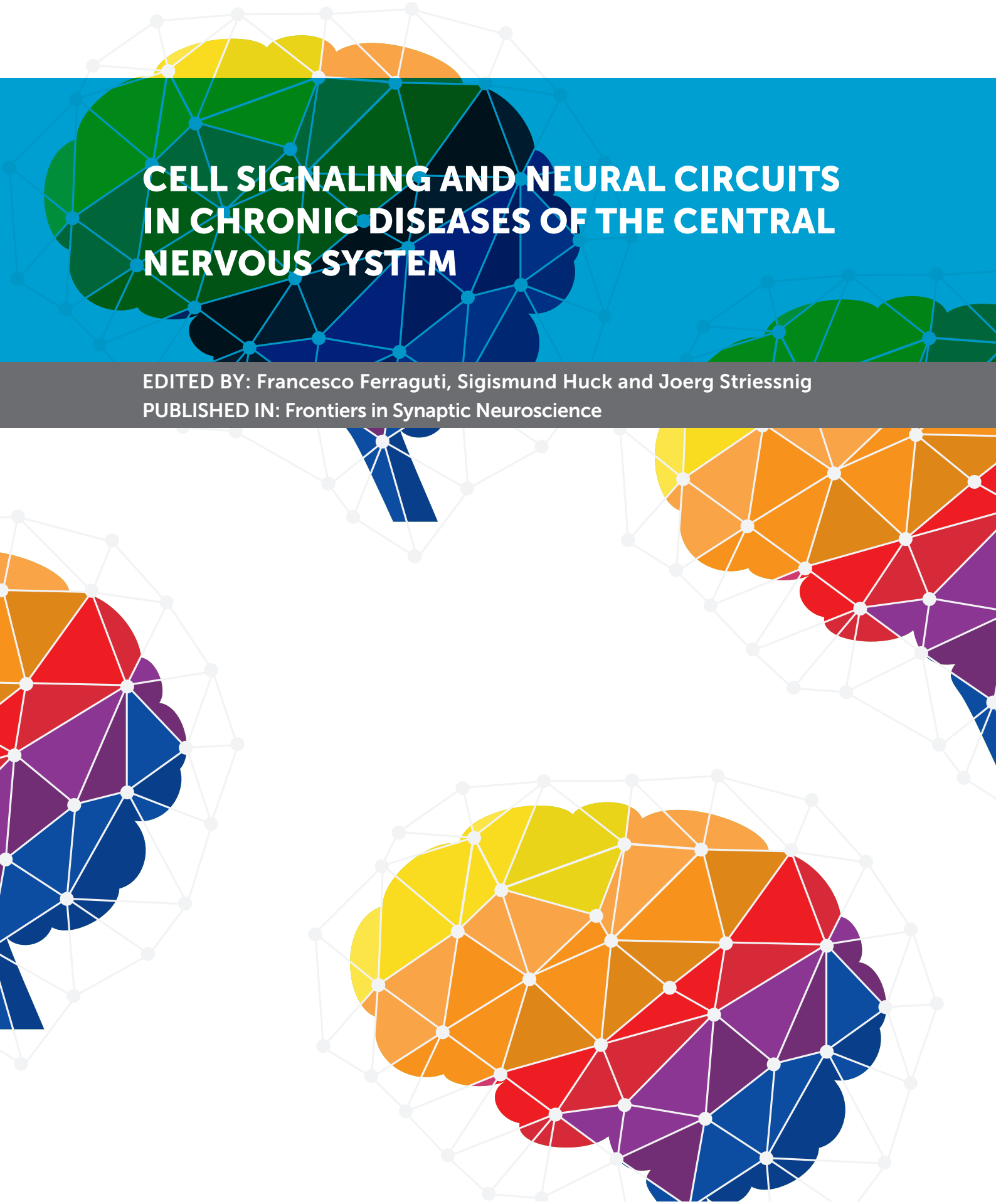

frontiers Research Topics

frontiers

Frontiers eBook Copyright Statement

The copyright in the text of individual articles in this eBook is the property of their respective authors or their respective institutions or funders. The copyright in graphics and images within each article may be subject to copyright of other parties. In both cases this is subject to a license granted to Frontiers.

The compilation of articles constituting this eBook is the property of Frontiers.

Each article within this eBook, and the eBook itself, are published under the most recent version of the Creative Commons CC-BY licence. The version current at the date of publication of this eBook is CC-BY 4.0. If the CC-BY licence is updated, the licence granted by Frontiers is automatically updated to the new version.

When exercising any right under the CC-BY licence, Frontiers must be attributed as the original publisher of the article or eBook, as applicable.

Authors have the responsibility of ensuring that any graphics or other materials which are the property of others may be included in the CC-BY licence, but this should be checked before relying on the CC-BY licence to reproduce those materials. Any copyright notices relating to those materials must be complied with.

Copyright and source acknowledgement notices may not be removed and must be displayed in any copy, derivative work or partial copy which includes the elements in question.

All copyright, and all rights therein, are protected by national and international copyright laws. The above represents a summary only. For further information please read Frontiers' Conditions for Website Use and Copyright Statement, and the applicable CC-BY licence.

ISSN 1664-8714
ISBN 978-2-88971-884-9
DOI 10.3389/978-2-88971-884-9

About Frontiers

Frontiers is more than just an open-access publisher of scholarly articles: it is a pioneering approach to the world of academia, radically improving the way scholarly research is managed. The grand vision of Frontiers is a world where all people have an equal opportunity to seek, share and generate knowledge. Frontiers provides immediate and permanent online open access to all its publications, but this alone is not enough to realize our grand goals.

Frontiers Journal Series

The Frontiers Journal Series is a multi-tier and interdisciplinary set of open-access, online journals, promising a paradigm shift from the current review, selection and dissemination processes in academic publishing. All Frontiers journals are driven by researchers for researchers; therefore, they constitute a service to the scholarly community. At the same time, the Frontiers Journal Series operates on a revolutionary invention, the tiered publishing system, initially addressing specific communities of scholars, and gradually climbing up to broader public understanding, thus serving the interests of the lay society, too.

Dedication to Quality

Each Frontiers article is a landmark of the highest quality, thanks to genuinely collaborative interactions between authors and review editors, who include some of the world's best academicians. Research must be certified by peers before entering a stream of knowledge that may eventually reach the public - and shape society; therefore, Frontiers only applies the most rigorous and unbiased reviews.
Frontiers revolutionizes research publishing by freely delivering the most outstanding research, evaluated with no bias from both the academic and social point of view. By applying the most advanced information technologies, Frontiers is catapulting scholarly publishing into a new generation.

What are Frontiers Research Topics?

Frontiers Research Topics are very popular trademarks of the Frontiers Journals Series: they are collections of at least ten articles, all centered on a particular subject. With their unique mix of varied contributions from Original Research to Review Articles, Frontiers Research Topics unify the most influential researchers, the latest key findings and historical advances in a hot research area! Find out more on how to host your own Frontiers Research Topic or contribute to one as an author by contacting the Frontiers Editorial Office: frontiersin.org/about/contact

CELL SIGNALING AND NEURAL CIRCUITS IN CHRONIC DISEASES OF THE CENTRAL NERVOUS SYSTEM

Topic Editors:
Francesco Ferraguti, Innsbruck Medical University, Austria
Sigismund Huck, Medical University of Vienna, Austria
Joerg Striessnig, University of Innsbruck, Austria

Citation: Ferraguti, F., Huck, S., Striessnig, J., eds. (2021). Cell Signaling and Neural Circuits in Chronic Diseases of the Central Nervous System. Lausanne: Frontiers Media SA. doi: 10.3389/978-2-88971-884-9

Table of Contents

05 ***Histone Deacetylase 6 and the Disease Mechanisms of α-Synucleinopathies***
Miguel Lemos and Nadia Stefanova

18 ***From Synaptic Protein to Prion: The Long and Controversial Journey of α-Synuclein***
Antonio Heras-Garvin and Nadia Stefanova

36 ***Two Distinct Populations of α1α6-Containing GABAA-Receptors in Rat Cerebellum***
Petra Scholze, Michael Pökl, Severin Längle, Friederike Steudle, Jure Fabjan and Margot Ernst

46 ***The Creatine Transporter Unfolded: A Knotty Premise in the Cerebral Creatine Deficiency Syndrome***
Clemens V. Farr, Ali El-Kasaby, Michael Freissmuth and Sonja Sucic

61 ***The Good, the Bad and the Unknown Aspects of Ghrelin in Stress Coping and Stress-Related Psychiatric Disorders***
Eva Maria Fritz, Nicolas Singewald and Dimitri De Bundel

84 ***The α5 Nicotinic Acetylcholine Receptor Subunit Differentially Modulates α4β2* and α3β4* Receptors***
Petra Scholze and Sigismund Huck

108 ***PKN1 Is a Novel Regulator of Hippocampal GluA1 Levels***
Motahareh Solina Safari, Dido Obexer, Gabriele Baier-Bitterlich and Stephanie zur Nedden

117 ***Phenotypic Characterization and Brain Structure Analysis of Calcium Channel Subunit $\alpha_2\delta$-2 Mutant (Ducky) and $\alpha_2\delta$ Double Knockout Mice***
Stefanie M. Geisler, Ariane Benedetti, Clemens L. Schöpf, Christoph Schwarzer, Nadia Stefanova, Arnold Schwartz and Gerald J. Obermair

140 ***Voltage-Gated Ca^{2+} Channels in Dopaminergic Substantia Nigra Neurons: Therapeutic Targets for Neuroprotection in Parkinson's Disease?***
Nadine J. Ortner

151 ***Multi-Electrode Array Analysis Identifies Complex Dopamine Responses and Glucose Sensing Properties of Substantia Nigra Neurons in Mouse Brain Slices***
Nadja Mannal, Katharina Kleiner, Michael Fauler, Antonios Dougalis, Christina Poetschke and Birgit Liss

170 ***Dopamine in Fear Extinction***
Ximena I. Salinas-Hernández and Sevil Duvarci

178 ***Voltage-Gated Ca^{2+}-Channel α1-Subunit* de novo *Missense Mutations: Gain or Loss of Function – Implications for Potential Therapies***
Jörg Striessnig

203 ***NPY Released From GABA Neurons of the Dentate Gyrus Specially Reduces Contextual Fear Without Affecting Cued or Trace Fear***
Lucas B. Comeras, Noa Hörmer, Pradeepa Mohan Bethuraj and Ramon O. Tasan

220 ***Fear Memory Retrieval Is Associated With a Reduction in AMPA Receptor Density at Thalamic to Amygdala Intercalated Cell Synapses***
Anna Seewald, Sabine Schönherr, Heide Hörtnagl, Ingrid Ehrlich, Claudia Schmuckermair and Francesco Ferraguti

frontiers in Synaptic Neuroscience

REVIEW
published: 11 September 2020
doi: 10.3389/fnsyn.2020.586453

Histone Deacetylase 6 and the Disease Mechanisms of α-Synucleinopathies

*Miguel Lemos and Nadia Stefanova**

Department of Neurology, Medical University of Innsbruck, Innsbruck, Austria

The abnormal accumulation of α-Synuclein (α-Syn) is a prominent pathological feature in a group of diseases called α-Synucleinopathies, such as Parkinson's disease, dementia with Lewy bodies (DLB), and multiple system atrophy (MSA). The formation of Lewy bodies (LBs) and glial cytoplasmic inclusions (GCIs) in neurons and oligodendrocytes, respectively, is highly investigated. However, the molecular mechanisms behind α-Syn improper folding and aggregation remain unclear. Histone deacetylase 6 (HDAC6) is a Class II deacetylase, containing two active catalytic domains and a ubiquitin-binding domain. The properties of HDAC6 and its exclusive cytoplasmic localization allow HDAC6 to modulate the microtubule dynamics, acting as a specific α-tubulin deacetylase. Also, HDAC6 can bind ubiquitinated proteins, facilitating the formation of the aggresome, a cellular defense mechanism to cope with higher levels of misfolded proteins. Several studies report that the aggresome shares similarities in size and composition with LBs and GCIs. HDAC6 is found to co-localize with α-Syn in neurons and in oligodendrocytes, together with other aggresome-related proteins. The involvement of HDAC6 in several neurodegenerative diseases is already under discussion, however, the results obtained by modulating HDAC6 activity are not entirely conclusive. The main goal of this review is to summarize and critically discuss previous *in vitro* and *in vivo* data regarding the specific role of HDAC6 in the context of α-Syn accumulation and protein aggregation in α-Synucleinopathies.

Keywords: histone deacetylase 6, α-synuclein, α-synucleinopathies, Parkinson's disease, multiple system atrophy, neurodegeneration, protein degradation

OPEN ACCESS

Edited by:
Joerg Striessnig, University of Innsbruck, Austria

Reviewed by:
Mattia Volta, Eurac Research, Italy
Graziella Cappelletti, University of Milan, Italy

***Correspondence:**
Nadia Stefanova
nadia.stefanova@i-med.ac.at

Received: *23 July 2020*
Accepted: *24 August 2020*
Published: *11 September 2020*

Citation:
Lemos M and Stefanova N (2020) Histone Deacetylase 6 and the Disease Mechanisms of α-Synucleinopathies. Front. Synaptic Neurosci. 12:586453. doi: 10.3389/fnsyn.2020.586453

Abbreviations: AD, Alzheimer's disease; ALS, amyotrophic lateral sclerosis; BDNF, brain-derived neurotrophic factor; CMA, chaperone-mediated autophagy; CNS, central nervous system; DD1, and DD2 HDAC6 deacetylase domain 1 and 2; DLB, dementia with Lewy bodies; GCIs, glial cytoplasmic inclusions; HAT, histone acetyltransferases; HD, Huntington's disease; HDAC6, histone deacetylase 6; HSF1, heat-shock transcription factor 1; HSP90, heat-shock protein 90; Htt, huntingtin protein; LBs, Lewy bodies; LNs, Lewy neurites; MPP+, 1-methyl-4-phenylpyridinium; MSA, multiple system atrophy; MTOC, microtubule-organizing center; NAC, non-Amyloid β component; PD, Parkinson's disease; SNc, substantia nigra pars compacta; TDP-43, TAR DNA-binding protein 43; TPPP/p25α, Tubulin polymerization-promoting protein; UPS, ubiquitin-proteasome system; α-Syn, α-Synuclein.

INTRODUCTION

Protein misfolding and consequent accumulation is a biological process that has been intensively studied for many years. To perform their function within the cell, the newly synthesized proteins must achieve the proper conformation in a three-dimensional structure. However, due to disturbances in the folding process, such as environmental insults or genetic mutations, certain proteins may fail to achieve the native conformation (Balchin et al., 2016). Through a mechanism that is still not well understood, those proteins can undergo a process of misfolding and aggregation, leading to the formation of neurotoxic inclusions, a feature of age-related neurodegenerative diseases (Ross and Poirier, 2004; Sweeney et al., 2017; Soto and Pritzkow, 2018).

In this review article, we focus exclusively on the process of α-synuclein (α-Syn) accumulation and aggregation, the pathological hallmark of a group of diseases like Parkinson's disease (PD), multiple system atrophy (MSA) and dementia with Lewy bodies (DLB), commonly known as α-Synucleinopathies (Duda et al., 2000; Goedert et al., 2017). To date, it is well-accepted that α-Syn is the major component of pathological aggregates, such as Lewy bodies (LBs), Lewy neurites (LNs), and glial cytoplasmic inclusions (GCIs; Spillantini and Goedert, 2000; Visanji et al., 2019). It is believed that these protein inclusions play a central role in the progression of the disease, contributing to neuronal dysfunction, neuroinflammation, and neurodegeneration (Vekrellis et al., 2011; Uchihara and Giasson, 2016). However, the molecular mechanisms involved in the formation of such inclusions are not fully understood.

To cope with higher amounts of pathological α-Syn aggregates, several protein quality control mechanisms are triggered to maintain the normal function and homeostasis of the neural cells (Ciechanover and Kwon, 2015). However, in a disease context, the exacerbated amount of pathological α-Syn leads to the dysfunction of the ubiquitin-proteasome system (UPS), resulting in a higher accumulation of toxic aggregates (Ciechanover and Kwon, 2015; Kaushik and Cuervo, 2015; da Fonseca et al., 2015; Zheng et al., 2016). As a consequence, the aggresome-autophagy pathway is stimulated, in which misfolded and aggregated proteins are transported to a perinuclear aggresome (Olzmann et al., 2008). Interestingly, LBs and aggresomes share several biochemical and morphological characteristics (Olanow et al., 2004; Miki et al., 2011).

One important regulator involved in the formation of the aggresome is the histone deacetylase 6 (HDAC6), by linking ubiquitinated proteins to the microtubule dynein motor complex (Boyault et al., 2007a,b; Ouyang et al., 2012). HDAC6 is a protein from the histone deacetylase superfamily, containing two active catalytic domains (Yang and Grégoire, 2005). It is mainly localized in the cytoplasm and mediates the deacetylation of non-histone proteins, more specifically α-tubulin, heat-shock protein 90 (HSP90) and cortactin, thus being involved in the regulation of the microtubule dynamics and in the transfer of misfolded proteins to the aggresome (Simões-Pires et al., 2013). In α-Synucleinopathies, HDAC6 co-localizes with α-Syn in LBs and GCIs from PD and MSA samples, respectively (Miki et al., 2011).

In this review article, we aim to highlight previous findings regarding α-Syn aggregation, together with *in vivo* and *in vitro* data focusing on the specific role of HDAC6 in the formation of such protein inclusions. These studies may open new avenues towards a promising therapeutic target in α-Synucleinopathies.

α-SYNUCLEIN: AN ENIGMATIC PROTEIN

α-Syn is a protein with 14 kDa (containing 140 amino acids residues), mostly found in the nucleus and in the presynaptic terminals of the central nervous system (CNS; Jakes et al., 1994). It is composed of three distinct regions: (1) an amino terminus containing lipid-binding motif, which allows membrane binding and facilitates the formation of α-helical structures; (2) a central hydrophobic region, also known as the non-Amyloid β component (NAC); and (3), an unstructured and negatively charged carboxyl terminus (Mochizuki et al., 2018). α-Syn, together with β- and γ-Synuclein compose the synuclein family, however, what makes α-Syn structurally unique is the presence of the NAC region, which in turn confers the β-sheet forming potential and facilitates its aggregation process (Wong and Krainc, 2017).

Under physiologic conditions, α-Syn is considered an intrinsically unstructured protein, lacking a defined conformation (Theillet et al., 2016). It has been described that α-Syn exists mostly as a monomer, however, due to its structural flexibility, α-Syn can transit between monomeric and oligomeric states, under a highly-balanced process (Lashuel et al., 2013). As a consequence of such conformational flexibility and its localization at the presynaptic terminals, it is believed that α-Syn has multifunctional properties in the CNS, consisting in the regulation of neurotransmitter release, synaptic function and synaptic plasticity (Lashuel et al., 2013; Ghiglieri et al., 2018).

The attention to this protein expanded upon the discovery of a mutation in the *SNCA* gene, associated with early-onset familial forms of PD (Polymeropoulos et al., 1997). Afterward, in 1997, α-Syn was identified as one of the major components of LBs and LNs, neuronal cytoplasmic inclusions considered to be the pathological hallmark of PD and DLB (Spillantini et al., 1997). A year later, α-Syn was confirmed as the main component of GCIs in MSA (Spillantini et al., 1998; Wakabayashi et al., 1998). To date, it is well-accepted that aggregated α-Syn represents a key feature in the pathogenesis of this group of diseases called α-Synucleinopathies (Stefanis, 2012; Visanji et al., 2019).

Mutations in the SNCA gene and the presence of stress-induced conditions within the cell can lead to increased levels of α-Syn and consequent disruption of the equilibrium between monomeric and oligomeric species (Auluck et al., 2010; Wales et al., 2013). Despite the presence of protein homeostasis mechanisms, α-Syn can undergo a process of uncontrolled oligomerization from soluble oligomeric species into large, insoluble fibrils, resulting in the formation of structures like LBs (Stefanis, 2012). The process of α-Syn aggregation can be potentiated in disease-induced stress conditions in the cells, such as changes in the pH, temperature, oxidative stress, mitochondria

dysfunction, and post-translational modifications (Hasegawa et al., 2002; Anderson et al., 2006). In the healthy brain, α-Syn homeostasis is promoted by combined actions of molecular chaperones, the UPS, and finally, the lysosome autophagy system (Ghiglieri et al., 2018). On the other hand, the accumulation of α-Syn into proteinaceous inclusions creates a scenario in which those protein quality control mechanisms become impaired, resulting in a vicious cycle that aggravates the neurodegeneration process (Djajadikerta et al., 2020).

Under pathological conditions, the failure of intracellular mechanisms of α-Syn clearance might contribute to the pathological release of toxic α-Syn oligomeric species to neighboring cells (Lee et al., 2013; da Fonseca et al., 2015). Recent findings show that soluble and insoluble α-Syn aggregates can be secreted and propagate through connected neuronal regions, in a stereotypical pattern, such as the hypothesis developed by Braak and colleagues, commonly known as the Braak's hypothesis for PD (Braak et al., 2003; McCann et al., 2016). This is evidenced by the presence of α-Syn aggregates in several areas of the CNS, and not only in brain regions where the level of neurodegeneration is more accentuated (Rey et al., 2019). Furthermore, these α-Syn aggregates can be transferred between different brain cells, triggering the oligomerization and aggregation of the native monomeric α-Syn species (Luk et al., 2012; Rey et al., 2019). Such pathological characteristic of α-Syn aggregates was observed upon the addition of recombinant α-Syn fibrils in cultured cells, resulting in the recruitment of the endogenous α-Syn and consequent formation of LBs (Luk et al., 2009).

α-SYNUCLEINOPATHIES

α-Synucleinopathies represent a group of neurodegenerative disorders characterized by the misfolding and aggregation of α-Syn forming LBs and LNs within neurons, or GCIs in oligodendrocytes (Jellinger, 2003; Peelaerts and Baekelandt, 2016). Primary α-Synucleinopathies include diseases such as PD, DLB, and MSA, distinguished by specific clinical and pathological manifestations (Galasko, 2017; Yang and Yu, 2017; Nussbaum, 2018).

PD is the most common motor neurodegenerative disorder, affecting mostly people over the age of 60 years. Clinical manifestations of PD include motor signs such as rigidity, bradykinesia, gait impairment, and resting tremor (Jankovic, 2008; Poewe et al., 2017; Del Rey et al., 2018). In addition to motor symptoms, patients suffering from PD also show several non-motor symptoms, including olfactory dysfunction, REM sleep abnormalities, cognitive impairment, and autonomic failure that may precede the onset of the motor symptoms (Fereshtehnejad et al., 2015; Kalia and Lang, 2015). Pathologically, PD is characterized by filamentous inclusions of α-Syn in neurons, named LBs or Lewy neurites. Also, selective neuronal loss is observed in multiple brain regions that define the clinical presentation of the disease. One of the most affected brain regions is the substantia nigra pars compacta (SNc; Jankovic, 2008; Stefanis, 2012).

In DLB, dementia is accompanied by motor symptoms similar to those in PD, however, the patients with DLB tend to have a poorer response to levodopa treatment (Burn et al., 2003). In most of the cases, autonomic features are also present, such as orthostatic hypotension (Yang and Yu, 2017). Opposed to PD, postmortem analysis of DLB brains reveals less neurodegeneration in the SNc, and an advanced Braak staging in the cerebral cortex and hippocampus, contributing to dementia and Alzheimer's disease (AD)-related symptoms (Dodel et al., 2008).

MSA is a unique α-Synucleinopathy, different from PD and DLB in several ways. It is characterized by a highly variable combination of Parkinsonism, cerebellar ataxia, and autonomic failure, which makes the correct diagnosis sometimes difficult (Jellinger, 2014; Fanciulli and Wenning, 2015). According to the predominance of the parkinsonian or the cerebellar features, the clinical presentation is divided into two subtypes: the MSA-P, where the striatonigral degeneration is more predominant, and MSA-C, where the olivopontocerebellar projections are mostly affected (Valera and Masliah, 2018). In both cases, the patients also show non-motor symptoms, with the most common being an autonomic failure (Fanciulli and Wenning, 2015). The pathological hallmark of MSA is the presence of aggregated α-Syn in the cytoplasm of oligodendrocytes, forming the so-called GCIs (Jellinger and Lantos, 2010). The source of α-Syn in MSA oligodendrocytes remains debatable to date (Miller et al., 2005; Asi et al., 2014; Djelloul et al., 2015). It is suggested that primary oligodendrogliopathy, α-Syn expression in oligodendroglia, and/or α-Syn uptake from surrounding neurons may play a role in the pathogenesis of MSA (Wenning et al., 2008; Fellner et al., 2011; Stefanova and Wenning, 2016).

THE HISTONE DEACETYLASE SUPERFAMILY: WHY IS HDAC6 UNIQUE?

Histone deacetylases (HDACs) are a group of enzymes that promote the deacetylation of lysine residues of histones, as well as cytoplasmic, nuclear, or mitochondrial proteins (Ruijter et al., 2003). The process of lysine deacetylation in histones has been extensively studied over the past years for its role in the regulation of epigenetic modifications and concerning certain types of cancer (Seidel et al., 2015). However, a growing number of identified non-histone substrates has been demonstrating that such enzymes can also regulate important cellular mechanisms such as cell proliferation, intracellular trafficking, and protein stability (Glozak et al., 2005; Haberland et al., 2011). As a consequence, selective HDAC inhibitors have been developed and contributed for a better understanding of the different functions and properties of several members of the HDAC superfamily (Prince et al., 2009; Dietz and Casaccia, 2010; Thaler and Mercurio, 2014; Didonna and Opal, 2015).

To date, HDAC enzymes are divided into four different classes based on their sequence homology to yeast deacetylases, cellular localization, and specific substrates (Ruijter et al., 2003). Class I HDACs include HDAC 1, 2, 3, and 8, which are ubiquitously expressed in the nucleus thus regulating the transcription of genes. Class II HDACs can shuttle between the cytoplasm and the nucleus and are expressed in specific body tissues. Class II is subdivided into Class IIa (HDAC 4, 5,

7, and 9), and Class IIb (HDAC 6 and 10). Class III HDACs are called Sirtuins. They are NAD^+-dependent enzymes and show different structural features. Finally, Class IV is composed only of HDAC11, showing similarities with some Class I and II HDACs. Classes I, II, and IV are referred to as "classical HDACs" due to their zinc-dependent catalytic activity (Ruijter et al., 2003).

The activity of HDAC enzymes is opposed to the functions of histone acetyltransferases (HATs; Saha and Pahan, 2006). In a disease context, an imbalance between HDACs and HATs has been described affecting histone deacetylation and the transcription of genes involved in neuroprotection and apoptosis (Saha and Pahan, 2006). The role of each HDAC enzyme depends on its specific cellular localization and molecular substrate. The involvement of several HDACs in brain disorders has already been described (Simões-Pires et al., 2013; Volmar and Wahlestedt, 2015).

Among all the HDAC enzymes, HDAC6 has emerged as a possible target for disease modification in neurodegenerative diseases over the past few years (Li et al., 2011; Simões-Pires et al., 2013; Van Helleputte et al., 2014). This particular interest in HDAC6 appears to be related to its structural and functional characteristics that make HDAC6 unique compared to other classical HDAC enzymes (Yang and Grégoire, 2005; Simões-Pires et al., 2013). For instance, HDAC6 is the only deacetylase with two functional N-terminal catalytic domains, a C-terminal zinc finger ubiquitin-binding domain, and a tetradecapeptide repeating domain, which together with two leucine-rich nuclear export sequences, contributes to the cytosolic expression of HDAC6 (Li et al., 2011). Such properties allow HDAC6 to interact mainly with cytoplasmic substrates, with particular functions in cellular signaling systems involving not only acetylation but also ubiquitination of proteins and consequent protein degradation (Zhang et al., 2003; Lee et al., 2010). This protein drew even more attention among the research community upon the discovery that it was identified as a component of several pathological inclusions associated with AD, PD, and MSA (Ding et al., 2008; Miki et al., 2011; Chiba et al., 2012). In post-mitotic cells, efficient protein degradation is a crucial step to maintain cellular homeostasis, however, the precise implications of HDAC6 as a therapeutic target in these neurodegenerative disorders remain undefined.

STRUCTURE AND FUNCTIONS OF HDAC6

HDAC6 was identified in 1999 as a protein composed of 1215 amino acids and the only HDAC enzyme containing a full duplication of Class I and II HDAC-homology domain (Grozinger et al., 1999; Verdel and Khochbin, 1999). It contains two active catalytic domains (DD1 and DD2), a ubiquitin zinc-dependent C-terminus domain and a conserved nuclear export signal (NES) at the N-terminus, responsible for the main expression of HDAC6 in the cytoplasm of different cell types (Bertos et al., 2004; Hai and Christianson, 2016; **Figure 1**). According to the literature, the implications of both catalytic domains in the deacetylase activity of HDAC6 are not well understood. Some studies report that both domains are needed for the deacetylation of α-tubulin, whereas others show that the inhibition of DD2 catalytic domain results in less α-tubulin deacetylation, suggesting that the second catalytic domain is responsible for the deacetylation of tubulin substrates (Haggarty et al., 2003; Zhang et al., 2006). Due to its unique structure and localization, HDAC6 is allowed to interact with a wide number of cytoplasmic substrates (Li et al., 2013). The most studied HDAC6 targets are α-tubulin, cortactin, and HSP90 (Hubbert et al., 2002; Zhang et al., 2003, 2007; Kovacs et al., 2005; **Figure 2**). The deacetylation of α-tubulin and cortactin makes HDAC6 an important regulator of the microtubule and actin cytoskeleton dynamics, respectively, contributing to the control of cell motility, adhesion and intracellular cargo trafficking (Zhang et al., 2007; Zilberman et al., 2009; Chen et al., 2010; **Figures 2A,B**). By promoting the deacetylation of HSP90, HDAC6 appears to have an important role in one of the main cellular mechanisms to cope with misfolded proteins (Boyault et al., 2007b; **Figure 2C**). Also, due to the ubiquitin zinc-dependent domain located at the C-terminal, HDAC6 can bind with high affinity to ubiquitinated proteins suggesting a pivotal role of HDAC6 in another cellular proteolysis mechanism (Boyault et al., 2006; **Figure 3**). Such features put HDAC6 on the list of therapeutic targets in neurodegenerative diseases, in which protein accumulation and aggregation leads to neurodegeneration in different regions of the brain.

HDAC6 INTERACTING PARTNERS AND SPECIFIC ROLE IN PROTEIN DEGRADATION

Newly synthesized proteins need the proper biological machinery to adopt the correct conformation. During this process, some proteins can incorrectly fold and form larger aggregates (Balchin et al., 2016). In turn, such aggregates are harmful and constitute one of the common features of neurodegenerative disorders (Ross and Poirier, 2004). Therefore, neuronal cells depend highly on proteolysis and other protein quality control mechanisms to maintain homeostasis in the CNS. As mentioned above, HDAC6 is an important player in several biological processes and it was observed that it is a key regulator of three cellular mechanisms triggered to cope with the accumulation of protein aggregates: (1) the formation of the aggresome and consequent autophagy; (2) the binding to poly-ubiquitinated chains of misfolded proteins; and (3) the deacetylation of HSP90. These mechanisms rely on HDAC6 either through its deacetylase activity, or ubiquitin-binding properties.

HDAC6 is involved in the regulation of the UPS, a cellular mechanism for the degradation of small, soluble, and non-aggregated proteins (Ciechanover and Brundin, 2003). Under physiological conditions, HDAC6 forms a complex with a chaperone-like 97 kDa p97/VCP protein, an adenosine triphosphatase with a pivotal role to transfer ubiquitinated proteins to the proteasome (Boyault et al., 2006; **Figure 3A**). In neurodegenerative disorders, the UPS is impaired, and consequently, poly-ubiquitin protein chains accumulate (Bence et al., 2001). HDAC6 binds the polyubiquitinated proteins to

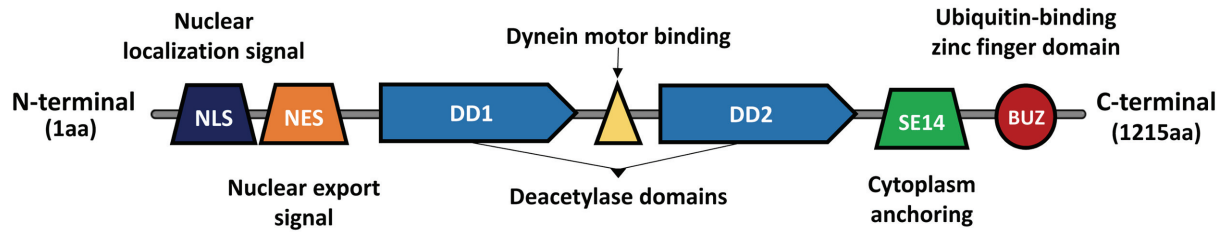

FIGURE 1 | Histone deacetylase 6 (HDAC6) structure and domains. HDAC6 is a Class II histone deacetylase, composed of 1,215 amino acids. It is the only member from the Class II deacetylases containing two active catalytic domains (DD1 and DD2), which allow it to interact with different substrates (e.g., α-tubulin, HSP90, cortactin, et cetera). Due to the nuclear localization signal (NLS) and the nuclear export signal (NES), HDAC6 can shuttle between the nucleus and cytoplasm, however, the presence of a cytoplasm anchoring domain (SE14) ensures that HDAC6 is stably present in the cytoplasm. Between DD1 and DD2 exists a dynein motor binding domain, which allows HDAC6 to interact with the dynein motor complex and modulate cargo trafficking alongside the microtubules. In the C-terminal exists a ubiquitin-binding zinc finger domain (BUZ) with a high affinity to poly-ubiquitinated protein chains.

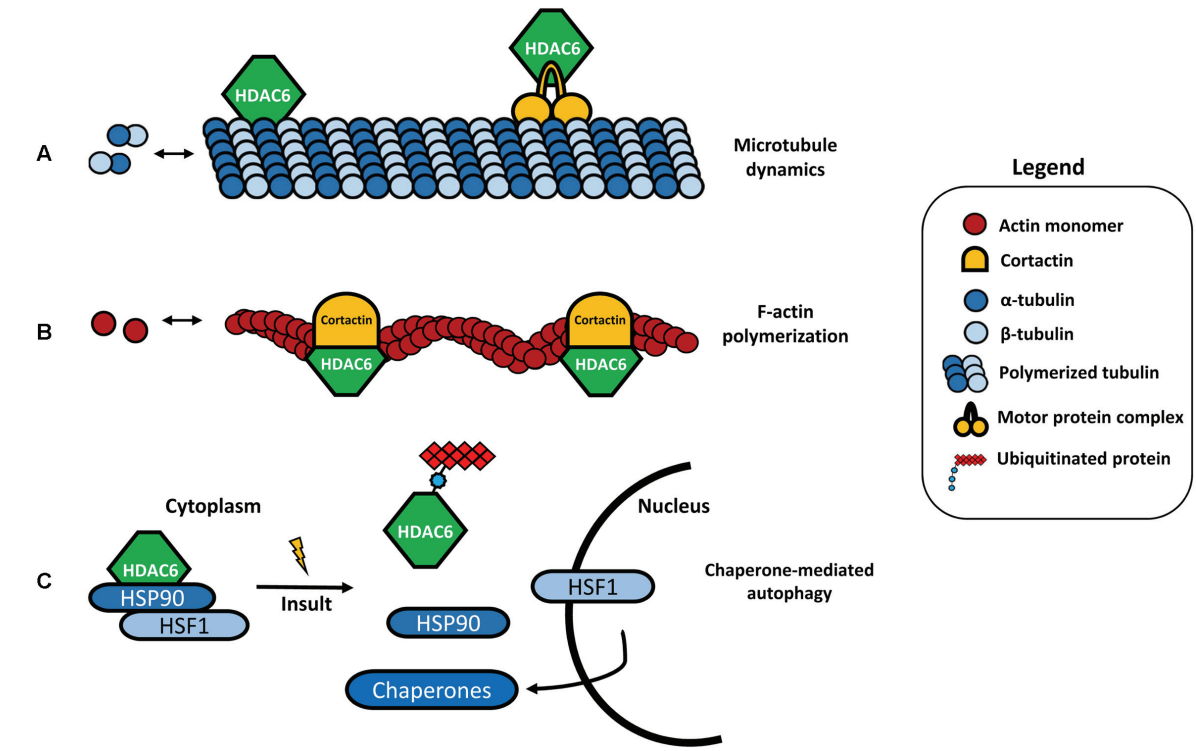

FIGURE 2 | HDAC6 substrates. **(A)** One of the most studied targets of HDAC6 deacetylation is α-tubulin, an important subunit from the microtubules network. By binding to α-tubulin and inducing its deacetylation, HDAC6 can modulate the microtubule dynamics and cell motility. HDAC6 is also able to bind specific protein motor complexes, thus interfering with protein and cargo trafficking. **(B)** Cortactin is also a target for HDAC6 deacetylation. The interaction between HDAC6 and cortactin can modulate actin polymerization. **(C)** HSP90 under basal conditions forms a complex with HDAC6 and heat-shock transcription factor 1 (HSF1), however, in the presence of ubiquitinated protein aggregates, HDAC6 dissociates from this complex, leading to HSF1 activation and translocation to the nucleus to trigger the expression of major cellular chaperones involved in chaperone-mediated autophagy (CMA).

mediate the formation of the aggresome and enable alternative protein degradation through the autophagy-lysosome pathway (Pandey et al., 2007; **Figure 3B**).

Under stress conditions, the activation of a heat-shock gene response complex is triggered, leading to the expression of several chaperones. The activity of the chaperones prevents the aggregate formation by assisting the delivery of misfolded proteins to the UPS, or by mediating the chaperone-mediated autophagy (CMA; Waza et al., 2006). One of these chaperones is the HSP90, another deacetylase target of HDAC6 (Kovacs et al., 2005). HSP90 forms a complex with HDAC6 and the heat-shock transcription factor 1 (HSF1), which remains inactive in normal conditions (Boyault et al., 2007b; **Figure 4A**). Again, the increased levels of ubiquitination will favor the deacetylation

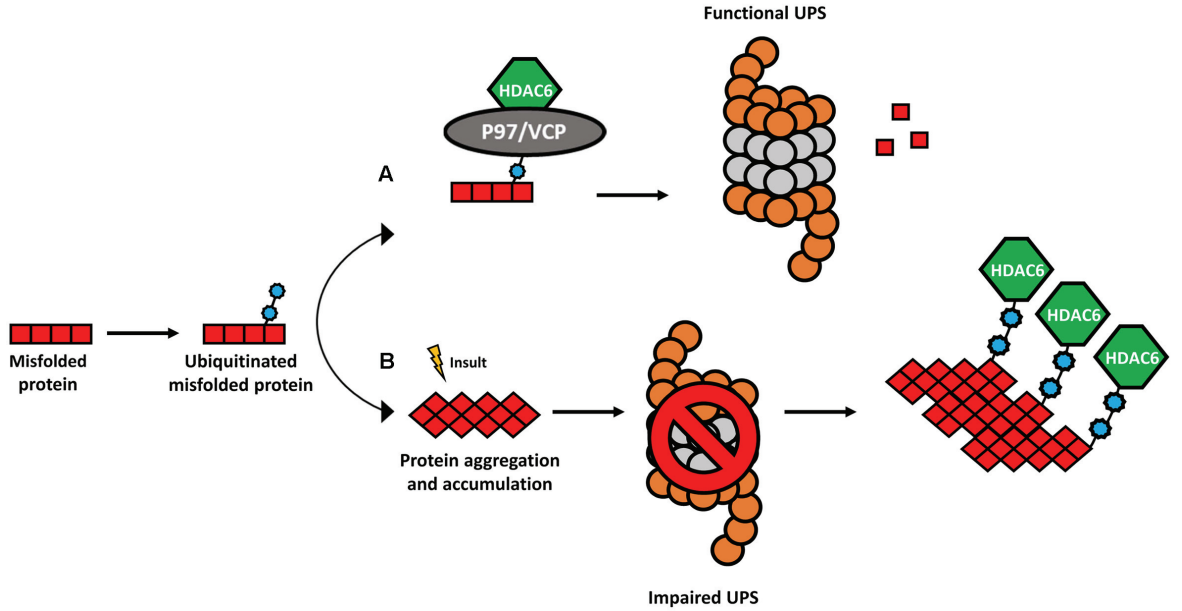

FIGURE 3 | The ubiquitin-binding activity of HDAC6. The presence of a ubiquitin-binding domain in HDAC6 allows it to interact with higher affinity to poly-ubiquitinated protein chains. **(A)** Under physiological conditions, HDAC6 and the chaperone-like P97/VCP constitute a complex whereas an excess of P97/VCP over HDAC6 facilitates the release of ubiquitinated proteins for degradation in the proteasome. **(B)** In several neurodegenerative disorders, the formation of protein aggregates leads to a dysfunctional ubiquitin-proteasome system (UPS) and consequent accumulation of poly-ubiquitinated proteins. HDAC6 senses the increase in poly-ubiquitin chains and binds to them with higher affinity coordinating an alternative cellular protein degradation pathway.

of HSP90 by HDAC6, leading to the dissociation of the complex. As a consequence, HSF1 is activated, induces the transcription of heat-shock proteins and co-chaperones, and initiates a process of CMA (Boyault et al., 2007b).

As already mentioned, one of the most studied deacetylase targets of HDAC6 is α-tubulin, an important subunit of microtubules. Acetylated α-tubulin plays an important role in axonal trafficking and cargo transfer, by promoting the interaction between the motor proteins dynein, kinesin-1, and the microtubule network, therefore interfering with both anterograde and retrograde trafficking of cargo (Reed et al., 2006; **Figure 4B**). For example, velocity and motility of the mitochondria and the transport of proteins have been shown to depend on both anterograde and retrograde axonal transports modulated by HDAC6 inhibition and tubulin acetylation (Bulinski, 2007; Dompierre et al., 2007; Chen et al., 2010; Kim et al., 2012). The formation of the aggresome and consequent autophagic clearance of protein aggregates also depends on the deacetylase activity of HDAC6 and the ability to bind poly-ubiquitinated protein chains (**Figure 4B**). Through the interaction with both ubiquitinated proteins and with the dynein motor complex, HDAC6 mediates the transfer of protein aggregates towards the microtubule organizing center (MTOC), the region where the aggresome formation takes place (Johnston et al., 1998; Kopito, 2000; Kawaguchi et al., 2003). Indeed, the knock-down of HDAC6 resulted in an impairment of the aggresome formation and increased apoptosis in cultured cells, suggesting an important role of the HDAC6-ubiquitin-dynein complex for the transportation of aggregated proteins and the formation of the aggresome (Kawaguchi et al., 2003; **Figure 4B**). Subsequently, lysosome-dependent macroautophagy is triggered to degrade the aggregated proteins of the aggresome (Fortun et al., 2003; Chin et al., 2010). It is believed that the autophagic machinery is recruited to the aggresome in the same way that substrates are accumulated at the MTOC (Iwata et al., 2005). Interestingly, by promoting the reorganization of the actin filaments through the deacetylation of cortactin, HDAC6 plays also an important role facilitating the fusion of lysosomes with autophagosomes, where the aggregates are degraded (Lee et al., 2010; Wang et al., 2018; **Figure 4B**). The depletion of HDAC6 prevents cortactin deacetylation, resulting in impaired lysosome-autophagosome fusion and consequent decrease of autophagic activity (Lee et al., 2010).

These observations suggest a decisive role of HDAC6 in the initiation of three main protein degradation mechanisms.

INVOLVEMENT OF HDAC6 IN NEURODEGENERATIVE DISORDERS

The involvement of HDAC6 in several neurodegenerative disorders has already been described, however, the functions of HDAC6 in the progression of neurodegeneration are not yet understood.

In AD, HDAC6 is significantly increased in the hippocampus and other relevant brain regions both in AD patients and in models of the disease (Zhang et al., 2013). However, the role of HDAC6 in the progression of AD pathology is still unclear. Some studies report that HDAC6 has a beneficial

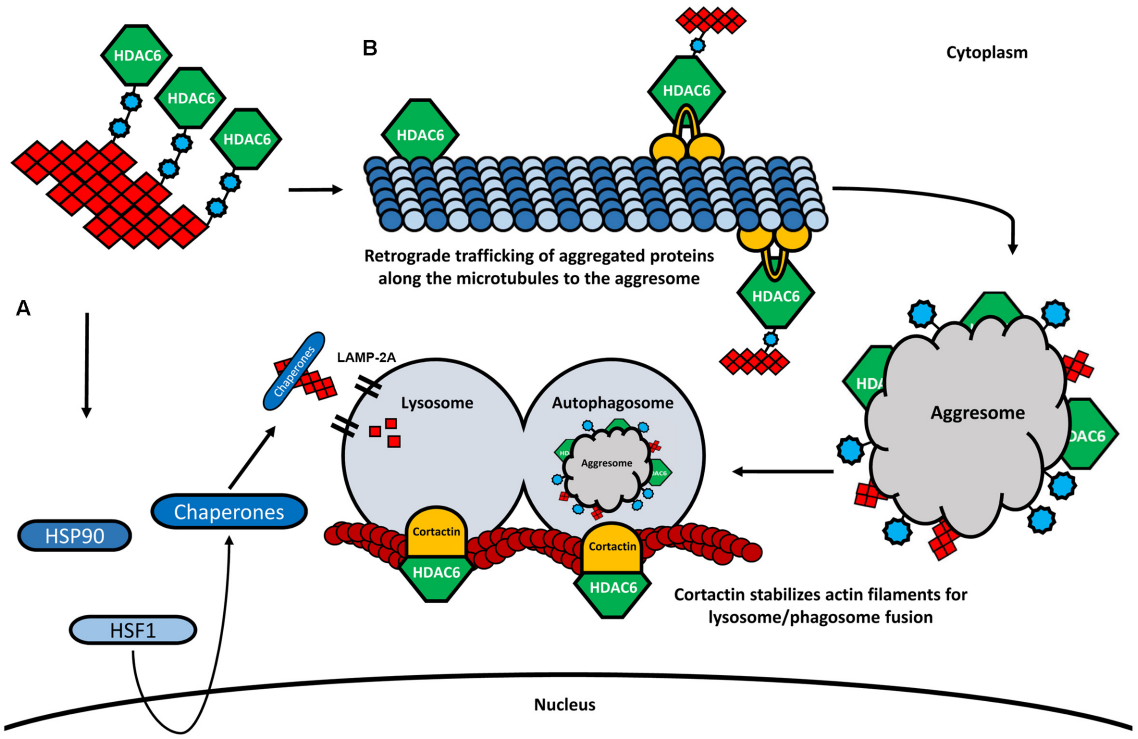

FIGURE 4 | HDAC6 and its involvement in CMA and aggresome formation. **(A)** In the presence of higher amounts of ubiquitinated proteins, HDAC6 dissociates from the HSP90/HSF1 complex, leading to the activation of heat-shock response and degradation of aggregated proteins by the lysosome *via* LAMP-2A. **(B)** HDAC6 binds to ubiquitinated proteins through its ubiquitin-binding domain. Also, HDAC6 interacts with the motor protein dynein and retrogradely transports the aggregated proteins along the microtubules to the perinuclear region where the aggresome is formed. The aggresome is then transferred to the autophagosome, which is fused to the lysosome. The fusion of the autophagosome and the lysosome is further modulated by HDAC6 through the deacetylation of cortactin.

effect by rescuing neurodegeneration while others believe that HDAC6 contributes to AD-associated neurodegeneration. One example of the detrimental role of HDAC6 associated with AD is the direct interaction with the microtubule-associated protein tau (Ding et al., 2008). *In vivo* and *in vitro* experiments show that HDAC6 can bind to tau and modulate its phosphorylation leading to the formation of neurofibrillary tau tangles (Ding et al., 2008; Cook et al., 2012, 2014). In contrast, HDAC6 can also rescue neurodegeneration by participating in the formation of tau-containing aggresomes. Proteasome inhibition *in vitro* resulted in the tau aggresome formation mediated by the ubiquitin-binding activity of HDAC6 (Guthrie and Kraemer, 2011). Therefore, HDAC6 in AD pathology may play a dual role: on one hand, it mediates the hyperphosphorylation of tau and formation of neurofibrillary tangles; on the other hand, it enables the formation of the aggresome and triggers alternative protein degradation by the autophagy-lysosomal pathway.

Huntington's disease (HD) is characterized by the accumulation of the huntingtin protein (htt) and disturbances in axonal transport, resulting in cognitive decline, dementia, and impairment in motor coordination (Walker, 2007). Also, microtubule-dependent transport and tubulin acetylation are decreased in HD, leading to impaired transport of neurotrophic factors and cell death (Gunawardena et al., 2003). The use of HDAC6 inhibitors in a cellular model of HD increased acetylated tubulin and enhanced the recruitment of the dynein motor complex to the microtubules, stimulating the transfer of brain-derived neurotrophic factor (BDNF), in the cells (Dompierre et al., 2007). Furthermore, HDAC6 appeared to have an important role in the degradation of htt by recruiting the autophagic machinery to inclusion bodies containing htt in a neuronal cell model of HD (Iwata et al., 2005). However, in a mouse of HD, the inhibition of HDAC6 showed contradictory effects. Despite increased levels of tubulin acetylation, the authors observed no effects on BDNF transport, nor on the levels of soluble mutant htt (Bobrowska et al., 2011).

HDAC6 is associated with familial cases of amyotrophic lateral sclerosis (ALS), in which mutations in the DNA binding protein TDP-43 result in impaired microtubule-dependent axonal trafficking of mRNAs and the formation of TDP-43 aggregates. Interestingly, TDP-43 can bind to HDAC6 mRNA, regulating its expression (Fiesel et al., 2011). Also, mutations in the chaperone-like p97/VCP are found in ALS cases, resulting in the accumulation of ubiquitin-positive aggregates found in ALS patients (Johnson et al., 2010). The interaction between HDAC6 and p97/VCP is known to orchestrate the degradation of ubiquitinated proteins through the UPS, suggesting a possible role of HDAC6 in ALS pathogenesis (Van Helleputte et al., 2014). It was observed that blocking

HDAC6 activity increased insoluble TDP-43 levels *in vitro*, suggesting that HDAC6 inhibition may exacerbate TDP-43 accumulation (Chen and Cohen, 2019).

THE ROLE OF HDAC6 IN α-SYNUCLEINOPATHIES

The association between HDAC6 and the pathogenesis of α-Synucleinopathies emerged when histopathological analysis in brain sections from PD patients revealed highly concentrated expression of HDAC6 within LBs, suggesting a possible role of HDAC6 in the formation of such inclusions (Kawaguchi et al., 2003; Miki et al., 2011). Besides, a recent study showed that not only HDAC6 but also its phosphorylated form was co-localized with α-Syn in inclusions derived from postmortem brains of PD and MSA patients (Mazzetti et al., 2020). Despite the small cohort of patients used in this study, the presence of phosphorylated HDAC6 seems to be a common feature of intracellular inclusions in α-Synucleinopathies, while it was absent in β-amyloid plaques derived from AD brains. The location of α-Syn inclusions in the brain of patients with PD and MSA is not only limited to the cytoplasm and can be found in the nucleus of neuronal and glial cells. Indeed, several studies have reported that epigenetic disturbances and dysregulation in histone deacetylation play a role in the pathogenesis of PD (Mazzocchi et al., 2020). The presence of α-Syn in the nucleus was shown to interfere with histone acetylation, resulting in gene expression alterations and neurotoxicity *in vitro* (Goers et al., 2003; Kontopoulos et al., 2006). Such neurotoxic effects were rescued upon the treatment with an HDAC inhibitor (Kontopoulos et al., 2006). Another study in a mouse model of MSA showed that histone deacetylation inhibition presented a neuroprotective role in the pathogenesis of MSA-like neurodegeneration (Sturm et al., 2016).

Although there are substantial findings regarding the potential neuroprotective effects in the modulation of HDACs activity in α-Synucleinopathies, the focus on HDAC6 increased with the demonstration that HDAC6 plays an important role in the regulation of different protein degradation mechanisms. As mentioned above, HDAC6 plays a pivotal role in the formation of the aggresome, a cellular defense mechanism to cope with higher amounts of misfolded proteins (Kawaguchi et al., 2003). Interestingly, LBs and aggresomes share important biochemical and morphological properties that led researchers to hypothesize that the formation of LBs is an aggresome-related process (Olanow et al., 2004; Tanaka et al., 2004). Indeed, proteins associated with the formation of the aggresome were found in LBs from PD and DLB patients (McNaught et al., 2002). Besides, LBs can sequester heat-shock proteins such as HSP70, together with proteins associated with the UPS system, also found in the aggresome to enhance protein degradation (Lee and Lee, 2002; McNaught et al., 2002).

Intriguingly, the involvement of HDAC6 in the pathogenesis of PD has been further supported in genetic cases. *ATP13A2*, a gene that is mutated in autosomal recessive juvenile PD, was experimentally shown to facilitate HDAC6 recruitment to the lysosome leading to disruption of autophagosome-lysosome fusion by increasing the cortactin acetylation (Wang et al., 2019).

In oligodendrocytes, the presence of aggresome-related proteins together with HDAC6 were found also co-localized with GCIs derived from brain samples of MSA patients, suggesting that oligodendrocytes may use the same aggresome machinery for the formation of such MSA-specific α-Syn inclusions (Chiba et al., 2012). However, GCIs and aggresomes present some differences. For instance, one important step for the aggresome formation is the redistribution of vimentin, an intermediate filament protein, forming a cage-like structure surrounding aggregated and ubiquitinated proteins in the perinuclear region (Johnston et al., 1998). According to the literature, mature oligodendrocytes are devoid of intermediate filament networks,

TABLE 1 | Current evidence on the effects of HDAC6 modulation on α-Syn aggregation.

Reference	α-Synucleinopathy model	HDAC6 modulation strategy	Effects on α-syn pathology
Du et al. (2010)	Human α-Syn expression in *Drosophila*	Knockout	• Reduced number of α-Syn inclusions • Increased levels of α-Syn oligomers
		Overexpression	• Increased number of α-Syn inclusions • Decreased levels of α-Syn oligomers
Su et al. (2011)	PC12 and SH-SY5Y cell lines with A53T mutant α-Syn overexpression + MPP+ treatment	siRNA Tubacin A	• Intracellular accumulation of α-Syn without the formation of inclusions
Ejlerskov et al. (2013)	The differentiated PC12 cell line with mutant A30P α-Syn overexpression + TPPP/p25α expression	shRNA Trichostatin A	• Increased levels of α-Syn in the nucleus • p25α inhibition of HDAC6 activity resulting in impaired autophagosome maturation and consequent α-Syn exophagy.
Du et al. (2014)	Lactacystin UPS-impairment in mice	Trichostatin A	• Increased α-Syn oligomers in SNc
	SK-N-SH neuroblastoma cell line with α-Syn overexpression	Knockdown	• Increased α-Syn oligomers levels
		Overexpression	• Decreased α-Syn oligomers levels • Increased α-Syn inclusion formation
Francelle et al. (2020)	AAV-α-Syn rat model	Tubastatin A	• Activation of autophagy pathways • Decreased α-Syn phosphorylation

suggesting that the presence of other cytoskeleton proteins may be involved in the formation of GCIs in oligodendrocytes (Chiba et al., 2012; Kaji et al., 2020). Taking this into consideration as well as the involvement of HDAC6 in different protein quality control mechanisms prompted researchers to investigate whether HDAC6 could be involved in the formation of α-Syn containing inclusions.

Therefore, further studies focused on the role of HDAC6 in α-Synucleinopathy models (**Table 1**). In general, the reported data have shown some controversies that may be related to the use of different models and different methods for HDAC6 modulation. Several studies suggested that HDAC6 deficit induced by either pharmacological inhibition (Tubastatin A, Tubacin, Trichostatin A) or genetic modification (knockout, siRNA, shRNA) leads to an increase of oligomeric α-Syn commonly associated with lower cell viability and reduction of the intracellular inclusion burden. These effects have been attributed to impaired aggresome formation and disruption of autophagy mechanisms (Du et al., 2010, 2014; Su et al., 2011; Ejlerskov et al., 2013). On the other hand, Francelle et al. (2020) reported that HDAC6 inhibition in an AAV-α-Syn overexpression model resulted in higher levels of HSP70 and LAMP-2A linked to lower α-syn phosphorylation suggesting a leading role of CMA in this setting, finally leading to the neuroprotection of dopaminergic neurons. Alternatively, HDAC6 overexpression was suggested to lower α-Syn oligomer levels but substantially increase the level of insoluble protein and inclusion formation, which the authors related to reduced cellular toxicity (Du et al., 2010, 2014). Importantly, the Class III HDAC, Sirtuin 2, expressed also in the cytoplasm, has been associated with the modulation of tubulin acetylation and its inhibition led to neuroprotection linked to enlargement of α-Syn aggregates in PD models (Outeiro et al., 2007). Whether HDAC6 and Sirtuin 2 may share common mechanisms of neuroprotection in α-Synucleinopathy is not completely clear. Recently, Mazzocchi and collaborators (Mazzocchi et al., 2020) proposed that the neuroprotective effects of HDAC6 may be due to the modulation of the proteinopathy, however, rescue effects may depend on the cellular context, e.g., linked to other processes dependent on the cytoskeletal dynamics like axonal transport of synaptic activity. Further studies will be needed to understand the interference of HDAC6 with α-Syn toxicity concerning its structure and interaction partners, which may tune the interaction outcome in the different experimental systems.

It is currently unclear whether the interaction between α-Syn and HDAC6 may be bidirectional. It was previously proposed that α-Syn in the nucleus may interfere with histone acetylation and HDAC inhibition may rescue the pathology in cell culture and in flies (Kontopoulos et al., 2006). Similar effects of α-Syn in the cytoplasm on the acetylation of other proteins have not been reported yet.

CONCLUDING REMARKS

To summarize, it becomes clear that HDAC6 is involved in the pathology of α-Synucleinopathies by interfering with the accumulation of α-Syn oligomers and the formation of protein aggregates. Importantly, LBs in neurons and GCIs in oligodendrocytes differ in the structure supporting the idea of a different origin and/or trigger of α-Syn aggregation. However, LBs and GCIs share common components including HDAC6, ubiquitin, and heat shock proteins. This fact suggests that the same protein clearance mechanisms may act to rescue the cells from the accumulating misfolded α-Syn, however remaining inefficient.

HDAC6 may represent an attractive target for the therapy of α-Synucleinopathies, however, the effects of its enzymatic (deacetylation activity) or non-enzymatic activity (binding to ubiquitin) on α-Syn inclusion formation are still not conclusive. Models, selectively modulating each of these activities may help decipher their involvement and roles in the pathogenesis of α-Synucleinopathies. Understanding the role of possible interaction partners may be crucial for the interpretation of the outcomes of HDAC6 modulation in the variable experimental systems. Finally, understanding how the effects of HDAC6 on other basic cellular mechanisms may interfere with the vulnerability to α-Syn will be crucial in the future search for strategies to target HDAC6 for disease modification in α-Synucleinopathies.

AUTHOR CONTRIBUTIONS

ML wrote the first draft of the manuscript. NS conceived the idea and made revisions to the text. Both authors have seen and approved the submitted version.

FUNDING

This work was supported by grants of the Austrian Science Fund (FWF) W1206-08 and F4414.

REFERENCES

Anderson, J. P., Walker, D. E., Goldstein, J. M., De Laat, R., Banducci, K., Caccavello, R. J., et al. (2006). Phosphorylation of Ser-129 is the dominant pathological modification of α-Synuclein in familial and sporadic Lewy body disease. *J. Biol. Chem.* 281, 29739–29752. doi: 10.1074/jbc.m600933200

Asi, Y. T., Simpson, J. E., Heath, P. R., Wharton, S. B., Lees, A. J., Revesz, T., et al. (2014). α-Synuclein mRNA expression in oligodendrocytes in MSA. *Glia* 62, 964–970. doi: 10.1002/glia.22653

Auluck, P. K., Caraveo, G., and Lindquist, S. (2010). α-Synuclein: membrane interactions and toxicity in Parkinson's disease. *Annu. Rev. Cell Dev. Biol.* 26, 211–233. doi: 10.1146/annurev.cellbio.042308.113313

Balchin, D., Hayer-Hartl, M., and Hartl, F. U. (2016). *In vivo* aspects of protein folding and quality control. *Science* 353:aac4354. doi: 10.1126/science.aac4354

Bence, N. F., Sampat, R. M., and Kopito, R. R. (2001). Impairment of the ubiquitin-proteasome system by protein aggregation. *Science* 292, 1552–1555. doi: 10.1126/science.292.5521.1552

Bertos, N. R., Gilquin, B., Chan, G. K. T., Yen, T. J., Khochbin, S., and Yang, X. J. (2004). Role of the tetradecapeptide repeat domain of human histone deacetylase 6 in cytoplasmic retention. *J. Biol. Chem.* 279, 48246–48254. doi: 10.1074/jbc.m408583200

Bobrowska, A., Paganetti, P., Matthias, P., and Bates, G. P. (2011). HDAC6 knock-out increases tubulin acetylation but does not modify disease progression in the R6/2 mouse model of Huntington's disease. *PLoS One* 6:e20696. doi: 10.1371/journal.pone.0020696

Boyault, C., Gilquin, B., Zhang, Y., Rybin, V., Garman, E., Meyer-Klaucke, W., et al. (2006). HDAC6–p97/VCP controlled polyubiquitin chain turnover. *EMBO J.* 25, 3357–3366. doi: 10.1038/sj.emboj.7601210

Boyault, C., Sadoul, K., Pabion, M., and Khochbin, S. (2007a). HDAC6, at the crossroads between cytoskeleton and cell signaling by acetylation and ubiquitination. *Oncogene* 26, 5468–5476. doi: 10.1038/sj.onc.1210614

Boyault, C., Zhang, Y., Fritah, S., Caron, C., Gilquin, B., Kwon, S. H., et al. (2007b). HDAC6 controls major cell response pathways to cytotoxic accumulation of protein aggregates. *Genes Dev.* 21, 2172–2181. doi: 10.1101/gad.436407

Braak, H., Del Tredici, K., Rüb, U., De Vos, R. A. I., Jansen Steur, E. N. H., and Braak, E. (2003). Staging of brain pathology related to sporadic Parkinson's disease. *Neurobiol. Aging* 24, 197–211. doi: 10.1016/s0197-4580(02)00065-9

Bulinski, J. C. (2007). Microtubule modification: acetylation speeds anterograde traffic flow. *Curr. Biol.* 17, R18–R20. doi: 10.1016/j.cub.2006.11.036

Burn, D. J., Rowan, E. N., Minett, T., Sanders, J., Myint, P., Richardson, J., et al. (2003). Extrapyramidal features in Parkinson's disease with and without dementia and dementia with Lewy bodies: a cross-sectional comparative study. *Mov. Disord.* 18, 884–889. doi: 10.1002/mds.10455

Chen, Y., and Cohen, T. J. (2019). Aggregation of the nucleic acid- binding protein TDP-43 occurs *via* distinct routes that are coordinated with stress granule formation. *J. Biol. Chem.* 294, 3696–3706. doi: 10.1074/jbc.ra118.006351

Chen, S., Owens, G. C., Makarenkova, H., and Edelman, D. B. (2010). HDAC6 Regulates mitochondrial transport in hippocampal neurons. *PLoS One* 5:e10848. doi: 10.1371/journal.pone.0010848

Chiba, Y., Takei, S., Kawamura, N., Kawaguchi, Y., Sasaki, K., Hasegawa-Ishii, S., et al. (2012). Immunohistochemical localization of aggresomal proteins in glial cytoplasmic inclusions in multiple system atrophy. *Neuropathol. Appl. Neurobiol.* 38, 559–571. doi: 10.1111/j.1365-2990.2011.01229.x

Chin, L. S., Olzmann, J. A., and Li, L. (2010). Parkin-mediated ubiquitin signalling in aggresome formation and autophagy. *Biochem. Soc. Trans.* 38, 144–149. doi: 10.1042/bst0380144

Ciechanover, A., and Brundin, P. (2003). The ubiquitin proteasome system in neurodegenerative diseases: sometimes the chicken, sometimes the egg. *Neuron* 40, 427–446. doi: 10.1016/s0896-6273(03)00606-8

Ciechanover, A., and Kwon, Y. T. A. (2015). Degradation of misfolded proteins in neurodegenerative diseases: therapeutic targets and strategies. *Exp. Mol. Med.* 47:e147. doi: 10.1038/emm.2014.117

Cook, C., Carlomagno, Y., Gendron, T. F., Dunmore, J., Scheffel, K., Stetler, C., et al. (2014). Acetylation of the KXGS motifs in tau is a critical determinant in modulation of tau aggregation and clearance. *Hum. Mol. Genet.* 23, 104–116. doi: 10.1093/hmg/ddt402

Cook, C., Gendron, T. F., Scheffel, K., Carlomagno, Y., Dunmore, J., DeTure, M., et al. (2012). Loss of HDAC6, a novel CHIP substrate, alleviates abnormal tau accumulation. *Hum. Mol. Genet.* 21, 2936–2945. doi: 10.1093/hmg/dds125

da Fonseca, T. L., Villar-Piqué, A., and Outeiro, T. F. (2015). The interplay between α-Synuclein clearance and spreading. *Biomolecules* 5, 435–471. doi: 10.3390/biom5020435

Del Rey, N. L. G., Quiroga-Varela, A., Garbayo, E., Carballo-Carbajal, I., Fernández-Santiago, R., Monje, M. H. G., et al. (2018). Advances in parkinson's disease: 200 years later. *Front. Neuroanat.* 12:113. doi: 10.3389/fnana.2018.00113

Didonna, A., and Opal, P. (2015). The promise and perils of HDAC inhibitors in neurodegeneration. *Ann. Clin. Transl. Neurol.* 2, 79–101. doi: 10.1002/acn3.147

Dietz, K. C., and Casaccia, P. (2010). HDAC inhibitors and neurodegeneration: at the edge between protection and damage. *Pharmacol. Res.* 62, 11–17. doi: 10.1016/j.phrs.2010.01.011

Ding, H., Dolan, P. J., and Johnson, G. V. W. (2008). Histone deacetylase 6 interacts with the microtubule-associated protein tau. *J. Neurochem.* 106, 2119–2130. doi: 10.1111/j.1471-4159.2008.05564.x

Djajadikerta, A., Keshri, S., Pavel, M., Prestil, R., Ryan, L., and Rubinsztein, D. C. (2020). Autophagy induction as a therapeutic strategy for neurodegenerative diseases. *J. Mol. Biol.* 432, 2799–2821. doi: 10.1016/j.jmb.2019.12.035

Djelloul, M., Holmqvist, S., Boza-Serrano, A., Azevedo, C., Yeung, M. S., Goldwurm, S., et al. (2015). α-Synuclein expression in the oligodendrocyte lineage: an *in vitro* and *in vivo* study using rodent and human models. *Stem Cell Reports* 5, 174–184. doi: 10.1016/j.stemcr.2015.07.002

Dodel, R., Csoti, I., Ebersbach, G., Fuchs, G., Hahne, M., Kuhn, W., et al. (2008). Lewy body dementia and Parkinson's disease with dementia. *J. Neurol.* 255, 39–47. doi: 10.1007/s00415-008-5007-0

Dompierre, J. P., Godin, J. D., Charrin, B. C., Cordelières, F. P., King, S. J., Humbert, S., et al. (2007). Histone deacetylase 6 inhibition compensates for the transport deficit in Huntington's disease by increasing tubulin acetylation. *J. Neurosci.* 27, 3571–3583. doi: 10.1523/JNEUROSCI.0037-07.2007

Du, G., Liu, X., Chen, X., Song, M., Yan, Y., Jiao, R., et al. (2010). Drosophila HDAC6 protects dopaminergic neurons against synuclein toxicity by promoting inclusion formation. *Mol. Biol. Cell* 21, 4325–4337. doi: 10.1091/mbc.e10-03-0200

Du, Y., Wang, F., Zou, J., Le, W., Dong, Q., Wang, Z., et al. (2014). Histone deacetylase 6 regulates cytotoxic α-Synuclein accumulation through induction of the heat shock response. *Neurobiol. Aging* 35, 2316–2328. doi: 10.1016/j.neurobiolaging.2014.04.029

Duda, J. E., Lee, V. M., and Trojanowski, J. Q. (2000). Neuropathology of synuclein aggregates: new insights into mechanisms of neurodegenerative diseases. *J. Neurosci. Res.* 61, 121–127. doi: 10.1002/1097-4547(20000715)61:2<121::aid-jnr1>3.0.co;2-4

Ejlerskov, P., Rasmussen, I., Nielsen, T. T., Bergström, A. L., Tohyama, Y., Jensen, P. H., et al. (2013). Tubulin polymerization-promoting protein (TPPP/p25α) promotes unconventional secretion of α-Synuclein through exophagy by impairing autophagosome-lysosome fusion. *J. Biol. Chem.* 288, 17313–17335. doi: 10.1074/jbc.M112.401174

Fanciulli, A., and Wenning, G. K. (2015). Multiple-system atrophy. *N. Eng. J. Med.* 372, 249–263. doi: 10.1056/NEJMra1311488

Fellner, L., Jellinger, K. A., Wenning, G. K., and Stefanova, N. (2011). Glial dysfunction in the pathogenesis of α-Synucleinopathies: emerging concepts. *Acta Neuropathol.* 121, 675–693. doi: 10.1007/s00401-011-0833-z

Fereshtehnejad, S. M., Shafieesabet, M., Farhadi, F., Hadizadeh, H., Rahmani, A., Naderi, N., et al. (2015). Heterogeneous determinants of quality of life in different phenotypes of Parkinson's disease. *PLoS One* 10:e0137081. doi: 10.1371/journal.pone.0137081

Fiesel, F. C., Schurr, C., Weber, S. S., and Kahle, P. J. (2011). TDP-43 knockdown impairs neurite outgrowth dependent on its target histone deacetylase 6. *Mol. Neurodegener.* 6:64. doi: 10.1186/1750-1326-6-64

Fortun, J., Dunn, W. A. Jr., Joy, S., Li, J., and Notterpek, L. (2003). Emerging role for autophagy in the removal of aggresomes in schwann cells. *J. Neurosci.* 23, 10672–10680. doi: 10.1523/JNEUROSCI.23-33-10672.2003

Francelle, L., Outeiro, T. F., and Rappold, G. A. (2020). Inhibition of HDAC6 activity protects dopaminergic neurons from α-Synuclein toxicity. *Sci. Rep.* 10:6064. doi: 10.1038/s41598-020-62678-5

Galasko, D. (2017). Lewy body disorders. *Neurol. Clin.* 35, 325–338. doi: 10.1016/j.ncl.2017.01.004

Ghiglieri, V., Calabrese, V., and Calabresi, P. (2018). α-Synuclein: from early synaptic dysfunction to neurodegeneration. *Front. Neurol.* 9:295. doi: 10.3389/fneur.2018.00295

Glozak, M. A., Sengupta, N., Zhang, X., and Seto, E. (2005). Acetylation and deacetylation of non-histone proteins. *Gene* 363, 15–23. doi: 10.1016/j.gene.2005.09.010

Goedert, M., Jakes, R., and Spillantini, M. G. (2017). The synucleinopathies: twenty years on. *J. Parkinsons Dis.* 7, S51–S69. doi: 10.3233/jpd-179005

Goers, J., Manning-Bog, A. B., McCormack, A. L., Millett, I. S., Doniach, S., Di Monte, D. A., et al. (2003). Nuclear localization of alpha-synuclein and its interaction with histones. *Biochemistry* 42, 8465–8471. doi: 10.1021/bi0341152

Grozinger, C. M., Hassig, C. A., and Schreiber, S. L. (1999). Three proteins define a class of human histone deacetylases related to yeast Hda1p. *Proc. Natl. Acad. Sci. U S A* 96, 4868–4873. doi: 10.1073/pnas.96.9.4868

Gunawardena, S., Her, L. S., Brusch, R. G., Laymon, R. A., Niesman, I. R., Gordesky-Gold, B., et al. (2003). Disruption of axonal transport by loss of

huntingtin or expression of pathogenic polyQ proteins in *Drosophila*. *Neuron* 40, 25–40. doi: 10.1016/s0896-6273(03)00594-4

Guthrie, C. R., and Kraemer, B. C. (2011). Proteasome inhibition drives HDAC6-dependent recruitment of tau to aggresomes. *J. Mol. Neurosci.* 45, 32–41. doi: 10.1007/s12031-011-9502-x

Haberland, M., Montgomery, R. L., and Olson, E. N. (2011). The many roles of histone deacetylases in development and physiology: implications for disease and therapy. *Nat. Rev. Genet.* 10, 32–42. doi: 10.1038/nrg2485

Haggarty, S. J., Koeller, K. M., Wong, J. C., Grozinger, C. M., and Schreiber, S. L. (2003). Domain-selective small-molecule inhibitor of tubulin deacetylation 6 (HDAC6)-mediated tubulin deacetylation. *Proc. Natl. Acad. Sci. U S A* 100, 4389–4394. doi: 10.1073/pnas.0430973100

Hai, Y., and Christianson, D. W. (2016). Histone deacetylase 6 structure and molecular basis of catalysis and inhibition. *Nat. Chem. Biol.* 12, 741–747. doi: 10.1038/nchembio.2134

Hasegawa, M., Fujiwara, H., Nonaka, T., Wakabayashi, K., Takahashi, H., Lee, V. M. Y., et al. (2002). Phosphorylated α-Synuclein is ubiquitinated in α-synucleinopathy lesions. *J. Biol. Chem.* 277, 49071–49076. doi: 10.1074/jbc.M208046200

Hubbert, C., Guardiola, A., Shao, R., Kawaguchi, Y., Ito, A., Nixon, A., et al. (2002). HDAC6 is a microtubule-associated deacetylase. *Nature* 417, 455–458. doi: 10.1038/417455a

Iwata, A., Riley, B. E., Johnston, J. A., and Kopito, R. R. (2005). HDAC6 and microtubules are required for autophagic degradation of aggregated Huntingtin. *J. Biol. Chem.* 280, 40282–40292. doi: 10.1074/jbc.m508786200

Jakes, R., Spillantini, M. G., and Goedert, M. (1994). Identification of two distinct synucleins from human brain. *FEBS Lett.* 345, 27–32. doi: 10.1016/0014-5793(94)00395-5

Jankovic, J. (2008). Parkinson's disease: clinical features and diagnosis. *J. Neurol. Neurosurg. Psychiatry* 79, 368–376. doi: 10.1136/jnnp.2007.131045

Jellinger, K. A. (2003). Neuropathological spectrum of synucleinopathies. *Mov. Disord.* 18, 2–12. doi: 10.1002/mds.10557

Jellinger, K. A. (2014). Neuropathology of multiple system atrophy: new thoughts about pathogenesis. *Mov. Disord.* 29, 1720–1741. doi: 10.1002/mds.26052

Jellinger, K. A., and Lantos, P. L. (2010). Papp-Lantos inclusions and the pathogenesis of multiple system atrophy: an update. *Acta Neuropathol.* 119, 657–667. doi: 10.1007/s00401-010-0672-3

Johnson, J. O., Mandrioli, J., Benatar, M., Deerlin, V. M. V., Trojanowski, J. Q., Gibbs, J. R., et al. (2010). Exome sequencing reveals VCP mutations as a cause of familial ALS. *Neuron* 68, 857–864. doi: 10.1016/j.neuron.2010.11.036

Johnston, J. A., Ward, C. L., and Kopito, R. R. (1998). A cellular response to misfolded proteins aggresomes. *J. Cell Biol.* 143, 1883–1898. doi: 10.1083/jcb.143.7.1883

Kaji, S., Maki, T., Ishimoto, T., Yamakado, H., and Takahashi, R. (2020). Insights into the pathogenesis of multiple system atrophy: focus on glial cytoplasmic inclusions. *Transl. Neurodegener.* 9:7. doi: 10.1186/s40035-020-0185-5

Kalia, L. V., and Lang, A. E. (2015). Parkinson's disease. *Lancet* 386, 896–912. doi: 10.1016/S0140-6736(14)61393-3

Kaushik, S., and Cuervo, A. M. (2015). Proteostasis and aging. *Nat. Med.* 21, 1406–1415. doi: 10.1038/nm.4001

Kawaguchi, Y., Kovacs, J. J., McLaurin, A., Vance, J. M., Ito, A., and Yao, T. P. (2003). The deacetylase HDAC6 regulates aggresome formation and cell viability in response to misfolded protein stress. *Cell* 115, 727–738. doi: 10.1016/s0092-8674(03)00939-5

Kim, C., Choi, H., Jung, E. S., Lee, W., Oh, S., and Jeon, N. L. (2012). HDAC6 inhibitor blocks amyloid β-induced impairment of mitochondrial transport in hippocampal neurons. *PLoS One* 7:e42983. doi: 10.1371/journal.pone.0042983

Kontopoulos, E., Parvin, J. D., and Feany, M. B. (2006). α-Synuclein acts in the nucleus to inhibit histone acetylation and promote neurotoxicity. *Hum. Mol. Genet.* 15, 3012–3023. doi: 10.1093/hmg/ddl243

Kopito, R. R. (2000). Aggresomes, inclusion bodies and protein aggregation. *Trends Cell Biol.* 10, 524–530. doi: 10.1016/s0962-8924(00)01852-3

Kovacs, J. J., Murphy, P. J. M., Gaillard, S., Zhao, X., Wu, J. T., Nicchitta, C. V., et al. (2005). HDAC6 regulates Hsp90 acetylation and chaperone-dependent activation of glucocorticoid receptor. *Mol. Cell* 18, 601–607. doi: 10.1016/j.molcel.2005.04.021

Lashuel, H. A., Overk, C. R., Oueslati, A., and Masliah, E. (2013). The many faces of α-Synuclein: from structure and toxicity to therapeutic target. *Nat. Rev. Neurosci.* 14, 38–48. doi: 10.1038/nrn3406

Lee, H. J., Cho, E. D., Lee, K. W., Kim, J. H., Cho, S. G., and Lee, S. J. (2013). Autophagic failure promotes the exocytosis and intercellular transfer of α-Synuclein. *Exp. Mol. Med.* 45:e22. doi: 10.1038/emm.2013.45

Lee, J. Y., Koga, H., Kawaguchi, Y., Tang, W., Wong, E., Gao, Y. S., et al. (2010). HDAC6 controls autophagosome maturation essential for ubiquitin-selective quality-control autophagy. *EMBO J.* 29, 969–980. doi: 10.1038/emboj.2009.405

Lee, H. J., and Lee, S. J. (2002). Characterization of cytoplasmic α-Synuclein aggregates. Fibril formation is tightly linked to the inclusion-forming process in cells. *J. Biol. Chem.* 277, 48976–48983. doi: 10.1074/jbc.M208192200

Li, G., Jiang, H., Chang, M., Xie, H., and Hu, L. (2011). HDAC6 α-tubulin deacetylase: a potential therapeutic target in neurodegenerative diseases. *J. Neurol. Sci.* 304, 1–8. doi: 10.1016/j.jns.2011.02.017

Li, Y., Shin, D., and Kwon, S. H. (2013). Histone deacetylase 6 plays a role as a distinct regulator of diverse cellular processes. *FEBS J.* 280, 775–793. doi: 10.1111/febs.12079

Luk, K. C., Kehm, V., Carroll, J., Zhang, B., Brien, P. O., Trojanowski, J. Q., et al. (2012). Pathological α-Synuclein transmission initiates Parkinson-like neurodegeneration in nontransgenic mice. *Science* 338, 949–954. doi: 10.1126/science.1227157

Luk, K. C., Song, C., Brien, P. O., Stieber, A., Branch, J. R., Brunden, K. R., et al. (2009). Exogenous α-Synuclein fibrils seed the formation of Lewy body-like intracellular inclusions in cultured cells. *Proc. Natl. Acad. Sci. U S A* 106, 20051–20056. doi: 10.1073/pnas.0908005106

Mazzetti, S., De Leonardis, M., Gagliardi, G., Calogero, A. M., Basellini, M. J., Madaschi, L., et al. (2020). Phospho-HDAC6 gathers into protein aggregates in Parkinson's disease and atypical Parkinsonisms. *Front. Neurosci.* 14:624. doi: 10.3389/fnins.2020.00624

Mazzocchi, M., Collins, L. M., Sullivan, A. M., and O'Keeffe, G. W. (2020). The class II histone deacetylases as therapeutic targets for Parkinson's disease. *Neuronal Signal.* 4:Ns20200001. doi: 10.1042/ns20200001

McCann, H., Cartwright, H., and Halliday, G. M. (2016). Neuropathology of α-Synuclein propagation and braak hypothesis. *Mov. Disord.* 31, 152–160. doi: 10.1002/mds.26421

McNaught, K. S. P., Shashidharan, P., Perl, D. P., Jenner, P., and Olanow, C. W. (2002). Aggresome-related biogenesis of Lewy bodies. *Eur. J. Neurosci.* 16, 2136–2148. doi: 10.1046/j.1460-9568.2002.02301.x

Miki, Y., Mori, F., Tanji, K., Kakita, A., Takahashi, H., and Wakabayashi, K. (2011). Accumulation of histone deacetylase 6, an aggresome-related protein, is specific to Lewy bodies and glial cytoplasmic inclusions. *Neuropathology* 31, 561–568. doi: 10.1111/j.1440-1789.2011.01200.x

Miller, D. W., Johnson, J. M., and Solano, S. M. (2005). Absence of α-Synuclein mRNA expression in normal and multiple system atrophy oligodendroglia. *J. Neural Transm.* 112, 1613–1624. doi: 10.1007/s00702-005-0378-1

Mochizuki, H., Choong, C. J., and Masliah, E. (2018). A refined concept: α-Synuclein dysregulation disease. *Neurochem. Int.* 119, 84–96. doi: 10.1016/j.neuint.2017.12.011

Nussbaum, R. L. (2018). Genetics of synucleinopathies. *Cold Spring Harb. Perspect. Med.* 8:a024109. doi: 10.1101/cshperspect.a024109

Olanow, C. W., Perl, D. P., DeMartino, G. N., and McNaught, K. S. P. (2004). Lewy-body formation is an aggresome-related process: a hypothesis. *Lancet Neurol.* 3, 496–503. doi: 10.1016/s1474-4422(04)00827-0

Olzmann, J. A., Li, L., and Chin, L. S. (2008). Aggresome formation and neurodegenerative diseases: therapeutic implications. *Curr. Med. Chem.* 15, 47–60. doi: 10.2174/092986708783330692

Outeiro, T. F., Kontopoulos, E., Altmann, S. M., Kufareva, I., Strathearn, K. E., Amore, A. M., et al. (2007). Sirtuin 2 inhibitors rescue α-Synuclein-mediated toxicity in models of Parkinson's disease. *Science* 317, 516–519. doi: 10.1126/science.1143780

Ouyang, H., Ali, Y. O., Ravichandran, M., Dong, A., Qiu, W., MacKenzie, F., et al. (2012). Protein aggregates are recruited to aggresome by histone deacetylase 6 *via* unanchored ubiquitin C termini. *J. Biol. Chem.* 287, 2317–2327. doi: 10.1074/jbc.m111.273730

Pandey, U. B., Nie, Z., Batlevi, Y., McCray, B. A., Ritson, G. P., Nedelsky, N. B., et al. (2007). HDAC6 rescues neurodegeneration and provides an

essential link between autophagy and the UPS. *Nature* 447, 859–863. doi: 10.1038/nature05853

Peelaerts, W., and Baekelandt, V. (2016). α-Synuclein strains and the variable pathologies of synucleinopathies. *J. Neurochem.* 139, 256–274. doi: 10.1111/jnc.13595

Poewe, W., Seppi, K., Tanner, C. M., Halliday, G. M., Brundin, P., Volkmann, J., et al. (2017). Parkinson disease. *Nat. Rev. Dis. Primers* 3, 1–21. doi: 10.1038/nrdp.2017.13

Polymeropoulos, M. H., Lavedan, C., Leroy, E., Ide, S. E., Dehejia, A., Dutra, A., et al. (1997). Mutation in the α-Synuclein gene identified in families with Parkinson's disease. *Science* 276, 2045–2047. doi: 10.1126/science.276.5321.2045

Prince, H. M., Bishton, M. J., and Harrison, S. J. (2009). Clinical studies of histone deacetylase inhibitors. *Clin. Cancer Res.* 15, 3958–3969. doi: 10.1158/1078-0432.CCR-08-2785

Reed, N. A., Cai, D., Blasius, T. L., Jih, G. T., Meyhofer, E., Gaertig, J., et al. (2006). Microtubule acetylation promotes kinesin-1 binding and transport. *Curr. Biol.* 16, 2166–2172. doi: 10.1016/j.cub.2006.09.014

Rey, N. L., Bousset, L., George, S., Madaj, Z., Meyerdirk, L., Schulz, E., et al. (2019). α-Synuclein conformational strains spread, seed and target neuronal cells differentially after injection into the olfactory bulb. *Acta Neuropathol. Commun.* 7:221. doi: 10.1186/s40478-019-0859-3

Ross, C. A., and Poirier, M. A. (2004). Protein aggregation and neurodegenerative disease. *Nat. Med.* 10, S10–S10. doi: 10.1038/nm1066

Ruijter, A. J. M. D., Gennip, A. H. V., Caron, H. N., Kemp, S., and Kuilenburg, A. B. P. V. (2003). Histone deacetylases (HDACs): characterization of the classical HDAC family. *Biochem. J.* 749, 737–749. doi: 10.1042/bj20021321

Saha, R. N., and Pahan, K. (2006). HATs and HDACs in neurodegeneration: a tale of disconcerted acetylation homeostasis. *Cell Death Differ.* 13, 539–550. doi: 10.1038/sj.cdd.4401769

Seidel, C., Schnekenburger, M., Dicato, M., and Diederich, M. (2015). Histone deacetylase 6 in health and disease. *Epigenomics* 7, 103–118. doi: 10.2217/epi.14.69

Simões-Pires, C., Zwick, V., Nurisso, A., Schenker, E., Carrupt, P. A., and Cuendet, M. (2013). HDAC6 as a target for neurodegenerative diseases: what makes it different from the other HDACs? *Mol. Neurodegener.* 8:7. doi: 10.1186/1750-1326-8-7

Soto, C., and Pritzkow, S. (2018). Protein misfolding, aggregation and conformational strains in neurodegenerative diseases. *Nat. Neurosci.* 21, 1332–1340. doi: 10.1038/s41593-018-0235-9

Spillantini, M. G., and Goedert, M. (2000). The α-Synucleinopathies: Parkinson's disease, dementia with Lewy bodies and multiple. *Ann. N Y Acad. Sci.* 920, 16–27. doi: 10.1111/j.1749-6632.2000.tb06900.x

Spillantini, M. G., Crowther, R., Jakes, R., Cairns, N. J., Lantos, P. L., and Goedert, M. (1998). Filamentous α-Synuclein inclusions link multiple system atrophy with Parkinson's disease and dementia with Lewy bodies. *Neurosci. Lett.* 251, 205–208. doi: 10.1016/s0304-3940(98)00504-7

Spillantini, M. G., Schmidt, M. L., Lee, V. M. Y., Trojanowski, J. Q., and Ross Jakes, M. G. (1997). α-Synuclein in Lewy bodies. *Nature* 388, 839–840. doi: 10.1038/42166

Stefanis, L. (2012). α-Synuclein in Parkinson's disease. *Cold Spring Harb. Perspect. Med.* 2:a009399. doi: 10.1101/cshperspect.a009399

Stefanova, N., and Wenning, G. K. (2016). Review: multiple system atrophy: emerging targets for interventional therapies. *Neuropathol. Appl. Neurobiol.* 42, 20–32. doi: 10.1111/nan.12304

Sturm, E., Fellner, L., Krismer, F., Poewe, W., Wenning, G. K., and Stefanova, N. (2016). Neuroprotection by epigenetic modulation in a transgenic model of multiple system atrophy. *Neurotherapeutics* 13, 871–879. doi: 10.1007/s13311-016-0447-1

Su, M., Shi, J. J., Yang, Y. P., Li, J., Zhang, Y. L., Chen, J., et al. (2011). HDAC6 regulates aggresome-autophagy degradation pathway of α-Synuclein in response to MPP+-induced stress. *J. Neurochem.* 117, 112–120. doi: 10.1111/j.1471-4159.2011.07180.x

Sweeney, P., Park, H., Baumann, M., Dunlop, J., Frydman, J., Kopito, R., et al. (2017). Protein misfolding in neurodegenerative diseases: implications and strategies. *Transl. Neurodegener.* 6:6. doi: 10.1186/s40035-017-0077-5

Tanaka, M., Kim, Y. M., Lee, G., Junn, E., Iwatsubo, T., and Mouradian, M. M. (2004). Aggresomes formed by α-Synuclein and synphilin-1 are cytoprotective. *J. Biol. Chem.* 279, 4625–4631. doi: 10.1074/jbc.M310994200

Thaler, F., and Mercurio, C. (2014). Towards selective inhibition of histone deacetylase isoforms: what has been achieved, where we are and what will be next. *ChemMedChem* 9, 523–536. doi: 10.1002/cmdc.201300413

Theillet, F. X., Binolfi, A., Bekei, B., Martorana, A., Rose, H. M., Stuiver, M., et al. (2016). Structural disorder of monomeric α-Synuclein persists in mammalian cells. *Nature* 530, 45–50. doi: 10.1038/nature16531

Uchihara, T., and Giasson, B. I. (2016). Propagation of α-Synuclein pathology: hypotheses, discoveries, and yet unresolved questions from experimental and human brain studies. *Acta Neuropathol.* 131, 49–73. doi: 10.1007/s00401-015-1485-1

Valera, E., and Masliah, E. (2018). The neuropathology of multiple system atrophy and its therapeutic implications. *Auton. Neurosci.* 211, 1–6. doi: 10.1016/j.autneu.2017.11.002

Van Helleputte, L., Benoy, V., and Van Den Bosch, L. (2014). The role of histone deacetylase 6 (HDAC6) in neurodegeneration. *Res. Rep. Biol.* doi: 10.2147/rrb.s35470 [Epub ahead of print]

Vekrellis, K., Xilouri, M., Emmanouilidou, E., Rideout, H. J., and Stefanis, L. (2011). Pathological roles of α-Synuclein in neurological disorders. *Lancet Neurol.* 10, 1015–1025. doi: 10.1016/S1474-4422(11)70213-7

Verdel, A., and Khochbin, S. (1999). Identification of a new family of higher eukaryotic histone deacetylases: coordinate expression of differentiation-dependent chromatin modifiers. *J. Biol. Chem.* 274, 2440–2445. doi: 10.1074/jbc.274.4.2440

Visanji, N. P., Lang, A. E., and Kovacs, G. G. (2019). Beyond the synucleinopathies: α-Synuclein as a driving force in neurodegenerative comorbidities. *Transl. Neurodegener.* 8:28. doi: 10.1186/s40035-019-0172-x

Volmar, C. H., and Wahlestedt, C. (2015). Histone deacetylases (HDACs) and brain function. *Neuroepigenetics* 1, 20–27. doi: 10.1016/j.nepig.2014.10.002

Wakabayashi, K., Hayashi, S., Kakita, A., Yamada, M., Toyoshima, Y., Yoshimoto, M., et al. (1998). Accumulation of α-Synuclein/NACP is a cytopathological feature common to Lewy body disease and multiple system atrophy. *Acta Neuropathol.* 96, 445–452. doi: 10.1007/s004010050918

Wales, P., Lázaro, D. F., Pinho, R., and Outeiro, T. F. (2013). Limelight on α-Synuclein: pathological and mechanistic implications in neurodegeneration. *J. Parkinsons Dis.* 3, 415–459. doi: 10.3233/jpd-130216

Walker, F. O. (2007). Huntington's disease. *Lancet* 369, 218–228. doi: 10.1016/S0140-6736(07)60111-1

Wang, R., Tan, J., Chen, T., Han, H., Tian, R., Tan, Y., et al. (2019). ATP13A2 facilitates HDAC6 recruitment to lysosome to promote autophagosome-lysosome fusion. *J. Cell Biol.* 218, 267–284. doi: 10.1083/jcb.201804165

Wang, X. X., Wan, R. Z., and Liu, Z. P. (2018). Recent advances in the discovery of potent and selective HDAC6 inhibitors. *Eur. J. Med. Chem.* 143, 1406–1418. doi: 10.1016/j.ejmech.2017.10.040

Waza, M., Adachi, H., Katsuno, M., Minamiyama, M., Tanaka, F., Doyu, M., et al. (2006). Modulation of Hsp90 function in neurodegenerative disorders: a molecular-targeted therapy against disease-causing protein. *J. Mol. Med.* 84, 635–646. doi: 10.1007/s00109-006-0066-0

Wenning, G. K., Stefanova, N., Jellinger, K. A., Poewe, W., and Schlossmacher, M. G. (2008). Multiple system atrophy: a primary oligodendrogliopathy. *Ann. Neurol.* 64, 239–246. doi: 10.1002/ana.21465

Wong, Y. C., and Krainc, D. (2017). α-Synuclein toxicity in neurodegeneration: mechanism and therapeutic strategies. *Nat. Med.* 23, 1–13. doi: 10.1038/nm.4269

Yang, X.-J., and Grégoire, S. (2005). Class II histone deacetylases: from sequence to function, regulation and clinical implication. *Mol. Cell. Biol.* 25, 2873–2884. doi: 10.1128/mcb.25.8.2873-2884.2005

Yang, W., and Yu, S. (2017). Synucleinopathies: common features and hippocampal manifestations. *Cell. Mol. Life Sci.* 74, 1485–1501. doi: 10.1007/s00018-016-2411-y

Zhang, L., Sheng, S., and Qin, C. (2013). The role of HDAC6 in Alzheimer's disease. *J. Alzheimers Dis.* 33, 283–295. doi: 10.3233/jad-2012-120727

Zhang, Y., Gilquin, B., and Khochbin, S. (2006). Required for protein. *J. Biol. Chem.* 281, 2401–2404. doi: 10.1074/jbc.C500241200

Zhang, Y., Li, N., Caron, C., Matthias, G., Hess, D., Khochbin, S., et al. (2003). HDAC-6 interacts with and deacetylates tubulin and microtubules *in vivo*. *EMBO J.* 22, 1168–1179. doi: 10.1093/emboj/cdg115

Zhang, X., Yuan, Z., Zhang, Y., Yong, S., Salas-Burgos, A., Koomen, J., et al. (2007). HDAC6 modulates cell motility by altering the acetylation level of cortactin. *Mol. Cell* 27, 197–213. doi: 10.1016/j.molcel.2007.05.033

Zheng, Q., Huang, T., Zhang, L., Zhou, Y., Luo, H., Xu, H., et al. (2016). Dysregulation of ubiquitin-proteasome system in neurodegenerative diseases. *Front. Aging Neurosci.* 8:303. doi: 10.3389/fnagi.2016.00303

Zilberman, Y., Ballestrem, C., Carramusa, L., Mazitschek, R., Khochbin, S., and Bershadsky, A. (2009). Regulation of microtubule dynamics by inhibition of the tubulin deacetylase HDAC6. *J. Cell Sci.* 122, 3531–3541. doi: 10.1242/jcs.046813

Conflict of Interest: The authors declare that the research was conducted in the absence of any commercial or financial relationships that could be construed as a potential conflict of interest.

Copyright © 2020 Lemos and Stefanova. This is an open-access article distributed under the terms of the Creative Commons Attribution License (CC BY). The use, distribution or reproduction in other forums is permitted, provided the original author(s) and the copyright owner(s) are credited and that the original publication in this journal is cited, in accordance with accepted academic practice. No use, distribution or reproduction is permitted which does not comply with these terms.

frontiers in Synaptic Neuroscience

REVIEW
published: 21 September 2020
doi: 10.3389/fnsyn.2020.584536

From Synaptic Protein to Prion: The Long and Controversial Journey of α-Synuclein

Antonio Heras-Garvin and Nadia Stefanova**

Division of Neurobiology, Department of Neurology, Medical University of Innsbruck, Innsbruck, Austria

Since its discovery 30 years ago, α-synuclein (α-syn) has been one of the most studied proteins in the field of neuroscience. Dozens of groups worldwide have tried to reveal not only its role in the CNS but also in other organs. α-syn has been linked to several processes essential in brain homeostasis such as neurotransmitter release, synaptic function, and plasticity. However, despite the efforts made in this direction, the main function of α-syn is still unknown. Moreover, α-syn became a protein of interest for neurologists and neuroscientists when mutations in its gene were found associated with Parkinson's disease (PD) and even more when α-syn protein deposits were observed in the brain of PD, dementia with Lewy bodies (DLB), and multiple system atrophy (MSA) patients. At present, the abnormal accumulation of α-syn constitutes one of the pathological hallmarks of these disorders, also referred to as α-synucleinopathies, and it is used for post-mortem diagnostic criteria. Whether α-syn aggregation is cause or consequence of the pathogenic events underlying α-synucleinopathies remains unclear and under discussion. Recently, different *in vitro* and *in vivo* studies have shown the ability of pathogenic α-syn to spread between cells, not only within the CNS but also from peripheral locations such as the gut, salivary glands, and through the olfactory network into the CNS, inducing abnormal misfolding of endogenous α-syn and leading to neurodegeneration and motor and cognitive impairment in animal models. Thus, it has been suggested that α-syn should be considered a prion protein. Here we present an update of what we know about α-syn function, aggregation and spreading, and its role in neurodegeneration. We also discuss the rationale and findings supporting the hypothetical prion nature of α-syn, its weaknesses, and future perspectives for research and the development of disease-modifying therapies.

Keywords: α-synuclein, α-synucleinopathies, Parkinson's disease, neurodegeneration, prion

OPEN ACCESS

Edited by:
Taher Darreh-Shori, Karolinska Institutet (KI), Sweden

Reviewed by:
Paolo Calabresi, Catholic University of the Sacred Heart, Italy
Qihui Wu, University of Pennsylvania, United States

****Correspondence:***
Antonio Heras-Garvin
antonio.heras@i-med.ac.at
Nadia Stefanova
nadia.stefanova@i-med.ac.at

Received: *17 July 2020*
Accepted: *26 August 2020*
Published: *21 September 2020*

Citation:
Heras-Garvin A and Stefanova N (2020) From Synaptic Protein to Prion: The Long and Controversial Journey of α-Synuclein. Front. Synaptic Neurosci. 12:584536. doi: 10.3389/fnsyn.2020.584536

INTRODUCTION

α-synuclein (α-syn) is one of the most abundant proteins in the nervous system, encoded by the *SNCA* gene. With a molecular mass of approximately 15 kDa, α-syn is composed of 140 amino acid residues (Lee and Trojanowski, 2006; Bendor et al., 2013). α-syn presents three domains: the C-terminal domain, the central domain, or "non-amyloid component" (NAC), which permits its oligomerization due to its hydrophobic composition, and the N-terminal domain, that forms an alpha helix allowing α-syn-lipid interaction (Lashuel et al., 2013). However, despite the efforts made

since its discovery, its precise native structure is still unclear and under discussion. It has been proposed that, in physiological conditions, α-syn is mainly found in its monomeric form, either as a soluble intrinsically disordered protein in the cytoplasm of neurons (Binolfi et al., 2012; Fauvet et al., 2012; Theillet et al., 2016), or in an alpha-helical conformation (Bartels et al., 2011; Wang et al., 2011), or a combination of the two (Burré et al., 2013). Moreover, α-syn can undergo a variety of post-translational modifications (PTM; i.e., phosphorylation, glycation, glycosylation, acetylation) that may affect protein structure and function (Giasson et al., 2000; Theillet et al., 2016; Burré et al., 2018; Meade et al., 2019).

At the cellular level, α-syn can be found in different cellular organelles, including synaptic terminals and the nucleus of neurons (Maroteaux et al., 1988), mitochondria (Li et al., 2007; Devi et al., 2008; Parihar et al., 2008), endoplasmic reticulum (Hoozemans et al., 2007; Guardia-Laguarta et al., 2014), Golgi apparatus (Gosavi et al., 2002; Mori et al., 2002), and in the endolysosomal system (Lee et al., 2004). In this regard, since its discovery, α-syn has been associated or involved in different cellular processes, such as neurotransmission, calcium homeostasis, vesicle transport, mitochondrial function, and gene regulation (**Figure 1**). However, the physiological function of α-syn in those subcellular compartments is not fully understood. It has been shown that α-syn is involved in the regulation of the membrane lipid content and curvature, therefore playing a role in vesicle budding and trafficking (Chandra et al., 2003; Varkey et al., 2010). Moreover, α-syn plays a role in SNARE complex assembly at presynaptic terminals (Burré et al., 2010). Studies based on *in situ* proximity ligation assay (PLA) in neurons have demonstrated proximity between α-syn and SNARE proteins in cell bodies and neurites, including VAMP-2, SNAP-25, and syntaxin-1 (Almandoz-Gil et al., 2018). α-syn is also involved in clathrin-mediated endocytosis (Ben Gedalya et al., 2009) and in dopamine content and metabolism (Sidhu et al., 2004; Yu et al., 2005; Al-Wandi et al., 2010). In association with its nuclear localization, α-syn functions as a regulator of gene expression through its direct interaction with DNA (Pinho et al., 2019), chromatin (Vasquez et al., 2017), and transcription factors involved in development, mitochondrial homeostasis and metabolism of energy (Zheng et al., 2010; Decressac et al., 2012; Eschbach et al., 2015; Davidi et al., 2020), as well as through epigenetic mechanism including DNA methylation or histone acetylation (Surguchev and Surguchov, 2017). Furthermore, α-syn directly controls mitochondrial activity and function by modulating membrane potential, calcium homeostasis, cytochrome release, ATP production, and mitochondrial fusion and fission (Vicario et al., 2018). Interestingly, α-syn is also present in blood cells including red blood cells, peripheral blood mononuclear cells, platelets, and in the plasma. However, the role of α-syn in those cells is unclear (Barbour et al., 2008).

The functions and the structure of α-syn have being intensively investigated during the last decades, leading to a better knowledge of the protein and its association with crucial pathways on different cell types in the central nervous system

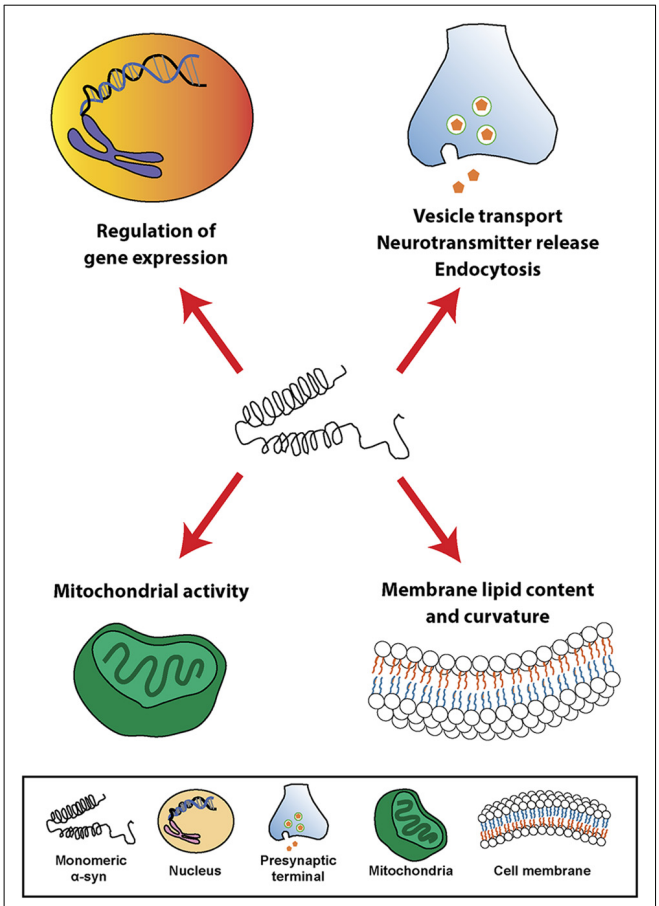

FIGURE 1 | Physiological roles of α-synuclein (α-syn). Schematic overview including some of the cellular processes linked to α-syn in physiological conditions.

(CNS), however α-syn research remains a priority not only for neuroscientist, but also for clinicians and pharmaceutical companies. The fact that α-syn aggregation and accumulation constitute the main pathological hallmark of a group of neurodegenerative disorders, referred to as α-synucleinopathies, and that mutations of its gene (*SNCA*) are associated with familiar forms of these disorders, has led α-syn to become one of the "most wanted" proteins in the biomedical field. Pre-clinical studies *in vitro* and *in vivo* have shown than α-syn oligomeric species and aggregates induce the impairment of different processes essential for cellular homeostasis, not only in neurons, but also in other cell types. Moreover, inoculation of α-syn oligomers, fibrils or aggregates in animal models, demonstrated the capability of pathogenic forms of α-syn to spread in a prion-like manner, inducing in some cases changes that replicated human pathology, including the clinical presentation. As a result of those observations, some authors have proposed that α-syn should be considered a prion protein. In this review, we discuss the role of α-syn in neurodegeneration, the different findings supporting the prion nature of α-syn, and its consequences for future therapeutic strategies.

α-SYN AND NEURODEGENERATION: α-SYNUCLEIONOPATHIES

The abnormal aggregation and accumulation of α-syn constitute the main pathological hallmark of Parkinson's disease (PD), multiple system atrophy (MSA), and dementia with Lewy bodies (DLB; Spillantini et al., 1997, 1998; Goedert and Spillantini, 1998). These three disorders are also known as α-synucleinopathies. Recently, pure autonomic failure (PAF) and REM sleep behavior disorder (RBD) have been suggested to represent prodromal α-synucleinopathies commonly preceding PD or MSA and showing α-syn aggregation in the peripheral and autonomic nervous system (Arai et al., 2000; Kaufmann et al., 2001, 2004; Iranzo et al., 2013; Barber et al., 2017). Polymeropoulos et al. (1996, 1997) first described the association between α-syn and PD, when they found that individuals with familiar forms of this disorder presented mutations in the SNCA gene (Polymeropoulos et al., 1996, 1997). Soon afterwards Spillantini et al. (1997, 1998) showed that the abnormal protein aggregates observed in α-synucleinopathies were strongly immunoreactive for α-syn (Spillantini et al., 1997, 1998; Goedert and Spillantini, 1998). Moreover, some *SNCA* gene allelic variants (i.e., SNCA locus triplication) were sufficient to develop a severe early onset PD and DLB (Singleton et al., 2003; Orme et al., 2018; Zafar et al., 2018). Since then, multiple *in vitro* and *in vivo* studies have tried to decipher the mechanisms underlying α-syn misfolding and aggregation, the following cellular and physiological consequences, and their influence in the human pathology.

α-synucleinopathies present a preference for affecting motor, cognitive and autonomic areas, leading to motor dysfunction, cognitive impairment and/or autonomic failure (Marti et al., 2003). Phenotypic diversity, symptom severity and disease duration varies among these disorders based on the affectation of different neuroanatomical regions, selective vulnerability of different cell types and the extent of the pathology (Marti et al., 2003). Pathologically, PD and DLB are characterized by the abnormal accumulation of α-syn in the cytoplasm of neurons, in the so-called Lewy bodies (LBs; Spillantini et al., 1998). Associated with the presence of LBs in cortical and subcortical areas, post-mortem evaluation of PD and DLB brains show a preferential loss of dopaminergic neurons in the substantia nigra pars compacta (SNpc), neuronal loss in the locus coeruleus (LC) and cortical atrophy (Dickson et al., 2009; Cheng et al., 2010; Jellinger, 2018). In addition to that, other neuronal populations in the brainstem accumulate LBs and degenerate, probably leading to many of the secondary clinical features of PD and DLB, such as autonomic dysfunction or sleep disturbances (Coon et al., 2018; Outeiro et al., 2019). In PAF, typical LBs are present in sympathetic ganglia, distal sympathetic nerves, substantia nigra, and locus ceruleus. In correlation with the presence of LBs, PAF patients present a significant unmyelinated nerve fiber density compared to healthy controls and neuronal degeneration in preganglionic sympathetic intermediolateral column and paravertebral ganglia (Kaufmann et al., 2001; Thaisetthawatkul, 2016). In MSA, however, α-syn mainly (but not exclusively) accumulates throughout the neocortex, hippocampus, brainstem, spinal cord, and dorsal root ganglia in the cytoplasm of oligodendrocytes, in the so-called glial cytoplasmic inclusions (GCIs), associating with striatonigral degeneration (SND), olivopontocerebellar atrophy and cell loss in LC and brainstem nuclei, leading to parkinsonism, cerebellar symptoms and autonomic dysfunction (Fanciulli and Wenning, 2015).

Despite the different clinical features of α-synucleinopathies, these disorders share characteristics such as neurodegeneration, neuroinflammation and demyelination, among others. Based on *in vitro* and *in vivo* studies, α-syn seems to play a central role in the pathological changes through a direct interaction with components of cellular pathways essential for cell homeostasis (**Figure 2**). Thus, pathological α-syn is able to bind and inhibit lysosomal function (Mazzulli et al., 2016; Flavin et al., 2017), proteasomal activity (Stefanis et al., 2001; Tanaka et al., 2001; Petrucelli et al., 2002; Snyder et al., 2003; Lindersson et al., 2004; Emmanouilidou et al., 2010), to impair axonal transport (Volpicelli-Daley, 2017), and to induce Ca^{2+} dyshomeostasis (Danzer et al., 2007; Chen Y. et al., 2015; Angelova et al., 2016) and mitochondrial dysfunction (Di Maio et al., 2016; Ganjam et al., 2019; Wang et al., 2019; Park et al., 2020). Latter promotes the generation of reactive oxygen species (ROS), and therefore oxidative stress, which may lead to mitochondrial damage, the release of cytochrome c to the cytoplasm, and cell death (Hsu et al., 2000; Smith et al., 2005; Parihar et al., 2008; Reeve et al., 2015; Tapias et al., 2017; Ludtmann et al., 2018). Associated with its nuclear localization or its capacity to promote oxidative stress, recent studies suggested an involvement of α-syn in DNA damage (Paiva et al., 2017; Vasquez et al., 2017; Milanese et al., 2018; Schaser et al., 2019). Pathological α-syn also promotes pathogenic redistribution of membrane proteins (Shrivastava et al., 2015, 2020) and interferes with the normal function of cell membranes, facilitating diffusion of molecules and ions, specially Ca^{2+}, and inducing cell damage (Tosatto et al., 2012; Tsigelny et al., 2012; Angelova et al., 2016; Fusco et al., 2017; Dong et al., 2018). The impairment of all these cellular processes may be especially significant in dopaminergic neurons, since dopamine promotes the formation of pathological α-syn species (Cappai et al., 2005; Lee et al., 2011; Mor et al., 2017). Thus, a multi-hit model has been proposed, in which the synergistic interaction between α-syn, dopamine and Ca^{2+} in neurons may underlie neuronal loss in SNpc and LC (Post et al., 2018). Neurodegeneration in the LC may induce a direct loss of norepinephrine (NE), however, α-syn is also able to translocate to the nucleus of NE-producing cells and interfere with transcription of dopamine ß-hydroxylase, the final enzyme in NE biosynthesis, disrupting NE production and leading to a reduction of neurotrophic factor signaling, indirectly altering innate and adaptive immune response and worsening central and peripheral inflammation (Butkovich et al., 2018).

Different *in vivo* and *in vitro* studies have also shown the ability of pathological α-syn to induce synaptic dysfunction, both at the presynaptic and postsynaptic terminal (Ghiglieri et al., 2018). At presynaptic level, pathological α-syn seems to affect synaptic vesicle pool, trafficking and endocytosis by interfering with the exo-endocytotic cycling machinery, thus

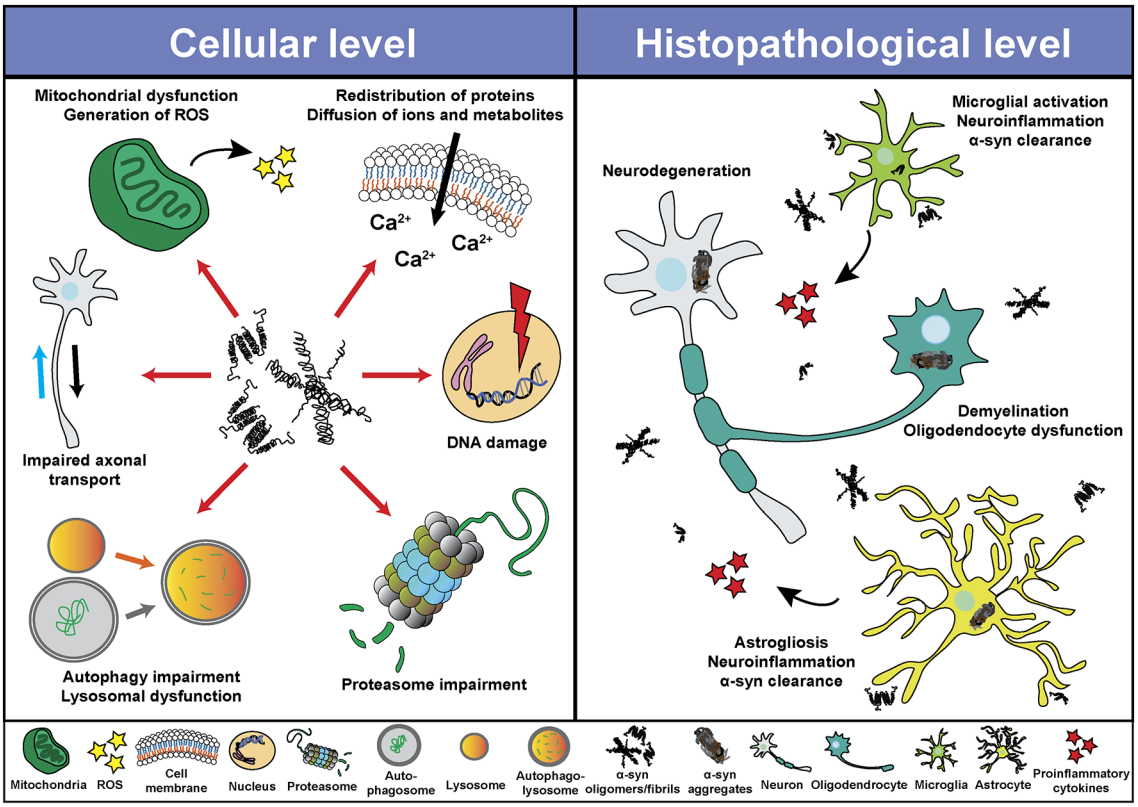

FIGURE 2 | Pathological roles of α-syn. Schematic overview including some of the cellular processes (left) and histopathological events (right) associated with the presence of pathogenic α-syn species.

suggesting the possible association between α-syn pathology and impaired synaptic function even in the absence of cell death (Bridi and Hirth, 2018; Froula et al., 2018; Wu et al., 2019). At a postsynaptic level, *in vivo* studies have shown that pathological α-syn reduces striatal dopamine, NMDA receptor-mediated synaptic currents, impairs early memory and motor learning, and prevents long-term potentiation of cholinergic interneurons and spiny projection neurons in the striatum even at early stages of the disease (Tozzi et al., 2016; Phan et al., 2017; Giordano et al., 2018; Durante et al., 2019).

Pathological α-syn can also modulate neuroinflammation (**Figure 2**) directly through different mechanism including the activation of microglial cells (Austin et al., 2006; Su et al., 2008; Theodore et al., 2008; Fellner et al., 2013; Choi et al., 2020), which induces a robust pro-inflammatory response (Kim et al., 2013; Sarkar et al., 2020) leading to increased α-syn aggregation and potentiating neurodegeneration (Zhang et al., 2005; Stefanova et al., 2007). In this regard, microgliosis has been shown in post-mortem studies and in PET imaging analysis of patients diagnosed with α-synucleinopathies (McGeer et al., 1988a; Gerhard et al., 2003, 2006; Doorn et al., 2014; Stokholm et al., 2017; Surendranathan et al., 2018). In addition, microgliosis paralleled system degeneration in patients and was associated with α-syn inclusions (Imamura et al., 2003; Ishizawa et al., 2004, 2008; Croisier et al., 2005; Kubler et al., 2019). A recent study with PD patients engrafted with foetal embryonic dopaminergic neurons showed microglia activation in all grafts before α-syn aggregates were detected (Olanow et al., 2019). The authors speculated that microglial activation could have been initiated by the presence of endogenous pathological α-syn in patients, by an immune reaction due to the implantation of foreign tissue or by the surgical procedure itself (Olanow et al., 2019). Moreover, we recently showed that targeting α-syn oligomerization in an animal model for MSA led to a decrease of α-syn aggregates which significantly correlated with neuroprotection and a reduction in microglial activation (Heras-Garvin et al., 2019).

Similar to microglial cells, pathological α-syn also induces activation of astrocytes (**Figure 2**), aggravating neuroinflammation (Lee et al., 2010; Fellner et al., 2013; Radford et al., 2015). Astrogliosis has also been described in α-synucleinopathies paralleling the neurodegenerative process (Ozawa et al., 2004; Miklossy et al., 2006; Radford et al., 2015). Moreover, α-syn inclusions are often found in the cytoplasm of astrocytes and may lead to astrocyte dysfunction (Song et al., 2009; Halliday and Stevens, 2011; Sorrentino et al., 2019). Even a role of the adaptive immune system in PD has been proposed. Post-mortem evaluation showed higher numbers of T cells in the ventral midbrain of PD brains and mouse models than in healthy controls, suggesting a targeted extravasation, and supporting a

role for T cells in disease pathogenesis (McGeer et al., 1988b; Theodore et al., 2008; Brochard et al., 2009; Sommer et al., 2018). Recent studies showed the presence of α-syn-specific T cells in PD patients, and therefore an autoimmune response to α-syn (Sulzer et al., 2017; Garretti et al., 2019). However, at present, α-syn-specific T cells have only been detected in the periphery of PD patients. Whether these cells are able to infiltrate into the CNS and cause dopaminergic neuron death remains to be determined.

Although most research on the pathogenic role of α-syn have been focused in neurons, microglia and astrocytes, there have also been studies that evaluated the deleterious effect of pathogenic α-syn in oligodendrocytes and oligodendroglial precursor cells (OPCs), which are essential to understand the cellular and molecular consequences of α-syn accumulation in MSA (**Figure 2**). Over-expression of α-syn or the addition of exogenous pathological α-syn severely impaired myelin formation *in vitro* and *in vivo* (Ettle et al., 2016; Mandel et al., 2017; Mavroeidi et al., 2019), corroborating the demyelination observed in MSA brains (Song et al., 2007; Don et al., 2014; Ettle et al., 2016). This effect seems to be mediated by the interference of α-syn with the expression of proteins associated with cholesterol and membrane biogenesis (Ettle et al., 2016; Kaji et al., 2018), and by the partial sequestration of the myelin basic protein (MBP) into GCIs in a process orchestrated by endogenous α-syn and the the oligodendroglial-specific phosphoprotein p25α (Mavroeidi et al., 2019). Moreover, α-syn impairs OPC maturation *in vitro* (Ettle et al., 2014) and in animal models of MSA, where an age-dependent increase of dividing OPCs within the striatum was observed (May et al., 2014). Latter was confirmed after postmortem analysis in MSA patients, revealing α-syn within OPCs and an increased number of striatal OPCs compared to healthy controls (May et al., 2014). α-syn also induces a distinct gene expression profile in oligodendrocytes, including upregulation of cytokines important for myeloid cell attraction and proliferation (Schafferer et al., 2016; Hoffmann et al., 2019), which constitutes an early crosstalk between neuroinflammation and α-syn-mediated oligodendrocyte dysfunction.

Overall, multiple cell populations and pathways can be affected by the abnormal misfolding, aggregation and accumulation of α-syn. Determining which events are primary or secondary in the pathogenesis of α-synucleinopathies will be essential in order to define potential strategies to prevent cell damage and, finally, neurodegeneration.

AGGREGATION AND SPREADING OF α-SYN

As stated before, the normal conformation of α-syn is either a disordered monomer, alpha-helical, or a combination of the two. But, under pathological conditions, monomers can convert to β-sheets by recruiting additional monomers, aggregating and giving rise to oligomers that, eventually, form protofilaments and amyloid fibrils (**Figure 3**), which can adopt different morphologies such as spherical, chain-like, annular (pore-like structure), and tubular (Cremades and Dobson, 2018). To define the process through which α-syn oligomers give rise to pathological inclusions is challenging due to their transient nature and their ability to rapidly recruit monomeric α-syn to form fibrils. Nevertheless, the recent description that α-syn oligomers can be kinetically trapped made possible to compare the contribution of oligomers and fibrils to different α-synucleinopathy phenotypes (Chen S. W. et al., 2015; Iljina et al., 2016; De Oliveira and Silva, 2019; Froula et al., 2019). It is believed that the formation of α-syn fibrils results from interactions between monomers and oligomers that are thermodynamically favorable and stabilizing (Alam et al., 2019). Despite several studies have associated the presence of α-syn oligomers and fibrillar species with cytotoxicity and neurodegeneration, thus supporting the idea that these α-syn forms are the responsible for the neurodegenerative process observed in α-synucleinoptahies (Alam et al., 2019), a recent publication by Mahul-Mellier et al. (2020) proposed that the process of LB formation, rather than simply fibril formation, is one of the major drivers of neurodegeneration through disruption of cellular functions, inducing mitochondria damage and deficits, and synaptic dysfunction. Therefore, which α-syn species or processes associated with α-syn aggregation and accumulation are the most toxic is still a matter of debate.

Mutations in the *SNCA* gene associated with familiar forms of α-synucleinopathies, such as A30P or A53T, are more prone to aggregate and form fibrillar α-syn oligomers (Lashuel et al., 2002; Bengoa-Vergniory et al., 2017). Different events promote α-syn aggregation (**Figure 3**), including low pH (Buell et al., 2014). Indeed, neutral pH inhibits the growth of α-syn fibrils, while acidic pH increases it (Grey et al., 2011). Other micro-environmental factors affecting α-syn aggregation include metal ions (Uversky et al., 2001), polyamines (Krasnoslobodtsev et al., 2012; Holmes et al., 2013), proteoglycans (Lashuel et al., 2013), nucleic acids (Hegde and Rao, 2007), poly-ADP ribose (Kam et al., 2018) and fatty acids (Fecchio et al., 2018). α-syn PTM play also a role in its aggregation process. Thus, glycation of α-syn potentiate toxicity and aggregation (Vicente Miranda et al., 2017). Phosphorylation at various sites contributes to α-syn aggregation (Zhang et al., 2019). In particular, phosphorylation at residue Ser129 constitutes one of the most studied α-syn PTM, however, there is contradictory data about its role in pathology, as it was shown to be both protective and toxic (Arawaka et al., 2017; Zhang et al., 2019). In physiological conditions, α-syn is constitutively acetylated in its N-terminal, which seems to make α-syn more resistant to oligomerization and aggregation (Gonzalez et al., 2019). C-terminal truncation of α-syn has been associated with an increase in self-assembly properties and constitutes 10–25% of the LBs (Li et al., 2005; Wang et al., 2016). As a result of oxidative stress, the generation of nitric oxide induces nitration of tyrosine residues of α-syn, promoting aggregation (Giasson et al., 2000). SUMOylation inhibits ubiquitin-mediated degradation of α-syn, which leads to an increase of α-syn concentration and aggregation (Rott et al., 2017). Lastly, the aggregation process of α-syn seems to be affected by the presence of other proteins. Although homotypic seeding is the preferred form of aggregation, α-syn can bind other natively unfolded proteins such as tau, PrP^C or Aβ, in

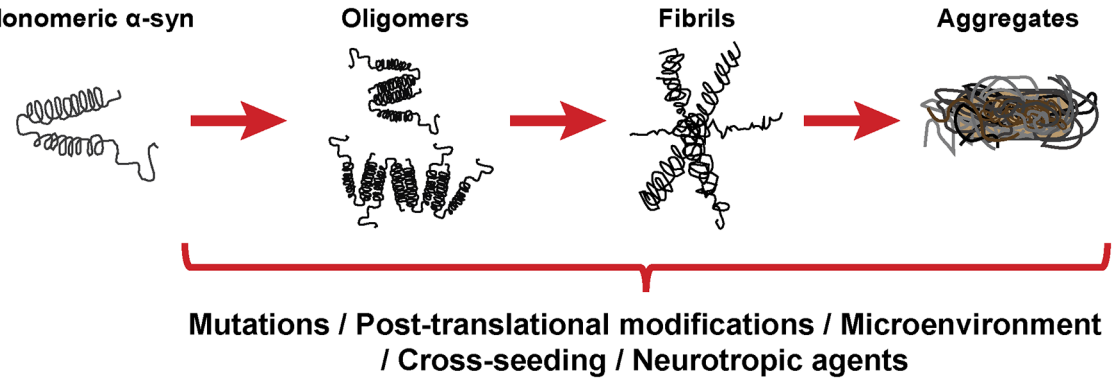

FIGURE 3 | α-synuclein aggregation process. Schematic overview of the hypothetical aggregation process of monomeric α-syn and the different events that can induce its misfolding and promote aggregation.

a process termed heterotypic cross-seeding, which accelerate aggregation and neuropathology (Clinton et al., 2010; Ono et al., 2012; Guo et al., 2013; Katorcha et al., 2017; Bassil et al., 2020). However, despite our knowledge about the different processes that may be involved in its abnormal aggregation, the initial event that triggers α-syn oligomer formation and accumulation remains unknown.

In 2003, after post-mortem evaluation of PD brains, Braak et al. (2003a) staged the pathology of this disorder. In that study, they defined the earliest phases of the disease, characterized by the presence of α-syn pathology in the anterior olfactory nucleus and in the dorsal motor nucleus of the vagal in the absence of motor symptoms. Based on those findings, Braak et al. (2003b) developed a theory in which PD might be initiated when a neurotropic agent enters the body by nasal route, through the olfactory epithelium to the olfactory bulb, or by gastric route, infiltrating the gut to the submucous plexus and traveling along preganglionic parasympathetic fibers to the dorsal motor nucleus of the vagus nerve. The presence of LBs in the enteric and peripheral nervous systems supported their claim (Braak et al., 2006, 2007; Shannon et al., 2012). The LB pathology would then travel through the CNS. The authors proposed that PD could be divided into six different stages, each one defined by abnormal pathology in particular neurological structures and specific symptom severity. Thus, early stages would be characterized by non-motor symptoms, including hyposmia and autonomic dysfunction, mid-stages would be characterized by the presence of motor symptoms and later stages by the presence of cognitive impairment (Braak et al., 2004). In their theory, the authors proposed as the possible neurotropic agent a virus or a pathogen composed of fragments of misfolded α-syn that could possess unconventional prion-like properties (Braak et al., 2003b). Over the last decade, different studies have shown that α-syn is in fact not only able to aggregate, but also to spread and propagate the synucleinopathy in a prion-like fashion. This new hypothesis and line of research was initially inspired by the observation that grafts of embryonic dopamine neurons into the brains of human PD patients developed α-syn pathology (Kordower et al., 2008; Li et al., 2008). The authors hypothesized that pathological α-syn from the host was transferred into the young grafted neurons in a prion-like manner (Brundin et al., 2008). Since then, different groups have proven that α-syn is able to be taken up by cells, including dopaminergic neurons (Luk et al., 2009; Volpicelli-Daley et al., 2011), be transmitted from neuron to neuron (Desplats et al., 2009; Freundt et al., 2012), from neurons to oligodendrocytes (Reyes et al., 2014), and to induce the formation of aggregates that share some of the LB features, i.e., a high degree of phosphorylation and polyubiquitination (Volpicelli-Daley et al., 2011). An early work demonstrated the presence of α-syn in plasma and cerebrospinal fluid of PD patients, thus supporting the hypothesis that α-syn may enter cells from the extracellular space (El-Agnaf et al., 2003). Moreover, the inoculation of recombinant α-syn preformed-fibrils (PFFs) or patient-derived pathological α-syn in wildtype and transgenic animals resulted in the development of widespread synucleinopathy throughout synaptically connected networks, neurodegeneration and behavioral deficits, following in some cases a similar pattern to the one define in Braak's hypothesis (Luk et al., 2012a,b; Masuda-Suzukake et al., 2013; Ulusoy et al., 2013; Holmqvist et al., 2014; Recasens et al., 2014; Paumier et al., 2015; Abdelmotilib et al., 2017; Manfredsson et al., 2018; Rey et al., 2018; Chu et al., 2019; Kim S. et al., 2019; Challis et al., 2020). Additional studies demonstrated that the spreading of α-syn pathology depended on the misfolding and recruitment of endogenous α-syn (Volpicelli-Daley et al., 2011; Kaji et al., 2018; Kim S. et al., 2019; Wu et al., 2019). Furthermore, a recent publication suggested that the inoculation site may determine the synucleinopathy, since autonomic ganglionic injection of α-syn fibrils resulted in a model of PAF (Wang et al., 2020). However, the mechanism involved in α-syn internalization remains unclear. In the last years, several membrane protein receptors have been proposed to play an important role in α-syn uptake, including lymphocyte-activation gene 3 (Mao et al., 2016), Rab proteins (Masaracchia et al., 2018) and flotillin-1 and dopamine transporter (DAT; Kobayashi et al., 2019).

In addition, recent publications have demonstrated the existence of different strains of pathological α-syn which cause

distinct synucleinopathies, targeting distinct brain regions and cell types (Bousset et al., 2013; Peelaerts et al., 2015; Rey et al., 2019; Lau et al., 2020). In particular, MSA and PD strains seem to have different structural and seed properties that may be used as differential diagnostic criteria and that could explain the more aggressive and rapid progression of MSA compared to other synucleinopathies (Peng et al., 2018b; Candelise et al., 2019; Yamasaki et al., 2019; Schweighauser et al., 2020; Shahnawaz et al., 2020; Van Der Perren et al., 2020). It is not yet clear how the different α-syn strains are generated, but the cellular micro-environment may play an important role (Candelise et al., 2020). Thus, a recent publication by the group of Virginia Lee showed that the α-syn extracted from GCIs presents a different proteolytic profile and more potent biological activity than the α-syn from LBs and that the specific cellular milieu of oligodendrocytes is responsible for the transformation of misfolded α-syn into the MSA strain (Peng et al., 2018a).

The identification of the mechanisms associated or responsible for α-syn uptake, processing, aggregation and release, and the contribution of different α-syn strains to inclusion formation and to the impairment of cellular pathways will be essential to completely understand the pathogenic process underlying α-synucleinopathies, to identify novel targets for disease modification, the development of new therapeutic strategies and to generate possible biomarkers which would allow the early diagnosis of these disorders.

α-SYN, A PRION PROTEIN?

The term prion was first described by Stanley Prusiner as a "small proteinaceous infectious particle which is resistant to inactivation by most procedures that modify nucleic acids" and resulted from the blend of "protein" and "infection" (Prusiner, 1982). Therefore, prions should constitute the underlying cause of an infectious disease that can be transmitted among individuals from the same or different species, and not a secondary consequence of the disease (Prusiner, 1998). In this regard, based on *in vivo* and *in vitro* studies, α-syn seems to exhibit some of the properties of prion proteins (**Figure 4**), such as the ability to undergo misfolding and to self-propagate, inducing aggregation of endogenous α-syn (Hijaz and Volpicelli-Daley, 2020), to exist as distinct strains (Bousset et al., 2013; Peelaerts et al., 2015; Candelise et al., 2019; Yamasaki et al., 2019; Lau et al., 2020; Schweighauser et al., 2020; Shahnawaz et al., 2020) and to be resistant to inactivation by formaldehyde (Schweighauser et al., 2015; Woerman et al., 2018). As discussed before, the fact that α-syn aggregates were found in human brain regions affected by the disease and that some studies, like the one conducted by Braak et al. (2004) showed the presence of inclusions in peripheral organs and described an association between disease stage and Lewy pathology, led the authors to propose that α-synucleinopathies could initiate in the gut or the olfactory bulb and slowly spread to the CNS (Beach et al., 2009). This evidence and the data demonstrating the ability of α-syn to propagate from the gut and other peripheral organs in animal models (Kim S. et al., 2019; Lohmann et al., 2019) as well as the finding of LBs in grafted dopaminergic neurons in PD patients (Kordower et al., 2008; Li et al., 2008) supported the prion nature of α-syn.

However, there is evidence that challenges some of these observations and the prion hypothesis for α-syn (**Figure 4**). On one hand, subsequent post-mortem studies showed that only half of PD cases present a pattern of Lewy pathology consistent with Braak's staging and that an important number do not even follow it (Kalaitzakis et al., 2008; Jellinger, 2009; Halliday et al., 2012). In many cases, the distribution of α-syn inclusions is sparse and discrete, even at late stages of the disease (Beach et al., 2009; Dijkstra et al., 2014), and some patients do not show aggregates at all (Berg et al., 2014). Moreover, no correlation has been observed between Braak's staging of Lewy pathology and severity of clinical progression (Jellinger, 2009). In addition, cells within the same region are not equally affected by Lewy pathology, which is only observed in a small percentage of neurons, mainly affecting catecholaminergic and cholinergic but not GABAergic neurons. Furthermore, the strength of connectivity between brain areas does not correlate with Lewy pathology patterns (Surmeier et al., 2017) and, in MSA, the trans-synaptic propagation of α-syn pathology proposed for PD cannot explain the spatial distribution of GCIs (Armstrong et al., 2004; Dhillon et al., 2019; Kaji et al., 2020).

The ability of α-syn to propagate and generate aggregates in humans is also a matter of debate since additional transplantation studies did not show α-syn accumulation in the engrafted dopaminergic cells (Mendez et al., 2008; Hallett et al., 2014). Interestingly, the main difference between these studies and the ones showing Lewy pathology was the use of dissociated neurons instead of cellular aggregates or tissue pieces. Moreover, independently of the absence or presence of α-syn aggregates, transplanted neurons generally survive and remain healthy and functional for decades (Li et al., 2016). The appearance of pathology in the engrafted cells has been, however, associated with an extensive microglial activation when cellular aggregates or tissue pieces are used (Kordower et al., 2008; Li et al., 2008). This effect was not observed when dissociated neurons were transplanted (Mendez et al., 2008). Nevertheless, it is still unclear from where was the pathology observed in transplanted cells coming from, and why the number of neurons affected did not change with time (Kordower et al., 2008; Li et al., 2008, 2016). It has been proposed that the graft's micro-environment together with the already stressed environment from the host may trigger the pathology in those cells (Surmeier et al., 2017). In fact, post-mortem studies have shown that brain regions presenting α-syn inclusions do not necessarily develop neuronal loss, in contrast, neurodegeneration sometimes occurs in areas with no α-syn pathology or before it appears (Leak et al., 2019). Furthermore, *in vitro* studies have shown that mutations in α-syn, such as A53E and G51D, which are associated with familiar forms of PD and MSA, attenuate aggregation and delay the pathology (Fares et al., 2014; Ghosh et al., 2014). Interestingly, different neuropathological reports have shown an absence of Lewy pathology in most patients with familiar forms of parkin-related PD and in a proportion of PD patients with mutations

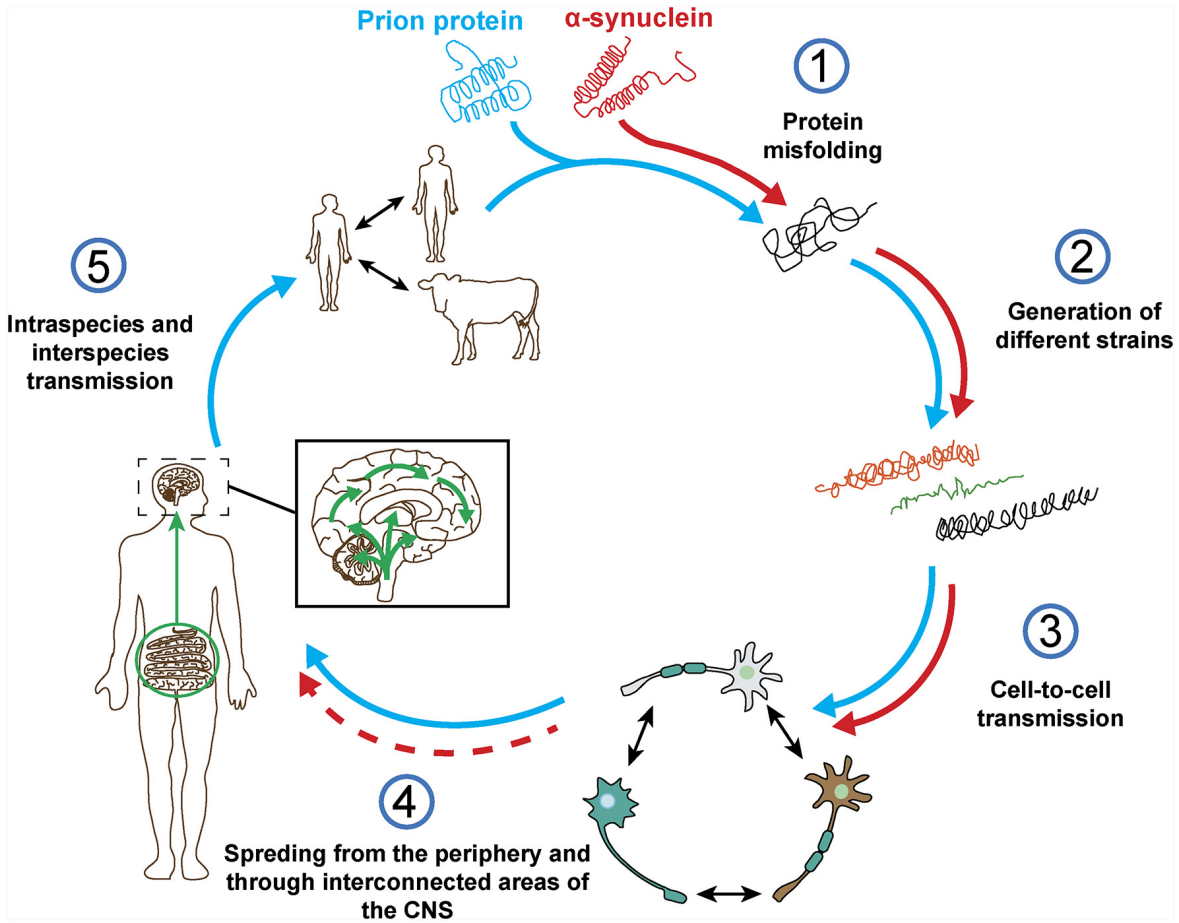

FIGURE 4 | Prion protein vs. α-synuclein: current knowledge. Both proteins can undergo misfolding (1) which leads to the formation of different pathogenic strains (2). The pathogenic forms of both proteins can be transferred cell-to-cell (3) and spread from the periphery into the CNS *in vivo* (4). However, based on post-mortem data from α-synucleinopathy patients and in contrast to the prion protein, it is not clear how and where does α-synuclein pathology start and if the spreading observed in *in vivo* studies really happens in humans (4). Finally, unlike prion protein, no evidence of intraspecies or interpecies transmission of α-syn has ever been reported (5).

in the *LRRK2* gene, which are respectively the most common cause of recessive and dominant forms of PD, and a small proportion of sporadic PD cases (Kalia and Lang, 2015; Tolosa et al., 2020).

Bonafide prions can spread from extraneural sites into the CNS and the molecular processes underlying their spreading have been evaluated in detail (Kara et al., 2018). Regarding α-syn, recent studies have demonstrated the presence of inclusions in peripheral sites, including cells of the enteric nervous system, nerve cells and fibers in the skin and submandibular salivary glands of α-synucleinopathies patients (Beach et al., 2010, 2016; Shannon et al., 2012; Kim J. Y. et al., 2019). Therefore, these data support the hypothesis that α-syn pathology may start in the periphery and ascend towards the CNS in a similar way to prions. In addition, it was reported that vagotomy reduces the risk of developing PD (Svensson et al., 2015), that may be explained by a disruption of α-syn spreading from the periphery to the brain. However, these observations were not replicated in a different study with the same cohort but extended follow-up (Tysnes et al., 2015). Therefore, the debate on the periphery as the possible initiation site of α-syn pathology remains unsolved, especially considering that: (i) α-syn is mainly expressed in the brain (Lashuel et al., 2013); (ii) some peripheral regions with α-syn pathology do not present a clear exposure route, such as the cardiac sympathetic nerve (Orimo et al., 2008); (iii) no cases have been found in post-mortem whole body studies with α-syn inclusions in the periphery without the brain being affected (Lionnet et al., 2018); and (iv) peripheral α-syn aggregates from PD patients show lack of pathogenic potential (Recasens et al., 2018; **Figure 4**).

Other exogenous and endogenous factors may trigger the pathological changes underlying α-synucleinopathies and α-syn aggregation (**Figure 3**). Thus, gut dysbiosis and microbiota have been associated with PD (Fitzgerald et al., 2019). Moreover, recent studies demonstrated that amyloid proteins produced by gut bacteria can induce α-syn aggregation and seeding (Sampson et al., 2016, 2020), and that viral infection disrupts cellular proteostasis and causes α-syn aggregation

(Marreiros et al., 2020). Several authors have therefore suggested that neurodegeneration and the neurological deficits observed in α-synucleinopathies may be triggered by factors other than α-syn, like inflammation or local micro environmental conditions (Engelender and Isacson, 2017) and that selective vulnerability of neuronal subpopulations may better explain the generation of α-syn inclusions throughout disease progression, rather than prion-like transmission (Surmeier et al., 2017). In this regard, a protective role of α-syn aggregates has been suggested, where they may be a consequence of the disease process rather than the cause (Olanow et al., 2004; Sian-Hulsmann et al., 2015). Based on these observations, and the fact that severity of clinical symptoms correlates with neurodegeneration rather than with α-syn inclusions in humans (Beach et al., 2009), the role of α-syn in these pathologies remains unclear.

It has to be mention that, to date, despite longitudinal studies with α-synucleinopathies patients have demonstrated clinical and biological changes throughout disease progression, they have not been able to show meaningful concordance between them, making difficult to properly define disease stages and, therefore, to evaluate the association between α-syn pathology and disease progression (Espay et al., 2020). In addition to that, the absence of significant correlation between α-syn pathology and cell loss in brain areas affected in these disorders could be due to a lack of sensitivity of current immunohistochemical methods. Further studies evaluating the presence of α-syn oligomers or early aggregation stages by novel techniques such as AS-PLA, RT-QuIC or PMCA may lead to a better understanding of the role of α-syn in α-synucleinopathies and clarify the possible pathological routes of α-syn propagation (Bengoa-Vergniory et al., 2017; Shahnawaz et al., 2020).

Finally, no evidences of α-syn transmission between humans has ever been reported, including iatrogenic (Irwin et al., 2013; Beekes et al., 2014), and there is no epidemiological data supporting this possibility for any α-synucleinopathy (Rajput et al., 2016; **Figure 4**). No evidences of transmission from animal to human have been found either (Wenning et al., 2018). Historically, prion infections have been a rarity whereas α-synucleinopathies present an important incidence that remains relatively stable over time in various ethnical populations (Pringsheim et al., 2014; Leak et al., 2019), however, *in vivo* studies show that the level of infectivity of α-syn aggregates per amount of protein might be orders of magnitude lower than that of prions (Watts, 2019).

Overall, despite α-syn shares several characteristics with prions, the absence of infectivity, the lack of human studies supporting the hypothesis and the existence of contradictory data must be taken in consideration. Thus, the term "prionoid" has been proposed to designate proteins that share propagative mechanisms with prions but may not be transmissible between individuals (Kara et al., 2018). At present, the most probable explanation regarding the start and progression of α-synucleionopathies would be that they are the consequence of a multifactorial process. This process would include the occurrence of exogenous and cellular micro-environmental changes in the affected regions that may trigger and modulate the pathology, and the presence of different α-syn strains that are able to spread through the organism in a cell type/susceptibility-dependent manner leading to different neuroanatomical spreading patterns.

FUTURES PERSPECTIVES IN α-SYN RESEARCH AND THERAPY

Although our knowledge about α-syn, its physiological functions, structure, properties and its pathological role in α-synucleinopathies have been extensively studied, there are still gaps that must be filled to completely understand the nature and the importance of this protein.

The characterization of α-syn interactions in the different subcellular compartments, not only in the CNS, but also in peripheral organs may be essential to fully understand its functions, the cellular and systemic changes that underlie α-synucleinopathies, and the possible deleterious consequences of therapeutic strategies targeting α-syn. The combination of novel super-resolution imaging, proteomics and computational techniques constitute a powerful approach to define α-syn interactome (Brás et al., 2020). A complete and detailed identification of all α-syn PTM, the different pathways involved in its clearance and the role of glial cells in this process represent other important targets for further studies (Lopes Da Fonseca et al., 2015; Gonzalez et al., 2019; Tremblay et al., 2019). Regarding the pathological role of α-syn, the absence of specific biomarkers and PET tracers constitute, at present, one of the most important disadvantages to identify its spatial and temporal contribution to disease progression in α-synucleinopathy patients. In addition, the biochemical composition and the molecular architecture of α-syn strains and inclusions and the cellular and environmental factors modulating their formation in the different disorders have not yet been completely revealed, mainly due to the lack of proper and highly sensitive protocols and tools. Elucidating the native conformation of α-syn and the different pathogenic strains by cryo-electron microscopy (Chen S. W. et al., 2015; Li et al., 2018; Guerrero-Ferreira et al., 2019), nuclear magnetic resonance (Galvagnion et al., 2019) or super-resolution imaging techniques (Nugent et al., 2017; Shahmoradian et al., 2019) will be essential to develop alternative drug-based disease modifying therapies. The establishment of brain banks of high-quality post-mortem brain tissue, CSF, plasma and fibroblast from clinically and pathologically well-defined patients and healthy controls will improve the potential of future studies. Moreover, the incorporation of induced-pluripotent stem cells (iPSCs) to those banks, to develop human patient-specific *in vitro* models of the disease, should be considered. Finally, further genetic and epigenetic studies will also provide important insights into the mechanism underlying α-synucleinopathies, the differences between them, as well as novel therapeutic targets.

Though the exact role of α-syn in the pathology has not yet been fully elucidated, an important number of preclinical studies and clinical trials have been focused on targeting directly α-syn and α-syn aggregation, or indirectly through the

modulation of processes associated with its accumulation. The use of small molecules to target α-syn aggregation have shown positive results in preclinical models of α-synucleionopathies by reducing aggregation and accumulation of α-syn inclusions, neurodegeneration and motor symptoms (Finkelstein et al., 2017; Price et al., 2018; Heras-Garvin et al., 2019; Wegrzynowicz et al., 2019). Antibiotics such as rifampicin also reduces α-syn aggregation and fibrillization (Li et al., 2004) and showed positive results in animal models (Ubhi et al., 2008). Different preclinical studies have demonstrated that α-syn immunotherapy enhances α-syn clearance, prevents spreading and neuronal loss and demyelination and improves motor function in animal models (Masliah et al., 2011; Mandler et al., 2014, 2015). Enhancing α-syn degradation by modulating cellular pathways and the activation of glial cell types associated with α-syn clearance constitute another promising strategy (Malagelada et al., 2010; Gao et al., 2019; Perrino et al., 2019). Stimulation of microglial-dependent clearance of α-syn reduces the number of inclusions, ameliorates motor symptoms and shows a neuroprotective effect in *in vivo* models of MSA and PD (Park et al., 2016; Venezia et al., 2017; Choi et al., 2020). Intriguingly, microglial activation and neuroinflammation can also promote α-syn aggregation and induce neurodegeneration, accelerating disease progression (Lema Tome et al., 2013), therefore, reduction of microglial activation have also been used for disease modification (Liu et al., 2019). Recently, the use of antisense nucleotides (ASO) to selectively inhibit proteins associated with α-syn pathology in specific brain regions or cell types has been proposed as an alternative approach to reduce α-syn accumulation in PD models (Zhao et al., 2017; Alarcón-Arís et al., 2018). This is particularly important since altering or removing α-syn gene expression in previous studies has shown profound and deleterious intracellular and developmental effects that in some cases could induce neuronal loss (Perez and Hastings, 2004; Benskey et al., 2016).

Most of these therapeutic strategies are currently under evaluation in human clinical trials (Heras-Garvin and Stefanova, 2020). Unfortunately, some of them have not shown ability to slow or halt disease progression (Heras-Garvin and Stefanova, 2020). The distinct efficacies observed between preclinical studies, based on *in vitro* and *in vivo* models, and the data from human studies could be explained by the neurobiological differences among species, but may be a consequence of current limitations to recruit patients at early stages of the disease, when significant neurodegeneration and motor symptoms are not yet present, to misdiagnosis and to the absence of specific biomarkers for α-syn.

CONCLUSIONS

It has been a long journey since α-syn was discovered 30 years ago. Many *in vitro* and *in vivo* studies have contributed to a better understanding of this versatile and multifaceted protein, its functions and its potential role in neurodegeneration. Moreover, the analysis of human material has indeed supported the idea that α-syn may contribute in some extent to the pathogenic events underlying the α-synucleionopathies. However, whether α-syn is the cause or main force driving these disorders or a mere secondary event is still a matter of debate. The use of novel highly sensitive tools and techniques in future studies, combined with the recruitment and collection of human material from well-characterized and documented cohorts, will definitely help us to finally define the pathogenic role of α-syn and to improve the development of proper therapeutic strategies.

AUTHOR CONTRIBUTIONS

AH-G: conception and design, drafting and revising the manuscript, and final approval of the submission. NS: conception and design, revising the manuscript, and final approval of the submission. All authors contributed to the article and approved the submitted version.

FUNDING

This work was supported by a grant of the Austrian Science Funds (FWF) F4414 and the grant "Fit for Science" of the Tyrol County.

REFERENCES

Abdelmotilib, H., Maltbie, T., Delic, V., Liu, Z., Hu, X., Fraser, K. B., et al. (2017). α-Synuclein fibril-induced inclusion spread in rats and mice correlates with dopaminergic Neurodegeneration. *Neurobiol. Dis.* 105, 84–98. doi: 10.1016/j.nbd.2017.05.014

Alam, P., Bousset, L., Melki, R., and Otzen, D. E. (2019). α-synuclein oligomers and fibrils: a spectrum of species, a spectrum of toxicities. *J. Neurochem.* 150, 522–534. doi: 10.1111/jnc.14808

Alarcón-Arís, D., Recasens, A., Galofre, M., Carballo-Carbajal, I., Zacchi, N., Ruiz-Bronchal, E., et al. (2018). Selective α-synuclein knockdown in monoamine neurons by intranasal oligonucleotide delivery: potential therapy for Parkinson's disease. *Mol. Ther.* 26, 550–567. doi: 10.1016/j.ymthe.2017.11.015

Almandoz-Gil, L., Persson, E., Lindstrom, V., Ingelsson, M., Erlandsson, A., and Bergstrom, J. (2018). *In situ* proximity ligation assay reveals co-localization of α-synuclein and SNARE proteins in murine primary neurons. *Front. Neurol.* 9:180. doi: 10.3389/fneur.2018.00180

Al-Wandi, A., Ninkina, N., Millership, S., Williamson, S. J., Jones, P. A., and Buchman, V. L. (2010). Absence of α-synuclein affects dopamine metabolism and synaptic markers in the striatum of aging mice. *Neurobiol. Aging* 31, 796–804. doi: 10.1016/j.neurobiolaging.2008.11.001

Angelova, P. R., Ludtmann, M. H., Horrocks, M. H., Negoda, A., Cremades, N., Klenerman, D., et al. (2016). Ca^{2+} is a key factor in α-synuclein-induced neurotoxicity. *J. Cell Sci.* 129, 1792–1801. doi: 10.1242/jcs.180737

Arai, K., Kato, N., Kashiwado, K., and Hattori, T. (2000). Pure autonomic failure in association with human α-synucleinopathy. *Neurosci. Lett.* 296, 171–173. doi: 10.1016/s0304-3940(00)01623-2

Arawaka, S., Sato, H., Sasaki, A., Koyama, S., and Kato, T. (2017). Mechanisms underlying extensive Ser129-phosphorylation in α-synuclein aggregates. *Acta Neuropathol. Commun.* 5:48. doi: 10.1186/s40478-017-0452-6

Armstrong, R. A., Lantos, P. L., and Cairns, N. J. (2004). Spatial patterns of α-synuclein positive glial cytoplasmic inclusions in multiple system atrophy. *Mov. Disord.* 19, 109–112. doi: 10.1002/mds.10637

Austin, S. A., Floden, A. M., Murphy, E. J., and Combs, C. K. (2006). α-synuclein expression modulates microglial activation phenotype. *J. Neurosci.* 26, 10558–10563. doi: 10.1523/JNEUROSCI.1799-06.2006

Barber, T. R., Lawton, M., Rolinski, M., Evetts, S., Baig, F., Ruffmann, C., et al. (2017). Prodromal Parkinsonism and neurodegenerative risk stratification in REM sleep behavior disorder. *Sleep* 40:zsx071. doi: 10.1093/sleep/zsx071

Barbour, R., Kling, K., Anderson, J. P., Banducci, K., Cole, T., Diep, L., et al. (2008). Red blood cells are the major source of α-synuclein in blood. *Neurodegener. Dis.* 5, 55–59. doi: 10.1159/000112832

Bartels, T., Choi, J. G., and Selkoe, D. J. (2011). α-Synuclein occurs physiologically as a helically folded tetramer that resists aggregation. *Nature* 477, 107–110. doi: 10.1038/nature10324

Bassil, F., Brown, H. J., Pattabhiraman, S., Iwasyk, J. E., Maghames, C. M., Meymand, E. S., et al. (2020). Amyloid-β (Aβ) plaques promote seeding and spreading of α-synuclein and tau in a mouse model of Lewy body disorders with Aβ pathology. *Neuron* 105, 260.e6–275.e6. doi: 10.1016/j.neuron.2019.10.010

Beach, T. G., Adler, C. H., Lue, L., Sue, L. I., Bachalakuri, J., Henry-Watson, J., et al. (2009). Unified staging system for Lewy body disorders: correlation with nigrostriatal degeneration, cognitive impairment and motor dysfunction. *Acta Neuropathol.* 117, 613–634. doi: 10.1007/s00401-009-0538-8

Beach, T. G., Adler, C. H., Serrano, G., Sue, L. I., Walker, D. G., Dugger, B. N., et al. (2016). Prevalence of submandibular gland synucleinopathy in Parkinson's disease, dementia with Lewy bodies and other Lewy body disorders. *J. Parkinsons Dis.* 6, 153–163. doi: 10.3233/JPD-150680

Beach, T. G., Adler, C. H., Sue, L. I., Vedders, L., Lue, L., White Iii, C. L., et al. (2010). Multi-organ distribution of phosphorylated α-synuclein histopathology in subjects with Lewy body disorders. *Acta Neuropathol.* 119, 689–702. doi: 10.1007/s00401-010-0664-3

Beekes, M., Thomzig, A., Schulz-Schaeffer, W. J., and Burger, R. (2014). Is there a risk of prion-like disease transmission by Alzheimer- or Parkinson-associated protein particles? *Acta Neuropathol.* 128, 463–476. doi: 10.1007/s00401-014-1324-9

Bendor, J. T., Logan, T. P., and Edwards, R. H. (2013). The function of α-synuclein. *Neuron* 79, 1044–1066. doi: 10.1016/j.neuron.2013.09.004

Ben Gedalya, T., Loeb, V., Israeli, E., Altschuler, Y., Selkoe, D. J., and Sharon, R. (2009). α-synuclein and polyunsaturated fatty acids promote clathrin-mediated endocytosis and synaptic vesicle recycling. *Traffic* 10, 218–234. doi: 10.1111/j.1600-0854.2008.00853.x

Bengoa-Vergniory, N., Roberts, R. F., Wade-Martins, R., and Alegre-Abarrategui, J. (2017). α-synuclein oligomers: a new hope. *Acta Neuropathol.* 134, 819–838. doi: 10.1007/s00401-017-1755-1

Benskey, M. J., Perez, R. G., and Manfredsson, F. P. (2016). The contribution of α-synuclein to neuronal survival and function—implications for Parkinson's disease. *J. Neurochem.* 137, 331–359. doi: 10.1111/jnc.13570

Berg, D., Postuma, R. B., Bloem, B., Chan, P., Dubois, B., Gasser, T., et al. (2014). Time to redefine PD? Introductory statement of the MDS Task Force on the definition of Parkinson's disease. *Mov. Disord.* 29, 454–462. doi: 10.1002/mds.25844

Binolfi, A., Theillet, F. X., and Selenko, P. (2012). Bacterial in-cell NMR of human α-synuclein: a disordered monomer by nature? *Biochem. Soc. Trans.* 40, 950–954. doi: 10.1042/bst20120096

Bousset, L., Pieri, L., Ruiz-Arlandis, G., Gath, J., Jensen, P. H., Habenstein, B., et al. (2013). Structural and functional characterization of two α-synuclein strains. *Nat. Commun.* 4:2575. doi: 10.3990/1.9789036529310

Braak, H., Del Tredici, K., Rub, U., De Vos, R. A., Jansen Steur, E. N., and Braak, E. (2003a). Staging of brain pathology related to sporadic Parkinson's disease. *Neurobiol. Aging* 24, 197–211. doi: 10.1016/s0197-4580(02)00065-9

Braak, H., Rüb, U., Gai, W. P., and Del Tredici, K. (2003b). Idiopathic Parkinson's disease: possible routes by which vulnerable neuronal types may be subject to neuroinvasion by an unknown pathogen. *J. Neural Transm.* 110, 517–536. doi: 10.1007/s00702-002-0808-2

Braak, H., De Vos, R. A., Bohl, J., and Del Tredici, K. (2006). Gastric α-synuclein immunoreactive inclusions in Meissner's and Auerbach's plexuses in cases staged for Parkinson's disease-related brain pathology. *Neurosci. Lett.* 396, 67–72. doi: 10.1016/j.neulet.2005.11.012

Braak, H., Ghebremedhin, E., Rub, U., Bratzke, H., and Del Tredici, K. (2004). Stages in the development of Parkinson's disease-related pathology. *Cell Tissue Res.* 318, 121–134. doi: 10.1007/s00441-004-0956-9

Braak, H., Sastre, M., Bohl, J. R., De Vos, R. A., and Del Tredici, K. (2007). Parkinson's disease: lesions in dorsal horn layer I, involvement of parasympathetic and sympathetic pre- and postganglionic neurons. *Acta Neuropathol.* 113, 421–429. doi: 10.1007/s00401-007-0193-x

Brás, I. C., Dominguez-Meijide, A., Gerhardt, E., Koss, D., Lazaro, D. F., Santos, P. I., et al. (2020). Synucleinopathies: where we are and where we need to go. *J. Neurochem.* 153, 433–454. doi: 10.1111/jnc.14965

Bridi, J. C., and Hirth, F. (2018). Mechanisms of α-synuclein induced synaptopathy in Parkinson's disease. *Front. Neurosci.* 12:80. doi: 10.3389/fnins.2018.00080

Brochard, V., Combadière, B., Prigent, A., Laouar, Y., Perrin, A., Beray-Berthat, V., et al. (2009). Infiltration of $CD4^+$ lymphocytes into the brain contributes to neurodegeneration in a mouse model of Parkinson disease. *J. Clin. Invest.* 119, 182–192. doi: 10.1172/JCI36470

Brundin, P., Li, J. Y., Holton, J. L., Lindvall, O., and Revesz, T. (2008). Research in motion: the enigma of Parkinson's disease pathology spread. *Nat. Rev. Neurosci.* 9, 741–745. doi: 10.1038/nrn2477

Buell, A. K., Galvagnion, C., Gaspar, R., Sparr, E., Vendruscolo, M., Knowles, T. P., et al. (2014). Solution conditions determine the relative importance of nucleation and growth processes in α-synuclein aggregation. *Proc. Natl. Acad. Sci. U S A* 111, 7671–7676. doi: 10.1073/pnas.1315346111

Burré, J., Sharma, M., and Sudhof, T. C. (2018). Cell biology and pathophysiology of α-synuclein. *Cold Spring Harb. Perspect. Med.* 8:a024091. doi: 10.1101/cshperspect.a024091

Burré, J., Sharma, M., Tsetsenis, T., Buchman, V., Etherton, M. R., and Sudhof, T. C. (2010). α-synuclein promotes SNARE-complex assembly *in vivo* and *in vitro*. *Science* 329, 1663–1667. doi: 10.1126/science.1195227

Burré, J., Vivona, S., Diao, J., Sharma, M., Brunger, A. T., and Sudhof, T. C. (2013). Properties of native brain α-synuclein. *Nature* 498, E4–6; discussion E6–E7. doi: 10.1038/nature12125

Butkovich, L. M., Houser, M. C., and Tansey, M. G. (2018). α-synuclein and noradrenergic modulation of immune cells in Parkinson's disease pathogenesis. *Front. Neurosci.* 12:626. doi: 10.3389/fnins.2018.00626

Candelise, N., Schmitz, M., Llorens, F., Villar-Pique, A., Cramm, M., Thom, T., et al. (2019). Seeding variability of different α-synuclein strains in synucleinopathies. *Ann. Neurol.* 85, 691–703. doi: 10.1002/ana.25446

Candelise, N., Schmitz, M., Thune, K., Cramm, M., Rabano, A., Zafar, S., et al. (2020). Effect of the micro-environment on α-synuclein conversion and implication in seeded conversion assays. *Transl. Neurodegener.* 9:5. doi: 10.1186/s40035-019-0181-9

Cappai, R., Leck, S. L., Tew, D. J., Williamson, N. A., Smith, D. P., Galatis, D., et al. (2005). Dopamine promotes α-synuclein aggregation into SDS-resistant soluble oligomers *via* a distinct folding pathway. *FASEB J.* 19, 1377–1379. doi: 10.1096/fj.04-3437fje

Challis, C., Hori, A., Sampson, T. R., Yoo, B. B., Challis, R. C., Hamilton, A. M., et al. (2020). Gut-seeded α-synuclein fibrils promote gut dysfunction and brain pathology specifically in aged mice. *Nat. Neurosci.* 23, 327–336. doi: 10.1038/s41593-020-0589-7

Chandra, S., Chen, X., Rizo, J., Jahn, R., and Sudhof, T. C. (2003). A broken α-helix in folded α-synuclein. *J. Biol. Chem.* 278, 15313–15318. doi: 10.1074/jbc.M213128200

Chen, S. W., Drakulic, S., Deas, E., Ouberai, M., Aprile, F. A., Arranz, R., et al. (2015). Structural characterization of toxic oligomers that are kinetically trapped during α-synuclein fibril formation. *Proc. Natl. Acad. Sci. U S A* 112, E1994–E2003. doi: 10.1073/pnas.1421204112

Chen, Y., Yang, W., Li, X., Li, X., Yang, H., Xu, Z., et al. (2015). α-Synuclein-induced internalization of NMDA receptors in hippocampal neurons is associated with reduced inward current and $Ca^{(2+)}$ influx upon NMDA stimulation. *Neuroscience* 300, 297–306. doi: 10.1016/j.neuroscience.2015.05.035

Cheng, H. C., Ulane, C. M., and Burke, R. E. (2010). Clinical progression in Parkinson disease and the neurobiology of axons. *Ann. Neurol.* 67, 715–725. doi: 10.1002/ana.21995

Choi, I., Zhang, Y., Seegobin, S. P., Pruvost, M., Wang, Q., Purtell, K., et al. (2020). Microglia clear neuron-released α-synuclein *via* selective autophagy and prevent neurodegeneration. *Nat. Commun.* 11:1386. doi: 10.1038/s41467-020-15119-w

Chu, Y., Muller, S., Tavares, A., Barret, O., Alagille, D., Seibyl, J., et al. (2019). Intrastriatal α-synuclein fibrils in monkeys: spreading, imaging and neuropathological changes. *Brain* 142, 3565–3579. doi: 10.1093/brain/awz296

Clinton, L. K., Blurton-Jones, M., Myczek, K., Trojanowski, J. Q., and Laferla, F. M. (2010). Synergistic interactions between Aβ, τ, and α-synuclein: acceleration of neuropathology and cognitive decline. *J. Neurosci.* 30, 7281–7289. doi: 10.1523/jneurosci.0490-10.2010

Coon, E. A., Cutsforth-Gregory, J. K., and Benarroch, E. E. (2018). Neuropathology of autonomic dysfunction in synucleinopathies. *Mov. Disord.* 33, 349–358. doi: 10.1002/mds.27186

Cremades, N., and Dobson, C. M. (2018). The contribution of biophysical and structural studies of protein self-assembly to the design of therapeutic strategies for amyloid diseases. *Neurobiol. Dis.* 109, 178–190. doi: 10.1016/j.nbd.2017.07.009

Croisier, E., Moran, L. B., Dexter, D. T., Pearce, R. K., and Graeber, M. B. (2005). Microglial inflammation in the parkinsonian substantia nigra: relationship to α-synuclein deposition. *J Neuroinflammation* 2:14. doi: 10.1186/1742-2094-2-14

Danzer, K. M., Haasen, D., Karow, A. R., Moussaud, S., Habeck, M., Giese, A., et al. (2007). Different species of α-synuclein oligomers induce calcium influx and seeding. *J. Neurosci.* 27, 9220–9232. doi: 10.1523/jneurosci.2617-07.2007

Davidi, D., Schechter, M., Elhadi, S. A., Matatov, A., Nathanson, L., and Sharon, R. (2020). α-synuclein translocates to the nucleus to activate retinoic-acid-dependent gene transcription. *iScience* 23:100910. doi: 10.2139/ssrn.3480698

De Oliveira, G. A. P., and Silva, J. L. (2019). α-synuclein stepwise aggregation reveals features of an early onset mutation in Parkinson's disease. *Commun. Biol.* 2:374. doi: 10.1038/s42003-019-0598-9

Decressac, M., Kadkhodaei, B., Mattsson, B., Laguna, A., Perlmann, T., and Bjorklund, A. (2012). α-Synuclein-induced down-regulation of Nurr1 disrupts GDNF signaling in nigral dopamine neurons. *Sci. Transl. Med.* 4:163ra156. doi: 10.1126/scitranslmed.3004676

Desplats, P., Lee, H. J., Bae, E. J., Patrick, C., Rockenstein, E., Crews, L., et al. (2009). Inclusion formation and neuronal cell death through neuron-to-neuron transmission of α-synuclein. *Proc. Natl. Acad. Sci. U S A* 106, 13010–13015. doi: 10.1073/pnas.0903691106

Devi, L., Raghavendran, V., Prabhu, B. M., Avadhani, N. G., and Anandatheerthavarada, H. K. (2008). Mitochondrial import and accumulation of α-synuclein impair complex I in human dopaminergic neuronal cultures and Parkinson disease brain. *J. Biol. Chem.* 283, 9089–9100. doi: 10.1074/jbc.m710012200

Dhillon, J. S., Trejo-Lopez, J. A., Riffe, C., Mcfarland, N. R., Hiser, W. M., Giasson, B. I., et al. (2019). Dissecting α-synuclein inclusion pathology diversity in multiple system atrophy: implications for the prion-like transmission hypothesis. *Lab. Invest.* 99, 982–992. doi: 10.1038/s41374-019-0198-9

Dickson, D. W., Braak, H., Duda, J. E., Duyckaerts, C., Gasser, T., Halliday, G. M., et al. (2009). Neuropathological assessment of Parkinson's disease: refining the diagnostic criteria. *Lancet Neurol.* 8, 1150–1157. doi: 10.1016/S1474-4422(09)70238-8

Dijkstra, A. A., Voorn, P., Berendse, H. W., Groenewegen, H. J., Netherlands Brain, B., Rozemuller, A. J., et al. (2014). Stage-dependent nigral neuronal loss in incidental Lewy body and Parkinson's disease. *Mov. Disord.* 29, 1244–1251. doi: 10.1002/mds.25952

Di Maio, R., Barrett, P. J., Hoffman, E. K., Barrett, C. W., Zharikov, A., Borah, A., et al. (2016). α-Synuclein binds to TOM20 and inhibits mitochondrial protein import in Parkinson's disease. *Sci. Transl. Med.* 8:342ra378. doi: 10.1126/scitranslmed.aaf3634

Don, A. S., Hsiao, J. H., Bleasel, J. M., Couttas, T. A., Halliday, G. M., and Kim, W. S. (2014). Altered lipid levels provide evidence for myelin dysfunction in multiple system atrophy. *Acta Neuropathol. Commun.* 2:150. doi: 10.1186/s40478-014-0150-6

Dong, C., Hoffmann, M., Li, X., Wang, M., Garen, C. R., Petersen, N. O., et al. (2018). Structural characteristics and membrane interactions of tandem α-synuclein oligomers. *Sci. Rep.* 8:6755. doi: 10.1038/s41598-018-25133-0

Doorn, K. J., Moors, T., Drukarch, B., Van De Berg, W., Lucassen, P. J., and Van Dam, A. M. (2014). Microglial phenotypes and toll-like receptor 2 in the substantia nigra and hippocampus of incidental Lewy body disease cases and Parkinson's disease patients. *Acta Neuropathol. Commun.* 2:90. doi: 10.1186/s40478-014-0090-1

Durante, V., De Iure, A., Loffredo, V., Vaikath, N., De Risi, M., Paciotti, S., et al. (2019). α-synuclein targets GluN2A NMDA receptor subunit causing striatal synaptic dysfunction and visuospatial memory alteration. *Brain* 142, 1365–1385. doi: 10.1093/brain/awz065

El-Agnaf, O. M., Salem, S. A., Paleologou, K. E., Cooper, L. J., Fullwood, N. J., Gibson, M. J., et al. (2003). α-synuclein implicated in Parkinson's disease is present in extracellular biological fluids, including human plasma. *FASEB J.* 17, 1945–1947. doi: 10.1096/fj.03-0098fje

Emmanouilidou, E., Stefanis, L., and Vekrellis, K. (2010). Cell-produced α-synuclein oligomers are targeted to and impair, the 26S proteasome. *Neurobiol. Aging* 31, 953–968. doi: 10.1016/j.neurobiolaging.2008.07.008

Engelender, S., and Isacson, O. (2017). The threshold theory for Parkinson's disease. *Trends Neurosci.* 40, 4–14. doi: 10.1016/j.tins.2016.10.008

Eschbach, J., Von Einem, B., Müller, K., Bayer, H., Scheffold, A., Morrison, B. E., et al. (2015). Mutual exacerbation of peroxisome proliferator-activated receptor γ coactivator 1α deregulation and α-synuclein oligomerization. *Ann. Neurol.* 77, 15–32. doi: 10.1002/ana.24294

Espay, A. J., Kalia, L. V., Gan-Or, Z., Williams-Gray, C. H., Bedard, P. L., Rowe, S. M., et al. (2020). Disease modification and biomarker development in Parkinson disease: revision or reconstruction? *Neurology* 94, 481–494. doi: 10.1212/WNL.0000000000009107

Ettle, B., Kerman, B. E., Valera, E., Gillmann, C., Schlachetzki, J. C., Reiprich, S., et al. (2016). α-Synuclein-induced myelination deficit defines a novel interventional target for multiple system atrophy. *Acta Neuropathol.* 132, 59–75. doi: 10.1007/s00401-016-1572-y

Ettle, B., Reiprich, S., Deusser, J., Schlachetzki, J. C., Xiang, W., Prots, I., et al. (2014). Intracellular α-synuclein affects early maturation of primary oligodendrocyte progenitor cells. *Mol. Cell. Neurosci.* 62, 68–78. doi: 10.1016/j.mcn.2014.06.012

Fanciulli, A., and Wenning, G. K. (2015). Multiple-system atrophy. *N. Engl. J. Med.* 372, 249–263. doi: 10.1056/NEJMra1311488

Fares, M. B., Ait-Bouziad, N., Dikiy, I., Mbefo, M. K., Jovicic, A., Kiely, A., et al. (2014). The novel Parkinson's disease linked mutation G51D attenuates *in vitro* aggregation and membrane binding of α-synuclein and enhances its secretion and nuclear localization in cells. *Hum. Mol. Genet.* 23, 4491–4509. doi: 10.1093/hmg/ddu165

Fauvet, B., Mbefo, M. K., Fares, M. B., Desobry, C., Michael, S., Ardah, M. T., et al. (2012). α-Synuclein in central nervous system and from erythrocytes, mammalian cells, and Escherichia coli exists predominantly as disordered monomer. *J. Biol. Chem.* 287, 15345–15364. doi: 10.1074/jbc.M111.318949

Fecchio, C., Palazzi, L., and De Laureto, P. P. (2018). α-synuclein and polyunsaturated fatty acids: molecular basis of the interaction and implication in neurodegeneration. *Molecules* 23:1531. doi: 10.3390/molecules23071531

Fellner, L., Irschick, R., Schanda, K., Reindl, M., Klimaschewski, L., Poewe, W., et al. (2013). Toll-like receptor 4 is required for α-synuclein dependent activation of microglia and astroglia. *Glia* 61, 349–360. doi: 10.1002/glia.22437

Finkelstein, D. I., Billings, J. L., Adlard, P. A., Ayton, S., Sedjahtera, A., Masters, C. L., et al. (2017). The novel compound PBT434 prevents iron mediated neurodegeneration and α-synuclein toxicity in multiple models of Parkinson's disease. *Acta Neuropathol. Commun.* 5:53. doi: 10.1186/s40478-017-0456-2

Fitzgerald, E., Murphy, S., and Martinson, H. A. (2019). α-synuclein pathology and the role of the microbiota in Parkinson's disease. *Front. Neurosci.* 13:369. doi: 10.3389/fnins.2019.00369

Flavin, W. P., Bousset, L., Green, Z. C., Chu, Y., Skarpathiotis, S., Chaney, M. J., et al. (2017). Endocytic vesicle rupture is a conserved mechanism of cellular invasion by amyloid proteins. *Acta Neuropathol.* 134, 629–653. doi: 10.1007/s00401-017-1722-x

Freundt, E. C., Maynard, N., Clancy, E. K., Roy, S., Bousset, L., Sourigues, Y., et al. (2012). Neuron-to-neuron transmission of α-synuclein fibrils through axonal transport. *Ann. Neurol.* 72, 517–524. doi: 10.1002/ana.23747

Froula, J. M., Castellana-Cruz, M., Anabtawi, N. M., Camino, J. D., Chen, S. W., Thrasher, D. R., et al. (2019). Defining α-synuclein species responsible for Parkinson's disease phenotypes in mice. *J. Biol. Chem.* 294, 10392–10406. doi: 10.1074/jbc.RA119.007743

Froula, J. M., Henderson, B. W., Gonzalez, J. C., Vaden, J. H., Mclean, J. W., Wu, Y., et al. (2018). α-Synuclein fibril-induced paradoxical structural and functional defects in hippocampal neurons. *Acta Neuropathol. Commun.* 6:35. doi: 10.1186/s40478-018-0537-x

Fusco, G., Chen, S. W., Williamson, P. T. F., Cascella, R., Perni, M., Jarvis, J. A., et al. (2017). Structural basis of membrane disruption and cellular toxicity by α-synuclein oligomers. *Science* 358, 1440–1443. doi: 10.1126/science.aan6160

Galvagnion, C., Topgaard, D., Makasewicz, K., Buell, A. K., Linse, S., Sparr, E., et al. (2019). Lipid dynamics and phase transition within α-synuclein amyloid fibrils. *J. Phys. Chem. Lett.* 10, 7872–7877. doi: 10.1021/acs.jpclett.9b03005

Ganjam, G. K., Bolte, K., Matschke, L. A., Neitemeier, S., Dolga, A. M., Hollerhage, M., et al. (2019). Mitochondrial damage by α-synuclein causes cell death in human dopaminergic neurons. *Cell Death Dis.* 10:865. doi: 10.1038/s41419-019-2091-2

Gao, J., Perera, G., Bhadbhade, M., Halliday, G. M., and Dzamko, N. (2019). Autophagy activation promotes clearance of α-synuclein inclusions in fibril-seeded human neural cells. *J. Biol. Chem.* 294, 14241–14256. doi: 10.1074/jbc.ra119.008733

Garretti, F., Agalliu, D., Lindestam Arlehamn, C. S., Sette, A., and Sulzer, D. (2019). Autoimmunity in Parkinson's disease: the role of α-synuclein-specific T cells. *Front. Immunol.* 10:303. doi: 10.3389/fimmu.2019.00303

Gerhard, A., Banati, R. B., Goerres, G. B., Cagnin, A., Myers, R., Gunn, R. N., et al. (2003). [^{11}C](R)-PK11195 PET imaging of microglial activation in multiple system atrophy. *Neurology* 61, 686–689. doi: 10.1212/01.wnl.0000078192.95645.e6

Gerhard, A., Pavese, N., Hotton, G., Turkheimer, F., Es, M., Hammers, A., et al. (2006). *In vivo* imaging of microglial activation with [^{11}C](R)-PK11195 PET in idiopathic Parkinson's disease. *Neurobiol. Dis.* 21, 404–412. doi: 10.1016/j.nbd.2005.08.002

Ghiglieri, V., Calabrese, V., and Calabresi, P. (2018). α-synuclein: from early synaptic dysfunction to neurodegeneration. *Front. Neurol.* 9:295. doi: 10.3389/fneur.2018.00295

Ghosh, D., Sahay, S., Ranjan, P., Salot, S., Mohite, G. M., Singh, P. K., et al. (2014). The newly discovered Parkinson's disease associated Finnish mutation (A53E) attenuates α-synuclein aggregation and membrane binding. *Biochemistry* 53, 6419–6421. doi: 10.1021/bi5010365

Giasson, B. I., Duda, J. E., Murray, I. V., Chen, Q., Souza, J. M., Hurtig, H. I., et al. (2000). Oxidative damage linked to neurodegeneration by selective α-synuclein nitration in synucleinopathy lesions. *Science* 290, 985–989. doi: 10.1126/science.290.5493.985

Giordano, N., Iemolo, A., Mancini, M., Cacace, F., De Risi, M., Latagliata, E. C., et al. (2018). Motor learning and metaplasticity in striatal neurons: relevance for Parkinson's disease. *Brain* 141, 505–520. doi: 10.1093/brain/awx351

Goedert, M., and Spillantini, M. G. (1998). Lewy body diseases and multiple system atrophy as alpha-synucleinopathies. *Mol. Psychiatry* 3, 462–465. doi: 10.1038/sj.mp.4000458

Gonzalez, N., Arcos-Lopez, T., Konig, A., Quintanar, L., Menacho Marquez, M., Outeiro, T. F., et al. (2019). Effects of α-synuclein post-translational modifications on metal binding. *J. Neurochem.* 150, 507–521. doi: 10.1111/jnc.14721

Gosavi, N., Lee, H. J., Lee, J. S., Patel, S., and Lee, S. J. (2002). Golgi fragmentation occurs in the cells with prefibrillar α-synuclein aggregates and precedes the formation of fibrillar inclusion. *J. Biol. Chem.* 277, 48984–48992. doi: 10.1074/jbc.m208194200

Grey, M., Linse, S., Nilsson, H., Brundin, P., and Sparr, E. (2011). Membrane interaction of α-synuclein in different aggregation states. *J. Parkinsons Dis.* 1, 359–371. doi: 10.3233/JPD-2011-11067

Guardia-Laguarta, C., Area-Gomez, E., Rub, C., Liu, Y., Magrane, J., Becker, D., et al. (2014). α-Synuclein is localized to mitochondria-associated ER membranes. *J. Neurosci.* 34, 249–259. doi: 10.1523/JNEUROSCI.2507-13.2014

Guerrero-Ferreira, R., Taylor, N. M., Arteni, A. A., Kumari, P., Mona, D., Ringler, P., et al. (2019). Two new polymorphic structures of human full-length α-synuclein fibrils solved by cryo-electron microscopy. *eLife* 8:e48907. doi: 10.7554/eLife.48907

Guo, J. L., Covell, D. J., Daniels, J. P., Iba, M., Stieber, A., Zhang, B., et al. (2013). Distinct α-synuclein strains differentially promote tau inclusions in neurons. *Cell* 154, 103–117. doi: 10.1016/j.cell.2013.05.057

Hallett, P. J., Cooper, O., Sadi, D., Robertson, H., Mendez, I., and Isacson, O. (2014). Long-term health of dopaminergic neuron transplants in Parkinson's disease patients. *Cell Rep.* 7, 1755–1761. doi: 10.1016/j.celrep.2014.05.027

Halliday, G., Mccann, H., and Shepherd, C. (2012). Evaluation of the Braak hypothesis: how far can it explain the pathogenesis of Parkinson's disease? *Expert Rev. Neurother.* 12, 673–686. doi: 10.1586/ern.12.47

Halliday, G. M., and Stevens, C. H. (2011). Glia: initiators and progressors of pathology in Parkinson's disease. *Mov. Disord.* 26, 6–17. doi: 10.1002/mds.23455

Hegde, M. L., and Rao, K. S. (2007). DNA induces folding in α-synuclein: understanding the mechanism using chaperone property of osmolytes. *Arch. Biochem. Biophys.* 464, 57–69. doi: 10.1016/j.abb.2007.03.042

Heras-Garvin, A., and Stefanova, N. (2020). MSA: from basic mechanisms to experimental therapeutics. *Parkinsonism Relat. Disord.* 73, 94–104. doi: 10.1016/j.parkreldis.2020.01.010

Heras-Garvin, A., Weckbecker, D., Ryazanov, S., Leonov, A., Griesinger, C., Giese, A., et al. (2019). Anle138b modulates α-synuclein oligomerization and prevents motor decline and neurodegeneration in a mouse model of multiple system atrophy. *Mov. Disord.* 34, 255–263. doi: 10.1002/mds.27562

Hijaz, B. A., and Volpicelli-Daley, L. A. (2020). Initiation and propagation of α-synuclein aggregation in the nervous system. *Mol. Neurodegener.* 15:19. doi: 10.1186/s13024-020-00368-6

Hoffmann, A., Ettle, B., Battis, K., Reiprich, S., Schlachetzki, J. C. M., Masliah, E., et al. (2019). Oligodendroglial α-synucleinopathy-driven neuroinflammation in multiple system atrophy. *Brain Pathol.* 29, 380–396. doi: 10.1111/bpa.12678

Holmes, B. B., Devos, S. L., Kfoury, N., Li, M., Jacks, R., Yanamandra, K., et al. (2013). Heparan sulfate proteoglycans mediate internalization and propagation of specific proteopathic seeds. *Proc. Natl. Acad. Sci. U S A* 110, E3138–E3147. doi: 10.1073/pnas.1301440110

Holmqvist, S., Chutna, O., Bousset, L., Aldrin-Kirk, P., Li, W., Bjorklund, T., et al. (2014). Direct evidence of Parkinson pathology spread from the gastrointestinal tract to the brain in rats. *Acta Neuropathol.* 128, 805–820. doi: 10.1007/s00401-014-1343-6

Hoozemans, J. J., Van Haastert, E. S., Eikelenboom, P., De Vos, R. A., Rozemuller, J. M., and Scheper, W. (2007). Activation of the unfolded protein response in Parkinson's disease. *Biochem. Biophys. Res. Commun.* 354, 707–711. doi: 10.1016/j.bbrc.2007.01.043

Hsu, L. J., Sagara, Y., Arroyo, A., Rockenstein, E., Sisk, A., Mallory, M., et al. (2000). α-synuclein promotes mitochondrial deficit and oxidative stress. *Am. J. Pathol.* 157, 401–410. doi: 10.1016/s0002-9440(10)64553-1

Iljina, M., Garcia, G. A., Horrocks, M. H., Tosatto, L., Choi, M. L., Ganzinger, K. A., et al. (2016). Kinetic model of the aggregation of α-synuclein provides insights into prion-like spreading. *Proc. Natl. Acad. Sci. U S A* 113, E1206–E1215. doi: 10.1073/pnas.1524128113

Imamura, K., Hishikawa, N., Sawada, M., Nagatsu, T., Yoshida, M., and Hashizume, Y. (2003). Distribution of major histocompatibility complex class II-positive microglia and cytokine profile of Parkinson's disease brains. *Acta Neuropathol.* 106, 518–526. doi: 10.1007/s00401-003-0766-2

Iranzo, A., Tolosa, E., Gelpi, E., Molinuevo, J. L., Valldeoriola, F., Serradell, M., et al. (2013). Neurodegenerative disease status and post-mortem pathology in idiopathic rapid-eye-movement sleep behaviour disorder: an observational cohort study. *Lancet Neurol.* 12, 443–453. doi: 10.1016/S1474-4422(13)70056-5

Irwin, D. J., Abrams, J. Y., Schonberger, L. B., Leschek, E. W., Mills, J. L., Lee, V. M., et al. (2013). Evaluation of potential infectivity of Alzheimer and Parkinson disease proteins in recipients of cadaver-derived human growth hormone. *JAMA Neurol.* 70, 462–468. doi: 10.1001/jamaneurol.2013.1933

Ishizawa, K., Komori, T., Arai, N., Mizutani, T., and Hirose, T. (2008). Glial cytoplasmic inclusions and tissue injury in multiple system atrophy: A quantitative study in white matter (olivopontocerebellar system) and gray matter (nigrostriatal system). *Neuropathology* 28, 249–257. doi: 10.1111/j.1440-1789.2007.00855.x

Ishizawa, K., Komori, T., Sasaki, S., Arai, N., Mizutani, T., and Hirose, T. (2004). Microglial activation parallels system degeneration in multiple system atrophy. *J. Neuropathol. Exp. Neurol.* 63, 43–52. doi: 10.1093/jnen/63.1.43

Jellinger, K. A. (2009). A critical evaluation of current staging of α-synuclein pathology in Lewy body disorders. *Biochim. Biophys. Acta* 1792, 730–740. doi: 10.1016/j.bbadis.2008.07.006

Jellinger, K. A. (2018). Dementia with Lewy bodies and Parkinson's disease-dementia: current concepts and controversies. *J. Neural Transm.* 125, 615–650. doi: 10.1007/s00702-017-1821-9

Kaji, S., Maki, T., Ishimoto, T., Yamakado, H., and Takahashi, R. (2020). Insights into the pathogenesis of multiple system atrophy: focus on glial cytoplasmic inclusions. *Transl. Neurodegener.* 9:7. doi: 10.1186/s40035-020-0185-5

Kaji, S., Maki, T., Kinoshita, H., Uemura, N., Ayaki, T., Kawamoto, Y., et al. (2018). Pathological endogenous α-synuclein accumulation in oligodendrocyte precursor cells potentially induces inclusions in multiple system atrophy. *Stem Cell Reports* 10, 356–365. doi: 10.1016/j.stemcr.2017.12.001

Kalaitzakis, M. E., Graeber, M. B., Gentleman, S. M., and Pearce, R. K. (2008). The dorsal motor nucleus of the vagus is not an obligatory trigger site of Parkinson's disease: a critical analysis of α-synuclein staging. *Neuropathol. Appl. Neurobiol.* 34, 284–295. doi: 10.1111/j.1365-2990.2007.00923.x

Kalia, L. V., and Lang, A. E. (2015). Parkinson's disease. *Lancet* 386, 896–912. doi: 10.1016/S0140-6736(14)61393-3

Kam, T. I., Mao, X., Park, H., Chou, S. C., Karuppagounder, S. S., Umanah, G. E., et al. (2018). Poly(ADP-ribose) drives pathologic α-synuclein neurodegeneration in Parkinson's disease. *Science* 362:eaat8407. doi: 10.1126/science.aat8407

Kara, E., Marks, J. D., and Aguzzi, A. (2018). Toxic protein spread in neurodegeneration: reality versus fantasy. *Trends Mol. Med.* 24, 1007–1020. doi: 10.1016/j.molmed.2018.09.004

Katorcha, E., Makarava, N., Lee, Y. J., Lindberg, I., Monteiro, M. J., Kovacs, G. G., et al. (2017). Cross-seeding of prions by aggregated α-synuclein leads to transmissible spongiform encephalopathy. *PLoS Pathog.* 13:e1006563. doi: 10.1371/journal.ppat.1006563

Kaufmann, H., Hague, K., and Perl, D. (2001). Accumulation of α-synuclein in autonomic nerves in pure autonomic failure. *Neurology* 56, 980–981. doi: 10.1212/wnl.56.7.980

Kaufmann, H., Nahm, K., Purohit, D., and Wolfe, D. (2004). Autonomic failure as the initial presentation of Parkinson disease and dementia with Lewy bodies. *Neurology* 63, 1093–1095. doi: 10.1212/01.wnl.0000138500.73671.dc

Kim, C., Ho, D. H., Suk, J. E., You, S., Michael, S., Kang, J., et al. (2013). Neuron-released oligomeric α-synuclein is an endogenous agonist of TLR2 for paracrine activation of microglia. *Nat. Commun.* 4:1562. doi: 10.1038/ncomms2534

Kim, J. Y., Illigens, B. M., Mccormick, M. P., Wang, N., and Gibbons, C. H. (2019). α-synuclein in skin nerve fibers as a biomarker for α-synucleinopathies. *J. Clin. Neurol.* 15, 135–142. doi: 10.3988/jcn.2019.15.2.135

Kim, S., Kwon, S. H., Kam, T. I., Panicker, N., Karuppagounder, S. S., Lee, S., et al. (2019). Transneuronal propagation of pathologic α-synuclein from the gut to the brain models Parkinson's disease. *Neuron* 103, 627.e7–641.e7. doi: 10.1016/j.neuron.2019.05.035

Kobayashi, J., Hasegawa, T., Sugeno, N., Yoshida, S., Akiyama, T., Fujimori, K., et al. (2019). Extracellular α-synuclein enters dopaminergic cells by modulating flotillin-1-assisted dopamine transporter endocytosis. *FASEB J.* 33, 10240–10256. doi: 10.1096/fj.201802051r

Kordower, J. H., Chu, Y., Hauser, R. A., Freeman, T. B., and Olanow, C. W. (2008). Lewy body-like pathology in long-term embryonic nigral transplants in Parkinson's disease. *Nat. Med.* 14, 504–506. doi: 10.1096/fj.20180 2051R

Krasnoslobodtsev, A. V., Peng, J., Asiago, J. M., Hindupur, J., Rochet, J. C., and Lyubchenko, Y. L. (2012). Effect of spermidine on misfolding and interactions of α-synuclein. *PLoS One* 7:e38099. doi: 10.1371/journal.pone.0038099

Kubler, D., Wachter, T., Cabanel, N., Su, Z., Turkheimer, F. E., Dodel, R., et al. (2019). Widespread microglial activation in multiple system atrophy. *Mov. Disord.* 34, 564–568. doi: 10.1002/mds.27620

Lashuel, H. A., Overk, C. R., Oueslati, A., and Masliah, E. (2013). The many faces of α-synuclein: from structure and toxicity to therapeutic target. *Nat. Rev. Neurosci.* 14, 38–48. doi: 10.1038/nrn3406

Lashuel, H. A., Petre, B. M., Wall, J., Simon, M., Nowak, R. J., Walz, T., et al. (2002). α-synuclein, especially the Parkinson's disease-associated mutants, forms pore-like annular and tubular protofibrils. *J. Mol. Biol.* 322, 1089–1102. doi: 10.1016/s0022-2836(02)00735-0

Lau, A., So, R. W. L., Lau, H. H. C., Sang, J. C., Ruiz-Riquelme, A., Fleck, S. C., et al. (2020). α-Synuclein strains target distinct brain regions and cell types. *Nat. Neurosci.* 23, 21–31. doi: 10.1038/s41593-019-0541-x

Leak, R. K., Frosch, M. P., Beach, T. G., and Halliday, G. M. (2019). α-synuclein: prion or prion-like? *Acta Neuropathol.* 138, 509–514. doi: 10.1007/s00401-019-02057-1

Lee, H. J., Baek, S. M., Ho, D. H., Suk, J. E., Cho, E. D., and Lee, S. J. (2011). Dopamine promotes formation and secretion of non-fibrillar α-synuclein oligomers. *Exp. Mol. Med.* 43, 216–222. doi: 10.3858/emm.2011.43.4.026

Lee, H. J., Khoshaghideh, F., Patel, S., and Lee, S. J. (2004). Clearance of α-synuclein oligomeric intermediates *via* the lysosomal degradation pathway. *J. Neurosci.* 24, 1888–1896. doi: 10.1523/jneurosci.3809-03.2004

Lee, H. J., Suk, J. E., Patrick, C., Bae, E. J., Cho, J. H., Rho, S., et al. (2010). Direct transfer of α-synuclein from neuron to astroglia causes inflammatory responses in synucleinopathies. *J. Biol. Chem.* 285, 9262–9272. doi: 10.1074/jbc.m109.081125

Lee, V. M., and Trojanowski, J. Q. (2006). Mechanisms of Parkinson's disease linked to pathological α-synuclein: new targets for drug discovery. *Neuron* 52, 33–38. doi: 10.1016/j.neuron.2006.09.026

Lema Tome, C. M., Tyson, T., Rey, N. L., Grathwohl, S., Britschgi, M., and Brundin, P. (2013). Inflammation and α-synuclein's prion-like behavior in Parkinson's disease--is there a link? *Mol. Neurobiol.* 47, 561–574. doi: 10.1007/s12035-012-8267-8

Li, B., Ge, P., Murray, K. A., Sheth, P., Zhang, M., Nair, G., et al. (2018). Cryo-EM of full-length α-synuclein reveals fibril polymorphs with a common structural kernel. *Nat. Commun.* 9:3609. doi: 10.1038/s41467-018-05971-2

Li, J., Zhu, M., Rajamani, S., Uversky, V. N., and Fink, A. L. (2004). Rifampicin inhibits α-synuclein fibrillation and disaggregates fibrils. *Chem. Biol.* 11, 1513–1521. doi: 10.1016/j.chembiol.2004.08.025

Li, J. Y., Englund, E., Holton, J. L., Soulet, D., Hagell, P., Lees, A. J., et al. (2008). Lewy bodies in grafted neurons in subjects with Parkinson's disease suggest host-to-graft disease propagation. *Nat. Med.* 14, 501–503. doi: 10.1038/nm1746

Li, W., Englund, E., Widner, H., Mattsson, B., Van Westen, D., Latt, J., et al. (2016). Extensive graft-derived dopaminergic innervation is maintained 24 years after transplantation in the degenerating parkinsonian brain. *Proc. Natl. Acad. Sci. U S A* 113, 6544–6549. doi: 10.1073/pnas.1605245113

Li, W., West, N., Colla, E., Pletnikova, O., Troncoso, J. C., Marsh, L., et al. (2005). Aggregation promoting C-terminal truncation of α-synuclein is a normal cellular process and is enhanced by the familial Parkinson's disease-linked mutations. *Proc. Natl. Acad. Sci. U S A* 102, 2162–2167. doi: 10.1073/pnas.0406976102

Li, W. W., Yang, R., Guo, J. C., Ren, H. M., Zha, X. L., Cheng, J. S., et al. (2007). Localization of α-synuclein to mitochondria within midbrain of mice. *Neuroreport* 18, 1543–1546. doi: 10.1097/WNR.0b013e3282f03db4

Lindersson, E., Beedholm, R., Hojrup, P., Moos, T., Gai, W., Hendil, K. B., et al. (2004). Proteasomal inhibition by α-synuclein filaments and oligomers. *J. Biol. Chem.* 279, 12924–12934. doi: 10.1074/jbc.M306390200

Lionnet, A., Leclair-Visonneau, L., Neunlist, M., Murayama, S., Takao, M., Adler, C. H., et al. (2018). Does Parkinson's disease start in the gut? *Acta Neuropathol.* 135, 1–12. doi: 10.1007/s00401-017-1777-8

Liu, C. Y., Wang, X., Liu, C., and Zhang, H. L. (2019). Pharmacological targeting of microglial activation: new therapeutic approach. *Front. Cell. Neurosci.* 13:514. doi: 10.3389/fncel.2019.00514

Lohmann, S., Bernis, M. E., Tachu, B. J., Ziemski, A., Grigoletto, J., and Tamguney, G. (2019). Oral and intravenous transmission of α-synuclein fibrils to mice. *Acta Neuropathol.* 138, 515–533. doi: 10.1007/s00401-019-02037-5

Lopes Da Fonseca, T., Villar-Pique, A., and Outeiro, T. F. (2015). The interplay between α-synuclein clearance and spreading. *Biomolecules* 5, 435–471. doi: 10.3390/biom5020435

Ludtmann, M. H. R., Angelova, P. R., Horrocks, M. H., Choi, M. L., Rodrigues, M., Baev, A. Y., et al. (2018). α-synuclein oligomers interact with ATP synthase and

open the permeability transition pore in Parkinson's disease. *Nat. Commun.* 9:2293. doi: 10.1038/s41467-018-04422-2

Luk, K. C., Kehm, V., Carroll, J., Zhang, B., O'brien, P., Trojanowski, J. Q., et al. (2012a). Pathological α-synuclein transmission initiates Parkinson-like neurodegeneration in nontransgenic mice. *Science* 338, 949–953. doi: 10.1126/science.1227157

Luk, K. C., Kehm, V. M., Zhang, B., O'brien, P., Trojanowski, J. Q., and Lee, V. M. (2012b). Intracerebral inoculation of pathological α-synuclein initiates a rapidly progressive neurodegenerative α-synucleinopathy in mice. *J. Exp. Med.* 209, 975–986. doi: 10.1084/jem.20112457

Luk, K. C., Song, C., O'Brien, P., Stieber, A., Branch, J. R., Brunden, K. R., et al. (2009). Exogenous α-synuclein fibrils seed the formation of Lewy body-like intracellular inclusions in cultured cells. *Proc. Natl. Acad. Sci. U S A* 106, 20051–20056. doi: 10.1073/pnas.0908005106

Mahul-Mellier, A. L., Burtscher, J., Maharjan, N., Weerens, L., Croisier, M., Kuttler, F., et al. (2020). The process of Lewy body formation, rather than simply α-synuclein fibrillization, is one of the major drivers of neurodegeneration. *Proc. Natl. Acad. Sci. U S A* 117, 4971–4982. doi: 10.1073/pnas.1913904117

Malagelada, C., Jin, Z. H., Jackson-Lewis, V., Przedborski, S., and Greene, L. A. (2010). Rapamycin protects against neuron death in *in vitro* and *in vivo* models of Parkinson's disease. *J. Neurosci.* 30, 1166–1175. doi: 10.1523/jneurosci.3944-09.2010

Mandel, R. J., Marmion, D. J., Kirik, D., Chu, Y., Heindel, C., Mccown, T., et al. (2017). Novel oligodendroglial α-synuclein viral vector models of multiple system atrophy: studies in rodents and nonhuman primates. *Acta Neuropathol. Commun.* 5:47. doi: 10.1186/s40478-017-0451-7

Mandler, M., Valera, E., Rockenstein, E., Mante, M., Weninger, H., Patrick, C., et al. (2015). Active immunization against α-synuclein ameliorates the degenerative pathology and prevents demyelination in a model of multiple system atrophy. *Mol. Neurodegener.* 10:10. doi: 10.1186/s13024-015-0008-9

Mandler, M., Valera, E., Rockenstein, E., Weninger, H., Patrick, C., Adame, A., et al. (2014). Next-generation active immunization approach for synucleinopathies: implications for Parkinson's disease clinical trials. *Acta Neuropathol.* 127, 861–879. doi: 10.1007/s00401-014-1256-4

Manfredsson, F. P., Luk, K. C., Benskey, M. J., Gezer, A., Garcia, J., Kuhn, N. C., et al. (2018). Induction of α-synuclein pathology in the enteric nervous system of the rat and non-human primate results in gastrointestinal dysmotility and transient CNS pathology. *Neurobiol. Dis.* 112, 106–118. doi: 10.1016/j.nbd.2018.01.008

Mao, X., Ou, M. T., Karuppagounder, S. S., Kam, T. I., Yin, X., Xiong, Y., et al. (2016). Pathological α-synuclein transmission initiated by binding lymphocyte-activation gene 3. *Science* 353:aah3374. doi: 10.1126/science.aah3374

Maroteaux, L., Campanelli, J. T., and Scheller, R. H. (1988). Synuclein: a neuron-specific protein localized to the nucleus and presynaptic nerve terminal. *J. Neurosci.* 8, 2804–2815. doi: 10.1523/jneurosci.08-08-02804.1988

Marreiros, R., Muller-Schiffmann, A., Trossbach, S. V., Prikulis, I., Hansch, S., Weidtkamp-Peters, S., et al. (2020). Disruption of cellular proteostasis by H1N1 influenza A virus causes α-synuclein aggregation. *Proc. Natl. Acad. Sci. U S A* 117, 6741–6751. doi: 10.1073/pnas.1906466117

Marti, M. J., Tolosa, E., and Campdelacreu, J. (2003). Clinical overview of the synucleinopathies. *Mov. Disord.* 18, S21–S27. doi: 10.1002/mds.10559

Masaracchia, C., Hnida, M., Gerhardt, E., Lopes Da Fonseca, T., Villar-Pique, A., Branco, T., et al. (2018). Membrane binding, internalization and sorting of α-synuclein in the cell. *Acta Neuropathol. Commun.* 6:79. doi: 10.1186/s40478-018-0578-1

Masliah, E., Rockenstein, E., Mante, M., Crews, L., Spencer, B., Adame, A., et al. (2011). Passive immunization reduces behavioral and neuropathological deficits in an α-synuclein transgenic model of Lewy body disease. *PLoS One* 6:e19338. doi: 10.1371/journal.pone.0019338

Masuda-Suzukake, M., Nonaka, T., Hosokawa, M., Oikawa, T., Arai, T., Akiyama, H., et al. (2013). Prion-like spreading of pathological α-synuclein in brain. *Brain* 136, 1128–1138. doi: 10.1093/brain/awt037

Mavroeidi, P., Arvanitaki, F., Karakitsou, A. K., Vetsi, M., Kloukina, I., Zweckstetter, M., et al. (2019). Endogenous oligodendroglial α-synuclein and TPPP/p25α orchestrate α-synuclein pathology in experimental multiple system atrophy models. *Acta Neuropathol.* 138, 415–441. doi: 10.1007/s00401-019-02068-y

May, V. E., Ettle, B., Poehler, A. M., Nuber, S., Ubhi, K., Rockenstein, E., et al. (2014). α-Synuclein impairs oligodendrocyte progenitor maturation in multiple system atrophy. *Neurobiol. Aging* 35, 2357–2368. doi: 10.1016/j.neurobiolaging.2014.02.028

Mazzulli, J. R., Zunke, F., Isacson, O., Studer, L., and Krainc, D. (2016). α-Synuclein-induced lysosomal dysfunction occurs through disruptions in protein trafficking in human midbrain synucleinopathy models. *Proc. Natl. Acad. Sci. U S A* 113, 1931–1936. doi: 10.1073/pnas.1520335113

McGeer, P. L., Itagaki, S., Boyes, B. E., and McGeer, E. G. (1988a). Reactive microglia are positive for HLA-DR in the substantia nigra of Parkinson's and Alzheimer's disease brains. *Neurology* 38, 1285–1291. doi: 10.1212/wnl.38.8.1285

McGeer, P. L., Itagaki, S., and McGeer, E. G. (1988b). Expression of the histocompatibility glycoprotein HLA-DR in neurological disease. *Acta Neuropathol.* 76, 550–557. doi: 10.1007/bf00689592

Meade, R. M., Fairlie, D. P., and Mason, J. M. (2019). α-synuclein structure and Parkinson's disease—lessons and emerging principles. *Mol. Neurodegener.* 14:29. doi: 10.1186/s13024-019-0329-1

Mendez, I., Vinuela, A., Astradsson, A., Mukhida, K., Hallett, P., Robertson, H., et al. (2008). Dopamine neurons implanted into people with Parkinson's disease survive without pathology for 14 years. *Nat. Med.* 14, 507–509. doi: 10.1038/nm1752

Miklossy, J., Doudet, D. D., Schwab, C., Yu, S., Mcgeer, E. G., and Mcgeer, P. L. (2006). Role of ICAM-1 in persisting inflammation in Parkinson disease and MPTP monkeys. *Exp. Neurol.* 197, 275–283. doi: 10.1016/j.expneurol.2005.10.034

Milanese, C., Cerri, S., Ulusoy, A., Gornati, S. V., Plat, A., Gabriels, S., et al. (2018). Activation of the DNA damage response *in vivo* in synucleinopathy models of Parkinson's disease. *Cell Death Dis.* 9:818. doi: 10.1038/s41419-018-0848-7

Mor, D. E., Tsika, E., Mazzulli, J. R., Gould, N. S., Kim, H., Daniels, M. J., et al. (2017). Dopamine induces soluble α-synuclein oligomers and nigrostriatal degeneration. *Nat. Neurosci.* 20, 1560–1568. doi: 10.1038/nn.4641

Mori, F., Inenaga, C., Yoshimoto, M., Umezu, H., Tanaka, R., Takahashi, H., et al. (2002). α-synuclein immunoreactivity in normal and neoplastic Schwann cells. *Acta Neuropathol.* 103, 145–151. doi: 10.1007/s004010100443

Nugent, E., Kaminski, C. F., and Kaminski Schierle, G. S. (2017). Super-resolution imaging of α-synuclein polymorphisms and their potential role in neurodegeneration. *Integr. Biol.* 9, 206–210. doi: 10.1039/c6ib00206d

Olanow, C. W., Perl, D. P., Demartino, G. N., and Mcnaught, K. S. (2004). Lewy-body formation is an aggresome-related process: a hypothesis. *Lancet Neurol.* 3, 496–503. doi: 10.1016/s1474-4422(04)00827-0

Olanow, C. W., Savolainen, M., Chu, Y., Halliday, G. M., and Kordower, J. H. (2019). Temporal evolution of microglia and α-synuclein accumulation following foetal grafting in Parkinson's disease. *Brain* 142, 1690–1700. doi: 10.1093/brain/awz104

Ono, K., Takahashi, R., Ikeda, T., and Yamada, M. (2012). Cross-seeding effects of amyloid β-protein and α-synuclein. *J. Neurochem.* 122, 883–890. doi: 10.1111/j.1471-4159.2012.07847.x

Orimo, S., Uchihara, T., Nakamura, A., Mori, F., Kakita, A., Wakabayashi, K., et al. (2008). Axonal α-synuclein aggregates herald centripetal degeneration of cardiac sympathetic nerve in Parkinson's disease. *Brain* 131, 642–650. doi: 10.1093/brain/awm302

Orme, T., Guerreiro, R., and Bras, J. (2018). The genetics of dementia with Lewy bodies: current understanding and future directions. *Curr. Neurol. Neurosci. Rep.* 18:67. doi: 10.1007/s11910-018-0874-y

Outeiro, T. F., Koss, D. J., Erskine, D., Walker, L., Kurzawa-Akanbi, M., Burn, D., et al. (2019). Dementia with Lewy bodies: an update and outlook. *Mol. Neurodegener.* 14:5. doi: 10.1186/s13024-019-0306-8

Ozawa, T., Paviour, D., Quinn, N. P., Josephs, K. A., Sangha, H., Kilford, L., et al. (2004). The spectrum of pathological involvement of the striatonigral and olivopontocerebellar systems in multiple system atrophy: clinicopathological correlations. *Brain* 127, 2657–2671. doi: 10.1093/brain/awh303

Paiva, I., Pinho, R., Pavlou, M. A., Hennion, M., Wales, P., Schutz, A. L., et al. (2017). Sodium butyrate rescues dopaminergic cells from α-synuclein-

induced transcriptional deregulation and DNA damage. *Hum. Mol. Genet.* 26, 2231–2246. doi: 10.1093/hmg/ddx114

Parihar, M. S., Parihar, A., Fujita, M., Hashimoto, M., and Ghafourifar, P. (2008). Mitochondrial association of α-synuclein causes oxidative stress. *Cell Mol. Life Sci.* 65, 1272–1284. doi: 10.1007/s00018-008-7589-1

Park, H. J., Oh, S. H., Kim, H. N., Jung, Y. J., and Lee, P. H. (2016). Mesenchymal stem cells enhance α-synuclein clearance *via* M2 microglia polarization in experimental and human parkinsonian disorder. *Acta Neuropathol.* 132, 685–701. doi: 10.1007/s00401-016-1605-6

Park, J. H., Burgess, J. D., Faroqi, A. H., Demeo, N. N., Fiesel, F. C., Springer, W., et al. (2020). α-synuclein-induced mitochondrial dysfunction is mediated *via* a sirtuin 3-dependent pathway. *Mol. Neurodegener.* 15:5. doi: 10.1101/357624

Paumier, K. L., Luk, K. C., Manfredsson, F. P., Kanaan, N. M., Lipton, J. W., Collier, T. J., et al. (2015). Intrastriatal injection of pre-formed mouse α-synuclein fibrils into rats triggers α-synuclein pathology and bilateral nigrostriatal degeneration. *Neurobiol. Dis.* 82, 185–199. doi: 10.1016/j.nbd.2015.06.003

Peelaerts, W., Bousset, L., Van Der Perren, A., Moskalyuk, A., Pulizzi, R., Giugliano, M., et al. (2015). α-Synuclein strains cause distinct synucleinopathies after local and systemic administration. *Nature* 522, 340–344. doi: 10.1038/nature14547

Peng, C., Gathagan, R. J., Covell, D. J., Medellin, C., Stieber, A., Robinson, J. L., et al. (2018a). Cellular milieu imparts distinct pathological α-synuclein strains in alpha-synucleinopathies. *Nature* 557, 558–563. doi: 10.1038/s41586-018-0104-4

Peng, C., Gathagan, R. J., and Lee, V. M. (2018b). Distinct α-Synuclein strains and implications for heterogeneity among alpha-Synucleinopathies. *Neurobiol. Dis.* 109, 209–218. doi: 10.1016/j.nbd.2017.07.018

Perez, R. G., and Hastings, T. G. (2004). Could a loss of α-synuclein function put dopaminergic neurons at risk? *J. Neurochem.* 89, 1318–1324. doi: 10.1111/j.1471-4159.2004.02423.x

Perrino, G., Wilson, C., Santorelli, M., and Di Bernardo, D. (2019). Quantitative characterization of α-synuclein aggregation in living cells through automated microfluidics feedback control. *Cell Rep.* 27, 916.e5–927.e5. doi: 10.1016/j.celrep.2019.03.081

Petrucelli, L., O'Farrell, C., Lockhart, P. J., Baptista, M., Kehoe, K., Vink, L., et al. (2002). Parkin protects against the toxicity associated with mutant α-synuclein: proteasome dysfunction selectively affects catecholaminergic neurons. *Neuron* 36, 1007–1019. doi: 10.1016/s0896-6273(02)01125-x

Phan, J. A., Stokholm, K., Zareba-Paslawska, J., Jakobsen, S., Vang, K., Gjedde, A., et al. (2017). Early synaptic dysfunction induced by α-synuclein in a rat model of Parkinson's disease. *Sci. Rep.* 7:6363. doi: 10.1038/s41598-017-06724-9

Pinho, R., Paiva, I., Jercic, K. G., Fonseca-Ornelas, L., Gerhardt, E., Fahlbusch, C., et al. (2019). Nuclear localization and phosphorylation modulate pathological effects of α-synuclein. *Hum. Mol. Genet.* 28, 31–50. doi: 10.1093/hmg/ddy326

Polymeropoulos, M. H., Higgins, J. J., Golbe, L. I., Johnson, W. G., Ide, S. E., Di Iorio, G., et al. (1996). Mapping of a gene for Parkinson's disease to chromosome 4q21–q23. *Science* 274, 1197–1199. doi: 10.1126/science.274.5290.1197

Polymeropoulos, M. H., Lavedan, C., Leroy, E., Ide, S. E., Dehejia, A., Dutra, A., et al. (1997). Mutation in the α-synuclein gene identified in families with Parkinson's disease. *Science* 276, 2045–2047. doi: 10.1126/science.276.5321.2045

Post, M. R., Lieberman, O. J., and Mosharov, E. V. (2018). Can interactions between α-synuclein, dopamine and calcium explain selective neurodegeneration in Parkinson's disease? *Front. Neurosci.* 12:161. doi: 10.3389/fnins.2018.00161

Price, D. L., Koike, M. A., Khan, A., Wrasidlo, W., Rockenstein, E., Masliah, E., et al. (2018). The small molecule α-synuclein misfolding inhibitor, NPT200–11, produces multiple benefits in an animal model of Parkinson's disease. *Sci. Rep.* 8:16165. doi: 10.1038/s41598-018-34490-9

Pringsheim, T., Jette, N., Frolkis, A., and Steeves, T. D. (2014). The prevalence of Parkinson's disease: a systematic review and meta-analysis. *Mov. Disord.* 29, 1583–1590. doi: 10.1002/mds.25945

Prusiner, S. B. (1982). Novel proteinaceous infectious particles cause scrapie. *Science* 216, 136–144. doi: 10.1126/science.6801762

Prusiner, S. B. (1998). Prions. *Proc. Natl. Acad. Sci. U S A* 95, 13363–13383. doi: 10.1073/pnas.95.23.13363

Radford, R., Rcom-H'cheo-Gauthier, A., Wong, M. B., Eaton, E. D., Quilty, M., Blizzard, C., et al. (2015). The degree of astrocyte activation in multiple system atrophy is inversely proportional to the distance to α-synuclein inclusions. *Mol. Cell. Neurosci.* 65, 68–81. doi: 10.1016/j.mcn.2015.02.015

Rajput, A. H., Ferguson, L. W., Robinson, C. A., Guella, I., Farrer, M. J., and Rajput, A. (2016). Conjugal parkinsonism—clinical, pathology and genetic study. No evidence of person-to-person transmission. *Parkinsonism Relat. Disord.* 31, 87–90. doi: 10.1016/j.parkreldis.2016.07.011

Recasens, A., Carballo-Carbajal, I., Parent, A., Bove, J., Gelpi, E., Tolosa, E., et al. (2018). Lack of pathogenic potential of peripheral α-synuclein aggregates from Parkinson's disease patients. *Acta Neuropathol. Commun.* 6:8. doi: 10.1186/s40478-018-0509-1

Recasens, A., Dehay, B., Bove, J., Carballo-Carbajal, I., Dovero, S., Perez-Villalba, A., et al. (2014). Lewy body extracts from Parkinson disease brains trigger α-synuclein pathology and neurodegeneration in mice and monkeys. *Ann. Neurol.* 75, 351–362. doi: 10.1002/ana.24066

Reeve, A. K., Ludtmann, M. H., Angelova, P. R., Simcox, E. M., Horrocks, M. H., Klenerman, D., et al. (2015). Aggregated α-synuclein and complex I deficiency: exploration of their relationship in differentiated neurons. *Cell Death Dis.* 6:e1820. doi: 10.1038/cddis.2015.166

Rey, N. L., Bousset, L., George, S., Madaj, Z., Meyerdirk, L., Schulz, E., et al. (2019). α-Synuclein conformational strains spread, seed and target neuronal cells differentially after injection into the olfactory bulb. *Acta Neuropathol. Commun.* 7:221. doi: 10.1186/s40478-019-0859-3

Rey, N. L., George, S., Steiner, J. A., Madaj, Z., Luk, K. C., Trojanowski, J. Q., et al. (2018). Spread of aggregates after olfactory bulb injection of α-synuclein fibrils is associated with early neuronal loss and is reduced long term. *Acta Neuropathol.* 135, 65–83. doi: 10.1007/s00401-017-1792-9

Reyes, J. F., Rey, N. L., Bousset, L., Melki, R., Brundin, P., and Angot, E. (2014). α-synuclein transfers from neurons to oligodendrocytes. *Glia* 62, 387–398. doi: 10.1002/glia.22611

Rott, R., Szargel, R., Shani, V., Hamza, H., Savyon, M., Abd Elghani, F., et al. (2017). SUMOylation and ubiquitination reciprocally regulate α-synuclein degradation and pathological aggregation. *Proc. Natl. Acad. Sci. U S A* 114, 13176–13181. doi: 10.1073/pnas.1704351114

Sampson, T. R., Challis, C., Jain, N., Moiseyenko, A., Ladinsky, M. S., Shastri, G. G., et al. (2020). A gut bacterial amyloid promotes α-synuclein aggregation and motor impairment in mice. *eLife* 9:e53111. doi: 10.7554/eLife.53111

Sampson, T. R., Debelius, J. W., Thron, T., Janssen, S., Shastri, G. G., Ilhan, Z. E., et al. (2016). Gut microbiota regulate motor deficits and neuroinflammation in a model of Parkinson's disease. *Cell* 167, 1469.e12–1480.e12. doi: 10.1016/j.cell.2016.11.018

Sarkar, S., Dammer, E. B., Malovic, E., Olsen, A. L., Raza, S. A., Gao, T., et al. (2020). Molecular signatures of neuroinflammation induced by α-synuclein aggregates in microglial cells. *Front. Immunol.* 11:33. doi: 10.3389/fimmu.2020.00033

Schafferer, S., Khurana, R., Refolo, V., Venezia, S., Sturm, E., Piatti, P., et al. (2016). Changes in the miRNA-mRNA regulatory network precede motor symptoms in a mouse model of multiple system atrophy: clinical implications. *PLoS One* 11:e0150705. doi: 10.1371/journal.pone.0150705

Schaser, A. J., Osterberg, V. R., Dent, S. E., Stackhouse, T. L., Wakeham, C. M., Boutros, S. W., et al. (2019). α-synuclein is a DNA binding protein that modulates DNA repair with implications for Lewy body disorders. *Sci. Rep.* 9:10919. doi: 10.1038/s41598-019-47227-z

Schweighauser, M., Bacioglu, M., Fritschi, S. K., Shimshek, D. R., Kahle, P. J., Eisele, Y. S., et al. (2015). Formaldehyde-fixed brain tissue from spontaneously ill α-synuclein transgenic mice induces fatal alpha-synucleinopathy in transgenic hosts. *Acta Neuropathol.* 129, 157–159. doi: 10.1007/s00401-014-1360-5

Schweighauser, M., Shi, Y., Tarutani, A., Kametani, F., Murzin, A. G., Ghetti, B., et al. (2020). Structures of α-synuclein filaments from multiple system atrophy. *Nature* doi: 10.1038/s41586-020-2317-6 [Epub ahead of print].

Shahmoradian, S. H., Lewis, A. J., Genoud, C., Hench, J., Moors, T. E., Navarro, P. P., et al. (2019). Lewy pathology in Parkinson's disease consists of crowded organelles and lipid membranes. *Nat. Neurosci.* 22, 1099–1109. doi: 10.1038/s41593-019-0423-2

Shahnawaz, M., Mukherjee, A., Pritzkow, S., Mendez, N., Rabadia, P., Liu, X., et al. (2020). Discriminating α-synuclein strains in Parkinson's disease and multiple system atrophy. *Nature* 578, 273–277. doi: 10.1038/s41586-020-1984-7

Shannon, K. M., Keshavarzian, A., Mutlu, E., Dodiya, H. B., Daian, D., Jaglin, J. A., et al. (2012). α-synuclein in colonic submucosa in early untreated Parkinson's disease. *Mov. Disord.* 27, 709–715. doi: 10.3410/f.717698045.793456802

Shrivastava, A. N., Bousset, L., Renner, M., Redeker, V., Savistchenko, J., Triller, A., et al. (2020). Differential membrane binding and seeding of distinct α-synuclein fibrillar polymorphs. *Biophys. J.* 118, 1301–1320. doi: 10.1016/j.bpj.2020.01.022

Shrivastava, A. N., Redeker, V., Fritz, N., Pieri, L., Almeida, L. G., Spolidoro, M., et al. (2015). α-synuclein assemblies sequester neuronal α3-Na^+/K^+-ATPase and impair Na+ gradient. *EMBO J.* 34, 2408–2423. doi: 10.15252/embj.201591397

Sian-Hulsmann, J., Monoranu, C., Strobel, S., and Riederer, P. (2015). Lewy bodies: a spectator or salient killer? *CNS Neurol. Disord. Drug Targets* 14, 947–955. doi: 10.2174/1871527314666150317225659

Sidhu, A., Wersinger, C., and Vernier, P. (2004). Does α-synuclein modulate dopaminergic synaptic content and tone at the synapse? *FASEB J.* 18, 637–647. doi: 10.1096/fj.03-1112rev

Singleton, A. B., Farrer, M., Johnson, J., Singleton, A., Hague, S., Kachergus, J., et al. (2003). α-Synuclein locus triplication causes Parkinson's disease. *Science* 302:841. doi: 10.1126/science.1090278

Smith, W. W., Jiang, H., Pei, Z., Tanaka, Y., Morita, H., Sawa, A., et al. (2005). Endoplasmic reticulum stress and mitochondrial cell death pathways mediate A53T mutant α-synuclein-induced toxicity. *Hum. Mol. Genet.* 14, 3801–3811. doi: 10.1093/hmg/ddi396

Snyder, H., Mensah, K., Theisler, C., Lee, J., Matouschek, A., and Wolozin, B. (2003). Aggregated and monomeric α-synuclein bind to the S6' proteasomal protein and inhibit proteasomal function. *J. Biol. Chem.* 278, 11753–11759. doi: 10.1074/jbc.m208641200

Sommer, A., Marxreiter, F., Krach, F., Fadler, T., Grosch, J., Maroni, M., et al. (2018). Th17 lymphocytes induce neuronal cell death in a human iPSC-based model of Parkinson's disease. *Cell Stem Cell* 23, 123.e6–131.e6. doi: 10.1016/j.stem.2018.06.015

Song, Y. J., Halliday, G. M., Holton, J. L., Lashley, T., O'sullivan, S. S., Mccann, H., et al. (2009). Degeneration in different parkinsonian syndromes relates to astrocyte type and astrocyte protein expression. *J. Neuropathol. Exp. Neurol.* 68, 1073–1083. doi: 10.1097/nen.0b013e3181b66f1b

Song, Y. J., Lundvig, D. M., Huang, Y., Gai, W. P., Blumbergs, P. C., Hojrup, P., et al. (2007). p25α relocalizes in oligodendroglia from myelin to cytoplasmic inclusions in multiple system atrophy. *Am. J. Pathol.* 171, 1291–1303. doi: 10.1016/s1353-8020(08)70483-8

Sorrentino, Z. A., Giasson, B. I., and Chakrabarty, P. (2019). α-Synuclein and astrocytes: tracing the pathways from homeostasis to neurodegeneration in Lewy body disease. *Acta Neuropathol.* 138, 1–21. doi: 10.1007/s00401-019-01977-2

Spillantini, M. G., Crowther, R. A., Jakes, R., Hasegawa, M., and Goedert, M. (1998). α-Synuclein in filamentous inclusions of Lewy bodies from Parkinson's disease and dementia with Lewy bodies. *Proc. Natl. Acad. Sci. U S A* 95, 6469–6473. doi: 10.1073/pnas.95.11.6469

Spillantini, M. G., Schmidt, M. L., Lee, V. M., Trojanowski, J. Q., Jakes, R., and Goedert, M. (1997). α-synuclein in Lewy bodies. *Nature* 388, 839–840. doi: 10.1038/42166

Stefanis, L., Larsen, K. E., Rideout, H. J., Sulzer, D., and Greene, L. A. (2001). Expression of A53T mutant but not wild-type α-synuclein in PC12 cells induces alterations of the ubiquitin-dependent degradation system, loss of dopamine release and autophagic cell death. *J. Neurosci.* 21, 9549–9560. doi: 10.1523/jneurosci.21-24-09549.2001

Stefanova, N., Reindl, M., Neumann, M., Kahle, P. J., Poewe, W., and Wenning, G. K. (2007). Microglial activation mediates neurodegeneration related to oligodendroglial alpha-synucleinopathy: implications for multiple system atrophy. *Mov. Disord.* 22, 2196–2203. doi: 10.1002/mds.21671

Stokholm, M. G., Iranzo, A., Ostergaard, K., Serradell, M., Otto, M., Svendsen, K. B., et al. (2017). Assessment of neuroinflammation in patients with idiopathic rapid-eye-movement sleep behaviour disorder: a case-control study. *Lancet Neurol.* 16, 789–796. doi: 10.1016/s1474-4422(17)30173-4

Su, X., Maguire-Zeiss, K. A., Giuliano, R., Prifti, L., Venkatesh, K., and Federoff, H. J. (2008). Synuclein activates microglia in a model of Parkinson's disease. *Neurobiol. Aging* 29, 1690–1701. doi: 10.1016/j.neurobiolaging.2007.04.006

Sulzer, D., Alcalay, R. N., Garretti, F., Cote, L., Kanter, E., Agin-Liebes, J., et al. (2017). T cells from patients with Parkinson's disease recognize α-synuclein peptides. *Nature* 546, 656–661. doi: 10.1038/nature22815

Surendranathan, A., Su, L., Mak, E., Passamonti, L., Hong, Y. T., Arnold, R., et al. (2018). Early microglial activation and peripheral inflammation in dementia with Lewy bodies. *Brain* 141, 3415–3427. doi: 10.1093/brain/awy265

Surguchev, A. A., and Surguchov, A. (2017). Synucleins and gene expression: ramblers in a crowd or cops regulating traffic? *Front. Mol. Neurosci.* 10:224. doi: 10.3389/fnmol.2017.00224

Surmeier, D. J., Obeso, J. A., and Halliday, G. M. (2017). Parkinson's disease is not simply a prion disorder. *J. Neurosci.* 37, 9799–9807. doi: 10.1523/jneurosci.1787-16.2017

Svensson, E., Horváth-Puhó, E., Thomsen, R. W., Djurhuus, J. C., Pedersen, L., Borghammer, P., et al. (2015). Vagotomy and subsequent risk of Parkinson's disease. *Ann. Neurol.* 78, 522–529. doi: 10.1002/ana.24448

Tanaka, Y., Engelender, S., Igarashi, S., Rao, R. K., Wanner, T., Tanzi, R. E., et al. (2001). Inducible expression of mutant α-synuclein decreases proteasome activity and increases sensitivity to mitochondria-dependent apoptosis. *Hum. Mol. Genet.* 10, 919–926. doi: 10.1093/hmg/10.9.919

Tapias, V., Hu, X., Luk, K. C., Sanders, L. H., Lee, V. M., and Greenamyre, J. T. (2017). Synthetic α-synuclein fibrils cause mitochondrial impairment and selective dopamine neurodegeneration in part *via* iNOS-mediated nitric oxide production. *Cell. Mol. Life Sci.* 74, 2851–2874. doi: 10.1007/s00018-017-2541-x

Thaisetthawatkul, P. (2016). Pure autonomic failure. *Curr. Neurol. Neurosci. Rep.* 16:74. doi: 10.1007/s11910-016-0673-2

Theillet, F. X., Binolfi, A., Bekei, B., Martorana, A., Rose, H. M., Stuiver, M., et al. (2016). Structural disorder of monomeric α-synuclein persists in mammalian cells. *Nature* 530, 45–50. doi: 10.1038/nature16531

Theodore, S., Cao, S., Mclean, P. J., and Standaert, D. G. (2008). Targeted overexpression of human α-synuclein triggers microglial activation and an adaptive immune response in a mouse model of Parkinson disease. *J. Neuropathol. Exp. Neurol.* 67, 1149–1158. doi: 10.1097/nen.0b013e31818e5e99

Tolosa, E., Vila, M., Klein, C., and Rascol, O. (2020). LRRK2 in Parkinson disease: challenges of clinical trials. *Nat. Rev. Neurol.* 16, 97–107. doi: 10.1038/s41582-019-0301-2

Tosatto, L., Andrighetti, A. O., Plotegher, N., Antonini, V., Tessari, I., Ricci, L., et al. (2012). α-synuclein pore forming activity upon membrane association. *Biochim. Biophys. Acta* 1818, 2876–2883. doi: 10.1016/j.bbamem.2012.07.007

Tozzi, A., De Iure, A., Bagetta, V., Tantucci, M., Durante, V., Quiroga-Varela, A., et al. (2016). α-synuclein produces early behavioral alterations *via* striatal cholinergic synaptic dysfunction by interacting with GluN2D N-methyl-D-aspartate receptor subunit. *Biol. Psychiatry* 79, 402–414. doi: 10.1016/j.biopsych.2015.08.013

Tremblay, M. E., Cookson, M. R., and Civiero, L. (2019). Glial phagocytic clearance in Parkinson's disease. *Mol. Neurodegener.* 14:16. doi: 10.1186/s13024-019-0314-8

Tsigelny, I. F., Sharikov, Y., Wrasidlo, W., Gonzalez, T., Desplats, P. A., Crews, L., et al. (2012). Role of α-synuclein penetration into the membrane in the mechanisms of oligomer pore formation. *FEBS J.* 279, 1000–1013. doi: 10.1111/j.1742-4658.2012.08489.x

Tysnes, O. B., Kenborg, L., Herlofson, K., Steding-Jessen, M., Horn, A., Olsen, J. H., et al. (2015). Does vagotomy reduce the risk of Parkinson's disease? *Ann. Neurol.* 78, 1011–1012. doi: 10.1097/01.nt.0000475926.46736.74

Ubhi, K., Rockenstein, E., Mante, M., Patrick, C., Adame, A., Thukral, M., et al. (2008). Rifampicin reduces α-synuclein in a transgenic mouse model of multiple system atrophy. *Neuroreport* 19, 1271–1276. doi: 10.1097/wnr.0b013e32830b3661

Ulusoy, A., Rusconi, R., Perez-Revuelta, B. I., Musgrove, R. E., Helwig, M., Winzen-Reichert, B., et al. (2013). Caudo-rostral brain spreading of α-

synuclein through vagal connections. *EMBO Mol. Med.* 5, 1119–1127. doi: 10.1002/emmm.201302475

Uversky, V. N., Li, J., and Fink, A. L. (2001). Metal-triggered structural transformations, aggregation and fibrillation of human α-synuclein. A possible molecular NK between Parkinson's disease and heavy metal exposure. *J. Biol. Chem.* 276, 44284–44296. doi: 10.1074/jbc.m105343200

Van Der Perren, A., Gelders, G., Fenyi, A., Bousset, L., Brito, F., Peelaerts, W., et al. (2020). The structural differences between patient-derived α-synuclein strains dictate characteristics of Parkinson's disease, multiple system atrophy and dementia with Lewy bodies. *Acta Neuropathol.* 139, 977–1000. doi: 10.1007/s00401-020-02157-3

Varkey, J., Isas, J. M., Mizuno, N., Jensen, M. B., Bhatia, V. K., Jao, C. C., et al. (2010). Membrane curvature induction and tubulation are common features of synucleins and apolipoproteins. *J. Biol. Chem.* 285, 32486–32493. doi: 10.1074/jbc.m110.139576

Vasquez, V., Mitra, J., Hegde, P. M., Pandey, A., Sengupta, S., Mitra, S., et al. (2017). Chromatin-bound oxidized α-synuclein causes strand breaks in neuronal genomes in in vitro models of Parkinson's disease. *J. Alzheimers Dis.* 60, S133–S150. doi: 10.3233/jad-170342

Venezia, S., Refolo, V., Polissidis, A., Stefanis, L., Wenning, G. K., and Stefanova, N. (2017). Toll-like receptor 4 stimulation with monophosphoryl lipid A ameliorates motor deficits and nigral neurodegeneration triggered by extraneuronal alpha-synucleinopathy. *Mol. Neurodegener.* 12:52. doi: 10.1186/s13024-017-0195-7

Vicario, M., Cieri, D., Brini, M., and Cali, T. (2018). The close encounter between α-synuclein and mitochondria. *Front. Neurosci.* 12:388. doi: 10.3389/fnins.2018.00388

Vicente Miranda, H., Cassio, R., Correia-Guedes, L., Gomes, M. A., Chegao, A., Miranda, E., et al. (2017). Posttranslational modifications of blood-derived α-synuclein as biochemical markers for Parkinson's disease. *Sci. Rep.* 7:13713. doi: 10.1038/s41598-017-14175-5

Volpicelli-Daley, L. A. (2017). Effects of α-synuclein on axonal transport. *Neurobiol. Dis.* 105, 321–327. doi: 10.1016/j.nbd.2016.12.008

Volpicelli-Daley, L. A., Luk, K. C., Patel, T. P., Tanik, S. A., Riddle, D. M., Stieber, A., et al. (2011). Exogenous α-synuclein fibrils induce Lewy body pathology leading to synaptic dysfunction and neuron death. *Neuron* 72, 57–71. doi: 10.1016/j.neuron.2011.08.033

Wang, W., Nguyen, L. T., Burlak, C., Chegini, F., Guo, F., Chataway, T., et al. (2016). Caspase-1 causes truncation and aggregation of the Parkinson's disease-associated protein α-synuclein. *Proc. Natl. Acad. Sci. U S A* 113, 9587–9592. doi: 10.1073/pnas.1610099113

Wang, W., Perovic, I., Chittuluru, J., Kaganovich, A., Nguyen, L. T., Liao, J., et al. (2011). A soluble α-synuclein construct forms a dynamic tetramer. *Proc. Natl. Acad. Sci. U S A* 108, 17797–17802. doi: 10.1073/pnas.1113260108

Wang, X., Becker, K., Levine, N., Zhang, M., Lieberman, A. P., Moore, D. J., et al. (2019). Pathogenic α-synuclein aggregates preferentially bind to mitochondria and affect cellular respiration. *Acta Neuropathol. Commun.* 7:41. doi: 10.1186/s40478-019-0696-4

Wang, X. J., Ma, M. M., Zhou, L. B., Jiang, X. Y., Hao, M. M., Teng, R. K. F., et al. (2020). Autonomic ganglionic injection of α-synuclein fibrils as a model of pure autonomic failure alpha-synucleinopathy. *Nat. Commun.* 11:934. doi: 10.1038/s41467-019-14189-9

Watts, J. C. (2019). Calling α-synuclein a prion is scientifically justifiable. *Acta Neuropathol.* 138, 505–508. doi: 10.1007/s00401-019-02058-0

Wegrzynowicz, M., Bar-On, D., Calo, L., Anichtchik, O., Iovino, M., Xia, J., et al. (2019). Depopulation of dense α-synuclein aggregates is associated with rescue of dopamine neuron dysfunction and death in a new Parkinson's disease model. *Acta Neuropathol.* 138, 575–595. doi: 10.1007/s00401-019-02023-x

Wenning, G., Trojanowski, J. Q., Kaufmann, H., Wisniewski, T., Rocca, W. A., and Low, P. A. (2018). Is multiple system atrophy an infectious disease? *Ann. Neurol.* 83, 10–12. doi: 10.1002/ana.25132

Woerman, A. L., Kazmi, S. A., Patel, S., Freyman, Y., Oehler, A., Aoyagi, A., et al. (2018). MSA prions exhibit remarkable stability and resistance to inactivation. *Acta Neuropathol.* 135, 49–63. doi: 10.1007/s00401-017-1762-2

Wu, Q., Takano, H., Riddle, D. M., Trojanowski, J. Q., Coulter, D. A., and Lee, V. M. (2019). α-synuclein (αSyn) preformed fibrils induce endogenous alphasyn aggregation, compromise synaptic activity and enhance synapse loss in cultured excitatory hippocampal neurons. *J. Neurosci.* 39, 5080–5094. doi: 10.1523/jneurosci.0060-19.2019

Yamasaki, T. R., Holmes, B. B., Furman, J. L., Dhavale, D. D., Su, B. W., Song, E. S., et al. (2019). Parkinson's disease and multiple system atrophy have distinct α-synuclein seed characteristics. *J. Biol. Chem.* 294, 1045–1058. doi: 10.1074/jbc.RA118.004471

Yu, S., Uéda, K., and Chan, P. (2005). α-synuclein and dopamine metabolism. *Mol. Neurobiol.* 31, 243–254. doi: 10.1385/MN:31:1-3:243

Zafar, F., Valappil, R. A., Kim, S., Johansen, K. K., Chang, A. L. S., Tetrud, J. W., et al. (2018). Genetic fine-mapping of the Iowan *SNCA* gene triplication in a patient with Parkinson's disease. *NPJ Parkinsons Dis.* 4:18. doi: 10.1038/s41531-018-0054-4

Zhang, J., Li, X., and Li, J. D. (2019). The roles of post-translational modifications on α-synuclein in the pathogenesis of Parkinson's diseases. *Front. Neurosci.* 13:381. doi: 10.3389/fnins.2019.00381

Zhang, W., Wang, T., Pei, Z., Miller, D. S., Wu, X., Block, M. L., et al. (2005). Aggregated α-synuclein activates microglia: a process leading to disease progression in Parkinson's disease. *FASEB J.* 19, 533–542. doi: 10.1096/fj.04-2751com

Zhao, H. T., John, N., Delic, V., Ikeda-Lee, K., Kim, A., Weihofen, A., et al. (2017). LRRK2 antisense oligonucleotides ameliorate α-synuclein inclusion formation in a Parkinson's disease mouse model. *Mol. Ther. Nucleic Acids* 8, 508–519. doi: 10.1016/j.omtn.2017.08.002

Zheng, B., Liao, Z., Locascio, J. J., Lesniak, K. A., Roderick, S. S., Watt, M. L., et al. (2010). PGC-1α, a potential therapeutic target for early intervention in Parkinson's disease. *Sci. Transl. Med.* 2:52ra73. doi: 10.1126/scitranslmed.3001059

Conflict of Interest: The authors declare that the research was conducted in the absence of any commercial or financial relationships that could be construed as a potential conflict of interest.

Copyright © 2020 Heras-Garvin and Stefanova. This is an open-access article distributed under the terms of the Creative Commons Attribution License (CC BY). The use, distribution or reproduction in other forums is permitted, provided the original author(s) and the copyright owner(s) are credited and that the original publication in this journal is cited, in accordance with accepted academic practice. No use, distribution or reproduction is permitted which does not comply with these terms.

frontiers in Synaptic Neuroscience

ORIGINAL RESEARCH
published: 06 October 2020
doi: 10.3389/fnsyn.2020.591129

Two Distinct Populations of α1α6-Containing GABAA-Receptors in Rat Cerebellum

Petra Scholze, Michael Pökl, Severin Längle, Friederike Steudle, Jure Fabjan and Margot Ernst*

Department of Pathobiology of the Nervous System, Center for Brain Research, Medical University of Vienna, Vienna, Austria

GABAA receptors are pentameric GABA-gated chloride channels. The existence of 19 different subunits (six α, three β, three γ, δ, ε, θ, π, and three ρ) in mammalian systems gives rise to an enormous theoretical diversity of GABAA receptor subtypes with distinct subunit composition and unique pharmacological properties. These receptors are already now the drug targets of several clinically used compounds, such as benzodiazepines, anesthetics, and many more. There is a constant quest to identify novel molecules and possible future drug targets: Currently, α6-containing GABAA receptors are being discussed in the context of treating sensorimotor gating deficits in neuropsychiatric disorders, such as tic disorders and schizophrenia. Therefore, we aim to learn more about α6-containing GABAA receptors. They are mostly expressed in the cerebellar granule cell layer, where they form the following subtypes: α6βxγ2, α1α6βxγ2, α6βxδ, and α1α6βxδ. In former studies, α1α6βxγ2-containing GABAA receptors were considered a single receptor population. In the current study, we investigate the possibility, that this population can consist of two subgroups with alternative arrangements depending if α1 neighbors γ2 (forming a "diazepam-sensitive" receptor), or if α6 neighbors γ2 (forming a "diazepam-insensitive" receptor) and aimed to prove the existence of both subtypes in native tissue. We performed immunoprecipitation experiments on rat cerebellar lysates using α1- or α6 subunit-specific antibodies followed by radioligand binding assays with either ^{3}H-flunitrazepam or ^{3}H-Ro 15-4513. Indeed, we were able to prove the existence of two distinct populations of α1α6-containing GABAA-receptors and could quantify the different receptor populations: α1βxγ2 receptors constitute approximately 60% of all γ2-containing receptors in the rat cerebellum, α6βxγ2 about 20%, and both isoforms of α1α6βxγ2 9–15% each. The simple classification of GABAA-receptors into αx-containing subtypes seems not to reflect the complexity of nature; those receptors are more diverse than previously thought.

Keywords: cerebellum, GABAA-receptor, receptor composition, radioligand binding, immunoprecipitation

OPEN ACCESS

Edited by:
Joerg Striessnig, University of Innsbruck, Austria

Reviewed by:
Christoph Schwarzer, Innsbruck Medical University, Austria
Nathan Absalom, The University of Sydney, Australia

****Correspondence:***
Petra Scholze
petra.scholze@meduniwien.ac.at

Received: *03 August 2020*
Accepted: *09 September 2020*
Published: *06 October 2020*

Citation:
Scholze P, Pökl M, Längle S, Steudle F, Fabjan J and Ernst M (2020) Two Distinct Populations of α1α6-Containing GABAA-Receptors in Rat Cerebellum. Front. Synaptic Neurosci. 12:591129. doi: 10.3389/fnsyn.2020.591129

INTRODUCTION

GABAA receptors are ligand-gated chloride ion channels assembled as pentamers of subunits coded by one out of 19 different mammalian genes, grouped into eight classes (α1-α6, β1-β3, γ1–3, δ, ε, θ, π, and ρ1–3; Sieghart, 2015). The existence of receptor pentamers with different subunit composition and arrangement, so-called subtypes, has produced great efforts towards the development of subtype-selective ligands (Sieghart and Savić, 2018). GABAA receptors containing α6-subunits are predominantly expressed in cerebellar granular cells and in the embryologically related granule cells of the cochlear nucleus (Laurie et al., 1992; Wisden et al., 1992; Pirker et al., 2000; Hortnagl et al., 2013). Those α6-containing receptors represent an interesting and diverse population of tonically active extrasynaptic δ- and phasic active synaptic γ2-containing groups. It was suggested that α6 subunits are recruited for the strengthening of synapses and added to α1 subunit containing postsynaptic densities (Accardi et al., 2015). Recent research has identified a number of putative pathophysiological roles which involve α6-containing receptors, and targeting these is considered an interesting strategy for disorders with sensorimotor gating deficits (Chiou et al., 2018), essential tremor (Handforth et al., 2018), and by way of receptors thought to be localized in the trigeminal ganglia, trigeminal neuropathic pain states (Puri et al., 2012; Vasović et al., 2019) and migraine (Fan et al., 2018).

Unlike in the rest of the brain, GABAA receptors in cerebellar granular cells are much less diverse, since only selected subunits are being expressed. In terms of mRNA-abundance, the most significant transcripts are α1, α6, β2, β3, γ2, and δ, with additional weak traces of α4, β1, and γ3 (Laurie et al., 1992; Wisden et al., 1992). These findings are supported by immunohistochemical analysis, indicating protein expression of these subunits in mice (Hortnagl et al., 2013) as well as in rats (Pirker et al., 2000). According to previous results, those subunits assemble to form α1βxγ2, α6βxγ2, α1α6βxγ2, α6βxδ, and α1α6βxδ as major GABAA receptors (Jechlinger et al., 1998; Tretter et al., 2001; Pöltl et al., 2003). The co-existence of the two different α-subunits α1 and α6 in one pentamer has been appreciated previously (Khan et al., 1996), as well as the fact that the benzodiazepine binding pharmacology is defined by the α-subunit, which contacts γ2 and forms the α/γ-interface (Sieghart, 1995). In former studies, α1α6βxγ2-containing GABAA receptors were considered a single receptor population (Jechlinger et al., 1998; Pöltl et al., 2003). However, soon it was appreciated that concatenated α1α6βxγ2 GABAA receptors of two different arrangements can be expressed in *Xenopus laevis* oocytes, either with α1 neighboring γ2 or with α6 neighboring γ2 (Minier and Sigel, 2004). Receptors with such alternative subunit arrangements carry unique drug binding sites. The development of ligands specific for such unique binding sites is facilitated by structural models of the pocket- ligand interactions and has seen a recent surge of experimental models from moderate resolution cryo-EM and crystal structures of heteromeric GABAA receptors (Zhu et al., 2018; Masiulis et al., 2019).

In the current study, we investigated the possibility, that not only in heterologous expression systems but also in the native rat cerebellum, α1α6βxγ2-containing GABAA receptors can consist of two subgroups with alternative arrangements and therefore unique pharmacological properties. Also, we compile current insights gained from ligand-bound α1βγ2 receptors and extrapolate to the α6 containing subtypes described in this study to examine the options for selective targeting of individual receptor species.

MATERIALS AND METHODS

Materials

Rabbit antibodies against GABAA receptor subunits came from a local collection, were all generated as described (Mossier et al., 1994) and characterized in detail and used in several previous studies (Jechlinger et al., 1998; Pöltl et al., 2003; Ogris et al., 2006). Pansorbin® cells were purchased from Merck (Darmstadt, Germany) and Pierce™ BCA protein assay kit from ThermoFisher Scientific (Waltham, MA, USA). ^{3}H-flunitrazepam (specific activity 76.0 Ci/mmol) and ^{3}H-Ro 15-4513 (specific activity 49.5 Ci/mmol) were purchased from Perkin Elmer NEN (New England Nuclear, Waltham, MA, USA). Diazepam (7-chloro-1,3-dihydro-1-methyl-5-phenyl-2H-1,4,benzodiazepine-2-one) was bought from Nycomed (Opfikon, Switzerland) and Ro15–1788 [Flumazenil, ethyl 8-fluoro-5,6-dihydro-5-methyl-6-oxo-4H-imidazo(1,5-a;1,4)benzodiazepine-3-carboxylate] from Tocris (Bio-techne Ltd., Abingdon, United Kingdom). Standard chemicals were from Sigma-Aldrich (St. Louis, MO, USA).

Culturing and Transfection of Human Embryonic Kidney 293 (HEK 293) Cells

Human embryonic kidney (HEK) 293 cells (American Type Culture Collection ATCC® CRL-1574TM) were maintained in Dulbecco's modified Eagle medium (DMEM, high glucose, GlutaMAX™ supplement, Gibco 61965-059, ThermoFisher, Waltham, MA, USA) supplemented with 10% fetal calf serum (Sigma-Aldrich F7524, St. Louis, MO, USA), 100 U/ml Penicillin-Streptomycin (Gibco 15140-122, ThermoFisher, Waltham, MA, USA) and MEM (Non-Essential Amino Acids Gibco 11140-035, ThermoFisher, Waltham, MA, USA) on 10 cm cell culture dishes (Cell+, Sarstedt, Nürnbrecht, Germany) at 37°C and 5% CO_2.

HEK 293 cells were transfected with cDNAs encoding rat GABAA receptor subunits subcloned into pCI expression vectors. The ratio of plasmids used for transfection with the calcium phosphate precipitation method (Chen and Okayama, 1987) were 3 μg α (1, 2, 3 or 5) : 3 μg β3: 15 μg γ2 per 10 cm dish. The medium was changed 4–6 h after transfection. Cells were harvested 72 h after transfection by scraping into phosphate-buffered saline and pelleted by centrifugation (10 min, 12,000 *g*, 4°C). For membrane binding experiments, cells were resuspended in TC50 (50 mM Tris-Citrate pH = 7.1), homogenized with an ULTRA-TURRAX® (IKA, Staufen, Germany), and centrifuged (20 min, 50,000 *g*). Membranes were washed three times in TC50 as described above and frozen at −20°C until use. For immunoprecipitation assays, cells

were lysed in sodium deoxycholate (DOC) buffer (10 mM Tris pH = 8.5, 150 mM NaCl, 0.5% DOC, 0.05% phosphatidylcholine, 0.08% protease inhibitor) at 4°C for 2 h, cleared by centrifugation and used immediately.

Preparation of Rat Cerebellar Membranes and Extracts

Four to six-week-old female rats were sacrificed by decapitation, the cerebella removed quickly, flash-frozen in liquid nitrogen, and stored at −80°C until needed. For immunoprecipitation experiments, a single cerebellum was thawed at room temperature, homogenized in sodium deoxycholate (DOC) buffer in a brain to buffer ratio of 1 g/10 ml using an Ultra-Turrax rotor-stator homogenizer (IKA, Staufen, Germany) for 10 s followed by syringe and needle homogenization. After incubation (4°C for 2 h) the lysate was cleared by centrifugation and used immediately. For membrane binding experiments rat cerebellum was homogenized with an Ultra-Turrax rotor-stator homogenizer for 30 s in an ice-cold homogenization buffer (10 mM Hepes, 1 mM EDTA, 300 mM Sucrose, protease inhibitor) and centrifuged at 45,000 *g* at 4°C for 30 min. The pellet was resuspended in wash buffer (10 mM Hepes, 1 mM EDTA, protease inhibitor), incubated on ice for 30 min and centrifuged at 45,000 *g* at 4°C for 30 min. The pellet was stored at −80°C o/n and the next day was washed five times by suspension in 50 mM Tris-citrate buffer, pH = 7.1, and subsequent centrifugation as described above. Membrane pellets were stored at −80°C until final use.

Radioligand Membrane Binding Assays

Frozen membranes were thawed, resuspended, and incubated for 90 min at 4°C in a total of 500 µl of TC50/NaCl (50 mM Tris-Citrate pH = 7.1; 150 mM NaCl), various concentrations of the drug to be studied, 2 nM ^{3}H-flunitrazepam or 5 nM ^{3}H-Ro 15-4513 in the absence or presence of either 5 µM diazepam or 50 µM Ro 15-1788 (to determine unspecific binding; final DMSO-concentration 0.5%). To study the pharmacology of the α1/γ2-interface membranes were incubated with ^{3}H-flunitrazepam; to study the α6/γ2-interface membranes were incubated with 5 nM ^{3}H-Ro 15-4513 in the presence of 5 µM diazepam (to saturate α1-containing receptors and target α6-containing receptors only). Membranes were filtered through Whatman GF/B filters and the filters were rinsed twice with 4 ml of ice-cold 50 mM Tris/citrate buffer. Filters were transferred to scintillation vials and subjected to scintillation counting after the addition of 3 ml Rotiszint Eco plus liquid scintillation cocktail.

Immunoprecipitation Assays

Transfected HEK 293 cells or rat cerebella were lysed in sodium deoxycholate (DOC) buffer (10 mM Tris pH = 8.5, 150 mM NaCl, 0.5% DOC, 0.05% phosphatidylcholine, 0.08% protease inhibitor) at 4°C for 2 h, cleared by centrifugation and used immediately. One hundred and fifty micro litre clear supernatant and 5 µg antibody in 20 µl phosphate-buffered saline (PBS: 10 mM Na_2HPO_4, 1.8 mM KH_2PO_4, 2.7 mM KCl, 140 mM NaCl, pH = 7.4) were incubated on a shaking platform at 4°C overnight. Heat-killed, formalin-fixed Staphylococcus aureus cells carrying protein A (Standardized Pansorbin-cells, Calbiochem) were centrifuged at 2,300 *g* for 5 min at 4°C. The pellets were washed twice with IP-High (50 mM Tris-HCl pH = 8.3, 600 mM NaCl, 1 mM EDTA, 0.5% Triton X-100), once in IP-Low (50 mM Tris-HCl pH = 8.0, 150 mM NaCl, 1 mM EDTA, 0.2% Triton X-100), and re-suspended with IP-Low. Twenty microlitre of this suspension of Pansorbin cells were added to the above-mentioned cocktail containing the antibody and the solubilized receptors, for 2 h at 4°C on a shaking platform. Samples were centrifuged at 2,300 *g* for 5 min at 4°C and washed twice with IP-High and once with IP-Low at 2,300 *g* for 1 min at 4°C. Pellets were resuspended in 500 µl TC50/NaCl (50 mM Tris-Citrate pH = 7.1; 150 mM NaCl), radioligand was added and the radioligand binding assays performed as described above.

Data Calculation

Radioligand displacement experiments were analyzed using GraphPad Prism version 8.3.0 for Mac OS X, GraphPad Software[1], La Jolla, CA, USA. Nonlinear regression analysis of the displacement curves used the equation: Y = Bottom + (Top-Bottom)/(1 + 10^((LogIC50-X)*Hill-slope). IC50 values were converted into Ki values using the Cheng-Prusoff relationship (Cheng and Prusoff, 1973) Ki = IC50/(1 + (S/KD)) with S being the concentration of the radioligand (2 nM for ^{3}H-flunitrazepam or 5 nM for ^{3}H-Ro 15-4513) and the KD values as described previously [4.8 nM for ^{3}H-flunitrazepam (Simeone et al., 2017) and 1.4 nM for ^{3}H-Ro 15-4513 in the presence of diazepam (Treven et al., 2018)].

Structure Rendering and Homology Modeling

PDB files 6HUP and 6D6U were analyzed and rendered with MOE [Molecular Operating Environment (MOE), 2019.01; Chemical Computing Group ULC, 1010 Sherbrooke St. West, Suite #910, Montreal, QC, Canada, H3A 2R7, 2019]. A representative model of an α6+/γ2− the interface is based on 6D6U.

RESULTS

All ligands used in this study require the presence of the γ2-subunit, and thus, the total pool of γ2-containing GABAA receptors in the cerebellar membrane preparations was subjected to a workflow of differential identification and quantification. The number of γ2-containing GABAA receptors precipitated from rat cerebellar extracts using different α-subunit-specific antibodies was quantified using ^{3}H-Ro 15-4513 binding studies and related to the total number of benzodiazepine-sensitive receptors as estimated by precipitation with anti-γ2 antibodies (see **Figure 1**). Receptors precipitated with α3, α4, and α5 were statistically not significantly different from zero (as determined by a one-sample *t* and Wilcoxon test). Since the precipitation efficiencies of our antibodies have been characterized on transfected HEK 293 cells (see **Figure 2**), we can conclude

[1]www.graphpad.com

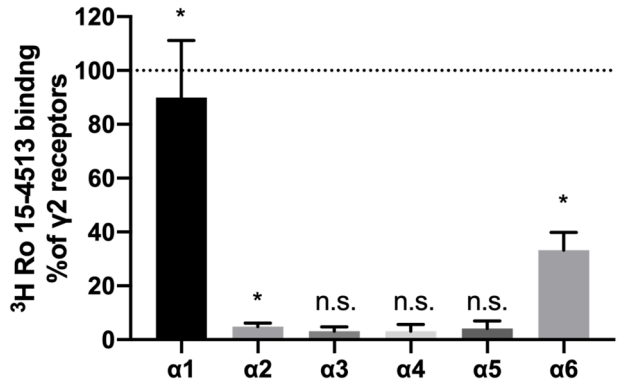

FIGURE 1 | α-subunits found in γ2-containing receptors in rat cerebellum. GABAA receptors were extracted from rat cerebellum, precipitated with subunit specific antibodies, and quantified using ^{3}H-Ro 15-4513 binding. Nonspecific binding was analyzed by the addition of 50 μM Ro 15-1788. Results are expressed concerning values obtained with parallel precipitation with specific anti-γ2 antibody. Shown are the mean ± SD of three independent experiments performed in duplicates each. Data were analyzed statistically, if they are significantly different from 0, following a one-sample *t* and Wilcoxon test (*$p < 0.05$; ns: $p > 0.05$; α1: $p = 0.0181$; α2: $p = 0.0260$; α6: $p = 0.0129$; α3, α4 and α5: $p > 0.05$).

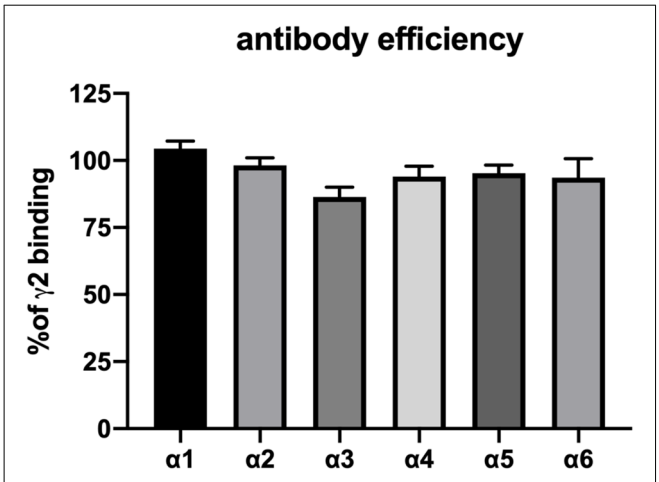

FIGURE 2 | Confirmation of the precipitation efficiency of subunit-specific antibodies used in this study. HEK 293 cells were transfected with the subunit combinations α1βγ2, α2βγ2, α3βγ2, α4βγ2, α5βγ2, and α6βγ2, lysed in deoxycholate (DOC) buffer and precipitated with 5 μg antibody in 20 μl phosphate-buffered saline as described in the "Materials and Methods" section. Precipitated pellets were subjected to radioligand binding assay with 2 nM ^{3}H-flunitrazepam (α1βγ2, α2βγ2, α3βγ2, and, α5βγ2) or 5 nM ^{3}H-Ro 15-4513 (α4βγ2 and α6βγ2). Nonspecific binding was analyzed by the addition of 5 μM diazepam or 50 μM Ro 15-1788. Results are expressed concerning values obtained with parallel precipitation with specific anti-γ2 antibody. Shown are the mean ± SD of three independent experiments performed in duplicates each. None of the results shown differ statistically from 100% (as determined by a one-sample *t* and Wilcoxon test), indicating that all antibodies precipitate their target receptor with high efficiency.

that we missed subunits due to poor antibody-quality. Only anti-α1, anti-α6, and anti-α2-antibodies precipitated significant amounts, the latter however only <5% of all receptors. This is in agreement with previous immunocytochemical studies, which found particularly high expression levels of α1 and notable levels of α6 in the cerebellar granule layer, and only weak or absent expression of the other α subunits (Pirker et al., 2000). Those other weakly expressed subunits such as α2 and α5 seem to be predominantly expressed in the molecular or the Purkinje layer of the cerebellum (Pirker et al., 2000; Hortnagl et al., 2013) and the Bergman glia (Wisden et al., 1992), but not in the granule cell layers, where α6 is being expressed. Therefore, when characterizing assembling partners for α6, only α1 will have to be accounted for.

So indeed, γ2-containing receptors in rat cerebellar granule cells contain α1, α6, and α1α6-subunit combinations. In former studies, α1α6βxγ2-containing GABAA receptors have been considered a single receptor population (Jechlinger et al., 1998; Pöltl et al., 2003). In the current study, we hypothesize that this population consists of two subgroups with alternative arrangements depending if α1 neighbors γ2 (forming a "diazepam-sensitive" receptor, short DS), or if α6 neighbors γ2 (forming a "diazepam-insensitive" receptor, short DI). In the rat cerebellum, we can therefore expect the four different receptor populations depicted in **Figure 3**.

To experimentally characterize the different distinct receptor populations found in the native rat cerebellum, radioligand displacement assays were performed. These experiments take advantage of the different subunit selectivity of the two radioligands ^{3}H-flunitrazepam, and ^{3}H-Ro 15-4513. Although both ligands bind to the benzodiazepine binding site at the α+/γ− -interface (Sieghart, 1995), ^{3}H-flunitrazepam, as well as diazepam act *via* the classical "diazepam-sensitive" DS-binding sites at α1βγ2, α2βγ2, α3βγ2, and α5βγ2, while ^{3}H-Ro 15-4513 as well as Ro 15-1788 (flumazenil) also bind to the "diazepam-insensitive" DI-binding sites at α4βγ2 and α6βγ2-receptors (Sieghart, 2015), see **Figure 3**. We performed radioligand displacement assays on rat cerebellar membranes using different radioligands, displacing ligands, and diazepam as DS-specific blocking ligand. First, ^{3}H-flunitrazepam was used to selectively label receptors containing an α1/γ-interface (circles in **Figures 4A,B**). Both compounds diazepam and Ro 15-1788 completely inhibited ^{3}H-flunitrazepam binding in a dose-dependent high-affinity one-site binding, as indicated by the Hill-slope of approximately −1. In a second experiment, the radioligand ^{3}H-Ro 15-4513 was used to label receptors with any α/γ-interface. Since diazepam only competes for binding at receptors, where α1 neighbors γ2, only partial displacement can be observed (open squares in **Figure 4A**). Ro 15-1788 on the other hand, can bind to any α/γ-interface, the affinities are however different, depending on if this α is an α1 or an α6. This leads to mixed pharmacology and a dose-response curve with a Hill-slope of −0.7 (closed squares in **Figure 4B**). To pharmacologically access receptors with an α6/γ-interface, membranes were incubated with ^{3}H-Ro 15-4513 in the presence of 5 μM diazepam. Diazepam does not bind to α6βxγ2-receptors under these conditions (data not shown), while Ro 15-1788 concentration-dependently displaced the radioligand in

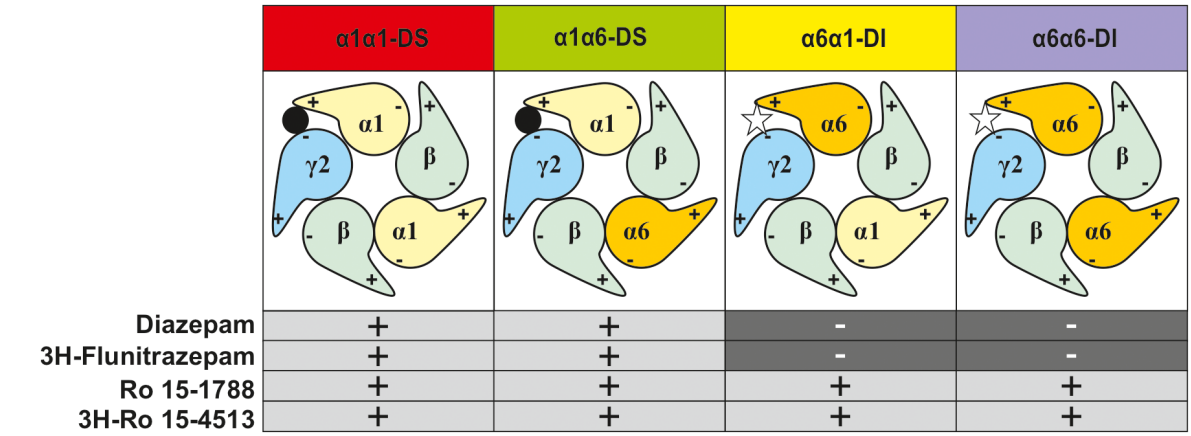

FIGURE 3 | Representation of the possible subtype combinations of γ2-containing GABAA-receptors found in rat cerebellar granule cells and their pharmacological profile. The first named α-subunit is the γ2-neighbor, and thus determines the drug sensitivity profile (diazepam-sensitive "DS" or diazepam-insensitive "DI").

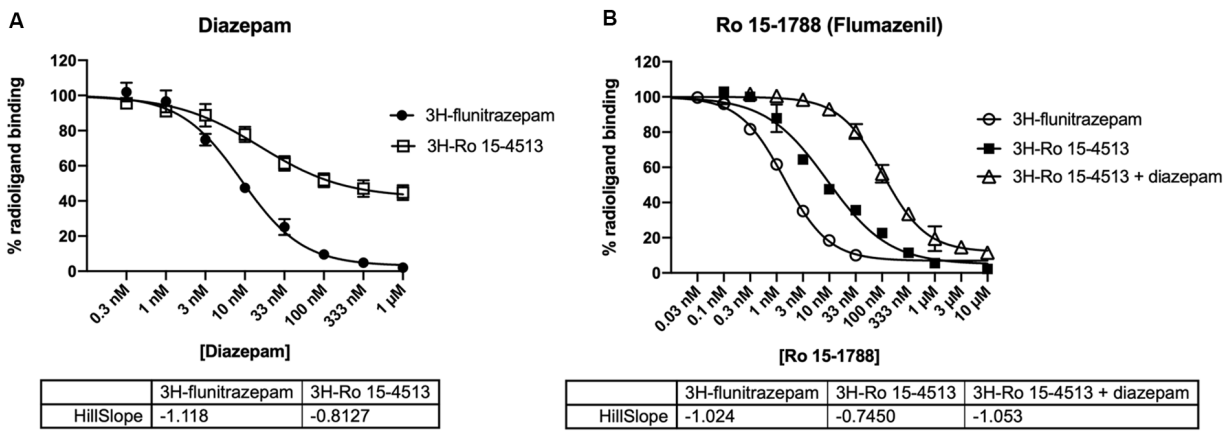

	3H-flunitrazepam	3H-Ro 15-4513
HillSlope	-1.118	-0.8127

	3H-flunitrazepam	3H-Ro 15-4513	3H-Ro 15-4513 + diazepam
HillSlope	-1.024	-0.7450	-1.053

FIGURE 4 | Inhibition of radioligand binding to rat cerebellar membranes. Rat cerebellar membranes were incubated with 2 nM ^{3}H-flunitrazepam (circles), 5 nM ^{3}H-Ro 15-4513 (squares), or 5 nM ^{3}H-Ro 15-4513 + 5 μM diazepam (triangles) in the presence of various concentrations of the displacing ligand [diazepam in panel **(A)** and Ro 15-1788 (flumazenil) in panel **(B)**]. The data shown are the mean ± SD of three independent experiments performed in duplicates each.

a low-affinity one-site binding with a Hill-slope of −1 (open triangles in **Figure 4B**).

Radioligand binding experiments as described in **Figure 4** can only give information about the α-subunit which contacts γ2. To gain information on the nature of the other second α-subunit in the pentamer, immunoprecipitation experiments with subtype-specific antibodies were performed, followed by a radioligand binding of the precipitate. Immunoprecipitation of cerebellar lysates with an anti-γ2 antibody followed by an unspecific ^{3}H-Ro 15-4513 binding will capture all γ2-containing receptors ("100%"). A similar immunoprecipitation with an anti-γ2 antibody followed by a ^{3}H-Ro 15-4513 binding in the presence of 5 μM diazepam will discriminate between diazepam-sensitive receptors with α1 neighboring γ2 (α1α1-DS and α1α6-DS) and the remaining diazepam-insensitive receptors with α6 neighboring γ2 (α6α1-DI and α6α6-DI). The latter proved to be 33.7 ± 1.7% (MW ± SEM, n = 6) of all γ2-containing receptors (see **Figure 5A**). The remaining 66% of receptors will therefore be diazepam-sensitive receptors with α1 neighboring γ2 (the receptors termed α1α1-DS and α1α6-DS). Immunoprecipitation with anti-α1 antibodies followed by an α6/γ2-interface-specific ^{3}H-Ro 15-4513 + 5 μM diazepam binding directly measures a receptor population with α6 neighboring γ2 and α1 as second α-subunit in the same pentamer (α6α1-DI and marked in yellow in **Figure 3**). Those receptors amount to 15.3 ± 1.1% (MW ± SEM, n = 7) of all γ2-containing receptors and are depicted as a yellow bar in **Figure 5A**.

To further analyze the population of diazepam sensitive receptors, with α1 next to γ2, we used immunoprecipitation experiments with subunit specific antibodies, followed by a radioligand binding with ^{3}H-flunitrazepam. As determined from the experiments shown in **Figure 5A**, diazepam-sensitive receptors with α1 neighboring γ2 (α1α1-DS and α1α6-DS)

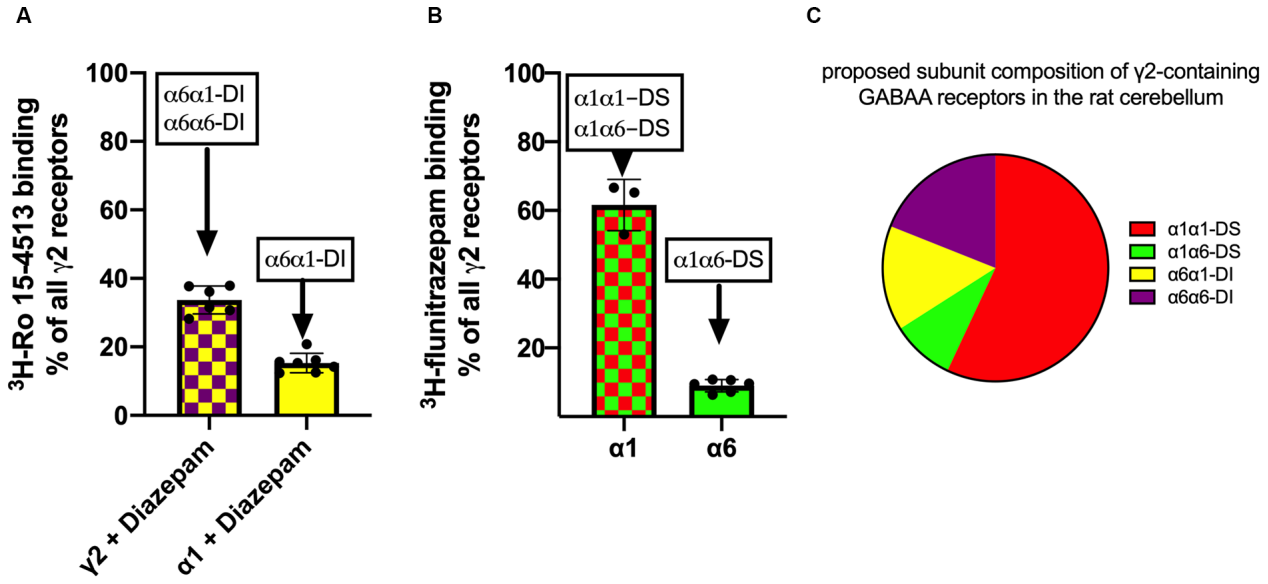

FIGURE 5 | Analysis of γ2-containing receptors in rat cerebellum. GABAA receptors were extracted from rat cerebellum, precipitated with subunit specific antibodies, and quantified using 5 nM ^{3}H-Ro 15-4513 with or without diazepam panel **(A)** or 2 nM ^{3}H-flunitrazepam panel **(B)**. The data shown are mean ± SD of 4–7 independent experiments performed in duplicates each. Panel **(C)**: the diagram illustrates the proposed subunit composition of γ2-containing GABAA receptors in the rat cerebellum. The pie chart is constructed from the data obtained from experiments depicted in panels **(A,B)**.

amount to 66% of all γ2-containing receptors. Those receptors will also be measured when immunoprecipitation with an anti-γ2 antibody followed by an α1/γ2-interface specific ^{3}H-flunitrazepam binding. The very same receptor population can also be captured when precipitating with anti- α1 antibodies followed by an α1/γ2-interface specific ^{3}H-flunitrazepam binding. Immunoprecipitation with anti-α6 antibodies followed by an α1/γ2-interface specific ^{3}H-flunitrazepam binding directly measures a receptor population with α1 neighboring γ2 and α6 as second α-subunit in the same pentamer (α1α6-DS, marked in green in **Figure 3**). Those receptors are depicted as a green bar in **Figure 5B** and amount to 13.5 ± 1.1% (MW ± SEM, n = 6) of all diazepam-sensitive receptors and, since diazepam-sensitive receptors amount to 66% of the total, they account for 9% of total γ2-containing receptors.

With those experiments, we can now define the composition of the bulk of γ2-containing receptors in rat cerebellum (see **Figure 5C**): 57% α1γ2βxα1βx (=α1α1-DS, red), 9% α1γ2βxα6βx (=α1α6-DS, green), 15% α6γ2βxα1βx (α6α1-DI, yellow), and 19% α6γ2βxα6βx (α6α6-DI, purple).

Those receptor subpopulations differ by their pharmacological properties: if ideally selective benzodiazepine-site ligands were available, receptors of the DS-arrangements could be targeted together, as well as those of the DI-arrangements. At this time, substances that interact selectively with DS sites are broadly available and include diazepam and flunitrazepam—and are also used in the current study. In contrast, ligands selective for the α6+/γ2− pocket so far are lacking. Existing experimental structures can provide some guidance towards the design of such ligands, see **Figures 6**, **7**.

A single amino acid on loop A causes the separation between DS and DI subunits, namely His in α1, α2, α3 and α5, and Arg in α4 and α6. A single amino acid in loop B causes zolpidem sensitivity in α1, α2, and α3, and renders α4, α5, and α6 zolpidem insensitive. Loop C displays unique variable amino acids for each α isoform, in theory enabling targeting of each subunit individually. Of all variable amino acids, which differ between α1 and α6, only some contribute directly to the pocket surface, see **Figure 7**.

DISCUSSION

Benzodiazepine type compounds have been used clinically as anesthetics, anticonvulsants, anxiolytics, hypnotics, and many more (Sieghart, 2015). They act by allosterically modulating GABAA receptors at the α/γ-interface. Existing experimental structures provide us with information about the molecular binding site of currently used ligands as well as some guidance towards the design of novel, more selective ligands. Computational modeling of potential drug binding sites found on a defined receptor species is however challenging since we lack the required knowledge of the receptor species existing in native tissue. Several receptor isoforms have been described to "exist," exist with "high probability," "tentatively" or "most likely" (Olsen and Sieghart, 2008; Mortensen et al., 2012), and this list is constantly being modified. In all of those studies, the nature of the α and γ-subunits is described precisely, there is however a complete lack of knowledge concerning the different β isoforms, which are mostly only listed as βx. Also, it is not fully known, whether all subunits can contribute to all interfaces or if there are assembly rules. It is therefore of uttermost

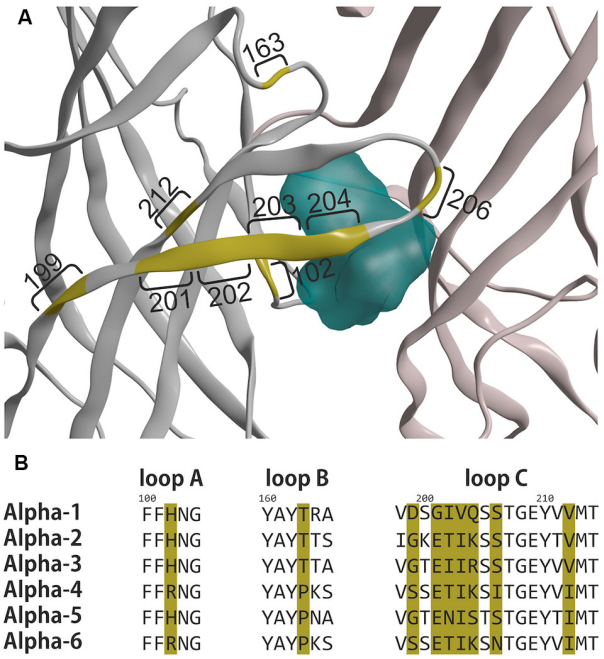

FIGURE 6 | Differences in the principal faces of α1 and α6 subunits. **(A)** Ribbon depiction of the α1+/γ2− ECD binding site from 6HUP. Segments colored in yellow represent amino acids, which differ between α1 and α6. Numbers indicate the number of the amino acid according to the numbering in 6HUP. The molecular surface of diazepam in the pocket is rendered in cyan to indicate the position of the variable amino acids concerning the space occupied by the ligand. **(B)** Partial alignment of sequences containing the different amino acids, depicted in **(A)**. All α isoforms are displayed with the positions of the amino acids, which differ between α1 and α6 colored in yellow. Amino acid numbering corresponds to 6HUP and represents the mature human α1 peptide.

importance to further identify subunit arrangements found in a given native tissue.

In the current study, we mostly focused on receptors containing the α6-subunit, which have gained recent attention as potential novel future drug targets. α6-containing GABAA receptors have been reported to contribute to the alleviation of sensorimotor gating deficits (Chiou et al., 2018) and orofacial pain and migraine (Fan et al., 2018) in animal and cell models. Moreover, models of essential tremor and trigeminal neuropathic pain also have been demonstrated to benefit from drugs that act on α6-containing GABAA receptors (Handforth et al., 2018; Vasović et al., 2019). α6βγ2-containing receptors can be discriminated from α1βγ2, α2βγ2, α3βγ2, and α5βγ2 since they are not sensitive to diazepam. This separation between diazepam-sensitive and diazepam-insensitive subunits is caused by a single amino acid on loop A, namely His in α1, α2, α3 and α5, and Arg in α4 and α6. Interestingly, the experimental structures of diazepam and Ro 15–1788 (flumazenil) in the α1+/γ2− ECD binding site do not indicate a common binding mode of these ligands. Diazepam as a prototypical ligand with selectivity for the DS subunits is close to the loop A residue His102 (see **Figure 6A**). In the homology model, the unselective flumazenil molecule leaves ample space for the bigger Arg100 sidechain in loop A, based on the unique orientation that was seen in the α1+/γ2− ECD binding site (Zhu et al., 2018). Ligands, which prefer α6 over α1 can theoretically exploit sequence differences not only in loop A, but also take advantage of the loop B difference that renders α6 zolpidem insensitive, and of amino acids unique to the C-loop of α6, see **Figures 6B** and **7D**. Seven amino acids on loop C differ, but two of these do not face the binding site at all. Of the remaining differences, only N204 near the loop tip is unique for the α6 subunit.

The receptors identified in this study could also be discriminated *via* their β-subunits, which may potentially differ in those receptor subtypes. Little is known about the alternative modulatory site which is present at the extracellular α+/β- interface (Ramerstorfer et al., 2011; Varagic et al., 2013a,b; Simeone et al., 2019). We have previously demonstrated that β-isoform-selective ligands can in principle be developed for this site (Simeone et al., 2017). We also have demonstrated that ligands which modulate *via* the α+/β− ECD interfaces can differentiate between α6+/β3− and α1+/β3− (Simeone et al., 2019). To take advantage of these alternative interfaces for selective targeting it would thus be of interest to identify the β-isoforms, which are between the two α subunits in the receptors described here. If they differ among the four receptors we have described here, there is a possibility that selective targeting of individual receptor species is possible. On the other hand, if all these receptors contain the same β isoform in the position between the α subunits, receptors α1α1-DS and α6α1-DI can be targeted together with α6+/β− selective ligands, while receptors α1α6-DS and α6α6-DI can be targeted with α1+/β− selective agents. In order to identify even further possible drug binding sites, we would need experimental structures with more subunits, as well as experimental structures with ligands bound to the α+/β− interfaces.

As mentioned above, for future drug development, it is necessary to precisely identify GABAA receptor subtypes found in a given native tissue. In the current study, we aimed to discriminate the different αβγ2-containing receptors found in rat cerebellum. First, we identified the α-subunits, which exist in the rat brain: α1, α6, and α2, with the latter, only found in <5% of all receptors. This finding is consistent with previous studies: Pöltl et al also find α1 and α6 and also only α2 being significantly different from zero to 7% of total muscimol-binding receptors in the rat (Pöltl et al., 2003). α2-containing receptors, however, seem to be predominantly expressed in the molecular layer (Hortnagl et al., 2013) and the Bergman glia (Wisden et al., 1992), but not in the granule cell layers. Therefore, α2 and α6 although both present in the cerebellum, will not co-assemble. Other studies also describe the (weak) expression of α5 in several different cerebellar cell layers (Pirker et al., 2000). It seems, however, that this subunit does not co-assemble with γ2, which would explain why we were not able to detect significant levels of α5γ2-containing receptors using our experimental conditions. Taking all those findings together, we can therefore expect the following αβγ2-containing receptors in the cerebellar granule cell layer: α1βxγ2, α6βxγ2, α1α6βxγ2. Although most articles only consider αx-containing receptors, the fact that two different α-subunits can co-assemble in one pentamer has been appreciated

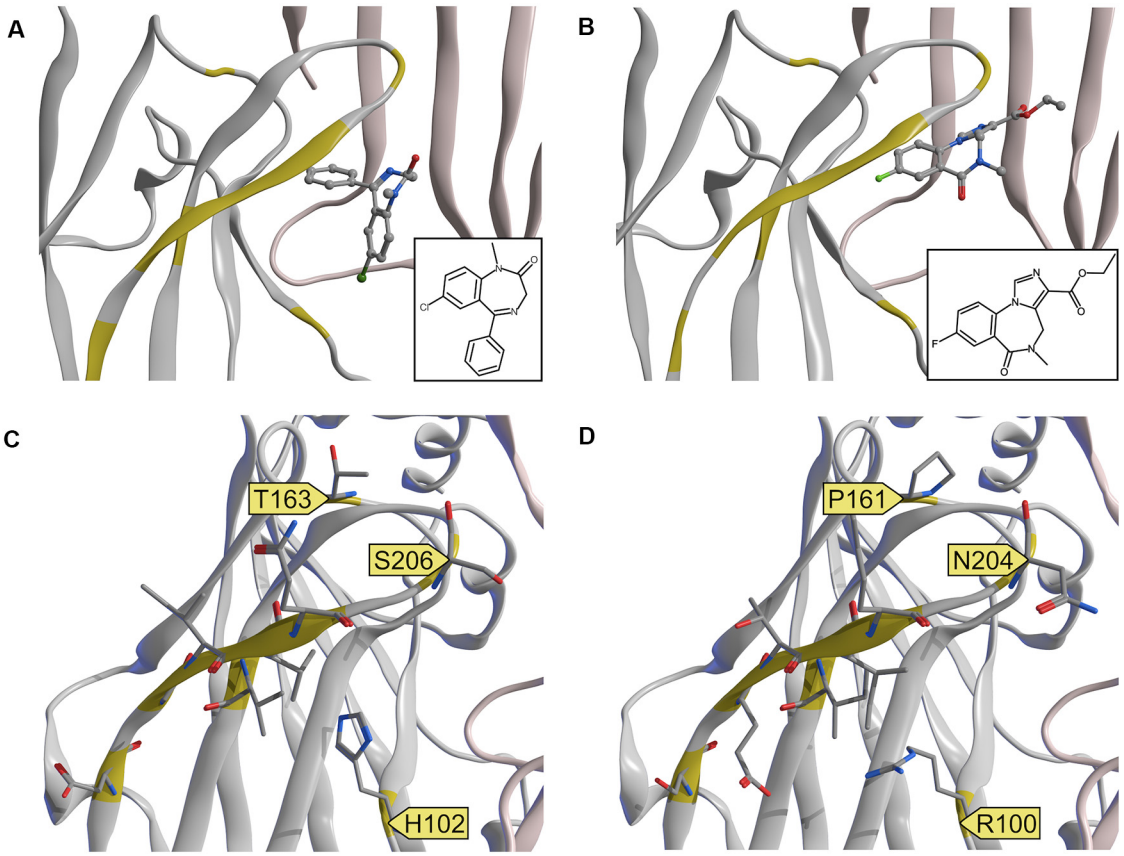

FIGURE 7 | Experimental structures and a homology model of the α6 subunit. **(A,B)** Comparison of experimental structures of diazepam and flumazenil at the α1+/γ2− ECD binding site. 6HUP **(A)** contains diazepam, 6D6U **(B)** contains flumazenil. The two ligands do not share a common binding mode. **(C)** 6HUP and **(D)** α6 homology model, both with amino acids, which differ between the two α isoforms in stick representation. Amino acids that could facilitate DI selective or even α6 selective targeting are highlighted with a yellow flag.

before: significant, however minor populations of α1α2, α1α3, and α2α3 have been described in the bovine cerebral cortex (Duggan et al., 1991) and α1α6 receptors even in rat brain (Khan et al., 1996). But even those studies do not consider the fact, that the arrangement of the different subunits will crucially influence the inter-subunit binding sites being formed, and therefore heavily influence the pharmacological properties of the receptor isoforms.

In the current study, we, therefore, aimed to further characterize α1α6βxγ2-containing GABAA receptors and hypothesize, that this population consists of two subgroups with alternative arrangements. We identified the γ2-containing GABAA receptors in the rat cerebellum as being composed of 57% α1γ2βxα1βx (=α1α1-DS, red), 9% α1γ2βxα6βx (=α1α6-DS, green), 15% α6γ2βxα1βx (α6α1-DI, yellow), and 19% α6γ2βxα6βx (α6α6-DI, purple; see **Figure 5C**). These findings are consistent with Ogris et al. (2006), who find that the majority (75%) of all GABAA receptors in the cerebellum contain α1. Among all α6 containing receptors, 30% have been described to contain δ (Jechlinger et al., 1998) but will not be detected using the radioligand binding experiments described in our current study. Jechlinger et al. (1998) describe the remaining non-δ-containing receptors to be distributed to about equal amounts to α6βxγ2 and α1α6βxγ2 (32% related to all α6 containing receptors). This is consistent with our finding, where we find α6α6-DI-receptors (purple segment in **Figure 5C**) being approximately equal to the sum of α1α6-DS and α6α1-DI (green and yellow segments in **Figure 5C**). We, however, in addition to these previous studies, can now specify the exact subunit arrangement and can show that indeed both α-positions are occupied by either α1 or α6.

Summarizing, the simple classification of GABAA-receptors into αx-containing subtypes seems not to reflect the complexity of nature; those receptors are more diverse than previously thought.

DATA AVAILABILITY STATEMENT

All datasets presented in this study are included in the article.

ETHICS STATEMENT

Ethical review and approval was not required for the animal study because The EU directive 210/63/EU,

which is also reflected by the Austrian federal law "Tierversuchsgesetz 2012", states that killing of animals solely for the use of their organs and tissues is not considered a "procedure" and does not require specific approval.

AUTHOR CONTRIBUTIONS

PS and ME participated in research design. MP, SL, FS, and JF conducted experiments. MP, SL, and FS performed data analysis. PS and ME wrote or contributed to the writing of the manuscript. All authors contributed to the article and approved the submitted version.

FUNDING

This study was supported by the Austrian Science Fund FWF, project number I2306.

ACKNOWLEDGMENTS

We thank Sabah Rehman for excellent technical assistance.

REFERENCES

Accardi, M. V., Brown, P. M., Miraucourt, L. S., Orser, B. A., and Bowie, D. (2015). α6-containing $GABA_A$ receptors are the principal mediators of inhibitory synapse strengthening by insulin in cerebellar granule cells. *J. Neurosci.* 35, 9676–9688. doi: 10.1523/JNEUROSCI.0513-15.2015

Chen, C., and Okayama, H. (1987). High-efficiency transformation of mammalian cells by plasmid DNA. *Mol. Cell. Biol.* 7, 2745–2752. doi: 10.1128/mcb.7.8.2745

Cheng, Y., and Prusoff, W. H. (1973). Relationship between the inhibition constant (K1) and the concentration of inhibitor which causes 50 per cent inhibition (I50) of an enzymatic reaction. *Biochem. Pharmacol.* 22, 3099–3108. doi: 10.1016/0006-2952(73)90196-2

Chiou, L.-C., Lee, H.-J., Ernst, M., Huang, W.-J., Chou, J.-F., Chen, H.-L., et al. (2018). Cerebellar α_6 -subunit-containing $GABA_A$ receptors: a novel therapeutic target for disrupted prepulse inhibition in neuropsychiatric disorders. *Br. J. Pharmacol.* 175, 2414–2427. doi: 10.1111/bph.14198

Duggan, M. J., Pollard, S., and Stephenson, F. A. (1991). Immunoaffinity purification of $GABA_A$ receptor α-subunit iso-oligomers. Demonstration of receptor populations containing α1α2, α1α3 and α2α3 subunit pairs. *J. Biol. Chem.* 266, 24778–24784.

Fan, P.-C., Lai, T.-H., Hor, C. C., Lee, M. T., Huang, P., Sieghart, W., et al. (2018). The α6 subunit-containing $GABA_A$ receptor: a novel drug target for inhibition of trigeminal activation. *Neuropharmacology* 140, 1–13. doi: 10.1016/j.neuropharm.2018.07.017

Handforth, A., Kadam, P. A., Kosoyan, H. P., and Eslami, P. (2018). Suppression of harmaline tremor by activation of an extrasynaptic $GABA_A$ receptor: implications for essential tremor. *Tremor Other Hyperkinet. Mov. (N Y)* 8:546. doi: 10.7916/D8JW9X9K

Hortnagl, H., Tasan, R. O., Wieselthaler, A., Kirchmair, E., Sieghart, W., and Sperk, G. (2013). Patterns of mRNA and protein expression for 12 $GABA_A$ receptor subunits in the mouse brain. *Neuroscience* 236, 345–372. doi: 10.1016/j.neuroscience.2013.01.008

Jechlinger, M., Pelz, R., Tretter, V., Klausberger, T., and Sieghart, W. (1998). Subunit composition and quantitative importance of hetero-oligomeric receptors: $GABA_A$ receptors containing α6 subunits. *J. Neurosci.* 18, 2449–2457. doi: 10.1523/JNEUROSCI.18-07-02449.1998

Khan, Z. U., Gutierrez, A., and De Blas, A. L. (1996). The α1 and α6 subunits can coexist in the same cerebellar $GABA_A$ receptor maintaining their individual benzodiazepine-binding specificities. *J. Neurochem.* 66, 685–691. doi: 10.1046/j.1471-4159.1996.66020685.x

Laurie, D. J., Seeburg, P. H., and Wisden, W. (1992). The distribution of 13 $GABA_A$ receptor subunit mRNAs in the rat brain. II. Olfactory bulb and cerebellum. *J. Neurosci.* 12, 1063–1076. doi: 10.1523/JNEUROSCI.12-03-01063.1992

Masiulis, S., Desai, R., Uchański, T., Serna Martin, I., Laverty, D., Karia, D., et al. (2019). $GABA_A$ receptor signalling mechanisms revealed by structural pharmacology. *Nature* 565, 454–459. doi: 10.1038/s41586-018-0832-5

Minier, F., and Sigel, E. (2004). Positioning of the α-subunit isoforms confers a functional signature to gamma-aminobutyric acid type a receptors. *Proc. Natl. Acad. Sci. U S A* 101, 7769–7774. doi: 10.1073/pnas.0400220101

Mortensen, M., Patel, B., and Smart, T. G. (2012). GABA potency at GABA(A) receptors found in synaptic and extrasynaptic zones. *Front. Cell. Neurosci.* 6:1. doi: 10.3389/fncel.2012.00001

Mossier, B., Tögel, M., Fuchs, K., and Sieghart, W. (1994). Immunoaffinity purification of gamma-aminobutyric acidA ($GABA_A$) receptors containing γ1-subunits. Evidence for the presence of a single type of γ-subunit in $GABA_A$ receptors. *J. Biol. Chem.* 269, 25777–25782.

Ogris, W., Lehner, R., Fuchs, K., Furtmüller, B., Höger, H., Homanics, G. E., et al. (2006). Investigation of the abundance and subunit composition of $GABA_A$ receptor subtypes in the cerebellum of α1-subunit-deficient mice. *J. Neurochem.* 96, 136–147. doi: 10.1111/j.1471-4159.2005.03509.x

Olsen, R. W., and Sieghart, W. (2008). International union of pharmacology. LXX. Subtypes of GABA(A) receptors: classification on the basis of subunit composition, pharmacology and function. Update. *Pharmacol. Rev.* 60, 243–260. doi: 10.1124/pr.108.00505

Pirker, S., Schwarzer, C., Wieselthaler, A., Sieghart, W., and Sperk, G. (2000). GABA(A) receptors: immunocytochemical distribution of 13 subunits in the adult rat brain. *Neuroscience* 101, 815–850. doi: 10.1016/s0306-4522(00)00442-5

Pöltl, A., Hauer, B., Fuchs, K., Tretter, V., and Sieghart, W. (2003). Subunit composition and quantitative importance of GABA(A) receptor subtypes in the cerebellum of mouse and rat. *J. Neurochem.* 87, 1444–1455. doi: 10.1046/j.1471-4159.2003.02135.x

Puri, J., Vinothini, P., Reuben, J., Bellinger, L. L., Ailing, L., Peng, Y. B., et al. (2012). Reduced GABA(A) receptor α6 expression in the trigeminal ganglion alters inflammatory TMJ hypersensitivity. *Neuroscience* 213, 179–190. doi: 10.1016/j.neuroscience.2012.03.059

Ramerstorfer, J., Furtmüller, R., Sarto-Jackson, I., Varagic, Z., Sieghart, W., and Ernst, M. (2011). The $GABA_A$ receptor α+β- interface: a novel target for subtype selective drugs. *J. Neurosci.* 31, 870–877. doi: 10.1523/JNEUROSCI.5012-10.2011

Sieghart, W. (1995). Structure and pharmacology of $GABA_A$ receptor subtypes. *Pharmacol. Rev.* 47, 181–234.

Sieghart, W. (2015). Allosteric modulation of $GABA_A$ receptors *via* multiple drug-binding sites. *Adv. Pharmacol.* 72, 53–96. doi: 10.1016/bs.apha.2014.10.002

Sieghart, W., and Savić, M. M. (2018). International union of basic and clinical pharmacology. CVI: $GABA_A$ receptor subtype- and function-selective ligands: key issues in translation to humans. *Pharmacol. Rev.* 70, 836–878. doi: 10.1124/pr.117.014449

Simeone, X., Iorio, M. T., Siebert, D. C. B., Rehman, S., Schnurch, M., Mihovilovic, M. D., et al. (2019). Defined concatenated α6α1β3γ2 $GABA_A$ receptor constructs reveal dual action of pyrazoloquinolinone allosteric modulators. *Bioorg. Med. Chem.* 27, 3167–3178. doi: 10.1016/j.bmc.2019.06.006

Simeone, X., Siebert, D. C. B., Bampali, K., Varagic, Z., Treven, M., Rehman, S., et al. (2017). Molecular tools for $GABA_A$ receptors: high affinity ligands for β1-containing subtypes. *Sci. Rep.* 7:5674. doi: 10.1038/s41598-017-05757-4

Tretter, V., Hauer, B., Nusser, Z., Mihalek, R. M., Höger, H., Homanics, G. E., et al. (2001). Targeted disruption of the GABA(A) receptor δ subunit gene leads to an up-regulation of γ2 subunit-containing receptors in cerebellar granule cells. *J. Biol. Chem.* 276, 10532–10538. doi: 10.1074/jbc.M011054200

Treven, M., Siebert, D. C. B., Holzinger, R., Bampali, K., Fabjan, J., Varagic, Z., et al. (2018). Towards functional selectivity for α6β3γ2 $GABA_A$ receptors: a series of novel pyrazoloquinolinones. *Br. J. Pharmacol.* 175, 419–428. doi: 10.1111/bph.14087

Varagic, Z., Ramerstorfer, J., Huang, S., Rallapalli, S., Sarto-Jackson, I., Cook, J., et al. (2013a). Subtype selectivity of α+β- site ligands of $GABA_A$ receptors: identification of the first highly specific positive modulators at α6β2/3γ2 receptors. *Br. J. Pharmacol.* 169, 384–399. doi: 10.1111/bph.12153

Varagic, Z., Wimmer, L., Schnürch, M., Mihovilovic, M. D., Huang, S., Rallapalli, S., et al. (2013b). Identification of novel positive allosteric modulators and null modulators at the $GABA_A$ receptor α+β− interface. *Br. J. Pharmacol.* 169, 371–383. doi: 10.1111/bph.12151

Vasović, D., Divović, B., Treven, M., Knutson, D. E., Steudle, F., Scholze, P., et al. (2019). Trigeminal neuropathic pain development and maintenance in rats are suppressed by a positive modulator of α6 $GABA_A$ receptors. *Eur. J. Pain* 23, 973–984. doi: 10.1002/ejp.1365

Wisden, W., Laurie, D. J., Monyer, H., and Seeburg, P. H. (1992). The distribution of 13 $GABA_A$ receptor subunit mRNAs in the rat brain. I. Telencephalon, diencephalon, mesencephalon. *J. Neurosci.* 12, 1040–1062. doi: 10.1523/JNEUROSCI.12-03-01040.1992

Zhu, S., Noviello, C. M., Teng, J., Walsh, R. M. Jr., Kim, J. J., and Hibbs, R. E. (2018). Structure of a human synaptic $GABA_A$ receptor. *Nature* 559, 67–72. doi: 10.1038/s41586-018-0255-3

Conflict of Interest: The authors declare that the research was conducted in the absence of any commercial or financial relationships that could be construed as a potential conflict of interest.

Copyright © 2020 Scholze, Pökl, Längle, Steudle, Fabjan and Ernst. This is an open-access article distributed under the terms of the Creative Commons Attribution License (CC BY). The use, distribution or reproduction in other forums is permitted, provided the original author(s) and the copyright owner(s) are credited and that the original publication in this journal is cited, in accordance with accepted academic practice. No use, distribution or reproduction is permitted which does not comply with these terms.

frontiers in Synaptic Neuroscience

REVIEW
published: 23 October 2020
doi: 10.3389/fnsyn.2020.588954

The Creatine Transporter Unfolded: A Knotty Premise in the Cerebral Creatine Deficiency Syndrome

*Clemens V. Farr, Ali El-Kasaby, Michael Freissmuth and Sonja Sucic**

Institute of Pharmacology, Center of Physiology and Pharmacology, Medical University of Vienna, Vienna, Austria

Creatine provides cells with high-energy phosphates for the rapid reconstitution of hydrolyzed adenosine triphosphate. The eponymous creatine transporter (CRT1/SLC6A8) belongs to a family of solute carrier 6 (SLC6) proteins. The key role of CRT1 is to translocate creatine across tissue barriers and into target cells, such as neurons and myocytes. Individuals harboring mutations in the coding sequence of the human CRT1 gene develop creatine transporter deficiency (CTD), one of the pivotal underlying causes of cerebral creatine deficiency syndrome. CTD encompasses an array of clinical manifestations, including severe intellectual disability, epilepsy, autism, development delay, and motor dysfunction. CTD is characterized by the absence of cerebral creatine, which implies an indispensable role for CRT1 in supplying the brain cells with creatine. CTD-associated variants dramatically reduce or abolish creatine transport activity by CRT1. Many of these are point mutations that are known to trigger folding defects, leading to the retention of encoded CRT1 proteins in the endoplasmic reticulum and precluding their delivery to the cell surface. Misfolding of several related SLC6 transporters also gives rise to detrimental pathologic conditions in people; e.g., mutations in the dopamine transporter induce infantile parkinsonism/dystonia, while mutations in the GABA transporter 1 cause treatment-resistant epilepsy. In some cases, folding defects are amenable to rescue by small molecules, known as pharmacological and chemical chaperones, which restore the cell surface expression and transport activity of the previously non-functional proteins. Insights from the recent molecular, animal and human case studies of CTD add toward our understanding of this complex disorder

OPEN ACCESS

Edited by:
Joerg Striessnig, University of Innsbruck, Austria

Reviewed by:
Matthew Skelton, University of Cincinnati College of Medicine, United States
Lara Gechijian, Jnana Therapeutics, United States

***Correspondence:**
Sonja Sucic
sonja.sucic@meduniwien.ac.at

Received: *30 July 2020*
Accepted: *18 September 2020*
Published: *23 October 2020*

Citation:
Farr CV, El-Kasaby A, Freissmuth M and Sucic S (2020) The Creatine Transporter Unfolded: A Knotty Premise in the Cerebral Creatine Deficiency Syndrome. Front. Synaptic Neurosci. 12:588954. doi: 10.3389/fnsyn.2020.588954

Abbreviations: ADHD, attention deficit hyperactivity disorder; AGAT, L-Arginine:glycine amidinotransferase; AMPK, AMP-activated protein kinase; BBB, blood-brain barrier; CCDS, cerebral creatine deficiency syndrome; CFTR, cystic fibrosis transmembrane conductance regulator; CK, creatine kinase; CNX, calnexin; CRT1, creatine transporter-1; CTD, creatine transporter deficiency; DAT, dopamine transporter; ER, endoplasmic reticulum; ERAD, ER-associated degradation; GAA, guanidino acetic acid; GABA, γ-aminobutyric acid; GAMT, guanidinoacetate N-methyltransferase; GAT-1, GABA transporter 1; GLYT, glycine transporter; GPA, β-guanidino propionic acid; NET, norepinephrine transporter; 4-PBA, 4-phenyl butyrate; SERT, serotonin transporter; SLC6, solute carrier 6; TMD, transmembrane domain.

and reveal the wide-ranging effects elicited upon CRT1 dysfunction. This grants novel therapeutic prospects for the treatment of patients afflicted with CTD, e.g., modifying the creatine molecule to facilitate CRT1-independent entry into brain cells, or correcting folding-deficient and loss-of-function CTD variants using pharmacochaperones and/or allosteric modulators. The latter justifies a search for additional compounds with a capacity to correct mutation-specific defects.

Keywords: creatine, intellectual disability, creatine transporter 1, creatine transporter deficiency, protein misfolding, pharmacochaperoning, SLC6A8

THE CREATINE TRANSPORTER DEFICIENCY (CTD) SYNDROME

Creatine transporter deficiency (CTD) is one of the known genetic causes of cerebral creatine deficiency syndromes (CCDS). In CTD, creatine is incapable of entering the brain cells *via* the designated creatine transporter 1 (CRT1). The remaining two CCDS disorders are caused by deficiencies in the enzymes arginine: glycine amidinotransferase (AGAT) and guanidinoacetate methyltransferase (GAMT), which are required for creatine synthesis in the body. All three deficiencies result in the absence of creatine in the brain. Because creatine is fundamental to normal brain development and function, the most frequent and core phenotype of CTD, and CCDS overall, is marked intellectual disability. Apart from this predicament, the clinical picture of the disease manifests in a complex spectrum of additional clinical symptoms including epileptic seizures, development delay (language and walking), behavior problems (autism, attention deficit hyperactivity disorder (ADHD), motor dysfunction (lack of coordination and dystonia), failure to thrive, and gastrointestinal problems (neonatal feeding difficulties, vomiting, constipation and ulcers).

AGAT and GAMT deficiencies affect males and females comparably, as they are inherited in an autosomal recessive manner. CTD, on the other hand, is an X-linked disease and as such predominantly impacts the male population. CTD is caused by mutations in the *SLC6A8* gene (mapped to Xq28), encoding the CRT1 protein. The mutations give rise to CRT1 variants, which dramatically reduce or abolish creatine uptake activity. To date, over 80 pathogenic variants have been identified in the human CRT1 gene. Detailed clinical indications have already been reported for specific point mutations (**Table 1**). The severity of CTD appears to correlate to residual CRT1 activity; e.g., A404P and P544L, both maintained 5–15% of wild type transporter creatine uptake levels in patient fibroblasts (Mancini et al., 2005; Alcaide et al., 2010) and HEK293 cells (El-Kasaby et al., 2019), and manifested in moderate intellectual disability. The fully inactive P382L variant, on the other hand, elicited a severe form of CTD in the afflicted patients (Mercimek-Mahmutoglu et al., 2009). According to van de Kamp and colleagues, the prevalence of CTD in males with intellectual disability lies between 0.4 and 1.4% (van de Kamp et al., 2014). The estimated carrier prevalence of CTD in females in the general population is a minimum of 0.024% (DesRoches et al., 2015). The true prevalence of CTD worldwide is probably underestimated, partly due to misdiagnosis (e.g., some patients diagnosed with autism, ADHD, or unexplained intellectual disability). Intellectual disability was estimated to have a prevalence of 1% in the general population (McKenzie et al., 2016), and although CTD is a rare disease, it is a significant and underappreciated cause of this condition.

About 20–30% of all CTD variants are thought to be caused by *de novo* mutations (DesRoches et al., 2015). The actual frequency of *de novo* mutations is unknown, but the emerging state-of-the-art genetic tests, such as trio (father, mother, child) based exome sequencing (Kreiman and Boles, 2020) ought to improve the diagnostic approaches for CTD. In the occurrence of CTD mutations, all males, and about 50% of the affected females, typically display intellectual and cognitive dysfunction (DesRoches et al., 2015). Despite CTD being an X-linked disease, females carrying heterozygous pathogenic mutations have been identified, albeit the extent of disease severity is comparatively mild, e.g., female relatives of CTD patients harboring the G381R and R514X mutations have only minor neuropsychological impairments. It is not entirely clear why some women are protected/asymptomatic carriers, while others are susceptible and develop CTD. The source of variability among female carriers can be rationalized by several factors. (i) Lyonisation or random X-inactivation (Davidson, 1964; Migeon, 2020), may clarify how a phenotypic consequence of the X chromosome can be manifested in mammalian females and males alike, despite females having two somatic X chromosomes and males only one. In females, one X chromosome undergoes inactivation during early embryonic development, such that the end quantities of X-linked gene products in females and males are similar. X-inactivation is random and incomplete, and some segments of the silenced X chromosome can escape inactivation. Females can thus be genetic mosaics, i.e., pathogenicity is ameliorated because the variant is not expressed in all their cells, in contrast to the hemizygous males, who express the pathogenic variant allele in every cell (Migeon, 2020). (ii) In some cases, females manifest the disease because the pathogenic variant interacts with the healthy allele in a dominant-negative manner. (iii) Clinical phenotypes can also be shaped by so-called modifier genes, which alter the expression of other genes, e.g., specific modifiers can differentially affect the incidence, severity as well as the time of onset of target gene diseases, as already reported for e.g., cystic fibrosis, epilepsy and sickle cell disorder (Riordan and Nadeau, 2017). Nonetheless, no such modifier genes have been identified in female carriers of pathogenic CRT1 mutations to date, and future studies may clarify the contribution of this mechanism to the clinical variability among female carriers of CTD.

TABLE 1 | Point mutations in human creatine transporter 1 (CRT-1) with the consequent CTD phenotypes.

Variant	Clinical phenotype	References
P31L	Seizures, speech and motor delay, and thalamus atrophy	Rostami et al. (2020)
G87R	Intellectual disability	Rosenberg et al. (2004)
G132V	Intellectual disability	Lion-François et al. (2006)
R207W	Global developmental delays, hypotonia, intellectual disability, and language apraxia	Ardon et al. (2016)
G253R	Mild intellectual disability and language delay	Battini et al. (2011)
N331K	Speech delay, seizures, and hyperactivity	Mencarelli et al. (2011)
C337W	Intellectual disability	Rosenberg et al. (2004)
G356V	Epilepsy and mild intellectual disability	Mercimek-Mahmutoglu et al. (2009)
G381R	Intellectual disability, seizures, speech, and behavioral disturbance, hypotonia, and gastrointestinal problems	Hahn et al. (2002)
P382L	Severe intellectual disability, speech delay, behavioral problems, and epilepsy	Mercimek-Mahmutoglu et al. (2009)
P390L	Intellectual disability, learning difficulties, seizures, hyperactive and impulsive behavior	Rosenberg et al. (2004) and Heussinger et al. (2017)
R391W	Seizures, hyperactivity, aggressiveness, and hyperphagia	Mencarelli et al. (2011)
T394K	Intellectual disabilities, severe developmental delay and speech impairment, seizures, and mild scale autism	Wang et al. (2018)
A404P	Mild psychomotor retardation and language impairments	Alcaide et al. (2010)
G424D	Speech and language delay, learning difficulties, mild autistic features, social anxiety and attention deficit, aggressiveness, impulsiveness, and hyperactivity	Puusepp et al. (2010)
G466R	Developmental delay, dystonia, no speech, and epilepsy	Alcaide et al. (2011)
D474G	Mild intellectual disability and occasional febrile seizures	Bruun et al. (2018)
C491W	Generalized tonic-clonic seizures	Lion-François et al. (2006)
M510K	Moderate intellectual disability, antiepileptic drug-responsive seizures, hypotonia, and dysarthria	Bruun et al. (2018)
P544L	Moderate intellectual disability, generalized hypotonia, delayed language, and speech skills, and multifocal epileptic waves	Mancini et al. (2005)
P554L	Intellectual disability, hypotonia, intellectual disability, severe speech delay, seizures, autism, and epilepsy	Rosenberg et al. (2004) and Nozaki et al. (2015)
G561A	Intellectual disability	Kato et al. (2014)
F315del	Intellectual disability, epilepsy, autism, and speech delay	Fons et al. (2009)
N336del	Intellectual disability, seizures, and motor dyspraxia	Battini et al. (2007)
I347del	Moderate intellectual disability, aggressive behavior, and seizures	Clark et al. (2006)
F354del	Intellectual disability	Betsalel et al. (2008)
F360del	Intellectual disability, epilepsy, autism, and speech delay	Fons et al. (2009) and Sempere et al. (2009)
F408del	Intellectual disability, epilepsy, autism, seizure, speech and language delay and a reduced interest in the surroundings	Bizzi et al. (2002) and Póo-Argüelles et al. (2006)

Only those CTD variants with identified clinical symptoms are listed, according to the reports available in the literature to date.

UNRAVELING THE INTRICATE CLINICAL PHENOTYPE OF CTD

The Brain as a Core Source of the Most Severe Symptoms in CTD

All individuals afflicted with CTD suffer from mild to severe impairment of brain function, which is explicable considering the lack of creatine supply to brain cells. Apart from the robust expression in the brain, CRT1 is also present in other tissues, justifying some of the peripheral symptoms of CTD in the affected individuals (**Figure 1**). In the human brain, CRT1 shows the highest expression in the pyramidal neurons in the cerebral cortex, Purkinje cells of the cerebellar cortex, hippocampus, and motor neurons of the somatic motor and visceromotor cranial nerve nuclei and the ventral horn of the spinal cord (Lowe et al., 2015). CTD impinges on many cerebral tasks, apart from the vital functions supported by the brainstem, which are selectively spared. The brainstem is phylogenetically a very old part of the brain, implying that CRT1 expression peaked only recently in hominid phylogeny. Moreover, CRT1 expression is much higher in the human brain compared to other primates, leading to the hypothesis that the energetic demand of encephalization (i.e., the emergence of intellect) was met by increased meat (that is, creatine) consumption during evolution (Pfefferle et al., 2011). Intellectual disability epitomizes the unifying symptom in all CTD cases, while other neural and extraneural functions remain affected to variable degrees.

Many of the brain symptoms of CTD were probed using mouse models of the disease. The hippocampus is a crucial neuroanatomical component in cognitive deficits related to CTD. Hippocampi of CRT1-deficient mice had lipofuscin accumulation, reduced volume, and reduced adult neurogenesis (Baroncelli et al., 2016). CRT1-knockout mice mirrored the cognitive phenotypes of CTD in people. The mice displayed poor performance in Morris Water Maze, novel object recognition, radial arm- and Y-maze tests (Skelton et al., 2011; Kurosawa et al., 2012; Baroncelli et al., 2014, 2016; Udobi et al., 2018; Molinaro et al., 2019). Collectively, these studies ratified the link between dysfunctional CRT1 and learning disabilities and impairments in declarative long-term as well as working memory. Importantly, it may also be concluded that the employed animal models accurately imitate the predominant human CTD symptoms (van

de Kamp et al., 2014). Cognitive deficiencies deteriorated with age in a murine model, alluding to the indispensable role of CRT1 in postnatal development of cognitive skills (Baroncelli et al., 2016; Molinaro et al., 2019). Conditional deletion of CRT1 in mice at postnatal day 5 led to cognitive deficits, whereas deletion at day 60 did not (Udobi et al., 2019). Therefore, cognitive symptoms in CTD may be preventable. Pre-symptomatic treatment with creatine in AGAT- and GAMT-deficiencies, in fact, did prevent further development of central nervous system symptoms in CCDS patients (Battini et al., 2006; Schulze et al., 2006).

Epileptic seizures are one of the most severe clinical symptoms of CTD, with many patients suffering from treatment-resistant epilepsies. The seizure phenotype has yet to be mimicked in the genetic mouse models of CTD. Likewise, autism is frequent among CTD patients (van de Kamp et al., 2014), but not entirely reflected in CRT1-deficient mice, possibly owing to the general difficulty of modeling autistic traits in rodents (Skelton et al., 2011; Baroncelli et al., 2016). ADHD is another common symptom of CTD (van de Kamp et al., 2014). CRT1-knockout mice exhibited hyperactive behavior (Kurosawa et al., 2012; Udobi et al., 2018, 2019; Molinaro et al., 2019). Hyperactivity was one of the few symptoms also observed in female mice (Hautman et al., 2014), closely reflecting the clinical portrait of CTD in people. The dopaminergic system was proposed to play a part in CTD-linked hyperactivity: CRT1-deletion from dopaminergic neurons was sufficient to trigger hyperactivity in mice (Abdulla et al., 2020a). However, this is difficult to reconcile with the low expression levels of CRT1 in dopaminergic neurons in people (Lowe et al., 2015). CTD may be linked to incoherent synaptic transmission, evident from patient fibroblasts having a discrepant expression pattern of synapse-linked genes (Nota et al., 2014). Studies of the monoaminergic system in the brains of CRT1 knockout mice revealed no major changes in dopamine, norepinephrine, or serotonin levels (Skelton et al., 2011; Abdulla et al., 2020b). The amount of γ-aminobutyric acid (GABA) and its metabolites was unfortunately not measured, although the GABAergic system is likely to be involved in CTD-related epilepsy. CRT1-deficient mice have less vesicular GABA transporters (Baroncelli et al., 2016). Also, succinate-semialdehyde dehydrogenase and GABA transaminase were upregulated, along with mitochondrial pyridoxal kinase in CRT1-deficient mouse brains (Giusti et al., 2019). Increased pyridoxal kinase activity in CRT1 knockout mice translates into higher levels of pyridoxal phosphate, a potent modulator of GABA synthesis, degradation, and uptake (Norris et al., 1983; Jung et al., 2019). Moreover, one clinical study reported drastically higher levels of guanidino acetic acid (GAA) in CTD patient brain tissues, with virtually no detectable creatine (Sijens et al., 2005). Increased GAA levels were also detected in CRT1-knockout mice (Baroncelli et al., 2016; Udobi et al., 2018). GAA is a biosynthetic precursor of creatine and may impose on the GABAergic signaling in CTD: it activates $GABA_A$ receptors (Neu et al., 2002) and decreases the expression of glutamate decarboxylase and $GABA_B$ receptors (Hanna-El-Daher et al., 2015). Wild type CRT1 transports GAA during cerebral creatine synthesis (Braissant et al., 2010) and out of the cerebrospinal fluid (Tachikawa et al., 2008). Accordingly, the lack of functional CRT1 in CTD could lead to cerebral accumulation of GAA which, being an endogenous convulsant, may trigger epileptic seizures in CTD patients.

Skeletal and Heart Muscles in CTD

CTD patients frequently display a slender physique and hypotonia (van de Kamp et al., 2014). In CRT1-deficient mice, muscles are reduced in size and are also entirely devoid of creatine (Russell et al., 2014; Stockebrand et al., 2018). Muscle fiber atrophy, or rather reduced myocyte numbers, explain the poorly developed muscle mass and low endurance experienced by many CTD patients. Creatine content in the skeletal muscles of two CTD patients was surprisingly not declined (De Grauw et al., 2003; Pyne-Geithman et al., 2004), possibly due to residual CRT1 function in these particular variants (e.g., delF107). This was also the case for some murine models of the disease and may originate from compensatory upregulation of AGAT in the skeletal muscle (Russell et al., 2014; Stockebrand et al., 2018). Moreover, CRT1-independent creatine uptake may occur in skeletal muscles due to the absence of a semipermeable endothelial barrier. In contrast, the brain is enveloped by the blood-brain-barrier, which does not permit the entry of hydrophilic creatine molecules, making the cerebral symptoms of CTD far more severe than muscular defects. Also, motor function is less affected in CTD mice harboring a brain-specific knockout, as opposed to a global CRT1 knockout (Kurosawa et al., 2012; Udobi et al., 2018; Molinaro et al., 2019).

Creatine promotes myoblast differentiation, although a direct role for CRT1 in embryofetal muscle development remains to be confirmed (Deldicque et al., 2007). Intact CRT1 activity allows for maternal creatine supply during the fetogenesis of AGAT-deficient mice, which is absent in CTD (Stockebrand et al., 2018). Relative to CTD, muscular pathologies in AGAT-deficient mice are less pronounced (Nabuurs et al., 2013). CRT1 is abundantly expressed in lower motor neurons (Mak et al., 2009; Lowe et al., 2015), and its deficiency in CTD may be responsible for the muscular atrophy symptoms in people. Furthermore, reduced CRT1 levels in the primary motor cortex might cause the central motor symptoms such as spastic paresis (Mak et al., 2009; Lowe et al., 2015). To date, only two CTD patients are known to suffer from spasticity (Ardon et al., 2016; Rostami et al., 2020). The motor system is also affected by CRT1-expressing cerebellar Purkinje cells, which rank among the highest CRT1-expressing brain regions (Mak et al., 2009; Lowe et al., 2015). CRT1-deficient mice lack cerebral creatine (Molinaro et al., 2019), and consequently display poor motor learning and coordination (Stockebrand et al., 2018). An outcome of compromised cerebellar function is its contribution to the delayed motor skill development, which occurs in most CTD patients (van de Kamp et al., 2014).

The effects on cardiac muscle have been identified in only a few CTD patients (van de Kamp et al., 2013). Under normal physiological conditions, the heart contains

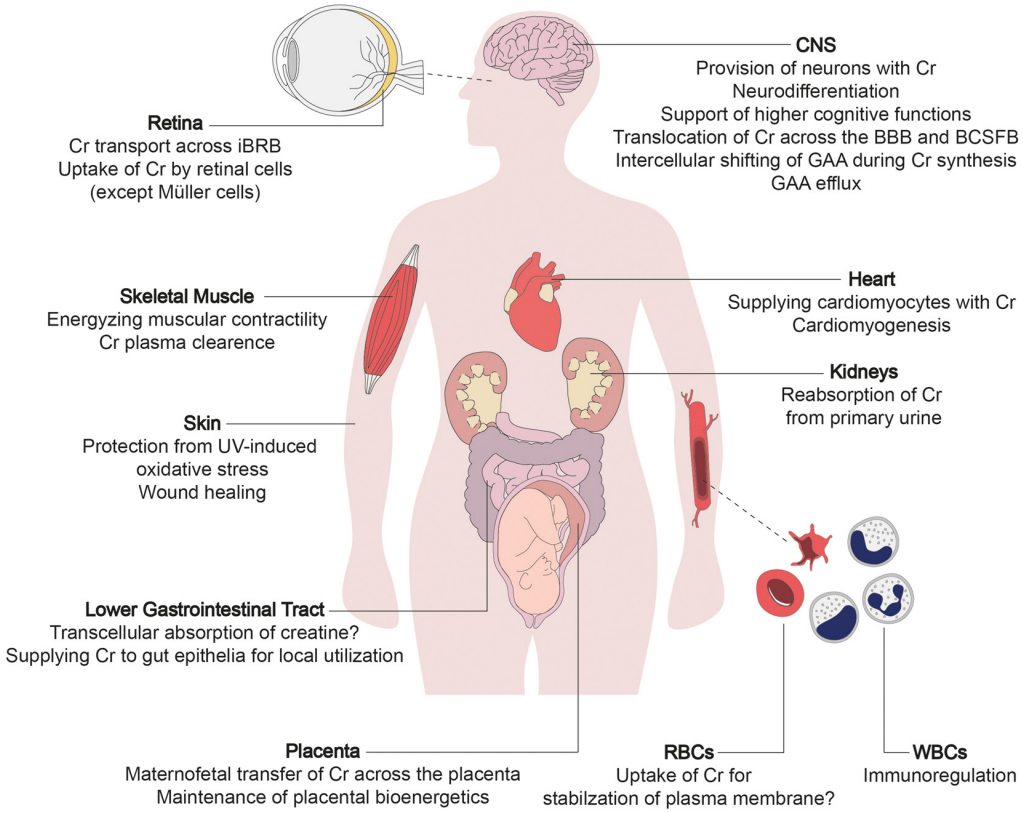

FIGURE 1 | The multi-layered physiological roles of creatine transporter 1 (CRT1). The primary function of creatine transporter 1 (CRT1) is to refill cellular creatine reserves, to compensate for its steady degradation (1.7% daily), in end-consumer cells incapable of self-synthesizing sufficient amounts of creatine (i.e., neurons, myocytes, and cardiomyocytes). CRT1 orchestrates creatine flux throughout the body by tuning the amount of creatine extracted from the blood by individual organs. CRT1 plays a key role in providing the brain with creatine, essential to higher cognitive functions. It shifts creatine across tissue barriers like the kidney tubules, the blood-brain barrier (BBB), and the inner blood-retinal barrier. It thus mediates reabsorption of creatine from the primary urine and facilitates the maintenance of cerebral and retinal tissue energetics, respectively. At the placenta, CRT1 takes up creatine, crucial for embryofetal development. It also supports the functioning and integrity of the intestinal barrier, and is an immunoregulator in leukocytes and stabilizes erythrocyte plasma membranes. Cr, creatine; BBB, blood-brain barrier; BCSFB, blood-cerebrospinal fluid barrier; iBRB, inner blood-retinal barrier; GAA, guanidinoacetate; RBC, red blood cell; WBC, white blood cell.

large amounts of creatine and expresses abundant amounts of CRT1. Yet, the heart seems to be one of the least affected organs in CTD (along with the retina, see below). Some CRT1-knockout mice have dramatically reduced heart tissue creatine levels, but do not display overt cardiac pathologies (Skelton et al., 2011; Baroncelli et al., 2014; Stockebrand et al., 2018). The discrepancies in human (and murine) cases of CTD may be down to the following: (i) underdiagnosis, i.e., CTD patients and animal models not undergoing appropriate medical examinations and experimental investigation, respectively; (ii) a later time of onset of the cardiac symptoms; (iii) heart tissues acquiring creatine in a CRT1-independent manner (as described above for skeletal muscles); and (iv) the cardiac phenotype may be contingent on the genetic background, which is consistent with the modifier gene concept. Such protective compensatory mechanisms on the heart add up because CRT1 is vital to cardiac function; i.e., the creatine-phosphocreatine circuit sustains cardiomyocytic bioenergetics (Guzun et al., 2011), and CRT1 plays a role in cardiomyogenesis, evident from enhanced myocardial expression of CRT1 upon cardiac maturation in rats (Fischer et al., 2010).

Effects on the Sensory Organs

High amounts of CRT1 are present in the retina (Acosta et al., 2005; Country, 2017), cochlea, and the auditory brainstem nuclei (Hiel et al., 1996; Wong et al., 2012). Still, this robust expression pattern does not inevitably provide a cue, as there is no evidence for impaired sight or hearing in CTD patients or in CRT1-deficient mouse models (Skelton et al., 2011). In CTD patients, the impaired hearing was proposed to contribute to the delay in speech development (van de Kamp et al., 2014). However, upon direct evaluation by brainstem auditory evoked potentials, the central auditory pathways appeared intact (Schiaffino et al., 2005; Rostami et al., 2020). Otoacoustic emission indicated hearing loss due to outer hair cell malfunction in one CTD patient (Hathaway et al., 2010). No major visual defects were reported in CTD patients, except for sporadic strabismus (Schiaffino et al., 2005; Yu et al., 2013), which can probably be ascribed to ocular myopathy. Visually evoked

potentials were assessed in a single CTD patient with no evidence of pathological changes, while compromised ocular fundus was reported in one out of three cases examined (Schiaffino et al., 2005; Anselm et al., 2006). The lack of the anticipated defects in the retina of CTD cases may ensue from compensatory processes such as cell-autonomous creatine synthesis in retinal neurons and/or glia, which presumably sustain adequate amounts of creatine.

Further Aspects of CTD: Immunity and Cellular Metabolic Networks

CRT1 supports the balance between two types of macrophage activation (Ji et al., 2019). Furthermore, creatine uptake was recently found to modulate CD8 T-cell response to antigen exposure (Di Biase et al., 2019). CRT1 is expressed in leukocytes (Taii et al., 2020) and macrophages (Loike et al., 1986; Lowe et al., 2015; Heinbockel et al., 2018; Ji et al., 2019). Since CRT1-activity was detected in lymphoblastoid cells derived from a CTD patient, it is conceivable that CRT1 has an immunoregulatory role in the body (Leuzzi et al., 2008). CTD mouse models also exhibit a marked increase in activated microglia (Baroncelli et al., 2016). Moreover, the brains of CRT1-deficient animals show an upregulation in cyclophilin A (Giusti et al., 2019), an immune effector molecule whose secretion is enhanced in many inflammatory conditions (Nigro et al., 2013). Both findings constitute unspecific reactions to cellular damage in CTD. Early and late apoptosis was observed in skin fibroblasts cultured from CTD patients with marked increases in reactive oxygen species levels (Alcaide et al., 2011). This is consistent with creatine having antiapoptotic and antioxidant properties (Lawler et al., 2002; Rahimi et al., 2015). In fact, creatine has been in clinical use for its neuroprotective effects (Sullivan et al., 2000; Sakellaris et al., 2006). Also of interest is a report of a novel CRT1 inhibitor, shown to suppress cancer growth and metastatic progression (Kurth et al., 2018), which implicates CRT1 in cancer and prompts a closer survey of cancer incidence among CTD patients.

Creatine is immersed in the metabolic network of cells. This balance is vulnerable and cells have developed compensatory mechanisms to cope with reduced creatine concentrations, e.g., upregulation of AGAT in kidneys and, albeit to an insufficient extent, in muscles of CRT1-deficient rodents (Russell et al., 2014; Stockebrand et al., 2018). Also, decreases in cellular energy reserves cause a multitude of mitochondrial adaptions in models of CTD. The upregulation of oxidative enzymes was confirmed by proteomic analysis of brain mitochondria in CRT1-knockout mice (Giusti et al., 2019). The increase in mitochondrial density may compensate for the lack of spatial ATP buffering, by decreasing the distance of diffusion (Oudman et al., 2013). Furthermore, inhibition of CRT1 leads to the upregulation of mitochondrial creatine kinase (CK) in striated muscles (Oudman et al., 2013). A rise in mitochondrial respiration in the hippocampus and skeletal muscle fibers was also observed in CRT1-deficient mice, accompanied by increased O_2 and CO_2 consumption assessed by whole-body calorimetry (Perna et al., 2016). Lastly, CRT1-deficient cells down-regulate the mitochondrial uncoupling protein 3, which is likely to limit energy dissipation in the form of heat (Stockebrand et al., 2018). Moreover, the AMP-activated protein kinase (AMPK) is activated by low energy levels and drives ATP production *via* multiple pathways. AMPK is activated in CRT1-deficient and β-guanidino propionic acid (GPA, CRT1 inhibitor)-fed animals (Oudman et al., 2013; Stockebrand et al., 2018). This response to low ATP levels likely aggravates the decreased creatine reabsorption from urine, since AMPK negatively regulates CRT1 expression in kidney epithelia (Li et al., 2010). Conversely, AMPK activation increases creatine uptake in cardiomyocytes (Darrabie et al., 2011). AMPK signaling may underlie the upregulation of fatty acid transporter proteins and glucose uptake *via* GLUT4 observed in animal models of CTD (Oudman et al., 2013; Stockebrand et al., 2018). In addition to stimulating the AMPK pathway, reduced creatine uptake triggers the activation of the mitogen-activated protein kinase 1 (MAPK/ERK) pathway (Giusti et al., 2019), and disturbed ERK1/2 activity has already been linked to intellectual disability (Kalkman, 2012; Pucilowska et al., 2015, 2018; Borrie et al., 2017). Many signaling pathways become activated in nerve and other cells, as they cannot meet their energy demands during sustained activity. Thus, changes in AMPK, MAPK/ERK, and other pathways reflect the malfunctioning of the brain and the altered synaptic transmission in CTD. Exploring cellular compensatory mechanisms as opportunities for alternative CTD treatments, though arduous, may be worthwhile.

MOLECULAR FEATURES OF CTD

CTD Effects on Neuron Cells: CRT1 Out-of-Place

The neurologic phenotype of CTD is by far the direst of all clinical manifestations of the disease. It is presumed that brain cells depend on local creatine synthesis since the expression levels of CRT1 at the blood-brain barrier (BBB) are comparatively low and the permeability of creatine through the BBB is limited. Indeed, AGAT and GAMT are expressed in neurons, oligodendrocytes, and astrocytes (Braissant et al., 2001, 2010; Tachikawa et al., 2004; Braissant and Henry, 2008). The two enzymes are rarely co-expressed, necessitating the intercellular translocation of the creatine precursor GAA (Braissant et al., 2010). This is most likely achieved by CRT1, which is predominantly expressed in the soma and proximal dendrites of neurons and to a lesser degree in oligodendrocytes and microglia (Braissant et al., 2010; Lowe et al., 2015). Cells with high energetic demands, such as hippocampal pyramidal neurons and Purkinje cells, all express AGAT, GAMT, and CRT1. CRT1 translocates GAA with an affinity 10-fold lower than that of creatine (Tachikawa et al., 2008). Plasma GAA levels are well below creatine levels (Almeida et al., 2004), so extracerebral GAA is not likely to contribute to neuronal creatine synthesis. Hence, in the absence of functional CRTs, brain cells are deprived of their essential energy resource, creatine. However, from a different perspective, one may argue that the capacity of BBB to translocate creatine must not be very high and is capable of sufficiently replacing the lost creatine.

Moreover, overexpression of CRT1 in the heart disrupts cardiac bioenergetics, implying that tight regulation of CRT1 expression prevents large increases in creatine concentrations (Wallis et al., 2005). Thus, although the hypothesis that the rodent brain can synthesize creatine is reasonably valid, further experimental evidence is required to grasp these mechanisms. One of the most highly CRT1-expressing cells in the brain are hippocampal neurons, whereby the transporter is delivered to both dendritic and axonal compartments (Dodd et al., 2010). We recently tracked fluorescently-tagged human CRT1 transiently transfected in primary rat hippocampal neurons: the transporter was targetted to the arborizations of neurite extensions and their distal tips. Quite an altered expression pattern was shown by the CTD variant P544L (**Table 1**), which was confined to the neuronal soma and reached only the proximal neurite segments (El-Kasaby et al., 2019). Thus, defective trafficking of variant CRT1 proteins poses one feasible trigger, at least for some CTD-linked variants. Disease mutations can elicit dysfunction either by interfering with cellular processing (e.g., P544L) or by disrupting protein function. A large number of CTD variants are known to cluster in the region encompassing transmembrane domains (TMDs) 7 and 8, a mutation hot spot (Freissmuth et al., 2018), which delineates the creatine translocation pathway in CRT1 (**Figure 2**). It is hence not surprising that mutations in this very region abolish transporter activity.

CTD and Key Insights From SLC6 Transporters Folding and Trafficking

Many CTD variants have been associated with aberrant glycosylation, intracellular retention, and reduced surface expression (Uemura et al., 2017; El-Kasaby et al., 2019). Evidence for proteostatic deficiencies in several CTD mutants was also substantiated by data from the Schlabach group (Salazar et al., 2020). Nascent membrane proteins in the endoplasmic reticulum (ER) are core-glycosylated. After export from the ER, they acquire mature N-linked glycans in the Golgi apparatus. We recently took advantage of glycosidases with different glycan cleavage patterns to demonstrate that 16 CTD-linked variants exhibit an immature glycosylation pattern (El-Kasaby et al., 2019). The mutant proteins also co-localized with the ER-resident chaperone calnexin (El-Kasaby et al., 2019), suggestive of misfolding and ER-retention. Much of the understanding of SLC6 protein folding and trafficking is shaped by paradigmatic studies of the serotonin transporter (SERT) in our laboratory (El-Kasaby et al., 2010; Koban et al., 2015; Kasture et al., 2019). Nascent SLC6 proteins are engaged by various ER-resident chaperones, such as calnexin and a relay of cytosolic chaperones that interact with the transporters' C-tail regions (Sucic et al., 2016), which serve as molecular folding sensors along the stringent ER quality control cascade. Hence, manipulating different components of the folding trajectory (detailed below) proved effective in the rescue of many misfolded SLC6 transporters, i.e., proper folding permits ER export and trafficking of the client proteins to their designated sites of action in cells.

The sequence of folding events taking place at the level of ER is meticulous. The ribosome is first recruited to the ER membrane *via* the signal recognition particle (SRP) and the SRP receptor, where the translation arrest is lifted and the transmembrane helices are co-translationally inserted into the translocon/SEC61 channel. In the translocon channel, hydrophobic residues of the nascent chain are shielded from the hydrophilic environment. After the lateral exit of transmembrane segments into the lipid bilayer and N-linked glycosylation, transporter proteins undergo the calnexin cycle on the lumenal side of the ER. On the cytosolic side, the C-terminus is engaged by a heat shock protein relay (e.g., HSP40, 70, and 90) to assist folding and impede premature engagement of the coat protein complex II (COPII)-coat. ER-resident, lumenal chaperones are recruited to the folding intermediates: calnexin recognizes the (re)glycosylated folding intermediates *via* its lectin domain. Upon reaching the minimum energy state (i.e., the stably folded conformation), the chaperones are released. The transporters subsequently form oligomeric complexes and recruit the cognate SEC23/SEC24-dimers (Sucic et al., 2011, 2013) to specific ER exit motifs located on their C-termini. The bow-tie shape of the COPII-component SEC23/SEC24 prompts membrane curvature of the budding COPII vesicles *en route* to the Golgi (**Figure 3**). Severely misfolded proteins remain bound to calnexin and HSPs and are at last destined for ER-associated degradation (ERAD).

The inheritance pattern of many folding diseases in SLC6 transporters can be rationalized by oligomerization, which takes place at the final stage of folding immediately before the concentrative export of COPII vesicles from the ER compartment. Synthetic ER export-deficient mutations in the C-terminal region of GAT1 elicit a dominant-negative effect on the wild type transporter (Just et al., 2004; Farhan et al., 2007), which also pertains to disease variants: i.e., dominant-negative phenotypes evident for misfolded variants NET-A457P (Hahn et al., 2002) and GLYT2-S510R (Rees et al., 2006; Giménez et al., 2012; Arribas-González et al., 2015). In recessive transmission, misfolded proteins remain trapped by lumenal chaperones in the ER, precluding oligomerization with wild type alleles; e.g., many hyperekplexia variants in GLYT2 (Eulenburg et al., 2006; Rees et al., 2006) or parkinsonism variants in DAT (Kurian et al., 2009, 2011; Ng et al., 2014).

The majority of CTD mutations are located in the hydrophobic core of CRT1 (**Figure 2**). This is predictable since the interaction of TMDs and the lipid bilayer represents a critical factor in SLC6 transporter folding. In the lipid bilayer, transmembrane segments of nascent SLC6 transporters rearrange to adopt an annular topology, which requires lipid displacement from surfaces of 12 α-helical TMDs, facing one another or away from the translocation pathway (Sucic et al., 2016). The same problem was observed for folding-disease variants in other SLC6 transporters (Freissmuth et al., 2018): e.g., infantile parkinsonism/dystonia in the dopamine transporter (DAT; Kurian et al., 2009, 2011; Ng et al., 2014), epilepsy in the GABA transporter 1 (GAT1), orthostatic intolerance in the transporter for norepinephrine (NET; Hahn et al., 2002) and hyperekplexia in the glycine transporter 2 (GLYT2; Eulenburg et al., 2006; Rees et al., 2006; Arribas-González et al., 2015). Remarkably, certain mutations occur at equivalent residues and give rise to diseases conveyed by the affected transporter:

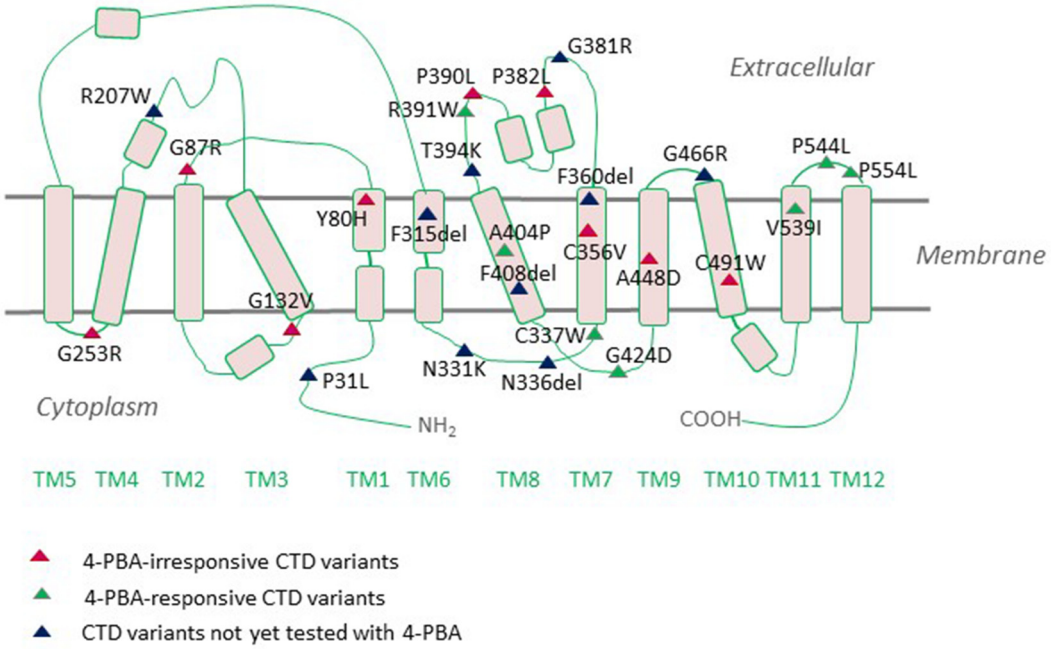

FIGURE 2 | Creatine transporter deficiency (CTD)-associated variants mapped onto a CRT1 topology. CRT1 adopts the common structural fold of SLC6 proteins with 12 transmembrane domains (TMs) and cytoplasmic N- and C-termini. Most of the reported sequence alterations in CTD cluster in the region encompassing TMDs 7 and 8. Only those variants with the ascertained clinical phenotypes are displayed on the topology. Sixteen mutations are known to be folding-deficient. Individual mutants vary in their response to the chemical chaperone 4-PBA.

e.g., the folding-deficient missense variant P554L reported both in CRT1 and DAT, triggers severe CTD and Parkinsonism, respectively. Then again, not all of the folding rules, founded on SERT and DAT, necessarily reconcile with CRT1. For example, most SLC6 relatives of CRT1 (DAT, SERT, NET, GAT1, and GLYTs), rely exclusively on their C-terminal domains for folding and trafficking (Farhan et al., 2007; El-Kasaby et al., 2010, 2014; Koban et al., 2015), with their N-termini being virtually dispensable (Sucic et al., 2010; Kern et al., 2017). CRT1 may be an exception to this rule, since the CTD variant P31L, located in the N-terminal region of the transporter, triggers severe functional deficits (Rostami et al., 2020).

THERAPEUTIC STRATEGIES FOR HANDLING CTD

The Explored Treatment Avenues: Modifying the Creatine Molecule

None of the treatment strategies explored to date have been effective in the long-term management of CTD. Oral supplementation with creatine or creatine precursors (i.e., arginine and glycine) improved the symptoms in some patients with mild CTD symptoms. This therapy appeared beneficial only in patients up to 9 years of age (Dunbar et al., 2014), possibly due to the remnant CRT1 activity in children (Taii et al., 2020) and some CTD variants exhibiting residual creatine uptake (Betsalel et al., 2012; El-Kasaby et al., 2019). Since creatine crosses the BBB very poorly (Ohtsuki et al., 2002; Perasso et al., 2003), some therapeutic approaches rely on boosting intracellular creatine pools using creatine analogs, capable of crossing the BBB and the neuronal plasma membrane (Adriano et al., 2017). Hence, salt-conjugated creatine formulations, which can cross BBB *via* transporters other than CRT1 [e.g., transporters for glucose (GLUTs) or ascorbic acid (SVCT2)], might prove beneficial in enhancing creatine concentrations in the brain. Creatine gluconate and creatine ascorbate increased the creatine content and delayed the population spike disappearance upon anoxia in mouse hippocampal slices, following the inhibition of CRT1 by GPA. But, both compounds failed to improve tissue levels of the energy reserve source, phosphocreatine (Adriano et al., 2017). An additional approach to facilitating creatine translocation into cells is by modifying its lipophilicity; e.g., a more lipophilic cyclocreatine may have therapeutic value, since it is also utilized by mitochondrial CK (Boehm et al., 2003). In CTD mouse models, a 9 week-treatment with a cGMP grade cyclocreatine led to its detection in the brain, hair and claws of the animals. Phosphocyclocreatine was also detected in the brain tissue of the treated mice, along with their spatial learning and memory also normalizing upon cyclocreatine treatment (Kurosawa et al., 2012). In studies carried out in human fibroblast cultures, the uptake of cyclocreatine, and the exchange rate of phosphocyclocreatine, was independent of CRT1, both in wild type and CTD patient cells (Gorshkov et al., 2019). On the other hand, high concentrations of cyclocreatine were associated

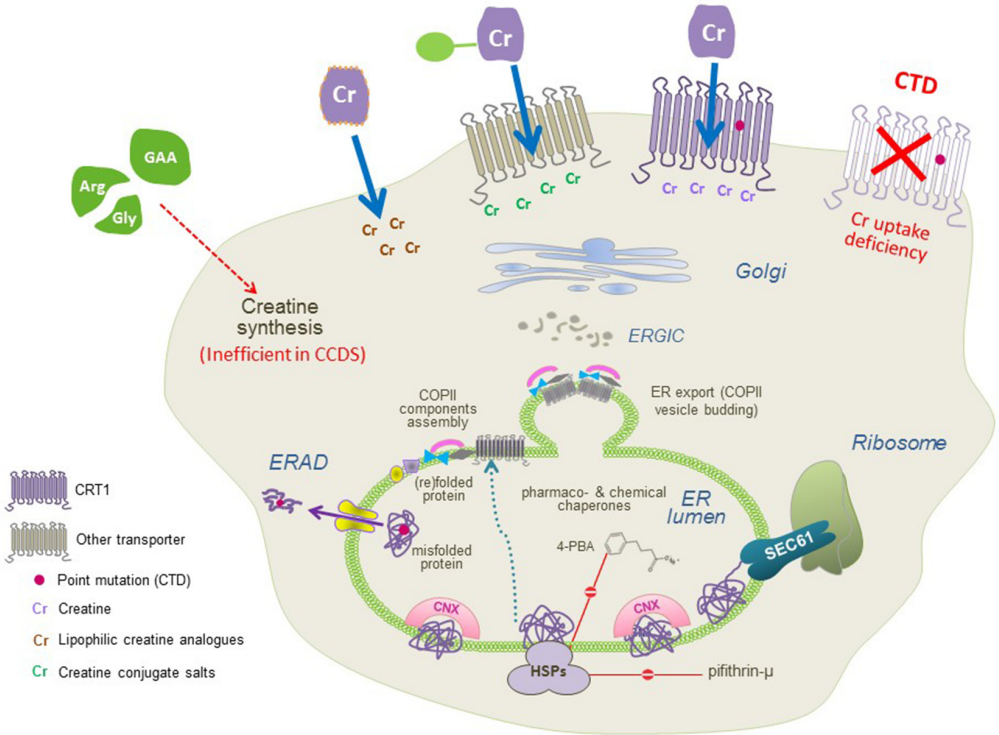

FIGURE 3 | A molecular view of CTD and the putative therapeutic approaches. CTD mutations trigger folding deficits or impair CRT1 substrate uptake activity (both resulting in the lack of functional CRT1 proteins at the cell surface; top right). Three approaches can be used to restore creatine supply in the cells: (1) conjugating creatine with salts, taken up by other transporters; and (2) creating lipophilic creatine analogs, to establish transporter-independent delivery of cyclocreatine, creatine benzyl, and fatty acid esters (top left), or (3) pharmacochaperoning to correct folding defects in CRT1 variants (recovering surface expression and creatine uptake activity of CTD mutant protein, top middle) by treatment with small molecules, that act either directly on the CRT1 itself (i.e., transporter ligands) or manipulate the cellular folding machinery (e.g., heat shock protein inhibitors and chemical chaperones).

with reduced ATP levels in both wild type and CTD patient fibroblasts, possibly owing to cyclocreatine dephosphorylation being slower than its phosphorylation (LoPresti and Cohn, 1989). Moreover, the clinical applicability of cyclocreatine is limited, since oral administration in rats set off seizures and showed histopathological changes in the thyroid, testes, and the brain (Kale et al., 2020). Creatine fatty esters were also tested for their ability to elevate cellular creatine levels. Incubating mouse hippocampal slices with creatine benzyl esters or with the phosphocreatine-magnesium acetate complex (at a ratio of 1:1), augmented the tissue creatine content in a CRT1-independent manner, albeit devoid of accompanying boosts in phosphocreatine levels (Lunardi et al., 2006). In CTD patient fibroblasts, dodecyl creatine ester accumulated in amounts comparable to healthy controls, and creatine content rose 20-fold relative to endogenous creatine amounts after a 1-hour treatment in CTD fibroblasts (Trotier-Faurion et al., 2013). Furthermore, lipid nanocapsules were used to overcome the action of plasma esterases, i.e., dodecyl creatine ester incorporated into lipid nanocapsules passed the BBB and increased creatine content in CTD fibroblasts (Trotier-Faurion et al., 2015). This approach may be beneficial in the therapeutic setting. Intracerebroventricular and intranasal administration of dodecyl creatine ester microemulsion to CTD mice, not only increased the creatine content in the brain but was also accompanied by enhanced learning and memory skills, evident from novel object recognition tests (Ullio-Gamboa et al., 2019). Significant efforts are ongoing in clinical programs conducted by Ultragenyx Pharmaceuticals, focusing on the development of new drug treatments for CTD.

Pharmacochaperoning: Rescue by Folding Correctors

Pharmacochaperoning is another putative treatment strategy for handling CTD, pertinent to the folding-deficient CRT1 variants. Pharmacological and chemical chaperones are small molecules that facilitate the folding and escape of misfolded proteins from the ER, consequently allowing their translocation to the appropriate cellular locations (Welch and Brown, 1996). Pharmacological chaperones are specific ligands (i.e., substrates or inhibitors) which bind to and stabilize the target proteins; e.g., noribogaine efficiently rescued several folding-deficient versions of SERT (El-Kasaby et al., 2014; Koban et al., 2015; Bhat et al., 2017) and parkinsonism variants of DAT (Kasture et al., 2019; Asjad et al., 2017). This is plausible since SLC6 protein folding proceeds *via* the inward-facing transporter conformation and noribogaine binds to the inward-facing conformation of monoamine transporters (Jacobs et al., 2007).

Noribogane treatment lowers the energy barrier between folding intermediates and facilitates the progression of transporter proteins along the folding trajectory. Inopportunely, the pharmacology of CRT1 is very modest compared to the rich ligand repertoire of the monoamine transporters (Kasture et al., 2017). Therefore, searching for potential pharmacochaperone (lead) compounds poses a challenge. The identification of lead molecules provides a platform for developing even more efficient pharmacochaperone analogs, which can bind to different protein conformations and hence correct additional misfolded mutants. Apart from the specific ligand, the rescue of folding-deficient proteins can also be achieved by manipulating/relaxing the ER quality control machinery, or by treatment with chemical chaperones (**Figure 3**). Pifithrin-μ and 17-dimethylaminoethylamino-17-demethoxygeldanamycin (17-DMAG) block HSP70 and HSP90β, respectively, which in turn permits the release of stalled transporter protein complexes (El-Kasaby et al., 2014). HSP blockers *per se* are not ideal chaperone compounds, because they do not act specifically on the misfolded transporters, and are predisposed to unwanted off target effects in a clinical setting.

Pharmacochaperoning has been proposed to work by one of the following four mechanisms: (i) binding to and stabilization of the native state; or (ii) of folding intermediate(s); (iii) suppression of aggregate formation; and (iv) dissolution of aggregates (Marinko et al., 2019). Most compounds, including noribogaine and bupropion (Beerepoot et al., 2016; Asjad et al., 2017), are thought to work *via* the first and/or second mechanism. Tafamidis, used in the treatment of transthyretin amyloidosis, is the only rationally designed drug known to work *via* mechanism (iv). The most effective molecule tested on folding-deficient CRT1 variants was the chemical chaperone 4-phenyl butyric acid (4-PBA) which, at least in part, falls into category (iii). Over a third of the 16 known misfolded CTD variants are amenable to the functional rescue by 4-PBA treatment (**Figures 2**, **3**; El-Kasaby et al., 2019). The rescue effect was also visible in hippocampal neurons expressing the P544L CTD variant, where exposure to 4-PBA promoted its delivery to neurite extensions (El-Kasaby et al., 2019).

Beyond CRT1, the chaperone activity of 4-PBA was also demonstrated on several synthetic misfolded versions of SERT (Fujiwara et al., 2013) and the cystic fibrosis transmembrane conductance regulator (CFTR; Rubenstein and Zeitlin, 2000). In CFTR, 4-PBA exerts its action by stabilizing the misfolded ΔF508-CFTR variant in the ER, subsequently promoting its delivery to the cell surface. 4-PBA also increased the ER-resident core- and mature-glycosylated species of wild type and responsive mutants of CRT1 (El-Kasaby et al., 2019). Interestingly, 4-PBA also helped overcome the dominant-negative effect of a hyperekplexia GLYT2 variant S512R on the wild type transporter, by disturbing oligomer formation between the two versions of the GLYT2 protein (Arribas-González et al., 2015). Classified as a hydrophobic chaperone, 4-PBA interacts with hydrophobic domains of unfolded proteins, thus preventing aggregation [i.e., mechanism (iii) above]. But, this small molecule is incredibly versatile and appears to have many putative mechanisms of action. For instance, it is known to reduce ER stress by downregulating or modulating HSC70 expression (Rubenstein and Zeitlin, 2000), modifying HSP70 levels or blocking histone deacetylases (Cousens et al., 1979), leading to transcriptional regulation of genes in the unfolded protein response system. Interestingly, 4-PBA was approved for clinical use almost 25 years ago. It is used in the chronic management of urea cycle disorders, where it acts as a nitrogen-scavenger assisting kidneys to excrete excess ammonia, as well as in handling sickle cell disease since it activates β-globin transcription (Dover et al., 1994). Over the last decade, the effects of 4-PBA have been tested in many disease models, e.g., Alzheimer's (Ricobaraza et al., 2009, 2012) and Parkinsons's disease (Inden et al., 2007; Huang et al., 2017). In light of our recent *in vitro* data on CRT1 variants, translational testing of 4-PBA effects in animal models of CTD would be invaluable, particularly in knock-in animal models harboring folding-defective CRT1 mutations. Since CTD induces irreversible damage already in the early stages of development, it is vital to begin the treatment as early as possible, preferentially throughout the pregnancy.

At the current stage, it is impossible to predict which variants are amenable to rescue by pharmacochaperoning. However, the evolving state-of-the-art computer simulation models, which explore the structural effects of mutations at the atomic level, may convey new insights and serve as a guide for biochemical and pharmacological studies. Such models may hold the predictive power to categorize CTD mutations into (i) folding-deficient variants, which preclude the delivery of CRT1 proteins to the cell surface; and (ii) inactive variants, which are capable of trafficking to the cell surface, but elicit their functional defects as a consequence of conformational alterations in CRT1 (e.g., disruption of the creatine binding site/translocation pathway). In addition to the pharmacochaperone approach, applicable to the misfolded CTD variants, other treatment strategies, which are particularly apt for the second group of mutations, include gene therapy and the use of allosteric modulators. A prominent example of the latter is ivacaftor, which acts as a potentiator of the cystic fibrosis transmembrane conductance regulator (CFTR), by increasing CFTR channel open probability in mutants associated with cystic fibrosis (Van Goor et al., 2009). Allosteric modulators acting on monoamine neurotransmitter transporters also hold potential, in the treatment of various neuropsychiatric disorders (Li et al., 2017; Niello et al., 2020). It is conceivable that effective potentiator molecules can be designed to restore creatine transport in the loss-of-function CRT1 variants linked to CTD.

CONCLUSION

Establishing effective long-term treatment schemes for CTD patients poses a major challenge to clinicians and researchers in the field. Current insights into the role(s) of CRT1 in health and disease and the molecular mechanisms underlying CTD have uncovered additional therapeutic avenues that may be worthwhile exploring. Pharmacochaperoning, for instance, ought to be a promising new approach in the treatment of misfolded CRT1 variants associated with CTD. This concept

was previously utilized to functionally rescue folding-deficient variants of the human dopamine transporter, which trigger infantile parkinsonism/dystonia, both *in vitro* (heterologous cells) and *in vivo* (*Drosophila melanogaster*). Ongoing endeavors in the rational design and development of novel small molecules with improved capacity for correcting folding deficiencies are of particular interest to those pathologic transporter variants shown to be irresponsive to the existing drugs.

AUTHOR CONTRIBUTIONS

SS and CF wrote the manuscript. MF contributed to the conceptual advice. SS, CF, and AE-K created the table and figures. All authors contributed to the article and approved the submitted version.

FUNDING

We acknowledge financial support from the Austrian Science Fund FWF (project P31255-B27 to SS and DOC 33-B27 to MF and CF).

ACKNOWLEDGMENTS

We thank Carmen Farr for her assistance with graphical illustrations in **Figure 1**.

REFERENCES

Abdulla, Z. I., Pahlevani, B., Lundgren, K. H., Pennington, J. L., Udobi, K. C., Seroogy, K. B., et al. (2020a). Deletion of the creatine transporter (Slc6a8) in dopaminergic neurons leads to hyperactivity in mice. *J. Mol. Neurosci.* 70, 102–111. doi: 10.1007/s12031-019-01405-w

Abdulla, Z. I., Pennington, J. L., Gutierrez, A., and Skelton, M. R. (2020b). Creatine transporter knockout mice (Slc6a8) show increases in serotonin-related proteins and are resilient to learned helplessness. *Behav. Brain Res.* 377:112254. doi: 10.1016/j.bbr.2019.112254

Acosta, M. L., Kalloniatis, M., and Christie, D. L. (2005). Creatine transporter localization in developing and adult retina: importance of creatine to retinal function. *Am. J. Physiol. Cell Physiol.* 289, C1015–C1023. doi: 10.1152/ajpcell.00137.2005

Adriano, E., Garbati, P., Salis, A., Damonte, G., Millo, E., and Balestrino, M. (2017). Creatine salts provide neuroprotection even after partial impairment of the creatine transporter. *Neuroscience* 340, 299–307. doi: 10.1016/j.neuroscience.2016.02.038

Alcaide, P., Merinero, B., Ruiz-Sala, P., Richard, E., Navarrete, R., Arias, Á., et al. (2011). Defining the pathogenicity of creatine deficiency syndrome. *Hum. Mutat.* 32, 282–291. doi: 10.1002/humu.21421

Alcaide, P., Rodriguez-Pombo, P., Ruiz-Sala, P., Ferrer, I., Castro, P., Ruiz Martin, Y., et al. (2010). A new case of creatine transporter deficiency associated with mild clinical phenotype and a novel mutation in the SLC6A8 gene. *Dev. Med. Child Neurol.* 52, 215–217. doi: 10.1111/j.1469-8749.2009.03480.x

Almeida, L. S., Verhoeven, N. M., Roos, B., Valongo, C., Cardoso, M. L., Vilarinho, L., et al. (2004). Creatine and guanidinoacetate: diagnostic markers for inborn errors in creatine biosynthesis and transport. *Mol. Genet. Metab.* 82, 214–219. doi: 10.1016/j.ymgme.2004.05.001

Anselm, I. M., Alkuraya, F. S., Salomons, G. S., Jakobs, C., Fulton, A. B., Mazumdar, M., et al. (2006). X-linked creatine transporter defect: a report on two unrelated boys with a severe clinical phenotype. *J. Inherit. Metab. Dis.* 29, 214–219. doi: 10.1007/s10545-006-0123-4

Ardon, O., Procter, M., Mao, R., Longo, N., Landau, Y. E., Shilon-Hadass, A., et al. (2016). Creatine transporter deficiency: novel mutations and functional studies. *Mol. Genet. Metab. Reports* 8, 20–23. doi: 10.1016/j.ymgmr.2016.06.005

Arribas-González, E., De Juan-Sanz, J., Aragón, C., and López-Corcuera, B. (2015). Molecular basis of the dominant negative effect of a glycine transporter 2 mutation associated with hyperekplexia. *J. Biol. Chem.* 290, 2150–2165. doi: 10.1074/jbc.M114.587055

Asjad, H. M. M., Kasture, A., El-Kasaby, A., Sackel, M., Hummel, T., Freissmuth, M., et al. (2017). Pharmacochaperoning in a Drosophila model system rescues human dopamine transporter variants associated with infantile/juvenile parkinsonism. *J. Biol. Chem.* 292, 19250–19265. doi: 10.1074/jbc.M117.797092

Baroncelli, L., Alessandrì, M. G., Tola, J., Putignano, E., Migliore, M., Amendola, E., et al. (2014). A novel mouse model of creatine transporter deficiency. *F1000Res.* 3:228. doi: 10.12688/f1000research.5369.1

Baroncelli, L., Molinaro, A., Cacciante, F., Alessandrì, M. G., Napoli, D., Putignano, E., et al. (2016). A mouse model for creatine transporter deficiency reveals early onset cognitive impairment and neuropathology associated with brain aging. *Hum. Mol. Genet.* 25, 4186–4200. doi: 10.1093/hmg/ddw252

Battini, R., Alessandrì, M. G., Leuzzi, V., Moro, F., Tosetti, M., Bianchi, M. C., et al. (2006). Arginine:glycine amidinotransferase (AGAT) deficiency in a newborn: early treatment can prevent phenotypic expression of the disease. *J. Pediatr.* 148, 828–830. doi: 10.1016/j.jpeds.2006.01.043

Battini, R., Chilosi, A. M., Casarano, M., Moro, F., Comparini, A., Alessandrì, M. G., et al. (2011). Language disorder with mild intellectual disability in a child affected by a novel mutation of SLC6A8 gene. *Mol. Genet. Metab.* 102, 153–156. doi: 10.1016/j.ymgme.2010.11.005

Battini, R., Chilosi, A., Mei, D., Casarano, M., Alessandrì, G. M., Leuzzi, V., et al. (2007). Mental retardation and verbal dyspraxia in a new patient with de novo creatine transporter (SLC6A8) mutation. *Am. J. Med. Genet. A.* 143A, 1771–1774. doi: 10.1002/ajmg.a.31827

Beerepoot, P., Lam, V. M., and Salahpour, A. (2016). Pharmacological chaperones of the dopamine transporter rescue dopamine transporter deficiency syndrome mutations in heterologous cells. *J. Biol. Chem.* 291, 22053–22062. doi: 10.1074/jbc.M116.749119

Betsalel, O. T., Pop, A., Rosenberg, E. H., Fernandez-Ojeda, M., Jakobs, C., and Salomons, G. S. (2012). Detection of variants in SLC6A8 and functional analysis of unclassified missense variants. *Mol. Genet. Metab.* 105, 596–601. doi: 10.1016/j.ymgme.2011.12.022

Betsalel, O. T., van de Kamp, J. M., Martínez-Muñoz, C., Rosenberg, E. H., de Brouwer, A. P. M., Pouwels, P. J. W., et al. (2008). Detection of low-level somatic and germline mosaicism by denaturing high-performance liquid chromatography in a EURO-MRX family with SLC6A8 deficiency. *Neurogenetics* 9, 183–190. doi: 10.1007/s10048-008-0125-5

Bhat, S., Hasenhuetl, P. S., Kasture, A., El-Kasaby, A., Baumann, M. H., Blough, B. E., et al. (2017). Conformational state interactions provide clues to the pharmacochaperone potential of serotonin transporter partial substrates. *J. Biol. Chem.* 292, 16773–16786. doi: 10.1074/jbc.M117.794081

Bizzi, A., Bugiani, M., Salomons, G. S., Hunneman, D. H., Moroni, I., Estienne, M., et al. (2002). X-linked creatine deficiency syndrome: a novel mutation in creatine transporter geneSLC6A8. *Ann. Neurol.* 52, 227–231. doi: 10.1002/ana.10246

Boehm, E., Chan, S., Monfared, M., Wallimann, T., Clarke, K., and Neubauer, S. (2003). Creatine transporter activity and content in the rat heart supplemented by and depleted of creatine. *Am. J. Physiol. Endocrinol. Metab.* 284, 399–406. doi: 10.1152/ajpendo.00259.2002

Borrie, S. C., Brems, H., Legius, E., and Bagni, C. (2017). Cognitive dysfunctions in intellectual disabilities: the contributions of the ras-MAPK and PI3K-AKT-mTOR pathways. *Annu. Rev. Genomics Hum. Genet.* 18, 115–142. doi: 10.1146/annurev-genom-091416-035332

Braissant, O., Béard, E., Torrent, C., and Henry, H. (2010). Dissociation of AGAT, GAMT and SLC6A8 in CNS: relevance to creatine deficiency syndromes. *Neurobiol. Dis.* 37, 423–433. doi: 10.1016/j.nbd.2009.10.022

Braissant, O., and Henry, H. (2008). AGAT, GAMT and SLC6A8 distribution in the central nervous system, in relation to creatine deficiency syndromes: a review. *J. Inherit. Metab. Dis.* 31, 230–239. doi: 10.1007/s10545-008-0826-9

Braissant, O., Henry, H., Loup, M., Eilers, B., and Bachmann, C. (2001). Endogenous synthesis and transport of creatine in the rat brain: an in situ hybridization study. *Mol. Brain Res.* 86, 193–201. doi: 10.1016/s0169-328x(00)00269-2

Bruun, T. U., Sidky, S., Bandeira, A. O., Debray, F., Ficicioglu, C., Goldstein, J., et al. (2018). Treatment outcome of creatine transporter deficiency: international retrospective cohort study. *Metab. Brain Dis.* 33, 875–884. doi: 10.1007/s11011-018-0197-3

Clark, A. J., Rosenberg, E. H., Almeida, L. S., Wood, T. C., Jakobs, C., Stevenson, R. E., et al. (2006). X-linked creatine transporter (SLC6A8) mutations in about 1% of males with mental retardation of unknown etiology. *Hum. Genet.* 119, 604–610. doi: 10.1007/s00439-006-0162-9

Country, M. W. (2017). Retinal metabolism: a comparative look at energetics in the retina. *Brain Res.* 1672, 50–57. doi: 10.1016/j.brainres.2017.07.025

Cousens, L. S., Gallwitz, D., and Alberts, B. M. (1979). Different accessibilities in chromatin to histone acetylase. *J. Biol. Chem.* 254, 1716–1723.

Darrabie, M. D., Arciniegas, A. J. L., Mishra, R., Bowles, D. E., Jacobs, D. O., and Santacruz, L. (2011). AMPK and substrate availability regulate creatine transport in cultured cardiomyocytes. *Am. J. Physiol. Endocrinol. Metab.* 300, E870–E876. doi: 10.1152/ajpendo.00554.2010

Davidson, R. G. (1964). The Lyon hypothesis. *J. Pediatr.* 65, 765–775. doi: 10.1016/s0022-3476(64)80163-3

De Grauw, T. J., Cecil, K. M., Byars, A. W., Salomons, G. S., Ball, W. S., and Jakobs, C. (2003). The clinical syndrome of creatine transporter deficiency. *Mol. Cell. Biochem.* 244, 45–48. doi: 10.1007/978-1-4615-0247-0_6

Deldicque, L., Theisen, D., Bertrand, L., Hespe, P., Hue, L., and Francaux, M. (2007). Creatine enhances differentiation of myogenic C2C12 cells by activating both p38 and Akt/PKB pathways. *Am. J. Physiol. Cell Physiol.* 293, 1263–1271. doi: 10.1152/ajpcell.00162.2007

DesRoches, C. L., Patel, J., Wang, P., Minassian, B., Salomons, G. S., Marshall, C. R., et al. (2015). Estimated carrier frequency of creatine transporter deficiency in females in the general population using functional characterization of novel missense variants in the SLC6A8 gene. *Gene* 565, 187–191. doi: 10.1016/j.gene.2015.04.011

Di Biase, S., Ma, X., Wang, X., Yu, J., Wang, Y., Smith, D. J., et al. (2019). Creatine uptake regulates CD8 T cell antitumor immunity. *J. Exp. Med.* 216, 2869–2882. doi: 10.1084/jem.20182044

Dodd, J. R., Birch, N. P., Waldvogel, H. J., and Christie, D. L. (2010). Functional and immunocytochemical characterization of the creatine transporter in rat hippocampal neurons. *J. Neurochem.* 115, 684–693. doi: 10.1111/j.1471-4159.2010.06957.x

Dover, G. J., Brusilow, S., and Charache, S. (1994). Induction of fetal hemoglobin production in subjects with sickle cell anemia by oral sodium phenylbutyrate. *Blood* 84, 339–343. doi: 10.1182/blood.v84.1.339.bloodjournal841339

Dunbar, M., Jaggumantri, S., Sargent, M., Stockler-Ipsiroglu, S., and van Karnebeek, C. D. M. (2014). Treatment of X-linked creatine transporter (SLC6A8) deficiency: systematic review of the literature and three new cases. *Mol. Genet. Metab.* 112, 259–274. doi: 10.1016/j.ymgme.2014.05.011

El-Kasaby, A., Just, H., Malle, E., Stolt-Bergner, P. C., Sitte, H. H., Freissmuth, M., et al. (2010). Mutations in the carboxyl-terminal SEC24 binding motif of the serotonin transporter impair folding of the transporter. *J. Biol. Chem.* 285, 39201–39210. doi: 10.1074/jbc.M110.118000

El-Kasaby, A., Kasture, A., Koban, F., Hotka, M., Asjad, H. M. M., Kubista, H., et al. (2019). Rescue by 4-phenylbutyrate of several misfolded creatine transporter-1 variants linked to the creatine transporter deficiency syndrome. *Neuropharmacology* 161:107572. doi: 10.1016/j.neuropharm.2019.03.015

El-Kasaby, A., Koban, F., Sitte, H. H., Freissmuth, M., and Sucic, S. (2014). A cytosolic relay of heat shock proteins HSP70–1A and HSP90β monitors the folding trajectory of the serotonin transporter. *J. Biol. Chem.* 289, 28987–29000. doi: 10.1074/jbc.M114.595090

Eulenburg, V., Becker, K., Gomeza, J., Schmitt, B., Becker, C. M., and Betz, H. (2006). Mutations within the human GLYT2 (SLC6A5) gene associated with hyperekplexia. *Biochem. Biophys. Res. Commun.* 348, 400–405. doi: 10.1016/j.bbrc.2006.07.080

Farhan, H., Reiterer, V., Korkhov, V. M., Schmid, J. A., Freissmuth, M., and Sitte, H. H. (2007). Concentrative export from the endoplasmic reticulum of the gamma-aminobutyric acid transporter 1 requires binding to SEC24D. *J. Biol. Chem.* 282, 7679–7689. doi: 10.1074/jbc.M609720200

Fischer, A., ten Hove, M., Sebag-Montefiore, L., Wagner, H., Clarke, K., Watkins, H., et al. (2010). Changes in creatine transporter function during cardiac maturation in the rat. *BMC Dev. Biol.* 10:70. doi: 10.1186/1471-213X-10-70

Fons, C., Sempere, A., Sanmartí, F. X., Arias, A., Póo, P., Pineda, M., et al. (2009). Epilepsy spectrum in cerebral creatine transporter deficiency. *Epilepsia* 50, 2168–2170. doi: 10.1111/j.1528-1167.2009.02142.x

Freissmuth, M., Stockner, T., and Sucic, S. (2018). "SLC6 transporter folding diseases and pharmacochaperoning," in *Handbook of Experimental Pharmacology: Targetting Trafficking in Drug Development*, eds Alfredo Ulloa-Aguirre and Ya-Xiong Tao (Cham, Switzerland: Springer), 249–270.

Fujiwara, M., Yamamoto, H., Miyagi, T., Seki, T., Tanaka, S., Hide, I., et al. (2013). Effects of the chemical chaperone 4-phenylbutylate on the function of the serotonin transporter (SERT) expressed in COS-7 cells. *J. Pharmacol. Sci.* 122, 71–83. doi: 10.1254/jphs.12194fp

Giménez, C., Pérez-Siles, G., Martínez-Villarreal, J., Arribas-González, E., and López-Corcuera, B. (2012). A novel dominant hyperekplexia mutation Y705C alters trafficking and biochemical properties of the presynaptic glycine transporter GlyT2. *J. Biol. Chem.* 287, 28986–29002. doi: 10.1074/jbc.M111.319244

Giusti, L., Molinaro, A., Alessandrì, M. G., Boldrini, C., Ciregia, F., Lacerenza, S., et al. (2019). Brain mitochondrial proteome alteration driven by creatine deficiency suggests novel therapeutic venues for creatine deficiency syndromes. *Neuroscience* 409, 276–289. doi: 10.1016/j.neuroscience.2019.03.030

Gorshkov, K., Wang, A. Q., Sun, W., Fisher, E., Frigeni, M., Singleton, M., et al. (2019). Phosphocyclocreatine is the dominant form of cyclocreatine in control and creatine transporter deficiency patient fibroblasts. *Pharmacol. Res. Perspect.* 7:e00525. doi: 10.1002/prp2.525

Guzun, R., Timohhina, N., Tepp, K., Gonzalez-Granillo, M., Shevchuk, I., Chekulayev, V., et al. (2011). Systems bioenergetics of creatine kinase networks: physiological roles of creatine and phosphocreatine in regulation of cardiac cell function. *Amino Acids* 40, 1333–1348. doi: 10.1007/s00726-011-0854-x

Hahn, K. A., Tackels-Horne, D., Wood, T. C., Taylor, H. A., Schroer, R. J., Lubs, H. A., et al. (2002). X-linked mental retardation with seizures and carrier manifestations is caused by a mutation in the creatine-transporter gene (SLC6A8) located in Xq28. *Am. J. Hum. Genet.* 70, 1349–1356. doi: 10.1086/340092

Hanna-El-Daher, L., Béard, E., Henry, H., Tenenbaum, L., and Braissant, O. (2015). Neurobiology of Disease Mild guanidinoacetate increase under partial guanidinoacetate methyltransferase de fi ciency strongly affects brain cell development. *Neurobiol. Dis.* 79, 14–27. doi: 10.1016/j.nbd.2015.03.029

Hathaway, S. C., Friez, M., Limbo, K., Parker, C., Salomons, G. S., Vockley, J., et al. (2010). X-linked creatine transporter deficiency presenting as a mitochondrial disorder. *J. Child Neurol.* 25, 1009–1012. doi: 10.1177/0883073809352109

Hautman, E. R., Kokenge, A. N., Udobi, K. C., Williams, M. T., Vorhees, C. V., and Skelton, M. R. (2014). Female mice heterozygous for creatine transporter deficiency show moderate cognitive deficits. *J. Inherit. Metab. Dis.* 37, 63–68. doi: 10.1007/s10545-013-9619-x

Heinbockel, L., Marwitz, S., Schromm, A., Watz, H., Kugler, C., Ammerpohl, O., et al. (2018). Identification of novel target genes in human lung tissue involved in chronic obstructive pulmonary disease. *Int. J. Chron. Obstruct. Pulmon. Dis.* 13, 2255–2259. doi: 10.2147/COPD.S161958

Heussinger, N., Saake, M., Mennecke, A., Dörr, H. G., and Trollmann, R. (2017). Variable white matter atrophy and intellectual development in a family with X-linked creatine transporter deficiency despite genotypic homogeneity. *Pediatr. Neurol.* 67, 45–52. doi: 10.1016/j.pediatrneurol.2016.10.007

Hiel, H., Happe, H. K., Warr, W. B., and Morley, B. J. (1996). Regional distribution of a creatine transporter in rat auditory brainstem: an in-situ hybridization study. *Hear. Res.* 98, 29–37. doi: 10.1016/0378-5955(96)00046-9

Inden, M., Kitamura, Y., Takeuchi, H., Yanagida, T., Takata, K., Kobayashi, Y., et al. (2007). Neurodegeneration of mouse nigrostriatal dopaminergic system induced by repeated oral administration of rotenone is prevented by 4-phenylbutyrate, a chemical chaperone. *J. Neurochem.* 101, 1491–1504. doi: 10.1111/j.1471-4159.2006.04440.x

Huang, L., Xue, Y., Feng, D., Yang, R., Nie, T., Zhu, G., et al. (2017). Blockade of RyRs in the ER attenuates 6-OHDA-induced calcium overload, cellular

hypo-excitability and apoptosis in dopaminergic neurons. *Front. Cell. Neurosci.* 11:52. doi: 10.3389/fncel.2017.00052

Jacobs, M. T., Zhang, Y. W., Campbell, S. D., and Rudnick, G. (2007). Ibogaine, a noncompetitive inhibitor of serotonin transport, acts by stabilizing the cytoplasm-facing state of the transporter. *J. Biol. Chem.* 282, 29441–29447. doi: 10.1074/jbc.M704456200

Ji, L., Zhao, X., Zhang, B., Kang, L., Song, W., Zhao, B., et al. (2019). Slc6a8-mediated creatine uptake and accumulation reprogram macrophage polarization *via* regulating cytokine responses. *Immunity* 51, 272.e7–284.e7.doi: 10.1016/j.immuni.2019.06.007

Jung, H. Y., Kwon, H. J., Kim, W., Nam, S. M., and Kim, J. W. (2019). Tissue and cell role of pyridoxine in GABA synthesis and degradation in the hippocampus. *Tissue Cell* 61, 72–78. doi: 10.1016/j.tice.2019.09.005

Just, H., Sitte, H. H., Schmid, J. A., Freissmuth, M., and Kudlacek, O. (2004). Identification of an additional interaction domain in transmembrane domains 11 and 12 that supports oligomer formation in the human serotonin transporter. *J. Biol. Chem.* 279, 6650–6657. doi: 10.1074/jbc.M306092200

Kale, V. P., Wallery, J., Novak, J., Gibbs, S., Bourdi, M., Do, M.-H. T., et al (2020). Evaluation of chronic toxicity of cyclocreatine, a creatine analog, in Sprague Dawley rat after oral gavage administration for up to 26 weeks. *Regul. Toxicol. Pharmacol.* 117:104750. doi: 10.1016/j.yrtph.2020.104750

Kalkman, H. O. (2012). Potential opposite roles of the extracellular signal-regulated kinase (ERK) pathway in autism spectrum and bipolar disorders. *Neurosci. Biobehav. Rev.* 36, 2206–2213. doi: 10.1016/j.neubiorev.2012.07.008

Kasture, A. S., Bartel, D., Steinkellner, T., Sucic, S., Hummel, T., and Freissmuth, M. (2019). Distinct contribution of axonal and somatodendritic serotonin transporters in drosophila olfaction. *Neuropharmacology* 161:107564. doi: 10.1016/j.neuropharm.2019.03.007

Kasture, A., Stockner, T., Freissmuth, M., and Sucic, S. (2017). An unfolding story: small molecules remedy misfolded monoamine transporters. *Int. J. Biochem. Cell Biol.* 92, 1–5. doi: 10.1016/j.biocel.2017.09.004

Kato, H., Miyake, F., Shimbo, H., Ohya, M., Sugawara, H., Aida, N., et al. (2014). Urine screening for patients with developmental disabilities detected a patient with creatine transporter deficiency due to a novel missense mutation in SLC6A8. *Brain Dev.* 36, 630–633. doi: 10.1016/j.braindev.2013.08.004

Kern, C., Erdem, F. A., El-Kasaby, A., Sandtner, W., Freissmuth, M., and Sucic, S. (2017). The N terminus specifies the switch between transport modes of the human serotonin transporter. *J. Biol. Chem.* 292, 3603–3613. doi: 10.1074/jbc.M116.771360

Koban, F., El-Kasaby, A., Häusler, C., Stockner, T., Simbrunner, B. M., Sitte, H. H., et al. (2015). A salt bridge linking the first intracellular loop with the C terminus facilitates the folding of the serotonin transporter. *J. Biol. Chem.* 290, 13263–13278. doi: 10.1074/jbc.M115.641357

Kreiman, B. L., and Boles, R. G. (2020). State of the art of genetic testing for patients with autism: a practical guide for clinicians. *Semin. Pediatr. Neurol.* 34:100804. doi: 10.1016/j.spen.2020.100804

Kurian, M. A., Li, Y., Zhen, J., Meyer, E., Hai, N., Christen, H. J., et al. (2011). Clinical and molecular characterisation of hereditary dopamine transporter deficiency syndrome: an observational cohort and experimental study. *Lancet Neurol.* 10, 54–62. doi: 10.1016/S1474-4422(10)70269-6

Kurian, M. A., Zhen, J., Cheng, S. Y., Li, Y., Mordekar, S. R., Jardine, P., et al. (2009). Homozygous loss-of-function mutations in the gene encoding the dopamine transporter are associated with infantile parkinsonism-dystonia. *J. Clin. Invest.* 119, 1595–1603. doi: 10.1172/JCI39060

Kurosawa, Y., DeGrauw, T. J., Lindquist, D. M., Blanco, V. M., Pyne-Geithman, G. J., Daikoku, T., et al. (2012). Cyclocreatine treatment improves cognition in mice with creatine transporter deficiency. *J. Clin. Invest.* 122, 2837–2846. doi: 10.1172/JCI59373

Kurth, I., Andreu, C., Takeda, S., Tian, H., Gonsalves, F., Leites, K., et al. (2018). "RGX-202, a first-in-class small-molecule inhibitor of the creatine transporter SLC6a8, is a robust suppressor of cancer growth and metastatic progression [abstract]," in *Proceedings of the American Association for Cancer Research Annual Meeting 2018*, Chicago, IL, Abstract no. 5863. doi: 10.1158/1538-7445.AM2018-5863

Lawler, J. M., Barnes, W. S., Wu, G., Song, W., and Demaree, S. (2002). Direct antioxidant properties of creatine. *Biochem. Biophys. Res. Commun.* 290, 47–52. doi: 10.1006/bbrc.2001.6164

Leuzzi, V., Alessandrì, M. G., Battini, R., and Cioni, G. (2008). Arginine and glycine stimulate creatine synthesis in creatine transporter 1-deficient lymphoblasts. *Anal. Biochem.* 375, 153–155. doi: 10.1016/j.ab.2008.01.018

Li, Y., Mayer, F. P., Hasenhuetl, P. S., Burtscher, V., Schicker, K., Sitte, H. H., et al. (2017). Occupancy of the zinc-binding site by transition metals decreases the substrate affinity of the human dopamine transporter by an allosteric mechanism. *J. Biol. Chem.* 292, 4235–4243. doi: 10.1074/jbc.M116.760140

Li, H., Thali, R. F., Smolak, C., Gong, F., Alzamora, R., Wallimann, T., et al. (2010). Regulation of the creatine transporter by AMP-activated protein kinase in kidney epithelial cells. *Am. J. Physiol. Physiol.* 299, F167–F177. doi: 10.1152/ajprenal.00162.2010

Lion-François, L., Cheillan, D., Pitelet, G., Acquaviva-Bourdain, C., Bussy, G., Cotton, F., et al. (2006). High frequency of creatine deficiency syndromes in patients with unexplained mental retardation. *Neurology* 67, 1713–1714. doi: 10.1212/01.wnl.0000239153.39710.81

Loike, J. D., Somes, M., and Silverstein, S. C. (1986). Creatine uptake, metabolism, and efflux in human monocytes and macrophages. *Am. J. Physiol. Cell Physiol.* 251, C128–C135. doi: 10.1152/ajpcell.1986.251.1.C128

LoPresti, P., and Cohn, M. (1989). Direct determination of creatine kinase equilibrium constants with creatine or cyclocreatine as substrate. *Biochim. Biophys. Acta* 998, 317–320. doi: 10.1016/0167-4838(89)90291-4

Lowe, M. T. J., Faull, R. L. M., Christie, D. L., and Waldvogel, H. J. (2015). Distribution of the creatine transporter throughout the human brain reveals a spectrum of creatine transporter immunoreactivity. *J. Comp. Neurol.* 523, 699–725. doi: 10.1002/cne.23667

Lunardi, G., Parodi, A., Perasso, L., Pohvozcheva, A. V., Scarrone, S., Adriano, E., et al. (2006). The creatine transporter mediates the uptake of creatine by brain tissue, but not the uptake of two creatine-derived compounds. *Neuroscience* 142, 991–997. doi: 10.1016/j.neuroscience.2006.06.058

Mak, C. S. W., Waldvogel, H. J., Dodd, J. R., Gilbert, R. T., Lowe, M. T. J., Birch, N. P., et al. (2009). Immunohistochemical localisation of the creatine transporter in the rat brain. *Neuroscience* 163, 571–585. doi: 10.1016/j.neuroscience.2009.06.065

Mancini, G. M. S., Catsman-Berrevoets, C. E., De Coo, I. F. M., Aarsen, F. K., Kamphoven, J. H. J., Huijmans, J. G., et al. (2005). Two novel mutations in SLC6A8 cause creatine transporter defect and distinctive X-linked mental retardation in two unrelated Dutch families. *Am. J. Med. Genet.* 132A, 288–295. doi: 10.1002/ajmg.a.30473

Marinko, J. T., Huang, H., Penn, W. D., Capra, J. A., Schlebach, J. P., and Sanders, C. R. (2019). Folding and misfolding of human membrane proteins in health and disease: from single molecules to cellular proteostasis. *Chem. Rev.* 119, 5537–5606. doi: 10.1021/acs.chemrev.8b00532

McKenzie, K., Milton, M., Smith, G., and Ouellette-Kuntz, H. (2016). Systematic review of the prevalence and incidence of intellectual disabilities: current trends and issues. *Curr. Dev. Disord. Rep.* 3, 104–115doi: 10.1007/s40474-016-0085-7

Mencarelli, M. A., Tassini, M., Pollazzon, M., Vivi, A., Calderisi, M., Falco, M., et al. (2011). Creatine transporter defect diagnosed by proton NMR spectroscopy in males with intellectual disability. *Am. J. Med. Genet. Part. A* 155, 2446–2452. doi: 10.1002/ajmg.a.34208

Mercimek-Mahmutoglu, S., Muehl, A., Salomons, G. S., Neophytou, B., Moeslinger, D., Struys, E., et al. (2009). Screening for X-linked creatine transporter (SLC6A8) deficiency *via* simultaneous determination of urinary creatine to creatinine ratio by tandem mass-spectrometry. *Mol. Genet. Metab.* 96, 273–275. doi: 10.1016/j.ymgme.2008.12.020

Migeon, B. R. (2020). X-linked diseases: susceptible females. *Genet. Med.* 22, 1156–1174. doi: 10.1038/s41436-020-0779-4

Molinaro, A., Alessandrì, M. G., Putignano, E., Leuzzi, V., Cioni, G., Baroncelli, L., et al. (2019). A nervous system-specific model of creatine transporter deficiency recapitulates the cognitive endophenotype of the disease: a longitudinal study. *Sci. Rep.* 9:62. doi: 10.1038/s41598-018-37303-1

Nabuurs, C. I., Choe, C. U., Veltien, A., Kan, H. E., van Loon, L. J. C., Rodenburg, R. J. T., et al. (2013). Disturbed energy metabolism and muscular dystrophy caused by pure creatine deficiency are reversible by creatine intake. *J. Physiol.* 591, 571–592. doi: 10.1113/jphysiol.2012.241760

Neu, A., Neuhoff, H., Trube, G., Fehr, S., Ullrich, K., Roeper, J., et al. (2002). Activation of GABAA receptors by guanidinoacetate: a novel

pathophysiological mechanism. *Neurobiol. Dis.* 11, 298–307. doi: 10.1006/nbdi.2002.0547

Ng, J., Zhen, J., Meyer, E., Erreger, K., Li, Y., Kakar, N., et al. (2014). Dopamine transporter deficiency syndrome: phenotypic spectrum from infancy to adulthood. *Brain* 137, 1107–1119. doi: 10.1093/brain/awu022

Niello, M., Gradisch, R., Loland, C. J., Stockner, T., and Sitte, H. H. (2020). Allosteric modulation of neurotransmitter transporters as a therapeutic strategy. *Trends Pharmacol. Sci.* 41, 446–463. doi: 10.1016/j.tips.2020.04.006

Nigro, P., Pompilio, G., and Capogrossi, M. C. (2013). Cyclophilin A: a key player for human disease. *Cell Death Dis.* 4:e888. doi: 10.1038/cddis.2013.410

Norris, D. K., Murphy, R. A., and Chung, S. H. (1983). Alteration of amino acid metabolism in epileptogenic mice by elevation of brain pyridoxal phosphate. *J. Neurochem.* 44, 1403–1410. doi: 10.1111/j.1471-4159.1985.tb08776.x

Nota, B., Ndika, J. D. T., van de Kamp, J. M., Kanhai, W. A., Van Dooren, S. J. M., Van de Wiel, M. A., et al. (2014). RNA sequencing of creatine transporter (SLC6A8) deficient fibroblasts reveals impairment of the extracellular matrix. *Hum. Mutat.* 35, 1128–1135. doi: 10.1002/humu.22609

Nozaki, F., Kumada, T., Shibata, M., Fujii, T., Wada, T., and Osaka, H. (2015). A family with creatine transporter deficiency diagnosed with urinary creatine/creatinine ratio and the family history: the third Japanese familial case. *Brain Dev.* 47, 49–52. doi: 10.11251/ojjscn.47.49

Ohtsuki, S., Tachikawa, M., Takanaga, H., Shimizu, H., Watanabe, M., Hosoya, K., et al. (2002). The blood-brain barrier creatine transporter is a major pathway for supplying creatine to the brain. *J. Cereb. Blood Flow Metab.* 22, 1327–1335. doi: 10.1097/01.WCB.0000033966.83623.7D

Oudman, I., Clark, J. F., and Brewster, L. M. (2013). The effect of the creatine analogue beta-guanidinopropionic acid on energy metabolism: a systematic review. *PLoS One* 8:e52879. doi: 10.1371/journal.pone.0052879

Perasso, L., Cupello, A., Lunardi, G. L., Principato, C., Gandolfo, C., and Balestrino, M. (2003). Kinetics of creatine in blood and brain after intraperitoneal injection in the rat. *Brain Res.* 974, 37–42. doi: 10.1016/s0006-8993(03)02547-2

Perna, M. K., Kokenge, A. N., Miles, K. N., Udobi, K. C., Joseph, F., Pyne-Geithman, G. J., et al. (2016). Creatine transporter deficiency leads to increased whole-body and cellular metabolism. *Amino Acids* 48, 2057–2065. doi: 10.1007/s00726-016-2291-3

Pfefferle, A. D., Warner, L. R., Wang, C. W., Nielsen, W. J., Babbitt, C. C., Fedrigo, O., et al. (2011). Comparative expression analysis of the phosphocreatine circuit in extant primates: implications for human brain evolution. *J. Hum. Evol.* 60, 205–212. doi: 10.1016/j.jhevol.2010.10.004

Póo-Argüelles, P., Arias, A., Vilaseca, M. A., Ribes, A., Artuch, R., Sans-Fito, A., et al. (2006). X-Linked creatine transporter deficiency in two patients with severe mental retardation and autism. *J. Inherit. Metab. Dis.* 29, 220–223. doi: 10.1007/s10545-006-0212-4

Pucilowska, J., Vithayathil, J., Pagani, M., Kelly, C., Karlo, J. C., Robol, C., et al. (2018). Pharmacological inhibition of ERK signaling rescues pathophysiology and behavioral phenotype associated with 16p11.2 chromosomal deletion in mice. *J. Neurosci.* 38, 6640–6652. doi: 10.1523/JNEUROSCI.0515-17.2018

Pucilowska, J., Vithayathil, J., Tavares, E. J., Kelly, C., Colleen Karlo, J., and Landreth, G. E. (2015). The 16p11.2 deletion mouse model of autism exhibits altered cortical progenitor proliferation and brain cytoarchitecture linked to the ERK MAPK pathway. *J. Neurosci.* 35, 3190–3200. doi: 10.1523/JNEUROSCI.4864-13.2015

Puusepp, H., Kall, K., Salomons, G. S., Talvik, I., Männamaa, M., Rein, R., et al. (2010). The screening of SLC6A8 deficiency among Estonian families with X-linked mental retardation. *J. Inherit. Metab. Dis.* 33, S5–S11. doi: 10.1007/s10545-008-1063-y

Pyne-Geithman, G. J., DeGrauw, T. J., Cecil, K. M., Chuck, G., Lyons, M. A., Ishida, Y., et al. (2004). Presence of normal creatine in the muscle of a patient with a mutation in the creatine transporter: a case study. *Mol. Cell. Biochem.* 262, 35–39. doi: 10.1023/b:mcbi.0000038213.15646.4a

Rahimi, R., Mirzaei, B., Rahmani-Nia, F., and Salehi, Z. (2015). Effects of creatine monohydrate supplementation on exercise-induced apoptosis in athletes: a randomized, double-blind, and placebo-controlled study. *J. Res. Med. Sci.* 20, 733–738. doi: 10.4103/1735-1995.168320

Rees, M. I., Harvey, K., Pearce, B. R., Chung, S. K., Duguid, I. C., Thomas, P., et al. (2006). Mutations in the gene encoding GlyT2 (SLC6A5) define a presynaptic component of human startle disease. *Nat. Genet.* 38, 801–806. doi: 10.1038/ng1814

Ricobaraza, A., Cuadrado-Tejedor, M., Marco, S., Pérez-Otaño, I., and García-Osta, A. (2012). Phenylbutyrate rescues dendritic spine loss associated with memory deficits in a mouse model of Alzheimer disease. *Hippocampus* 22, 1040–1050. doi: 10.1002/hipo.20883

Ricobaraza, A., Cuadrado-Tejedor, M., Pérez-Mediavilla, A., Frechilla, D., Del Río, J., and García-Osta, A. (2009). Phenylbutyrate ameliorates cognitive deficit and reduces tau pathology in an Alzheimer's disease mouse model. *Neuropsychopharmacology* 34, 1721–1732. doi: 10.1038/npp.2008.229

Riordan, J. D., and Nadeau, J. H. (2017). From peas to disease: modifier genes, network resilience, and the genetics of health. *Am. J. Hum. Genet.* 101, 177–191. doi: 10.1016/j.ajhg.2017.06.004

Rosenberg, E. H., Almeida, L. S., Kleefstra, T., DeGrauw, R. S., Yntema, H. G., Bahi, N., et al. (2004). High prevalence of SLC6A8 deficiency in X-linked mental retardation. *Am. J. Hum. Genet.* 75, 97–105. doi: 10.1086/422102

Rostami, P., Hosseinpour, S., Ashrafi, M. R., Alizadeh, H., Garshasbi, M., and Tavasoli, A. R. (2020). Primary creatine deficiency syndrome as a potential missed diagnosis in children with psychomotor delay and seizure: case presentation with two novel variants and literature review. *Acta Neurol. Belg.* 120, 511–516. doi: 10.1007/s13760-019-01168-6

Rubenstein, R. C., and Zeitlin, P. L. (2000). Sodium 4-phenylbutyrate downregulates Hsc70: implications for intracellular trafficking of ΔF508-CFTR. *Am. J. Physiol. Physiol.* 278, C259–C267. doi: 10.1152/ajpcell.2000.278.2.C259

Russell, A. P., Ghobrial, L., Wright, C. R., Lamon, S., Brown, E., Kon, M., et al. (2014). Creatine transporter (SLC6A8) knock out mice display an increased capacity for *in vitro* creatine biosynthesis in skeletal muscle. *Front. Physiol.* 5:314. doi: 10.3389/fphys.2014.00314

Sakellaris, G., Kotsiou, M., Tamiolaki, M., Kalostos, G., Tsapaki, E., Spanaki, M., et al. (2006). Prevention of complications related to traumatic brain injury in children and adolescents with creatine administration: an open label randomized pilot study. *J. Trauma* 61, 322–329. doi: 10.1097/01.ta.0000230269.46108.d5

Salazar, M. D., Zelt, N. B., Saldivar, R., Kuntz, C. P., Chen, S., Penn, W. D., et al. (2020). Classification of the molecular defects associated with pathogenic variants of the SLC6A8 creatine transporter. *Biochemistry* 59, 1367–1377. doi: 10.1021/acs.biochem.9b00956

Schiaffino, M. C., Bellini, C., Costabello, L., Caruso, U., Jakobs, C., Salomons, G. S., et al. (2005). X-linked creatine transporter deficiency: clinical description of a patient with a novel SLC6A8 gene mutation. *Neurogenetics* 6, 165–168. doi: 10.1007/s10048-005-0002-4

Schulze, A., Hoffmann, G. F., Bachert, P., Kirsch, S., Salomons, G. S., Verhoeven, N. M., et al. (2006). Presymptomatic treatment of neonatal guanidinoacetate methyltransferase deficiency. *Neurology* 67, 719–721. doi: 10.1212/01.wnl.0000230152.25203.01

Sempere, A., Fons, C., Arias, A., Rodríguez-Pombo, P., Colomer, R., Merinero, B., et al. (2009). Creatine transporter deficiency in two adult patients with static encephalopathy. *J. Inherit. Metab. Dis.* 32, 91–96. doi: 10.1007/s10545-009-1083-2

Sijens, P. E., Verbruggen, K. T., Oudkerk, M., van Spronsen, F. J., and Soorani-Lunsing, R. J. (2005). 1H MR spectroscopy of the brain in Cr transporter defect. *Mol. Genet. Metab.* 86, 421–422. doi: 10.1016/j.ymgme.2005.08.004

Skelton, M. R., Schaefer, T. L., Graham, D. L., deGrauw, T. J., Clark, J. F., Williams, M. T., et al. (2011). Creatine transporter (CrT; Slc6a8) knockout mice as a model of human CrT deficiency. *PLoS One* 6:e16187. doi: 10.1371/journal.pone.0016187

Stockebrand, M., Sasani, A., Das, D., Hornig, S., Hermans-Borgmeyer, I., Lake, H. A., et al. (2018). A mouse model of creatine transporter deficiency reveals impaired motor function and muscle energy metabolism. *Front. Physiol.* 9:773. doi: 10.3389/fphys.2018.00773

Sucic, S., Dallinger, S., Zdrazil, B., Weissensteiner, R., Jørgensen, T. N., Holy, M., et al. (2010). The N terminus of monoamine transporters is a lever required for the action of amphetamines. *J. Biol. Chem.* 285, 10924–10938. doi: 10.1074/jbc.M109.083154

Sucic, S., El-Kasaby, A., Kudlacek, O., Sarker, S., Sitte, H. H., Marin, P., et al. (2011). The serotonin transporter is an exclusive client of the coat protein

complex II (COPII) component SEC24C. *J. Biol. Chem.* 286, 16482–16490. doi: 10.1074/jbc.M111.230037

Sucic, S., Kasture, A., Asjad, H. M. M., Kern, C., El-kasaby, A., and Freissmuth, M. (2016). When transporters fail to be transported: how to rescue folding- deficient SLC6 transporters. *Neurol. Neuromedicine* 1, 34–40. doi: 10.29245/2572.942x/2016/9.1098

Sucic, S., Koban, F., El-Kasaby, A., Kudlacek, O., Stockner, T., Sitte, H. H., et al. (2013). Switching the clientele: a lysine residing in the C terminus of the serotonin transporter specifies its preference for the coat protein complex II component SEC24C. *J. Biol. Chem.* 288, 5330–5341. doi: 10.1074/jbc.M112.408237

Sullivan, P. G., Geiger, J. D., Mattson, M. P., and Scheff, S. W. (2000). Dietary supplement creatine protects against traumatic brain injury. *Ann. Neurol.* 48, 723–729. doi: 10.1002/1531-8249(200011)48:5<723::aid-ana5>3.0.co;2-w

Tachikawa, M., Fujinawa, J., Takahashi, M., Kasai, Y., Fukaya, M., Sakai, K., et al. (2008). Expression and possible role of creatine transporter in the brain and at the blood-cerebrospinal fluid barrier as a transporting protein of guanidinoacetate, an endogenous convulsant. *J. Neurochem.* 107, 768–778. doi: 10.1111/j.1471-4159.2008.05652.x

Tachikawa, M., Fukaya, M., Terasaki, T., Ohtsuki, S., and Watanabe, M. (2004). Distinct cellular expressions of creatine synthetic enzyme GAMT and creatine kinases uCK-Mi and CK-B suggest a novel neuron-glial relationship for brain energy homeostasis. *Eur. J. Neurosci.* 20, 144–160. doi: 10.1111/j.1460-9568.2004.03478.x

Taii, A., Tachikawa, M., Ohta, Y., Hosoya, K., and Terasaki, T. (2020). Determination of intrinsic creatine transporter (Slc6a8) activity and creatine transport function of leukocytes in rats. *Biol. Pharm. Bull.* 43, 474–479. doi: 10.1248/bpb.b19-00807

Trotier-Faurion, A., Dézard, S., Taran, F., Valayannopoulos, V., de Lonlay, P., and Mabondzo, A. (2013). Synthesis and biological evaluation of new creatine fatty esters revealed dodecyl creatine ester as a promising drug candidate for the treatment of the creatine transporter deficiency. *J. Med. Chem.* 56, 5173–5181. doi: 10.1021/jm400545n

Trotier-Faurion, A., Passirani, C., Béjaud, J., Dézard, S., Valayannopoulos, V., Taran, F., et al. (2015). Dodecyl creatine ester and lipid nanocapsule: a double strategy for the treatment of creatine transporter deficiency. *Nanomedicine* 10, 185–191. doi: 10.2217/nnm.13.205

Udobi, K. C., Delcimmuto, N., Kokenge, A. N., Abdulla, Z. I., Perna, M. K., and Skelton, M. R. (2019). Deletion of the creatine transporter gene in neonatal, but not adult, mice leads to cognitive deficits. *J. Inherit. Metab. Dis.* 42, 966–974. doi: 10.1002/jimd.12137

Udobi, K. C., Kokenge, A. N., Hautman, E. R., Ullio, G., Coene, J., Williams, M. T., et al. (2018). Cognitive deficits and increases in creatine precursors in a brain-specific knockout of the creatine transporter gene Slc6a8. *Genes Brain Behav.* 17:e12461. doi: 10.1111/gbb.12461

Uemura, T., Ito, S., Ohta, Y., Tachikawa, M., Wada, T., Terasaki, T., et al. (2017). Abnormal N-glycosylation of a novel missense creatine transporter mutant, G561R, associated with cerebral creatine deficiency syndromes alters transporter activity and localization. *Biol. Pharm. Bull.* 40, 49–55. doi: 10.1248/bpb.b16-00582

Ullio-Gamboa, G., Udobi, K. C., Dezard, S., Perna, M. K., Miles, K. N., Costa, N., et al. (2019). Dodecyl creatine ester-loaded nanoemulsion as a promising therapy for creatine transporter deficiency. *Nanomedicine* 14, 1579–1593. doi: 10.2217/nnm-2019-0059

van de Kamp, J. M., Jakobs, C., Gibson, K. M., and Salomons, G. S. (2013). New insights into creatine transporter deficiency: the importance of recycling creatine in the brain. *J. Inherit. Metab. Dis.* 36, 155–156. doi: 10.1007/s10545-012-9537-3

van de Kamp, J. M., Mancini, G. M., and Salomons, G. S. (2014). X-linked creatine transporter deficiency: clinical aspects and pathophysiology. *J. Inherit. Metab. Dis.* 37, 715–733. doi: 10.1007/s10545-014-9713-8

Van Goor, F., Hadida, S., Grootenhuis, P. D., Burton, B., Cao, D., Neuberger, T., et al. (2009). Rescue of CF airway epithelial cell function *in vitro* by a CFTR potentiator, VX-770. *Proc. Natl. Acad. Sci. U S A* 106, 18825–18830. doi: 10.1073/pnas.0904709106

Wallis, J., Lygate, C. A., Fischer, A., ten Hove, M., Schneider, J. E., Sebag-Montefiore, L., et al. (2005). Supranormal myocardial creatine and phosphocreatine concentrations lead to cardiac hypertrophy and heart failure: insights from creatine transporter-overexpressing transgenic mice. *Circulation* 112, 3131–3139. doi: 10.1161/CIRCULATIONAHA.105.572990

Wang, Q., Yang, J., Liu, Y., Li, X., Luo, F., and Xie, J. (2018). A novel SLC6A8 mutation associated with intellectual disabilities in a Chinese family exhibiting creatine transporter deficiency: case report 06 Biological Sciences 0604 Genetics. *BMC Med. Genet.* 19:193. doi: 10.1186/s12881-018-0707-5

Welch, W. J., and Brown, C. R. (1996). Influence of molecular and chemical chaperones on protein folding. *Cell Stress Chaperones* 1:109. doi: 10.1379/1466-1268(1996)001<0109:iomacc>2.3.co;2

Wong, A. C. Y., Velamoor, S., Skelton, M. R., Thorne, P. R., and Vlajkovic, S. M. (2012). Expression and distribution of creatine transporter and creatine kinase (brain isoform) in developing and mature rat cochlear tissues. *Histochem. Cell Biol.* 137, 599–613. doi: 10.1007/s00418-012-0922-7

Yu, H., van Karnebeek, C., Sinclair, G., Hill, A., Cui, H., Zhang, V. W., et al. (2013). Detection of a novel intragenic rearrangement in the creatine transporter gene by next generation sequencing. *Mol. Genet. Metab.* 110, 465–471. doi: 10.1016/j.ymgme.2013.09.018

Conflict of Interest: The authors declare that the research was conducted in the absence of any commercial or financial relationships that could be construed as a potential conflict of interest.

Copyright © 2020 Farr, El-Kasaby, Freissmuth and Sucic. This is an open-access article distributed under the terms of the Creative Commons Attribution License (CC BY). The use, distribution or reproduction in other forums is permitted, provided the original author(s) and the copyright owner(s) are credited and that the original publication in this journal is cited, in accordance with accepted academic practice. No use, distribution or reproduction is permitted which does not comply with these terms.

frontiers in Synaptic Neuroscience

REVIEW
published: 27 October 2020
doi: 10.3389/fnsyn.2020.594484

The Good, the Bad and the Unknown Aspects of Ghrelin in Stress Coping and Stress-Related Psychiatric Disorders

Eva Maria Fritz[1], *Nicolas Singewald*[1] *and Dimitri De Bundel*[2]*

[1] *Department of Pharmacology and Toxicology, Institute of Pharmacy and CMBI, University of Innsbruck, Innsbruck, Austria,* [2] *Department of Pharmaceutical Sciences, Research Group Experimental Pharmacology, Center for Neurosciences (C4N), Vrije Universiteit Brussel, Brussels, Belgium*

Ghrelin is a peptide hormone released by specialized X/A cells in the stomach and activated by acylation. Following its secretion, it binds to ghrelin receptors in the periphery to regulate energy balance, but it also acts on the central nervous system where it induces a potent orexigenic effect. Several types of stressors have been shown to stimulate ghrelin release in rodents, including nutritional stressors like food deprivation, but also physical and psychological stressors such as foot shocks, social defeat, forced immobilization or chronic unpredictable mild stress. The mechanism through which these stressors drive ghrelin release from the stomach lining remains unknown and, to date, the resulting consequences of ghrelin release for stress coping remain poorly understood. Indeed, ghrelin has been proposed to act as a stress hormone that reduces fear, anxiety- and depression-like behaviors in rodents but some studies suggest that ghrelin may - in contrast - promote such behaviors. In this review, we aim to provide a comprehensive overview of the literature on the role of the ghrelin system in stress coping. We discuss whether ghrelin release is more than a byproduct of disrupted energy homeostasis following stress exposure. Furthermore, we explore the notion that ghrelin receptor signaling in the brain may have effects independent of circulating ghrelin and in what way this might influence stress coping in rodents. Finally, we examine how the ghrelin system could be utilized as a therapeutic avenue in stress-related psychiatric disorders (with a focus on anxiety- and trauma-related disorders), for example to develop novel biomarkers for a better diagnosis or new interventions to tackle relapse or treatment resistance in patients.

Keywords: ghrelin, GHSR, stress, anxiety disorders, PTSD, central ghrelin resistance, food intake

OPEN ACCESS

Edited by:
Sigismund Huck,
Medical University of Vienna, Austria

Reviewed by:
Wulf Eckhard Haubensak,
Research Institute of Molecular Pathology (IMP), Austria
Harriet Schellekens,
University College Cork, Ireland

***Correspondence:**
Dimitri De Bundel
dimitri.de.bundel@vub.be

Received: *13 August 2020*
Accepted: *14 September 2020*
Published: *27 October 2020*

Citation:
Fritz EM, Singewald N and De Bundel D (2020) The Good, the Bad and the Unknown Aspects of Ghrelin in Stress Coping and Stress-Related Psychiatric Disorders. Front. Synaptic Neurosci. 12:594484. doi: 10.3389/fnsyn.2020.594484

Abbreviations: ACTH, adrenocorticotropic hormone; AG, acyl ghrelin; AGRP, agouti-related peptide; ARC, arcuate nucleus; CPP, conditioned place preference; CRF, corticotropin-releasing factor; CSDS, chronic social defeat stress; CUMS, chronic mild unpredictable stress; DAG, desacyl ghrelin; GABA, gamma aminobutyric acid; GHSR, ghrelin receptor (growth hormone secretagogue receptor); GOAT, ghrelin-O-acyltransferase; HFD, high-fat diet; HPA, hypothalamic-pituitary-adrenal; KO, knockout; LEAP2, liver-expressed antimicrobial peptide 2; LPS, lipopolysaccharide; MDD, major depressive disorder; NAc, nucleus accumbens; NG, nodose ganglion; NPY, neuropeptide Y; NTS, nucleus tractus solitarius; PTSD, post-traumatic stress disorder; PVN, paraventricular nucleus; TSST, Trier social stress test; VTA, ventral tegmental area.

THE GHRELIN SYSTEM

Ghrelin

Ghrelin is a stomach-derived peptide hormone that is tonically released into the blood stream with peak concentrations in response to a negative energy balance (Kojima et al., 1999; Kojima and Kangawa, 2005). The 28-amino-acid hormone is primarily produced by X/A-like oxyntic gland cells in the gastric mucosa from its precursor pre-proghrelin (117 amino acids) (Kojima et al., 1999; Date et al., 2000). In addition, ghrelin expression has also been described in other organs such as the pancreas, kidneys, lungs, heart and placenta (Mori et al., 2000; Gualillo et al., 2001; Gnanapavan et al., 2002; Iglesias et al., 2004; Kageyama et al., 2005).

Ghrelin O-acyltransferase (GOAT) is the enzyme present in the endoplasmatic reticulum of ghrelin-producing cells that ensures the post-translational acylation of desacyl ghrelin (DAG) at the serine-3 residue, resulting in the formation of acyl ghrelin (AG) (Gutierrez et al., 2008). Both, DAG and AG, are released into the blood stream where AG is rapidly converted to DAG (De Vriese et al., 2004), resulting in an AG/DAG ratio of 0.1–0.4 in plasma compared to 2.5 in stomach tissue (Hassouna et al., 2014). While DAG has received less attention in literature, an increasing amount of evidence indicates that it is not only a byproduct of AG synthesis but may act as a separate hormone that modulates or even opposes the effects of AG (for review see Delhanty et al., 2014). For example, DAG was shown to impair the feeding response to peripherally injected AG (Fernandez et al., 2016) and its actions on anxiety and other stress-related behaviors may also be distinct from those of AG (Stark et al., 2016; Mahbod et al., 2018). In this review, we aim to analyze the effects of AG and DAG separately and use the term 'ghrelin' whenever it was not possible to make a clear distinction or acylation status was not specified by the authors.

Ghrelin Receptors (GHSR)

The N-terminus of AG binds with high affinity to the growth hormone secretagogue receptor (GHSR) (Willesen et al., 1999; Cowley et al., 2003), of which two different transcripts have been identified: GHSR-1a and GHSR-1b (McKee et al., 1997). The GHSR-1a, also known as ghrelin receptor (and hereafter simply referred to as 'GHSR'), is a Gq-protein coupled receptor comprising seven transmembrane α-helical domains to which constitutive activity has been ascribed (Holst et al., 2003). The GHSR-1b form, a truncated splice variant, contains five transmembrane domains and while its physiological role remains poorly understood, it may negatively influence GHSR function by hindering conformational changes (Leung et al., 2007). AG is the main known high-affinity agonist for the GHSR, while (in physiological concentrations) DAG does not appear to act on the GHSR (Bednarek et al., 2000). A recent study indicates that the octanoyl chain is essential for the pharmacological action of AG and that DAG, while it might bind to the GHSR with very low affinity, is unlikely to stabilize an active GHSR conformation (Ferre et al., 2019). Several binding studies propose the existence of a separate receptor specific for DAG in different tissues and also the brain (e.g., Lear et al., 2010; Togliatto et al., 2010; Fernandez et al., 2016). However, such a receptor has not yet been identified (for review see Callaghan and Furness, 2014).

The GHSR is expressed in several organs such as the brain, the anterior pituitary, adrenal and thyroid glands, pancreas and the heart (Guan et al., 1997; Gnanapavan et al., 2002). Within the brain, GHSR expression has been described in several areas including the arcuate nucleus (ARC) and other subregions of the hypothalamus, the ventral tegmental area (VTA), the nucleus tractus solitarius (NTS), the hippocampus and the amygdala (Zigman et al., 2006; Mani et al., 2014). The function the GHSR has in those brain areas and whether they are accessible for circulating ghrelin is not yet fully understood (Perello et al., 2018). Thus, it is essential to note that the GHSR is constitutively active, signaling at 50% of its maximal activity in the absence of its ligand (Holst et al., 2003; Petersen et al., 2009). It is very likely that the function of the ghrelin/GHSR system is not solely dependent on the binding of AG to its receptor, but that also changes in GHSR expression levels might have pervasive biological effects. Furthermore, there is evidence that the GHSR can form heterodimers with various other receptors like for example those for dopamine, serotonin or oxytocin (Schellekens et al., 2013b; Kern et al., 2015; Wallace Fitzsimons et al., 2019), which affects downstream signaling and receptor trafficking (for review see Schellekens et al., 2013a; Abizaid and Hougland, 2020). Recent findings also suggest that the liver-expressed antimicrobial peptide 2 (LEAP2) acts as an endogenous antagonist/inverse agonist of the GHSR that modulates ghrelin function in response to the feeding status (Ge et al., 2018).

The Ghrelin System and Energy Homeostasis

Ghrelin is most widely known for its orexigenic effects. Following its release into the bloodstream, AG can diffuse passively through fenestrated capillaries of the median eminence into the ARC (Schaeffer et al., 2013) where it binds to GHSR that are expressed abundantly on neuropeptide Y/agouti-related peptide (NPY/AGRP) neurons (**Figure 1**) (Willesen et al., 1999; Cowley et al., 2003). Activation of these hypothalamic neurons by AG potently increases food intake and regulates homeostatic feeding behavior in order to maintain energy balance (Kamegai et al., 2000; Nakazato et al., 2001). Indeed, re-expression of GHSR in AGRP neurons of GHSR KO mice restores, albeit incompletely, the effect of systemic administration of AG on food intake (Wang et al., 2014). In addition, ghrelin also plays an important role in reward-based, hedonic eating behaviors (as reviewed in Perello and Zigman, 2012; Al Massadi et al., 2019), which are very likely mediated by GHSR on dopaminergic neurons of the VTA (Cornejo et al., 2020).

In humans, plasma ghrelin levels are typically increased under low-calorie conditions before meals and fall back to baseline levels after food consumption (Cummings, 2006). Also in rodents, ghrelin plasma levels rise during fasting periods and follow a diurnal rhythm peaking shortly after onset of the dark period, which is the major feeding time for rodents (Murakami et al., 2002; Bodosi et al., 2004). Peripherally circulating ghrelin

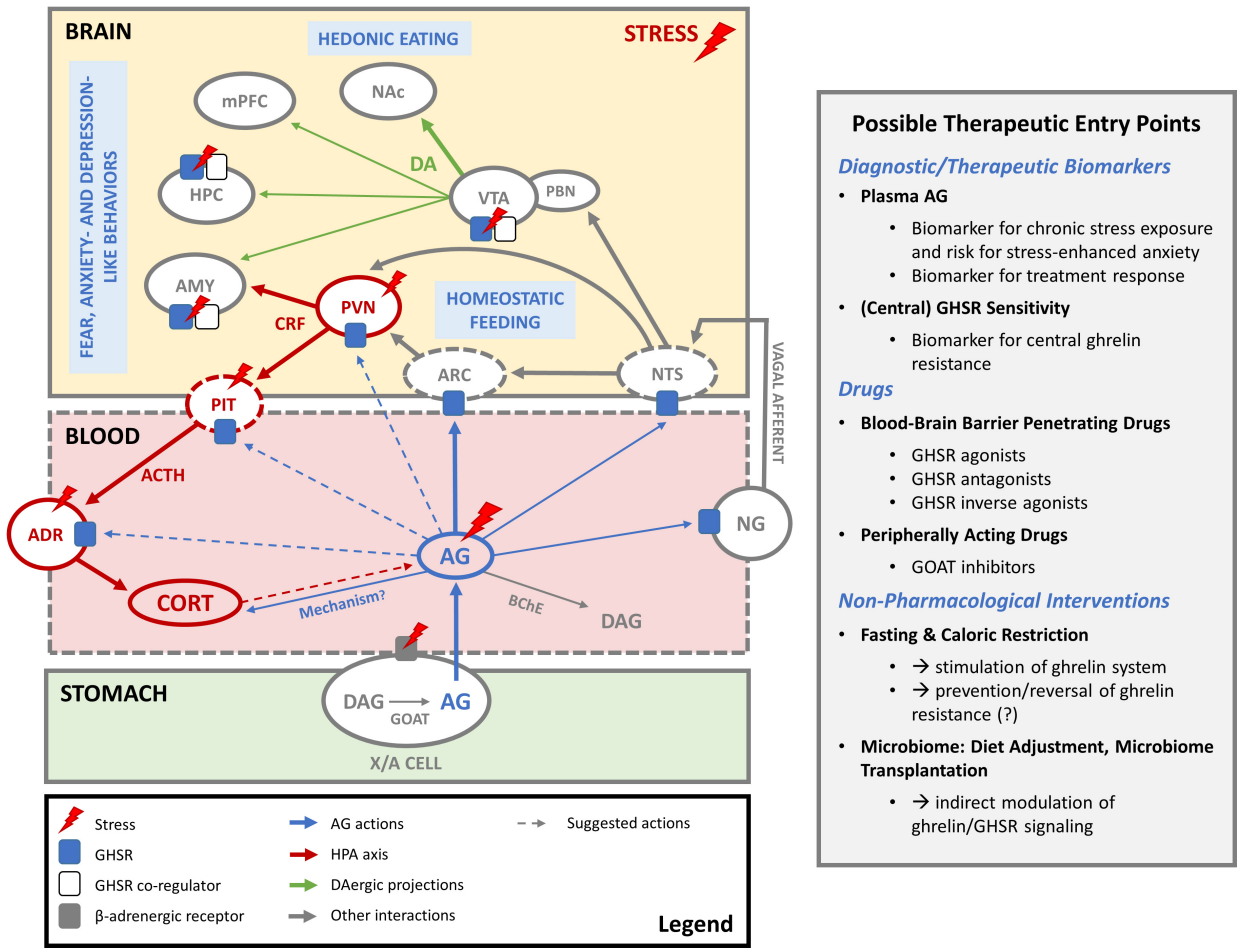

FIGURE 1 | The ghrelin system in stress coping. In periods of hunger and stress, AG is produced by acylation of DAG by GOAT in gastric X/A cells and released into the blood stream. Before it is degraded to DAG, it acts on GHSR in the arcuate nucleus of the hypothalamus (ARC) to regulate homeostatic feeding. Increased AG levels during stress also seem to amplify HPA axis activation and induce corticosterone (CORT) release. The exact mechanism is not clear and could involve indirect activation of CRF-producing neurons in the PVN by inhibition of the local GABAergic tone, modulation of ACTH production in the pituitary (PIT) or direct effects on the adrenal cortex (ADR). AG may also indirectly influence the HPA axis via GHSR in the nodose ganglion (NG) of the vagal nerve or in the nucleus tractus solitarius (NTS). Conversely, whether HPA axis activity during stress has an impact on ghrelin release remains a subject of debate. Elevated AG levels following stress may also be secondary to activation of the sympathetic nervous system and beta receptors on ghrelin-producing X/A cells. Whether AG can pass the blood-brain barrier to act on stress-relevant brain areas where GHSR are expressed is not clear. However, constitutive activity of central GHSR may be regulated via changes in GHSR expression levels or formation of heterodimers with other receptors (e.g., dopamine, serotonin) as co-regulators. Such mechanisms might play a role in stress-related changes in feeding and fear, anxiety- and depression like behaviors, possibly via GHSR in the ventral tegmental area (VTA), hippocampus (HPC) and amygdala (AMY). Also mesocorticolimbic dopaminergic projections (DA) of the VTA to nucleus accumbens (NAc), medial prefrontal cortex (mPFC), HPC and AMY may play a role here. *Abbreviations:* AG, acyl ghrelin; DAG, desacyl ghrelin; GOAT, ghrelin O-acyltransferase; BChE, butyryl cholinesterase; ARC, arcuate nucleus of the hypothalamus; PVN, paraventricular nucleus of the hypothalamus; CRF, corticotropin releasing factor; PIT, pituitary gland; ACTH, adrenocorticotropic hormone; CORT, corticosterone/cortisol; ADR, adrenal cortex; NTS, nucleus tractus solitarius; NG, nodose ganglion; VTA, ventral tegmental area; PBN, parabrachial nucleus; DA, dopamine; NAc, nucleus accumbens; mPFC, medial prefrontal cortex; HPC, hippocampus; AMY, amygdala.

has various effects on the gastrointestinal tract: it modulates intestinal motility, gastric emptying and gastric acid secretion as well as insulin release from the pancreas (for review see Kojima and Kangawa, 2005).

Overall, the role of ghrelin in driving food intake and energy homeostasis seems well established: it communicates with the brain and the gastrointestinal tract to promote feeding and ensure efficient energy storage and metabolism, lowering the risk of hypoglycemia (reviewed comprehensively by Yanagi et al., 2018). Importantly, while ghrelin signaling stimulates food intake, the effects of a loss of ghrelin signaling on feeding behavior are more subtle if detectable at all (as reviewed in Uchida et al., 2013). Nevertheless, ghrelin appears critical in the regulation of systemic glucose homeostasis and ensures survival after prolonged starvation (Goldstein et al., 2011; McFarlane et al., 2014), potentially through GHSR signaling in the nodose ganglion (NG) of the vagal nerve and the NTS (Scott et al., 2012; Okada et al., 2018) (**Figure 1**). Projections of the NTS to the parabrachial nucleus (Roman et al., 2016) and to the ARC (Aklan et al., 2020) were shown to regulate

food intake in anorectic or hypoglycemic conditions, but it remains poorly understood how the ghrelin system modulates activity in these neurochemically distinct pathways. The effect of ghrelin on glucose homeostasis also involves the release of growth hormone in response to low blood glucose if body fat stores are depleted, which in turn increases glucose release from the liver and contributes to stabilization of blood glucose levels (Goldstein et al., 2011). Moreover, ghrelin modulates pancreatic insulin secretion and regulates its peripheral actions, although the exact mechanisms involved are still a matter of debate (as reviewed by Gray et al., 2019). Interestingly, it has been proposed that a decline in ghrelin system activity may play a role in age-dependent impairment of energy homeostasis and associated disease patterns like reduced appetite, obesity, diabetes or hepatic steatosis, but also cardiovascular dysfunction and neurodegenerative diseases (for review see Stoyanova, 2014; Yin and Zhang, 2016; Amitani et al., 2017).

Ghrelin/GHSR Interactions With the HPA Axis

Beyond its well-established role as a mediator of feeding behavior, the ghrelin system has also been implicated in many other functions. Notably, it has been proposed as a regulator of stress responses, as its function seems to be closely entwined with that of the hypothalamic-pituitary-adrenal (HPA) axis (for review see Spencer et al., 2015), as illustrated in **Figure 1**.

Several studies have demonstrated that systemic or central administration of ghrelin increases the plasma concentration of corticosterone in rodents or cortisol in humans (Asakawa et al., 2001a; Stevanovic et al., 2007; Lambert et al., 2011; Cabral et al., 2012, 2016; Jensen et al., 2016). The effects of ghrelin on plasma adrenocorticotropic hormone (ACTH), however, appear inconsistent. One study reported elevated ACTH and an increased volume of ACTH-producing cells in the pituitary following central ghrelin administration (Stevanovic et al., 2007), but another study found no influence of ghrelin on plasma ACTH levels (Jensen et al., 2016). In line with the notion that the ghrelin system may increase activity of the HPA axis, a blunted release of ACTH and corticosterone after exposure to a brief period of immobilization stress was previously observed in ghrelin KO mice (Spencer et al., 2012). Similarly, one study showed lower corticosterone levels in GHSR KO compared to wild type mice in a chronic social defeat stress (CSDS) paradigm (Chuang et al., 2011). In contrast to the aforementioned studies, a more recent publication reported higher corticosterone release after acute restraint stress in non-handled ghrelin KO mice versus wild type controls (Mahbod et al., 2018). Moreover, more elevated plasma corticosterone levels have also been observed in GHSR KO mice following acute and chronic stress paradigms (Patterson et al., 2013a; Mahbod et al., 2018). Interestingly, administration of DAG increased plasma corticosterone levels in non-stressful conditions in ghrelin KO mice, but attenuated corticosterone release during acute stress exposure (Stark et al., 2016), suggesting that the effects of DAG on HPA axis activity may depend on prior stress exposure.

Taken together, the influence of the ghrelin system on HPA axis activity is not fully resolved yet and the underlying mechanisms remain poorly understood. Cabral and colleagues demonstrated that peripheral AG administration induces c-Fos expression not only in the ARC but also in corticotropin releasing factor (CRF)-producing cells in the paraventricular nucleus (PVN) of the hypothalamus (Cabral et al., 2012). These cells, however, do not express GHSR, so in a further study the authors suggested that AG may indirectly activate CRF neurons in the PVN via inhibition of the local GABAergic tone (Cabral et al., 2012, 2016), which was confirmed by a more recent electrophysiological study (Dos-Santos et al., 2018). Ghrelin may also influence the HPA axis through other mechanisms (**Figure 1**). Intravenous administration of ghrelin appears to inhibit vagal afferents (Asakawa et al., 2001b; Date et al., 2006) and stimulate vagal efferents (Fujitsuka et al., 2011). The influence of the ghrelin system on activity of the vagal nerve remains controversial (Arnold et al., 2006) and may involve activation of GHSR in the NG of the vagal nerve or central mechanisms with activation of GHSR in the NTS (Bansal et al., 2012; Swartz et al., 2014; Su et al., 2019). Further elucidation of the interaction of the ghrelin system with the vagus nerve may be relevant in this context, given that vagal nerve stimulation influences HPA axis activity in rodents (De Herdt et al., 2009) and humans (Warren et al., 2019). Moreover, ghrelin may also have an impact on glucocorticoid production through direct effects on the adrenal gland (Rucinski et al., 2009).

Conversely, how activity in the HPA axis may influence the ghrelin system also remains subject of debate (**Figure 1**). Administration of an ACTH analog was shown to increase plasma ghrelin levels in humans by increasing cortisol levels (Azzam et al., 2017). On the other hand, chronic immobilization stress increased plasma AG levels in adrenalectomized rats (Meyer et al., 2014), indicating that stress can drive AG release independently of glucocorticoid production. Interestingly, a recent study demonstrated that elevated AG levels following chronic stress exposure could be reversed by the beta receptor antagonist atenolol (Gupta et al., 2019). This hydrophilic beta receptor antagonist does not readily cross the blood-brain barrier, suggesting that stress-induced elevations in plasma AG may be secondary to activation of the sympathetic nervous system.

The notion that ghrelin is released upon stress exposure and mediates at least some behavioral adaptations to stress, which we review and discuss in the following two sections, supports the idea of ghrelin as a novel stress hormone, acting in concert with but also partially independent of the central HPA axis.

THE ROLE OF THE GHRELIN SYSTEM IN STRESS-RELATED BEHAVIORS IN RODENTS

Effects of Stress on Plasma Ghrelin Levels in Rodents

There is ample evidence showing that plasma ghrelin levels are affected by various acute and chronic stressors, as summarized

in **Table 1**. Increased total ghrelin levels were reported following acute water avoidance stress in rats (Kristenssson et al., 2006, Kristenssson et al., 2007) or maternal separation in mice (Schmidt et al., 2006), while elevated DAG but not AG was observed in plasma of rats following a short immobilization stress episode (Nahata et al., 2014). A number of publications also showed no changes in AG or total ghrelin levels after a single exposure to foot shocks (Harmatz et al., 2016; Rostamkhani et al., 2016) or immobilization stress in rats (Gul et al., 2017). Importantly, nutritional status may also play a role, given that acute stressors such as novelty stress (Saegusa et al., 2011) or a single injection of lipopolysaccharide (LPS) (Stengel et al., 2010) led to a decrease in plasma AG alone or both, DAG and AG, when blood samples were collected in food-deprived conditions.

In subchronic stress paradigms like exposure of rats to a flooded cage, elevated AG levels were found (Ochi et al., 2008). Also socially isolated male but not female mice showed increased plasma AG in fasted conditions (Yamada et al., 2015). However, no changes or even decreases in serum ghrelin levels were reported following subchronic social stress or social isolation in rats in a fasted state (Izadi et al., 2018). The effects of stress exposure on plasma ghrelin levels may be dependent on developmental stage and sex, given that subchronic stress induced by limited nesting material seemed to affect plasma ghrelin levels differently in male and female mice, with minor alterations in male pups versus pronounced changes in serum DAG in female pups (Yam et al., 2017).

Regarding chronic stressors, a number of studies reported increased plasma AG levels following CSDS in mice (Lutter et al., 2008; Chuang et al., 2011; Patterson et al., 2013a; Guo et al., 2019; Han et al., 2019). Only one study in mice found decreased total ghrelin levels following CSDS (Razzoli et al., 2015), however, the decrease in total plasma ghrelin was not observed when the food intake was restricted throughout the CSDS paradigm. Similarly, chronic mild unpredictable stress (CUMS) protocols were shown to induce elevated total serum ghrelin levels in rats (Lopez Lopez et al., 2018) and plasma AG levels in mice (Patterson et al., 2010; Huang et al., 2017). Also chronic immobilization stress increased ghrelin or AG levels in rats (Elbassuoni, 2014; Meyer et al., 2014). A recent study showed that elevated plasma AG levels following chronic immobilization stress in adolescent rats persisted up to four months after stress exposure (Yousufzai et al., 2018). Only one study reported decreased total ghrelin levels following repeated exposure to foot shocks (Rostamkhani et al., 2016). In summary, while literature on the effects of acute or subchronic stress exposure on plasma ghrelin levels is conflicting, chronic exposure to stress relatively consistently increases plasma AG levels.

Effects of Stress on Food Intake and Body Weight in Rodents and the Possible Role of Ghrelin and GHSR Signaling

Exposure to acute and chronic stressors impacts on food intake and body weight in rodents and the ghrelin system has been proposed a role in stress-related feeding behaviors, which, however, is not fully established yet. In **Table 2** we give an extensive, although certainly not exhaustive, overview of the effects of different acute and chronic stress paradigms on food intake and body weight.

Acute stressors such as a single session of social defeat (Meerlo et al., 1996), immobilization stress (Gul et al., 2017), novelty stress (Saegusa et al., 2011; Matsumoto et al., 2017) but also LPS injection (Stengel et al., 2010) were mostly found to reduce food intake. While only a few of these studies measured body weight, they reported a decrease following exposure to an acute stressor (Meerlo et al., 1996; Gul et al., 2017).

Also in subchronic and chronic stress paradigms food intake and body weight are typically negatively affected. For example, repeated immobilization stress decreased food intake (Jeong et al., 2013; Jiang and Eiden, 2016) and in parallel decreased (Li et al., 2015; Jiang and Eiden, 2016; Mograbi et al., 2020) or had no effect on body weight (Jeong et al., 2013). Also exposure to a flooded cage for five days decreased body weight (Ochi et al., 2008) and, similarly, social isolation for a week (Izadi et al., 2018) or chronic administration of foot shocks (Rostamkhani et al., 2016) reduced food intake and body weight. Early life stress induced by limited access to bedding and nesting material for a week led to attenuated weight gain during stress exposure in male and female pups, which was compensated by an increased weight gain after termination of the stress exposure (Yam et al., 2017). As an exception, only one study found increased food intake and body weight gain during immobilization stress over a period of three weeks, which was more pronounced in male than female rats (Elbassuoni, 2014).

Exposure to CUMS, which utilizes a battery of different stressors over a time course of several weeks, relatively consistently led to decreases in food intake (Patterson et al., 2010; Yao et al., 2016; He et al., 2018; Yan et al., 2018) and body weight in mice and rats (Forbes et al., 1996; Harris et al., 1997; Patterson et al., 2010; Lopez Lopez et al., 2018; Simas et al., 2018; Yan et al., 2018; Li et al., 2019; Yun et al., 2020). A few studies reported decreases in body weight or body weight gain, while food intake was not significantly altered (Harris et al., 1997; Lopez Lopez et al., 2018; Simas et al., 2018). Only one study found an increase in daily chow consumption and no differences in body weight between CUMS and non-CUMS mice after eight weeks of stress exposure (Huang et al., 2017). Interestingly, Simas et al. reported a decreased food intake in mice exposed to CUMS compared to non-stressed mice when only a high-fat diet (HFD) was provided, but not when fed a standard diet (Simas et al., 2018). This suggests that the rewarding properties of calorically dense food are abolished during CUMS. In line with this notion, several of the previously mentioned studies also evaluated sucrose or saccharine preference. Some found no differences (Forbes et al., 1996; Harris et al., 1997; Yun et al., 2020), but in several studies CUMS exposure led to reduced sucrose or saccharine intake (Yao et al., 2016; Huang et al., 2017; He et al., 2018; Yan et al., 2018), which may reflect stress-induced anhedonia.

On the other hand, CSDS in mice quite robustly led to increases in food intake (Lutter et al., 2008; Patterson et al., 2013a,b; Razzoli et al., 2015), associated with an increase in body weight in some studies (Patterson et al., 2013a; Razzoli et al., 2015) but not in others (Lutter et al., 2008;

TABLE 1 | Effect of stressors on ghrelin levels in rodents.

References	Animals	Feeding status	Duration	Stress paradigm	Ghrelin levels	Time point
(Kristenssson et al., 2006) (Kristenssson et al., 2007)	**rats (WKY, SPD)** f	*ad libitum* fed	**acute**	**water avoidance** 1 h	TG ↑ **(WKY > SPD)**	–
(Schmidt et al., 2006)	**mice (CD1)** m/f, pups (p8)	not specified	**acute**	**maternal separation** 4 h, 8 h, 12 h	?G ↑	–
(Nahata et al., 2014)	**mice (ICR)** m	fasted + fed (16 h + 20 min)	**acute**	**immobilization stress** 1 h	AG ↔ DAG ↑	@ during immobilization
		fasted (16 h)	**acute**	**immobilization stress** 1 h	AG ↔ DAG ↑	@ during immobilization
(Harmatz et al., 2016)	**rats (LE)** m	*ad libitum* fed	**acute**	**foot shock** 3 × 2s	AG ↔	–
(Rostamkhani et al., 2016)	**rats (WST)** m	*ad libitum* fed	**acute**	**foot shock** 60 × 10s	TG ↔	–
(Gul et al., 2017)	**rats (WST)** m	*ad libitum* fed	**acute**	**immobilization stress** 2 h	?G ↔	–
(Saegusa et al., 2011)	**mice (C57BL/6J)** m	fasted (24 h)	**acute**	**novelty (single housing)** 3 h	AG ↓	–
(Stengel et al., 2010)	**rats (SPD)** m	fasted (17 h)	**acute**	**LPS injection** 100 μg/kg	AG ↓ \ ↔ DAG ↓ \ ↔	@ 2 h, 5 h, 7 h \ 24 h
(Ochi et al., 2008)	**rats (WST)** m	*ad libitum* fed	**subchronic**	**water cage** 5 d	TG ↔ \ ↔ AG ↔ \ ↑ DAG ↔ \ ↔	@ 4 h, 8h, 24 h \ 3 d, 5 d
(Yamada et al., 2015)	**mice (C57BL/6)** m/f	fasted (18 h)	**subchronic**	**social isolation** 7 d	AG ↑ **m** vs. ↔ **f**	–
(Izadi et al., 2018)	**rats (WST)** m	fasted (16–18 h)	**subchronic**	**social stress** 7 d	?G ↔	–
			subchronic	**social isolation** 7 d	?G ↓	–
(Yam et al., 2017)	**mice (C57BL/6J)** m/f, pups (p2-p14)	not specified	**subchronic**	**early chronic stress** 7 d (p2-p9)	TG ↔ \ ↔ **m** vs. ↑ \ ↓ **f** AG ↔ \ ↔ **m** vs. ↔ \ ↔ **f** DAG ↔ \ ↔ **m** vs. ↑ \ ↓ **f**	@ p9 \ p14
(Lutter et al., 2008)	**mice (C57BL/6J)** m	*ad libitum* fed	**chronic**	**CSDS** 10 d	AG ↑ \ ↑	@ 11d \ 39d
(Chuang et al., 2011)	**mice (GHSR WT/KO)** m, C57BL/6J bckg	*ad libitum* fed	**chronic**	**CSDS** 10 d	AG ↑ (**GHSR KO** and **WT**) DAG ↔ (**GHSR KO** and **WT**)	
(Patterson et al., 2013a)	**mice (C57BL/6J)** m	*ad libitum* fed (STD + HFD)	**chronic**	**CSDS** 21 d	AG ↑ \ ↔	@ 22d \ 62d
	mice (GHSR WT/KO) m, C57BL/6J bckg	*ad libitum* fed (STD + HFD)	**chronic**	**CSDS** 21 d	AG ↑ (**GHSR WT** only)	–
(Guo et al., 2019)	**mice (GHSR KO/WT)** m	*ad libitum* fed	**chronic**	**CSDS** 10 d	TG ↑ (**GHSR KO** and **WT**)	–
(Han et al., 2019)	**C57BL/6J mice** m	*ad libitum* fed	**chronic**	**CSDS** 10 d	AG ↑	–

(Continued)

TABLE 1 | Continued

References	Animals	Feeding status	Duration	Stress paradigm	Ghrelin levels	Time point
(Razzoli et al., 2015)	**mice (CD1)** m	*ad libitum* fed	**chronic**	**CSDS** 28 d	TG ↓	–
(Lopez Lopez et al., 2018)	**rats (WST)** m	*ad libitum* fed	**chronic**	**CUMS** 20 d, 40 d, 60 d	TG ↔ \ ↑ \ ↔	@ 20 d \ 40 d \ 60 d
(Patterson et al., 2010)	**mice (GHSR WT/KO)** m, C57BL/6J-DBA bckg	*ad libitum* fed (STD + HFD)	**chronic**	**CUMS** 14 d	AG ↑ (**GHSR KO** and **WT**)	–
(Huang et al., 2017)	**mice (C57BL/6J)** m	*ad libitum* fed	**chronic**	**CUMS** 8 w	AG ↑	–
(Elbassuoni, 2014)	**rats (SPD)** m/f	fasted (10h)	**chronic**	**immobilization stress** 20 min/d, 21 d	?G ↑ (**f** > **m**)	–
(Meyer et al., 2014)	**rats (LE)** m	*ad libitum* fed	**chronic**	**immobilization stress** 4 h/d, 14 d	AG ↑	–
(Rostamkhani et al., 2016)	**rats (WST)** m	*ad libitum* fed	**chronic**	**foot shock** 60 × 10s, 15 d	TG ↓	–
(Yousufzai et al., 2018)	**rats (LE)** m	*ad libitum* fed	**chronic**	**immobilization stress** 4 h/d, 14 d	AG ↑	@ 130 d

Measurements after stressor cessation unless stated otherwise (@ x h/d; 1 = start of stressor). Abbreviations: WKY, Wistar-Kyoto; SPD, Sprague-Dawley; LE, Long-Evans; WST, Wistar; p, postnatal day; bckg, background; STD, standard diet; HFD, high-fat diet; LPS, lipopolysaccharide; CSDS, chronic social defeat stress; CUMS, chronic mild unpredictable stress; TG, total ghrelin; AG, acyl ghrelin; DAG, desacyl ghrelin; ?G, ghrelin (not specified).

Patterson et al., 2013b). Chuang and colleagues showed that conditioned place preference (CPP) for HFD was significantly increased in CSDS-exposed mice, which was associated with a higher intake of HFD chow and a greater weight gain over the course of the CPP paradigm (Chuang et al., 2011). However, in contrast to these studies in mice, subchronic and chronic social defeat paradigms in rats resulted in decreases in daily food intake (Berton et al., 1998) and body weight (Berton et al., 1998; Fanous et al., 2011; Patki et al., 2013).

Some of the aforementioned studies also investigated the role of the GHSR in stress-related changes in feeding behavior and found that both increases (CSDS) or decreases (CUMS) in food intake and body weight gain were abolished in GHSR KO mice (Lutter et al., 2008; Patterson et al., 2010, 2013a). Moreover, increased CPP for and higher intake of HFD and an associated weight gain after CSDS exposure were not present in GHSR KO mice (Chuang et al., 2011), indicating a central role of ghrelin signaling in these stress-induced changes. The increased CPP, however, could be reinstated by selective re-expression of GHSR in tyrosine hydroxylase-positive neurons, which the authors concluded are very likely involved in mediating stress-induced food reward. Interestingly, a recent study used re-expression of GHSR in dopamine transporter (DAT)-positive neurons of GHSR KO mice to confirm that GHSR signaling in dopaminergic neurons controls appetitive and consummatory behaviors toward HFD in *ad libitum* fed mice (Cornejo et al., 2020). Indeed, it has been proposed previously that the ghrelin system may play an important role in stress-induced food reward behavior and act as a critical modulator at the interface of homeostatic control of appetite and food reward during stress, promoting hyperphagia and hedonic intake of calorically dense 'comfort foods' (Schellekens et al., 2012).

Even though stress paradigms typically increase AG levels and in some instances increase feeding, paradoxically, exposure to stress may also be associated with a decrease in food intake and body weight. During acute stress exposure, it is likely that the orexigenic effects of high plasma AG are overcome by other factors, such as stress-induced changes in CRF signaling in the brain (Jochman et al., 2005; Haque et al., 2013; Dunn et al., 2015; Mogami et al., 2016). Chronic stress, on the other hand, might induce central ghrelin resistance, associated with lower GHSR expression in particular brain areas (Harmatz et al., 2016), which then may further contribute to reduced food intake and anhedonia-like behaviors in a GHSR-dependent manner, but irrespective of high circulating AG concentrations. This may apply for physical stressors like foot shocks, immobilization stress or various stressors used during CUMS which are typically associated with reduced food intake and decreases in body weight. The same hypothesis, however, does not seem to hold true for CSDS in mice, where high plasma AG is mostly associated with increases in food intake and where GHSR signaling in dopaminergic neurons has been proposed to mediate stress-induced food reward as a coping mechanism (Chuang et al., 2011). The observation that CSDS increases food intake and/or body weight specifically in mice but not in rats could be attributed to species differences in social dominance behavior (Kondrakiewicz et al., 2019). The question remains what impact

TABLE 2 | Effect of stressors on food intake in rodents.

References	Animals	Paradigm *(Feeding status)*	Food intake (FI)	Time point *Measurement*	Body weight (BW)	Time point *Measurement*
			Acute stress paradigms			
(Meerlo et al., 1996)	**rats (TMDS3)** m	**social defeat** 1x or 2x	↓ (**2x** only)	@ 1 d-3 d *FI daily*	↔ \ ↓ (**2x** > **1x**)	@ 1 d \ 2 d-3 d *BW g*
(Gul et al., 2017)	**rats (WST)** m	**immobilization stress** 2 h *(fed)*	↓	@ 24 h *FI cumul*	↓	@ 24h *BW change %*
(Saegusa et al., 2011)	**mice (C57BL/6J)** m	**novelty** 3 h *(fasted, 24h)*	↓ \ ↔	@ 1 h, 3 h \ 6 h *FI cumul*	-	-
(Matsumoto et al., 2017)	**mice (C57BL/6)** f, aged	**novelty** 3 h *(fasted, 18 h)*	↓	@ 1 h, 3 h *FI cumul*	-	-
	mice (C57BL/6) m/f, aged	**novelty** 3 h *(fed)*	↓ **m** vs. ↔ **f**	@ 6 h, 24 h *FI cumul*	-	-
(Stengel et al., 2010)	**rats (SPD)** m	**LPS injection** 100 μg/kg *(fasted, 16h)*	↓	@ 2 h, 5 h, 7 h, 24 h *FI per time period*	-	-
			(Sub)chronic stress paradigms			
(Jeong et al., 2013)	**mice (ICR)** m	**immobilization stress** 2 h/d, 15 d	↓ \ $(\downarrow)^{ns}$	@ 2 d-6 d \ 7 d-15 d *FI daily*	↔	@ 2 d-15 d *BW g*
(Jiang and Eiden, 2016)	**mice (PACAP WT)** m, C57BL/6N bckg	**immobilization stress** 1 h/d, 7 d	↓	@ 7 d *FI cumul*	↓	@ 7 d *BW loss %*
(Li et al., 2015)	**mice (ICR)** f, maternal	**immobilization stress** ? h/d, 21 d	$(\downarrow)^{ns}$	@ 1 d-16 d *FI daily*	↓	@ 3 d-16 d *BW g*
(Mograbi et al., 2020)	**rats (WST)** m	**immobilization stress** 2,4 or 6 h/d, 21 d	-	-	↓	@ 1 w, 2 w, 3 w *BW gain %*
(Ochi et al., 2008)	**rats (WST)** m	**water cage** 5 d	-	-	↓	@ d1-d5 *BW change %*
(Izadi et al., 2018)	**rats (WST)** m	**social stress** 7 d	↔	@ 8 d *FI cumul (3 h)*	↔	@ 7 d *BW change g*
	rats (WST) m	**social isolation** 7 d	↓	@ 8 d *FI cumul (3 h)*	↓	@ 7 d *BW change g*
(Rostamkhani et al., 2016)	**rats (WST)** m	**foot shock** 60 × 10 s, 15 d	↔ \ ↓ \ $(\downarrow)^{ns}$	@ 2 d \ 7 d \ 15 d *FI cumul (24 h)*	↔ \ ↓	@ d1 \ d15 *BW g*
(Yam et al., 2017)	**mice (C57BL/6J)** m/f, pups (p2-p14)	**early chronic stress** 7 d (p2-p9)	-	-	↓ \ ↑	@ p2-p9 \ p9-p14 *BW gain g*
(Elbassuoni, 2014)	**rats (SPD)** m/f	**immobilization stress** 20 min/d, 21 d	↑ (**m** > **f**)	@ 1 d-21 d *FI daily avgd*	↑ (**m** > **f**)	@ 21d *BW gain g*

(Continued)

TABLE 2 | Continued

References	Animals	Paradigm *(Feeding status)*	Food intake (FI)	Time point *Measurement*	Body weight (BW)	Time point *Measurement*
(Patterson et al., 2010)	**mice (GHSR WT/KO)** m, C57BL/6J-DBA bckg	**CUMS** 14 d *(STD + HFD)*	↓ ↔ **GHSR-KO**	@ 1 d-14 d *kcal daily avgd*	↓ ↔ **GHSR-KO**	@ d14 *BW change g*
(Yao et al., 2016)	**mice (C57BL/6N)** m	**CUMS + social isolation** 21 d *(fasted, 12 h)*	↓	@ 21 d *FI cumul (24 h)/BW*	-	-
(He et al., 2018)	**rats (SPD)** f	**CUMS** 4 w	-	-	↓	@ 1 w, 2 w, 3 w, 4 w *BW change %*
(Yan et al., 2018)	**mice (C57BL/6J)** m	**CUMS** 21 d	↔ \ ↓	@ 7 d, 14 d \ 21 d *FI cumul (24 h) ?*	↔ \ ↓	@ 7 d, 14 d \ 21 d *BW g*
(Forbes et al., 1996)	**rats (LH)** m	**CUMS** 6 w	-	-	↓	@ 1 w-6 w *BW g*
(Harris et al., 1997)	**rats (WST)** m	**CUMS** 40 d	↔	@ 1 d-40 d *FI daily*	↔ \ ↓	@ 1 d-3 d \ 4 d-40 d *BW g*
(Lopez Lopez et al., 2018)	**rats (WST)** m	**CUMS** 60 d	↔	@ 1 d-60 d *FI daily*	↔ \ ↓	@ 1 d-40 d \ 40 d-60 d *BW g*
(Simas et al., 2018)	**rats (WST)** m	**CUMS** 4 w *(STD)*	↔	@ 1 w, 2 w, 3 w, 4 w *FI daily avgd*	↔ (but no BW gain from 0w as control)	@ 1 w, 2 w, 3 w, 4 w *BW g*
		CUMS 4 w *(HFD)*	↔ \ ↓ \ (↓)^{ns}	@ 1 w, 2 w \ 3 w \ 4 w *FI daily avgd*	↔ \ ↓	@ 1 w, 2 w, 3 w \ 4 w *BW g*
(Li et al., 2019)	**rats (WST)** m	**CUMS** 4 w	-	-	↔ \ ↓ (and ↓ BW gain from 1 w)	@ 1 w \ 2 w, 3 w, 4 w *BW g*
(Yun et al., 2020)	**mice (C57BL/6N)** m	**CUMS** 6 w	-	-	↔ \ ↓	@ 2 w \ 4 w, 6 w *BW change g*
(Huang et al., 2017)	**mice (C57BL/6J)** m	**CUMS** 8 w	↑	@ 0 w-8 w *(1x/w) FI daily avgd*	↔	@ 8 w *BW change g*
(Lutter et al., 2008)	**mice (GHSR WT/KO)** m, C57BL/6 J bckg	**CSDS** 10 d	↑ ↔ **GHSR KO**	@ 1 d-10 d, 11 d-13 d *FI daily avgd*	↔	@ 1 d-13 d *BW change g*
(Patterson et al., 2013a)	**mice (C57BL/6J)** m	**CSDS** 21 d *(STD + HFD 4h/d)*	↑ **STD** vs. ↓ **HFD**	@ 1 d-21 d *FI daily avgd*	↑	@ 1 d-21 d *BW g avgd*
	mice (GHSR WT/KO) m, C57BL/6J bckg	**CSDS** 21 d *(STD + HFD 4h/d)*	↑ ↔ **GHSR KO**	@ 1 d-21 d *kcal daily avgd*	↑ ↔ **GHSR KO**	@ 21 d *BW gain g*
(Patterson et al., 2013b)	**mice (C57BL/6J)** m	**CSDS** 21 d	↑	@ 1 d-21 d *FI and kcal daily avgd*	↔	@ 21 d *BW, BW change g*
(Razzoli et al., 2015)	**mice (C57BL/6J)** m	**CSDS** 4 w	↑	@ 1 w-4 w ? *FI daily avgd*	-	-
	mice (CD1) m	**CSDS** 4 w *(STD 1 w, HFD 3 w)*	↑ \ ↔	@ 1 w, 2 w, 3 w \ 4 w *kcal daily avgd ?*	↔ \ ↑	@ 1 w \ 2 w, 3 w, 4 w *BW g*

(Continued)

TABLE 2 | Continued

References	Animals	Paradigm *(Feeding status)*	Food intake (FI)	Time point *Measurement*	Body weight (BW)	Time point *Measurement*
(Chuang et al., 2011)	**mice (GHSR WT/KO)** m, C57BL/6J bckg	**CSDS** 10 d	**STD** ↔ vs. **HFD** ↑ ↔ **GHSR KO**	@ 26 d (during CPP) *FI cumul (CPP)*	↑ ↔ **GHSR KO**	@ 26 d (during CPP) *BW change % (CPP)*
(Berton et al., 1998)	**rats (LEW)** m	**RI SDS** 7 d	↓ \ (↓)^{ns}	@ 1 d-5 d \ 6 d-7 d *FI daily (g/100g)*	↓ \ ↔	@ 1 d-4 d \ 5 d-6 d *BW change %*
(Fanous et al., 2011)	**rats (SPD)** m	**RI SDS** every 3 d, 10 d	-	-	↓	@ 10 d *BW gain g*
(Patki et al., 2013)	**rats (SPD)** m	**RI SDS** 7 d	↔	@ 1 d-7 d *FI daily avgd*	↓	@ 7 d *BW gain g*

Acute paradigms: Measurements after stressor cessation (@ x h/d/w; 1 = start of stressor). Chronic paradigms: Measurements during paradigm and/or after stressor cessation as indicated (@ x h/d). Abbreviations: TMDS3, Tryon Maze Dull S3; WST, Wistar; SPD, Sprague-Dawley; bckg, background; p, postnatal day; LH, Lister hooded; LEW, Lewis; LPS, lipopolysaccharide; CUMS, chronic mild unpredictable stress; STD, standard diet; HFD, high-fat diet; CSDS, chronic social defeat stress; RI, resident-intruder; SDS, social defeat stress; FI, food intake; cumul, cumulative; avgd, averaged; BW, body weight; ()^{ns}, non-significant.

circulating ghrelin and central GHSR signaling may have on other stress-related behaviors in rodents.

Role of Circulating Ghrelin in Fear, Anxiety- and Depression-Like Behaviors

While some studies propose that ghrelin reduces fear, anxiety- and depression-like behaviors in rodents, others actually suggest an opposite role. One early study showed that central administration of ghrelin antisense DNA had anxiolytic and antidepressant-like effects and reduced the retrieval of conditioned fear in unstressed rats (Kanehisa et al., 2006). Similarly, Spencer and colleagues found reduced anxiety-like behaviors in ghrelin KO mice under baseline conditions, but increased anxiety scores following acute immobilization stress (Spencer et al., 2012). However, a more recent study also found higher anxiety-like behavior in ghrelin KO mice under non-stressed conditions (Mahbod et al., 2018). A genetic deletion of GOAT and thus attenuated AG levels (Zhao et al., 2010) reduced anxiety-like behavior prior to stress exposure (Mahbod et al., 2018) or was anxiogenic regardless of stress conditions (Stark et al., 2016).

Pharmacological studies investigating the effects of AG and other GHSR ligands have also delivered contradictory results. Systemic or central injection of a single dose of AG has been shown to induce anxiety- and depression-like behaviors in mice and rats that were not previously subjected to stress (Asakawa et al., 2001a; Carlini et al., 2002, 2004; Currie et al., 2012, 2014; Brockway et al., 2016; Jackson et al., 2019). Similarly, central infusion of ghrelin for one month increased anxiety- and depression-like behavior in rats (Hansson et al., 2011). In contrast, a few other studies reported anxiolytic and antidepressant-like effects of a single systemic dose of AG in non-stressed mice (Lutter et al., 2008; Jensen et al., 2016). In a recent publication, the administration of AG into the dorsal raphe nucleus was anxiolytic in an inhibitory avoidance test but facilitated learned escape behavior in rats (Cavalcante et al., 2019).

In studies where AG is administered systemically, it should generally be considered that it can be converted to DAG (De Vriese et al., 2004). This could be relevant, given that DAG was found to have anxiogenic effects in ghrelin KO mice which were not previously subjected to stress (Stark et al., 2016). Moreover, the effects of exogenous AG administration may also depend on feeding state. An injection of ghrelin into the amygdala had no significant effect in fed mice, but was anxiolytic when no food was available (Alvarez-Crespo et al., 2012), suggesting that AG may promote foraging and risk-taking in response to a negative energy balance.

When focusing on the effects of exogenously administered ghrelin following stress exposure, an anxiolytic effect appears more evident. Peripherally administered AG attenuated anxiety-like behavior and stress responses after exposure to air puffs or immobilization stress (Jensen et al., 2016). Interestingly, DAG also produced anxiolytic-like effects following stress exposure in ghrelin KO mice (Stark et al., 2016). Moreover, anxiety- and depression-like behaviors induced by CUMS were at least partly rescued by administration of ghrelin or the ghrelin agonist GHRP-6 (Huang et al., 2017, 2019). A recent study demonstrated that intra-hippocampal administration of ghrelin fully and intraperitoneal injection partly normalized stress-enhanced anxiety- and depression-like phenotypes in a CSDS paradigm (Han et al., 2019). However, another study found that reduced social interaction following CSDS exposure could not be rescued by subcutaneous administration of AG or ghrelin agonist GHRP-2 (Gupta et al., 2019).

A number of studies also investigated how GHSR ligands affect fear conditioning and extinction. Administration of the GHSR agonist MK0677, systemically or directly into the basolateral amygdala, around the time of fear conditioning reduced contextual and cued fear memory strength in unstressed rats, while the GHSR antagonist D-Lys3 increased it (Harmatz et al., 2016). An earlier study of the same group, however, showed that repeated systemic or intra-amygdalar injection of MK0677 led to an enhancement of cued fear memory strength (Meyer et al., 2014). In rats that were subjected to chronic immobilization stress, stress-induced increases in cued fear were abolished when

the GHSR antagonist D-Lys3-GHRP-6 was administered daily before stress exposure (Meyer et al., 2014). In their 2016 study, this group reported that increased cued fear in chronically stress-exposed rats was associated with reduced binding of fluorescently labeled ghrelin in the basolateral amygdala, which they defined as central ghrelin resistance (Harmatz et al., 2016). Therefore, the authors hypothesized that a stress-induced elevation of AG levels and prolonged GHSR activation may lead to impaired GHSR signaling in the brain via downregulation of GHSR expression (Harmatz et al., 2016). Interestingly, infusion of MK0677 into the lateral amygdala was also shown to improve cued fear extinction in non-stressed mice (Huang et al., 2016). However, in our recently published study, we did not find significant effects of systemic or intra-VTA administration of MK0677 on cued fear expression or extinction in non-stressed mice (Pierre et al., 2020). Importantly, as the GHSR is constitutively active in the absence of ghrelin (Holst et al., 2003; Petersen et al., 2009), it is therefore important to consider the effects of central GHSR signaling independently of circulating AG or exogenous administration of an GHSR agonist.

Role of GHSR Signaling in Fear, Anxiety- and Depression-Like Behaviors

Under non-stressed conditions, no or only marginal effects on fear, anxiety- and depression like behaviors were observed in GHSR KO mice compared to wild type controls (Mahbod et al., 2018; Guo et al., 2019; Lu et al., 2019; Pierre et al., 2019). Nevertheless, one study found anxiolytic and antidepressant-like effects following overexpression of GHSR in the basolateral amygdala in non-stressed mice (Jensen et al., 2016). Another study reported reduced fear memory retention after contextual fear conditioning in unstressed GHSR KO mice (Albarran-Zeckler et al., 2012), but this observation was not confirmed in a more recent study (Hornsby et al., 2016).

Clearer evidence for behavioral effects in mice lacking the GHSR was obtained following stress exposure, where most studies reported impaired stress coping. For example, mild stressors like air puffs induced an exacerbated avoidance response in GHSR KO mice (Jensen et al., 2016). Similarly, CSDS resulted in more pronounced depression-like behavior in GHSR KO mice, as assessed by a social avoidance test (Lutter et al., 2008; Chuang et al., 2011). A local knockdown of the GHSR in the hippocampus also aggravated anxiety- and depression-like behaviors in mice following exposure to a CSDS or CUMS paradigm (Han et al., 2019; Huang et al., 2019), pointing to a protective role of the GHSR during chronic stress.

Effects of Caloric Restriction on Fear, Anxiety- and Depression-Like Behaviors

Caloric restriction and food deprivation paradigms typically increase plasma ghrelin levels and were also used in several studies to manipulate the endogenous ghrelin system and thus indirectly study its effects on fear, anxiety- and depression-related behaviors in rodents. An initial study demonstrated anxiolytic and antidepressant-like effects of caloric restriction that were abolished in GHSR KO mice (Lutter et al., 2008). In a later publication, the same group showed that the neuroprotective agent P7C3 restored the antidepressant-like effect of caloric restriction in GHSR KO mice, potentially by increasing hippocampal neurogenesis (Walker et al., 2015). This suggests that the effects of caloric restriction on depression-like behaviors may depend on GHSR signaling in the hippocampus and ensuing neurogenesis. Recently, a study reported that acute food deprivation for 24 h and chronic caloric restriction had anxiolytic- and antidepressant-like effects in wild type mice, which were abolished after re-feeding (Lu et al., 2019). In GHSR-KO mice, however, acute food deprivation enhanced, while only chronic caloric restriction reduced anxiety- and depression-like responses. This led the authors to conclude that the positive effect of acute but not chronic fasting was GHSR-dependent (Lu et al., 2019). The finding that the anxiolytic-like action of 24 h food deprivation in wild type mice was neutralized by administration of a GHSR antagonist further supported this conclusion (Lu et al., 2019).

In fear conditioning paradigms, caloric restriction and overnight fasting before extinction training were shown to enhance fear extinction and suppress return of fear in mice (Riddle et al., 2013; Huang et al., 2016; Verma et al., 2016), an effect that was abolished by administration of the GHSR antagonist D-Lys3 into the lateral amygdala (Huang et al., 2016). Interestingly, also in humans spontaneous recovery and reinstatement of fear were reduced after an overnight fast, which was correlated with ghrelin plasma levels (Shi et al., 2018). However, we could not confirm the extinction-promoting effect of overnight fasting using a weak extinction protocol and also found no difference between wild type and GHSR KO mice (Pierre et al., 2020). Thus, while manipulation of GHSR signaling may be an interesting avenue to curb fear expression or promote fear extinction, it appears that the experimental conditions under which such effects can be observed remain uncertain.

Summary, Shortcomings and Future Directions of Rodent Studies Investigating the Role of the Ghrelin System in Stress-Related Behaviors

The often mixed findings of rodent studies make it challenging to draw a general conclusion about the role of ghrelin and GHSR in stress-related behaviors. Possible reasons for these inconsistencies are diverse: the use of different mouse or rat strains, different age or sex of the animals, varying breeding, handling or habituation conditions, different time of day for testing and use of diverse behavioral and stress paradigms. The feeding status of the animals during testing may be of particular importance, as administration of exogenous ghrelin or GHSR agonists may confound the readout of behavioral assays by the instatement of hunger.

In summary, published literature suggests that the ghrelin system plays a different role in individuals depending on the amount and quality of previous stress exposure. This seems most obvious for GHSR signaling, which does not appear to affect fear, anxiety- and depression-like behaviors under non-stressed

conditions but may exert mostly protective effects during chronic stress. A similar trend can be observed in pharmacological studies using GSHR ligands, where, without prior stress exposure, GHSR agonists predominantly promote anxiety- and depression-like behaviors, but seem to reduce chronic stress-related phenotypes. Also, caloric restriction may have beneficial effects on fear, anxiety- and depression-like behaviors in unstressed rodents through activation of GHSR. Nevertheless, the response of rodents to the potentially stressful nature of food deprivation might additionally challenge stress coping mechanisms and, together with differences in fasting procedures, contribute to inconsistencies in literature.

It has been proposed that prolonged elevation of plasma AG levels during chronic stress induces a central ghrelin resistance with reduced GHSR expression (Harmatz et al., 2016), which would impede ligand-dependent as well as ligand-independent GHSR signaling and thereby eliminate its protective role during stress. In the face of central ghrelin resistance, a rescue of stress-related phenotypes by AG or GHSR agonists as well as caloric restriction, which elevates endogenous ghrelin levels, seems unlikely. Nevertheless, many studies suggest beneficial effects of GHSR agonism and fasting on fear, anxiety-, and depression-like behaviors.

Only a few studies have considered the role of DAG in stress coping, although it constitutes the majority of total circulating plasma ghrelin and may have behavioral effects that are distinct from those of AG. This applies not only for feeding behaviors (Fernandez et al., 2016) but also for stress-related behaviors (Stark et al., 2016). This may be relevant during chronic stress and associated central ghrelin resistance, as AG can be rapidly converted to DAG (De Vriese et al., 2004), which appears to not act via the GHSR (Bednarek et al., 2000; Ferre et al., 2019). Thus, the reported beneficial effects of exogenous AG administration during chronic stress paradigms in rodents may be attributed to DAG rather than AG action. In this context, it also can be noted that the way of reporting plasma ghrelin levels has not been consistent in existing literature. Studies often report either only total or AG levels or do not specify acylation status at all, thereby hindering the overview of ghrelin alterations in baseline versus stressed conditions.

One more point to consider is that the GHSR may have functions independent from binding of AG, which is of particular importance since accessibility of many GHSR-expressing brain areas for the ghrelin peptide is not resolved yet (Perello et al., 2018). While the endogenous peptide LEAP2 has been shown to act as an antagonist/inverse agonist of the GHSR (Ge et al., 2018), it remains unknown to what extent it influences GHSR activity in different brain areas. Because of its high constitutive activity (Holst et al., 2003; Petersen et al., 2009) also changes in GHSR expression levels will accordingly alter activation of downstream signaling pathways as well as a possible formation of heterodimers with other receptors, such as receptors for dopamine and serotonin (Schellekens et al., 2013b; Kern et al., 2015). Given that heterodimer formation influences receptor signaling and trafficking (for review see Schellekens et al., 2013a; Abizaid and Hougland, 2020), this could serve to fine-tune GHSR signaling in response to certain neurotransmitters and, conversely, GHSR signaling would also affect these neurotransmitter systems. These complex (inter)actions of the GHSR could further result in individual differences, where an impairment of GHSR signaling occurs in stress-susceptible but not stress-resilient individuals, in which GHSR agonism still would have beneficial effects. Therefore, it might be useful to identify such individual differences in GHSR sensitivity and investigate which factors contribute to constitutive GHSR signaling.

Furthermore, this requires a clear distinction between findings from studies manipulating peptide hormone levels or using GHSR ligands (e.g., ghrelin KO mice, GOAT KO mice, pharmacological studies) versus studies conducted in GHSR KO mice. For a comprehensive dissection of the role of GHSR signaling in distinct neuronal populations, the development of new biomolecular tools like GHSR-Cre mice is indispensable in order to perform targeted pharmaco- and optogenetic manipulations and selectively employ new viral techniques. Such novel genetic and viral tools could also be used to create conditional knockouts of GHSR, GOAT or ghrelin. It cannot be excluded that in conventional germ-line knockouts compensatory mechanisms are at play that disguise the loss-of-function effect, thereby confounding results and leading to mixed findings and wrong conclusions.

THE GHRELIN SYSTEM AS A NOVEL THERAPEUTIC AVENUE IN STRESS-RELATED PSYCHIATRIC DISORDERS?

A Need for New Treatment Strategies: Ghrelin as a Vantage Point?

In this review, we aimed to provide an overview of the current literature on the role of ghrelin system in stress coping. We summarized findings on fear, anxiety- and depression-like behaviors in rodent models and in this final chapter, we want to discuss the possible therapeutic utility of the ghrelin system in stress-related psychiatric disorders, with a focus on anxiety disorders and post-traumatic stress disorder (PTSD). They are the most common cause of psychiatric illness, with an estimated lifetime prevalence of up to 30% (Kessler et al., 2005a, 2012) and women being affected almost twice as often as men (Baxter et al., 2013). Besides reducing the quality of life of patients and their families dramatically, they cause an immense socioeconomic burden in modern western societies (Wittchen et al., 2011; Olesen et al., 2012). However, a lack of major advances in psychopharmacotherapy over the past three decades as well as limited validity of current symptom-based diagnostic manuals (Lang et al., 2016) leave anxiety disorders and PTSD poorly diagnosed and undertreated (Craske et al., 2017). Moreover, a large number of anxiety patients do not show long-term benefit from currently available treatments and fail to achieve full remission or often relapse with time (Hofmann and Smits,

2008; Bandelow et al., 2015; Koek et al., 2016; Craske et al., 2017). Currently, there are also no biomarkers for the measurement of treatment response available (Craske et al., 2017). Thus, there is an urgent need for the development of novel strategies to augment existing diagnostic and treatment options to improve their efficiency and tackle under- and misdiagnosis as well as treatment resistance (Singewald et al., 2015; Sartori and Singewald, 2019).

There is a growing interest in the involvement and therapeutic potential of the ghrelin system in psychiatric diseases. Positioned at the interface between feeding circuitry, metabolism and the HPA axis, its dysregulation could not only potentially influence food intake and energy homeostasis but also stress vulnerability. This involvement of the ghrelin system in different physiological processes has sparked a discussion about its role in a variety of pathological conditions like obesity and eating disorders, but also addictive disorders as well as anxiety disorders, PTSD and mood disorders (for review see Labarthe et al., 2014; Wittekind and Kluge, 2015; Bali and Jaggi, 2016; Stievenard et al., 2016; Jiao et al., 2017; Shi et al., 2017). The potential role of the ghrelin system is further underscored by the notion that mood-, anxiety- and trauma-related disorders are often associated with metabolic dysregulation and also show a high level of comorbidity with obesity or eating disorders (Scott et al., 2008; Ng et al., 2013; Mason et al., 2014; Meng and D'Arcy, 2015; Aaseth et al., 2019). It is very likely that comorbid diseases share a common neurobiological pathology, which could be of use to gain a better understanding of underlying disease mechanisms and to identify potential therapeutic targets.

(Dysregulation of) the Ghrelin System in Stress-Related Psychiatric Disorders

In humans, acute exposure to stressors is associated with elevated plasma ghrelin concentrations. In healthy individuals but also in obese patients with binge-eating disorder, total plasma ghrelin levels were elevated in those individuals who also had a high cortisol response to a Trier social stress test (TSST) (Rouach et al., 2007). Similarly, two studies with only female participants found elevated plasma cortisol and AG levels in healthy women (Raspopow et al., 2010) and higher saliva ghrelin but not cortisol levels in women suffering from bulimia nervosa (Monteleone et al., 2012) after stress exposure in a TSST. Other studies with only male participants reported no changes or, after alcohol consumption, even decreased AG levels following a TSST (Zimmermann et al., 2007) and no changes in total plasma ghrelin levels before and after a forced arithmetic task in a cohort of lean and obese men (Lambert et al., 2011). Taken together, these studies strongly suggest that the effects of acute stress exposure on plasma ghrelin levels may be dependent on sex. While the effects of chronic stress exposure have not been investigated explicitly in humans, one translational study reported elevated AG in teenagers 4.5 years after experiencing a severe traumatic event and proposed high plasma AG levels as a long-lasting biomarker for chronic stress exposure and a perpetuating risk factor for stress-enhanced fear (Yousufzai et al., 2018).

In line with the notion that alterations of the ghrelin system may be a biomarker for stress exposure, several other studies have investigated possible dysregulations of the ghrelin system in stress-related psychiatric disorders such as anxiety disorders, PTSD or major depressive disorder (MDD). The Gln90Le polymorphism in the pre-proghrelin gene has been linked to an increased risk of panic disorder (Hansson et al., 2013), while, in contrast, the Leu72Met variant of the pre-proghrelin gene was not associated with panic disorder (Nakashima et al., 2008) but with symptom severity in PTSD (Li et al., 2018) and MDD (Nakashima et al., 2008). A recent study reported elevated plasma ghrelin levels in children with a diagnosis of an anxiety disorder, which was more pronounced in girls than boys (Ozmen et al., 2019). Interestingly, ghrelin levels, serum cortisol and anxiety scores together with body mass index were more reduced in obese children following a combined dietary and mindfulness intervention in comparison to a control group that only underwent a dietary intervention (Lopez-Alarcon et al., 2020). However, in female patients diagnosed with anorexia nervosa or obesity, ghrelin levels were not correlated with depression- and anxiety-like symptoms independently of weight and body fat (Lawson et al., 2012). Numerous studies investigated plasma ghrelin levels in patients with MDD, which is often comorbid with anxiety- and trauma-related disorders and associated with stress-induced changes in food intake (Kessler, 1997, Kessler et al., 2005b; Kendler et al., 1999; Grant et al., 2013). They found increased fasting AG (Kurt et al., 2007; Algul and Ozcelik, 2018) and total ghrelin (Ozsoy et al., 2014), but also decreased fasting AG and DAG (Barim et al., 2009) or no changes in fasting AG or total ghrelin levels at all (Schanze et al., 2008; Kluge et al., 2010; Gimenez-Palop et al., 2012; Matsuo et al., 2012). Two of these studies showed a positive correlation of eating behavior with total ghrelin levels in MDD patients (Schanze et al., 2008; Matsuo et al., 2012), while another one reported lower AG levels in depressed patients with increased appetite (Simmons et al., 2020), indicating that plasma AG may not be good predictor for appetite or food intake in depressed patients.

The effect of treatment on ghrelin plasma levels in stress-related psychiatric disorders (mainly MDD) has also been examined. One study that found reduced plasma AG and DAG when comparing untreated MDD patients with healthy controls reported no effect of citalopram on ghrelin levels (Barim et al., 2009). Maprotiline treatment in male lean MDD patients, on the other hand, resulted in mildly increased plasma ghrelin levels (Pinar et al., 2008). In a mixed patient group suffering from bipolar disorder or MDD, serum AG levels were elevated compared to controls and decreased after electroconvulsive therapy (Kurt et al., 2007). A similar decrease in total ghrelin levels was reported in another study where patients received electroconvulsive therapy and/or different antidepressant drugs (Ozsoy et al., 2014). Interestingly, one study found, that therapy resistance in MDD and panic disorder was correlated with elevated AG (Ishitobi et al., 2012) and the effect of lithium augmentation treatment in treatment-resistant MDD could be characterized by a slight decrease in plasma AG in responders compared to an increase in non-responders (Ricken et al., 2017).

The conflicting findings in these studies probably result from confounding factors like nutritional status and time of day at sample collection, gender, age, body mass index, comorbid disorders and drug treatments, such as the type of antidepressant. Moreover, not all studies distinguished between AG and DAG and only measured total ghrelin levels or did not specify acylation status. Overall, it remains inconclusive whether genetic variants in the ghrelin system are causally involved in stress-related psychiatric disorders and whether altered ghrelin plasma levels are a predisposing factor for or just a byproduct of these diseases. Elevated plasma AG could indicate prior chronic stress exposure (Yousufzai et al., 2018), which in turn may enhance the risk for mental health disorders. Nevertheless, plasma AG appears to correlate with treatment resistance, suggesting more than mere association. Moreover, experiments in rodents indicate that stress-induced activation of the ghrelin system not only influences feeding but may also have a direct impact on fear, anxiety- and depression-like behaviors.

Therapeutic Potential of Targeting the Ghrelin System in Stress-Related Psychiatric Disorders

Despite the role of the ghrelin system in stress-related psychiatric disorders is not fully resolved yet, it provides a new and interesting vantage point in the search for more efficient diagnostic and therapeutic strategies (also see **Figure 1**). It remains unknown whether a modulation of the ghrelin system could be beneficial in the treatment of stress-related psychiatric disorders, however multiple pharmacological tools to do so have become available over the last two decades (McGovern et al., 2016; Lee et al., 2020; Moose et al., 2020). This includes GHSR agonists and antagonists as well as inverse agonists and GOAT inhibitors, although no authorized medicine is commercially available to date. The pharmacological characterization of many ligands has only just begun and it will be of great importance to consider their central penetrance and possible signaling bias and further elucidate downstream signaling in order to allow targeted predictive modeling and the design of future ghrelin-based therapies (Ramirez et al., 2019; Howick et al., 2020). To our knowledge, there are currently no studies published that directly investigated the effect of ghrelin-targeted interventions in stress-related psychiatric conditions. One study in healthy human participants found enhanced extinction memory retention and reduced return of fear following an overnight fast, which was negatively correlated with ghrelin plasma levels (Shi et al., 2018). Whether fasting may improve exposure-based psychotherapy outcomes in patients with anxiety disorders or PTSD and whether this would be associated with changes in plasma AG concentrations or brain GHSR function remains to be established.

As a biomarker, high plasma AG could indicate prior stress exposure (Yousufzai et al., 2018), which in turn may enhance the risk for stress-related psychiatric disorders. While plasma AG concentrations were not consistently associated with disease, they may predict treatment resistance (Ishitobi et al., 2012; Ricken et al., 2017). In several studies, a decrease in plasma AG or total ghrelin levels during therapy was also associated with treatment response (Kurt et al., 2007; Ozsoy et al., 2014; Ricken et al., 2017; Lopez-Alarcon et al., 2020). A lack of changes in plasma AG concentrations may thus reflect decreased sensitivity of the GHSR and dysregulation of its feedback system. In light of our previous discussion that GHSR in the brain may act partly independent of circulating AG, this highlights the therapeutic potential for the development of diagnostic tools to study brain GHSR function in order to aid further stratification of patients for an optimization of treatment strategies.

It also should be kept in mind that potentially beneficial effects associated with activation of the ghrelin system, as observed in some rodent experiments, may be lost in patients with impaired GHSR function (Harmatz et al., 2016). To this end, a precise definition of the phenomenon of central ghrelin resistance and corresponding neurobiological correlates is indispensable. Present literature merely suggests an impaired feeding response following ghrelin (agonist) administration, associated with reduced c-Fos expression in the ARC (Briggs et al., 2010) and a reduction of AG binding (Harmatz et al., 2016) as markers for disrupted GHSR function. In addition, it is presently unclear whether fasting or other interventions could rapidly reverse central ghrelin resistance. A loss of GHSR function in hypothalamic NPY/AgRP neurons as a result of diet-induced obesity could be rescued by caloric restriction (Briggs et al., 2010, 2013), but so far no study investigated whether this can be extrapolated to stress-induced central ghrelin resistance in brain regions beyond the hypothalamus. Instead of treatment, also a prevention of central ghrelin resistance could be considered. For example, a study in rats showed that administration of a GHSR antagonist during a chronic immobilization paradigm prevented the emergence of stress-enhanced fear (Meyer et al., 2014), while the same paradigm without GHSR antagonist administration led to reduced GHSR expression in the basolateral amygdala, which hampered the attenuation of stress-enhanced fear memories by a GHSR agonist (Harmatz et al., 2016). Therefore, preservation of GHSR function during chronic stress may keep the ghrelin system targetable for treatment interventions.

Also indirect targeting of the ghrelin system by other approaches may be of relevance in stress-related psychiatric disorders, for example via the gut microbiome (Schalla and Stengel, 2020). Changes in diet and gut microbiota composition have been linked to changes in plasma ghrelin levels in rodents and humans (for review see Lach et al., 2018). Moreover, it has been proposed that short-chain fatty acids produced by gastrointestinal microbiota may compete with octanoate for binding at the GOAT and interfere with the acylation of ghrelin (Heiman and Greenway, 2016). A recent study showed that different microbiota-derived metabolites, amongst them also short-chain fatty acids, may also directly attenuate GHSR signaling (Torres-Fuentes et al., 2019). Interestingly, one clinical study demonstrated that the use of dietary capsaicin altered gut microbiota composition and reduced ghrelin levels in healthy subjects (Kang et al., 2016). This is of particular interest, given that elevated plasma AG may reflect a higher risk for the development of stress-related psychiatric conditions (Yousufzai

et al., 2018). Overall, this highlights the possibility of utilizing the gut microbiome to influence ghrelin signaling and thereby modulate the gut-brain axis in stress, although the underlying mechanisms how gut microbiota interact with the ghrelin system are not fully resolved yet.

We believe that the therapeutic potential of ghrelin-targeted interventions in stress-related psychiatric disorders is just starting to be explored. Especially a better understanding of the interactions of ghrelin with the HPA axis, the role of DAG versus AG and factors that control constitutive GHSR activity or lead to ghrelin resistance in the brain may uncover novel diagnostic and therapeutic avenues that have not been considered so far.

Interaction of Ghrelin With Neurotransmitter Systems as a Gateway to the Treatment of Psychiatric Disorders

Abundant evidence demonstrates interaction of the ghrelin system with different neurotransmitters, neuromodulators and their receptors, including monoamines, neuropeptides and endocannabinoids (Brunetti et al., 2002; Skibicka et al., 2012b; Edwards and Abizaid, 2016; Hedegaard and Holst, 2020). One possibility how the ghrelin system may affect behaviors relevant for psychiatric disorders is through its effect on the limbic system. These effects may result from direct activation of GHSR in different limbic areas like hippocampus or amygdala but may also be the consequence of activation of GHSR in neurotransmitter systems projecting to these limbic areas. In this regard, the effect of ghrelin signaling on the release of noradrenalin, serotonin and dopamine merits further discussion. Only few studies have investigated the effect of ghrelin on noradrenalin and serotonin release. One study found that peripheral ghrelin may activate the noradrenergic pathway from the hindbrain to the hypothalamus (Date et al., 2006) and another study reported that food deprivation and central administration of ghrelin augmented the increase of noradrenalin release in the PVN following foot shock stress in rats (Kawakami et al., 2008). Concerning ghrelin's effects on serotonin signaling, one study showed that ghrelin postsynaptically depolarized serotonin neurons in rat brain slices containing the dorsal raphe nucleus (Ogaya et al., 2011), while a second study found that ghrelin reduced the firing rate of dorsal raphe neurons in brain slices prepared from rats chronically treated with ghrelin (Hansson et al., 2011). Interestingly, acute central administration of ghrelin in mice was shown to increase serotonin turnover and the expression of serotonin-related genes in the amygdala (Hansson et al., 2014). While these studies demonstrate that ghrelin influences serotonin and noradrenaline signaling, the direct implications for fear, anxiety- and mood-related behaviors remain unclear.

Because the interaction of the ghrelin with the dopamine system is studied more extensively, we will further highlight certain aspects of this interaction and, as an example, discuss possible therapeutic relevance. Ghrelin was shown to modulate the spontaneous firing frequency of mesolimbic dopaminergic neurons in the VTA (Abizaid et al., 2006) and trigger dopamine release in the nucleus accumbens (NAc), predominantly in the shell region (Jerlhag et al., 2007; Jerlhag, 2008; Quarta et al., 2009; Cone et al., 2014). Associated with this rise of extracellular dopamine levels in the NAc following systemic or intra-VTA administration of ghrelin, stimulation of locomotor activity and conditioned place preference was observed (Jerlhag et al., 2007; Jerlhag, 2008). GHSR antagonism or a ghrelin KO, on the other hand, attenuated alcohol-, cocaine-, amphetamine- or morphine-induced locomotor stimulation and CPP and abolished the associated increase of accumbal dopamine release (Jerlhag et al., 2010; Jerlhag et al., 2011; Engel et al., 2015). In paradigms offering a free choice between standard chow and rewarding (palatable) food, ghrelin in the VTA stimulated hedonic feeding, but not homeostatic food intake (Egecioglu et al., 2010; Skibicka et al., 2011, 2013; Schele et al., 2016). The mechanism via which ghrelin entrains the midbrain dopaminergic system, however, is not fully resolved yet. Recently, it was shown that ghrelin-binding cells are present in most subnuclei of the VTA, but not in the NAc (Cornejo et al., 2018). Moreover, Cornejo and colleagues demonstrated that centrally but not peripherally injected ghrelin recruits specific subsets of dopaminergic neurons in the parabrachial nucleus and GABAergic neurons in the interfascicular nucleus of the VTA (Cornejo et al., 2018). As for many other brain areas where the GHSR is expressed, there is no clear evidence whether peripherally circulating ghrelin reaches the VTA and directly acts on midbrain dopaminergic neurons (Perello et al., 2018). Also indirect mechanisms of activation (e.g., via orexigenic neurons in the lateral hypothalamus) have yet to be elucidated (Quarta and Smolders, 2014; Al Massadi et al., 2019). Furthermore, it has been proposed that (hippocampal) dopamine signaling is dependent on heterodimerization between dopamine D1 (DRD1) and GHS receptors, regulating DRD1-induced hippocampal synaptic plasticity and learning (Kern et al., 2015).

The role of ghrelin signaling on mesolimbic dopamine was previously reviewed extensively in the context of food reward (Skibicka and Dickson, 2011; Perello and Zigman, 2012; Skibicka et al., 2012a; Liu and Borgland, 2015; Al Massadi et al., 2019). However, these actions of ghrelin may also be relevant for stress-related psychiatric disorders. A possible role in mood disorders seems likely, given that ghrelin has been proposed to mediate CSDS-induced food reward (Chuang et al., 2011) and protect against depressive-like symptoms following CSDS in mice (Lutter et al., 2008). This is further corroborated by the observation that hyperphagic depressed patients showed a greater change in AG in response to a meal, which was associated with increased activity in the VTA (Cerit et al., 2019). As such, ghrelin signaling on mesolimbic dopamine neurons may indeed constitute the interface of stress, mood and food reward (Schellekens et al., 2012). With respect to anxiety disorders and PTSD, the abundant expression of the GHSR and GHSR mRNA on/in midbrain dopamine neurons of the VTA (Zigman et al., 2006; Mani et al., 2014) is particularly interesting (**Figure 1**), as accumulating evidence suggests midbrain dopaminergic signaling as an important player in fear extinction (Abraham et al., 2014; Kalisch et al., 2019). The extinction of fear is the driving mechanism behind the reduction of fear responses and very basis of exposure-based cognitive behavioral therapy (Milad and Quirk, 2012),

which is first-line in the treatment of anxiety- and trauma-related disorders (Craske, 2010; Craske et al., 2017). Also translationally, this paradigm is very appealing as it is easy to model in the laboratory in rodent models as well as humans (Milad and Quirk, 2012; Singewald and Holmes, 2019). Moreover, impaired fear extinction was suggested as a relevant endophenotype for anxiety disorders and PTSD (Singewald and Holmes, 2019). Recently, it has been proposed that during extinction learning midbrain dopaminergic neurons encode a quasi-appetitive reward prediction error, signaling the omission of the aversive unconditioned stimulus as a 'better-than-expected' outcome (Luo et al., 2018; Salinas-Hernandez et al., 2018; Cai et al., 2020). Besides this temporally restricted role in extinction acquisition, dopamine was also suggested to play a key role in the consolidation phase in a human fMRI study (Gerlicher et al., 2018). In a collaborative study, our lab has previously shown that enhancing dopaminergic signaling by L-DOPA treatment helps the formation of long-lasting extinction memories and prevents return of fear in extinction-competent mice and healthy humans (Haaker et al., 2013). Moreover, we were able to show that L-DOPA treatment can rescue deficient fear extinction in a mouse model for refractory anxiety disorders (Whittle et al., 2016).

Despite this clear evidence of interaction of the two systems, very few studies have investigated the possible benefits of targeting the ghrelin-dopamine axis in stress-related psychiatric disorders. We were able to show recently, that administration of the ghrelin agonist MK0677 directly into the VTA induces dopamine release in the NAc but also in amygdala and medial prefrontal cortex, which are important parts of fear and anxiety circuitries (Pierre et al., 2020). But despite increasing dopamine release in VTA projection areas, in our hands, MK0677 did not influence fear acquisition or extinction and extinction memory retrieval in unstressed mice. One explanation could be that the achieved rise in dopamine may not have been sufficient or not timed adequately, which may be enhanced by optimizing ghrelin agonists, dosage and ways of administration. Since the elucidation of the exact role of dopamine during fear extinction has only begun, advances in this field could help to utilize the ghrelin-dopamine axis in a more targeted manner (e.g., timing, individual differences) in future studies.

CONCLUSION AND FUTURE DIRECTIONS

Although the body of literature about the ghrelin system is growing rapidly, a great amount of questions regarding its effect on brain function remain unanswered. This complicates the evaluation of pathological relevance and therapeutic utility of ghrelin and GHSR in stress-related psychiatric disorders. To this end, a better understanding of the role of the ghrelin system in stress coping and its interplay with the HPA axis will be important. Further studies will be necessary to characterize brain GHSR signaling beyond the action of AG on its receptor, as DAG and ligand-independent GHSR activity have received little attention in existing literature. Moreover, the phenomenon of central ghrelin resistance in chronic stress needs to be studied more intensely in order to establish associated neurobiological correlates. The notion that ghrelin modulates fear, anxiety- and depression-like behaviors as a stress hormone seems to arise mostly from rodent experiments, while evidence from human studies is sparse and inconclusive. Nevertheless, it appears evident that ghrelin is much more than a 'hunger hormone' and represents an interesting target for novel interventions in stress-related psychiatric disorders that will become more accessible once its dynamics in the context of stress are better understood.

AUTHOR CONTRIBUTIONS

EMF and DDB conceptualized the review and performed literature research. EMF wrote the manuscript with contributions and supervision from DDB. DDB and NS reviewed and revised all sections. All authors read and approved the final manuscript.

FUNDING

This work was supported by the Austrian Science Fund (FWF, I2433-B26 and DKW-1206-B18) and the Fund for Scientific Research Flanders (FWO-G001816N and FWO-11ZL616N) and the Strategic Research Programme of the Vrije Universiteit Brussel (SRP49).

REFERENCES

Aaseth, J., Roer, G. E., Lien, L., and Bjorklund, G. (2019). Is there a relationship between PTSD and complicated obesity? A review of the literature. *Biomed. Pharmacother.* 117:108834. doi: 10.1016/j.biopha.2019.108834

Abizaid, A., and Hougland, J. L. (2020). Ghrelin signaling: GOAT and GHS-R1a take a LEAP in complexity. *Trends Endocrinol. Metab.* 31, 107–117. doi: 10.1016/j.tem.2019.09.006

Abizaid, A., Liu, Z. W., Andrews, Z. B., Shanabrough, M., Borok, E., Elsworth, J. D., et al. (2006). Ghrelin modulates the activity and synaptic input organization of midbrain dopamine neurons while promoting appetite. *J. Clin. Invest.* 116, 3229–3239. doi: 10.1172/jci29867

Abraham, A. D., Neve, K. A., and Lattal, K. M. (2014). Dopamine and extinction: a convergence of theory with fear and reward circuitry. *Neurobiol. Learn. Mem.* 108, 65–77. doi: 10.1016/j.nlm.2013.11.007

Aklan, I., Sayar Atasoy, N., Yavuz, Y., Ates, T., Coban, I., Koksalar, F., et al. (2020). NTS catecholamine neurons mediate hypoglycemic hunger via medial hypothalamic feeding pathways. *Cell Metab.* 31, 313–326.e5. doi: 10.1016/j.cmet.2019.11.016

Al Massadi, O., Nogueiras, R., Dieguez, C., and Girault, J. A. (2019). Ghrelin and food reward. *Neuropharmacology* 148, 131–138. doi: 10.1016/j.neuropharm.2019.01.001

Albarran-Zeckler, R. G., Brantley, A. F., and Smith, R. G. (2012). Growth hormone secretagogue receptor (GHS-R1a) knockout mice exhibit improved spatial memory and deficits in contextual memory. *Behav. Brain Res.* 232, 13–19. doi: 10.1016/j.bbr.2012.03.012

Algul, S., and Ozcelik, O. (2018). Evaluating the levels of nesfatin-1 and ghrelin hormones in patients with moderate and severe major depressive disorders. *Psychiatry Investig.* 15, 214–218. doi: 10.30773/pi.2017.05.24

Alvarez-Crespo, M., Skibicka, K. P., Farkas, I., Molnar, C. S., Egecioglu, E., Hrabovszky, E., et al. (2012). The amygdala as a neurobiological target for

ghrelin in rats: neuroanatomical, electrophysiological and behavioral evidence. *PLoS One* 7:e46321. doi: 10.1371/journal.pone.0046321

Amitani, M., Amitani, H., Cheng, K. C., Kairupan, T. S., Sameshima, N., Shimoshikiryo, I., et al. (2017). The role of ghrelin and ghrelin signaling in aging. *Int. J. Mol. Sci.* 18:1511. doi: 10.3390/ijms18071511

Arnold, M., Mura, A., Langhans, W., and Geary, N. (2006). Gut vagal afferents are not necessary for the eating-stimulatory effect of intraperitoneally injected ghrelin in the rat. *J. Neurosci.* 26, 11052–11060. doi: 10.1523/jneurosci.2606-06.2006

Asakawa, A., Inui, A., Kaga, T., Yuzuriha, H., Nagata, T., Fujimiya, M., et al. (2001a). A role of ghrelin in neuroendocrine and behavioral responses to stress in mice. *Neuroendocrinology* 74, 143–147. doi: 10.1159/000054680

Asakawa, A., Inui, A., Kaga, T., Yuzuriha, H., Nagata, T., Ueno, N., et al. (2001b). Ghrelin is an appetite-stimulatory signal from stomach with structural resemblance to motilin. *Gastroenterology* 120, 337–345. doi: 10.1053/gast.2001.22158

Azzam, I., Gilad, S., Limor, R., Stern, N., and Greenman, Y. (2017). Ghrelin stimulation by hypothalamic-pituitary-adrenal axis activation depends on increasing cortisol levels. *Endocr. Connect.* 6, 847–855. doi: 10.1530/EC-17-0212

Bali, A., and Jaggi, A. S. (2016). An integrative review on role and mechanisms of ghrelin in stress, anxiety and depression. *Curr. Drug Targets* 17, 495–507. doi: 10.2174/1389450116666150518095650

Bandelow, B., Reitt, M., Rover, C., Michaelis, S., Gorlich, Y., and Wedekind, D. (2015). Efficacy of treatments for anxiety disorders: a meta-analysis. *Int. Clin. Psychopharmacol.* 30, 183–192. doi: 10.1097/yic.0000000000000078

Bansal, V., Ryu, S. Y., Lopez, N., Allexan, S., Krzyzaniak, M., Eliceiri, B., et al. (2012). Vagal stimulation modulates inflammation through a ghrelin mediated mechanism in traumatic brain injury. *Inflammation* 35, 214–220. doi: 10.1007/s10753-011-9307-7

Barim, A. O., Aydin, S., Colak, R., Dag, E., Deniz, O., and Sahin, I. (2009). Ghrelin, paraoxonase and arylesterase levels in depressive patients before and after citalopram treatment. *Clin. Biochem.* 42, 1076–1081. doi: 10.1016/j.clinbiochem.2009.02.020

Baxter, A. J., Scott, K. M., Vos, T., and Whiteford, H. A. (2013). Global prevalence of anxiety disorders: a systematic review and meta-regression. *Psychol. Med.* 43, 897–910. doi: 10.1017/s003329171200147x

Bednarek, M. A., Feighner, S. D., Pong, S. S., Mckee, K. K., Hreniuk, D. L., Silva, M. V., et al. (2000). Structure-function studies on the new growth hormone-releasing peptide, ghrelin: minimal sequence of ghrelin necessary for activation of growth hormone secretagogue receptor 1a. *J. Med. Chem.* 43, 4370–4376. doi: 10.1021/jm0001727

Berton, O., Aguerre, S., Sarrieau, A., Mormede, P., and Chaouloff, F. (1998). Differential effects of social stress on central serotonergic activity and emotional reactivity in Lewis and spontaneously hypertensive rats. *Neuroscience* 82, 147–159. doi: 10.1016/s0306-4522(97)00282-0

Bodosi, B., Gardi, J., Hajdu, I., Szentirmai, E., Obal, F. Jr., Krueger, J. M. (2004). Rhythms of ghrelin, leptin, and sleep in rats: effects of the normal diurnal cycle, restricted feeding, and sleep deprivation. *Am. J. Physiol. Regul. Integr. Comp. Physiol.* 287, R1071–R1079. doi: 10.1152/ajpregu.00294.2004

Briggs, D. I., Enriori, P. J., Lemus, M. B., Cowley, M. A., and Andrews, Z. B. (2010). Diet-induced obesity causes ghrelin resistance in arcuate NPY/AgRP neurons. *Endocrinology* 151, 4745–4755. doi: 10.1210/en.2010-0556

Briggs, D. I., Lockie, S. H., Wu, Q., Lemus, M. B., Stark, R., and Andrews, Z. B. (2013). Calorie-restricted weight loss reverses high-fat diet-induced ghrelin resistance, which contributes to rebound weight gain in a ghrelin-dependent manner. *Endocrinology* 154, 709–717. doi: 10.1210/en.2012-1421

Brockway, E. T., Krater, K. R., Selva, J. A., Wauson, S. E., and Currie, P. J. (2016). Impact of [d-Lys(3)]-GHRP-6 and feeding status on hypothalamic ghrelin-induced stress activation. *Peptides* 79, 95–102. doi: 10.1016/j.peptides.2016.03.013

Brunetti, L., Recinella, L., Orlando, G., Michelotto, B., Di Nisio, C., and Vacca, M. (2002). Effects of ghrelin and amylin on dopamine, norepinephrine and serotonin release in the hypothalamus. *Eur. J. Pharmacol.* 454, 189–192. doi: 10.1016/s0014-2999(02)02552-9

Cabral, A., Portiansky, E., Sanchez-Jaramillo, E., Zigman, J. M., and Perello, M. (2016). Ghrelin activates hypophysiotropic corticotropin-releasing factor neurons independently of the arcuate nucleus. *Psychoneuroendocrinology* 67, 27–39. doi: 10.1016/j.psyneuen.2016.01.027

Cabral, A., Suescun, O., Zigman, J. M., and Perello, M. (2012). Ghrelin indirectly activates hypophysiotropic CRF neurons in rodents. *PLoS One* 7:e31462. doi: 10.1371/journal.pone.0031462

Cai, L. X., Pizano, K., Gundersen, G. W., Hayes, C. L., Fleming, W. T., Holt, S., et al. (2020). Distinct signals in medial and lateral VTA dopamine neurons modulate fear extinction at different times. *eLife* 9:e54936. doi: 10.7554/eLife.54936

Callaghan, B., and Furness, J. B. (2014). Novel and conventional receptors for ghrelin, desacyl-ghrelin, and pharmacologically related compounds. *Pharmacol. Rev.* 66, 984–1001. doi: 10.1124/pr.113.008433

Carlini, V. P., Monzon, M. E., Varas, M. M., Cragnolini, A. B., Schioth, H. B., Scimonelli, T. N., et al. (2002). Ghrelin increases anxiety-like behavior and memory retention in rats. *Biochem. Biophys. Res. Commun.* 299, 739–743. doi: 10.1016/s0006-291x(02)02740-7

Carlini, V. P., Varas, M. M., Cragnolini, A. B., Schioth, H. B., Scimonelli, T. N., and De Barioglio, S. R. (2004). Differential role of the hippocampus, amygdala, and dorsal raphe nucleus in regulating feeding, memory, and anxiety-like behavioral responses to ghrelin. *Biochem. Biophys. Res. Commun.* 313, 635–641. doi: 10.1016/j.bbrc.2003.11.150

Cavalcante, D. P., Turones, L. C., Camargo-Silva, G., Santana, J. S., Colugnati, D. B., Pansani, A. P., et al. (2019). Role of dorsal raphe nucleus GHS-R1a receptors in the regulation of inhibitory avoidance and escape behaviors in rats. *Behav. Brain Res.* 365, 178–184. doi: 10.1016/j.bbr.2019.03.017

Cerit, H., Christensen, K., Moondra, P., Klibanski, A., Goldstein, J. M., and Holsen, L. M. (2019). Divergent associations between ghrelin and neural responsivity to palatable food in hyperphagic and hypophagic depression. *J. Affect. Disord.* 242, 29–38. doi: 10.1016/j.jad.2018.07.088

Chuang, J. C., Perello, M., Sakata, I., Osborne-Lawrence, S., Savitt, J. M., Lutter, M., et al. (2011). Ghrelin mediates stress-induced food-reward behavior in mice. *J. Clin. Invest.* 121, 2684–2692. doi: 10.1172/jci57660

Cone, J. J., Mccutcheon, J. E., and Roitman, M. F. (2014). Ghrelin acts as an interface between physiological state and phasic dopamine signaling. *J. Neurosci.* 34, 4905–4913. doi: 10.1523/jneurosci.4404-13.2014

Cornejo, M. P., Barrile, F., Cassano, D., Aguggia, J. P., Garcia Romero, G., Reynaldo, M., et al. (2020). Growth hormone secretagogue receptor in dopamine neurons controls appetitive and consummatory behaviors towards high-fat diet in ad-libitum fed mice. *Psychoneuroendocrinology* 119:104718. doi: 10.1016/j.psyneuen.2020.104718

Cornejo, M. P., Barrile, F., De Francesco, P. N., Portiansky, E. L., Reynaldo, M., and Perello, M. (2018). Ghrelin recruits specific subsets of dopamine and gaba neurons of different ventral tegmental area sub-nuclei. *Neuroscience* 392, 107–120. doi: 10.1016/j.neuroscience.2018.09.027

Cowley, M. A., Smith, R. G., Diano, S., Tschop, M., Pronchuk, N., Grove, K. L., et al. (2003). The distribution and mechanism of action of ghrelin in the CNS demonstrates a novel hypothalamic circuit regulating energy homeostasis. *Neuron* 37, 649–661. doi: 10.1016/s0896-6273(03)00063-1

Craske, M. G. (2010). *Cognitive–Behavioral Therapy*. Washington, DC: American Psychological Association.

Craske, M. G., Stein, M. B., Eley, T. C., Milad, M. R., Holmes, A., Rapee, R. M., et al. (2017). Anxiety disorders. *Nat. Rev. Dis. Primers* 3:17024.

Cummings, D. E. (2006). Ghrelin and the short- and long-term regulation of appetite and body weight. *Physiol. Behav.* 89, 71–84. doi: 10.1016/j.physbeh.2006.05.022

Currie, P. J., Khelemsky, R., Rigsbee, E. M., Dono, L. M., Coiro, C. D., Chapman, C. D., et al. (2012). Ghrelin is an orexigenic peptide and elicits anxiety-like behaviors following administration into discrete regions of the hypothalamus. *Behav. Brain Res.* 226, 96–105. doi: 10.1016/j.bbr.2011.08.037

Currie, P. J., Schuette, L. M., Wauson, S. E., Voss, W. N., and Angeles, M. J. (2014). Activation of urocortin 1 and ghrelin signaling in the basolateral amygdala induces anxiogenesis. *Neuroreport* 25, 60–64.

Date, Y., Kojima, M., Hosoda, H., Sawaguchi, A., Mondal, M. S., Suganuma, T., et al. (2000). Ghrelin, a novel growth hormone-releasing acylated peptide, is synthesized in a distinct endocrine cell type in the gastrointestinal tracts of rats and humans. *Endocrinology* 141, 4255–4261. doi: 10.1210/endo.141.11.7757

Date, Y., Shimbara, T., Koda, S., Toshinai, K., Ida, T., Murakami, N., et al. (2006). Peripheral ghrelin transmits orexigenic signals through the noradrenergic

pathway from the hindbrain to the hypothalamus. *Cell Metab.* 4, 323–331. doi: 10.1016/j.cmet.2006.09.004

De Herdt, V., Puimege, L., De Waele, J., Raedt, R., Wyckhuys, T., El Tahry, R., et al. (2009). Increased rat serum corticosterone suggests immunomodulation by stimulation of the vagal nerve. *J. Neuroimmunol.* 212, 102–105. doi: 10.1016/j.jneuroim.2009.04.013

De Vriese, C., Gregoire, F., Lema-Kisoka, R., Waelbroeck, M., Robberecht, P., and Delporte, C. (2004). Ghrelin degradation by serum and tissue homogenates: identification of the cleavage sites. *Endocrinology* 145, 4997–5005. doi: 10.1210/en.2004-0569

Delhanty, P. J., Neggers, S. J., and Van Der Lely, A. J. (2014). Should we consider des-acyl ghrelin as a separate hormone and if so, what does it do? *Front. Horm. Res.* 42, 163–174. doi: 10.1159/000358345

Dos-Santos, R. C., Grover, H. M., Reis, L. C., Ferguson, A. V., and Mecawi, A. S. (2018). Electrophysiological effects of ghrelin in the hypothalamic paraventricular nucleus neurons. *Front. Cell. Neurosci.* 12:275. doi: 10.3389/fncel.2018.00275

Dunn, I. C., Wilson, P. W., D'eath, R. B., and Boswell, T. (2015). Hypothalamic agouti-related peptide mRNA is elevated during natural and stress-induced anorexia. *J. Neuroendocrinol.* 27, 681–691. doi: 10.1111/jne.12295

Edwards, A., and Abizaid, A. (2016). Driving the need to feed: insight into the collaborative interaction between ghrelin and endocannabinoid systems in modulating brain reward systems. *Neurosci. Biobehav. Rev.* 66, 33–53. doi: 10.1016/j.neubiorev.2016.03.032

Egecioglu, E., Jerlhag, E., Salome, N., Skibicka, K. P., Haage, D., Bohlooly, Y. M., et al. (2010). Ghrelin increases intake of rewarding food in rodents. *Addict. Biol.* 15, 304–311. doi: 10.1111/j.1369-1600.2010.00216.x

Elbassuoni, E. A. (2014). Gender differences in ghrelin response to chronic immobilization stress in rats: possible role of estrogen. *Gen. Physiol. Biophys.* 33, 111–120. doi: 10.4149/gpb_2013061

Engel, J. A., Nylander, I., and Jerlhag, E. (2015). A ghrelin receptor (GHS-R1A) antagonist attenuates the rewarding properties of morphine and increases opioid peptide levels in reward areas in mice. *Eur. Neuropsychopharmacol.* 25, 2364–2371. doi: 10.1016/j.euroneuro.2015.10.004

Fanous, S., Terwilliger, E. F., Hammer, R. P. Jr., and Nikulina, E. M. (2011). Viral depletion of VTA BDNF in rats modulates social behavior, consequences of intermittent social defeat stress, and long-term weight regulation. *Neurosci. Lett.* 502, 192–196. doi: 10.1016/j.neulet.2011.07.043

Fernandez, G., Cabral, A., Cornejo, M. P., De Francesco, P. N., Garcia-Romero, G., Reynaldo, M., et al. (2016). Des-acyl ghrelin directly targets the arcuate nucleus in a ghrelin-receptor independent manner and impairs the orexigenic effect of ghrelin. *J. Neuroendocrinol.* 28:12349.

Ferre, G., Louet, M., Saurel, O., Delort, B., Czaplicki, G., M'kadmi, C., et al. (2019). Structure and dynamics of G protein-coupled receptor-bound ghrelin reveal the critical role of the octanoyl chain. *Proc. Natl. Acad. Sci. U.S.A.* 116, 17525–17530. doi: 10.1073/pnas.1905105116

Forbes, N. F., Stewart, C. A., Matthews, K., and Reid, I. C. (1996). Chronic mild stress and sucrose consumption: validity as a model of depression. *Physiol. Behav.* 60, 1481–1484. doi: 10.1016/s0031-9384(96)00305-8

Fujitsuka, N., Asakawa, A., Uezono, Y., Minami, K., Yamaguchi, T., Niijima, A., et al. (2011). Potentiation of ghrelin signaling attenuates cancer anorexia-cachexia and prolongs survival. *Transl. Psychiatry* 1:e23. doi: 10.1038/tp.2011.25

Ge, X., Yang, H., Bednarek, M. A., Galon-Tilleman, H., Chen, P., Chen, M., et al. (2018). LEAP2 is an endogenous antagonist of the ghrelin receptor. *Cell Metab.* 27, 461–469.e6.

Gerlicher, A. M. V., Tuscher, O., and Kalisch, R. (2018). Dopamine-dependent prefrontal reactivations explain long-term benefit of fear extinction. *Nat. Commun.* 9:4294.

Gimenez-Palop, O., Coronas, R., Cobo, J., Gallart, L., Barbero, J. D., Parra, I., et al. (2012). Fasting plasma peptide YY concentrations are increased in patients with major depression who associate weight loss. *J. Endocrinol. Invest.* 35, 645–648.

Gnanapavan, S., Kola, B., Bustin, S. A., Morris, D. G., Mcgee, P., Fairclough, P., et al. (2002). The tissue distribution of the mRNA of ghrelin and subtypes of its receptor, GHS-R, in humans. *J. Clin. Endocrinol. Metab.* 87:2988. doi: 10.1210/jcem.87.6.8739

Goldstein, J. L., Zhao, T. J., Li, R. L., Sherbet, D. P., Liang, G., and Brown, M. S. (2011). Surviving starvation: essential role of the ghrelin-growth hormone axis. *Cold Spring Harb. Symp. Quant. Biol.* 76, 121–127. doi: 10.1101/sqb.2011.76.010447

Grant, F., Guille, C., and Sen, S. (2013). Well-being and the risk of depression under stress. *PLoS One* 8:e67395. doi: 10.1371/journal.pone.0067395

Gray, S. M., Page, L. C., and Tong, J. (2019). Ghrelin regulation of glucose metabolism. *J. Neuroendocrinol.* 31:e12705.

Gualillo, O., Caminos, J., Blanco, M., Garcia-Caballero, T., Kojima, M., Kangawa, K., et al. (2001). Ghrelin, a novel placental-derived hormone. *Endocrinology* 142, 788–794. doi: 10.1210/endo.142.2.7987

Guan, X. M., Yu, H., Palyha, O. C., Mckee, K. K., Feighner, S. D., Sirinathsinghji, D. J., et al. (1997). Distribution of mRNA encoding the growth hormone secretagogue receptor in brain and peripheral tissues. *Brain Res. Mol. Brain Res.* 48, 23–29. doi: 10.1016/s0169-328x(97)00071-5

Gul, S., Saleem, D., Haleem, M. A., and Haleem, D. J. (2017). Inhibition of hormonal and behavioral effects of stress by tryptophan in rats. *Nutr. Neurosci.* 22, 409–417. doi: 10.1080/1028415x.2017.1395551

Guo, L., Niu, M., Yang, J., Li, L., Liu, S., Sun, Y., et al. (2019). GHS-R1a deficiency alleviates depression-related behaviors after chronic social defeat stress. *Front. Neurosci.* 13:364. doi: 10.3389/fnins.2019.00364

Gupta, D., Chuang, J. C., Mani, B. K., Shankar, K., Rodriguez, J. A., Osborne-Lawrence, S., et al. (2019). beta1-adrenergic receptors mediate plasma acyl-ghrelin elevation and depressive-like behavior induced by chronic psychosocial stress. *Neuropsychopharmacology* 44, 1319–1327. doi: 10.1038/s41386-019-0334-7

Gutierrez, J. A., Solenberg, P. J., Perkins, D. R., Willency, J. A., Knierman, M. D., Jin, Z., et al. (2008). Ghrelin octanoylation mediated by an orphan lipid transferase. *Proc. Natl. Acad. Sci. U.S.A.* 105, 6320–6325. doi: 10.1073/pnas.0800708105

Haaker, J., Gaburro, S., Sah, A., Gartmann, N., Lonsdorf, T. B., Meier, K., et al. (2013). Single dose of L-dopa makes extinction memories context-independent and prevents the return of fear. *Proc. Natl. Acad. Sci. U.S.A.* 110, E2428–E2436.

Han, Q. Q., Huang, H. J., Wang, Y. L., Yang, L., Pilot, A., Zhu, X. C., et al. (2019). Ghrelin exhibited antidepressant and anxiolytic effect via the p38-MAPK signaling pathway in hippocampus. *Prog. Neuropsychopharmacol. Biol. Psychiatry* 93, 11–20. doi: 10.1016/j.pnpbp.2019.02.013

Hansson, C., Alvarez-Crespo, M., Taube, M., Skibicka, K. P., Schmidt, L., Karlsson-Lindahl, L., et al. (2014). Influence of ghrelin on the central serotonergic signaling system in mice. *Neuropharmacology* 79, 498–505. doi: 10.1016/j.neuropharm.2013.12.012

Hansson, C., Annerbrink, K., Nilsson, S., Bah, J., Olsson, M., Allgulander, C., et al. (2013). A possible association between panic disorder and a polymorphism in the preproghrelingene. *Psychiatry Res.* 206, 22–25. doi: 10.1016/j.psychres.2012.09.051

Hansson, C., Haage, D., Taube, M., Egecioglu, E., Salome, N., and Dickson, S. L. (2011). Central administration of ghrelin alters emotional responses in rats: behavioural, electrophysiological and molecular evidence. *Neuroscience* 180, 201–211. doi: 10.1016/j.neuroscience.2011.02.002

Haque, Z., Akbar, N., Yasmin, F., Haleem, M. A., and Haleem, D. J. (2013). Inhibition of immobilization stress-induced anorexia, behavioral deficits, and plasma corticosterone secretion by injected leptin in rats. *Stress* 16, 353–362. doi: 10.3109/10253890.2012.736047

Harmatz, E. S., Stone, L., Lim, S. H., Lee, G., Mcgrath, A., Gisabella, B., et al. (2016). Central ghrelin resistance permits the overconsolidation of fear memory. *Biol. Psychiatry* 81, 1003–1013. doi: 10.1016/j.biopsych.2016.11.009

Harris, R. B., Zhou, J., Youngblood, B. D., Smagin, G. N., and Ryan, D. H. (1997). Failure to change exploration or saccharin preference in rats exposed to chronic mild stress. *Physiol. Behav.* 63, 91–100. doi: 10.1016/s0031-9384(97)00425-3

Hassouna, R., Zizzari, P., Tomasetto, C., Veldhuis, J. D., Fiquet, O., Labarthe, A., et al. (2014). An early reduction in GH peak amplitude in preproghrelin-deficient male mice has a minor impact on linear growth. *Endocrinology* 155, 3561–3571. doi: 10.1210/en.2014-1126

He, D., Sai, X., Wang, N., Li, X., Wang, L., and Xu, Y. (2018). Camellia euphlebia exerts its antidepressant-like effect via modulation of the hypothalamic-pituitary-adrenal axis and brain monoaminergic systems. *Metab. Brain Dis.* 33, 301–312. doi: 10.1007/s11011-017-0167-1

Hedegaard, M. A., and Holst, B. (2020). The complex signaling pathways of the ghrelin receptor. *Endocrinology* 161:bqaa020.

Heiman, M. L., and Greenway, F. L. (2016). A healthy gastrointestinal microbiome is dependent on dietary diversity. *Mol. Metab.* 5, 317–320. doi: 10.1016/j.molmet.2016.02.005

Hofmann, S. G., and Smits, J. A. (2008). Cognitive-behavioral therapy for adult anxiety disorders: a meta-analysis of randomized placebo-controlled trials. *J. Clin. Psychiatry* 69, 621–632. doi: 10.4088/jcp.v69n0415

Holst, B., Cygankiewicz, A., Jensen, T. H., Ankersen, M., and Schwartz, T. W. (2003). High constitutive signaling of the ghrelin receptor–identification of a potent inverse agonist. *Mol. Endocrinol.* 17, 2201–2210. doi: 10.1210/me.2003-0069

Hornsby, A. K., Redhead, Y. T., Rees, D. J., Ratcliff, M. S., Reichenbach, A., Wells, T., et al. (2016). Short-term calorie restriction enhances adult hippocampal neurogenesis and remote fear memory in a Ghsr-dependent manner. *Psychoneuroendocrinology* 63, 198–207. doi: 10.1016/j.psyneuen.2015.09.023

Howick, K., Chruscicka, B., Felice, D., Ramirez, V. T., Van Leuven, L., Pietra, C., et al. (2020). Behavioural characterization of ghrelin ligands, anamorelin and HM01: appetite and reward-motivated effects in rodents. *Neuropharmacology* 168:108011. doi: 10.1016/j.neuropharm.2020.108011

Huang, C. C., Chou, D., Yeh, C. M., and Hsu, K. S. (2016). Acute food deprivation enhances fear extinction but inhibits long-term depression in the lateral amygdala via ghrelin signaling. *Neuropharmacology* 101, 36–45. doi: 10.1016/j.neuropharm.2015.09.018

Huang, H. J., Chen, X. R., Han, Q. Q., Wang, J., Pilot, A., Yu, R., et al. (2019). The protective effects of Ghrelin/GHSR on hippocampal neurogenesis in CUMS mice. *Neuropharmacology* 155, 31–43. doi: 10.1016/j.neuropharm.2019.05.013

Huang, H. J., Zhu, X. C., Han, Q. Q., Wang, Y. L., Yue, N., Wang, J., et al. (2017). Ghrelin alleviates anxiety- and depression-like behaviors induced by chronic unpredictable mild stress in rodents. *Behav. Brain Res.* 326, 33–43. doi: 10.1016/j.bbr.2017.02.040

Iglesias, M. J., Pineiro, R., Blanco, M., Gallego, R., Dieguez, C., Gualillo, O., et al. (2004). Growth hormone releasing peptide (ghrelin) is synthesized and secreted by cardiomyocytes. *Cardiovasc. Res.* 62, 481–488. doi: 10.1016/j.cardiores.2004.01.024

Ishitobi, Y., Kohno, K., Kanehisa, M., Inoue, A., Imanaga, J., Maruyama, Y., et al. (2012). Serum ghrelin levels and the effects of antidepressants in major depressive disorder and panic disorder. *Neuropsychobiology* 66, 185–192. doi: 10.1159/000339948

Izadi, M. S., Radahmadi, M., Ghasemi, M., and Rayatpour, A. (2018). Effects of isolation and social subchronic stresses on food intake and levels of leptin, ghrelin, and glucose in male rats. *Adv. Biomed. Res.* 7:118. doi: 10.4103/abr.abr_28_18

Jackson, T. M., Ostrowski, T. D., and Middlemas, D. S. (2019). Intracerebroventricular ghrelin administration increases depressive-like behavior in male juvenile rats. *Front. Behav. Neurosci.* 13:77. doi: 10.3389/fnbeh.2019.00077

Jensen, M., Ratner, C., Rudenko, O., Christiansen, S. H., Skov, L. J., Hundahl, C., et al. (2016). Anxiolytic-like effects of increased ghrelin receptor signaling in the amygdala. *Int. J. Neuropsychopharmacol.* 19:pyv123. doi: 10.1093/ijnp/pyv123

Jeong, J. Y., Lee, D. H., and Kang, S. S. (2013). Effects of chronic restraint stress on body weight, food intake, and hypothalamic gene expressions in mice. *Endocrinol. Metab.* 28, 288–296. doi: 10.3803/EnM.2013.28.4.288

Jerlhag, E. (2008). Systemic administration of ghrelin induces conditioned place preference and stimulates accumbal dopamine. *Addict. Biol.* 13, 358–363. doi: 10.1111/j.1369-1600.2008.00125.x

Jerlhag, E., Egecioglu, E., Dickson, S. L., Douhan, A., Svensson, L., and Engel, J. A. (2007). Ghrelin administration into tegmental areas stimulates locomotor activity and increases extracellular concentration of dopamine in the nucleus accumbens. *Addict. Biol.* 12, 6–16. doi: 10.1111/j.1369-1600.2006.00041.x

Jerlhag, E., Egecioglu, E., Dickson, S. L., and Engel, J. A. (2010). Ghrelin receptor antagonism attenuates cocaine- and amphetamine-induced locomotor stimulation, accumbal dopamine release, and conditioned place preference. *Psychopharmacology* 211, 415–422. doi: 10.1007/s00213-010-1907-7

Jerlhag, E., Landgren, S., Egecioglu, E., Dickson, S. L., and Engel, J. A. (2011). The alcohol-induced locomotor stimulation and accumbal dopamine release is suppressed in ghrelin knockout mice. *Alcohol* 45, 341–347. doi: 10.1016/j.alcohol.2010.10.002

Jiang, S. Z., and Eiden, L. E. (2016). Activation of the HPA axis and depression of feeding behavior induced by restraint stress are separately regulated by PACAPergic neurotransmission in the mouse. *Stress* 19, 374–382. doi: 10.1080/10253890.2016.1174851

Jiao, Q., Du, X., Li, Y., Gong, B., Shi, L., Tang, T., et al. (2017). The neurological effects of ghrelin in brain diseases: beyond metabolic functions. *Neurosci. Biobehav. Rev.* 73, 98–111. doi: 10.1016/j.neubiorev.2016.12.010

Jochman, K. A., Newman, S. M., Kalin, N. H., and Bakshi, V. P. (2005). Corticotropin-releasing factor-1 receptors in the basolateral amygdala mediate stress-induced anorexia. *Behav. Neurosci.* 119, 1448–1458. doi: 10.1037/0735-7044.119.6.1448

Kageyama, H., Funahashi, H., Hirayama, M., Takenoya, F., Kita, T., Kato, S., et al. (2005). Morphological analysis of ghrelin and its receptor distribution in the rat pancreas. *Regul. Pept.* 126, 67–71. doi: 10.1016/j.regpep.2004.08.031

Kalisch, R., Gerlicher, A. M. V., and Duvarci, S. (2019). A dopaminergic basis for fear extinction. *Trends Cogn. Sci.* 23, 274–277. doi: 10.1016/j.tics.2019.01.013

Kamegai, J., Tamura, H., Shimizu, T., Ishii, S., Sugihara, H., and Wakabayashi, I. (2000). Central effect of ghrelin, an endogenous growth hormone secretagogue, on hypothalamic peptide gene expression. *Endocrinology* 141, 4797–4800. doi: 10.1210/endo.141.12.7920

Kanehisa, M., Akiyoshi, J., Kitaichi, T., Matsushita, H., Tanaka, E., Kodama, K., et al. (2006). Administration of antisense DNA for ghrelin causes an antidepressant and anxiolytic response in rats. *Prog. Neuropsychopharmacol. Biol. Psychiatry* 30, 1403–1407. doi: 10.1016/j.pnpbp.2006.05.005

Kang, C., Zhang, Y., Zhu, X., Liu, K., Wang, X., Chen, M., et al. (2016). Healthy subjects differentially respond to dietary capsaicin correlating with specific gut enterotypes. *J. Clin. Endocrinol. Metab.* 101, 4681–4689. doi: 10.1210/jc.2016-2786

Kawakami, A., Okada, N., Rokkaku, K., Honda, K., Ishibashi, S., and Onaka, T. (2008). Leptin inhibits and ghrelin augments hypothalamic noradrenaline release after stress. *Stress* 11, 363–369. doi: 10.1080/10253890701820257

Kendler, K. S., Karkowski, L. M., and Prescott, C. A. (1999). Causal relationship between stressful life events and the onset of major depression. *Am. J. Psychiatry* 156, 837–841. doi: 10.1176/ajp.156.6.837

Kern, A., Mavrikaki, M., Ullrich, C., Albarran-Zeckler, R., Brantley, A. F., and Smith, R. G. (2015). Hippocampal Dopamine/DRD1 signaling dependent on the ghrelin receptor. *Cell* 163, 1176–1190. doi: 10.1016/j.cell.2015.10.062

Kessler, R. C. (1997). The effects of stressful life events on depression. *Annu. Rev. Psychol.* 48, 191–214. doi: 10.1146/annurev.psych.48.1.191

Kessler, R. C., Berglund, P., Demler, O., Jin, R., Merikangas, K. R., and Walters, E. E. (2005a). Lifetime prevalence and age-of-onset distributions of DSM-IV disorders in the National Comorbidity Survey Replication. *Arch. Gen. Psychiatry* 62, 593–602. doi: 10.1001/archpsyc.62.6.593

Kessler, R. C., Chiu, W. T., Demler, O., Merikangas, K. R., and Walters, E. E. (2005b). Prevalence, severity, and comorbidity of 12-month DSM-IV disorders in the National Comorbidity Survey Replication. *Arch. Gen. Psychiatry* 62, 617–627. doi: 10.1001/archpsyc.62.6.617

Kessler, R. C., Petukhova, M., Sampson, N. A., Zaslavsky, A. M., and Wittchen, H. U. (2012). Twelve-month and lifetime prevalence and lifetime morbid risk of anxiety and mood disorders in the United States. *Int. J. Methods Psychiatr. Res.* 21, 169–184. doi: 10.1002/mpr.1359

Kluge, M., Gazea, M., Schussler, P., Genzel, L., Dresler, M., Kleyer, S., et al. (2010). Ghrelin increases slow wave sleep and stage 2 sleep and decreases stage 1 sleep and REM sleep in elderly men but does not affect sleep in elderly women. *Psychoneuroendocrinology* 35, 297–304. doi: 10.1016/j.psyneuen.2009.07.007

Koek, R. J., Schwartz, H. N., Scully, S., Langevin, J. P., Spangler, S., Korotinsky, A., et al. (2016). Treatment-refractory posttraumatic stress disorder (TRPTSD): a review and framework for the future. *Prog. Neuropsychopharmacol. Biol. Psychiatry* 70, 170–218. doi: 10.1016/j.pnpbp.2016.01.015

Kojima, M., Hosoda, H., Date, Y., Nakazato, M., Matsuo, H., and Kangawa, K. (1999). Ghrelin is a growth-hormone-releasing acylated peptide from stomach. *Nature* 402, 656–660. doi: 10.1038/45230

Kojima, M., and Kangawa, K. (2005). Ghrelin: structure and function. *Physiol. Rev.* 85, 495–522. doi: 10.1152/physrev.00012.2004

Kondrakiewicz, K., Kostecki, M., Szadzinska, W., and Knapska, E. (2019). Ecological validity of social interaction tests in rats and mice. *Genes Brain Behav.* 18:e12525. doi: 10.1111/gbb.12525

Kristenssson, E., Sundqvist, M., Hakanson, R., and Lindstrom, E. (2007). High gastrin cell activity and low ghrelin cell activity in high-anxiety Wistar Kyoto rats. *J. Endocrinol.* 193, 245–250. doi: 10.1677/JOE-07-0028

Kristenssson, E., Sundqvist, M., Astin, M., Kjerling, M., Mattsson, H., Dornonville De La Cour, C., et al. (2006). Acute psychological stress raises plasma ghrelin in the rat. *Regul. Pept.* 134, 114–117. doi: /10.1016/j.regpep.2006.02.003

Kurt, E., Guler, O., Serteser, M., Cansel, N., Ozbulut, O., Altinbas, K., et al. (2007). The effects of electroconvulsive therapy on ghrelin, leptin and cholesterol levels in patients with mood disorders. *Neurosci. Lett.* 426, 49–53. doi: 10.1016/j.neulet.2007.08.018

Labarthe, A., Fiquet, O., Hassouna, R., Zizzari, P., Lanfumey, L., Ramoz, N., et al. (2014). Ghrelin-derived peptides: A link between appetite/reward, GH axis, and psychiatric disorders? *Front. Endocrinol.* 5:163. doi: 10.3389/fendo.2014.00163

Lach, G., Schellekens, H., Dinan, T. G., and Cryan, J. F. (2018). Anxiety, depression, and the microbiome: a role for gut peptides. *Neurotherapeutics* 15, 36–59. doi: 10.1007/s13311-017-0585-0

Lambert, E., Lambert, G., Ika-Sari, C., Dawood, T., Lee, K., Chopra, R., et al. (2011). Ghrelin modulates sympathetic nervous system activity and stress response in lean and overweight men. *Hypertension* 58, 43–50. doi: 10.1161/HYPERTENSIONAHA.111.171025

Lang, P. J., Mcteague, L. M., and Bradley, M. M. (2016). RDoC, DSM, and the reflex physiology of fear: a biodimensional analysis of the anxiety disorders spectrum. *Psychophysiology* 53, 336–347. doi: 10.1111/psyp.12462

Lawson, E. A., Miller, K. K., Blum, J. I., Meenaghan, E., Misra, M., Eddy, K. T., et al. (2012). Leptin levels are associated with decreased depressive symptoms in women across the weight spectrum, independent of body fat. *Clin. Endocrinol.* 76, 520–525. doi: 10.1111/j.1365-2265.2011.04182.x

Lear, P. V., Iglesias, M. J., Feijoo-Bandin, S., Rodriguez-Penas, D., Mosquera-Leal, A., Garcia-Rua, V., et al. (2010). Des-acyl ghrelin has specific binding sites and different metabolic effects from ghrelin in cardiomyocytes. *Endocrinology* 151, 3286–3298. doi: 10.1210/en.2009-1205

Lee, M. R., Tapocik, J. D., Ghareeb, M., Schwandt, M. L., Dias, A. A., Le, A. N., et al. (2020). The novel ghrelin receptor inverse agonist PF-5190457 administered with alcohol: preclinical safety experiments and a phase 1b human laboratory study. *Mol. Psychiatry* 25, 461–475. doi: 10.1038/s41380-018-0064-y

Leung, P. K., Chow, K. B., Lau, P. N., Chu, K. M., Chan, C. B., Cheng, C. H., et al. (2007). The truncated ghrelin receptor polypeptide (GHS-R1b) acts as a dominant-negative mutant of the ghrelin receptor. *Cell. Signal.* 19, 1011–1022. doi: 10.1016/j.cellsig.2006.11.011

Li, B., Xu, Y., Pan, D., Xiao, Q., Gao, Q., Chen, X., et al. (2015). Effect of immobilization stress on the appetite and stomach ghrelin expression in maternal mice. *Int. J. Clin. Exp. Pathol.* 8, 15993–15999.

Li, G., Zhang, K., Wang, L., Cao, C., Fang, R., Liu, P., et al. (2018). The preliminary investigation of orexigenic hormone gene polymorphisms on posttraumatic stress disorder symptoms. *Psychoneuroendocrinology* 100, 131–136. doi: 10.1016/j.psyneuen.2018.09.042

Li, H., Wang, P., Huang, L., Li, P., and Zhang, D. (2019). Effects of regulating gut microbiota on the serotonin metabolism in the chronic unpredictable mild stress rat model. *Neurogastroenterol. Motil.* 31:e13677. doi: 10.1111/nmo.13677

Liu, S., and Borgland, S. L. (2015). Regulation of the mesolimbic dopamine circuit by feeding peptides. *Neuroscience* 289, 19–42. doi: 10.1016/j.neuroscience.2014.12.046

Lopez Lopez, A. L., Escobar Villanueva, M. C., Brianza Padilla, M., Bonilla Jaime, H., and Alarcon Aguilar, F. J. (2018). Chronic unpredictable mild stress progressively disturbs glucose metabolism and appetite hormones in rats. *Acta Endocrinol.* 14, 16–23. doi: 10.4183/aeb.2018.16

Lopez-Alarcon, M., Zurita-Cruz, J. N., Torres-Rodriguez, A., Bedia-Mejia, K., Perez-Guemez, M., Jaramillo-Villanueva, L., et al. (2020). Mindfulness affects stress, ghrelin, and BMI of obese children: a clinical trial. *Endocr. Connect.* 9, 163–172. doi: 10.1530/EC-19-0461

Lu, Y., Niu, M., Qiu, X., Cao, H., Xing, B., Sun, Y., et al. (2019). Acute but not chronic calorie restriction defends against stress-related anxiety and despair in a GHS-R1a-dependent manner. *Neuroscience* 412, 94–104. doi: 10.1016/j.neuroscience.2019.05.067

Luo, R., Uematsu, A., Weitemier, A., Aquili, L., Koivumaa, J., Mchugh, T. J., et al. (2018). A dopaminergic switch for fear to safety transitions. *Nat. Commun.* 9:2483. doi: 10.1038/s41467-018-04784-7

Lutter, M., Sakata, I., Osborne-Lawrence, S., Rovinsky, S. A., Anderson, J. G., Jung, S., et al. (2008). The orexigenic hormone ghrelin defends against depressive symptoms of chronic stress. *Nat. Neurosci.* 11, 752–753. doi: 10.1038/nn.2139

Mahbod, P., Smith, E. P., Fitzgerald, M. E., Morano, R. L., Packard, B. A., Ghosal, S., et al. (2018). Desacyl Ghrelin decreases anxiety-like behavior in male mice. *Endocrinology* 159, 388–399. doi: 10.1210/en.2017-00540

Mani, B. K., Walker, A. K., Lopez Soto, E. J., Raingo, J., Lee, C. E., Perello, M., et al. (2014). Neuroanatomical characterization of a growth hormone secretagogue receptor-green fluorescent protein reporter mouse. *J. Comp. Neurol.* 522, 3644–3666. doi: 10.1002/cne.23627

Mason, S. M., Flint, A. J., Roberts, A. L., Agnew-Blais, J., Koenen, K. C., and Rich-Edwards, J. W. (2014). Posttraumatic stress disorder symptoms and food addiction in women by timing and type of trauma exposure. *JAMA Psychiatry* 71, 1271–1278. doi: 10.1001/jamapsychiatry.2014.1208

Matsumoto, C., Yamada, C., Sadakane, C., Nahata, M., Hattori, T., and Takeda, H. (2017). Psychological stress in aged female mice causes acute hypophagia independent of central serotonin 2C receptor activation. *PLoS One* 12:e0187937. doi: 10.1371/journal.pone.0187937

Matsuo, K., Nakano, M., Nakashima, M., Watanuki, T., Egashira, K., Matsubara, T., et al. (2012). Neural correlates of plasma acylated ghrelin level in individuals with major depressive disorder. *Brain Res.* 1473, 185–192. doi: 10.1016/j.brainres.2012.07.027

McFarlane, M. R., Brown, M. S., Goldstein, J. L., and Zhao, T. J. (2014). Induced ablation of ghrelin cells in adult mice does not decrease food intake, body weight, or response to high-fat diet. *Cell Metab.* 20, 54–60. doi: 10.1016/j.cmet.2014.04.007

McGovern, K. R., Darling, J. E., and Hougland, J. L. (2016). Progress in small molecule and biologic therapeutics targeting Ghrelin signaling. *Mini Rev. Med. Chem.* 16, 465–480. doi: 10.2174/1389557515666150722101329

McKee, K. K., Palyha, O. C., Feighner, S. D., Hreniuk, D. L., Tan, C. P., Phillips, M. S., et al. (1997). Molecular analysis of rat pituitary and hypothalamic growth hormone secretagogue receptors. *Mol. Endocrinol.* 11, 415–423. doi: 10.1210/mend.11.4.9908

Meerlo, P., Overkamp, G. J., Daan, S., Van Den Hoofdakker, R. H., and Koolhaas, J. M. (1996). Changes in behaviour and body weight following a single or double social defeat in rats. *Stress* 1, 21–32. doi: 10.3109/10253899609001093

Meng, X., and D'Arcy, C. (2015). Comorbidity between lifetime eating problems and mood and anxiety disorders: results from the Canadian Community Health Survey of Mental Health and Well-being. *Eur. Eat Disord. Rev.* 23, 156–162. doi: 10.1002/erv.2347

Meyer, R. M., Burgos-Robles, A., Liu, E., Correia, S. S., and Goosens, K. A. (2014). A ghrelin-growth hormone axis drives stress-induced vulnerability to enhanced fear. *Mol. Psychiatry* 19, 1284–1294. doi: 10.1038/mp.2013.135

Milad, M. R., and Quirk, G. J. (2012). Fear extinction as a model for translational neuroscience: ten years of progress. *Annu. Rev. Psychol.* 63, 129–151. doi: 10.1146/annurev.psych.121208.131631

Mogami, S., Sadakane, C., Nahata, M., Mizuhara, Y., Yamada, C., Hattori, T., et al. (2016). CRF receptor 1 antagonism and brain distribution of active components contribute to the ameliorative effect of rikkunshito on stress-induced anorexia. *Sci. Rep.* 6:27516. doi: 10.1038/srep27516

Mograbi, K. M., Suchecki, D., Da Silva, S. G., Covolan, L., and Hamani, C. (2020). Chronic unpredictable restraint stress increases hippocampal pro-inflammatory cytokines and decreases motivated behavior in rats. *Stress* 23, 427–436. doi: 10.1080/10253890.2020.1712355

Monteleone, P., Tortorella, A., Scognamiglio, P., Serino, I., Monteleone, A. M., and Maj, M. (2012). The acute salivary ghrelin response to a psychosocial stress is enhanced in symptomatic patients with bulimia nervosa: a pilot study. *Neuropsychobiology* 66, 230–236. doi: 10.1159/000341877

Moose, J. E., Leets, K. A., Mate, N. A., Chisholm, J. D., and Hougland, J. L. (2020). An overview of ghrelin O-acyltransferase inhibitors: a literature and patent review for 2010-2019. *Expert Opin. Ther. Pat.* doi: 10.1080/13543776.2020.1776263 [Epub ahead of print].

Mori, K., Yoshimoto, A., Takaya, K., Hosoda, K., Ariyasu, H., Yahata, K., et al. (2000). Kidney produces a novel acylated peptide, ghrelin. *FEBS Lett.* 486, 213–216. doi: 10.1016/S0014-5793(00)02308-5

Murakami, N., Hayashida, T., Kuroiwa, T., Nakahara, K., Ida, T., Mondal, M. S., et al. (2002). Role for central ghrelin in food intake and secretion profile of stomach ghrelin in rats. *J. Endocrinol.* 174, 283–288. doi: 10.1677/joe.0.1740283

Nahata, M., Saegusa, Y., Sadakane, C., Yamada, C., Nakagawa, K., Okubo, N., et al. (2014). Administration of exogenous acylated ghrelin or rikkunshito, an endogenous ghrelin enhancer, improves the decrease in postprandial gastric motility in an acute restraint stress mouse model. *Neurogastroenterol. Motil.* 26, 821–831. doi: 10.1111/nmo.12336

Nakashima, K., Akiyoshi, J., Hatano, K., Hanada, H., Tanaka, Y., Tsuru, J., et al. (2008). Ghrelin gene polymorphism is associated with depression, but not panic disorder. *Psychiatr. Genet.* 18:257. doi: 10.1097/YPG.0b013e328306c979

Nakazato, M., Murakami, N., Date, Y., Kojima, M., Matsuo, H., Kangawa, K., et al. (2001). A role for ghrelin in the central regulation of feeding. *Nature* 409, 194–198. doi: 10.1038/35051587

Ng, I. S., Cheung, K. C., and Chou, K. L. (2013). Correlates of eating disorder in middle-aged and older adults: evidence from 2007 British National Psychiatric Morbidity Survey. *J. Aging Health* 25, 1106–1120. doi: 10.1177/0898264313494798

Ochi, M., Tominaga, K., Tanaka, F., Tanigawa, T., Shiba, M., Watanabe, T., et al. (2008). Effect of chronic stress on gastric emptying and plasma ghrelin levels in rats. *Life Sci.* 82, 862–868. doi: 10.1016/j.lfs.2008.01.020

Ogaya, M., Kim, J., and Sasaki, K. (2011). Ghrelin postsynaptically depolarizes dorsal raphe neurons in rats *in vitro*. *Peptides* 32, 1606–1616. doi: 10.1016/j.peptides.2011.07.001

Okada, T., Waise, T. M. Z., Toshinai, K., Mita, Y., Sakoda, H., and Nakazato, M. (2018). Analysis of peripheral ghrelin signaling via the vagus nerve in ghrelin receptor-restored GHSR-null mice. *Neurosci. Lett.* 681, 50–55. doi: 10.1016/j.neulet.2018.05.035

Olesen, J., Gustavsson, A., Svensson, M., Wittchen, H. U., Jonsson, B., Group, C. S., et al. (2012). The economic cost of brain disorders in Europe. *Eur. J. Neurol.* 19, 155–162. doi: 10.1111/j.1468-1331.2011.03590.x

Ozmen, S., Seker, A., and Demirci, E. (2019). Ghrelin and leptin levels in children with anxiety disorders. *J. Pediatr. Endocrinol. Metab.* 32, 1043–1047. doi: 10.1515/jpem-2019-0229

Ozsoy, S., Besirli, A., Abdulrezzak, U., and Basturk, M. (2014). Serum ghrelin and leptin levels in patients with depression and the effects of treatment. *Psychiatry Investig.* 11, 167–172. doi: 10.1515/jpem-2019-0229

Patki, G., Solanki, N., Atrooz, F., Allam, F., and Salim, S. (2013). Depression, anxiety-like behavior and memory impairment are associated with increased oxidative stress and inflammation in a rat model of social stress. *Brain Res.* 1539, 73–86. doi: 10.1016/j.brainres.2013.09.033

Patterson, Z. R., Ducharme, R., Anisman, H., and Abizaid, A. (2010). Altered metabolic and neurochemical responses to chronic unpredictable stressors in ghrelin receptor-deficient mice. *Eur. J. Neurosci.* 32, 632–639. doi: 10.1111/j.1460-9568.2010.07310.x

Patterson, Z. R., Khazall, R., Mackay, H., Anisman, H., and Abizaid, A. (2013a). Central ghrelin signaling mediates the metabolic response of C57BL/6 male mice to chronic social defeat stress. *Endocrinology* 154, 1080–1091. doi: 10.1210/en.2012-1834

Patterson, Z. R., Parno, T., Isaacs, A. M., and Abizaid, A. (2013b). Interruption of ghrelin signaling in the PVN increases high-fat diet intake and body weight in stressed and non-stressed C57BL6J male mice. *Front. Neurosci.* 7:167. doi: 10.3389/fnins.2013.00167

Perello, M., Cabral, A., Cornejo, M. P., De Francesco, P. N., Fernandez, G., and Uriarte, M. (2018). Brain accessibility delineates the central effects of circulating ghrelin. *J. Neuroendocrinol.* 31:e12677. doi: 10.1111/jne.12677

Perello, M., and Zigman, J. M. (2012). The role of ghrelin in reward-based eating. *Biol. Psychiatry* 72, 347–353. doi: 10.1016/j.biopsych.2012.02.016

Petersen, P. S., Woldbye, D. P., Madsen, A. N., Egerod, K. L., Jin, C., Lang, M., et al. (2009). In vivo characterization of high Basal signaling from the ghrelin receptor. *Endocrinology* 150, 4920–4930. doi: 10.1210/en.2008-1638

Pierre, A., Regin, Y., Van Schuerbeek, A., Fritz, E. M., Muylle, K., Beckers, T., et al. (2019). Effects of disrupted ghrelin receptor function on fear processing, anxiety and saccharin preference in mice. *Psychoneuroendocrinology* 110:104430. doi: 10.1016/j.psyneuen.2019.104430

Pierre, A., Van Schuerbeek, A., Allaoui, W., Van Laere, S., Singewald, N., Van Eeckhaut, A., et al. (2020). Effects of ghrelin receptor activation on forebrain dopamine release, conditioned fear and fear extinction in C57BL/6J mice. *J. Neurochem.* 154:e14996. doi: 10.1111/jnc.14996

Pinar, M., Gulsun, M., Tasci, I., Erdil, A., Bolu, E., Acikel, C., et al. (2008). Maprotiline induced weight gain in depressive disorder: changes in circulating ghrelin and adiponectin levels and insulin sensitivity. *Prog. Neuropsychopharmacol. Biol. Psychiatry* 32, 135–139. doi: 10.1016/j.pnpbp.2007.07.028

Quarta, D., Di Francesco, C., Melotto, S., Mangiarini, L., Heidbreder, C., and Hedou, G. (2009). Systemic administration of ghrelin increases extracellular dopamine in the shell but not the core subdivision of the nucleus accumbens. *Neurochem. Int.* 54, 89–94. doi: 10.1016/j.neuint.2008.12.006

Quarta, D., and Smolders, I. (2014). Rewarding, reinforcing and incentive salient events involve orexigenic hypothalamic neuropeptides regulating mesolimbic dopaminergic neurotransmission. *Eur. J. Pharm. Sci.* 57, 2–10. doi: 10.1016/j.ejps.2014.01.008

Ramirez, V. T., Van Oeffelen, W., Torres-Fuentes, C., Chruscicka, B., Druelle, C., Golubeva, A. V., et al. (2019). Differential functional selectivity and downstream signaling bias of ghrelin receptor antagonists and inverse agonists. *FASEB J.* 33, 518–531. doi: 10.1096/fj.201800655R

Raspopow, K., Abizaid, A., Matheson, K., and Anisman, H. (2010). Psychosocial stressor effects on cortisol and ghrelin in emotional and non-emotional eaters: influence of anger and shame. *Horm. Behav.* 58, 677–684. doi: 10.1016/j.yhbeh.2010.06.003

Razzoli, M., Sanghez, V., and Bartolomucci, A. (2015). Chronic subordination stress induces hyperphagia and disrupts eating behavior in mice modeling binge-eating-like disorder. *Front. Nutr.* 1:30. doi: 10.3389/fnut.2014.00030

Ricken, R., Bopp, S., Schlattmann, P., Himmerich, H., Bschor, T., Richter, C., et al. (2017). Ghrelin serum concentrations are associated with treatment response during lithium augmentation of antidepressants. *Int. J. Neuropsychopharmacol.* 20, 692–697. doi: 10.1093/ijnp/pyw082

Riddle, M. C., Mckenna, M. C., Yoon, Y. J., Pattwell, S. S., Santos, P. M., Casey, B. J., et al. (2013). Caloric restriction enhances fear extinction learning in mice. *Neuropsychopharmacology* 38, 930–937. doi: 10.1038/npp.2012.268

Roman, C. W., Derkach, V. A., and Palmiter, R. D. (2016). Genetically and functionally defined NTS to PBN brain circuits mediating anorexia. *Nat. Commun.* 7:11905. doi: 10.1038/ncomms11905

Rostamkhani, F., Zardooz, H., Goshadrou, F., Baveisi, M., and Hedayati, M. (2016). Stress increased ghrelin secretion from pancreatic isolated islets in male rats. *Gen. Physiol. Biophys.* 35, 109–117.

Rouach, V., Bloch, M., Rosenberg, N., Gilad, S., Limor, R., Stern, N., et al. (2007). The acute ghrelin response to a psychological stress challenge does not predict the post-stress urge to eat. *Psychoneuroendocrinology* 32, 693–702. doi: 10.1016/j.psyneuen.2007.04.010

Rucinski, M., Ziolkowska, A., Tyczewska, M., and Malendowicz, L. K. (2009). Expression of prepro-ghrelin and related receptor genes in the rat adrenal gland and evidences that ghrelin exerts a potent stimulating effect on corticosterone secretion by cultured rat adrenocortical cells. *Peptides* 30, 1448–1455. doi: 10.1016/j.peptides.2009.04.016

Saegusa, Y., Takeda, H., Muto, S., Nakagawa, K., Ohnishi, S., Sadakane, C., et al. (2011). Decreased plasma ghrelin contributes to anorexia following novelty stress. *Am. J. Physiol. Endocrinol. Metab.* 301, E685–E696. doi: 10.1152/ajpendo.00121.2011

Salinas-Hernandez, X. I., Vogel, P., Betz, S., Kalisch, R., Sigurdsson, T., and Duvarci, S. (2018). Dopamine neurons drive fear extinction learning by signaling the omission of expected aversive outcomes. *eLife* 7:e38818. doi: 10.7554/eLife.38818.024

Sartori, S. B., and Singewald, N. (2019). Novel pharmacological targets in drug development for the treatment of anxiety and anxiety-related disorders. *Pharmacol. Ther.* 204:107402. doi: 10.1016/j.pharmthera.2019.107402

Schaeffer, M., Langlet, F., Lafont, C., Molino, F., Hodson, D. J., Roux, T., et al. (2013). Rapid sensing of circulating ghrelin by hypothalamic appetite-modifying neurons. *Proc. Natl. Acad. Sci. U.S.A.* 110, 1512–1517. doi: 10.1073/pnas.1212137110

Schalla, M. A., and Stengel, A. (2020). Effects of microbiome changes on endocrine ghrelin signaling - A systematic review. *Peptides* 133:170388. doi: 10.1016/j.peptides.2020.170388

Schanze, A., Reulbach, U., Scheuchenzuber, M., Groschl, M., Kornhuber, J., and Kraus, T. (2008). Ghrelin and eating disturbances in psychiatric disorders. *Neuropsychobiology* 57, 126–130. doi: 10.1159/000138915

Schele, E., Bake, T., Rabasa, C., and Dickson, S. L. (2016). Centrally administered ghrelin acutely influences food choice in rodents. *PLoS One* 11:e0149456. doi: 10.1371/journal.pone.0149456

Schellekens, H., Dinan, T. G., and Cryan, J. F. (2013a). Taking two to tango: a role for ghrelin receptor heterodimerization in stress and reward. *Front. Neurosci.* 7:148. doi: 10.3389/fnins.2013.00148

Schellekens, H., Finger, B. C., Dinan, T. G., and Cryan, J. F. (2012). Ghrelin signalling and obesity: at the interface of stress, mood and food reward. *Pharmacol. Ther.* 135, 316–326. doi: 10.1016/j.pharmthera.2012.06.004

Schellekens, H., Van Oeffelen, W. E., Dinan, T. G., and Cryan, J. F. (2013b). Promiscuous dimerization of the growth hormone secretagogue receptor (GHS-R1a) attenuates ghrelin-mediated signaling. *J. Biol. Chem.* 288, 181–191. doi: 10.1074/jbc.M112.382473

Schmidt, M. V., Levine, S., Alam, S., Harbich, D., Sterlemann, V., Ganea, K., et al. (2006). Metabolic signals modulate hypothalamic-pituitary-adrenal axis activation during maternal separation of the neonatal mouse. *J. Neuroendocrinol.* 18, 865–874. doi: 10.1111/j.1365-2826.2006.01482.x

Scott, K. M., Mcgee, M. A., Wells, J. E., and Oakley Browne, M. A. (2008). Obesity and mental disorders in the adult general population. *J. Psychosom. Res.* 64, 97–105. doi: 10.1016/j.jpsychores.2007.09.006

Scott, M. M., Perello, M., Chuang, J. C., Sakata, I., Gautron, L., Lee, C. E., et al. (2012). Hindbrain ghrelin receptor signaling is sufficient to maintain fasting glucose. *PLoS One* 7:e44089. doi: 10.1371/journal.pone.0044089

Shi, L., Deng, J., Chen, S., Que, J., Sun, Y., Wang, Z., et al. (2018). Fasting enhances extinction retention and prevents the return of fear in humans. *Transl. Psychiatry* 8:214. doi: 10.1038/s41398-018-0260-1

Shi, L., Du, X., Jiang, H., and Xie, J. (2017). Ghrelin and neurodegenerative disorders-a review. *Mol. Neurobiol.* 54, 1144–1155. doi: 10.1007/s12035-016-9729-1

Simas, B. B., Nunes, E. A., Crestani, C. C., and Speretta, G. F. (2018). Cardiovascular and metabolic consequences of the association between chronic stress and high-fat diet in rats. *Stress* 21, 247–256. doi: 10.1080/10253890.2018.1437413

Simmons, W. K., Burrows, K., Avery, J. A., Kerr, K. L., Taylor, A., Bodurka, J., et al. (2020). Appetite changes reveal depression subgroups with distinct endocrine, metabolic, and immune states. *Mol. Psychiatry* 25, 1457–1468. doi: 10.1038/s41380-018-0093-6

Singewald, N., and Holmes, A. (2019). Rodent models of impaired fear extinction. *Psychopharmacology* 236, 21–32. doi: 10.1007/s00213-018-5054-x

Singewald, N., Schmuckermair, C., Whittle, N., Holmes, A., and Ressler, K. J. (2015). Pharmacology of cognitive enhancers for exposure-based therapy of fear, anxiety and trauma-related disorders. *Pharmacol. Ther.* 149, 150–190. doi: 10.1016/j.pharmthera.2014.12.004

Skibicka, K. P., and Dickson, S. L. (2011). Ghrelin and food reward: the story of potential underlying substrates. *Peptides* 32, 2265–2273. doi: 10.1016/j.peptides.2011.05.016

Skibicka, K. P., Hansson, C., Alvarez-Crespo, M., Friberg, P. A., and Dickson, S. L. (2011). Ghrelin directly targets the ventral tegmental area to increase food motivation. *Neuroscience* 180, 129–137. doi: 10.1016/j.neuroscience.2011.02.016

Skibicka, K. P., Hansson, C., Egecioglu, E., and Dickson, S. L. (2012a). Role of ghrelin in food reward: impact of ghrelin on sucrose self-administration and mesolimbic dopamine and acetylcholine receptor gene expression. *Addict. Biol.* 17, 95–107. doi: 10.1111/j.1369-1600.2010.00294.x

Skibicka, K. P., Shirazi, R. H., Hansson, C., and Dickson, S. L. (2012b). Ghrelin interacts with neuropeptide Y Y1 and opioid receptors to increase food reward. *Endocrinology* 153, 1194–1205. doi: 10.1210/en.2011-1606

Skibicka, K. P., Shirazi, R. H., Rabasa-Papio, C., Alvarez-Crespo, M., Neuber, C., Vogel, H., et al. (2013). Divergent circuitry underlying food reward and intake effects of ghrelin: dopaminergic VTA-accumbens projection mediates ghrelin's effect on food reward but not food intake. *Neuropharmacology* 73, 274–283. doi: 10.1016/j.neuropharm.2013.06.004

Spencer, S. J., Emmerzaal, T. L., Kozicz, T., and Andrews, Z. B. (2015). Ghrelin's role in the hypothalamic-pituitary-adrenal axis stress response: implications for mood disorders. *Biol. Psychiatry* 78, 19–27. doi: 10.1016/j.biopsych.2014.10.021

Spencer, S. J., Xu, L., Clarke, M. A., Lemus, M., Reichenbach, A., Geenen, B., et al. (2012). Ghrelin regulates the hypothalamic-pituitary-adrenal axis and restricts anxiety after acute stress. *Biol. Psychiatry* 72, 457–465. doi: 10.1016/j.biopsych.2012.03.010

Stark, R., Santos, V. V., Geenen, B., Cabral, A., Dinan, T., Bayliss, J. A., et al. (2016). Des-Acyl Ghrelin and Ghrelin O-Acyltransferase Regulate Hypothalamic-Pituitary-Adrenal Axis Activation and Anxiety in Response to Acute Stress. *Endocrinology* 157, 3946–3957. doi: 10.1210/en.2016-1306

Stengel, A., Goebel, M., Wang, L., Reeve, J. R. Jr., Tache, Y., and Lambrecht, N. W. G. (2010). Lipopolysaccharide differentially decreases plasma acyl and desacyl ghrelin levels in rats: potential role of the circulating ghrelin-acylating enzyme GOAT. *Peptides* 31, 1689–1696. doi: 10.1016/j.peptides.2010.06.015

Stevanovic, D., Milosevic, V., Starcevic, V. P., and Severs, W. B. (2007). The effect of centrally administered ghrelin on pituitary ACTH cells and circulating ACTH and corticosterone in rats. *Life Sci.* 80, 867–872. doi: 10.1016/j.lfs.2006.11.018

Stievenard, A., Mequinion, M., Andrews, Z. B., Destee, A., Chartier-Harlin, M. C., Viltart, O., et al. (2016). Is there a role for ghrelin in central dopaminergic systems? Focus on nigrostriatal and mesocorticolimbic pathways. *Neurosci. Biobehav. Rev.* 73, 255–275. doi: 10.1016/j.neubiorev.2016.11.021

Stoyanova, I. (2014). Ghrelin: a link between ageing, metabolism and neurodegenerative disorders. *Neurobiol. Dis.* 72(Pt A), 72–83. doi: 10.1016/j.nbd.2014.08.026

Su, M., Yan, M., and Gong, Y. (2019). Ghrelin fiber projections from the hypothalamic arcuate nucleus into the dorsal vagal complex and the regulation of glycolipid metabolism. *Neuropeptides* 78:101972. doi: 10.1016/j.npep.2019.101972

Swartz, E. M., Browning, K. N., Travagli, R. A., and Holmes, G. M. (2014). Ghrelin increases vagally mediated gastric activity by central sites of action. *Neurogastroenterol. Motil.* 26, 272–282. doi: 10.1111/nmo.12261

Togliatto, G., Trombetta, A., Dentelli, P., Baragli, A., Rosso, A., Granata, R., et al. (2010). Unacylated ghrelin rescues endothelial progenitor cell function in individuals with type 2 diabetes. *Diabetes* 59, 1016–1025. doi: 10.2337/db09-0858

Torres-Fuentes, C., Golubeva, A. V., Zhdanov, A. V., Wallace, S., Arboleya, S., Papkovsky, D. B., et al. (2019). Short-chain fatty acids and microbiota metabolites attenuate ghrelin receptor signaling. *FASEB J.* 33, 13546–13559. doi: 10.1096/fj.201901433R

Uchida, A., Zigman, J. M., and Perello, M. (2013). Ghrelin and eating behavior: evidence and insights from genetically-modified mouse models. *Front. Neurosci.* 7:121. doi: 10.3389/fnins.2013.00121

Verma, D., Wood, J., Lach, G., Herzog, H., Sperk, G., and Tasan, R. (2016). Hunger promotes fear extinction by activation of an amygdala microcircuit. *Neuropsychopharmacology* 41, 431–439. doi: 10.1038/npp.2015.163

Walker, A. K., Rivera, P. D., Wang, Q., Chuang, J. C., Tran, S., Osborne-Lawrence, S., et al. (2015). The P7C3 class of neuroprotective compounds exerts antidepressant efficacy in mice by increasing hippocampal neurogenesis. *Mol. Psychiatry* 20, 500–508. doi: 10.1038/mp.2014.34

Wallace Fitzsimons, S. E., Chruscicka, B., Druelle, C., Stamou, P., Nally, K., Dinan, T. G., et al. (2019). A ghrelin receptor and oxytocin receptor heterocomplex impairs oxytocin mediated signalling. *Neuropharmacology* 152, 90–101. doi: 10.1016/j.neuropharm.2018.12.022

Wang, Q., Liu, C., Uchida, A., Chuang, J. C., Walker, A., Liu, T., et al. (2014). Arcuate AgRP neurons mediate orexigenic and glucoregulatory actions of ghrelin. *Mol. Metab.* 3, 64–72. doi: 10.1016/j.molmet.2013.10.001

Warren, C. M., Tona, K. D., Ouwerkerk, L., Van Paridon, J., Poletiek, F., Van Steenbergen, H., et al. (2019). The neuromodulatory and hormonal effects of transcutaneous vagus nerve stimulation as evidenced by salivary alpha amylase, salivary cortisol, pupil diameter, and the P3 event-related potential. *Brain Stimul.* 12, 635–642. doi: 10.1016/j.brs.2018.12.224

Whittle, N., Maurer, V., Murphy, C., Rainer, J., Bindreither, D., Hauschild, M., et al. (2016). Enhancing dopaminergic signaling and histone acetylation promotes long-term rescue of deficient fear extinction. *Transl. Psychiatry* 6:e974. doi: 10.1038/tp.2016.231

Willesen, M. G., Kristensen, P., and Romer, J. (1999). Co-localization of growth hormone secretagogue receptor and NPY mRNA in the arcuate nucleus of the rat. *Neuroendocrinology* 70, 306–316. doi: 10.1159/000054491

Wittchen, H. U., Jacobi, F., Rehm, J., Gustavsson, A., Svensson, M., Jonsson, B., et al. (2011). The size and burden of mental disorders and other disorders

of the brain in Europe 2010. *Eur. Neuropsychopharmacol.* 21, 655–679. doi: 10.1016/j.euroneuro.2011.07.018

Wittekind, D. A., and Kluge, M. (2015). Ghrelin in psychiatric disorders - A review. *Psychoneuroendocrinology* 52, 176–194. doi: 10.1016/j.psyneuen.2014.11.013

Yam, K. Y., Ruigrok, S. R., Ziko, I., De Luca, S. N., Lucassen, P. J., Spencer, S. J., et al. (2017). Ghrelin and hypothalamic NPY/AgRP expression in mice are affected by chronic early-life stress exposure in a sex-specific manner. *Psychoneuroendocrinology* 86, 73–77. doi: 10.1016/j.psyneuen.2017.09.006

Yamada, C., Saegusa, Y., Nahata, M., Sadakane, C., Hattori, T., and Takeda, H. (2015). Influence of aging and gender differences on feeding behavior and Ghrelin-related factors during social isolation in mice. *PLoS One* 10:e0140094. doi: 10.1371/journal.pone.0140094

Yan, Z., Jiao, H., Ding, X., Ma, Q., Li, X., Pan, Q., et al. (2018). Xiaoyaosan improves depressive-like behaviors in mice through regulating Apelin-APJ system in hypothalamus. *Molecules* 23:1073. doi: 10.3390/molecules23051073

Yanagi, S., Sato, T., Kangawa, K., and Nakazato, M. (2018). The Homeostatic Force of Ghrelin. *Cell Metab.* 27, 786–804. doi: 10.1016/j.cmet.2018.02.008

Yao, L., Chen, J., Chen, H., Xiang, D., Yang, C., Xiao, L., et al. (2016). Hypothalamic gastrin-releasing peptide receptor mediates an antidepressant-like effect in a mouse model of stress. *Am. J. Transl. Res.* 8, 3097–3105.

Yin, Y., and Zhang, W. (2016). The role of Ghrelin in senescence: a mini-review. *Gerontology* 62, 155–162. doi: 10.1159/000433533

Yousufzai, M., Harmatz, E. S., Shah, M., Malik, M. O., and Goosens, K. A. (2018). Ghrelin is a persistent biomarker for chronic stress exposure in adolescent rats and humans. *Transl. Psychiatry* 8:74. doi: 10.1038/s41398-018-0135-5

Yun, B., Yoo, J. Y., Park, M. R., Ryu, S., Lee, W. J., Choi, H. J., et al. (2020). Ingestion of Gouda cheese ameliorates the chronic unpredictable mild stress in mice. *Food Sci. Anim. Resour.* 40, 145–153. doi: 10.5851/kosfa.2019.e81

Zhao, T. J., Liang, G., Li, R. L., Xie, X., Sleeman, M. W., Murphy, A. J., et al. (2010). Ghrelin O-acyltransferase (GOAT) is essential for growth hormone-mediated survival of calorie-restricted mice. *Proc. Natl. Acad. Sci. U.S.A.* 107, 7467–7472. doi: 10.1073/pnas.1002271107

Zigman, J. M., Jones, J. E., Lee, C. E., Saper, C. B., and Elmquist, J. K. (2006). Expression of ghrelin receptor mRNA in the rat and the mouse brain. *J. Comp. Neurol.* 494, 528–548. doi: 10.1002/cne.20823

Zimmermann, U. S., Buchmann, A., Steffin, B., Dieterle, C., and Uhr, M. (2007). Alcohol administration acutely inhibits ghrelin secretion in an experiment involving psychosocial stress. *Addict. Biol.* 12, 17–21. doi: 10.1111/j.1369-1600.2006.00026.x

Conflict of Interest: The authors declare that the research was conducted in the absence of any commercial or financial relationships that could be construed as a potential conflict of interest.

Copyright © 2020 Fritz, Singewald and De Bundel. This is an open-access article distributed under the terms of the Creative Commons Attribution License (CC BY). The use, distribution or reproduction in other forums is permitted, provided the original author(s) and the copyright owner(s) are credited and that the original publication in this journal is cited, in accordance with accepted academic practice. No use, distribution or reproduction is permitted which does not comply with these terms.

frontiers in Synaptic Neuroscience

REVIEW
published: 03 December 2020
doi: 10.3389/fnsyn.2020.607959

The α5 Nicotinic Acetylcholine Receptor Subunit Differentially Modulates α4β2* and α3β4* Receptors

*Petra Scholze and Sigismund Huck**

Department of Pathobiology of the Nervous System, Center for Brain Research, Medical University of Vienna, Vienna, Austria

Nicotine, the principal reinforcing compound in tobacco, acts in the brain by activating neuronal nicotinic acetylcholine receptors (nAChRs). This review summarizes our current knowledge regarding how the α5 accessory nAChR subunit, encoded by the *CHRNA5* gene, differentially modulates α4β2* and α3β4* receptors at the cellular level. Genome-wide association studies have linked a gene cluster in chromosomal region 15q25 to increased susceptibility to nicotine addiction, lung cancer, chronic obstructive pulmonary disease, and peripheral arterial disease. Interestingly, this gene cluster contains a non-synonymous single-nucleotide polymorphism (SNP) in the human *CHRNA5* gene, causing an aspartic acid (D) to asparagine (N) substitution at amino acid position 398 in the α5 nAChR subunit. Although other SNPs have been associated with tobacco smoking behavior, efforts have focused predominantly on the D398 and N398 variants in the α5 subunit. In recent years, significant progress has been made toward understanding the role that the α5 nAChR subunit—and the role of the D398 and N398 variants—plays on nAChR function at the cellular level. These insights stem primarily from a wide range of experimental models, including receptors expressed heterologously in *Xenopus* oocytes, various cell lines, and neurons derived from human induced pluripotent stem cells (iPSCs), as well as endogenous receptors in genetically engineered mice and—more recently—rats. Despite providing a wealth of available data, however, these studies have yielded conflicting results, and our understanding of the modulatory role that the α5 subunit plays remains incomplete. Here, we review these reports and the various techniques used for expression and analysis in order to examine how the α5 subunit modulates key functions in α4β2* and α3β4* receptors, including receptor trafficking, sensitivity, efficacy, and desensitization. In addition, we highlight the strikingly different role that the α5 subunit plays in Ca^{2+} signaling between α4β2* and α3β4* receptors, and we discuss whether the N398 α5 subunit variant can partially replace the D398 variant.

Keywords: nACh receptor, CHRNA5 polymorphism, subunit composition, heterologous expression, endogenous receptors, calcium

OPEN ACCESS

Edited by:
Francisco J. Barrantes, Instituto de Investigaciones Biomédicas (BIOMED UCA-CONICET), Argentina

Reviewed by:
Michael David Scofield, Medical University of South Carolina, United States
Anna M. Lee, University of Minnesota Twin Cities, United States

***Correspondence:**
Sigismund Huck
sigismund.huck@meduniwien.ac.at

Received: *18 September 2020*
Accepted: *11 November 2020*
Published: *03 December 2020*

Citation:
Scholze P and Huck S (2020) The α5 Nicotinic Acetylcholine Receptor Subunit Differentially Modulates α4β2 and α3β4* Receptors. Front. Synaptic Neurosci. 12:607959. doi: 10.3389/fnsyn.2020.607959*

INTRODUCTION

Nicotinic acetylcholine receptors (nAChRs) are homo- and hetero-pentamers that can be distinguished by their sensitivity to α-bungarotoxin. Receptors containing an α4β2*[1] or α3β4* backbone are insensitive to α-bungarotoxin and often referred to as central nervous system (CNS) and peripheral nervous system (PNS) nAChRs, respectively (Millar and Gotti, 2009). Despite this relatively loose distinction, α3β4* receptors have also been found in distinct brain regions such as the medial habenula (MHb) and interpeduncular nucleus (IPN), where they play a central role in nicotine addiction. Moreover, so-called "neuronal" nAChRs are also expressed in non-neuronal cells, where they play both physiological and pathological roles (reviewed by Zoli et al., 2018).

In the PNS, nAChRs mediate synaptic transmission in sympathetic and parasympathetic ganglia. In contrast, nAChRs in the CNS primarily modulate and/or trigger the release of a wide variety of neurotransmitters from presynaptic sites, and the functional impact of this modulation depends on the transmitter system involved (e.g., glutamate, GABA, or catecholamines) and the role these transmitter systems play in brain circuitry.

As ionotropic receptors, nAChRs are ligand-gated cation channels activated by the neurotransmitter acetylcholine (ACh) binding to canonical (orthosteric) binding sites at the N-terminal interface of two subunits with a primary and complementary component (Zoli et al., 2018). The α subunit contains the primary ligand-binding site, and the β subunit contains the complementary site. To maximally activate heteromeric nAChRs, ACh must bind to two binding sites in receptors; in contrast, homomeric α7 receptors require binding to a single site for maximal activation (reviewed by Zoli et al., 2018).

The α3, α4, β2, and β4 subunits can co-assemble to produce a fairly wide range of functional receptor subtypes with various stoichiometries. In the CNS, both high-affinity $(\alpha4\beta2)_2\beta2$ and low-affinity $(\alpha4\beta2)_2\alpha4$ receptors have been reported (Grady et al., 2010; Marks et al., 2010; Harpsoe et al., 2011). Peripheral-type $(\alpha3\beta4)_2\beta4$ and $(\alpha3\beta4)_2\alpha3$ receptors have been expressed in *Xenopus* oocytes (Grishin et al., 2010; Krashia et al., 2010; George et al., 2012) and HEK293 cells (Krashia et al., 2010); however, the stoichiometry of α3β4* receptors in the CNS and/or PNS is currently unknown. The fifth subunit—e.g., α4 and β2 in $(\alpha4\beta2)_2\alpha4$ and $(\alpha4\beta2)_2\beta2$ receptors, and α3 and β4 in $(\alpha3\beta4)_2\alpha3$ and $(\alpha3\beta4)_2\beta4$ receptors, respectively—may contribute to allosteric binding sites. Receptor complexity is increased further by additional subunits such as the α2, α5, α6, and β3 subunits, which can co-assemble into the two principal types of PNS and/or CNS receptors.

Because both the α5 and β3 subunits lack a primary or complementary component (Le Novere et al., 2002), they cannot contribute to the orthosteric binding site and are therefore often referred to as "accessory" subunits; nevertheless, these subunits contribute to the channel's lining, as well as potential allosteric binding sites and distinct properties conferred by the large cytoplasmic loop between the third and fourth transmembrane domains (i.e., the M3–M4 loop).

Below, we discuss the role of the cytoplasmic loop in the α5 subunit on the receptor's assembly, trafficking, and targeting to the plasma membrane. However, the cytoplasmic loop may also affect other receptor properties beyond its effects on membrane trafficking. For example, Kabbani and colleagues found that the β2 subunit can form a complex with at least 21 different cellular proteins identified using MALDI-TOF-TOF MS/MS analysis (Kabbani et al., 2007).

In addition to their ionotropic properties, nAChRs also mediate G protein signaling via the cytoplasmic loop, as reviewed extensively by Kabbani et al. (2013). The majority of research in this respect has focused on α7-containing nAChRs and found that α7 receptors can act via ionotropic signaling, as well as Gαq-mediated metabotropic signaling via a G protein–binding cluster in the subunit's M3–M4 loop (King et al., 2015). Interestingly, the α3, α5, and β2 subunits have also be been found to bind Goα and Gβγ proteins (Fischer et al., 2005a).

Several putative CaMKII and PKA sites, as well as novel nicotine-induced phosphorylation sites, have been identified in the cytoplasmic loop of α4/β2* nAChRs (Miller et al., 2018). Non-ionic signaling events triggered by nAChR-coupled protein kinases appear to play a particularly prominent role in non-excitable cells, in which receptor activation has been linked to cancer (for review, see Grando, 2014). Although the functional role of α5 phosphorylation has yet to be fully explored, studies involving small molecule kinase inhibitors suggest that kinases do play a functional role related to the α5 subunit (Ray et al., 2017).

The general structure, properties, and function of nAChRs have been covered thoroughly by a large number of reviews (e.g., McGehee and Role, 1995; Le Novere et al., 2002; Gotti et al., 2006; Stokes et al., 2015; Bertrand and Terry, 2018; Zoli et al., 2018). Here, we focus on the α5 accessory subunit, given that human genome-wide association studies have shown that polymorphisms in the gene cluster in chromosomal region 15q25, which includes genes that encode the α5, α3, and β4 nAChR subunits, are linked to susceptibility to nicotine addiction and certain forms of cancer. For example, in the human *CHRNA5* gene, which encodes the α5 nAChR subunit, the single-nucleotide polymorphism (SNP) rs16969968 replaces an aspartic acid with an asparagine in the resulting protein and has been strongly correlated with excessive and compulsive nicotine abuse and lung cancer (see below). On the other hand, the SNP rs16969968 may confer a protective effect against cocaine dependence (Grucza et al., 2008; Forget et al., in press), possibly due to the more general role that the α5 subunit plays in α3β4* and α4β2* receptors, determining whether the function of these receptors

Abbreviations: ACh, acetylcholine; α-CtxMII, α-conotoxin MII; CAP, compound action potential; CNS, central nervous system; DhβE, dihydro-β-erythroidine; DMPP, dimethylphenylpiperazinium; EPSC, excitatory postsynaptic current; EPSP, excitatory postsynaptic potential; HEK, human embryonic kidney; IPN, interpeduncular nucleus; iPSC, induced pluripotent stem cell; KO, knockout; MHb, medial habenula; nAChR, nicotinic acetylcholine receptor; PFC, prefrontal cortex; PNS; peripheral nervous system; SCG, superior cervical ganglion; SNP, single-nucleotide polymorphism; TTX, tetrodotoxin; VIP, vasoactive intestinal polypeptide; VTA, ventral tegmental area; WT, wild-type.

[1]The asterisk denotes that the two subunits listed (e.g., α4 and β2) comprise the backbone, with an additional subunit completing the pentamer. The additional subunit can be an "accessory" subunit such as α5 or a "complementary" subunit such as α4 or β2, giving rise to $(\alpha4\beta2)_2\alpha4$ or $(\alpha4\beta2)_2\beta2$ pentamers, respectively.

is increased or reduced by the presence of an α5 subunit. We will therefore address the role that the α5 subunit plays in α4β2* and α3β4* receptors with respect to their expression, targeting, activation, and desensitization, as well as how the α5 subunit modulates receptor's ability to raise intracellular Ca^{2+}.

Considerable insight into the function of the α5 subunit has come from studying recombinant receptors expressed in a wide range of cell types and systems, including *Xenopus* oocytes, HEK293 cells, and rat pituitary GH4C1 cells. In addition, studies using transgenic knockout (KO) mice—and more recently, rats—lacking the α5 subunit have provided new insights into the role of α5 subunits in endogenous receptors. These studies may explain—at least to some extent—the considerable receptor diversity highlighted in **Tables 1**, **2**. However, because the proper assembly and processing of nAChRs in the endoplasmic reticulum is supported by a variety of chaperone proteins, which may not be present in heterologous expression systems, nAChRs should ideally be analyzed in their endogenous physiological context. To date, the properties of native receptors were investigated primarily in mice, whereas the majority of studies involving human nAChRs used heterologous expression systems. As noted above, heterologous expression systems such as the highly popular HEK293 cell line may lack the necessary chaperone proteins such as NACHO required for the assembly and trafficking of nAChRs (Matta et al., 2017). Moreover, heterologous expression systems generally also lack proteins specific to neurons such as the Lynx1 protein (Miwa et al., 1999), which affect the membrane targeting and function of both α3β4* and α4β2* receptors (see below, Nichols et al., 2014; George et al., 2017). Finally, differences in receptor function were found when expressing fully pentameric nAChR concatemer constructs compared to expressing the α3, β4, and α5 subunits in *Xenopus* oocytes (George et al., 2012). Still, some properties of α3β4* receptors differ between human and rodent receptors, as shown by expressing these subunits in *Xenopus* oocytes (Stokes and Papke, 2012). Recently, Maskos reviewed the differences in the properties of receptors containing the N398 α5 subunit variant compared to the more common D398 variant in both α4β2* and α3β4* receptors (Maskos, 2020); we will therefore touch on this subject only briefly. In our review, we focus on the functional effect of the α5 subunit at the cellular level, referring to studies assessing nAChR pathways in nicotine addiction (Leslie et al., 2013; Picciotto and Kenny, 2013; Antolin-Fontes et al., 2015; Pistillo et al., 2015; Molas et al., 2017; Arvin et al., 2019) and variants at the *CHRNA5*/*CHRNA3*/*CHRNB4* gene locus on chromosome 15q25 (Bierut et al., 2008; Stevens et al., 2008; Thorgeirsson et al., 2008; Improgo et al., 2010; Tuesta et al., 2011; Berrettini and Doyle, 2012; Slimak et al., 2014; Lassi et al., 2016; Forget et al., 2018; Besson et al., 2019; Maskos, 2020).

The vast majority of heteropentameric neuronal nAChRs consist of two α subunit and two β subunits that comprise the backbone, with an additional subunit completing the pentamer (reviewed in Zoli et al., 2018). This additional subunit can be an "accessory" subunit such as α5 or β3, or it can be a "complementary" subunit such as α4 or β2 (primarily in CNS-type receptors), or α3 or β4 (primarily in PNS-type receptors). The two receptor backbones into which the α5 subunit can co-assemble, namely α4β2* (see **Table 1**) and α3β4* (see **Table 2**), differ fundamentally with respect to both their activation and desensitization properties and are discussed separately. These differences in receptor properties have consequences with respect to tobacco use, as nicotine concentrations typically reached while smoking tobacco primarily activate—and equally important, inactivate—α4β2* receptors (Benowitz and Jacob, 1990; Wooltorton et al., 2003; Brody et al., 2006). It is therefore interesting to examine how the α5 subunit affects the properties of these two receptor subtypes, and how the D398 and N398 α5 subunit variants differ in this respect. A graphical summary of the effects of α5 is provided in **Figure 1**.

WHAT WE ALREADY KNOW FROM HETEROLOGOUSLY EXPRESSED AND ENDOGENOUS RECEPTORS

The α5 Subunit Co-assembles With α4 and β2 in the Central Nervous System

The presence of the α5 subunit may affect the functional properties of nAChRs in several ways, including: (i) altering the potency and efficacy of ligands; (ii) affecting the receptor's Ca^{2+} permeability (or altering other mechanisms that increase intracellular Ca^{2+}); (iii) altering the receptor's desensitization properties; (iv) regulating receptor expression, posttranslational processing, and/or trafficking to the cell membrane; and (v) modulating Ca^{2+}-independent downstream signaling. Moreover, the anatomical distribution of α5 affects the functional role of nAChRs in the CNS.

Distribution of α5-Containing Receptors in the Central Nervous System

Our knowledge regarding the distribution of α5-containing receptors is based on *in situ* hybridization (Wada et al., 1990; Azam et al., 2002; Winzer-Serhan and Leslie, 2005), antibody-based techniques such as immunoprecipitation (Mao et al., 2006; Grady et al., 2009; David et al., 2010) and solid-phase radioimmunoassay (Conroy and Berg, 1995; Wang et al., 1998), expressing reporter genes under the control of the *CHRNA5* promoter (Hsu et al., 2013; Morton et al., 2018), and electrophysiology and optical recordings in specific regions of the nervous system (e.g., Morel et al., 2014). Unfortunately, reliable anti-α5 antibodies for use in immunocytochemistry are not currently available.

A recent RNAseq study revealed that 9 out of 16 nAChR subunits genes (among them most notably *CHRNA4* and *CHRNB2*, but also at moderate levels *CHRNA5*) are already expressed early in human brain development between 7.5 and 12 post-conceptional weeks (Alzu'bi et al., 2020). In adult rodent brain, immunoprecipitation experiments using α5-specific antibodies have shown the presence of α5-containing receptors—but not an association between α5 subunits and α4 and/or β2 subunits—in certain regions in the rodent brain, including the MHb, IPN, hippocampus, striatum, thalamus, prefrontal cortex (PFC), substantia nigra, ventral tegmental area (VTA), brainstem, and spinal cord (Brown et al., 2007; Counotte

TABLE 1 | Effects of α5 in α4β2* receptors.

Receptor without α5 or with $\alpha5^{N398}$	Receptor with $\alpha5^{D398}$	Expression system or preparation	Expression level	Potency	Efficacy[1]	Desensitization acute	Desensitization chronic	Assay	References
Chick α4β2*[2]	$(\alpha4\beta2)_2\alpha5$	*Xenopus*		ACh current ↓[3]	ACh current ↑			Voltage clamp	Ramirez-Latorre et al., 1996
Chick α4β2*	$(\alpha4\beta2)_2\alpha5$	*Xenopus*		ACh current ↓	ACh current ↔			Voltage clamp	Fucile et al., 1997
Human $(\alpha4\beta2)_2\beta2$	$(\alpha4\beta2)_2\alpha5$	*Xenopus*		ACh current ↔	ACh Ca^{2+} permeability ↑			Voltage clamp	Tapia et al., 2007
Human $(\alpha4\beta2)_2\alpha4$	$(\alpha4\beta2)_2\alpha5$	*Xenopus*		ACh current ↑	ACh Ca^{2+} permeability ↑			Voltage clamp	Tapia et al., 2007
Human $(\alpha4\beta2)_2\alpha5^{N398}$	$(\alpha4\beta2)_2\alpha5^{D398}$	*Xenopus*		ACh current ↔	ACh Ca^{2+} permeability ↑	↓		Voltage clamp	Kuryatov et al., 2011
Human $(\alpha4\beta2)_2\beta2$	$(\alpha4\beta2)_2\alpha5$	*Xenopus*		ACh current ↔ Saz-A current ↓	ACh current ↓			Voltage clamp	Prevost et al., 2020
Human $(\alpha4\beta2)_2\alpha4$	$(\alpha4\beta2)_2\alpha5$	*Xenopus*		ACh current ↑	ACh current ↓ Saz-A current↑			Voltage clamp	Prevost et al., 2020
Human $(\alpha4\beta2)_2\alpha5^{N398}$	$(\alpha4\beta2)_2\alpha5^{D398}$	*Xenopus*		ACh current ↔	ACh current ↔	↔		Voltage clamp	Prevost et al., 2020
Mouse $(\alpha4\beta2)_2\beta2$ $(\alpha4\beta2)_2\alpha4$	$(\alpha4\beta2)_2\alpha5$	*Xenopus*		ACh current ↑	ACh current ↓			Voltage clamp	Nichols et al., 2016
Mouse $(\alpha4\beta2)_2\beta2$	$(\alpha4\beta2)_2\alpha5$	HEK293		ACh ↓				Membrane potential assay kit	Nichols et al., 2016
Human $(\alpha4\beta2)_2\beta2$	$(\alpha4\beta2)_2\alpha5$	*Xenopus*		ACh current ↔	ACh current ↓			Voltage clamp	Jin et al., 2014
Human $(\alpha4\beta2)_2\alpha4$	$(\alpha4\beta2)_2\alpha5$	*Xenopus*		ACh current ↑	ACh current ↓			Voltage clamp	Jin et al., 2014
Human $(\alpha4\beta2)_2\beta2^4$ $(\alpha4\beta2)_2\alpha4$	$(\alpha4\beta2)_2\alpha5$	tsA201	↑ Overall ↓ Cell surface	ACh ↓ Nic ↓		↑	↔[5]	Membrane potential and Ca^{2+} assay kits $[^3H]$-epibatidine (mAb295, mAb210)	Kuryatov et al., 2008
Mouse[6] $(\alpha4\beta2)_2\alpha5^{N397}$	$(\alpha4\beta2)_2\alpha5^{D397}$	HEK293T	↔ Overall	Epi Ca^{2+} ↔	Epi Ca^{2+} ↑			Aequorin $[^{125}I]$-epibatidine	Bierut et al., 2008
α5 KO Mouse	WT Mouse[7]	Thalamus, striatum synaptosomes	↔ Overall	ACh ↔	ACh ↑[8]			$^{86}Rb^+$ efflux $[^{125}I]$-epibatidine	Brown et al., 2007
α5 KO Mouse	WT Mouse	Thalamus, hindbrain synaptosomes	↔ Overall		ACh ↑[9]			$^{86}Rb^+$ efflux $[^{125}I]$-epibatidine	Jackson et al., 2010
α5 KO Mouse	WT Mouse	Striatum synaptosomes		ACh ↔	ACh ↑[10]			$[^3H]$-DA release	Salminen et al., 2004
α5 KO Mouse	WT Mouse	Dorsal striatum slice			Electrical stimulation ↑[11]			DA release, fast-scan cyclic voltammetry	Exley et al., 2012

(Continued)

TABLE 1 | Continued

Receptor without α5 or with $\alpha5^{N398}$	Receptor with $\alpha5^{D398}$	Expression system or preparation	Expression level	Potency	Efficacy	Desensitization acute	Desensitization chronic	Assay	References
α5 KO Mouse	WT Mouse	Prefrontal cortex synaptosomes		ACh ↔	ACh ↑[12]			[^{3}H]-GABA release	McClure-Begley et al., 2009
α5 KO Mouse	WT Mouse	Habenula, IPN intact tissue	↔ Overall	Nic ↑				[^{3}H]-NE release [^{3}H]-epibatidine	Beiranvand et al., 2014
α5 KO Mouse	WT Mouse	Prefrontal cortex synaptosomes					↓[13]	[^{3}H]-GABA release	Grady et al., 2012
α5 KO Mouse	WT Mouse	Striatum synaptosomes					↓[14]	[^{3}H]-DA release	Wageman et al., 2014
[15]$(\alpha4\beta2)_2\alpha5^{N397}$ $(\alpha3\beta4)_2\alpha5^{N397}$	WT Mouse	Habenula synaptosomes	↑[16] Overall	ACh ↔	ACh ↔			$^{86}Rb^+$ efflux [^{125}I]-epibatidine	O'Neill et al., 2018
$(\alpha4\beta2)_2\alpha5^{N397}$	WT Mouse	Striatum synaptosomes	↔ Overall		ACh ↑[17]			[^{3}H]-DA release [^{125}I]-epibatidine	O'Neill et al., 2018
α5 KO Mouse	WT Mouse	Habenula, IPN synaptosomes			ACh ↑[18]			$^{86}Rb^+$ efflux	Fowler et al., 2011
α5 KO Mouse	WT Mouse	PFC layer VI pyramidal cells, slice		ACh ↑ current	ACh current ↑		↓	Patch clamp	Bailey et al., 2009
α5 KO Mouse	WT Mouse	VTA slice	↑ Overall		ACh current ↑		↓	Patch clamp α4YFP	Chatterjee et al., 2013
α5 KO Mouse	WT Mouse	VTA slice Anesthetized mouse		Firing rate ↑ Nic intravenously	DMPP current ↑			Patch clamp Extracellular recordings	Morel et al., 2014
[19]$(\alpha4\beta2)_2\alpha5^{N397}$	WT Mouse	VTA slice Anesthetized mouse		Firing rate ↑ Nic intravenously	DMPP current ↔			Patch clamp Extracellular recordings	Morel et al., 2014
α5 KO Rat	WT Rat	VTA slice Anesthetized rat	↔ Overall	Firing rate ↑ Nic intravenously	DMPP current ↑			Patch clamp Extracellular recordings	Forget et al., 2018
[20]$(\alpha4\beta2)_2\alpha5^{N397}$	WT Rat	VTA slice Anesthetized rat	↔ Overall	Firing rate ↔ Nic intravenously	DMPP current ↔			Patch clamp Extracellular recordings	Forget et al., 2018
α5 KO Rat	WT Rat	IPN slice			Nic current ↑			Patch clamp	Forget et al., 2018
$(\alpha4\beta2)_2\alpha5^{N397}$	WT Rat	IPN slice			Nic current ↑			Patch clamp	Forget et al., 2018
Human $(\alpha4\beta2)_2\alpha4$	$(\alpha4\beta2)_2\alpha5^{D398}$	GH4C1			Nic current ↓ ↓[21] Ca^{2+}	↔		Patch clamp Fura-2 Ca^{2+} assay	Sciaccaluga et al., 2015
Human $(\alpha4\beta2)_2\alpha5^{N398}$	$(\alpha4\beta2)_2\alpha5^{D398}$	GH4C1			Nic current ↔ ↔ Ca^{2+}	↓	↑[22]	Patch clamp Fura-2 Ca^{2+} assay	Sciaccaluga et al., 2015
α5 KO Mouse[23]	WT Mouse	Ventral midbrain cell culture			Nic ↑↑[24] Ca^{2+}			Fura-2 Ca^{2+} assay	Sciaccaluga et al., 2015
[25]$(\alpha4\beta2)_2\alpha5^{N397}$	WT Mouse	Ventral midbrain cell culture			Nic ↑[26] Ca^{2+}			Fura-2 Ca^{2+} assay	Sciaccaluga et al., 2015
α5 KO Mouse	WT Mouse	Ventral midbrain slice			Nic current ↑[27]			Patch clamp	Sciaccaluga et al., 2015
$(\alpha4\beta2)_2\alpha5^{N397}$	WT Mouse	Ventral midbrain slice			Nic current ↑[28]			Patch clamp	Sciaccaluga et al., 2015

(Continued)

TABLE 1 | Continued

Receptor without α5 or with $\alpha5^{N398}$	Receptor with $\alpha5^{D398}$	Expression system or preparation	Expression level	Potency	Efficacy	Desensitization acute	Desensitization chronic	Assay	References
$(\alpha4\beta2)_2\alpha5^{N398}$	$(\alpha4\beta2)_2\alpha5^{D398}$	Dopaminergic iPSC Glutamatergic iPSC		Nic ↓ EPSC frequency			↓[29]	Patch clamp	Oni et al., 2016
α5 KO Mouse	WT Mouse	PFC layer II/III VIP neurons		Firing rate ↑ of VIP interneurons				*In vivo* two-photon calcium imaging	Koukouli et al., 2017
	WT Mouse [30]$(\alpha4\beta2)_2\alpha5^{N397}$	PFC layer II/III VIP neurons		Firing rate ↑ of VIP interneurons				*In vivo* two-photon calcium imaging	Koukouli et al., 2017
α5 KO Mouse	WT Mouse	Rostral IPN slice		Nic current ↑ Nic firing rate ↑	ACh, Nic current ↑			Patch clamp Extracellular recordings	Morton et al., 2018

[1]*Deduced from maximal effect at saturating agonist concentration. Unless specifically excluded, an increased efficacy may also result from a higher number of plasma membrane receptors.*
[2]*The asterisk means that the two subunits build a backbone, and that an additional subunit will contribute to the fifth position.*
[3]*Downward arrow means reduced effect of receptors shown in column 2 (receptor with α5 D398) compared to column 1 (receptor without α5 or with α5 N398).*
[4]*The parent cell line contains a mixture of high-affinity $(\alpha4\beta2)_2\beta2$ and low-affinity $(\alpha4\beta2)_2\alpha4$ receptors.*
[5]*Similar nicotine IC_{50} values.*
[6]*In the mouse and rat homologs, amino acid 397 corresponds to amino acid 398 in the human α5 protein.*
[7]*WT mice have $(\alpha4\beta2)_2\alpha5$ together with $(\alpha4\beta2)_2\beta2$ and $(\alpha4\beta2)_2\alpha4$ receptors.*
[8]*The α5 KO reduces the DHβE-sensitive component of $^{86}Rb^+$ efflux.*
[9]*$^{86}Rb^+$ efflux by 30 μM ACh (high-sensitivity component) is enhanced in WT mice.*
[10]*The α-CtxMII–resistant (non-α6) component of dopamine release is reduced in α5 KO mice.*
[11]*α4(non-α6) receptors.*
[12]*The high-sensitivity component of [^{3}H]-GABA release is reduced in α5 KO mice, predominantly in the cortex.*
[13]*Higher nicotine IC_{50} values for WT mice.*
[14]*$(\alpha4\beta2)_2\beta2$ (non-α6) are more potently inactivated by nicotine, and recover more slowly from inactivation than $(\alpha4\beta2)_2\alpha5$.*
[15]*Mice engineered to express the α5 N397 variant.*
[16]*Offsprings were tested: Data show increased cytisine-resistant [^{125}I]-epibatidine binding for offsprings from dams with nicotine in drinking water.*
[17]*Offsprings were tested. Efficacy for the α-CtxMII resistant component was low for $(\alpha4\beta2)_2\alpha5^{N397}$ mice, regardless whether dams had 0.2% saccharin, or nicotine in drinking water; efficacy for α-CtxMII sensitive component was highest in D397 offsprings of dams with 0.2% saccharin in drinking water.*
[18]*Injections of Lenti-CHRNA5 into the MHb of knockout mice attenuated the deficits in ^{86}Rb efflux in the IPN, but not in the MHb.*
[19]*Mice expressing the α5 N397 in the VTA.*
[20]*Rats engineered to express the α5 N397 variant.*
[21]*Number of cells responding to nicotine; intracellular Ca^{2+} signal likely due to voltage-gated rather than nAChR-mediated Ca^{2+} influx.*
[22]*Repetitive application of 100 μM nicotine at one minute intervals with 0.5 mM BAPTA intracellularly.*
[23]*Possibly expressing both $(\alpha4\beta2)_2\alpha4$ and $(\alpha4\beta2)_2\beta2$ receptors.*
[24]*None of the α5 KO mouse cells responded to nicotine.*
[25]*Mice engineered to possess the α5 N397 variant.*
[26]*More WT cells respond to nicotine and also with a higher increase of Ca^{2+}.*
[27]*No cells with a ≈40 pA (high amplitude) current response in the α5 KO mouse.*
[28]*The number of cells with a ≈40 pA current response is significantly reduced in the α5 N397 variant.*
[29]*Cells with α5 D398 variant, but not cells with the N398 variant, respond to higher nicotine concentrations by an increase of EPSC frequency.*
[30]*Mice engineered to possess the α5 N397 variant.*
ACh, acetylcholine; DA, dopamine, dopaminergic; Cyt, cytisine; DMPP, dimethylphenylpiperazinium; Epi, epibatidine; EPSC, excitatory postsynaptic current; HEK, human embryonic kidney cells; IPN, interpeduncular nucleus; iPSC, induced pluripotent stem cell; KO, knockout; MHb, medial habenula; NE, norepinephrine; Nic, nicotine; PFC, prefrontal cortex; Saz-A, sazetidine-A; SCG, superior cervical ganglion; Var, varenicline; VIP, vasoactive intestinal polypeptide; VTA ventral tegmental area; WT, wild type.

TABLE 2 | Effects of α5 in α3β4* receptors.

Receptor without α5 or with α5 N398	Receptor with α5 D398	Expression system or preparation	Expression level	Potency	Efficacy[1]	Desensitization acute	Desensitization chronic	Assay	Reference
Human $\alpha3\beta4^{*2}$	$(\alpha3\beta4)_2\alpha5$	*Xenopus*	Cell surface ↔	ACh, Nic ↔	ACh, Nic current ↔	↑[3]		[^{125}I]-mAb210 Voltage clamp	Wang et al., 1996
Chick α3β4*	$(\alpha3\beta4)_2\alpha5$	*Xenopus*		ACh ↔	ACh current ↔			Voltage clamp	Fucile et al., 1997
Chick α3β4*	$(\alpha3\beta4)_2\alpha5$	BOSC-23		ACh ↓[4]	ACh current ↓	↔		Patch clamp	Fucile et al., 1997
Human α3β4*	$(\alpha3\beta4)_2\alpha5$	*Xenopus*		ACh, DMPP, Cyt ↔	DMPP current ↓ Ca^{2+} permeability ↑	↑		Voltage clamp	Gerzanich et al., 1998
Human $(\alpha3\beta4)_2\alpha5^{N398}$	$(\alpha3\beta4)_2\alpha5^{D398}$	*Xenopus*		ACh ↔	Ach Ca^{2+} permeability ↔	↔		Voltage clamp	Kuryatov et al., 2011
Human α3β4*	$(\alpha3\beta4)_2\alpha5$	*Xenopus*		ACh ↔	ACh current ↔	↑		Voltage clamp	Groot-Kormelink et al., 2001
Mouse α3β4*	$(\alpha3\beta4)_2\alpha5$	*Xenopus*		ACh ↔[5]				Voltage clamp	Papke et al., 2010
Human $(\alpha3\beta4)_2\beta4$	$(\alpha3\beta4)_2\alpha5$	*Xenopus*		ACh, Nic, Cyt, Var ↔[6]				Voltage clamp	Stokes and Papke, 2012
Human $(\alpha3\beta4)_2\alpha5^{N398}$	$(\alpha3\beta4)_2\alpha5^{D398}$	*Xenopus*		ACh, Nic, Cyt, Var ↔				Voltage clamp	Stokes and Papke, 2012
Human $(\alpha3\beta4)_2\beta4$	$(\alpha3\beta4)_2\alpha5$	*Xenopus*		ACh, Nic, Cyt ↔	ACh, Nic, Cyt current ↑			Voltage clamp	George et al., 2012
Human $(\alpha3\beta4)_2\alpha3$	$(\alpha3\beta4)_2\alpha5$	*Xenopus*		ACh, Nic, Cyt ↔	ACh, Nic, Cyt current ↑			Voltage clamp	George et al., 2012
Human $(\alpha3\beta4)_2\alpha5^{N398}$	$(\alpha3\beta4)_2\alpha5^{D398}$	*Xenopus*		ACh, Nic, Cyt ↔	ACh, Nic, Cyt current ↔ ↑[7]			Voltage clamp	George et al., 2012
Mouse $(\alpha3\beta4)_2\beta4$	$(\alpha3\beta4)_2\alpha5$	*Xenopus*			ACh current ↓[8]			Voltage clamp	Frahm et al., 2011
Mouse $(\alpha3\beta4)_2\alpha5^{N397}$	$(\alpha3\beta4)_2\alpha5^{D397}$	*Xenopus*			ACh current ↑[9]			Voltage clamp	Frahm et al., 2011
Human α3β4*	$(\alpha3\beta4)_2\alpha5$[10]	tsA201	Overall ↔	ACh, Nic ↔		↔		[^{3}H]-epibatidine Patch clamp	Wang et al., 1998
Human α3β4*	$(\alpha3\beta4)_2\alpha5$[11]	tsA201		ACh, Nic, Cyt, DMPP ↔		ACh ↔		Patch clamp	Nelson et al., 2001
Human α3β4*	[12]$(\alpha3\beta4)_2\alpha5^{D398}$	HEK293		ACh, Nic, Cyt, DMPP ↔		↔ ↓[13]	↔[14]	Patch clamp	Li et al., 2011
Human $(\alpha3\beta4)_2\alpha5^{N398}$	$(\alpha3\beta4)_2\alpha5^{D398}$	HEK293		ACh, Nic, Cyt, DMPP ↔		↔	↔[15]	Patch clamp	Li et al., 2011
Human α3β4*	$(\alpha3\beta4)_2\alpha5$	HEK293	Overall ↔ Cell surface ↔	Nic, ACh, Var ↔	Nic, Var Ca^{2+} ↓	↔[16]	↔	mAb35 [^{125}I]-epibatidine Aequorin Ca^{2+} assay	Tammimaki et al., 2012
Human $(\alpha3\beta4)_2\alpha5^{N398}$	$(\alpha3\beta4)_2\alpha5^{D398}$	HEK293	Overall ↔ Cell surface ↔	Nic ↑[17] ACh, Var ↔	Nic, ACh, Var Ca^{2+} ↔	↔[18]	↔	mAb35 [^{125}I]-epibatidine Patch clamp Aequorin Ca^{2+} assay	Tammimaki et al., 2012

(Continued)

TABLE 2 | Continued

Receptor without α5 or with α5 N398	Receptor with α5 D398	Expression system or preparation	Expression level	Potency	Efficacy	Desensitization acute	Desensitization chronic	Assay	Reference
Human α3β4*	$(\alpha3\beta4)_2\alpha5$	HEK293	Cell surface ↓		Nic Ca^{2+} ↓		↓	Tagged subunits Aequorin Ca^{2+} assay	Ray et al., 2017
Human $(\alpha3\beta4)_2\alpha5^{N398}$	$(\alpha3\beta4)_2\alpha5^{D398}$	HEK293			Nic Ca^{2+} ↑			Tagged subunits Aequorin Ca^{2+} assay	Ray et al., 2017
Human $(\alpha3\beta4)_2\alpha5^{N398}$	$(\alpha3\beta4)_2\alpha5^{D398}$	DA iPSC		ACh, Nic ↑	ACh, Nic current ↓	↔		Patch clamp	Deflorio et al., 2016
Human α3β4*	$(\alpha3\beta4)_2\alpha5$	Rat kidney cells	Cell surface ↓					Confocal microscopy	Crespi et al., 2018b
α5 KO Mouse	WT mouse	Habenula intact tissue	Overall ↔					[^{3}H]-epibatidine	Scholze et al., 2012
Chick[19]α3β4*	Chick $(\alpha3\beta4)_2\alpha5$	Sympathetic neurons			ACh, Cyt ↓			Patch clamp	Yu and Role, 1998
α5β2 KO Mouse[20]	β2 KO Mouse[21]	SCG cell culture	Overall ↔	Cyt, DMPP current ↔	ACh, Cyt, DMPP current ↔	↔		[^{3}H]-epibatidine Patch clamp	David et al., 2010
α5 KO Mouse	WT mouse	SCG cell culture		ACh, Nic, Cyt, DMPP, Epi ↔	ACh, Nic, Cyt, DMPP, Epi ↓			[^{3}H]-NE release Fura-2 Ca^{2+} assay	Fischer et al., 2005b
α5 KO Mouse	WT mouse	SCG intact ganglion		↔[22]	↔		↓	Transganglionic transmission	Simeone et al., 2019

[1]*Deduced from maximal effect at saturating agonist concentration. Unless specifically excluded, the increased efficacy may also result from a higher number of plasma membrane receptors.*
[2]*The asterisk means that the two subunits build a backbone, and that an additional subunit will contribute to the fifth position.*
[3]*Upward arrow means enhanced effect of receptors shown in column 2 (receptor with α5 D398) compared to column 1 (receptor without α5 or with α5 N398).*
[4]*Co-expression of α5 leads to a biphasic concentration-response curve due to the appearance of a second low-affinity component.*
[5]*By comparison of EC_{50} values of peak currents; the α3β4* concentration-response curve for net charge is biphasic.*
[6]*Comparison of EC_{50} values of peak currents.*
[7]*Significantly different for ACh; enhanced but not significantly different for nicotine and cytisine in WT.*
[8]*With ratios of 10:10:1 for α5:β4:α3 injected cRNA, α5 will reduce currents compared to oocytes injected with β4:α3 at a ratio of 10:1.*
[9]*With ratios of 10:10:1 for α5:β4:α3 injected cRNA, currents by α5 D397 are larger than currents by α5 N397.*
[10]*Only 14% of α3β4* receptors contain the α5 subunit.*
[11]*Only 14% of α3β4* receptors contain the α5 subunit.*
[12]*A FLAG epitope was inserted near the amino terminus of the α5 subunit. Cells were selected by binding to beads coated with antibody to the FLAG epitope.*
[13]*Decay time not significantly different for 1 mM ACh; significantly prolonged for 100 μM nicotine.*
[14]*Recovery from desensitization.*
[15]*Recovery from desensitization.*
[16]*Residual current after a 40 s pulse of 100 μM ACh, recorded by patch clamp electrophysiology (bath solution with 2 mM Ca^{2+}).*
[17]*$(\alpha3\beta4)_2\alpha5^{D398}$ is significantly more sensitive than $(\alpha3\beta4)_2\alpha5^{N398}$.*
[18]*Residual current after a 40 s pulse of 100 μM ACh, recorded by patch clamp electrophysiology (bath solution with 2 mM Ca^{2+}).*
[19]*AS: antisense oligonucleotide treatment.*
[20]*Remaining receptors are 100% α3β4.*
[21]*Remaining receptors are 75% α3β4 and 25% $(\alpha3\beta4)_2\alpha5$.*
[22]*Unaltered amplitude of compound action potential and EPSC.*
ACh, acetylcholine; DA, dopamine, dopaminergic; Cyt, cytisine; DMPP, dimethylphenylpiperazinium; Epi, epibatidine; EPSC, excitatory postsynaptic current; HEK, human embryonic kidney cells; IPN, interpeduncular nucleus; iPSC, induced pluripotent stem cell; KO, knockout; MHb, medial habenula; NE, norepinephrine; Nic, nicotine; PFC, prefrontal cortex; Saz-A, sazetidine-A; SCG, superior cervical ganglion; Var, varenicline; VIP, vasoactive intestinal polypeptide; VTA ventral tegmental area; WT, wild type.

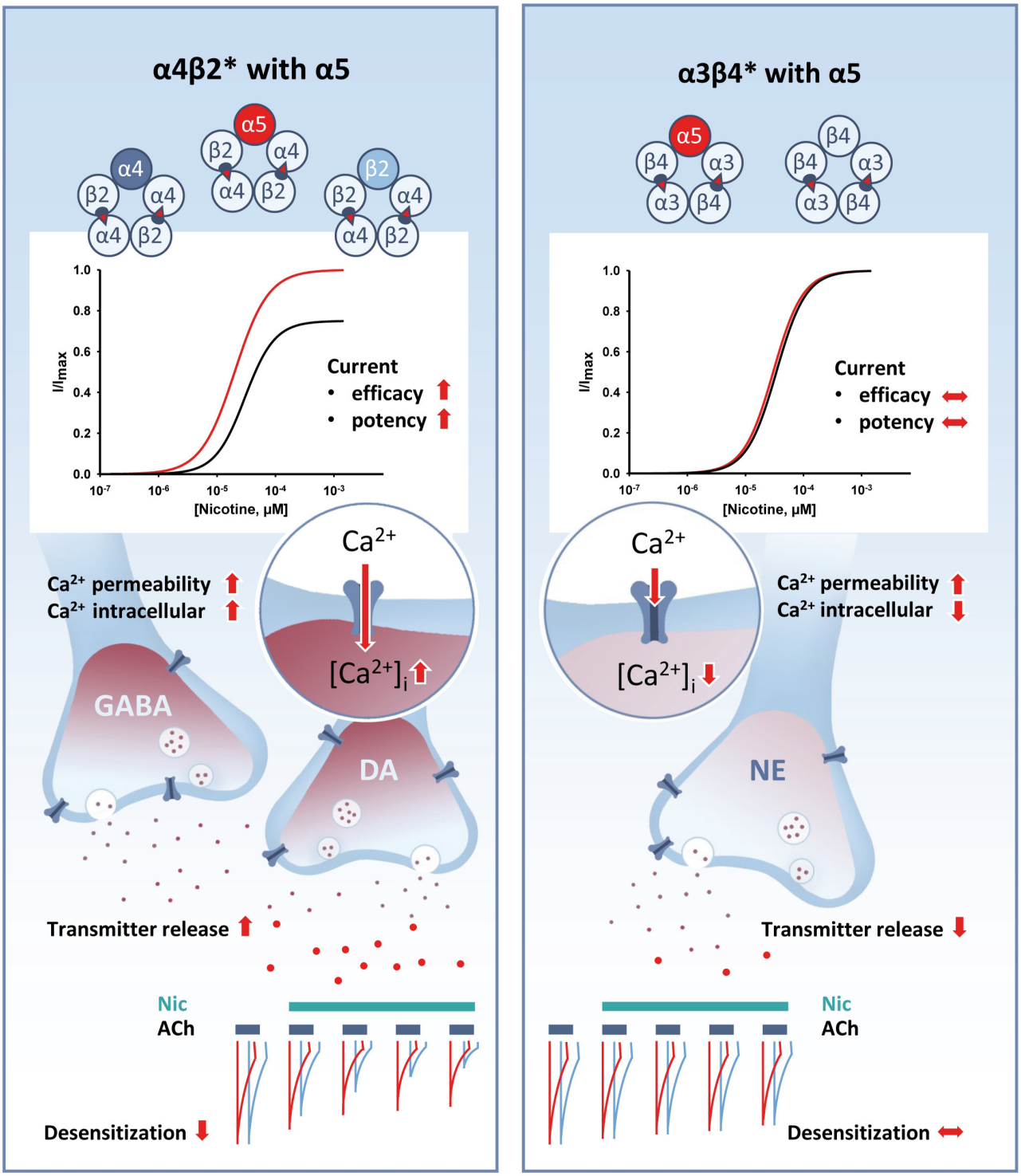

FIGURE 1 | Graphical summary of the key effects of the α5 subunit on various receptor properties when co-assembled with either α4β2* or α3β4* receptors. Red arrows indicate effects mediated by the presence of α5. Left: addition of the α5 subunit to α4β2* receptors increases ligand efficacy and potency (top), increases Ca^{2+} permeability and transmitter release (middle), and decreases receptor desensitization (bottom). Right: in contrast, addition of the α5 subunit to α3β4* receptors has no effect on efficacy or potency (top), increases Ca^{2+} permeability while decreasing intracellular Ca^{2+} and transmitter release (middle), and has no significant effect on receptor desensitization (bottom). Note: that in cases in which the reported effects of the α5 subunit differed between exogenously expressed receptors and endogenous receptors, we report the results observed for endogenous receptors.

et al., 2012; Xanthos et al., 2015; Forget et al., 2018). In addition, measuring α5 subunits in mice lacking specific nAChR subunits (e.g., α4 or β2) has provided evidence that α5 associates with the α4 and β2 subunits (Champtiaux et al., 2003; Grady et al., 2009; Scholze et al., 2012; Beiranvand et al., 2014; Xanthos et al., 2015). The direct association between α5 and the α4β2* backbone was demonstrated using a combination of immunopurification and immunoprecipitation of [^{3}H]-epibatidine–labeled receptors with subunit-specific antibodies. Studies in the rat CNS indicate that $(\alpha4\beta2)_2\alpha5$ receptors are expressed robustly in several regions, including the hippocampus, striatum, cerebral cortex, thalamus, and superior colliculus (Zoli et al., 2002; Mao et al., 2008; Grady et al., 2009). Similar experiments in mice revealed that these receptors are expressed in the striatum (Champtiaux et al., 2003), superior colliculus, and lateral geniculate nucleus (Gotti et al., 2005). Finally, sequential immunoprecipitation experiments revealed the expression of $(\alpha4\beta2)_2\alpha5$ receptors in the chick brain (Conroy and Berg, 1998) and human neocortex (Gerzanich et al., 1998).

Two brain regions in which α5-containing receptors are expressed have been shown to play a key role in the reinforcing effects of nicotine; these regions are the MHb-IPN system, which accounts primarily for withdrawal mechanisms, and the VTA, which principal role consists in mediating reward (Tuesta et al., 2011; Leslie et al., 2013; Picciotto and Kenny, 2013; Antolin-Fontes et al., 2015; Pistillo et al., 2015; Molas et al., 2017; Arvin et al., 2019). Additional evidence suggests that—irrespective of the α5 subunit—α4β2 and α6β2 receptors in the VTA are necessary and sufficient for systemic nicotine reinforcement (Pons et al., 2008). Finally, Champtiaux and colleagues reported that the α5 subunit preferentially associates with the α4 and β2 subunits in dopaminergic neurons (Champtiaux et al., 2003).

Interestingly, α5-containing receptors in the MHb-IPN system have been linked to tobacco abuse and thus warrant special attention. No other region in the CNS has such a high density of nAChRs, and no region expresses more α5-containing receptors than the IPN. For example, the IPN of adolescent or adult rat contains ∼350 fmol of overall receptor protein/mg total protein (Grady et al., 2009; Forget et al., 2018), and even though the reported amount of α5-containing receptors differs between studies, ranging from 23 fmol/mg protein (Forget et al., 2018) to 200 fmol/mg protein (Grady et al., 2009), direct comparisons between various brain regions support the notion that α5-containing receptors are highly enriched in both the rat (Forget et al., 2018) and mouse IPN (Beiranvand et al., 2014; Xanthos et al., 2015). Immunodepletion using an anti-β2 antibody significantly reduced the number of α5-containing receptors in the rat IPN, suggesting that the α5 subunit co-assembles into β2-containing receptors (Grady et al., 2009). In contrast, α5-containing receptors are not reduced in the IPN of β2 KO mice (Grady et al., 2009), although a different study found that α5-containing receptors were significantly reduced in β2 KO mice, but not in β4 KO mice (Beiranvand et al., 2014). Given that the levels of α4—but not α3—subunits are significantly reduced in both β2 KO mice (Grady et al., 2009; Beiranvand et al., 2014) and β2-immunodepleted rats (Grady et al., 2009), we conclude that α5 predominantly, if not exclusively, assembles into α4β2* receptors in the rodent IPN. As summarized below, a strikingly different picture emerges with respect to the MHb, in which the α5 subunit serves as the accessory subunit in α3β4* receptors (Scholze et al., 2012).

Using a transgenic $\alpha5^{GFP}$ mouse, Hsu and colleagues found that α5-containing receptors are robustly expressed in several IPN subnuclei, but not in the MHb; the α5-containing neurons in the IPN were identified as predominantly GABAergic neurons that project to distinct raphe nuclei (Hsu et al., 2013). In a follow-up study by the same group, these findings were confirmed and expanded using *Chrna5*^{Cre} mice with the *Ai6* reporter gene (Morton et al., 2018). Specifically, they performed electrophysiological recordings in acute brain slices and found that the α5 subunit co-assembles with α4 and β2 subunits in these neurons, and currents induced by applying 1 mM ACh were significantly reduced by 10 μM dihydro-β-erythroidine (DhβE), which preferentially inhibits α4β2* receptors at this concentration (Morton et al., 2018).

Functional evidence supporting the presence of α5-containing nAChRs in distinct cell types in the CNS comes from both *in vivo* and *in vitro* (e.g., brain slices, transmitter release, etc.) experiments. For example, experiments combining patch-clamp recordings with single-cell PCR found that the nicotine-induced activation of interneurons is mediated by nAChRs composed of α4, α5, and β2 subunits in layers II, III, and V in acute rat brain slices containing the motor neocortex (Porter et al., 1999). Moreover, nAChR agonists induced larger, DhβE-sensitive currents in layer VI pyramidal neurons in slices containing the medial PFC taken from mice expressing the α5 subunit compared to slices obtained from α5 KO mice (Bailey et al., 2009). More recently, Koukouli and colleagues performed two-photon Ca^{2+} imaging in awake α5 KO mice and found reduced activity of VIP (vasoactive intestinal polypeptide)–expressing GABAergic interneurons, affecting the firing rate in layer II/III pyramidal cells (Koukouli et al., 2017). Finally, the α5 subunit has been shown to play a critical role in midbrain VTA neurons, in which the presence of this subunit significantly increased both the overall number of α4-containing receptors and the magnitude of ACh-induced, DhβE-sensitive currents (Chatterjee et al., 2013).

In summary, the α5 subunit co-assembles with the α4 and β2 subunits in different regions throughout the CNS; the medial habenula also expresses relatively low levels of $(\alpha3\beta4)_2\alpha5$ nAChRs.

Receptor Affinity and Efficacy

The functional properties of α4β2* receptors, and how these properties are affected by the presence of the α5 accessory subunit, have been studied in detail using heterologous expression systems. For example, seminal work by Ramirez-Latorre and colleagues showed that chick α5 subunits require both the α4 and β2 subunits to form functional receptors when expressed in *Xenopus* oocytes, and the concentration-response curve of ACh-induced currents in α4β2 receptors was significantly right-shifted, with larger current amplitude, when the α5 subunit was expressed (Ramirez-Latorre et al., 1996). These early observations were confirmed partially by individual constructs or the pairwise expression of human α4β2

concatemers together with α4, β2, or α5 subunits in *Xenopus* oocytes; specifically $(\alpha4\beta2)_2\alpha5$ receptors were as sensitive to ACh as $(\alpha4\beta2)_2\beta2$ receptors, while the concentration-response curve was significantly right-shifted for $(\alpha4\beta2)_2\alpha4$ receptors compared to $(\alpha4\beta2)_2\beta2$ receptors (Tapia et al., 2007; Jin et al., 2014). More recently, Nichols and colleagues injected *Xenopus* oocytes with α5, α4, and β2 mRNA at a 10:1:1 ratio (i.e., a 10-fold excess of α5) and found that 100% of the receptors were high-affinity (i.e., α5 subunit-containing), with an ACh EC_{50} of 0.26 μM); in contrast, oocytes injected with only α4 and β2 (at a 1:1 ratio) had a biphasic concentration-response, with 65% high-affinity receptors (ACh EC_{50}: 0.67 μM) and 35% low-affinity receptors (ACh EC_{50}: 190 μM) (Nichols et al., 2016).

Lately, Prevost and colleagues used pentameric concatemer constructs for expression in *Xenopus* oocytes (Prevost et al., 2020). Similar to previous reports they observed no difference in ACh potency between human $(\alpha4\beta2)_2\beta2$ and $(\alpha4\beta2)_2\alpha5$ receptors, whereas $(\alpha4\beta2)_2\alpha4$ receptors showed a biphasic concentration response curve with an overall significantly reduced ACh potency. However, current amplitudes in response to saturating ACh concentrations were significantly reduced for α5 containing concatemers. Sazetidine-A, on the other hand, was a partial agonist for $(\alpha4\beta2)_2\alpha4$ but a full agonist for $(\alpha4\beta2)_2\beta2$ and $(\alpha4\beta2)_2\alpha5$ receptors, albeit with lower potency for $(\alpha4\beta2)_2\alpha5$ receptors. Of interest, α5-containing nAChRs were irreversibly blocked by methanethiosulfonate reagents through a covalent reaction with a cysteine present at the second transmembrane segment only in α5 at position 261. By using this approach, the authors showed that reconstitution of nAChRs from loose α5, α4 and β2 subunits was inefficient and highly variable (Prevost et al., 2020).

Importantly, the presence of the α5 subunit also significantly increases the receptor's Ca^{2+} permeability. With Ca^{2+} as the only cation available in the superfusion buffer, peak currents recorded in $(\alpha4\beta2)_2\alpha5$–expressing *Xenopus* oocytes were even larger than currents measured in oocytes expressing α7 receptors, the nAChR subtype with the highest Ca^{2+} permeability; $(\alpha4\beta2)_2\alpha4$ receptors also showed high Ca^{2+} permeability, whereas $(\alpha4\beta2)_2\beta2$ receptors were hardly Ca^{2+}-permeable (Tapia et al., 2007). Using stable nAChR-expressing tsA201 cell lines, Kuryatov and colleagues found that $(\alpha4\beta2)_2\beta2$ receptors were most sensitive to nicotine and ACh, followed by $(\alpha4\beta2)_2\alpha5$, and then $(\alpha4\beta2)_2\alpha4$, similar to the previously reported overall ranking measured in *Xenopus* oocytes (Kuryatov et al., 2008). Moreover, immunoisolation experiments revealed that 100% of receptors in the $(\alpha4\beta2)_2\alpha5$-expressing cell line indeed contained the α5 subunit (Kuryatov et al., 2008).

Any increase in Ca^{2+} permeability will affect downstream Ca^{2+}-dependent processes such as nAChR-induced transmitter release. Consistent with this notion, ACh-induced, DhβE-sensitive ^{86}Rb efflux was significantly smaller in thalamic synaptosomes prepared from α5 KO mice compared to wild-type (WT) mice[2]. The finding that [^{125}I]-epibatidine binding was not affected in the α5 KO mice—indicating that the overall number of receptors is unchanged—suggests impaired function in α4β2* receptors that lack the α5 accessory subunit (Brown et al., 2007; Jackson et al., 2010). Although ^{86}Rb efflux measures the overall function of synaptic release, independent of the underlying transmitter system, these results are supported by the finding that α-conotoxin MII (α-CtxMII)–resistant, DhβE-sensitive [^{3}H]-dopamine efflux from mouse striatal synaptosomes was also reduced in the α5 KO mouse (Salminen et al., 2004). These observations were subsequently confirmed by showing that dopamine release (measured using fast-scan cyclic voltammetry) requires the α5 subunit in the dorsal striatum, but not in the nucleus accumbens (Exley et al., 2012). Finally, the high-affinity component of ACh-induced GABA release from synaptic vesicles, which was abolished in several brain regions in α4 and β2 KO mice, was significantly reduced in the PFC—as well as in the hippocampus and striatum, albeit to a lesser extent—upon deletion of the α5 subunit (McClure-Begley et al., 2009).

In both the MHb and IPN, the nicotine concentration-response curves for the release of norepinephrine were right-shifted in α5 KO mice compared to control mice, suggesting that the α5 subunit increases the receptor's ligand sensitivity (Beiranvand et al., 2014). However, nAChR-stimulated norepinephrine release requires action potentials (Sacaan et al., 1995; Scholze et al., 2007) and is blocked by tetrodotoxin (TTX), similar to nicotine-induced norepinephrine release in the hippocampus (Sacaan et al., 1995; Scholze et al., 2007; Beiranvand et al., 2014). Moreover, the Ca^{2+} required for synaptic vesicle fusion (and hence, transmitter release) in presynaptic terminals may come either via nACh receptors (if they are positioned closely enough to the release site) or via voltage-gated Ca^{2+} channels (along with the action potentials generated by nAChRs); these two mechanisms have been termed "transmitter release by presynaptic nAChRs receptors" and "transmitter release by preterminal nAChRs receptors," respectively (Wonnacott, 1997). In addition, norepinephrine release was also abolished in β2 KO mice, suggesting that this release is mediated by α4β2* receptors (Scholze et al., 2007; Beiranvand et al., 2014). Importantly, both the MHb (Lecourtier and Kelly, 2007) and the IPN (Antolin-Fontes et al., 2015) receive noradrenergic input from the locus coeruleus, where most nicotinic subunits, including α5, are expressed (Lena et al., 1999).

Patch-clamp recordings revealed significantly smaller currents in response to 1 mM ACh in brain slices containing the VTA prepared from α5 KO mice compared to WT mice (Chatterjee et al., 2013). Likewise, stimulating nAChRs in VTA brain slices with a saturating concentration of dimethylphenylpiperazinium (DMPP) induced smaller currents in α5 KO mice compared to WT mice, and restoring the α5 subunit in α5 KO mice by lentiviral infection restored the DMPP-induced response in VTA neurons to WT levels (Morel et al., 2014). Consistent with these results, an 8-fold higher dose of intravenous nicotine was required to significantly increase the *in vivo* firing rate of dopaminergic VTA neurons in α5 KO mice compared to WT mice, and the sensitivity to intravenous nicotine was restored by expressing the α5 subunit in α5 KO VTA dopaminergic neurons (Morel et al., 2014). These observations in mice were later supported in a follow-up study using α5 KO rats, in which

[2]Thalamic neurons in WT mice express $(\alpha4\beta2)_2\alpha4$, $(\alpha4\beta2)_2\beta2$, and $(\alpha4\beta2)_2\alpha5$ receptors.

currents induced with 100 μM DMPP were significantly smaller in VTA brain slices prepared from KO rats compared to WT rats (Forget et al., 2018). Similarly, a 3-fold higher intravenous dose of nicotine was needed to increase the firing frequency of VTA neurons in KO rats compared to WT rats. Consistent with affecting function but not expression, the overall number of nAChRs in nine specific brain regions (measured using immunoprecipitation) was similar between WT and KO animals (Forget et al., 2018). Finally, currents elicited with 30 μM nicotine were significantly smaller in IPN slices prepared from α5 KO rats compared to WT rats (Forget et al., 2018). Taken together, these findings suggest that the α5 accessory subunit increases the receptor's sensitivity and efficacy.

Interestingly, cells recorded in VTA slices prepared from α5 KO mice lacked an additional "large" (40 pA) current component measured in response to 100 μM nicotine, a feature that was present in WT slices (Sciaccaluga et al., 2015). In addition, the authors also found that applying 100 μM nicotine increased intracellular Ca^{2+} in cultured VTA neurons prepared from WT mice, but not in neurons prepared from α5 KO mice (Sciaccaluga et al., 2015). Overall, these findings suggest that the α5 subunit increases the receptor's efficacy.

On the other hand, Sciaccaluga and colleagues found that expressing the α5 subunit in rat pituitary GH4C1 cells significantly reduced receptor efficacy compared to cells expressing $(\alpha4\beta2)_2\alpha4$ receptors. Hence, cells expressing $(\alpha4\beta2)_2\alpha5$ receptors had smaller currents and less increase in intracellular Ca^{2+} in response to 100 μM nicotine (Sciaccaluga et al., 2015). This finding is consistent with reduced receptor efficacy (measured using voltage-clamp recordings) in *Xenopus* oocytes expressing $(\alpha4\beta2)_2\alpha5$ receptors compared to $(\alpha4\beta2)_2\alpha4$ receptors (Jin et al., 2014). Nevertheless, given the increased Ca^{2+} permeability of $(\alpha4\beta2)_2\alpha5$ receptors (Tapia et al., 2007), one would have expected increased Ca^{2+} signals in GH4C1 cells expressing these receptors.

The α5 subunit is also expressed in VIP interneurons in layer II/III, which inhibit both somatostatin and parvalbumin interneurons in the PFC. Given that both somatostatin and parvalbumin GABAergic neurons reduce the firing rate of layer II/III pyramidal neurons, reduced activity of VIP interneurons would be expected to reduce the firing frequency of pyramidal neurons. Consistent with this hypothesis, Koukouli and colleagues performed *in vivo* two-photon Ca^{2+} imaging in awake mice and found that pyramidal cells in α5 KO mice fire at a reduced frequency, and targeted virus-mediated expression of the α5 subunit in VIP GABAergic neurons restored both the normal firing rate of VIP interneurons and the firing frequency of pyramidal cells (Koukouli et al., 2017). Together with the *in vitro* data above, these *in vivo* results suggest that $(\alpha4\beta2)_2\alpha5$ receptors have a robust response to endogenous ACh compared to receptors lacking the α5 subunit.

The presence of the α5 subunit in α4β2* receptors also appears to have a major effect on neuronal activity in the rostral IPN, as currents elicited in response to 1 μM nicotine or 1 mM ACh are smaller in slices prepared from α5 KO mice compared to WT mice; in contrast, no difference was observed in the ventral MHb (Morton et al., 2018). The reduced response in α5 KO IPN neurons could be due to a reduced number of receptors and/or reduced efficacy; based on previously published [^{3}H]-epibatidine radioligand binding experiments in WT and α5 KO mice, the authors concluded that reduced efficacy of receptors lacking the α5 subunit is the more likely explanation (Morton et al., 2018). Thus, the reduced DhβE-sensitive ACh-induced currents in layer VI pyramidal neurons in α5 KO mice are likely also due to reduced efficacy, rather than reduced receptor expression or membrane trafficking (Bailey et al., 2009). Finally, Bailey and colleagues found that ACh is not only less efficacious but also less potent in eliciting currents in layer VI pyramidal neurons in α5 KO mice compared to WT mice (Bailey et al., 2009).

In summary $(\alpha4\beta2)_2\alpha5$ and $(\alpha4\beta2)_2\beta2$ receptors have similar sensitivity, and both receptor subtypes are significantly more sensitive than $(\alpha4\beta2)_2\alpha4$ receptors, which are also found in the CNS. Moreover, agonists are more efficacious at activating $(\alpha4\beta2)_2\alpha5$ receptors compared to α4β2* receptors lacking the α5 subunit, while $(\alpha4\beta2)_2\alpha5$ receptors have higher Ca^{2+} permeability compared to both $(\alpha4\beta2)_2\beta2$ and $(\alpha4\beta2)_2\alpha4$ receptors. Taken together, these properties explain the fact that $(\alpha4\beta2)_2\alpha5$ receptors are highly efficacious at mediating transmitter release in the CNS.

Desensitization Properties

Unlike acute receptor desensitization, seen as the decay of current during ligand application, "prolonged" desensitization may actually be more physiologically relevant. Receptors enter and maintain a state of prolonged desensitization when exposed to ligands such as nicotine (at concentrations measured in smokers) for an extended period of time (Quick and Lester, 2002; Wooltorton et al., 2003).

The effect of the α5 subunit on prolonged desensitization in nAChRs has been studied in both heterologously expressed and endogenous receptors, with partially conflicting results. When expressed in tsA201 cells, for example, long-term (e.g., 6 h) desensitization was similar between cells expressing $(\alpha4\beta2)_2\alpha5$ and cells expressing a combination of $(\alpha4\beta2)_2\alpha4$ and $(\alpha4\beta2)_2\beta2$ receptors (Kuryatov et al., 2008). In contrast, several reports found that the α5 subunit reduces desensitization when assembled in α4β2* receptors. For example $(\alpha4\beta2)_2\beta2$ receptors mediating GABA release in cortical synaptosomes isolated from α5 KO mice had significantly more nicotine-induced desensitization compared to the $(\alpha4\beta2)_2\alpha5$ receptors present in WT synaptosomes (Grady et al., 2012). Similarly, the IC_{50} values of 11 agonists for desensitizing α-CtxMII-resistant (i.e., non-α6*) receptors that mediate [^{3}H]-dopamine release were significantly lower in α5 KO striatal synaptosomes compared to WT (Wageman et al., 2014).

By measuring currents induced by applying 1 mM ACh to layer VI pyramidal cells in the medial PFC, Bailey and colleagues found that neurons in α5 KO mice had ∼2-fold more desensitization following a 10-min pretreatment with 100 or 300 nM nicotine compared to WT neurons (Bailey et al., 2010). In extending this observation by optogenetic stimulation of cholinergic fibers, Venkatesan and Lambe recently reported that in α5 WT mice, the optogenetic cholinergic response of layer VI pyramidal cells is unchanged by application of 100 nM nicotine,

whereas the optogenetic response is rapidly attenuated in α5 KO mice (Venkatesan and Lambe, 2020). Interesting, 300 nM nicotine cause complete desensitization of receptors in layer II/III and layer VI interneurons measured using patch-clamp recordings in PFC slice preparations; in contrast, the cholinergic responses in layer V interneurons and layer VI pyramidal cells had less desensitization, possibly due to the expression of the α5 subunit in these neurons (Poorthuis et al., 2013). Finally, Chatterjee and colleagues found significantly more nicotine-induced desensitization in VTA neurons in slices prepared from α5 KO compared to WT mice (Chatterjee et al., 2013).

In summary, α5 KO neurons are more sensitive to chronic agonist-induced desensitization compared to WT neurons.

Receptor Expression and Membrane Trafficking

Using tsA201 cell lines expressing either α4β2* or $(\alpha4\beta2)_2\alpha5$ receptors, Kuryatov and colleagues found that cells expressing $(\alpha4\beta2)_2\alpha5$ receptors had 40% more epibatidine binding sites compared to cells expressing α4β2* receptors [i.e., $(\alpha4\beta2)_2\alpha4$ and $(\alpha4\beta2)_2\beta2$ receptors], suggesting that the presence of the α5 subunit increases overall receptor expression; in contrast, plasmic membrane targeting [which in cells expressing $(\alpha4\beta2)_2\alpha5$ receptors represents ∼20% of the total [^{3}H]-epibatidine–binding pool] was significantly reduced compared to cells expressing α4β2* receptors (Kuryatov et al., 2008). The α5 subunit has been shown to play a role in the expression of α4-containing receptors midbrain VTA neurons, increasing the overall expression and trafficking of α4β2* receptors (Chatterjee et al., 2013). In contrast, [^{125}I]-epibatidine binding measured at a high enough concentration to bind both high-affinity and low-affinity receptors was similar between WT and α5 KO mice in all brain regions investigated (Salas et al., 2003). A subsequent study by Baddick and Marks using semi-quantitative visual analysis in WT and additional mouse KO models confirmed these results (Baddick and Marks, 2011). As discussed above, Brown and colleagues found that deleting the α5 subunit in α5 KO mice significantly reduced DhβE-sensitive ^{86}Rb efflux in thalamic synaptosomes without affecting [^{125}I]-epibatidine binding, suggesting reduced receptor efficacy, rather than reduced expression of presynaptic receptors (Brown et al., 2007). Interestingly, Nichols and colleagues found that introducing the V287L mutation in the β2 subunit (a mutation linked to autosomal dominant nocturnal frontal lobe epilepsy) reduced the total surface expression of α4β2* receptors expressed in HEK293 cells but caused a 4-fold increase in $(\alpha4\beta2)_2\alpha5$ receptors at the plasma membrane (Nichols et al., 2016).

In summary, in both mice and rats, loss of α5 does not affect the overall expression of α4β2* receptors measured using either [^{125}I]-epibatidine or [^{3}H]-epibatidine binding.

Do the Functional Properties Differ Between $(\alpha4\beta2)_2\alpha5^{N398}$ and $(\alpha4\beta2)_2\alpha5^{D398}$ Receptors?

Kuryatov and colleagues compared the properties of $(\alpha4\beta2)\alpha5$ receptors containing either the α5 N398 or D398 variant expressed in *Xenopus* oocytes (Kuryatov et al., 2011). In the α5 subunit, amino acid 398 resides in the large cytoplasmic domain adjacent to the conserved amphipathic α-helix that immediately precedes the fourth transmembrane domain (**Figure 2**). The authors speculated that in this region, the negatively charged aspartic acid at position 398 in the D398 variant might increase Ca^{2+} permeability, whereas the amide group in the asparagine in the rare N398 variant might reduce Ca^{2+} permeability. Indeed, they found that the N398 α5 variant has significantly lower Ca^{2+} permeability—but similar sensitivity—compared to the D398 variant (Kuryatov et al., 2011). The authors observed no difference in ACh potency between receptors incorporating either the N398 or the D398 α5 variant. However, desensitization in the presence of 3 μM ACh was significantly larger for $(\alpha4\beta2)_2\alpha5^{N398}$ than for $(\alpha4\beta2)_2\alpha5^{D398}$ receptors, suggesting that the already narrow concentration range for activatable α4β2* receptors relevant at smoking may be further reduced by the N398 variant ("smoldering activation range," Kuryatov et al., 2011).

In contrast to the tetrameric β2-α4-β2-α4 concatemers with added either N398 or D398 α5, Prevost and colleagues used full pentameric concatemers for expression in *Xenopus* oocytes. Still, no difference was observed in ACh potency, efficacy or acute desensitization when comparing $(\alpha4\beta2)_2\alpha5^{D398}$ with $(\alpha4\beta2)_2\alpha5^{N398}$ receptors (Prevost et al., 2020). The reduced Ca^{2+} permeability mentioned above explain the smaller Ca^{2+} signal measured using the Ca^{2+}-sensing photoprotein aequorin in HEK293T cells transfected with mouse α4, β2, and $\alpha5^{N397}$ subunits[3], compared to cells transfected with α4, β2, and $\alpha5^{D397}$ subunits (Bierut et al., 2008).

Using qPCR analysis, Oni and colleagues found that *CHRNA3*, *CHRNA4*, *CHRNA5*, *CHRNB2*, and *CHRNB4* mRNA levels (encoding the α3, α4, α5, β2, and β4 nAChR subunits, respectively), were similar in human iPSCs differentiated to primarily dopaminergic neurons, irrespective of whether the *CHRNA5* gene carried the D398 or N398 allele (Oni et al., 2016). Compared to D398-expressing neurons, N398-expressing neurons exhibited greater postsynaptic activity, indicated by the increased frequency and the amplitudes of the spontaneous postsynaptic currents. When the authors differentiated the iPSCs into glutamatergic cells, they found that 0.1 μM nicotine significantly increased the frequency of spontaneous excitatory postsynaptic currents (EPSCs) in neurons carrying the N398 variant, but had no effect in neurons carrying the D398 variant. Higher concentrations of nicotine increased the frequency of EPSCs in neurons carrying the D398 variant, but had no effect in neurons carrying the N398 variant, which could be explained by receptor desensitization at these concentrations. Given the response to sub-micromolar concentrations of nicotine, these differences are likely due to the presence of high-affinity $(\alpha4\beta2)_2\alpha5$ receptors containing either the D398 or N398 α5 variant. Based on gene expression profiling using RNA-seq analysis, the authors speculated that genes specific for the ligand-receptor interaction, Ca^{2+} signaling, and axon guidance are enriched in neurons carrying the N398 α5 variant, thus accounting for the observed differences (Oni et al., 2016). Interestingly, however, the differences observed between neurons

[3]In the mouse and rat homologs, amino acid 397 corresponds to amino acid 398 in the human α5 protein.

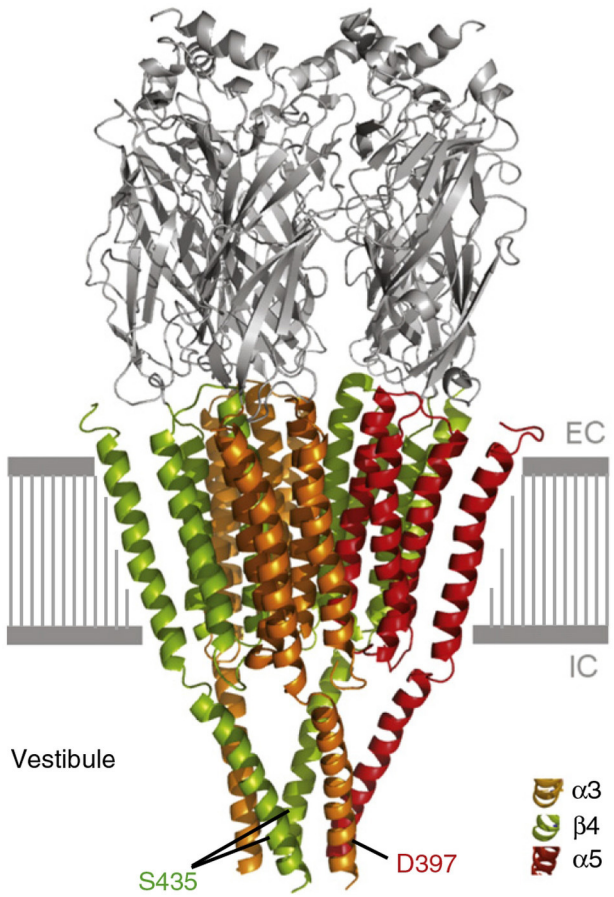

FIGURE 2 | Model of the 3D structure of the $(\alpha3\beta4)_2\alpha5$ nAChR. Transmembrane and intracellular domains of α3, α5, and β4 subunits are shown in orange, red, and green, respectively. The S435 residue in β4 and the D397 residue in α5 are located at the tip of the intracellular vestibule. Note the close apposition between S435 in the β4 subunit and D397 (corresponding to amino acid 398 in the human ortholog) in the α5 subunit. Changing the serine at position 435 in the β4 subunit to the arginine present in the corresponding residue in β2 abolished the β4-specific trafficking of the receptor to the plasma membrane. EC, extracellular space; IC, intracellular space. Reproduced with permission from Frahm et al. (2011).

carrying the N398 variant and neurons carrying the D398 variant were independent of preceding nAChR activation.

More recently, O'Neill and colleagues found that exposing pregnant mice to nicotine significantly affected the offspring's consumption of nicotine. Nicotine in the drinking water of dames reduced the nicotine consumption of offsprings carrying the α5(D397) gene, whereas consumption was enhanced in offsprings carrying the α5(N397) gene. By examining the underlying cellular and molecular mechanisms, the authors observed that exposure to nicotine during development differentially affected both the function of α4β2* nAChRs in the striatum and the expression of α3β4* nAChRs in the habenula of offsprings (O'Neill et al., 2018).

In VTA slice preparations, application of 100 μM nicotine revealed two distinct neuronal populations; one population responded with a relatively large current of ∼40 pA, and the other population responded with a much smaller current (∼8 pA). Interestingly, the 40-pA cell population was significantly reduced in mice carrying the N397 α5 variant and missing entirely in α5 KO mice (Sciaccaluga et al., 2015). Furthermore, the number of cultured ventral midbrain cells that responded to 100 μM nicotine, as well as the extent of the increase in intracellular Ca^{2+}, was significantly reduced in neurons carrying the N397 variant compared to neurons carrying the D397 variant. Since nicotine application failed to induce an increase in intracellular Ca^{2+} in cultures prepared from α5 KO mice, these observations indicate that the N397 variant can partially substitute for the more common D397 variant in $(\alpha4\beta2)_2\alpha5$ receptors (Sciaccaluga et al., 2015). This notion is supported by experiments with transiently transfected rat pituitary GH4C1 cells, which suggests that the N397 variant can indeed replace the D397 variant; compared to cells expressing $(\alpha4\beta2)_2\beta2$ receptors, both the current and the number of cells with an increase in intracellular Ca^{2+} in response to 100 μM nicotine were reduced to similar levels in cells expressing either $(\alpha4\beta2)_2\alpha5^{N397}$ or $(\alpha4\beta2)_2\alpha5^{D397}$ nAChRs (Sciaccaluga et al., 2015).

As discussed above, the firing rates of VIP interneurons and pyramidal cells in layer II/III of the PFC are regulated by α5-containing receptors, likely containing the α4β2* backbone. In α5 KO mice, the reduced firing frequency in these neurons is fully restored by expressing the D397 α5 variant, but is only partially restored by expressing the N397 variant, suggesting that the N397 variant can functionally replace—at least partially—the D397 α5 variant (Koukouli et al., 2017).

In separate experiments, Morel and colleagues used targeted lentiviral infection to express the N397 or D397 α5 variant in α5 KO mice and found that both variants restored DMPP-induced currents in VTA brain slices to the same extent. However, they found that increasing the firing rate of *in vivo* recorded VTA dopaminergic neurons required a 2-fold higher dose of intravenous nicotine in α5 KO mice virally transfected with the N397 α5 variant compared to α5 KO mice transfected with the D397 variant. Together with the previous observation that an 8-fold higher dose of nicotine was required to achieve the same effect in uninfected α5 KO mice, these results indicate that the N397 variant is less potent than the D397 variant at driving nicotine dependence (Morel et al., 2014).

Recently, these findings in mice were confirmed in rats genetically engineered to express the N397 α5 variant on an α5 KO background (Forget et al., 2018). Stimulating nAChRs in VTA brain slices with a saturating concentration of DMPP concentration induced currents that were similar between WT and $\alpha5^{N397}$ rats (Forget et al., 2018). Similarly, and unlike the α5 KO rat, WT and $\alpha5^{N397}$ rats required the same dose of intravenous nicotine in order to increase the firing frequency of VTA neurons. These observations suggest that nAChRs expressed in VTA neurons have similar sensitivity and efficacy regardless of whether they contain the D397 or N397 α5 variant. However, compared to WT rats, the current amplitude measured in IPN neurons stimulated with 30 μM nicotine was significantly reduced in both α5 KO rats and in $\alpha5^{N397}$ rats. Finally, the authors found that $\alpha5^{N397}$ rats self-administered more nicotine

at higher doses and exhibited higher levels of nicotine-induced reinstatement of nicotine-seeking behavior compared to WT rats, confirming that the IPN plays a critical role in this behavior (Forget et al., 2018).

In summary $(\alpha4\beta2)_2\alpha5^{N397}$ receptors are less sensitive to agonists compared to $(\alpha4\beta2)_2\alpha5^{D397}$ receptors. Moreover $(\alpha4\beta2)_2\alpha5^{N398}$ receptors have less Ca^{2+} permeability compared to $(\alpha4\beta2)_2\alpha5^{D398}$ receptors.

THE α5 SUBUNIT CO-ASSEMBLES WITH α3 AND β4 IN THE CENTRAL AND PERIPHERAL NERVOUS SYSTEMS

Regional Distribution

Receptors containing α3 and β4 nAChR subunits are predominately expressed in the autonomic nervous system, and the α5 subunits co-assembles with these two subunits to a significant extent (Conroy and Berg, 1995; Mao et al., 2006; David et al., 2010). Moreover, the α3 and β4 subunits are present in several regions in the rodent brain, particularly the MHb and IPN (Sheffield et al., 2000; Grady et al., 2009; Scholze et al., 2012; Beiranvand et al., 2014). In the MHb, α5, although expressed at relatively low levels, co-assembles primarily with α3β4* receptors, as deleting the β4 subunit eliminates all of the [^{3}H]-epibatidine-labeled receptors pulled down using an anti-α5 antibody (Scholze et al., 2012). In contrast, mice lacking the β2 subunit have normal levels of α5-containing receptors (Grady et al., 2009; Scholze et al., 2012). Despite this finding, some receptors in the MHb may contain the β2 subunit, as pre-clearing this subunit using an anti-β2 antibody also removes α5-containing receptors in both mice (Scholze et al., 2012) and rats (Grady et al., 2009). Nevertheless, a previous report based on nAChR agonist and antagonist profiling suggested that nAChRs in the rat MHb consist primarily of α3β4* receptors (Quick et al., 1999). Specifically, they found that cytisine was the most efficacious agonist, and the α3β4-specific antagonist α-conotoxin AuIB inhibited ∼75% of nicotine-induced currents. Given that the α3β2-specific antagonist α-CtxMII also inhibited currents to a certain extent, the authors proposed that the β2 subunit may contribute to these receptors (Quick et al., 1999), consistent with the above-mentioned immunoprecipitation studies (Grady et al., 2009; Scholze et al., 2012). On the other hand, α5-containing receptors were not detected in the MHb of transgenic $\alpha5^{GFP}$ mice (Hsu et al., 2013), and along with its relatively low expression in the MHb (Morton et al., 2018), *Chrna5* mRNA could not be detected in this brain region using *in situ* hybridization (Wada et al., 1990).

Although the notion that α3β4* receptors are expressed predominantly in the MHb is undisputed, the effect of the α5 accessory subunit on receptor function in the MHb has been a matter of debate (Morton et al., 2018). Transgenic mice overexpressing Chrnb4 exhibit a strong aversion to nicotine, which can be reversed by expressing the N397 α5 variant in the MHb (Frahm et al., 2011). On the other hand, the aversive effects of high nicotine doses on the brain's reward systems are abolished in mice with a targeted loss of α5 subunits, and this effect was reversed by restoring α5 expression in the MHb (Fowler et al., 2011). The converse experiment—knocking down α5 expression using a lentivirus-mediated shRNA injected into the MHb of rats—support the findings in α5 KO mice (Fowler et al., 2011). The authors also found that Fos immunoreactivity (a marker for neuronal activity) was significantly increased in the IPN following an aversively high dose of nicotine in WT mice, but not in α5 KO mice, leading to the conclusion that the α5 subunit has a facilitating effect on receptor function. This effect may be indirect, as nicotine increased the intrinsic excitability of MHb neurons in brain slices, and this increase was mimicked by the application of the neurokinin 1 receptor ligand substance P and the neurokinin 3 receptor agonist neurokinin B, but was prevented by preincubation with the neurokinin 1 receptor antagonist L-732138 and the neurokinin 3 receptor antagonist SB222200, and was absent in α5 KO mice (Dao et al., 2014). Moreover, ^{86}Rb efflux induced with 30 μM ACh was significantly reduced in synaptosomes isolated from several brain regions in α5 KO mice, including the habenula and IPN (Fowler et al., 2011). Interestingly, injections of Lenti-*Chrna5* into the MHb attenuated the deficits in ^{86}Rb efflux in the IPN, but not in the MHb, of knockout mice.

The IPN receives major cholinergic input from MHb afferents, which release glutamate and ACh (Ren et al., 2011), and studies have shown that the release of ACh from either intact IPN tissue or IPN synaptosomes in response to nAChR activation requires β4-containing receptors (Grady et al., 2009; Beiranvand et al., 2014), suggesting receptors consisting of the α3β4* backbone. The finding that ACh release was also reduced in β3 KO mice suggests that β3β4* receptors also contribute to this release (Grady et al., 2009). On the other hand, the agonist-induced release of ACh is not facilitated by α4, α5, or β2 subunits (Grady et al., 2009; Beiranvand et al., 2014). With respect to norepinephrine release from the IPN and MHb, however, the concentration-response curves depended on β2-containing receptors; moreover, the curves were right-shifted in α5 KO mice, and norepinephrine release was abolished in the presence of TTX (Beiranvand et al., 2014).

In the autonomic nervous system, α3β4* receptors form the predominant receptor backbone, unlike in the CNS. In both mouse and rat ganglia, ∼25% of these receptors contain the α5 subunit (Mandelzys et al., 1994; Mao et al., 2006; Putz et al., 2008; David et al., 2010). Given the finite number of possibly nAChR subunit combinations, and given the availability of various mouse—and more recently, rat—KO models, the ganglia in the autonomic nervous system are an ideal system for studying the composition and function of specific endogenous nAChRs.

In summary, the α5 subunit co-assembles with the α3 and β4 subunits throughout the autonomic nervous system. However, nAChRs in the medial habenula contain $(\alpha3\beta4)_2\alpha5$ receptors at low levels.

Receptor Affinity and Efficacy

Like α4β2* receptors discussed above, the properties of α3β4* receptors, and how these properties are affected by the presence of the α5 subunit, have been studied in heterologous expression systems. For example, Wang and colleagues reported no

significant difference in the potency or efficacy of ACh and nicotine between human α3β4* receptors lacking the α5 subunit and $(α3β4)_2α5$ receptors when expressed in *Xenopus* oocytes (Wang et al., 1996). On the other hand, expressing α5 with α3 and β4 receptors at a 1:1:1 ratio in *Xenopus* oocytes significantly increased Ca^{2+} permeability and the rate of receptor desensitization (Gerzanich et al., 1998). These observations were later confirmed by Groot-Kormelink and colleagues, who also observed an increase in apparent receptor desensitization and no difference in ACh potency or efficacy between α3β4* and $(α3β4)_2α5$ receptors expressed in *Xenopus* oocytes; to maximize the number of $(α3β4)_2α5$ receptors, the α5, α3, and β4 subunits were expressed at a ratio of 20:1:1 (Groot-Kormelink et al., 2001). In a separate study in which *Xenopus* oocytes expressed mouse α3 and β4 subunits (at a 1:1 ratio), ACh produced a monophasic concentration-response curve when peak current was measured, but a biphasic curve when net charge was measured, suggesting the expression of both high-affinity and low-affinity receptors; the addition of α5 expression (at a 1:1:1 ratio with α3 and β4) had no effect on the ACh EC_{50} value for peak current, but produced a monophasic ACh concentration-response curve for net charge, consistent with the hypothesis that α5 co-expression shifts receptors toward a single α5-containing form (Papke et al., 2010). In follow-up experiments by the same group, none of the agonists studied, including ACh, nicotine, cytisine, and varenicline, differed in potency between human $(α3β4)_2β4$ and $(α3β4)_2α5$ receptors expressed in *Xenopus* oocytes by injecting the dimeric α3-β4 concatemer together with either β4 or α5 (Stokes and Papke, 2012).

Similarly, no significant difference was found with respect to the potency of ACh, nicotine, or cytisine among $(α3β4)_2β4$, $(α3β4)_2α3$, and $(α3β4)_2α5$ receptors expressed as pentameric concatemers in *Xenopus* oocytes, although the nAChR agonists ACh, nicotine, and cytisine had higher efficacy in α5-containing receptors compared to α3- and β4-containing receptors (George et al., 2012). In contrast, when α3 and β4 were injected separately, the addition of α5 at a ratio of 1:1:1 significantly reduced the expression of functional receptors, possibly due to an adverse effect of separate α5 subunits with respect to forming functional nAChRs (George et al., 2012). Interestingly, the potency of mecamylamine decreased by an order of magnitude between $(α3β4)_2β4$ and $(α3β4)_2α5$ receptors, regardless of whether they were expressed as separate subunits or as concatemers (George et al., 2012). These observations are similar to results obtained regarding the effect of hexamethonium on inhibiting transganglionic transmission in the superior cervical ganglion (SCG) of WT mice and α5β2 KO mice (i.e., expressing α3β4* receptors), with IC_{50} values of 389.2 and 126.7 μM, respectively (Simeone et al., 2019). By taking into consideration the contribution of $(α3β4)_2β4$ receptors in WT mice, the authors calculated an IC_{50} of 568.6 μM for $(α3β4)_2α5$ receptors (Simeone et al., 2019).

Studies have found no difference in the potency or efficacy of agonists between α3β4* receptors expressed either with or without the α5 subunit in tsA201 cells (Wang et al., 1998; Nelson et al., 2001). The presence of the α5 subunit also had no effect on the decay of currents elicited by 300 μM ACh (Wang et al., 1998). However, immunoprecipitation studies using a cell line expressing $(α3β4)_2α5$ receptors showed that only 14% of all nAChRs contained the α5 subunit (Wang et al., 1998; Nelson et al., 2001), which may be too low to reveal any meaningful effect of the α5 subunit. To overcome this issue, Li and colleagues transiently transfected α3β4-expressing HEK293 cells with a FLAG-tagged α5 subunit, allowing them to selectively study cells that bound to small beads coated with an anti-FLAG antibody (Li et al., 2011). Using this strategy combined with patch-clamp recording, the authors found that the presence of the α5 subunit had no effect on the potency of ACh, nicotine, cytisine, or DMPP (Li et al., 2011). In BOSC-23 cells (a human kidney cell line derived from the 293T cell line), co-expressing the α5 subunit with α3β4 receptors caused a significant right-shift in the ACh concentration-response curve, as well as a reduction in the peak amplitude of the response; in contrast, when α5 was co-expressed with α3 and β4 in *Xenopus* oocytes, no observable difference was found with respect to ACh potency or efficacy (Fucile et al., 1997).

Decreased agonist efficacy in the presence of the α5 subunit was also observed when receptor function was measured using the bioluminescent Ca^{2+} indicator aequorin. At saturating concentrations of the agonists nicotine and varenicline, together with 20 mM Ca^{2+} in the recording solution, the increase in intracellular Ca^{2+} concentration was significantly higher in HEK293 cells stably expressing α3β4* compared to cells expressing $(α3β4)_2α5$; importantly, this effect of the α5 subunit was not due to a change in either the total or surface expression of the receptors (Tammimaki et al., 2012). Interestingly, and in contrast to results obtained with *Xenopus* oocytes (George et al., 2012), Tammimaki and colleagues found that the potency of mecamylamine was somewhat higher in cells expressing the α5 subunit (Tammimaki et al., 2012). Recently, the reduced efficacy of nicotine at activating $(α3β4)_2α5$ receptors compared to $(α3β4)_2β4$ receptors was confirmed by measuring aequorin luminescence in HEK293 cells stably transfected with human α3 and β4 subunits and cells stably expressing α3, β4, and α5 subunits (Ray et al., 2017).

Yu and Role studied the effect of α5 on α3β4* receptors in chick sympathetic neurons by functionally deleting the α5 subunit with antisense oligonucleotide treatment. The deletion of α5 significantly increased the potency of both ACh and cytisine. ACh was more efficacious than cytisine both with and without antisense treatment, but the difference was significantly larger upon deletion of α5. As deletion of α5 also eliminated channels that were blocked by the α7-specific antagonist methyllycaconitine while increasing the percentage of current carried by nAChRs that are sensitive to α-bungarotoxin, the authors inferred that native sympathetic neurons express heteromeric nAChRs that include both α5 and α7 (Yu and Role, 1998).

In β2 KO mice, the SCG neurons express ∼75% α3β4* receptors and ∼25% $(α3β4)_2α5$ receptors, whereas α5β2 double-KO mice express exclusively α3β4* hetero-pentameric receptors, making these ideal models for investigating the role of the α5 subunit in endogenous α3β4* receptors (David et al., 2010). Moreover, as discussed below, experiments showed that the percentage of $(α3β4)_2α5$ receptors in the plasma membrane is

significantly higher than the percentage of the overall receptor pool determined by immunoprecipitation (Simeone et al., 2019). With respect to ligand potency, David and colleagues found no difference in either the potency or efficacy of cytisine or DMPP between cultured neurons prepared from either α5β2 double-KO mice or β2 KO mice, and the total number of nACh receptors was not reduced in either α5β2 double-KO mice or β2 KO mice (David et al., 2010). With respect to the single-channel properties, unitary conductance was similar between α5-containing receptors and α3β4* hetero-pentameric receptors; however, α5-containing receptors had a longer open dwell time and longer burst duration (Ciuraszkiewicz et al., 2013).

In cultured SCG neurons, both α3β4* hetero-pentameric receptors and $(\alpha3\beta4)_2\alpha5$ receptors are present at presynaptic sites, where receptor activation by ACh, nicotine, cytisine, DMPP, or epibatidine in the presence of TTX (for blocking voltage-gated Na^+ channels) or Cd^{2+} (for blocking voltage-gated Ca^{2+} channels) triggers the release of preloaded [^{3}H]-norepinephrine (Kristufek et al., 1999; Fischer et al., 2005b). Although agonist potency differed slightly between SCG cultures prepared from α5 KO mice and WT mice, the agonists' efficacy was considerably higher in α5 KO neurons (Fischer et al., 2005b). Importantly, the release of [^{3}H]-norepinephrine required extracellular Ca^{2+} in the superfusion buffer, suggesting that Ca^{2+} entry via nAChRs triggers exocytosis and transmitter release, and intracellular Ca^{2+} imaging revealed that nAChR agonists induce a larger Ca^{2+} transient in α5 KO neurons compared to WT neurons (Fischer et al., 2005b). Given that the peak current amplitudes elicited in response to saturating concentrations of ACh, DMPP, and cytisine were similar between α3β4* hetero-pentameric receptors and $(\alpha3\beta4)_2\alpha5$ receptors (David et al., 2010), the above-mentioned findings suggest that receptors lacking the α5 subunit have increased Ca^{2+} permeability, increased Ca^{2+} release from intracellular stores, or an increase in additional downstream mechanisms, rather than a general increase in receptor efficacy. These findings are reminiscent of the results obtained using HEK293 cells expressing α3 and β4 subunits vs. cells expressing α3, β4, and α5 subunits (Tammimaki et al., 2012; Ray et al., 2017).

In summary, the α5 subunit does not significantly affect the sensitivity of α3β4* receptors expressed with concatemer constructs in *Xenopus* oocytes. However, heterologously expressed human receptors containing the α5 subunit are activated at higher efficacy than either (α3β4)2α3 or (α3β4)2β4 receptors. In contrast, endogenous receptors recorded in SCG neurons in α5 KO mice do not differ significantly from WT neurons with respect to either activation sensitivity or efficacy. Activation of α3β4* leads to a significantly higher increase in intracellular Ca^{2+} compared to $(\alpha3\beta4)_2\alpha5$ receptors expressed in HEK293 cells. Likewise, SCG neurons taken from α5 KO mice show a significantly higher increase in intracellular Ca^{2+} upon receptor activation compared SCG neurons taken from WT mice, and receptor activation also induces a significantly higher release of preloaded [^{3}H]-norepinephrine in SCG neurons taken from α5 KO mice. This contrasts observations in *Xenopus* oocytes, where $(\alpha3\beta4)_2\alpha5$ receptors have higher Ca^{2+} permeability compared to α3β4* receptors.

Desensitization Properties

When expressed in *Xenopus* oocytes, the addition of the α5 subunit to the α3 and β4 subunits increased the rate of apparent receptor desensitization during ACh application (Gerzanich et al., 1998; Groot-Kormelink et al., 2001). Indeed, expressing the α5 subunit in a tsA201 cell line stably expressing human α3β4 receptors had no effect on the decay of currents elicited in response to 300 μM ACh (Nelson et al., 2001). Similarly, no difference in decay was observed using a higher concentration of ACh (1 mM), whereas 100 μM nicotine prolonged the current decay in HEK293 cells transfected with α5, α3, and β4 subunits compared to cells expressing only the α3 and β4 subunits (Li et al., 2011).

When HEK293 cells expressing either α3β4* or α3β4α5 receptors were incubated for 30 s with 1 mM ACh or 100 μM nicotine, the time course of recovery from desensitization measured using patch-clamp recording was similar between the two receptor subtypes (Li et al., 2011). Moreover, using the intracellular Ca^{2+}-sensing photoprotein aequorin, Tammimaki and colleagues found no significant difference in nicotine IC_{50} values between α3β4* and $(\alpha3\beta4)_2\alpha5$ receptors stably expressed in HEK293 cells upon prolonged exposed to nicotine (Tammimaki et al., 2012).

The current decay measured in response to 300 μM ACh and fit with the sum of two exponential functions was similar between α5 single-KO and α5β2 double-KO mice, which express α3β4* hetero-pentameric receptors and $(\alpha3\beta4)_2\alpha5$ receptors, respectively (David et al., 2010). These KO mouse models were also used to measure receptor desensitization during prolonged exposure to nicotine in an intact SCG preparation in which compound action potentials (CAPs) were recorded from the postganglionic nerve in response to supramaximal stimulation of the preganglionic nerve. Nicotine added to the superfusion buffer at increasing concentrations yielded IC_{50} values of 3.01 μM for α3β4* receptors and 3.67 μM for $(\alpha3\beta4)_2\alpha5$ receptors (Simeone et al., 2019). This small, yet statistically significant difference indicates that the presence of the α5 subunit provides a slight degree of protection from receptor desensitization, although these levels of nicotine are not achieved, even with heavy smoking (Moreyra et al., 1992).

Varying the stimulation frequency of the preganglionic nerve also revealed differences in CAP amplitude between ganglia expressing α3β4* receptors and ganglia expressing $(\alpha3\beta4)_2\alpha5$ receptors (Simeone et al., 2019). With a stimulation frequency of 5 Hz, CAP amplitude increased significantly in WT ganglia but not in α5β2 KO ganglia; with 10-Hz stimulation, however, CAP amplitude decreased in α5β2 KO ganglia but not in WT ganglia, suggesting differences in activation and/or desensitization properties between these two receptors (Simeone et al., 2019).

In summary, the α5 subunit has just minor effects, if at all, on the desensitization properties of α3β4* receptors.

Receptor Expression and Membrane Trafficking

Measuring the total number of receptors using methods such as radiolabeled ligands (Brown et al., 2007; Baddick and

Marks, 2011) or immunoprecipitation of solubilized [^{125}I]-epibatidine–labeled receptors (Tammimaki et al., 2012) does not necessarily provide information regarding the number of functional receptors that actually reach the cell surface, requiring morphological, biochemical, and/or functional techniques in order to monitor receptor trafficking to the plasma membrane. Studies have shown that a number of chaperone proteins and regulatory proteins play a role in the trafficking of homo- and hetero-pentameric nAChR receptors to the plasma membrane (Millar and Harkness, 2008; St John, 2009; Crespi et al., 2018a). Because heterologous expression systems provide a robust model for studying receptor processing and trafficking, our current knowledge regarding the role of the α5 subunit in these processes stems primarily from studies involving cell lines (e.g., HEK293 cells), normal rat kidney cells, and *Xenopus* oocytes.

Combining [^{125}I]-mAb210 immunolabeling, two-electrode voltage clamp, and single-channel electrophysiology, George and colleagues reported differential effects of lynx1 on surface expression and functional properties of $(\alpha3\beta4)_2\alpha3$, $(\alpha3\beta4)_2\beta4$, and $(\alpha3\beta4)_2\alpha5$ in oocytes (George et al., 2017). Lynx family proteins are related to elapid snake venom toxin genes, such as α-bungarotoxin, consisting of a three-fingered folding motif and multiple internal disulfide bonds (Miwa et al., 2019). Lynx1 was previously shown to directly bind to α4β2* nAChRs (Ibanez-Tallon et al., 2002) and to shift nAChR stoichiometry to low sensitivity $(\alpha4\beta2)_2\alpha4$ pentamers (Nichols et al., 2014). Lynx1 reduced $(\alpha3\beta4)_2\beta4$ nAChR function principally by lowering cell-surface expression, whereas decreased unitary conductance, enhanced closed dwell times, and reduction in the proportion of long bursts accounted for reduced function of $(\alpha3\beta4)_2\alpha3$ receptors. Alterations in both cell-surface expression and single-channel properties mediated by lynx1 accounted for the reduction in $(\alpha3\beta4)_2\alpha5$ function (George et al., 2017).

Using [^{125}I]-epibatidine binding of solubilized receptors and an mAb35-based ELISA assay in intact cells, Tammimaki and colleagues found no difference in the number of receptors between HEK293 cells stably expressing α3 and β4 subunits and cells expressing α3, β4, and α5 subunits (Tammimaki et al., 2012), suggesting that the α5 subunit does not interfere with the assembly and membrane trafficking of these receptors. In contrast, Ray and colleagues reported that co-expressing the human α5 subunit significantly reduced the number of α3β4* receptors at the plasma membrane in HEK293 cells (Ray et al., 2017). For their experiments, the authors inserted an N-terminal HA, cMYC, and V5 tag in the α3, β4, and α5 subunits, respectively, finding that 98% of receptors were $(\alpha3\beta4)_2\beta4$ receptors in cells expressing α3 and β4, whereas 50% of the receptors were $(\alpha3\beta4)_2\beta4$ and 50% were $(\alpha3\beta4)_2\alpha5$ receptors in cells expressing α3, β4, and α5 subunits (Ray et al., 2017). Strikingly different results were obtained in rat kidney cells co-transfected with a dimeric plasmid expressing α3β4 together with a plasmid expressing α3, β4, or α5 (Crespi et al., 2018b). Using this approach, the authors found that including the β4-expressing construct resulted in $(\alpha3\beta4)_2\beta4$ receptors that reached the plasma membrane; in contrast, combining the dimeric construct with α3 resulted in $(\alpha3\beta4)_2\alpha3$ receptors that failed to exit the endoplasmic reticulum, and combining the dimeric construct with α5 resulted in $(\alpha3\beta4)_2\alpha5$ receptors were unable to exit the Golgi apparatus and were shuttled back to the endoplasmic reticulum (Crespi et al., 2018b).

An indirect method for measuring nAChRs at the cell surface is to record whole-cell currents in response to a saturating concentration of agonists; this approach has been used to determine whether the α5 subunit plays a role in receptor trafficking to the plasma membrane (e.g., Frahm et al., 2011; George et al., 2012). Using 2-electrode voltage-clamp recordings in *Xenopus* oocytes, Frahm and colleagues identified structural components in nAChR subunits critical for the trafficking of α3β4* receptors to the plasma membrane (Frahm et al., 2011). They found that injecting mouse β4—but not β2—cRNA in excess of α3 cRNA significantly increased currents elicited by 100 μM nicotine; if they included an excess amount α5 cRNA, nicotine-induced currents were reduced. They also found that the apparent potentiating effect of β4 was specific to amino acid S435, as it was eliminated by changing this serine to an arginine, the amino acid present in the equivalent position (R431) in the β2 subunit. Conversely, expressing a β2 subunit with a serine at position 431 results in a potentiation of nicotine-induced currents, giving the β2 subunit "β4-like" properties (Frahm et al., 2011). These results may explain the finding that the total number of nAChRs in the SCG is reduced by ∼90% in β4 KO mice, while deleting the β2 subunit has no effect (David et al., 2010). Homology modeling by Frahm and colleagues using the *Torpedo* nAChR suggests that the receptor's five subunits form a vestibule in which residue S435 in the β4 subunit is in apposition to residue D397—corresponding to residue 398 in the human ortholog—in the α5 subunit (**Figure 2**) (Frahm et al., 2011). Notably, when expressed in *Xenopus* oocytes, the α5 subunit reduced receptor trafficking only when the non-concatenated forms of human α3 and β4 cRNA were used; expressing the α5 subunit had no effect when concatenated α3-β4 cRNA was used (George et al., 2012).

Interestingly, SCG neurons obtained from α5 KO mice did not differ from WT neurons with respect to the total number of receptors measured using immunoprecipitation or peak currents measured in response to ACh, cytisine, or DMPP, suggesting that the α5 subunit does not affect expression and membrane trafficking of endogenous α3β4* receptors (David et al., 2010). Conversely, the authors found that β4 KO mice do not express α5-containing receptors, with the small number of remaining receptors (corresponding to ∼10% of the number of receptors measured in WT mice) comprised of α3β2* receptors (David et al., 2010). This finding differs from several heterologous systems, in which the receptors can be "forced" into an $(\alpha3\beta2)_2\alpha5$ configuration (Wang et al., 1996, 1998; Fucile et al., 1997; Nelson et al., 2001; Papke et al., 2010).

As noted above, only 25% of all receptors in the SCG of β2 KO mice contain the α5 subunit, and this relatively small contribution to the total receptor pool may not be sufficient to reveal differences at the whole-cell level. However, the non-competitive nAChR antagonist hexamethonium was significantly less potent at blocking $(\alpha3\beta4)_2\alpha5$ receptors compared to the α3β4* hetero-pentameric receptors expressed in α5β2 double-KO mice (see also Wang et al., 2002; Simeone et al., 2019). Using the difference in the right-shift in the concentration-response

curve allowed Simeone and colleagues to calculate the potency of hexamethonium at blocking a hypothetical "pure" population of $(\alpha3\beta4)_2\alpha5$ receptors, as well as the percentage of these receptors present at the cell surface. Interestingly, the authors found that hexamethonium inhibited transganglionic transmission in intact ganglia to the same extent as cultured SCG neurons stimulated with 100 μM ACh, suggesting that α5-containing receptors are dispersed along the surface of SCG neurons and are not specifically targeted to synaptic sites (Simeone et al., 2019). The finding that 72 and 63% of surface receptors are $(\alpha3\beta4)_2\alpha5$ receptors in intact ganglia and cultured SCG neurons, respectively, indicates that α5-containing receptors are enriched at the plasma membrane (Simeone et al., 2019).

In summary, the majority of studies show that the α5 subunit does not significantly affect either the total number of receptors or the number of receptors expressed at the plasma membrane.

Do the Functional Properties Differ Between $(\alpha3\beta4)_2\alpha5^{N398}$ and $(\alpha3\beta4)_2\alpha5^{D398}$ Receptors?

In *Xenopus* oocytes, the agonists ACh, nicotine, cytisine, and varenicline had similar potencies at activating $(\alpha3\beta4)_2\alpha5^{D398}$ receptors vs. $(\alpha3\beta4)_2\alpha5^{N398}$ receptors expressed by injecting the α3-β4 concatemer together with the respective α5 variant (Stokes and Papke, 2012). Similarly, Kuryatov and colleagues found no difference with respect to ACh EC_{50} values, Ca^{2+} permeability, or short-term desensitization in response to a 3-s exposure to 100 μM ACh when separately injecting α3, β4, and either $\alpha5^{D398}$ or $\alpha5^{N398}$ cRNA at a ratio of 1:1:2 in *Xenopus* oocytes (Kuryatov et al., 2011).

As discussed above, nAChR expression in *Xenopus* oocytes can be significantly increased by injecting an excess amount of mouse β4 cRNA compared to α3 cRNA. However, this increased expression can be reduced by co-injecting α5 cRNA, suggesting that this residue in the α5 subunit may play a role in receptor assembly, processing, and/or trafficking. Moreover, when α3, β4, and α5 cRNA was injected at a 1:10:10 ratio, the N397 α5 variant was significantly more effective at decreasing receptor expression compared to the D397 variant (Frahm et al., 2011). Consistent with this finding, George and colleagues found that receptors expressed using the fully pentameric β4-α3-β4-α3-α5 concatemer differed significantly in their ACh-induced peak currents depending on whether the α5 subunit was the N398 or D398 variant (George et al., 2012). Still, none of the nAChR ligands tested differed in potency between the two α5 variants, regardless of whether the receptors were expressed using concatemers or separate constructs (George et al., 2012).

By taking advantage of the fusion proteins encoding concatemers of human α3, β4, $\alpha5^{D398}$, and $\alpha5^{N398}$ subunits, Ochoa and colleagues tested the effects of the co-expressed protoxin LYPD6B on distinct nAChRs in *Xenopus* oocytes. LYPD6B enhanced ACh potency for $(\alpha3\beta4)_2\alpha3$ while reducing efficacy for $(\alpha3\beta4)_2\alpha3$ and $(\alpha3\beta4)_2\alpha5^{D398}$ receptors, whereas the properties $(\alpha3\beta4)_2\beta4$ and $(\alpha3\beta4)_2\alpha5^{N398}$ remained unaffected (Ochoa et al., 2016).

Interestingly, both the peak current amplitude and the EC_{50} values for nicotine and acetylcholine were slightly but significantly higher in human iPSC-derived dopaminergic neurons carrying the N398 α5 variant compared to cells carrying the D398 variant (Deflorio et al., 2016). However, RT-PCR analysis revealed that these cells express both α4β2* and α3β4* receptors (Deflorio et al., 2016), suggesting that the polymorphism may have affected α4β2* as well as α3β4*receptors, although the ACh EC_{50} values of 63.4 μM (in cells with the D398 variant) and 93.9 μM (in cells with the N398 variant) suggest that the difference in currents primarily reflected the properties measured for the low-affinity α3β4* receptors.

Using patch-clamp recording, Li and colleagues found no significant differences in the functional properties (e.g., agonist potency and efficacy, receptor desensitization, or time course of recovery from desensitization) between α3 and β4 subunits co-expressed in HEK293 cells with either the D398 or N398 α5 variant (Li et al., 2011). In contrast, Tammimaki and colleagues measured changes in intracellular Ca^{2+} using aequorin and found significant differences between HEK293 cells expressing $(\alpha3\beta4)_2\alpha5^{N398}$, $(\alpha3\beta4)_2\alpha5^{D398}$, and α3β4* receptors, with cells expressing α3β4* receptors having the highest response (Tammimaki et al., 2012). In these cells, IP_3 receptors and ryanodine receptors contribute to the increase in intracellular Ca^{2+}, although the role of IP_3 receptors was larger in the two cell lines expressing $(\alpha3\beta4)_2\alpha5$ receptors compared to the cell line expressing α3β4* receptors; paradoxically, however, the cell lines expressing α3β4* receptors had the largest agonist-induced increase in intracellular Ca^{2+} (Tammimaki et al., 2012).

Recently, Ray and colleagues performed a comprehensive directed screen of a large library of potential nAChR ligands and small molecule kinase inhibitors in order to identify candidate compounds that can distinguish between $(\alpha3\beta4)_2\beta4$, $(\alpha3\beta4)_2\alpha5^{D398}$, and $(\alpha3\beta4)_2\alpha5^{N398}$ receptors. The authors used aequorin to measure the effect of 100 μM nicotine in HEK293 cell lines stably expressing the various receptors, finding 8 antagonists that differed between the various receptors, with some compounds able to distinguish between $(\alpha3\beta4)_2\alpha5^{D398}$ and $(\alpha3\beta4)_2\alpha5^{N398}$ receptors (Ray et al., 2017). Moreover, some molecules such as the EGF receptor tyrosine kinase inhibitor tyrphostin-25 and Zaprinast, an inhibitor of cGMP-specific phosphodiesterases V an VI, prevented the nicotine-induced increase in intracellular Ca^{2+} in cells expressing $(\alpha3\beta4)_2\beta4$ receptors, but had no effect in cells expressing either $(\alpha3\beta4)_2\alpha5^{D398}$ or $(\alpha3\beta4)_2\alpha5^{N398}$ receptors (Ray et al., 2017). Finally, the authors found that some molecules such as the protein tyrosine kinase inhibitor genistein and the protein kinase C inhibitor hypocrellin A differentially affected cells expressing $(\alpha3\beta4)_2\alpha5^{D398}$ vs. $(\alpha3\beta4)_2\alpha5^{N398}$ receptors (Ray et al., 2017).

In summary $(\alpha3\beta4)_2\alpha5^{D398}$ and $(\alpha3\beta4)_2\alpha5^{N398}$ receptors have similar properties with respect to sensitivity and efficacy; in contrast, these receptors differ significantly with respect to the effect of specific kinase inhibitors.

SUMMARY AND PERSPECTIVES

$(\alpha4\beta2)_2\alpha5$ Receptors

A growing body of evidence based on both heterologously expressed and endogenous nAChR subunits indicates that the addition of the α5 subunit to α4β2* receptors significantly increases the receptor's Ca^{2+} permeability; for example, assays that measure intracellular Ca^{2+} have shown an increased efficacy of $(\alpha4\beta2)_2\alpha5$ receptors compared to α4β2* receptors. This increased permeability affects downstream Ca^{2+}-dependent signaling, including nAChR-mediated transmitter release. Studies using electrophysiology have also shown that native $(\alpha4\beta2)_2\alpha5$ receptors have increased efficacy compared to α4β2* receptors.

The ligand affinity of $(\alpha4\beta2)_2\alpha5$ receptors is similar to high-affinity $(\alpha4\beta2)_2\beta2$ receptors. Thus, replacing low-affinity $(\alpha4\beta2)_2\alpha4$ receptors with $(\alpha4\beta2)_2\alpha5$ receptors in a mixed population containing both $(\alpha4\beta2)_2\alpha4$ and $(\alpha4\beta2)_2\beta2$ receptors will result in an overall population consisting of highly sensitive (i.e., high-affinity) receptors. In addition, the presence of the α5 subunit "protects" α4β2* receptors from chronic desensitization in the prolonged presence of even low concentrations of nicotine. In various heterologous expression systems, although the number of α4β2* receptors may be increased by expressing the α5 subunit, membrane trafficking of the resulting $(\alpha4\beta2)_2\alpha5$ receptors may be reduced, leading to fewer receptors at the cell surface.

Most—but not all—cellular assays suggest that $(\alpha4\beta2)_2\alpha5$ receptors containing the N398 α5 variant may have reduced functionality (i.e., reduced sensitivity and/or efficacy) compared to receptors containing the D398 variant, but increased functionality compared to α4β2* hetero-pentameric receptors. Thus, the N398 α5 variant appears to be able to replace—at least partially—the D398 variant in α4β2* receptors. Moreover, neither knocking out the α5 subunit nor replacing the D398 variant with the N398 variant significantly affects the overall expression of nAChRs in the CNS. Although recent studies involving both mice and rats have shown differences in drug-seeking behavior between WT animals (i.e., carrying the D398 variant) and animals carrying the N398 variant, the underlying cellular mechanisms remain poorly understood and warrant future study.

$(\alpha3\beta4)_2\alpha5$ Receptors

In various heterologous expression systems, the presence of the α5 subunit has been found to increase, reduce, or have no effect on the number of α3β4* receptors, depending on the expression system used. In sympathetic neurons in α5 KO mice, loss of the α5 subunit does not affect currents induced by saturating concentrations of agonists, suggesting that the α5 subunit does not affect the number of functional receptors that traffic to the plasma membrane in these neurons. However, studies have shown that the α5 subunit requires the β4 subunit for proper expression of endogenous receptors, as β4 KO mice lack α5-containing receptors. Although $(\alpha3\beta4)_2\alpha5$ receptors do not differ significantly from α3β4* hetero-pentameric receptors with respect to agonist potency or desensitization, nAChR antagonists such as mecamylamine and hexamethonium can distinguish between α3β4* and $(\alpha3\beta4)_2\alpha5$ receptors.

Interestingly, the increase in intracellular Ca^{2+} upon receptor activation is differentially affected by the addition of the α5 subunit to α4β2* vs. α3β4* receptors. With respect to α3β4* receptors, addition of the α5 subunit decreases the Ca^{2+} response, despite the paradoxical finding that α5-containing receptors have increased Ca^{2+} permeability measured using voltage-clamp recordings in *Xenopus* oocytes. Thus, compared to $(\alpha3\beta4)_2\alpha5$ receptors, activating α3β4* hetero-pentameric receptors cause a larger increase in intracellular Ca^{2+} and increased transmitter release. A review of the published literature suggests that this increase is unlikely to be due solely to an increased number of receptors at the plasma membrane when α5 is knocked out. Finally, evidence suggests that $(\alpha3\beta4)_2\alpha5$ receptors containing the N398 α5 variant are more effective than receptors containing the D398 variant with respect to preventing the increase in intracellular Ca^{2+}.

Perspectives

The growing list of compounds that can distinguish between α3β4*, $(\alpha3\beta4)_2\alpha5^{D398}$, and/or $(\alpha3\beta4)_2\alpha5^{N398}$ receptors based on inhibiting the receptor directly or inhibiting downstream signaling provide a robust set of tools for studying how the α5 subunit—and its two variants—affects the function of α4β2* and α3β4* receptors. A key to resolving the underlying mechanisms may be the intracellular loop connecting the third and fourth transmembrane domains, the site in which where nAChR subunits have the highest diversity, containing putative phosphorylation and protein-binding sites. As eloquently summarized by Stokes and colleagues (p. 522), "if we want insights into the functional roles of specific nAChR subtypes, we will have to make efforts to reveal the hidden functions of their intracellular domains" (Stokes et al., 2015).

AUTHOR CONTRIBUTIONS

Both authors contributed to the writing of this review.

FUNDING

Major parts of our own work cited in this review were supported by the Austrian Science Fund (Projects P-11607MED and P19325-B09), the Medizinische - Wissenschaftliche Fonds des Bürgermeisters des Bundeshauptstadt Wien (Grant 08070), and the Austrian Ministry for Education, Science, and Culture (GZ 70.072/2-PR/4/2000).

ACKNOWLEDGMENTS

The authors would like to thank Uwe Maskos for critical reading of the manuscript and Theresa König for designing the artwork used in **Figure 1**.

REFERENCES

Alzu'bi, A., Middleham, W., Shoaib, M., and Clowry, G. J. (2020). Selective expression of nicotinic receptor sub-unit mRNA in early human fetal forebrain. *Front. Mol. Neurosci.* 13:72. doi: 10.3389/fnmol.2020.00072

Antolin-Fontes, B., Ables, J. L., Gorlich, A., and Ibanez-Tallon, I. (2015). The habenulo-interpeduncular pathway in nicotine aversion and withdrawal. *Neuropharmacol.* 96(Pt B), 213–222. doi: 10.1016/j.neuropharm.2014.11.019

Arvin, M. C., Jin, X. T., Yan, Y., Wang, Y., Ramsey, M. D., Kim, V. J., et al. (2019). Chronic nicotine exposure alters the neurophysiology of habenulo-interpeduncular circuitry. *J. Neurosci.* 39, 4268–4281. doi: 10.1523/JNEUROSCI.2816-18.2019

Azam, L., Winzer-Serhan, U. H., Chen, Y., and Leslie, F. M. (2002). Expression of neuronal nicotinic acetylcholine receptor subunit mRNAs within midbrain dopamine neurons. *J. Comp. Neurol.* 444, 260–274. doi: 10.1002/cne.10138

Baddick, C. G., and Marks, M. J. (2011). An autoradiographic survey of mouse brain nicotinic acetylcholine receptors defined by null mutants. *Biochem. Pharmacol.* 82, 828–841. doi: 10.1016/j.bcp.2011.04.019

Bailey, C. D., Alves, N. C., De Biasi, M., and Lambe, E. K. (2009). Nicotine persistently activates prefrontal layer VI pyramidal neurons through α5 subunit-containing α4β2*nicotinic acetylcholine receptors. *Biochem. Pharmacol.* 78, 915–915. doi: 10.1016/j.bcp.2009.06.069

Bailey, C. D., De, B. M., Fletcher, P. J., and Lambe, E. K. (2010). The nicotinic acetylcholine receptor α5 subunit plays a key role in attention circuitry and accuracy. *J. Neurosci.* 30, 9241–9252. doi: 10.1523/JNEUROSCI.2258-10.2010

Beiranvand, F., Zlabinger, C., Orr-Urtreger, A., Ristl, R., Huck, S., and Scholze, P. (2014). Nicotinic acetylcholine receptors control acetylcholine and noradrenaline release in the rodent habenulo-interpeduncular complex. *Br. J. Pharmacol.* 171, 5209–5224. doi: 10.1111/bph.12841

Benowitz, N. L., and Jacob, P. 3rd (1990). Intravenous nicotine replacement suppresses nicotine intake from cigarette smoking. *J. Pharmacol. Exp. Ther.* 254, 1000–1005.

Berrettini, W. H., and Doyle, G. A. (2012). The CHRNA5-A3-B4 gene cluster in nicotine addiction. *Mol. Psychiatry* 17, 856–866. doi: 10.1038/mp.2011.122

Bertrand, D., and Terry, A. V. Jr. (2018). The wonderland of neuronal nicotinic acetylcholine receptors. *Biochem. Pharmacol.* 151, 214–225. doi: 10.1016/j.bcp.2017.12.008

Besson, M., Forget, B., Correia, C., Blanco, R., and Maskos, U. (2019). Profound alteration in reward processing due to a human polymorphism in CHRNA5: a role in alcohol dependence and feeding behavior. *Neuropsychopharmacology* 44, 1906–1916. doi: 10.1038/s41386-019-0462-0

Bierut, L. J., Stitzel, J. A., Wang, J. C., Hinrichs, A. L., Grucza, R. A., Xuei, X., et al. (2008). Variants in nicotinic receptors and risk for nicotine dependence. *Am. J. Psychiatry* 165, 1163–1171. doi: 10.1176/appi.ajp.2008.07111711

Brody, A. L., Mandelkern, M. A., London, E. D., Olmstead, R. E., Farahi, J., Scheibal, D., et al. (2006). Cigarette smoking saturates brain α4β2 nicotinic acetylcholine receptors. *Arch. Gen. Psychiatry* 63, 907–915. doi: 10.1001/archpsyc.63.8.907

Brown, R. W. B., Collins, A. C., Lindstrom, J. M., and Whiteaker, P. (2007). Nicotinic α5 subunit deletion locally reduces high-affinity agonist activation without altering nicotinic receptor numbers. *J. Neurochem.* 103, 204–215. doi: 10.1111/j.1471-4159.2007.04700.x

Champtiaux, N., Gotti, C., Cordero-Erausquin, M., David, D. J., Przybylski, C., Lena, C., et al. (2003). Subunit composition of functional nicotinic receptors in dopaminergic neurons investigated with knock-out mice. *J. Neurosci.* 23, 7820–7829. doi: 10.1523/JNEUROSCI.23-21-07820.2003

Chatterjee, S., Santos, N., Holgate, J., Haass-Koffler, C. L., Hopf, F. W., Kharazia, V., et al. (2013). The α5 subunit regulates the expression and function of α4*-containing neuronal nicotinic acetylcholine receptors in the ventral-tegmental area. *PLoS ONE* 8:e68300. doi: 10.1371/journal.pone.0068300

Ciuraszkiewicz, A., Schreibmayer, W., Platzer, D., Orr-Urtreger, A., Scholze, P., and Huck, S. (2013). Single-channel properties of α3β4, α3β4α5 and α3β4β2 nicotinic acetylcholine receptors in mice lacking specific nicotinic acetylcholine receptor subunits. *J. Physiol.* 591(Pt 13), 3271–3288. doi: 10.1113/jphysiol.2012.246595

Conroy, W. G., and Berg, D. K. (1995). Neurons can maintain multiple classes of nicotinic acetylcholine receptors distinguished by different subunit compositions. *J. Biol. Chem.* 270, 4424–4431. doi: 10.1074/jbc.270.9.4424

Conroy, W. G., and Berg, D. K. (1998). Nicotinic receptor subtypes in the developing chick brain: appearance of a species containing the α4, β2, and α5 gene products. *Mol. Pharmacol.* 53, 392–401. doi: 10.1124/mol.53.3.392

Counotte, D. S., Goriounova, N. A., Moretti, M., Smoluch, M. T., Irth, H., Clementi, F., et al. (2012). Adolescent nicotine exposure transiently increases high-affinity nicotinic receptors and modulates inhibitory synaptic transmission in rat medial prefrontal cortex. *FASEB J.* 26, 1810–1820. doi: 10.1096/fj.11-198994

Crespi, A., Colombo, S. F., and Gotti, C. (2018a). Proteins and chemical chaperones involved in neuronal nicotinic receptor expression and function: an update. *Br. J. Pharmacol.* 175, 1869–1879. doi: 10.1111/bph.13777

Crespi, A., Plutino, S., Sciaccaluga, M., Righi, M., Borgese, N., Fucile, S., et al. (2018b). The fifth subunit in α3β4 nicotinic receptor is more than an accessory subunit. *FASEB J.* 32, 4190–4202. doi: 10.1096/fj.201701377R

Dao, D. Q., Perez, E. E., Teng, Y., Dani, J. A., and De Biasi, M. (2014). Nicotine enhances excitability of medial habenular neurons via facilitation of neurokinin signaling. *J. Neurosci.* 34, 4273–4284. doi: 10.1523/JNEUROSCI.2736-13.2014

David, R., Ciuraszkiewicz, A., Simeone, X., Orr-Urtreger, A., Papke, R. L., McIntosh, J. M., et al. (2010). Biochemical and functional properties of distinct nicotinic acetylcholine receptors in the superior cervical ganglion of mice with targeted deletions of nAChR subunit genes. *Eur. J. Neurosci.* 31, 978–993. doi: 10.1111/j.1460-9568.2010.07133.x

Deflorio, C., Blanchard, S., Carisi, M. C., Bohl, D., and Maskos, U. (2016). Human polymorphisms in nicotinic receptors: a functional analysis in iPS-derived dopaminergic neurons. *FASEB J.* 31, 828–839. doi: 10.1096/fj.201600932R

Exley, R., McIntosh, J. M., Marks, M. J., Maskos, U., and Cragg, S. J. (2012). Striatal α5 nicotinic receptor subunit regulates dopamine transmission in dorsal striatum. *J. Neurosci.* 32, 2352–2356. doi: 10.1523/JNEUROSCI.4985-11.2012

Fischer, H., Liu, D. M., Lee, A., Harries, J. C., and Adams, D. J. (2005a). Selective modulation of neuronal nicotinic acetylcholine receptor channel subunits by G(o)-protein subunits. *J. Neurosci.* 25, 3571–3577. doi: 10.1523/JNEUROSCI.4971-04.2005

Fischer, H., Orr-Urtreger, A., Role, L. W., and Huck, S. (2005b). Selective deletion of the α5 subunit differentially affects somatic-dendritic versus axonally targeted nicotinic ACh receptors in mouse. *J. Physiol.* 563, 119–137. doi: 10.1113/jphysiol.2004.075788

Forget, B., Icick, R., Robert, J., Correia, C., Prevost, M. S., Gielen, M., et al. (in press). Alterations in nicotinic receptor alpha5 subunit gene differentially impact early and later stages of cocaine addiction: a translational study in transgenic rats and patients. *Prog. Neurobiol.* 101898. doi: 10.1016/j.pneurobio.2020.101898

Forget, B., Scholze, P., Langa, F., Morel, C., Pons, S., Mondoloni, S., et al. (2018). A human polymorphism in CHRNA5 is linked to relapse to nicotine seeking in transgenic rats. *Curr. Biol.* 28:3244. doi: 10.1016/j.cub.2018.08.044

Fowler, C. D., Lu, Q., Johnson, P. M., Marks, M. J., and Kenny, P. J. (2011). Habenular α5 nicotinic receptor subunit signalling controls nicotine intake. *Nature* 471, 597–601. doi: 10.1038/nature09797

Frahm, S., Slimak, M. A., Ferrarese, L., Santos-Torres, J., Antolin-Fontes, B., Auer, S., et al. (2011). Aversion to nicotine is regulated by the balanced activity of β4 and α5 nicotinic receptor subunits in the medial habenula. *Neuron* 70, 522–535. doi: 10.1016/j.neuron.2011.04.013

Fucile, S., Barabino, B., Palma, E., Grassi, F., Limatola, C., Mileo, A. M., et al. (1997). α5 Subunits forms functional α3β4α5 nAChRs in transfected human cells. *Neuroreport* 8, 2433–2436. doi: 10.1097/00001756-199707280-00005

George, A. A., Bloy, A., Miwa, J. M., Lindstrom, J. M., Lukas, R. J., and Whiteaker, P. (2017). Isoform-specific mechanisms of α3β4*-nicotinic acetylcholine receptor modulation by the prototoxin lynx1. *FASEB J.* 31, 1398–1420. doi: 10.1096/fj.201600733R

George, A. A., Lucero, L. M., Damaj, M. I., Lukas, R. J., Chen, X., and Whiteaker, P. (2012). Function of human α3β4α5 nicotinic acetylcholine receptors is reduced by the α5(D398N) variant. *J. Biol. Chem.* 287, 25151–25162. doi: 10.1074/jbc.M112.379339

Gerzanich, V., Wang, F., Kuryatov, A., and Lindstrom, J. (1998). α5 Subunit alters desensitization, pharmacology, Ca^{++} permeability and Ca^{++} modulation of human neuronal α3 nicotinic receptors. *J. Pharmacol. Exp. Ther.* 286, 311–320.

Gotti, C., Moretti, M., Zanardi, A., Gaimarri, A., Champtiaux, N., Changeux, J.-P., et al. (2005). Heterogeneity and selective targeting of neuronal nicotinic acetylcholine receptor (nAChR) subtypes expressed on retinal afferents of the superior colliculus and lateral geniculate neucleus: identification of a new native

nAChR subtype α3β2(α5 or β3) enriched in retinocollicular afferents. *Mol. Pharmacol.* 68, 1162–1171. doi: 10.1124/mol.105.015925

Gotti, C., Zoli, M., and Clementi, F. (2006). Brain nicotinic acetylcholine receptors: native subtypes and their relevance. *Trends Pharmacol. Sci.* 27, 482–491. doi: 10.1016/j.tips.2006.07.004

Grady, S. R., Moretti, M., Zoli, M., Marks, M. J., Zanardi, A., Pucci, L., et al. (2009). Rodent habenulo-interpeduncular pathway expresses a large variety of uncommon nAChR subtypes, but only the α3β4* and α3β3β4* subtypes mediate acetylcholine release. *J. Neurosci.* 29, 2272–2282. doi: 10.1523/JNEUROSCI.5121-08.2009

Grady, S. R., Salminen, O., McIntosh, J. M., Marks, M. J., and Collins, A. C. (2010). Mouse striatal dopamine nerve terminals express α4α5β2 and two stoichiometric forms of α4β2*-nicotinic acetylcholine receptors. *J. Mol. Neurosci.* 40, 91–95. doi: 10.1007/s12031-009-9263-y

Grady, S. R., Wageman, C. R., Patzlaff, N. E., and Marks, M. J. (2012). Low concentrations of nicotine differentially desensitize nicotinic acetylcholine receptors that include α5 or α6 subunits and that mediate synaptosomal neurotransmitter release. *Neuropharmacology* 62, 1935–1943. doi: 10.1016/j.neuropharm.2011.12.026

Grando, S. A. (2014). Connections of nicotine to cancer. *Nat. Rev. Cancer* 14, 419–429. doi: 10.1038/nrc3725

Grishin, A. A., Wang, C. I., Muttenthaler, M., Alewood, P. F., Lewis, R. J., and Adams, D. J. (2010). α-conotoxin AuIB isomers exhibit distinct inhibitory mechanisms and differential sensitivity to stoichiometry of α3β4 nicotinic acetylcholine receptors. *J. Biol. Chem.* 285, 22254–22263. doi: 10.1074/jbc.M110.111880

Groot-Kormelink, P. J., Boorman, J. P., and Sivilotti, L. G. (2001). Formation of functional α3β4α5 human neuronal nicotinic receptors in *Xenopus* oocytes: a reporter mutation approach. *Br. J. Pharmacol.* 134, 789–796. doi: 10.1038/sj.bjp.0704313

Grucza, R. A., Wang, J. C., Stitzel, J. A., Hinrichs, A. L., Saccone, S. F., Saccone, N. L., et al. (2008). A risk allele for nicotine dependence in CHRNA5 is a protective allele for cocaine dependence. *Biol. Psychiatry* 64, 922–929. doi: 10.1016/j.biopsych.2008.04.018

Harpsoe, K., Ahring, P. K., Christensen, J. K., Jensen, M. L., Peters, D., and Balle, T. (2011). Unraveling the high- and low-sensitivity agonist responses of nicotinic acetylcholine receptors. *J. Neurosci.* 31, 10759–10766. doi: 10.1523/JNEUROSCI.1509-11.2011

Hsu, Y. W., Tempest, L., Quina, L. A., Wei, A. D., Zeng, H., and Turner, E. E. (2013). Medial habenula output circuit mediated by α5 nicotinic receptor-expressing GABAergic neurons in the interpeduncular nucleus. *J. Neurosci.* 33, 18022–18035. doi: 10.1523/JNEUROSCI.2927-13.2013

Ibanez-Tallon, I., Miwa, J. M., Wang, H. L., Adams, N. C., Crabtree, G. W., Sine, S. M., et al. (2002). Novel modulation of neuronal nicotinic acetylcholine receptors by association with the endogenous prototoxin lynx1. *Neuron* 33, 893–903. doi: 10.1016/S0896-6273(02)00632-3

Improgo, M. R., Scofield, M. D., Tapper, A. R., and Gardner, P. D. (2010). The nicotinic acetylcholine receptor CHRNA5/A3/B4 gene cluster: dual role in nicotine addiction and lung cancer. *Prog. Neurobiol.* 92, 212–226. doi: 10.1016/j.pneurobio.2010.05.003

Jackson, K. J., Marks, M. J., Vann, R. E., Chen, X., Gamage, T. F., Warner, J. A., et al. (2010). Role of α5 nicotinic acetylcholine receptors in pharmacological and behavioral effects of nicotine in mice. *J. Pharmacol. Exp. Ther.* 334, 137–146. doi: 10.1124/jpet.110.165738

Jin, X., Bermudez, I., and Steinbach, J. H. (2014). The nicotinic α5 subunit can replace either an acetylcholine-binding or nonbinding subunit in the α4β2* neuronal nicotinic receptor. *Mol. Pharmacol.* 85, 11–17. doi: 10.1124/mol.113.089979

Kabbani, N., Nordman, J. C., Corgiat, B. A., Veltri, D. P., Shehu, A., Seymour, V. A., et al. (2013). Are nicotinic acetylcholine receptors coupled to G proteins? *Bioessays* 35, 1025–1034. doi: 10.1002/bies.201300082

Kabbani, N., Woll, M. P., Levenson, R., Lindstrom, J. M., and Changeux, J. P. (2007). Intracellular complexes of the β2 subunit of the nicotinic acetylcholine receptor in brain identified by proteomics. *Proc. Natl. Acad. Sci. U.S.A.* 104, 20570–20575. doi: 10.1073/pnas.0710314104

King, J. R., Nordman, J. C., Bridges, S. P., Lin, M. K., and Kabbani, N. (2015). Identification and characterization of a G protein-binding cluster in α7 nicotinic acetylcholine receptors. *J. Biol. Chem.* 290, 20060–20070. doi: 10.1074/jbc.M115.647040

Koukouli, F., Rooy, M., Tziotis, D., Sailor, K. A., O'Neill, H. C., Levenga, J., et al. (2017). Nicotine reverses hypofrontality in animal models of addiction and schizophrenia. *Nat. Med.* 23, 347–354. doi: 10.1038/nm.4274

Krashia, P., Moroni, M., Broadbent, S., Hofmann, G., Kracun, S., Beato, M., et al. (2010). Human α3β4 neuronal nicotinic receptors show different stoichiometry if they are expressed in *Xenopus* oocytes or mammalian HEK293 cells. *PLoS ONE* 5:e13611. doi: 10.1371/journal.pone.0013611

Kristufek, D., Stocker, E., Boehm, S., and Huck, S. (1999). Somatic and prejunctional nicotinic receptors in cultured rat sympathetic neurones show different agonist profiles. *J. Physiol.* 516, 739–756. doi: 10.1111/j.1469-7793.1999.0739u.x

Kuryatov, A., Berrettini, W., and Lindstrom, J. (2011). Acetylcholine receptor (AChR) α5 subunit variant associated with risk for nicotine dependence and lung cancer reduces (α4β2)(2)α5 AChR function. *Mol. Pharmacol.* 79, 119–125. doi: 10.1124/mol.110.066357

Kuryatov, A., Onksen, J., and Lindstrom, J. (2008). Roles of accessory subunits in α4β2*nicotinic receptors. *Mol. Pharmacol.* 74, 132–143. doi: 10.1124/mol.108.046789

Lassi, G., Taylor, A. E., Timpson, N. J., Kenny, P. J., Mather, R. J., Eisen, T., et al. (2016). The CHRNA5-A3-B4 gene cluster and smoking: from discovery to therapeutics. *Trends Neurosci.* 39, 851–861. doi: 10.1016/j.tins.2016.10.005

Le Novere, N., Corringer, P. J., and Changeux, J. P. (2002). The diversity of subunit composition in nAChRs: evolutionary origins, physiologic and pharmacologic consequences. *J. Neurobiol.* 53, 447–456. doi: 10.1002/neu.10153

Lecourtier, L., and Kelly, P. H. (2007). A conductor hidden in the orchestra? Role of the habenular complex in monoamine transmission and cognition. *Neurosci. Biobehav. Rev.* 31, 658–672. doi: 10.1016/j.neubiorev.2007.01.004

Lena, C., de Kerchove d'Exaerde, A., Cordero-Erausquin, M., Le Novere, N., del Mar Arroyo-Jimenez, M., and Changeux, J.-P. (1999). Diversity and distribution of nicotinic acetylcholine receptors in the locus ceruleus neurons. *Proc. Natl. Acad. Sci. U.S.A.* 96, 12126–12131. doi: 10.1073/pnas.96.21.12126

Leslie, F. M., Mojica, C. Y., and Reynaga, D. D. (2013). Nicotinic receptors in addiction pathways. *Mol. Pharmacol.* 83, 753–758. doi: 10.1124/mol.112.083659

Li, P., McCollum, M., Bracamontes, J., Steinbach, J. H., and Akk, G. (2011). Functional characterization of the α5(Asn398) variant associated with risk for nicotine dependence in the α3β4α5 nicotinic receptor. *Mol. Pharmacol.* 80, 818–827. doi: 10.1124/mol.111.073841

Mandelzys, A., Pie, B., Deneris, E. S., and Cooper, E. (1994). The developmental increase in ACh current densities on rat sympathetic neurons correlates with changes in nicotinic ACh receptor subunit gene expression and occurs independent of innervation. *J. Neurosci.* 14, 2357–2364. doi: 10.1523/JNEUROSCI.14-04-02357.1994

Mao, D., Perry, D. C., Yasuda, R. P., Wolfe, B. B., and Kellar, K. J. (2008). The α4β2α5 nicotinic cholinergic receptor in rat brain is resistant to up-regulation by nicotine *in vivo*. *J. Neurochem.* 104, 446–456. doi: 10.1111/j.1471-4159.2007.05011.x

Mao, D., Yasuda, R. P., Fan, H., Wolfe, B. B., and Kellar, K. J. (2006). Heterogeneity of nicotinic cholinergic receptors in rat superior cervical and nodosa ganglia. *Mol. Pharmacol.* 70, 1693–1699. doi: 10.1124/mol.106.027458

Marks, M. J., Meinerz, N. M., Brown, R. W., and Collins, A. C. (2010). $86Rb^+$ efflux mediated by α4β2*-nicotinic acetylcholine receptors with high and low-sensitivity to stimulation by acetylcholine display similar agonist-induced desensitization. *Biochem. Pharmacol.* 80, 1238–1251. doi: 10.1016/j.bcp.2010.06.040

Maskos, U. (2020). The nicotinic receptor α5 coding polymorphism rs16969968 as a major target in disease: functional dissection and remaining challenges. *J. Neurochem.* 154, 241–250. doi: 10.1111/jnc.14989

Matta, J. A., Gu, S., Davini, W. B., Lord, B., Siuda, E. R., Harrington, A. W., et al. (2017). NACHO mediates nicotinic acetylcholine receptor function throughout the brain. *Cell Rep.* 19, 688–696. doi: 10.1016/j.celrep.2017.04.008

McClure-Begley, T. D., King, N. M., Collins, A. C., Stitzel, J. A., Wehner, J. M., and Butt, C. M. (2009). Acetylcholine-stimulated [3H]GABA release from mouse brain synaptosomes is modulated by α4β2 and α4α5β2 nicotinic receptor subtypes. *Mol. Pharmacol.* 75, 918–926. doi: 10.1124/mol.108.052274

McGehee, D. S., and Role, L. W. (1995). Physiological diversity of nicotinic acetylcholine receptors expressed by vertebrate neurons. *Annu. Rev. Physiol.* 57, 521–546. doi: 10.1146/annurev.ph.57.030195.002513

Millar, N. S., and Gotti, C. (2009). Diversity of vertebrate nicotinic acetylcholine receptors. *Neuropharmacology* 56, 237–246. doi: 10.1016/j.neuropharm.2008.07.041

Millar, N. S., and Harkness, P. C. (2008). Assembly and trafficking of nicotinic acetylcholine receptors (review). *Mol. Membr. Biol.* 25, 279–292. doi: 10.1080/09687680802035675

Miller, M. B., Wilson, R. S., Lam, T. T., Nairn, A. C., and Picciotto, M. R. (2018). Evaluation of the phosphoproteome of mouse α4/β2-containing nicotinic acetylcholine receptors *in vitro* and *in vivo*. *Proteomes* 6:42. doi: 10.3390/proteomes6040042

Miwa, J. M., Anderson, K. R., and Hoffman, K. M. (2019). Lynx prototoxins: roles of endogenous mammalian neurotoxin-like proteins in modulating nicotinic acetylcholine receptor function to influence complex biological processes. *Front. Pharmacol.* 10:343. doi: 10.3389/fphar.2019.00343

Miwa, J. M., Ibanez-Tallon, I., Crabtree, G. W., Sanchez, R., Sali, A., Role, L. W., et al. (1999). lynx1, an endogenous toxin-like modulator of nicotinic acetylcholine receptors in the mammalian CNS. *Neuron* 23, 105–114. doi: 10.1016/S0896-6273(00)80757-6

Molas, S., DeGroot, S. R., Zhao-Shea, R., and Tapper, A. R. (2017). Anxiety and nicotine dependence: emerging role of the habenulo-interpeduncular axis. *Trends Pharmacol. Sci.* 38, 169–180. doi: 10.1016/j.tips.2016.11.001

Morel, C., Fattore, L., Pons, S., Hay, Y. A., Marti, F., Lambolez, B., et al. (2014). Nicotine consumption is regulated by a human polymorphism in dopamine neurons. *Mol. Psychiatry* 19, 930–936. doi: 10.1038/mp.2013.158

Moreyra, A. E., Lacy, C. R., Wilson, A. C., Kumar, A., and Kostis, J. B. (1992). Arterial blood nicotine concentration and coronary vasoconstrictive effect of low-nicotine cigarette smoking. *Am. Heart J.* 124, 392–397. doi: 10.1016/0002-8703(92)90603-S

Morton, G., Nasirova, N., Sparks, D. W., Brodsky, M., Sivakumaran, S., Lambe, E. K., et al. (2018). Chrna5-expressing neurons in the interpeduncular nucleus mediate aversion primed by prior stimulation or nicotine exposure. *J. Neurosci.* 38, 6900–6920. doi: 10.1523/JNEUROSCI.0023-18.2018

Nelson, M. E., Wang, F., Kuryatov, A., Choi, C. H., Gerzanich, V., and Lindstrom, J. (2001). Functional properties of human nicotinic AChRs expressed by IMR-32 neuroblastoma cells resemble those of a3b4 AChRs expressed in permanently transfected HEK cells. *J. Gen. Physiol.* 118, 563–582. doi: 10.1085/jgp.118.5.563

Nichols, W. A., Henderson, B. J., Marotta, C. B., Yu, C. Y., Richards, C., Dougherty, D. A., et al. (2016). Mutation linked to autosomal dominant nocturnal frontal lobe epilepsy reduces low-sensitivity α4β2, and increases α5α4β2, nicotinic receptor surface expression. *PLoS ONE* 11:e0158032. doi: 10.1371/journal.pone.0158032

Nichols, W. A., Henderson, B. J., Yu, C., Parker, R. L., Richards, C. I., Lester, H. A., et al. (2014). Lynx1 shifts α4β2 nicotinic receptor subunit stoichiometry by affecting assembly in the endoplasmic reticulum. *J. Biol. Chem.* 289, 31423–31432. doi: 10.1074/jbc.M114.573667

Ochoa, V., George, A. A., Nishi, R., and Whiteaker, P. (2016). The prototoxin LYPD6B modulates heteromeric α3β4-containing nicotinic acetylcholine receptors, but not α7 homomers. *FASEB J.* 30, 1109–1119. doi: 10.1096/fj.15-274548

O'Neill, H. C., Wageman, C. R., Sherman, S. E., Grady, S. R., Marks, M. J., and Stitzel, J. A. (2018). The interaction of the Chrna5 D398N variant with developmental nicotine exposure. *Genes Brain Behav.* 17:e12474. doi: 10.1111/gbb.12474

Oni, E. N., Halikere, A., Li, G., Toro-Ramos, A. J., Swerdel, M. R., Verpeut, J. L., et al. (2016). Increased nicotine response in iPSC-derived human neurons carrying the CHRNA5 N398 allele. *Sci. Rep.* 6:34341. doi: 10.1038/srep34341

Papke, R. L., Wecker, L., and Stitzel, J. A. (2010). Activation and inhibition of mouse muscle and neuronal nicotinic acetylcholine receptors expressed in *Xenopus* oocytes. *J. Pharmacol. Exp. Ther.* 333, 501–518. doi: 10.1124/jpet.109.164566

Picciotto, M. R., and Kenny, P. J. (2013). Molecular mechanisms underlying behaviors related to nicotine addiction. *Cold Spring Harb. Perspect. Med.* 3:a012112. doi: 10.1101/cshperspect.a012112

Pistillo, F., Clementi, F., Zoli, M., and Gotti, C. (2015). Nicotinic, glutamatergic and dopaminergic synaptic transmission and plasticity in the mesocorticolimbic system: focus on nicotine effects. *Prog. Neurobiol.* 124, 1–27. doi: 10.1016/j.pneurobio.2014.10.002

Pons, S., Fattore, L., Cossu, G., Tolu, S., Porcu, E., McIntosh, J. M., et al. (2008). Crucial role of α4 and α6 nicotinic acetylcholine receptor subunits from ventral tegmental area in systemic nicotine self-administration. *J. Neurosci.* 28, 12318–12327. doi: 10.1523/JNEUROSCI.3918-08.2008

Poorthuis, R. B., Bloem, B., Verhoog, M. B., and Mansvelder, H. D. (2013). Layer-specific interference with cholinergic signaling in the prefrontal cortex by smoking concentrations of nicotine. *J. Neurosci.* 33, 4843–4853. doi: 10.1523/JNEUROSCI.5012-12.2013

Porter, J. T., Cauli, B., Tsuzuki, K., Lambolez, B., Rossier, J., and Audinat, E. (1999). Selective excitation of subtypes of neocortical interneurons by nicotinic receptors. *J. Neurosci.* 19, 5228–5235. doi: 10.1523/JNEUROSCI.19-13-05228.1999

Prevost, M. S., Bouchenaki, H., Barilone, N., Gielen, M., and Corringer, P. J. (2020). Concatemers to re-investigate the role of alpha5 in alpha4beta2 nicotinic receptors. *Cell Mol. Life Sci.* doi: 10.1007/s00018-020-03558-z

Putz, G., Kristufek, D., Orr-Urtreger, A., Changeux, J. P., Huck, S., and Scholze, P. (2008). Nicotinic acetylcholine receptor-subunit mRNAs in the mouse superior cervical ganglion are regulated by development but not by deletion of distinct subunit genes. *J. Neurosci. Res.* 86, 972–981. doi: 10.1002/jnr.21559

Quick, M. W., Ceballos, R. M., Kasten, M., McIntosh, J. M., and Lester, R. A. (1999). α3β4 subunit-containing nicotinic receptors dominate function in rat medial habenula neurons. *Neuropharmacol.* 38, 769–783. doi: 10.1016/S0028-3908(99)00024-6

Quick, M. W., and Lester, R. A. J. (2002). Desensitization of neuronal nicotinic receptors. *J. Neurobiol.* 53, 457–478. doi: 10.1002/neu.10109

Ramirez-Latorre, J., Yu, C. R., Qu, X., Perin, F., Karlin, A., and Role, L. W. (1996). Functional contributions of α5 subunit to neuronal acetylcholine receptor channels. *Nature* 380, 347–351. doi: 10.1038/380347a0

Ray, C., Soderblom, E. J., Bai, Y., Carroll, F. I., Caron, M. G., and Barak, L. S. (2017). Probing the allosteric role of the α5 subunit of α3β4α5 nicotinic acetylcholine receptors by functionally Selective modulators and ligands. *ACS Chem. Biol.* 12, 702–714. doi: 10.1021/acschembio.6b01117

Ren, J., Qin, C., Hu, F., Tan, J., Qiu, L., Zhao, S., et al. (2011). Habenula "cholinergic" neurons co-release glutamate and acetylcholine and activate postsynaptic neurons via distinct transmission modes. *Neuron* 69, 445–452. doi: 10.1016/j.neuron.2010.12.038

Sacaan, A. I., Dunlop, J. L., and Lloyd, G. K. (1995). Pharmacological characterization of neuronal acetylcholine gated ion channel receptor-mediated hippocampal norepinephrine and striatal dopamine release from rat brain slices. *J. Pharmacol. Exp. Ther.* 274, 224–230.

Salas, R., Orr-Urtreger, A., Broide, R. S., Beaudet, A., Paylor, R., and De Biasi, M. (2003). The nicotinic acetylcholine receptor subunit α5 mediates short-term effects of nicotine in *vivo*. *Mol. Pharmacol.* 63, 1059–1066. doi: 10.1124/mol.63.5.1059

Salminen, O., Murphy, K. L., McIntosh, J. M., Drago, J., Marks, M. J., Collins, A. C., et al. (2004). Subunit composition and pharmacology of two classes of striatal presynaptic nicotinic acetylcholine receptors mediating dopamine release in mice. *Mol. Pharmacol.* 65, 1526–1535. doi: 10.1124/mol.65.6.1526

Scholze, P., Koth, G., Orr-Urtreger, A., and Huck, S. (2012). Subunit composition of α5-containing nicotinic receptors in the rodent habenula. *J. Neurochem.* 121, 551–560. doi: 10.1111/j.1471-4159.2012.07714.x

Scholze, P., Orr-Urtreger, A., Changeux, J. P., McIntosh, J. M., and Huck, S. (2007). Catecholamine outflow from mouse and rat brain slice preparations evoked by nicotinic acetylcholine receptor activation and electrical field stimulation. *Br. J. Pharmacol.* 151, 414–422. doi: 10.1038/sj.bjp.0707236

Sciaccaluga, M., Moriconi, C., Martinello, K., Catalano, M., Bermudez, I., Stitzel, J. A., et al. (2015). Crucial role of nicotinic α5 subunit variants for Ca^{2+} fluxes in ventral midbrain neurons. *FASEB J.* 29, 3389–3398. doi: 10.1096/fj.14-268102

Sheffield, E. B., Quick, M. W., and Lester, R. A. (2000). Nicotinic acetylcholine receptor subunit mRNA expression and channel function in medial habenula neurons. *Neuropharmacology* 39, 2591–2603. doi: 10.1016/S0028-3908(00)00138-6

Simeone, X., Karch, R., Ciuraszkiewicz, A., Orr-Urtreger, A., Lemmens-Gruber, R., Scholze, P., et al. (2019). The role of the nAChR subunits α5, β2, and β4 on synaptic transmission in the mouse superior cervical ganglion. *Physiol. Rep.* 7:e14023. doi: 10.14814/phy2.14023

Slimak, M. A., Ables, J. L., Frahm, S., Antolin-Fontes, B., Santos-Torres, J., Moretti, M., et al. (2014). Habenular expression of rare missense variants of the β4 nicotinic receptor subunit alters nicotine consumption. *Front. Hum. Neurosci.* 8:12. doi: 10.3389/fnhum.2014.00012

St John, P. A. (2009). Cellular trafficking of nicotinic acetylcholine receptors. *Acta Pharmacol. Sin.* 30, 656–662. doi: 10.1038/aps.2009.76

Stevens, V. L., Bierut, L. J., Talbot, J. T., Wang, J. C., Sun, J., Hinrichs, A. L., et al. (2008). Nicotinic receptor gene variants influence susceptibility to heavy smoking. *Cancer Epidemiol. Biomarkers Prev.* 17, 3517–3525. doi: 10.1158/1055-9965.EPI-08-0585

Stokes, C., and Papke, R. L. (2012). Use of an α3β4 nicotinic acetylcholine receptor subunit concatamer to characterize ganglionic receptor subtypes with specific subunit composition reveals species-specific pharmacologic properties. *Neuropharmacology* 63, 538–546. doi: 10.1016/j.neuropharm.2012.04.035

Stokes, C., Treinin, M., and Papke, R. L. (2015). Looking below the surface of nicotinic acetylcholine receptors. *Trends Pharmacol. Sci.* 36, 514–523. doi: 10.1016/j.tips.2015.05.002

Tammimaki, A., Herder, P., Li, P., Esch, C., Laughlin, J. R., Akk, G., et al. (2012). Impact of human D398N single nucleotide polymorphism on intracellular calcium response mediated by α3β4α5 nicotinic acetylcholine receptors. *Neuropharmacology* 63, 1002–1011. doi: 10.1016/j.neuropharm.2012.07.022

Tapia, L., Kuryatov, A., and Lindstrom, J. (2007). Ca^{2+} permeability of the (α4)(3)(β2)(2) stoichiometry greatly exceeds that of (α4)(2)(β2)(3) human acetylcholine receptors. *Mol. Pharmacol.* 71, 769–776. doi: 10.1124/mol.106.030445

Thorgeirsson, T. E., Geller, F., Sulem, P., Rafnar, T., Wiste, A., Magnusson, K. P., et al. (2008). A variant associated with nicotine dependence, lung cancer and peripheral arterial disease. *Nature* 452, 638–642. doi: 10.1038/nature 06846

Tuesta, L. M., Fowler, C. D., and Kenny, P. J. (2011). Recent advances in understanding nicotinic receptor signaling mechanisms that regulate drug self-administration behavior. *Biochem. Pharmacol.* 82, 984–995. doi: 10.1016/j.bcp.2011.06.026

Venkatesan, S., and Lambe, E. K. (2020). Chrna5 is essential for a rapid and protected response to optogenetic release of endogenous acetylcholine in prefrontal cortex. *J. Neurosci.* 40, 7255–7268. doi: 10.1523/JNEUROSCI.1128-20.2020

Wada, E., McKinnon, D., Heinemann, S., Patrick, J., and Swanson, L. W. (1990). The distribution of mRNA encoded by a new member of the neuronal nicotinic acetylcholine receptor gene family α5 in the rat central nervous system. *Brain Res.* 526, 45–53. doi: 10.1016/0006-8993(90)90248-A

Wageman, C. R., Marks, M. J., and Grady, S. R. (2014). Effectiveness of nicotinic agonists as desensitizers at presynaptic α4β2- and α4α5β2-nicotinic acetylcholine receptors. *Nicotine. Tob. Res.* 16, 297–305. doi: 10.1093/ntr/ntt146

Wang, F., Gerzanich, V., Wells, G. B., Anand, R., Peng, X., Keyser, K., et al. (1996). Assembly of human neuronal nicotinic receptor α5 subunits with α3, β2, and β4 subunits. *J. Biol. Chem.* 271, 17656–17665. doi: 10.1074/jbc.271.30.17656

Wang, F., Nelson, M. E., Kuryatov, A., Olale, F., Cooper, J., Keyser, K., et al. (1998). Chronic nicotine treatment up-regulates human α3β2 but not α3β4 acetylcholine receptors stably transfected in human embryonic kidney cells. *J. Biol. Chem.* 273, 28721–28732. doi: 10.1074/jbc.273.44.28721

Wang, N., Orr-Urtreger, A., Chapman, J., Rabinowitz, R., Nachmann, R., and Korczyn, A. D. (2002). Autonomic function in mice lacking α5 neuronal nicotinic acetylcholine receptor subunit. *J. Physiol.* 542, 347–354. doi: 10.1113/jphysiol.2001.013456

Winzer-Serhan, U. H., and Leslie, F. M. (2005). Expression of alpha5 nicotinic acetylcholine receptor subunit mRNA during hippocampal and cortical development. *J. Comp. Neurol.* 481, 19–30. doi: 10.1002/cne.20357

Wonnacott, S. (1997) Presynaptic nicotinic ACh receptors. *Trends Neurosci.* 20, 92–98. doi: 10.1016/s0166-2236(96)10073-4

Wooltorton, J. R., Pidoplichko, V. I., Broide, R. S., and Dani, J. A. (2003). Differential desensitization and distribution of nicotinic acetylcholine receptor subtypes in midbrain dopamine areas. *J. Neurosci.* 23, 3176–3185. doi: 10.1523/JNEUROSCI.23-08-03176.2003

Xanthos, D. N., Beiersdorf, J. W., Thrun, A., Ianosi, B., Orr-Urtreger, A., Huck, S., et al. (2015). Role of α5-containing nicotinic receptors in neuropathic pain and response to nicotine. *Neuropharmacology* 95, 37–49. doi: 10.1016/j.neuropharm.2015.02.012

Yu, C. R., and Role, L. W. (1998). Functional contribution of the α5 subunit to neuronal nicotinic channels expressed by chick sympathetic ganglion neurones. *J. Physiol.* 509 (Pt 3), 667–681. doi: 10.1111/j.1469-7793.1998.667bm.x

Zoli, M., Moretti, M., Zanardi, A., McIntosh, J. M., Clementi, F., and Gotti, C. (2002). Identification of the nicotinic receptor subtypes expressed on dopaminergic terminals in the rat striatum. *J. Neurosci.* 22, 8785–8789. doi: 10.1523/JNEUROSCI.22-20-08785.2002

Zoli, M., Pucci, S., Vilella, A., and Gotti, C. (2018). Neuronal and extraneuronal nicotinic acetylcholine receptors. *Curr. Neuropharmacol.* 16, 338–349. doi: 10.2174/1570159X15666170912110450

Conflict of Interest: The authors declare that the research was conducted in the absence of any commercial or financial relationships that could be construed as a potential conflict of interest.

Copyright © 2020 Scholze and Huck. This is an open-access article distributed under the terms of the Creative Commons Attribution License (CC BY). The use, distribution or reproduction in other forums is permitted, provided the original author(s) and the copyright owner(s) are credited and that the original publication in this journal is cited, in accordance with accepted academic practice. No use, distribution or reproduction is permitted which does not comply with these terms.

frontiers in Synaptic Neuroscience

BRIEF RESEARCH REPORT
published: 05 February 2021
doi: 10.3389/fnsyn.2021.640495

PKN1 Is a Novel Regulator of Hippocampal GluA1 Levels

Motahareh Solina Safari, Dido Obexer, Gabriele Baier-Bitterlich and Stephanie zur Nedden**

CCB-Biocenter, Institute of Neurobiochemistry, Medical University of Innsbruck, Innsbruck, Austria

Alterations in the processes that control α-Amino-3-hydroxy-5-methyl-4-isoxazolepropionic acid receptor (AMPAR) expression, assembly and trafficking are closely linked to psychiatric and neurodegenerative disorders. We have recently shown that the serine/threonine kinase Protein kinase N1 (PKN1) is a developmentally active regulator of cerebellar synaptic maturation by inhibiting AKT and the neurogenic transcription factor neurogenic differentiation factor-2 (NeuroD2). NeuroD2 is involved in glutamatergic synaptic maturation by regulating expression levels of various synaptic proteins. Here we aimed to study the effect of *Pkn1* knockout on AKT phosphorylation and NeuroD2 levels in the hippocampus and the subsequent expression levels of the NeuroD2 targets and AMPAR subunits: glutamate receptor 1 (GluA1) and GluA2/3. We show that PKN1 is expressed throughout the hippocampus. Interestingly, not only postnatal but also adult hippocampal phospho-AKT and NeuroD2 levels were significantly elevated upon *Pkn1* knockout. Postnatal and adult $Pkn1^{-/-}$ hippocampi showed enhanced expression of the AMPAR subunit GluA1, particularly in area CA1. Surprisingly, GluA2/3 levels were not different between both genotypes. In addition to higher protein levels, we also found an enhanced GluA1 content in the membrane fraction of postnatal and adult $Pkn1^{-/-}$ animals, while GluA2/3 levels remained unchanged. This points toward a very specific regulation of GluA1 expression and/or trafficking by the novel PKN1-AKT-NeuroD2 axis. Considering the important role of GluA1 in hippocampal development as well as the pathophysiology of several disorders, ranging from Alzheimer's, to depression and schizophrenia, our results validate PKN1 for future studies into neurological disorders related to altered AMPAR subunit expression in the hippocampus.

Keywords: AMPA receptor, PKN1, NeuroD2, GluA1, hippocampus

OPEN ACCESS

Edited by:
Joerg Striessnig, University of Innsbruck, Austria

Reviewed by:
Tommaso Patriarchi, University of Zurich, Switzerland
Alexandra Pinggera, MRC Laboratory of Molecular Biology (LMB), United Kingdom

****Correspondence:***
Gabriele Baier-Bitterlich
gabriele.baier-bitterlich@i-med.ac.at
Stephanie zur Nedden
stephanie.zur-Nedden@i-med.ac.at

Received: *11 December 2020*
Accepted: *18 January 2021*
Published: *05 February 2021*

Citation:
Safari MS, Obexer D, Baier-Bitterlich G and zur Nedden S (2021) PKN1 Is a Novel Regulator of Hippocampal GluA1 Levels. Front. Synaptic Neurosci. 13:640495. doi: 10.3389/fnsyn.2021.640495

Abbreviations: AMPAR, α-amino-3-hydroxy-5-methyl-4-isoxazolepropionic acid receptor; Aβ, amyloid-β; BSA, bovine serum albumin; Cgc, cerebellar granule cells; CA1-3, Cornu Ammonis area 1-3; DG, dentate gyrus; EAAT3, excitatory amino acid transporter 3; GABA, gamma aminobutyric acid subtype A ($GABA_A$) receptors; GAPDH, glyceraldehyde 3-phosphate dehydrogenase; GluA1, glutamate receptor 1; GluA2/3, glutamate receptor 2/3; HCl, hydrochloric acid; NeuroD2, neurogenic differentiation factor-2; NMDA, N-methyl-D-aspartate; PFA, paraformaldehyde; PF, Parallel fiber; P, postnatal day; PBS, phosphate buffered saline; pAKT, phosphorylated AKT; PMSF, phenylmethylsulfonyl fluoride; PKN1, Protein kinase N1; PSD-95, postsynaptic density protein 95; SDS, Sodium dodecyl sulfate; NaF, sodium fluoride; SNAP-25, Synaptosomal-Associated Protein 25 kDa; TBS-T, Tris buffered saline with Tween 20; VAMP2, vesicle associated membrane protein 2; VGlut 1 and 2, vesicular glutamate transporter 1 and 2.

INTRODUCTION

We have recently identified the serine threonine kinase Protein kinase N1 (PKN1) as a developmentally active enzyme regulating axon growth, presynaptic maturation, and synapse formation in the Parallel fiber (PF)-forming cerebellar granule cells (Cgc). We discovered that PKN1-mediated AKT inhibition during critical stages of PF-maturation results in a reduction of the transcription factor neurogenic differentiation factor-2 (NeuroD2) and a subsequent increase in presynaptic specifications along PF. Consequently, *Pkn1* knockout leads to AKT hyperactivation as well as enhanced NeuroD2 protein levels, which results in a defective developmental synapse formation, a degeneration of cerebellar neurons and ataxia in adult animals (zur Nedden et al., 2018). *Neurod2* knockout animals exhibit morphological and physiological defects in various brain regions, including thalamocortical connections, hippocampal synaptogenesis, axonal guidance of callosal axons, development of amygdalar nuclei, cortical fasciculation, targeted axogenesis of compact fiber tracts as well as differences in intrinsic excitability during cortical development (Olson et al., 2001; Lin et al., 2005; Ince-Dunn et al., 2006; Wilke et al., 2012; Bormuth et al., 2013; Chen et al., 2016). Accordingly, disruption of NeuroD2 function has been implicated in several neurodevelopmental, neuropsychiatric and mood disorders, such as autism (Runge et al., 2020), depression (Bagot et al., 2016), schizophrenia (Spellmann et al., 2017), or epilepsy (Sega et al., 2019).

One striking role of NeuroD2 is the regulation of the subunit expression levels of ionotropic AMPARs. AMPARs are assemblies of four core subunits termed GluA1-4 (Collingridge et al., 2009), which mediate fast excitatory neurotransmission. Developmentally- and activity-regulated changes in AMPAR number and subunit composition are crucial for excitatory synapse formation, synaptic plasticity and neuronal circuit formation (Henley and Wilkinson, 2016). *Neurod2*$^{-/-}$ animals showed a marked reduction of GluA2/3 protein levels in layer IV of the cortex and cultured *Neurod2*$^{-/-}$ neurons had a decreased surface expression of GluA1 and GluA2 subunits (Ince-Dunn et al., 2006). The effect of NeuroD2 was AMPAR-specific, since N-methyl-D-aspartate (NMDA) or kainate receptor expression was not affected. This implies that NeuroD2 controls the expression of AMPAR subunit proteins and/or proteins involved in the trafficking and surface retention of AMPARs. Indeed, NeuroD2 has been shown to regulate several genes involved in vesicle and receptor trafficking (Olson et al., 2001; Molnár and Molnár, 2006). Besides AMPARs, NeuroD2 has also been shown to regulate vesicular glutamate transporter 1 (VGlut1) (Bormuth et al., 2013), Synaptosomal-Associated Protein 25 kDa (SNAP-25) (Messmer et al., 2012), and postsynaptic density protein 95 (PSD-95) expression levels (Wilke et al., 2012).

The aim of this study was to analyze if PKN1 regulates hippocampal AKT and NeuroD2 and subsequently the protein levels and membrane-association of several synaptic proteins, with particular focus on GluA1 and GluA2/3.

MATERIALS AND METHODS

Animals

The generation of *Pkn1* knockout mice (*Pkn1*$^{-/-}$ mice) has been described previously (Quétier et al., 2016). Animals were kindly provided by P. Parker and A. Cameron. Mice were backcrossed to C57BL/6N for more than 10 generations. C57BL/6N wildtype (WT) and C57BL/6N *Pkn1*$^{-/-}$ animals were derived from the same heterozygous crosses and then bred separately, but kept under same housing and experimental conditions in the same room. C57BL/6N were derived from Jackson Laboratory. Animals younger than postnatal day (P)12 were killed by decapitation and animals older than P12 were killed by cervical dislocation. For studies in adult animals only 2–5 month old males were used.

Preparation of Hippocampal Sections

After decapitation, brains were quickly removed, hemispheres were separated and a small block of tissue containing cortical and hippocampal regions was fixed in 4% PFA for 4–5 h.

Cryosections

After washing in PBS, hemispheres were incubated in 30% sucrose for a minimum of 24 h, embedded in optimal cutting temperature compound (Carl Roth) and stored at −80°C until analysis. 20 μm thick sagittal sections were cut with a cryostat (CM1950, Leica), transferred onto lysine-coated coverslips (Thermo Scientific) and allowed to dry for a minimum of 2 h at 37°C for further analysis or stored at −20°C. Sections were used for *in situ* hybridization.

Free-Floating Sections

After fixation hemispheres were washed in PBS and 50 μm thick sagittal sections were prepared with a Vibratome (VT1200S, Leica). Sections were used for antibody staining as described below.

In situ Hybridization

In situ hybridization was performed employing the RNAScope Fluorescent Multiplex Assay kit (ACDBio). Cryosections from WT mice were dried (30 min, 60°C) and fixed for an additional 15 min in 4% PFA. Sections were processed as per manufacturers instructions, embedded in Mowiol (Sigma-Aldrich) and imaged with a widefield microscope (Axio, Axiocam 305, Zeiss and DMi8, Leica). The mean intensity of mRNA transcript was analyzed in Fiji (Schindelin et al., 2012) by tracing the dentate gyrus (DG) granule cell layer, CA3 and CA1 pyramidal cell layers. For comparability between experiments data was expressed as fold of the mean intensity of the DG for each experiment.

Immunofluorescence Staining and Analysis of Mean GluA1 Intensity

Free-floating sections were subjected to antigen retrieval (10 mM sodium citrate, pH 6.0, 10 min at 100°C), washed in PBS, permeabilized (0.3% Triton-X-100, 45 min), blocked (10% goat serum, 2% BSA, 1 h), and primary antibodies (diluted in 0.1%

Triton-X-100, 1% BSA, 5% goat serum in PBS) were added at room temperature overnight. After washing in PBS + 0.05% Tween for 30 min, sections were incubated with secondary antibodies (goat-anti rabbit Alexa-488 and goat anti-mouse Alexa-555) and Hoechst (8 μM) for 3 h at room temperature. After thorough washing in PBS + 0.05% Tween for 45 min, sections were placed on a microscope slide and embedded in Mowiol. To ensure comparable results all samples were processed on the same day using the same solutions. Images were taken with a widefield microscope (Axio, Axiocam 305, Zeiss), using the same exposure time, or a confocal microscope (SP8, Leica), using the same laser intensity for WT and *Pkn1*$^{-/-}$ GluA1 stainings. Mean GluA1 intensity was analyzed in widefield images with Fiji by placing and measuring four 150 × 150 μm squares throughout CA1 stratum radiatum and oriens.

Preparation of Subcellular Fractions and Western Blotting

For extraction of the detergent-soluble cytosolic and detergent-insoluble membrane fraction we followed the protocol of Takagi et al. (2010). Hippocampi of P12 or adult animals were carefully homogenized in TRIS-Buffer (20 mM Tris/HCl pH 7.5, 1 mM NaF, 10 μg/ml aprotinin, 10 μg/ml leupeptin, 50 μM PMSF, 2 mM sodium orthovanadate) and kept on ice for 30 min. After centrifugation (3000 × *g*, 10 min, 4°C) the supernatant was collected as cytosolic fraction. Pellets were washed once in TRIS-Buffer and resuspended in membrane extraction buffer (0.5% NP-40, 0.1% deoxycholate, 0.1% Brij 35, 10 mM DTT, 50 μM PMSF). Samples were incubated at 4°C for 60 min with gentle agitation. After centrifugation (10730 × *g*, 5 min, RT) supernatants were collected and resuspended in 4xLaemmli buffer (8% SDS, 40% glycerol, 20% β-mercaptoethanol, 0.01% bromophenol blue, and 250 mM Tris HCl, pH 6.8), boiled at 95°C for 5 min and stored at −20°C.

For whole cell extracts hippocampi were carefully dissected out in ice cold PBS and protein extraction was performed as described previously (zur Nedden et al., 2018). Protein contents were measured with a BCA assay kit (Thermo Fisher Scientific) and 35–70 μg protein was loaded onto self-made 10% or 12.5% continuous polyacrylamide gels. Western blotting was performed as described earlier (zur Nedden et al., 2018). Primary antibodies were added overnight in 5% BSA in TBS-T at 4°C and secondary antibodies (Li-Cor, anti-mouse 680 nm and anti-rabbit 800 nm) were added for 90 min at room temperature in 5% Milk in TBS-T. Membranes were imaged and analyzed with an Odyssey Clx infrared imager (Li-Cor). Stripping was not performed, however, for gels in **Figures 3A,B** a second blot in the same order was done to probe for PKN1, which would have otherwise masked the weak GluA1 signal. The correct separation of both fractions was assessed with appropriate loading controls.

Antibodies

Clone numbers and RRID, where known, as well as catalog numbers (#) are provided in brackets. The following antibodies were from Cell signaling: AKT (40D4, #2920, RRID: AB_1147620), Na/K-ATPase (#3010, RRID: AB_2060983), GAPDH (D16H11, #5174, RRID: AB_10622025), phospho-AKT(T308) (D25E6, #13038, RRID: AB_2629447), PSD-95 (D27E11, #3450, RRID: AB_2292883 as well as 7E3, #36233, RRID: AB_2721262), Synapsin-1 (D12G5, #5297, RRID: AB_2616578), and VAMP2 (D601A, #13508, RRID: AB_2798240). VGlut1 (#48-2400, RRID: AB_2533843), goat anti-rabbit Alexa-488 (#A11070, RRID: AB_142134), and goat anti-mouse Alexa-555 (#A21425, RRID: AB_1500751) were purchased from Thermo Fisher Scientific. GluA1 (G-12, #sc-55509; RRID: AB_629532) and NeuroD2 (G-10, #sc-365896, RRID: AB_10843361) were from Santa Cruz. PKN1 (clone 49/PRK1, #610687, RRID: AB_398012) was from BD Transduction Laboratories. Actin (clone C4, #MAB1501, RRID: AB_2223041), VGlut2 (8G9.2, #ab79157, RRID: AB_1603114), tyrosine hydroxylase (#AB152, RRID: AB_390204), GluA2/3 (#AB1506, RRID: AB_90710), and $GABA_A$β2/3 (#MAB341, RRID: AB_2109419) were from Merck Millipore. Znt3 (#197 011, RRID: AB_2189665) was purchased from Synaptic Systems. The secondary antibodies for the Odyssey infrared Imager, IR680 LT mouse (#92668020, RRID: AB_10706161) and IR800CW (#92632211, RRID: AB_621843) were purchased from Li-Cor. $GABA_A$α4 was kindly provided by Gerald Obermair [a4N (1-14), (Hörtnagl et al., 2013)].

Statistics

All data is presented as individual *n*-values with mean ± S.E.M., with *n*-values referring to different animals. For comparison of two independent groups a two-tailed unpaired *t*-test was used, for comparison of three or more groups a one-way ANOVA with Tukey's multiple comparisons test was used and for comparison of two variables of two groups a two-way ANOVA was used. *P*-values smaller than 0.05 were considered as statistically significant. All analyses were performed in GraphPad prism 8.

RESULTS

PKN1 Is Highly Expressed Throughout the Hippocampal Formation and Regulates AKT Phosphorylation and NeuroD2 Levels in Juvenile and Adult Animals

Protein kinase N1 *in situ* hybridization revealed that PKN1 is abundantly expressed in the hippocampus in P10 old and adult animals. PKN1 mRNA was found in all hippocampal areas (**Figure 1A**). There was no difference in mean intensity levels between hippocampal layers in P10 old (mean intensity expressed as fold of DG mean intensity: 1 ± 00 for DG, 1.0 ± 0.08 for CA3, and 0.9 ± 0.01 for CA1, *n* = 3/genotype, $P > 0.05$, one way ANOVA, data not shown) or in adult animals (mean intensity expressed as fold of DG mean intensity: 1 for DG, 0.91 and 0.82 for CA3, 0.74 and 1.09 for CA1, *n* = 2/genotype, data not shown). Western blot analysis of WT whole cell hippocampal protein extracts revealed a significant reduction in PKN1 expression from P1 to P15 (**Figure 1B**) and a further decrease from P15 to adult animals (PKN1/Actin

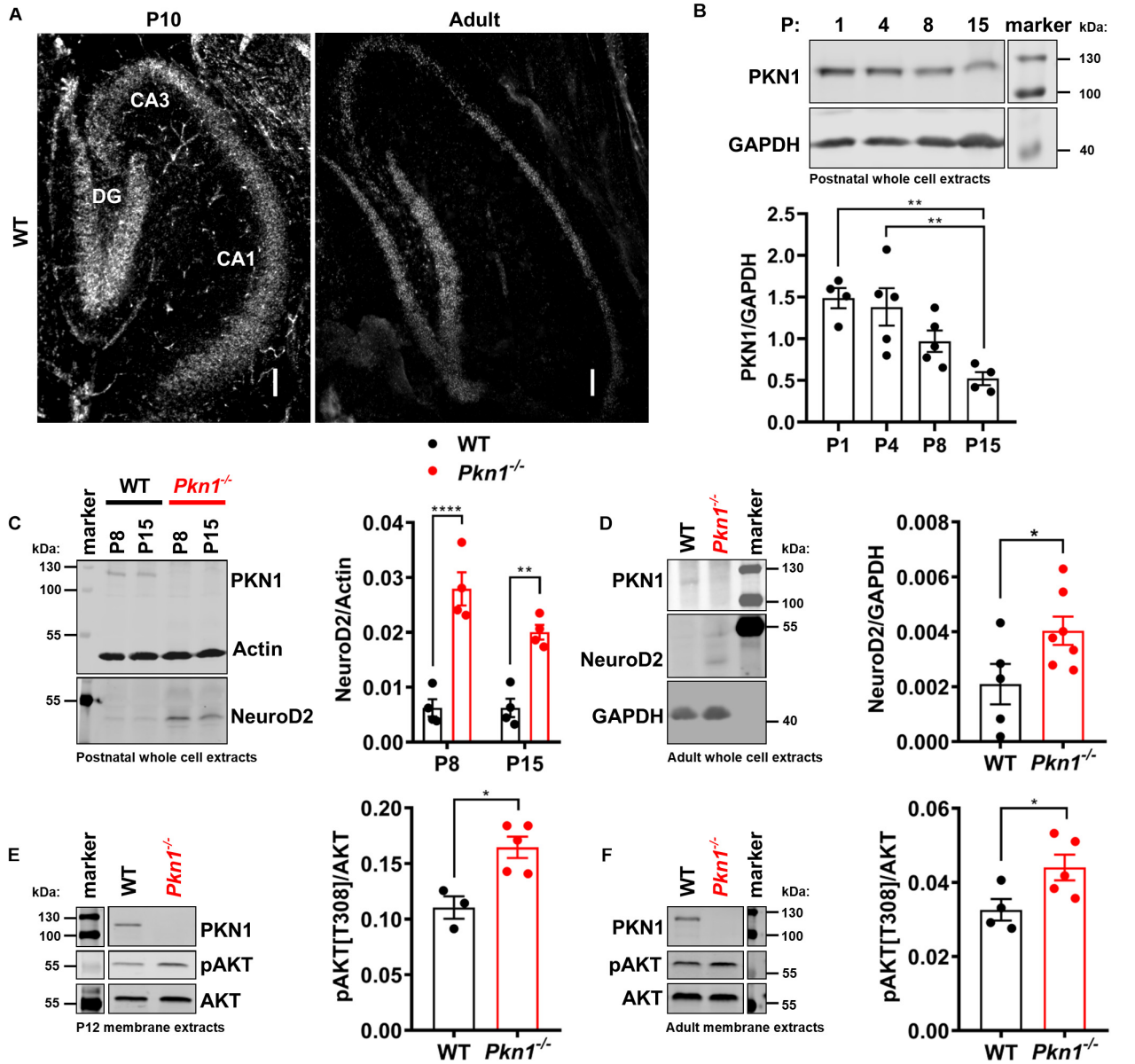

FIGURE 1 | PKN1 regulates AKT phosphorylation and NeuroD2 levels in postnatal and adult hippocampi. **(A)** P10 and adult hippocampal sections from WT animals were tested for PKN1 expression by *in situ* hybridization. Pictures are representative of 2–3 separate WT animals. Scale bar refers to 100 μm. **(B)** PKN1 expression levels from P1 to P15 old WT hippocampi were assessed by western blotting (**$P < 0.01$, one way ANOVA with Tukey's multiple comparisons test). **(C)** NeuroD2 expression in hippocampal whole cell protein extracts of P8 and P15 old WT and *Pkn1*$^{-/-}$ animals was assessed by western blotting (two way ANOVA: Interaction: $P = 0.0745$, Age: $P = 0.0747$, Genotype: $P < 0.0001$, Sidak's multiple comparisons test: P8: $P < 0.0001$, P15: $P = 0.0025$). **(D)** NeuroD2 expression in adult WT and *Pkn1*$^{-/-}$ hippocampal whole cells extracts (*$P = 0.0496$, unpaired *t*-test). **(E)** Hippocampi from P12 old WT and *Pkn1*$^{-/-}$ animals were separated into cytosolic and membrane fractions. Membrane extracts were probed for phosphorylated AKT[T308] (pAKT[T308]) and total AKT and the ratio was calculated (*$P = 0.0104$, unpaired *t*-test). **(F)** Membrane fractions of adult WT and *Pkn1*$^{-/-}$ animals were probed for pAKT[T308] and AKT (*$P = 0.045$, unpaired *t*-test). The markers in the representative blots in **(E,F)** are shown in separate lanes as samples were not directly next to the markers in the blots. Data is presented as individual *n*-values with mean ± S.E.M.

ratio was 0.026 ± 0.0007 for P15, $n = 3$, and 0.018 ± 0.0008 for adult WT animals, $n = 4$, **$P = 0.0011$, unpaired *t*-test, data not shown), suggesting an important role of PKN1 during postnatal development. The gross hippocampal morphology was not altered, and the layer thickness of all hippocampal layers was similar between both genotypes (**Supplementary Figures 1A,B**). The infrapyramidal mossy fiber projection was slightly enlarged upon *Pkn1* knockout (**Supplementary Figures 1A,B**). We did not detect aberrant sprouting of mossy fibers into the inner molecular layer of the DG in *Pkn1*$^{-/-}$ animals (**Supplementary Figure 1C**). We next tested the effect of *Pkn1* knockout on hippocampal AKT phosphorylation and NeuroD2 levels. In agreement with

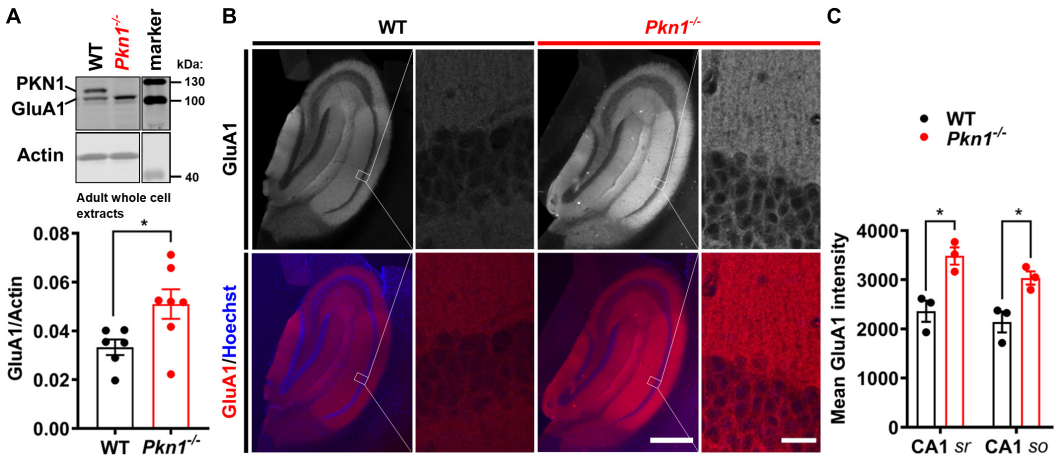

FIGURE 2 | Adult *Pkn1*$^{-/-}$ animals have enhanced GluA1 protein levels **(A)** Whole cell protein extracts from adult WT and *Pkn1*$^{-/-}$ hippocampi were prepared, probed for GluA1 and the ratio to the loading control actin was calculated (*P = 0.0321, unpaired t-test). The marker in the representative blot is shown in a separate lane as samples were not directly next to the marker in the blot. **(B)** Hippocampal GluA1 levels were further assessed by immunofluorescence staining. Pictures are representative of 3 animals/genotype. Scale bar in overview images refers to 500 μm and scale bar in high resolution inserts refers to 20 μm. **(C)** The mean intensity of hippocampal GluA1 levels from **(B)** was quantified in Fiji. CA1 *sr* refers to CA1 stratum radiatum, CA1 *so* refers to CA1 stratum oriens. (CA1 *sr* *P = 0.0156, unpaired t-test, CA1 *so* *P = 0.0233, unpaired t-test). All data is presented as individual n-values with mean ± S.E.M.

our earlier findings in the cerebellum hippocampal NeuroD2 levels in postnatal *Pkn1*$^{-/-}$ animals were strongly elevated at P8 and P15 (**Figure 1C**), suggesting that PKN1-mediated inhibition of NeuroD2 is important in various brain areas during development. Interestingly, we also observed an elevation of NeuroD2 levels in adult *Pkn1*$^{-/-}$ hippocampi, even though this was less pronounced than during development (**Figure 1D**). AKT is primarily activated at the plasma membrane, and subsequently exerts its role at the plasma membrane or several subcellular compartments (Ebner et al., 2017; Lučić et al., 2018). To investigate if *Pkn1* knockout results in enhanced AKT phosphorylation, we prepared detergent-soluble (cytosolic) and detergent-insoluble fractions (membrane-associated proteins) of P12 old and adult WT and *Pkn1*$^{-/-}$ hippocampi. The proper separation of fractions was assessed by appropriate loading controls. Importantly, the membrane-bound proteins Na^+/K^+-ATPase and PSD-95 were only found in the membrane extract (data not shown). We chose P12 as an intermediate age between P8 and P15. Interestingly we found that particularly membrane-associated AKT was hyper-phosphorylated upon *Pkn1* knockout in P12 old (**Figure 1E**) as well as in adult animals (**Figure 1F**). AKT phosphorylation in the cytosolic fraction was not different at both ages (**Supplementary Figure 2**). This contrasts with our findings in the cerebellum, where neither phospho-AKT nor NeuroD2 levels were different in adult animals, and suggests that this novel PKN1-AKT-NeuroD2 axis remains relevant for hippocampal function in adult animals.

Pkn1$^{-/-}$ Hippocampi Have Higher GluA1 Levels

It has been previously reported that *Neurod2* knockout animals show a reduction in GluA1, GluA2/3, PSD-95, and VGlut1 expression (Ince-Dunn et al., 2006; Wilke et al., 2012; Bormuth et al., 2013). Additionally, NeuroD2 controls the excitatory/inhibitory synaptic balance in pyramidal cortical neurons (Chen et al., 2016). We therefore probed adult hippocampal extracts from WT and *Pkn1*$^{-/-}$ animals for a series of glutamatergic, gamma aminobutyric acid (GABA)-ergic and general synaptic markers (**Figure 2** and **Table 1**). Adult *Pkn1*$^{-/-}$ animals showed significantly elevated GluA1 levels (**Figure 2A**), however, GluA2/3 levels were not different between both genotypes (**Table 1**). Immunofluorescence staining revealed that GluA1 levels in *Pkn1*$^{-/-}$ animals were particularly elevated in the CA1 area of the hippocampus (**Figures 2B,C**). Another protein significantly upregulated upon *Pkn1* knockout was VGlut 1 (**Table 1**), however, several other synaptic proteins (such as PSD-95, Znt-3, $GABA_A$ receptor subtypes, see **Table 1**) were not, or only moderately affected by *Pkn1* knockout (such as SNAP-25).

Pkn1$^{-/-}$ Animals Show Higher Membrane-Associated GluA1 Levels

In addition to decreased protein expression levels, *Neurod2* knockout neurons showed a reduction in GluA1 surface expression (Ince-Dunn et al., 2006). To test if hippocampal extracts from young postnatal and adult animals show differences in cytosolic and membrane-associated GluA1 levels, we analyzed the detergent-soluble cytosolic [contains soluble cytosolic enzymes, as well as, due to the low g force and centrifugation duration transport/recycling vesicles (Jeppesen et al., 2014)] and the detergent-insoluble membrane protein fraction (contains plasma membrane-associated proteins and vesicles) of P12 old and adult WT and *Pkn1*$^{-/-}$ hippocampi by immunoblotting. While we did not find a significant difference in the GluA1 content in the cytosolic fraction of P12 old animals (**Figure 3A**), we observed a significant increase in GluA1 levels in the membrane fraction of *Pkn1*$^{-/-}$ hippocampi (**Figure 3B**). In

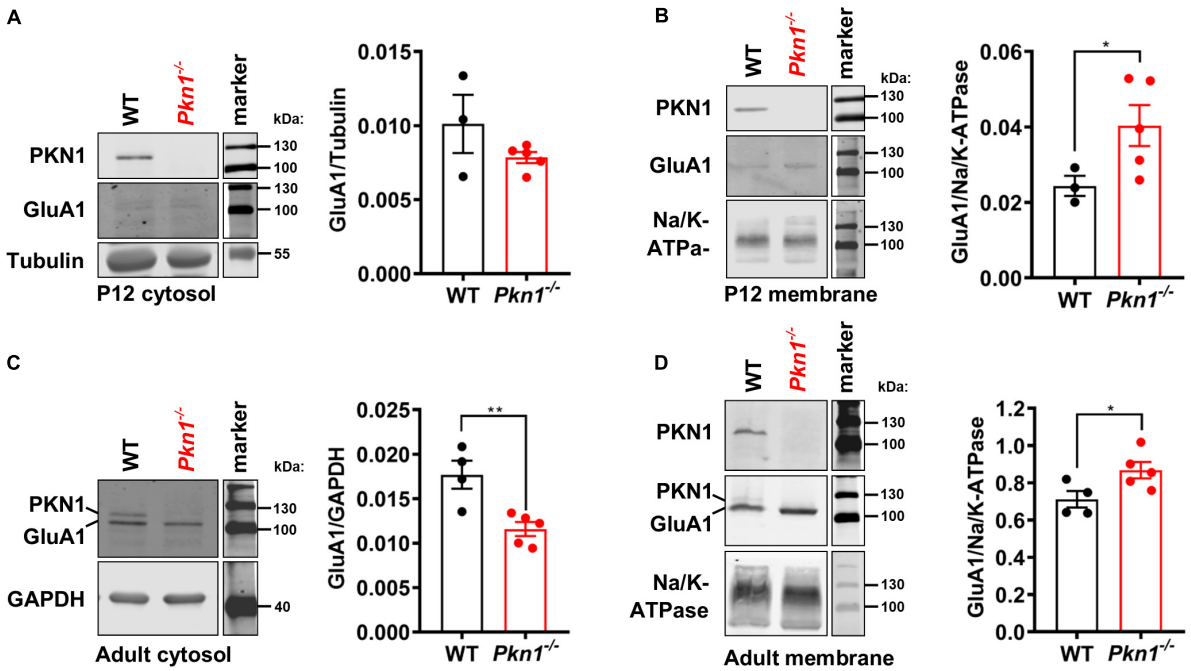

FIGURE 3 | Postnatal and adult *Pkn1*$^{-/-}$ animals show enhanced membrane-association of GluA1. **(A)** The detergent-soluble cytosolic fraction of extracts prepared from P12 old WT and *Pkn1*$^{-/-}$ hippocampi was probed for the loading control Tubulin and GluA1 ($P = 0.393$, unpaired *t*-test). **(B)** The detergent-insoluble membrane fraction of extracts prepared from P12 old WT and *Pkn1*$^{-/-}$ hippocampi was probed for the loading control Na^+/K^+-ATPase and GluA1 (*$P = 0.0416$, unpaired *t*-test). **(C)** The detergent-soluble cytosolic fraction of extracts prepared from adult WT and *Pkn1*$^{-/-}$ hippocampi was probed for the loading control GAPDH and GluA1 (**$P = 0.0075$, unpaired *t*-test). **(D)** The detergent-insoluble membrane fraction of extracts prepared from adult WT and *Pkn1*$^{-/-}$ hippocampi was probed for the loading control Na^+/K^+-ATPase and GluA1 (*$P = 0.0430$, unpaired *t*-test). All data is presented as individual *n*-values with mean ± S.E.M. Images of PKN1 in **(A,B)** were derived from a second blot, loaded in the same order. All markers in the representative blots are shown in separate lanes as samples were not next to the markers in the blots.

accordance with our results in adult animals we found that VGlut1 and VGlut2 were significantly elevated upon *Pkn1* knockout in P12 old animals (**Table 1**). In adult *Pkn1*$^{-/-}$ animals GluA1 levels in the cytosolic fraction were significantly reduced (**Figure 3C**) while the membrane-associated content of GluA1 was significantly increased (**Figure 3D**). This suggests that besides differences in protein levels, GluA1 trafficking might be affected by *Pkn1* knockout in adult animals. GluA2/3 levels in the cytosolic or membrane fraction of P12 old and adult animals were not different between both genotypes (**Table 1**). Likewise, the content of several other synaptic proteins (such as PSD-95, synapsin 1, Znt-3, $GABA_A$ Receptor subtypes) was not significantly affected by *Pkn1* knockout (**Table 1**).

DISCUSSION

Here we establish PKN1 as a novel regulator of hippocampal GluA1 levels and GluA1 membrane/cytosol trafficking. Mechanistically we provide evidence that phosphorylated AKT and the transcription factor NeuroD2, which has been shown to regulate AMPAR subunit expression and membrane insertion (Olson et al., 2001; Ince-Dunn et al., 2006; Molnár and Molnár, 2006; Wilke et al., 2012), are strongly elevated upon *Pkn1* knockout in postnatal and adult animals.

We have recently shown that PKN1 regulates NeuroD2 levels in an AKT-dependent manner, thereby controlling the precise balance between axonal growth and presynaptic differentiation in early postnatal cerebellar development (zur Nedden et al., 2018). Accordingly, *Pkn1*$^{-/-}$ animals showed AKT hyperphosphorylation, higher NeuroD2 protein levels and subsequently a decrease in presynaptic specifications accompanied by a defective PF-Purkinje cell synapse formation. The fact that the hippocampus shows a similar dysregulation of AKT and NeuroD2 upon *Pkn1* knockout suggests that the tight control of postnatal AKT/NeuroD2 levels by PKN1 constitutes a general and important regulatory mechanism in the development of several brain areas. However, we also observed significantly increased AKT phosphorylation and NeuroD2 levels in adult *Pkn1*$^{-/-}$ hippocampi. This contrasts our results obtained in the cerebellum, where neither phospho-AKT nor NeuroD2 were elevated in adult animals, and shows that PKN1-mediated AKT and NeuroD2 inhibition remains important in the hippocampus beyond postnatal development.

Pkn1$^{-/-}$ animals showed a specific elevation of hippocampal GluA1 levels, while GluA2/3 levels as well as other NeuroD2 downstream targets such as PSD-95 were not altered. These findings are surprising, since it was reported that NeuroD2 controls both, thalamocortical GluA1/2/3 (Ince-Dunn et al., 2006) as well as hippocampal PSD-95 expression and mossy

TABLE 1 | Expression levels of synaptic proteins in whole cell, cytosolic, and membrane fractions of P12 and adult animals.

	WT (*n*-number)	*Pkn1*$^{-/-}$ (*n*-number)	*P*-Value
Adult whole cell extract			
GluA2/3/Actin	0.145 ± 0.017 (6)	0.145 ± 0.014 (7)	0.836
VGlut1	0.003 ± 0.0005 (6)	0.005 ± 0.001 (7)	0.038 (*)
SNAP-25/Actin	0.572 ± 0.024 (6)	0.638 ± 0.020 (7)	0.0596
PSD-95/Actin	0.018 ± 0.002 (6)	0.019 ± 0.002 (7)	0.775
Znt-3/Actin	0.008 ± 0.002 (6)	0.011 ± 0.001 (7)	0.255
$GABA_A\beta2/3$/Actin	0.000718 ± 0.002 (3)	0.00054 ± 0.0002 (4)	0.587
Tyrosine Hydroxylase/Actin	0.139 ± 0.026 (4)	0.128 ± 0.005 (4)	0.682
P12 membrane/cytosolic fraction			
VGlut1/Na/K-ATPase	0.000492 ± 0.0005 (3)	0.001075 ± 0.00009 (4)	0.012 (*)
VGlut2/Na/K-ATPase	0.456 ± 0.0798 (5)	0.641 ± 0.001 (4)	0.041 (*)
Membrane: GluA2/3/Actin$^{\#}$	0.037 ± 0.0066 (5)	0.038 ± 0.0052 (4)	0.815
Cytosol: GluA2/3/Actin	0.003 ± 0.0005 (5)	0.003 ± 0.0007 (4)	0.856
PSD-95/Na/K-ATPase	0.085 ± 0.007 (5)	0.103 ± 0.004 (4)	0.079
$GABA_A\alpha4$/Na/K-ATPase	0.101 ± 0.011 (5)	0.100 ± 0.022 (4)	0.968
$GABA_A\beta2/3$/Na/K-ATPase	0.288 ± 0.043 (5)	0.391 ± 0.0345 (4)	0.117
Znt-3/Na/K-ATPase	0.002 ± 0.0004 (5)	0.003 ± 0.0002 (4)	0.124
Adult membrane/cytosolic fraction			
Membrane: GluA2/3/Actin$^{\#}$	0.2484 ± 0.025 (4)	0.2886 ± 0.037 (5)	0.425
Cytosol: GluA2/3/Actin	0.0218 ± 0.003 (4)	0.019 ± 0.003 (5)	0.537
PSD-95/Na/K-ATPase	28.6 ± 1.65 (4)	25.3 ± 1.80 (5)	0.226
$GABA_A\alpha4$/Na/K-ATPase	0.37 ± 0.03 (4)	0.34 ± 0.04 (5)	0.517
Znt-3/Na/K-ATPase	0.44 ± 0.03 (4)	0.49 ± 0.02 (5)	0.114
VAMP2/Na/K-ATPase	6.07 ± 0.83 (4)	7.30 ± 0.91 (5)	0.362
Synapsin 1/Na/K-ATPase	3.45 ± 0.22 (4)	4.08 ± 0.27 (5)	0.122

Whole cell extracts and cytosolic extracts are expressed in relation to the loading controls actin. Membrane extracts are expressed in relation to the loading control Na^+/K^+-ATPase. $^{\#}$Since GluA2/3 and Na^+/K^+-ATPase had the same size (∼100 kDa) and host species we used Actin as a loading control for both fractions. (*) $P < 0.05$, unpaired t-test.

fiber-CA3 synaptic maturation (Wilke et al., 2012). We have not analyzed mossy fiber-CA3 synapse number or CA3-specific PSD-95 expression, which might reveal more subtle differences between WT and *Pkn1*$^{-/-}$ animals. Nevertheless, a possible explanation for these apparent differences might be that PKN1 controls NeuroD2 activity in a very targeted manner. This is further supported by the fact that only very few synaptic downstream targets of NeuroD2 were elevated upon *Pkn1* knockout, such as VGlut1. Besides PKN1, the activity/expression of NeuroD2 is controlled by other basic helix-loop-helix factors (neurogenin 1) (Lin et al., 2004), various signaling cascades and posttranslational modifications, such as phosphorylation (Dennis et al., 2019). Furthermore, calcium acts as an activity-dependent regulator of NeuroD2 (Ince-Dunn et al., 2006). Therefore, an altered synaptic protein content could have a secondary influence on NeuroD2-mediated transcription upon *Pkn1* knockout. Moreover, there are brain area-specific differences in the effect of NeuroD2 overexpression versus deficiency on synaptic maturation. In the cerebellum, our (zur Nedden et al., 2018) and an earlier report (Yang et al., 2009) showed that in Cgc, NeuroD2 levels are high during axonal/dendritic growth, where it prevents premature synaptogenesis but need to be degraded in order to drive presynaptic maturation of PFs. On the contrary, *Neurod2*-deficient Cgc functionally integrate into the cerebellar circuit (Pieper et al., 2019), suggesting that NeuroD2 is redundant and/or not essential for correct PF-synaptic maturation. In the hippocampus, however, *Neurod2*-deficiency results in reduced expression of PSD-95 and a defective CA3-mossy fiber synapse formation, establishing NeuroD2 as a non-redundant and important regulator of synaptic maturation in that brain area (Wilke et al., 2012). Therefore, *Neurod2*-deficiency versus overactivation might not be directly comparable and result in diverse outcomes in different brain areas.

Besides higher GluA1 levels we also found an elevated GluA1 content in the membrane fraction of postnatal and adult *Pkn1*$^{-/-}$ animals. While we cannot deduce if this is related to enhanced surface expression of GluA1, it points toward enhanced transportation of GluA1 to the plasma membrane. Additionally, adult animals showed significantly lower GluA1 levels in the cytosolic fraction (which contains transport/recycling vesicles), suggesting a potential difference in GluA1 trafficking. NeuroD2 regulates different populations of target genes in the embryonal and postnatal cortex (Guzelsoy et al., 2019). Therefore, the difference between P12 and adult animals might lie in differently regulated downstream genes involved in receptor trafficking and surface retention (Olson et al., 2001; Molnár and Molnár, 2006). Alternatively, PKN1 itself might be involved in the regulation of GluA1 trafficking and/or degradation. PKN1 belongs to the PKC superfamily, and PKCs as well as PKA are well known for their roles in phosphorylation of GluA1, thereby regulating channel conductance, internalization, and receptor trafficking (Buonarati et al., 2019).

The functional implications of enhanced GluA1 protein levels/membrane-association in *Pkn1*$^{-/-}$ animals remain to be elucidated. AMPAR subunit composition determines the conductance, trafficking and calcium permeability of these receptors. Calcium permeability is mainly conferred by the presence or absence of the calcium impermeable GluA2 subunit. Hippocampal AMPAR primarily exist as either GluA1/2 (>80%) or GluA2/3 heteromers (Lu et al., 2009). Calcium permeable (CP) GluA1 homomers are particularly abundant in immature CA1 synapses (Stubblefield and Benke, 2010; Henley and Wilkinson, 2016; Benke and Traynelis, 2019). Although less frequent, CP-AMPAR are also found in adult neurons where they contribute to the induction of long term potentiation, to homeostatic synaptic scaling and potentially long term depression (Henley and Wilkinson, 2016). Defects in the regulation of AMPAR subunit expression, assembly, trafficking, and membrane insertion are

closely linked to psychiatric conditions as well as cognitive decline and neurodegenerative diseases, including Alzheimer's disease (Walsh and Selkoe, 2007; Whitcomb et al., 2015) or mood disorders (Naylor et al., 1996; Martinez-Turrillas et al., 2002; Du et al., 2008). Addition of only 5% homomeric GluA1 to the pool of AMPAR in hippocampal neurons can already account for a conductance change (Guire et al., 2008). Therefore, it would be interesting to study if and how extrasynaptic and synaptic AMPAR composition is affected by the enhanced GluA1 protein levels upon *Pkn1* knockout.

Recently it was shown that PKN1 promotes synapse maturation by inhibiting type I metabotropic glutamate receptor-dependent long term depression through regulation of excitatory amino acid transporter 3 (EAAT3) in area CA1 (Yasuda et al., 2020). Knockdown of PKN1 to 1/10th of WT levels results in immature synaptic transmission, more silent synapses and fewer spines with shorter postsynaptic densities in juvenile CA1 neurons. While there might be a difference between our complete *Pkn1* knockout animals and the reduction of PKN1 to 1/10th of WT animals, this report would imply that (1) enhanced protein levels of GluA1 and VGlut1 are not due to an increase in synapse number, which is further supported by unchanged PSD-95 levels, but rather reflect a selective increase in protein concentrations of these specific synaptic proteins; and (2) enhanced GluA1 expression might not be translated into a higher synaptic content of GluA1 homomers. However, authors did not analyze AMPAR subunit composition or adult *Pkn1* knockdown animals, and considering EAAT3 expression drops during development (Bjørn-Yoshimoto and Underhill, 2016), electrophysiological properties in adult $Pkn1^{-/-}$ or *Pkn1* knockdown animals might reveal differences in AMPAR function and/or composition.

Taken together our data validate PKN1 as a novel regulator of hippocampal GluA1 levels and GluA1 membrane-association, thereby providing a new tool to understand the functional consequences of this specific subunit as well as raising the potential for the modulation of GluA1 as a possible strategy for therapeutic intervention. In that context, it is worth noting that non-specific PKN1 inhibitors have already been validated for safe use in humans (Shibuya et al., 2005; Cohen et al., 2017) and the development of specific PKN1 inhibitors is a focus of cancer research (Ostrovskyi et al., 2016).

DATA AVAILABILITY STATEMENT

The raw data supporting the conclusions of this article will be made available by the authors, without undue reservation.

ETHICS STATEMENT

Ethical review and approval was not required for the animal study because they are classified as *in vitro*. However, we are monitored and certified (FELASA) by Austrian authorities with regard to animal handling, cervical dislocation, and decapitation. Every effort was taken to minimize the number of animals used. Written informed consent was obtained from the owners for the participation of their animals in this study.

AUTHOR CONTRIBUTIONS

SzN, MS, and GB-B developed the study concept and design. MS, DO, and SzN performed immunoblotting, immunohistochemistry, and analysis of all data. MS and SzN prepared the figures. SzN and GB-B supervised the project and wrote the manuscript with critical input from all authors. All authors approved the manuscript.

FUNDING

This study was supported by the Austrian Science Fund (FWF)-funded projects: T1091 and P31085.

ACKNOWLEDGMENTS

We thank L. Krimbacher and M. Klose for technical assistance.

SUPPLEMENTARY MATERIAL

The Supplementary Material for this article can be found online at: https://www.frontiersin.org/articles/10.3389/fnsyn.2021.640495/full#supplementary-material

REFERENCES

Bagot, R. C., Cates, H. M., Purushothaman, I., Lorsch, Z. S., Walker, D. M., Wang, J., et al. (2016). Circuit-wide transcriptional profiling reveals brain region-specific gene networks regulating depression susceptibility. *Neuron* 90, 969–983. doi: 10.1016/j.neuron.2016.04.015

Benke, T., and Traynelis, S. F. (2019). AMPA-type glutamate receptor conductance changes and plasticity: still a lot of noise. *Neurochem. Res.* 44, 539–548. doi: 10.1007/s11064-018-2491-1

Bjørn-Yoshimoto, W. E., and Underhill, S. M. (2016). The importance of the excitatory amino acid transporter 3 (EAAT3). *Neurochem. Int.* 98, 4–18. doi: 10.1016/j.neuint.2016.05.007

Bormuth, I., Yan, K., Yonemasu, T., Gummert, M., Zhang, M., Wichert, S., et al. (2013). Neuronal basic helix-loop-helix proteins Neurod2/6 regulate cortical commissure formation before midline interactions. *J. Neurosci.* 33, 641–651. doi: 10.1523/JNEUROSCI.0899-12.2013

Buonarati, O. R., Hammes, E. A., Watson, J. F., Greger, I. H., and Hell, J. W. (2019). Mechanisms of postsynaptic localization of AMPA-type glutamate receptors and their regulation during long-term potentiation. *Sci. Signal.* 12:eaar6889. doi: 10.1126/scisignal.aar6889

Chen, F., Moran, J. T., Zhang, Y., Ates, K. M., Yu, D., Schrader, L. A., et al. (2016). The transcription factor NeuroD2 coordinates synaptic innervation and cell intrinsic properties to control excitability of cortical pyramidal neurons. *J. Physiol.* 594, 3729–3744. doi: 10.1113/JP271953

Cohen, S. B., Tanaka, Y., Mariette, X., Curtis, J. R., Lee, E. B., Nash, P., et al. (2017). Long-term safety of tofacitinib for the treatment of rheumatoid arthritis up to 8.5 years: integrated analysis of data from the global clinical trials. *Ann. Rheum. Dis.* 76, 1253–1262. doi: 10.1136/annrheumdis-2016-210457

Collingridge, G. L., Olsen, R. W., Peters, J., and Spedding, M. (2009). A nomenclature for ligand-gated ion channels. *Neuropharmacology* 56, 2–5. doi: 10.1016/j.neuropharm.2008.06.063

Dennis, D. J., Han, S., and Schuurmans, C. (2019). bHLH transcription factors in neural development, disease, and reprogramming. *Brain Res.* 1705, 48–65. doi: 10.1016/j.brainres.2018.03.013

Du, J., Creson, T. K., Wu, L.-J., Ren, M., Gray, N. A., Falke, C., et al. (2008). The role of hippocampal GluR1 and GluR2 receptors in manic-like behavior. *J. Neurosci.* 28, 68–79. doi: 10.1523/JNEUROSCI.3080-07.2008

Ebner, M., Lučić, I., Leonard, T. A., and Yudushkin, I. (2017). PI(3,4,5)P3 engagement restricts Akt activity to cellular membranes. *Mol. Cell* 65, 416–431.e416. doi: 10.1016/j.molcel.2016.12.028

Guire, E. S., Oh, M. C., Soderling, T. R., and Derkach, V. A. (2008). Recruitment of calcium-permeable AMPA receptors during synaptic potentiation is regulated by CaM-kinase I. *J. Neurosci.* 28, 6000–6009. doi: 10.1523/jneurosci.0384-08.2008

Guzelsoy, G., Akkaya, C., Atak, D., Dunn, C. D., Kabakcioglu, A., Ozlu, N., et al. (2019). Terminal neuron localization to the upper cortical plate is controlled by the transcription factor NEUROD2. *Sci. Rep.* 9:19697. doi: 10.1038/s41598-019-56171-x

Henley, J. M., and Wilkinson, K. A. (2016). Synaptic AMPA receptor composition in development, plasticity and disease. *Nat. Rev. Neurosci.* 17, 337–350. doi: 10.1038/nrn.2016.37

Hörtnagl, H., Tasan, R. O., Wieselthaler, A., Kirchmair, E., Sieghart, W., and Sperk, G. (2013). Patterns of mRNA and protein expression for 12 GABAA receptor subunits in the mouse brain. *Neuroscience* 236, 345–372. doi: 10.1016/j.neuroscience.2013.01.008

Ince-Dunn, G., Hall, B. J., Hu, S. C., Ripley, B., Huganir, R. L., Olson, J. M., et al. (2006). Regulation of thalamocortical patterning and synaptic maturation by NeuroD2. *Neuron* 49, 683–695. doi: 10.1016/j.neuron.2006.01.031

Jeppesen, D. K., Hvam, M. L., Primdahl-Bengtson, B., Boysen, A. T., Whitehead, B., Dyrskjøt, L., et al. (2014). Comparative analysis of discrete exosome fractions obtained by differential centrifugation. *J. Extracell. Vesicles* 3:25011. doi: 10.3402/jev.v3.25011

Lin, C.-H., Hansen, S., Wang, Z., Storm, D. R., Tapscott, S. J., and Olson, J. M. (2005). The dosage of the neuroD2 transcription factor regulates amygdala development and emotional learning. *Proc. Natl. Acad. Sci. U.S.A.* 102, 14877–14882. doi: 10.1073/pnas.0506785102

Lin, C.-H., Stoeck, J., Ravanpay, A. C., Guillemot, F., Tapscott, S. J., and Olson, J. M. (2004). Regulation of neuroD2 expression in mouse brain. *Dev. Biol.* 265, 234–245. doi: 10.1016/j.ydbio.2003.08.027

Lu, W., Shi, Y., Jackson, A. C., Bjorgan, K., During, M. J., Sprengel, R., et al. (2009). Subunit composition of synaptic AMPA receptors revealed by a single-cell genetic approach. *Neuron* 62, 254–268. doi: 10.1016/j.neuron.2009.02.027

Lučić, I., Rathinaswamy, M. K., Truebestein, L., Hamelin, D. J., Burke, J. E., and Leonard, T. A. (2018). Conformational sampling of membranes by Akt controls its activation and inactivation. *Proc. Natl. Acad. Sci. U.S.A.* 115, E3940–E3949. doi: 10.1073/pnas.1716109115

Martinez-Turrillas, R., Frechilla, D., and Del Río, J. (2002). Chronic antidepressant treatment increases the membrane expression of AMPA receptors in rat hippocampus. *Neuropharmacology* 43, 1230–1237. doi: 10.1016/S0028-3908(02)00299-X

Messmer, K., Shen, W. B., Remington, M., and Fishman, P. S. (2012). Induction of neural differentiation by the transcription factor neuroD2. *Int. J. Dev. Neurosci.* 30, 105–112. doi: 10.1016/j.ijdevneu.2011.12.006

Molnár, Z., and Molnár, E. (2006). Calcium and NeuroD2 control the development of thalamocortical communication. *Neuron* 49, 639–642. doi: 10.1016/j.neuron.2006.02.012

Naylor, P., Stewart, C. A., Wright, S. R., Carl, A., Pearson, R., and Reid, I. C. (1996). Repeated ECS induces GluR1 mRNA but not NMDAR1A-G mRNA in the rat hippocampus. *Mol. Brain Res.* 35, 349–353. doi: 10.1016/0169-328X(95)00264-S

Olson, J. M., Asakura, A., Snider, L., Hawkes, R., Strand, A., Stoeck, J., et al. (2001). NeuroD2 Is necessary for development and survival of central nervous system neurons. *Dev. Biol.* 234, 174–187. doi: 10.1006/dbio.2001.0245

Ostrovskyi, D., Rumpf, T., Eib, J., Lumbroso, A., Slynko, I., Klaeger, S., et al. (2016). Tofacitinib and analogs as inhibitors of the histone kinase PRK1 (PKN1). *Future Med. Chem.* 8, 1537–1551. doi: 10.4155/fmc-2016-0132

Pieper, A., Rudolph, S., Wieser, G. L., Götze, T., Mießner, H., Yonemasu, T., et al. (2019). NeuroD2 controls inhibitory circuit formation in the molecular layer of the cerebellum. *Sci. Rep.* 9:1448. doi: 10.1038/s41598-018-37850-7

Quétier, I., Marshall, J. J. T., Spencer-Dene, B., Lachmann, S., Casamassima, A., Franco, C., et al. (2016). Knockout of the PKN family of Rho effector kinases reveals a non-redundant role for PKN2 in developmental mesoderm expansion. *Cell Reports* 14, 440–448. doi: 10.1016/j.celrep.2015.12.049

Runge, K., Mathieu, R., Bugeon, S., Lafi, S., Beurrier, C., Sahu, S., et al. (2020). Disruption of the transcription factor NEUROD2 causes an autism syndrome via cell-autonomous defects in cortical projection neurons. *bioRxiv* [Preprint]. doi: 10.1101/296889

Schindelin, J., Arganda-Carreras, I., Frise, E., Kaynig, V., Longair, M., Pietzsch, T., et al. (2012). Fiji: an open-source platform for biological-image analysis. *Nat. Methods* 9, 676–682. doi: 10.1038/nmeth.2019

Sega, A. G., Mis, E. K., Lindstrom, K., Mercimek-Andrews, S., Ji, W., Cho, M. T., et al. (2019). De novo pathogenic variants in neuronal differentiation factor 2 (NEUROD2) cause a form of early infantile epileptic encephalopathy. *J. Med. Genet.* 56:113. doi: 10.1136/jmedgenet-2018-105322

Shibuya, M., Hirai, S., Seto, M., Satoh, S., and Ohtomo, E. (2005). Effects of fasudil in acute ischemic stroke: results of a prospective placebo-controlled double-blind trial. *J. Neurol. Sci.* 238, 31–39. doi: 10.1016/j.jns.2005.06.003

Spellmann, I., Riedel, M., Städtler, J., Zill, P., Obermeier, M., Cerovecki, A., et al. (2017). Associations of NEUROD2 polymorphisms and change of cognitive dysfunctions in schizophrenia and schizoaffective disorder after eight weeks of antipsychotic treatment. *Cogn. Neuropsychiatry* 22, 280–297. doi: 10.1080/13546805.2017.1322502

Stubblefield, E. A., and Benke, T. A. (2010). Distinct AMPA-type glutamatergic synapses in developing rat CA1 hippocampus. *J. Neurophysiol.* 104, 1899–1912. doi: 10.1152/jn.00099.2010

Takagi, H., Hsu, C.-P., Kajimoto, K., Shao, D., Yang, Y., Maejima, Y., et al. (2010). Activation of PKN mediates survival of cardiac myocytes in the heart during ischemia/reperfusion. *Circulation Res.* 107, 642–649. doi: 10.1161/CIRCRESAHA.110.217554

Walsh, D. M., and Selkoe, D. J. (2007). Aβ Oligomers – a decade of discovery. *J. Neurochem.* 101, 1172–1184. doi: 10.1111/j.1471-4159.2006.04426.x

Whitcomb, D. J., Hogg, E. L., Regan, P., Piers, T., Narayan, P., Whitehead, G., et al. (2015). Intracellular oligomeric amyloid-beta rapidly regulates GluA1 subunit of AMPA receptor in the hippocampus. *Sci. Rep.* 5:10934. doi: 10.1038/srep10934

Wilke, S. A., Hall, B. J., Antonios, J. K., Denardo, L. A., Otto, S., Yuan, B., et al. (2012). NeuroD2 regulates the development of hippocampal mossy fiber synapses. *Neural. Dev.* 7:9. doi: 10.1186/1749-8104-7-9

Yang, Y., Kim, A. H., Yamada, T., Wu, B., Bilimoria, P. M., Ikeuchi, Y., et al. (2009). A Cdc20-APC ubiquitin signaling pathway regulates presynaptic differentiation. *Science* 326, 575–578. doi: 10.1126/science.1177087

Yasuda, H., Yamamoto, H., Hanamura, K., Mehruba, M., Kawamata, T., Morisaki, H., et al. (2020). PKN1 promotes synapse maturation by inhibiting mGluR-dependent silencing through neuronal glutamate transporter activation. *Commun. Biol.* 3:710. doi: 10.1038/s42003-020-01435-w

zur Nedden, S., Eith, R., Schwarzer, C., Zanetti, L., Seitter, H., Fresser, F., et al. (2018). Protein kinase N1 critically regulates cerebellar development and long-term function. *J. Clin. Invest.* 128, 2076–2088. doi: 10.1172/JCI96165

Conflict of Interest: The authors declare that the research was conducted in the absence of any commercial or financial relationships that could be construed as a potential conflict of interest.

Copyright © 2021 Safari, Obexer, Baier-Bitterlich and zur Nedden. This is an open-access article distributed under the terms of the Creative Commons Attribution License (CC BY). The use, distribution or reproduction in other forums is permitted, provided the original author(s) and the copyright owner(s) are credited and that the original publication in this journal is cited, in accordance with accepted academic practice. No use, distribution or reproduction is permitted which does not comply with these terms.

frontiers in Synaptic Neuroscience

ORIGINAL RESEARCH
published: 19 February 2021
doi: 10.3389/fnsyn.2021.634412

Phenotypic Characterization and Brain Structure Analysis of Calcium Channel Subunit $\alpha_2\delta$-2 Mutant (Ducky) and $\alpha_2\delta$ Double Knockout Mice

*Stefanie M. Geisler[1,2], Ariane Benedetti[1†], Clemens L. Schöpf[1], Christoph Schwarzer[3], Nadia Stefanova[4], Arnold Schwartz[5] and Gerald J. Obermair[1,6]**

[1]Institute of Physiology, Medical University Innsbruck, Innsbruck, Austria, [2]Department of Pharmacology and Toxicology, Center for Molecular Biosciences, University of Innsbruck, Innsbruck, Austria, [3]Department of Pharmacology, Medical University Innsbruck, Innsbruck, Austria, [4]Division of Neurobiology, Department of Neurology, Medical University Innsbruck, Innsbruck, Austria, [5]Department of Pharmacology and Systems Physiology, College of Medicine, University of Cincinnati, Cincinnati, OH, United States, [6]Division Physiology, Karl Landsteiner University of Health Sciences, Krems an der Donau, Austria

OPEN ACCESS

Edited by:
Sigismund Huck,
Medical University of Vienna, Austria

Reviewed by:
Gary Stephens,
University of Reading,
United Kingdom
Ricardo Felix,
Instituto Politécnico Nacional de México (CINVESTAV), Mexico

***Correspondence:**
Gerald J. Obermair
gerald.obermair@kl.ac.at

†Present address:
Ariane Benedetti
Institute of Experimental Neuroregeneration, Spinal Cord Injury and Tissue Regeneration Center Salzburg (SCI-TReCS), Paracelsus Medical University, Salzburg, Austria

Received: 27 November 2020
Accepted: 11 January 2021
Published: 19 February 2021

Citation:
Geisler SM, Benedetti A, Schöpf CL, Schwarzer C, Stefanova N, Schwartz A and Obermair GJ (2021) Phenotypic Characterization and Brain Structure Analysis of Calcium Channel Subunit $\alpha_2\delta$-2 Mutant (Ducky) and $\alpha_2\delta$ Double Knockout Mice. Front. Synaptic Neurosci. 13:634412. doi: 10.3389/fnsyn.2021.634412

Auxiliary $\alpha_2\delta$ subunits of voltage-gated calcium channels modulate channel trafficking, current properties, and synapse formation. Three of the four isoforms ($\alpha_2\delta$-1, $\alpha_2\delta$-2, and $\alpha_2\delta$-3) are abundantly expressed in the brain; however, of the available knockout models, only $\alpha_2\delta$-2 knockout or mutant mice display an obvious abnormal neurological phenotype. Thus, we hypothesize that the neuronal $\alpha_2\delta$ isoforms may have partially specific as well as redundant functions. To address this, we generated three distinct $\alpha_2\delta$ double knockout mouse models by crossbreeding single knockout ($\alpha_2\delta$-1 and -3) or mutant ($\alpha_2\delta$-2/ducky) mice. Here, we provide a first phenotypic description and brain structure analysis. We found that genotypic distribution of neonatal litters in distinct $\alpha_2\delta$-1/-2, $\alpha_2\delta$-1/-3, and $\alpha_2\delta$-2/-3 breeding combinations did not conform to Mendel's law, suggesting premature lethality of single and double knockout mice. Notably, high occurrences of infant mortality correlated with the absence of specific $\alpha_2\delta$ isoforms ($\alpha_2\delta$-2 > $\alpha_2\delta$-1 > $\alpha_2\delta$-3), and was particularly observed in cages with behaviorally abnormal parenting animals of $\alpha_2\delta$-2/-3 cross-breedings. Juvenile $\alpha_2\delta$-1/-2 and $\alpha_2\delta$-2/-3 double knockout mice displayed a waddling gate similar to ducky mice. However, in contrast to ducky and $\alpha_2\delta$-1/-3 double knockout animals, $\alpha_2\delta$-1/-2 and $\alpha_2\delta$-2/-3 double knockout mice showed a more severe disease progression and highly impaired development. The observed phenotypes within the individual mouse lines may be linked to differences in the volume of specific brain regions. Reduced cortical volume in ducky mice, for example, was associated with a progressively decreased space between neurons, suggesting a reduction of total synaptic connections. Taken together, our findings show that $\alpha_2\delta$ subunits differentially regulate premature survival, postnatal growth, brain development, and behavior, suggesting specific neuronal functions in health and disease.

Keywords: brain disease, CACNA2D, cortical lamination, over-grooming, stereology, voltage-gated calcium channels

INTRODUCTION

In the central nervous system (CNS) the second messenger calcium regulates a variety of pivotal functions including neurotransmitter release, gene regulation, and synaptic plasticity (Nanou and Catterall, 2018). In healthy neurons, the entry of calcium is tightly controlled by voltage-gated calcium channels (VGCCs). Neuronal VGCCs are hetero-multimeric protein complexes consisting of a transmembrane pore-forming α_1 subunit, which conducts Ca^{2+} upon membrane depolarization, and cytoplasmic β and extracellular $\alpha_2\delta$ subunits (Catterall, 2000; Zamponi et al., 2015). In vertebrates, four genes (Cacna2d1-4) encode four $\alpha_2\delta$ subunit isoforms ($\alpha_2\delta$-1 to -4), which are post-translationally processed into highly glycosylated α_2 and δ peptides linked to each other by disulfide bonds (De Jongh et al., 1990; Sandoval et al., 2004; Calderon-Rivera et al., 2012). The distinct isoforms share a protein sequence identity of approximately 60% ($\alpha_2\delta$-3 vs. $\alpha_2\delta$-4), 55% ($\alpha_2\delta$-1 vs. $\alpha_2\delta$-2), and 30% ($\alpha_2\delta$-1/$\alpha_2\delta$-2 vs. $\alpha_2\delta$-3/$\alpha_2\delta$-4; Klugbauer et al., 1999; Qin et al., 2002). Nevertheless, all $\alpha_2\delta$ subunit isoforms display a related topology with a rather similar domain structure (reviewed in Geisler et al., 2015; Dolphin, 2018).

Studies on the mRNA expression of the four $\alpha_2\delta$ subunit isoforms have revealed a partially differential and partially overlapping distribution in distinct organs including the heart, skeletal muscle, and pancreas (Ellis et al., 1988; Klugbauer et al., 1999; Gao et al., 2000; Arikkath and Campbell, 2003; Mastrolia et al., 2017). Notably, three out of four isoforms ($\alpha_2\delta$-1, $\alpha_2\delta$-2, and $\alpha_2\delta$-3) are abundantly expressed in the brain (Klugbauer et al., 1999; Cole et al., 2005; Schlick et al., 2010; Geisler et al., 2019). $\alpha_2\delta$-4 is the major isoform of retinal photoreceptor cells (Knoflach et al., 2013) and its expression in other CNS neurons seems negligible (Schlick et al., 2010). $\alpha_2\delta$-1 has gained particular attention during the past years, as it contains a high-affinity binding site for the widely used anti-allodynic and anti-epileptic drugs gabapentin (Neurontin) and pregabalin (Lyrica; Gee et al., 1996; Gong et al., 2001; Fuller-Bicer et al., 2009).

Heterologous co-expression studies uncovered all $\alpha_2\delta$ subunit isoforms as potent modulators of calcium currents and membrane trafficking (Felix et al., 1997; Klugbauer et al., 1999; Hobom et al., 2000; Geisler et al., 2015; Dolphin, 2018). Beyond this principal role, isoform-specific synaptic functions have been proposed for $\alpha_2\delta$-1 (Eroglu et al., 2009; Tong et al., 2017; Brockhaus et al., 2018; Chen et al., 2018; Risher et al., 2018), $\alpha_2\delta$-2 (Fell et al., 2016; Tedeschi et al., 2016; Geisler et al., 2019), $\alpha_2\delta$-3 (Pirone et al., 2014), and $\alpha_2\delta$-4 (Wang et al., 2017; Kerov et al., 2018). Despite this increasing number of examples for $\alpha_2\delta$-isoform specificity, it is unclear why distinct brain regions express three distinct isoforms (Cole et al., 2005; Schlick et al., 2010; Geisler et al., 2019). Moreover, all three neuronal isoforms could rescue a major defect in glutamatergic synapse formation observed in a cellular triple loss-of-function model (Schoepf et al., 2019).

Existing mouse models with spontaneous mutations and targeted deletions for all individual $\alpha_2\delta$ subunits enabled novel insights into their potential functional redundancy as well as specificity: deletion of $\alpha_2\delta$-1 impaired synaptic NMDA receptor (NMDAR) recruitment, excitatory synaptogenesis, and spine morphology (Risher et al., 2018), and LTP-associated learning and memory (Zhou et al., 2018). Loss of full-length $\alpha_2\delta$-2 in four distinct mouse strains with naturally occurring mutations [ducky: Barclay et al., 2001; Brodbeck et al., 2002; entla: Brill et al., 2004; and ducky(2J): Donato et al., 2006] and targeted deletions in Cacna2d2 (Ivanov et al., 2004) induced epilepsy, dyskinesia, cerebellar atrophy, and high mortality in juvenile mice. $\alpha_2\delta$-3 knockout mice display altered pain processing (Neely et al., 2010), abnormal hearing (Pirone et al., 2014), anxiety-like behavior (Landmann et al., 2018a), and sensory cross-activation (Neely et al., 2010; Landmann et al., 2018b). Finally, distinct mouse strains with spontaneous mutations (Wycisk et al., 2006) and targeted deletions (Wang et al., 2017; Kerov et al., 2018) in the $\alpha_2\delta$-4 isoform are associated with retinal degeneration and night blindness. Notably, of these existing mouse models, only $\alpha_2\delta$-2 mutant mice display a highly decreased life span associated with severe neurological disease. This is insofar surprising as neurological disorders have been linked to aberrant $\alpha_2\delta$ subunit expression in humans: mutations in CACNA2D1 and CACNA2D2 with epilepsy (Chioza et al., 2009; Edvardson et al., 2013; Pippucci et al., 2013; Vergult et al., 2015; Butler et al., 2018), CACNA2D3 is a potential risk gene for autism spectrum disorders (Iossifov et al., 2012; De Rubeis et al., 2014), and all three genes with schizophrenia (Purcell et al., 2014; Moons et al., 2016; reviewed in Ablinger et al., 2020).

Thus, to provide novel insights into $\alpha_2\delta$ subunit specificity and redundancy we generated three double knockout mouse models by cross-breeding $\alpha_2\delta$-1, $\alpha_2\delta$-2, or $\alpha_2\delta$-3 mouse strains. Here, we provide a phenotypic characterization and brain structure analysis of these newly established $\alpha_2\delta$ double knockout models. Moreover, we also included the characterization of adult ducky mice (8–10-weeks), as previous analyzes were restricted to young mice (∼1 month). Our findings underpin the general importance of $\alpha_2\delta$ subunits for normal development and survival. However, we further show that loss of distinct combinations of two isoforms differentially affected postnatal growth and brain development, which was associated with neurological disease including gait abnormalities, repetitive behaviors, and the occurrence of seizure symptoms. Together, these data support the conclusion that $\alpha_2\delta$ subunits are critically involved in both, partially redundant and also isoform-specific functions.

MATERIALS AND METHODS

Breeding and Genotyping Procedures

Generation and Breeding of $\alpha_2\delta$ Double Knockout Mice

Double knockout mice lacking different combinations of $\alpha_2\delta$ subunit isoforms (referred to as $\alpha_2\delta$-1/-3, $\alpha_2\delta$-1/-2, and $\alpha_2\delta$-2/-3 double knockout mice) were generated by cross-breeding

previously established conventional mouse models with targeted deletions or spontaneous mutations for individual $\alpha_2\delta$ subunits.

$\alpha_2\delta$-1 Knockout Mouse (Referred to as $\alpha_2\delta$-1$^{-/-}$)

The $\alpha_2\delta$-1 knockout mouse was generated by introducing a targeted insertion into exon 2 of the Cacna2d1 gene (Fuller-Bicer et al., 2009). The original strain was maintained in a C57BL/6 genetic background and knockout mice displayed a cardiovascular phenotype (Fuller-Bicer et al., 2009) as well as deficits in mechanical and cold sensitivity (Patel et al., 2013). For our breeding colony, mice heterozygous for $\alpha_2\delta$-1 were kept in a mixed 129J × C57BL/6N background. Male knockout animals could not be used for breeding double knockout mice due to their reduced life span caused by their progressing diabetic phenotype (Mastrolia et al., 2017).

$\alpha_2\delta$-2 Null Mouse (Referred to as $\alpha_2\delta$-2 Mutant, $\alpha_2\delta$-2$^{du/du}$ or Ducky Mice)

The naturally occurring ducky mutation was formerly discovered in a breeding stock at the Jackson Laboratory (Bar Harbor, ME, USA; Snell, 1955). It represents a spontaneous recessive autosomal mutation that is linked to a genomic rearrangement within the Cacna2d2 gene resulting in loss of the full-length protein (Cacna2d2^{du}). Previous studies showed that affected homozygous mice display growth retardation, an ataxic waddling gate, paroxysmal dyskinesia, and absence epilepsy, as well as dysgenesis of selective regions of the CNS, especially of hindbrain structures including the brainstem and cerebellum (Snell, 1955; Meier, 1968; Brodbeck et al., 2002). The original strain was purchased from the Jackson Laboratory (strain: TKDU/DnJ, #000575: Bar Harbor, ME, USA) and carried a spontaneous tail kink mutation (tk) in repulsion with the ducky mutation (du). We backcrossed the mice into a C57BL/6N background for more than eight generations to eliminate the tail kink mutation and select for the ducky allele. We provided the Jackson Laboratory with these mice (backcrossed for three generations) as the original stock was lost (strain: B6N; TKDU-Myo5ad Cacna2d2du/J, #012889: Bar Harbor, ME, USA).

$\alpha_2\delta$-3 Knockout Mouse (Referred to as $\alpha_2\delta$-3$^{-/-}$)

The $\alpha_2\delta$-3 knockout mouse was generated and characterized by Deltagen (strain: B6.129P2-Cacna2d3tm1Dgen; San Mateo, CA, USA; Neely et al., 2010). Knockout was obtained by targeted insertion of a bacterial LacZ cassette into exon 15 of the Cacna2d3 gene, and a deletion of 11 base pairs (bp 1,521 to base 1,531), enabling concomitant expression of β galactosidase under the endogenous promoter (last accessed in January 2021[1]). Previous studies showed that $\alpha_2\delta$-3 knockout mice display hearing deficits (Pirone et al., 2014) as well as anxiety-like behavior (Landmann et al., 2018a). Mice for our breeding colony were provided by Jutta Engel (Saarland University, Germany) with the consent of the Jackson Laboratory (#005780: Bar Harbor, ME, USA), and backcrossed for more than eight generations into a C57BL/6N background.

$\alpha_2\delta$-1/-2, $\alpha_2\delta$-1/-3, and $\alpha_2\delta$-2/-3 double knockout mice and littermate controls were obtained by cross-breeding single knockout or heterozygous mice as described below [(see Results section: "Generation of $\alpha_2\delta$ Double Knockout Mice") and in Schoepf et al. (2019)]. Both $\alpha_2\delta$-2 and $\alpha_2\delta$-3 mice were backcrossed into a C57BL/6N background for more than 10 generations before double knockout breedings. Breedings for $\alpha_2\delta$-1/-2 and $\alpha_2\delta$-1/-3 double knockouts were maintained in a mixed 129J × C57BL/6N background ($\alpha_2\delta$-1) repeatedly crossed with C57BL/6N ($\alpha_2\delta$-2 or $\alpha_2\delta$-3). Thus, progeny displayed either an agouti (129J) or black (C57BL/6N) fur color, the latter being primarily selected for breeding cages.

Animal Care and Husbandry

Animal procedures for wildtype BALB/c and $\alpha_2\delta$ mutant mice were performed at the Medical University Innsbruck following institutional guidelines that follow national and international laws and policies (European council directive for laboratory animals 2010/63/EU). The animal studies were reviewed and approved by the Austrian Federal Ministry of Education, Science and Research (formerly bmwfw), license numbers BMWFW-66.011/0113-WF/V/3b/2014 and BMWFW-66.011/0114-WF/V/3b/2014. Mouse numbers used for this project were regularly reported to the Austrian Federal Ministry of Education, Science, and Research. All mouse lines were maintained at the central animal facility in Innsbruck (ZVTA) under standard housing conditions with a temperature-and-humidity-controlled environment, food and water *ad libitum*, and a 12 h light/dark cycle. Generally, we tried to avoid unnecessary handling and resultant stress (see signs for stress and anxiety-related behavior below) by adapting distinct husbandry strategies for all or individual mouse lines as described below.

Breeding

Breeding cages normally consisted of one male and one female mouse, kept together for the entire breeding period. During the entire mating and breeding time, we preferentially monitored mice using undisturbed observation whenever applicable. Double knockout breeding cages were left completely undisturbed and cleaned/monitored by the researcher only. In addition to the standard cage equipment including wood bedding, nesting material, and polycarbonate houses, the environment of breeding cages was further enriched with cardboard houses (Ehret, Tulln, Austria). Whenever individual mice showed progressing signs of stress/anxiety-like behavior—obvious by head trembling, excessive grooming, and increased jumping/activity upon handling—we ensured the application of humane endpoints ($\alpha_2\delta$-2/-3; see "Results" section). To increase the postnatal survival chance of litters from $\alpha_2\delta$-2/-3 inter-crosses, pregnant females displaying anxiety-like behavior were kept together with BALB/c foster mothers.

Weaning

Offspring derived from $\alpha_2\delta$-2 and $\alpha_2\delta$-1/-3 breeding pairs was housed in the parental cage until weaning between postnatal days (P) 21–28. Thereafter, weanlings were kept in groups of same-sex littermates. Since the high mortality previously reported for $\alpha_2\delta$-2 mutant mice relates at least to some extent to difficulties in obtaining food and water (Snell, 1955), dried and moistened chow, as well as water gels (HydroGel, H007-

[1]http://www.informatics.jax.org/knockout _mice/deltagen/12_MolBio.html

70015; ssniff Spezialdiäten, Germany), were placed on the bottom of the cage twice a week. Moreover, in addition to the standard cage equipment described above, the environment of weaned $\alpha_2\delta$-2 mutant mice was further enriched with cardboard houses which also aided in accessing surplus food from wire bar lids at the top of the cage. In a previous study, we showed that the majority of $\alpha_2\delta$-1/-2 and $\alpha_2\delta$-2/-3 double knockout mice required the application of humane endpoints (Schoepf et al., 2019). The underlying cause was found to be most likely multifactorial, including infanticide, malnutrition associated with a poor general condition, and seizures linked to the loss of the $\alpha_2\delta$-2 isoform (Meier, 1968; Barclay et al., 2001). Thus, the health condition of individual animals was monitored and graded according to general signs of well-being including activity, body posture, and grooming behavior[2]. Accordingly, some $\alpha_2\delta$-1/-2 and $\alpha_2\delta$-2/-3 double knockout mice required the use of humane endpoints and experiments were done slightly before weaning age [between P17 and 21, referred to as juvenile (3–4-week-old) for simplicity] or at weaning age.

Genotyping of $\alpha_2\delta$ Mutant Mice

Mice were genotyped for the respective $\alpha_2\delta$ alleles at weaning age or when used for experiments. To this end, DNA was either extracted from 1 to 2 mm tail (until October 2014) or ear punch biopsies (after October 2014; according to BMWFW guidelines) by applying the HOTSHOT method (Truett et al., 2000). Two microliter of the resultant DNA solution was used as a template for PCR genotyping following the GoTaq Flexi protocol (Promega, Fitchburg, WI, USA) as described (Geisler et al., 2019). *$\alpha_2\delta$-1 genotyping*: genotyping for the Cacna2d1 gene was done by use of standard PCR conditions (annealing at 52°C for 30 s). Forward (F) and reverse (R) primers were: wildtype-F1: 5′-GAGCTTTCTTTCTTCTGATTCCAC-3′, mutant-F2: 5′-CTGCACGAGACTAGTGAGACG-3′, R: 5′-ACATTCTCAAGACTGTAGGCAGAG-3′. Expected band sizes were 346 bp for wildtype ($\alpha_2\delta$-$1^{+/+}$) and 635 bp for knockout ($\alpha_2\delta$-$1^{-/-}$) animals, respectively, and heterozygous mice showed both bands. *$\alpha_2\delta$-2 genotyping*: genotyping for the ducky mutation was adapted from Brodbeck et al. (2002) by use of standard PCR conditions (annealing at 56°C for 30 s). Primers F: 5′–ACCTATCAGGCAAAAGGACG-3′ and R: 5′-AGGGATGGTGATTGGTTGGA-3′ produced a fragment of 541 bp from a region duplicated in the ducky allele. Subsequent enzymatic digestion of the mutant allele with BspHI (New England Biolabs, Ipswich, MA, USA) and gel electrophoresis resulted in two fragments (286 and 273 bp) while the wildtype allele remained uncut. Heterozygous mice could be distinguished from $\alpha_2\delta$-2 mutant mice according to the relative intensities of the double band. To confirm the genomic duplication of the Cacna2d2 gene in potential $\alpha_2\delta$-2 null mice a previously established copy number (CN) qPCR assay was used (Schoepf et al., 2019). To this end, DNA was extracted from sacrificed putative knockout and littermate controls by incubating tissue biopsies at 55°C and 550 rpm in 250 µl Direct PCR Tail Lysis reagent (VWR, Radnor, PA, USA) containing 2.5 µl Protease K (20 mg/ml, Roche, Basel, Switzerland). Following overnight lysis, samples were heated to 85°C for 45 min at 550 rpm to inactivate Protease K, centrifuged at 16,800× *g* for 1 min and DNA content was measured using a NanoDrop 2000 Spectrophotometer (Thermo Fisher Scientific, Waltham, MA, USA). Samples were run in triplicates on a 7,500 fast real-time PCR machine (50 cycles). For each reaction 8 µl DNA (5 ng/µl), 1 µl FAM-dye labeled Cacna2d2 CN (ID: Mm00270662-cn) and 1 µl Vic-dye labeled transferrin receptor (Tfrc, #4458370) assay were added to 10 µl TaqMan Universal PCR Master Mix. All products were purchased from Thermo Fisher Scientific (Waltham, MA, USA; formerly Applied Biosystems). Relative gene expression of Cacna2d2 was calculated with the ΔΔCt-method ($2^{\Delta\Delta CT}$), were ΔCt was defined as Ct (gene) – Ct (Tfrc, housekeeping gene) and ΔΔCt as ΔCt (putative homozygous) – ΔCt (WT control). Thus, expected ratios between ducky and Tfrc alleles were 1 for wildtype samples (2 du alleles), 1.5 for heterozygous samples (3 du alleles), and 2 for homozygous ducky samples (4 du alleles). *$\alpha_2\delta$-3 genotyping*: wildtype-F1: 5′–TAGAAAAGATGCACTGGTCACCAGG-3′, mutant-F2: 5′-GGGCCAGCTCATTCCTCCCACTCAT-3′, R: 5′–GCAGAAGGCACATTGCCATACTCAC-3′ (annealing at 63°C for 30 s. Expected band sizes were 183 bp for wildtype ($\alpha_2\delta$-$3^{+/+}$) and 331 bp for knockout ($\alpha_2\delta$-$3^{-/-}$) animals, respectively, and heterozygous mice showed both bands.

Genotype Distribution in Neonatal Litters

Breeding cages containing female mice in their late gestation period were examined once daily for litters *via* undisturbed observation when applicable. Cages containing BALB/c foster mothers were not included in this analysis to avoid potential bias caused by differences in maternal caretaking abilities. Pups were considered newly born when first found, giving a 0–24-h variability in actual age (P0–1). Because some of the new-born pups obtained from $\alpha_2\delta$-2 and $\alpha_2\delta$-2/-3 breeding combinations were required at P1–P2 for another project (Schoepf et al., 2019), they were immediately marked on the paws using green tattoo ink (Ketchum Manufacturing Inc., Brockville, ON, Canada) and genotyped as described above. Alternatively, the number of pups was counted when first found (P0–1), followed by genotyping at weaning age or when needed for experiments (defined by scientific or humane endpoints, see above). In this case, subsequent analysis of expected and observed neonatal genotype ratios was solely done on litters with complete numbers at weaning. While this approach may give biased results in that it underestimates total numbers, excessive handling stress was reduced in the behaviorally sensitive $\alpha_2\delta$ mutant parenting animals. Statistical analysis for neonatal genotype ratios was calculated using the Chi-square test.

The General Assessment of Behavioral Phenotypes

Pre-weaning Development

Initial observations on phenotypes of $\alpha_2\delta$-1/-2, $\alpha_2\delta$-1/-3, and $\alpha_2\delta$-2/-3 double knockout pups were done once weekly when cleaning cages to reduce handling stress and increase survival chances of double knockout animals. General health was

[2]https://www.humane-endpoints.info

assessed by examining the grooming state of fur, posture, and responsiveness to handling. Since previous studies showed that ducky mice display ataxia and absence epilepsy (Snell, 1955; Meier, 1968; Brodbeck et al., 2002), we evaluated during handling if double knockout mice show symptoms which are typically associated with ataxic and epileptic conditions (wide based gait, whisker trembling during the behavioral arrest, loss of balance, falling to the side, and behavioral immobility; Ding et al., 2017; Van Erum et al., 2019).

Behavior in Breeding Pairs

It has been previously reported that $\alpha_2\delta$-3 single knockout mice display an increased anxiety-like behavior (Landmann et al., 2018a), and CACNA2D3 is mentioned as a potential risk gene for autism spectrum disorders (Iossifov et al., 2012; De Rubeis et al., 2014). During weekly cleaning of cages we therefore monitored $\alpha_2\delta$-1/-3 and $\alpha_2\delta$-2/-3 breeding pairs for obvious signs of stress, anxiety, and repetitive behavior (e.g., excessive grooming, head tremble, hesitant behavior when opening the cage, and increased jumping/activity upon handling; Bolivar et al., 2007; Kalueff et al., 2016; Landmann et al., 2018a; Lee et al., 2018).

Neuroanatomical Studies

Brain to Bodyweight Ratios

Body weights of juvenile or adult male mice were measured and subsequently mice were killed by CO_2, decapitated, and the whole brains were quickly removed from the skull and immediately weighted. Samples comprised anterior tissue starting from the olfactory bulb to the posterior brainstem including the medulla. The spinal cord was cut off at the cerebellum. The relative weight of brain, body, and brain to body ratios of single and double knockout mice were calculated as a percentage of control.

Brain Tissue Preparation

Fresh whole brains of single/double knockouts and respective controls were removed from the skull as described above. To obtain sagittal sections, hemispheres were separated with a cut along the midline and placed medial side down on a flat piece of thin acryl glass (Geisler et al., 2019). Subsequently, mounted hemispheres were submerged for 1 min in 2-methylbutan (Carl Roth, Karlsruhe, Germany) cooled to −50°C. Frozen samples were stored in sealed vials at −80°C until further processing and transferred to −20°C 1 day before sectioning. Brain samples were mounted on a tissue holder using Tissue-Tek® O.C.T.™ Compound (A. Hartenstein, Würzburg, Germany). Consecutive sections (20 μm) of one hemisphere were obtained with a cryotome (NX50: Histocom, Vienna, Austria), collected on polysine coated glass slides (Lactan, Graz, Austria), and stored at −20°C until further use.

Nissl Staining and Volumetric Analysis

Nissl staining of every 15th slide was performed as described previously (Paxinos and Franklin, 2012) with some modifications. Briefly, sections were air-dried at room temperature (RT) for 15 min and fixed with freshly prepared cold 4% paraformaldehyde (pF) diluted in 1× phosphate-buffered saline (PBS, pH 7.4) for 10 min. After dipping slides in 1× PBS and Milli-Q (MQ) water, sections were dehydrated by an ascending ethanol series, followed by immersion in *n*-butyl acetate (Roth, Germany) for 10 min. Thereafter, samples were rehydrated by a descending ethanol series ending in MQ water. Nissl staining was performed for 20 min *via* incubation in a staining solution consisting of 0.5% cresyl violet acetate (Sigma–Aldrich, St. Louis, MO, USA), three parts MQ water, 1.7 parts 1 M acetic acid, and 0.3 parts sodium acetate. Staining was stopped by shortly immersing sections in MQ water and excess solution was removed *via* an ascending ethanol series followed by clearing with *n*-butyl acetate. The slides were mounted with Eukitt (Christine Gröpl, Tulln, Austria) and air-dried for subsequent volumetric analysis. Representative images of distinct brain regions were recorded with a BX53 microscope (Olympus, Tokyo, Japan) equipped with an SC100 color-camera (Olympus, Tokyo, Japan) using a 10× 0.40 NA objective. 8-bit panorama pictures were created by scanning specimens with a 4× 0.16 NA objective and using the manual multiple image alignment (MIA) function in cellSens Dimension software (Olympus, Tokyo, Japan).

Volumetric analysis of individual brain regions of interest (ROIs) was obtained with a Nikon Eclipse E800 microscope equipped with a Nikon camera DXM1200 and a Stereo Investigator Software driving a motorized stage (Micro Bright Field Europe, Magdeburg, Germany). The first section analyzed comprised the hippocampus and corpus callosum (∼0.225 mm lateral to Bregma), and the last slide included the external capsule (∼3.725 mm lateral to Bregma). Thus, 7–11 sections were analyzed per animal by an experimenter blinded to the genotypes. To select brain structures of interest we used the following criteria: (1) clearly outlined on Nissl-stained sections; and/or (2) previously shown to express brain $\alpha_2\delta$ subunit isoforms ($\alpha_2\delta$-1, $\alpha_2\delta$-2, and $\alpha_2\delta$-3; Cole et al., 2005; Schlick et al., 2010); and/or (3) abnormal $\alpha_2\delta$ expression associated with consequences on structure or function (Brodbeck et al., 2002; Landmann et al., 2018b). Borders of the individual regions of interest were delineated according to the Mouse Brain Atlas (Paxinos and Franklin, 2012) and Redwine et al. (2003) as follows: cerebellum (rostral border: flocculus, middle cerebellar peduncle, and central lobule two—ventral border: dorsal to the fourth ventricle); corpus callosum (gray-white matter border); hippocampus (gray/white matter border with the fimbria/corpus callosum); whole hemisphere (rostral border: excluding olfactory bulbs—caudal border: medulla/spinal cord boundary at the most caudal point of the cerebellum); neocortex (dorsal border: corpus callosum—rostral border: rhinal fissure). The counter tracer option of the software was used to outline and measure the distinct ROIs on each slide. Subsequently, volumes were calculated according to the Cavalieri principle (Glaser and Glaser, 2000) by multiplying the sum of the areas with the uniform distance between the sections (15 × 20 μm).

Antibody Characterization

Cortical lamination was analyzed using well-established markers for transcription factors specifically expressed in distinct cortical layers (Nieto et al., 2004; Hevner, 2007; Molyneaux et al., 2007). Information on primary antibodies, which have been published

and validated previously as described below, is summarized in **Supplementary Table 1**. The chicken ovalbumin upstream promoter transcription factor-interacting protein 2 antibody (Ctip2, also known as Bcl11b; amino acid residues 1–150: MSRRKQGNPQHLSQRELITPEADHVEAAILEEDEGLEIEEPS GLGLMVGG) detects two bands at about 120 kD on Western blots prepared from Jurkat cell lysates (T-cell line), possibly representing two CTIP2 isoforms (Senawong et al., 2003). Immunofluorescence analysis performed in the present study displayed immunopositive neurons in cortex layers V and VI, as well as hippocampus and striatum. Thus, the staining patterns reported here are in accordance with numerous studies using the same antibody on mouse brain sections (Arlotta et al., 2005; Chen et al., 2005; Huang et al., 2012; Betancourt et al., 2014; Chang et al., 2018).

The Homeobox protein Cut Like 1 antibody (Cux1, also known as Cutl1 or CDP; amino acid residues 1111–1332, C-terminal) detects the full-length 200-kDa protein (p200) as well as several truncated isoforms (p55 and p75) on Western blots prepared from nuclear extracts isolated from testes (Kroll et al., 2011). Moreover, a band of 200-kDa was detected in whole-cell protein extracts isolated from lungs of wildtype, but not of Cux1 knockout mice (Luong et al., 2002). In the present study, immunopositive neurons were identified in cortex layers II–IV, replicating staining patterns shown previously for this antibody (Jaitner et al., 2016; Abdurakhmanova et al., 2017; Chang et al., 2018).

The T-box brain 1 antibody (Tbr1, to amino acid residues 50–150: SPLKKITRGMTNQSDTDNFPDSKDSPGDVQRSK LSPVLDGVSELRHSFDGS) was previously validated for chromatin immunoprecipitation (Chip) on embryonic mouse cortices, further revealing specific binding to the deep-layer transcription factor Fezf2 (McKenna et al., 2011). Immunofluorescence analysis performed in the present study displayed immunopositive neurons in cortex layer II–IV, V, and VI, thus replicating the staining pattern reported in previous studies using the same antibody on mouse brain sections (Favero et al., 2013; Betancourt et al., 2014).

Primary antibodies were detected by fluorochrome-conjugated secondary goat-anti-rabbit Alexa Fluor 488 (1:4,000; Thermo Fisher Scientific, Waltham, MA, USA; Cat# A-11094, RRID: AB_221544) and goat-anti-rat Alexa Fluor 594 (1:4,000; Thermo Fisher Scientific, Waltham, MA, USA; Cat# A-11007, RRID: AB_10561522). The specificity of secondary antibodies was verified on cryosections by omitting primary antibody incubation, which gave no signal.

Immunohistochemistry and Cortex Analysis

Consecutive slides of sagittal cryosections obtained from $\alpha_2\delta$-2 mutant ($\alpha_2\delta$-$2^{du/du}$) and control ($\alpha_2\delta$-$2^{+/+}$) mice were processed for immunohistochemistry as follows: brain slices were air-dried at RT for 15 min, surrounded with a hydrophobic liquid barrier (Roti®-Liquid Barrier Marker, colorless; Carl Roth, Karlsruhe, Germany) and fixed in 4% pF/4% sucrose in PBS for 5 min. Following washing with three changes of PBS and permeabilization in PBS containing 0.2% bovine serum albumin (BSA) and 0.2% Triton X-100 (PBS/BSA/Triton) for 5 min, samples were incubated in blocking solution (5% normal goat serum in PBS/BSA/Triton) for 2 h. Thereafter, slides were incubated in a blocking buffer containing the following combinations of primary antibodies (**Supplementary Table 1**): rat-anti-Ctip2 with rabbit-anti-Cux1 or rat-anti-Ctip2 and rabbit-anti-Tbr1, applied at 4°C overnight. After three subsequent washes in PBS/BSA/Triton for 10 min, primary antibodies were detected by fluorochrome-conjugated secondary goat-anti-rabbit Alexa Fluor 488 and goat-anti-rat Alexa Fluor 594, incubated for 2 h (diluted in blocking solution). Following three repeated washes with PBS/BSA/Triton for 30 min, cell nuclei were counterstained with Höchst33342 (1:10,000; #B2261: Sigma–Aldrich, St. Louis, MO, USA) for 5 min. Finally, slides were rinsed several times with PBS and MilliQ water, mounted with Vectashield (adult; #H-100: Szabo-Scandic, Vienna, Austria) or Fluoromount-G (juvenile; #0100-01: SouthernBiotech, Birmingham, AL, USA) and sealed with nail polish. All steps were done at RT except primary antibody incubation. For all subsequent analyzes described below, anatomically matched sections of $\alpha_2\delta$-2 mutant mice and control animals were analyzed by an experimenter blind to the genotype.

Cortical Length. 8-bit panorama pictures were recorded with a BX53 microscope (Olympus, Tokyo, Japan) equipped with a cooled CCD camera (XM10, Olympus, Tokyo, Japan) as follows: specimens counterstained with Höchst were scanned with a 4× 0.16 NA objective lens. The MIA function in cellSens Dimension software (Olympus, Tokyo, Japan) was applied for image stitching to comprise the entire cortex in one image. The anteroposterior distance was measured from olfactory bulb/frontal cortex boundary (rhinal fissure) to posterior cortex/superior colliculus boundary (Mairet-Coello et al., 2012) using MetaMorph software (Molecular Devices, Sunnyvale, CA, USA). Measurements of two to four consecutive sections per brain were averaged in MS excel (total of two to four ROIs per sample), and two (adult) and four (juvenile) brains per genotype were analyzed (total of 4–16 ROIs per genotype).

Cortical and Laminar Thickness. 14-bit color images from triple fluorescence-labeled sections were acquired from Ctip2 (red; layer V), Cux1 (green; layer II–IV), or Tbr1 (green; layer VI), and Höchst (blue) channels using a BX53 microscope (Olympus, Tokyo, Japan) equipped with an SC100 color-camera (Olympus, Tokyo, Japan) and a 10× 0.40 NA objective lense. After the acquisition, corresponding Ctip, Cux/Tbr, and Höchst images were superimposed in Adobe Photoshop CS6 and analyzed in MetaMorph (Molecular Devices, Sunnyvale, CA, USA) and MS Excel. To this end, whole cortical thickness (layer I–VI) and laminar thickness (layer I, II–IV, V, and VI) were measured at the level of somatosensory cortex at three anteroposterior positions randomly selected within a region spanning from the anterior part of the lateral ventricle to the rostral hippocampus. two samples (adult; wildtype and knockout) were excluded from the analysis of laminar thickness, as they were not at a comparable cortical level. Three measurements per section and two to four consecutive sections per brain were averaged (total of 6–12 ROIs per sample), and

two to three (adult) and four (juvenile) brains per genotype were analyzed (total of 12–48 ROIs per genotype). Finally, the absolute laminar thickness of individual layers of $\alpha_2\delta$-2 mutant mice was calculated as the percentage change to control.

Cell Density. Calculation of cell densities was done using ImageJ software (NIH[3]; Schneider et al., 2012) as follows: Ctip (red), Tbr (green), and Höchst (blue) images were superimposed and a region comprising the entire cortical area was drawn, as well as a selection for background subtraction. Subsequently, the individual color images were thresholded (Image > Adjust > Threshold) to solely include cells positive for the respective marker. Background mean intensity was measured in distinct channels and the ROI surrounding the cortex was transferred to the thresholded Höchst image. The watershed function (Process > Binary > Watershed) was used to separate single cell nuclei. Thus, using the "analyze particle function," thresholded cells exclusively within the cortical area were selected automatically as ROIs and counted (parameters: particle size: 0-infinity, excluding edges). ROIs were transferred to the Ctip/Tbr channel images and individual mean gray value intensities were measured in all three channels and further analyzed in MS Excel. Background subtractions for distinct channels were applied, providing the absolute number of positively stained cells. Cell numbers were then divided by the cortex area (mm^2) to quantify the cellular density as the number of cells per mm^2 cortex. The proportion of the following four categories was calculated as the percentage of $Höchst^+$ cells (total cells = neurons and non-neuronal cells): (1) $Ctip^-/Tbr^-/Höchst^+$ (layer I–IV neurons and non-neuronal cells); (2) $Ctip^+/Tbr^+/Höchst^+$ (layer V–VI neurons); (3) $Ctip^+/Tbr^-/Höchst^+$ (layer V neurons); (4) $Ctip^-/Tbr^+/Höchst^+$ (layer VI neurons). Measurements of 2-4 consecutive sections per brain were averaged in MS excel (total of two to four ROIs per sample), and two (adult) and four (juvenile) brains per genotype were analyzed (total of 12–48 ROIs per genotype).

Experimental Design and Statistical Analysis

According to the 3R principle, the minimum number of mice necessary for a statistical representative analysis was used. Humane endpoints and resultant experimental ages were chosen for the individual mouse lines according to the severity of the phenotype. Thus, research was primarily conducted on either juvenile (3–4-week-old; ducky, $\alpha_2\delta$-1/-2 and $\alpha_2\delta$-2/-3) or adult mice (8–13-week-old; ducky and $\alpha_2\delta$-1/-3). The utilized controls were wildtype, heterozygous, or single knockout for a given $\alpha_2\delta$ isoform and included in most cases littermates or age-matched individuals. Mouse numbers, genotypes, and ages used for individual experiments are given in the figure legends. Where indicated, investigators were blinded during experiments and analyzes (see respective sections above). Data are depicted either as bar graphs showing means of mice ± SEM, or dot plots representing values of individual mice (dots) and means (line) ± SEM. *N*-numbers to calculate SEMs were given by the number of animals used. Before statistical analysis, the normality of data sets was evaluated with histograms (Sigma Plot, Systat Software GmbH, Erkrath, Germany). Significance levels (*p*-values) are presented in the respective figure legends or tables. *p*-values were calculated using an unpaired *t*-test or ANOVA with Holm–Sidak *posthoc* analysis (>2 groups). For the data presented in **Figure 4**, volumes of individual brain regions between controls and mutants were first compared using unpaired *t*-tests. Subsequently, *p*-values of all analyzed brain regions were manually corrected for multiple comparisons using Holm–Sidak *posthoc* adjustment (**Supplementary Table 2**). Data and graphs were organized and analyzed using MS Excel, Graph Pad Prism 6 (GraphPad Software, La Jolla, CA, USA), and Sigma Plot (Systat Software GmbH, Erkrath, Germany). Figures were assembled in Adobe Photoshop CS6 and linear adjustments were done to correct black level and contrast.

[3]https://imagej.net/ImageJ

RESULTS

Generation of $\alpha_2\delta$ Double Knockout Mice

Loss-of-function models such as knockout or mutant animals allow conclusions on the potential roles of the affected proteins. Of the existing $\alpha_2\delta$ subunit loss-of-function mouse models only the $\alpha_2\delta$-2 mutant mice, in our case ducky ($\alpha_2\delta$-$2^{du/du}$), essentially an $\alpha_2\delta$-2 null mouse (see "Materials and Methods" section), display a severe neurological CNS phenotype and decreased life span (Meier, 1968; Barclay et al., 2001; Brodbeck et al., 2002). Thus, we hypothesized that the neuronal $\alpha_2\delta$ isoforms ($\alpha_2\delta$-1, $\alpha_2\delta$-2, and $\alpha_2\delta$-3) may have partially redundant as well as specific functions. To address this hypothesis, we generated three distinct $\alpha_2\delta$ double knockout mouse models by crossbreeding single knockout ($\alpha_2\delta$-1 and -3) or mutant (ducky) mice (see below and parental genotypes in **Figure 1**).

Due to the phenotypes of the distinct single knockout mice—ducky mice are infertile and male $\alpha_2\delta$-1 knockout mice exhibit a progressive form of diabetes (Snell, 1955; Mastrolia et al., 2017)—successful generation of double knockouts was inherently difficult and accomplished only by employing the following strategies: ducky mice ($\alpha_2\delta$-$2^{du/du}$) were generated by breeding heterozygous mice ($\alpha_2\delta$-$2^{du/+}$ × $\alpha_2\delta$-$2^{du/+}$; **Figure 1A**). $\alpha_2\delta$-1/-3 double knockout mice ($\alpha_2\delta$-$1^{-/-}$, $\alpha_2\delta$-$3^{-/-}$) were either obtained by inter-crossing double heterozygous animals ($\alpha_2\delta$-$1^{+/-}$, $\alpha_2\delta$-$3^{+/-}$), or mice heterozygous for $\alpha_2\delta$-1 ($\alpha_2\delta$-$1^{+/-}$) and homozygous knockout for $\alpha_2\delta$-3 ($\alpha_2\delta$-$3^{-/-}$; **Figure 1B**). $\alpha_2\delta$-1/-2 double knockout/mutant mice ($\alpha_2\delta$-$1^{-/-}$, $\alpha_2\delta$-$2^{du/du}$) were generated by cross-breeding double heterozygous animals ($\alpha_2\delta$-$1^{+/-}$, $\alpha_2\delta$-$2^{du/+}$), or mice heterozygous for $\alpha_2\delta$-2 ($\alpha_2\delta$-$2^{du/+}$) and homozygous knockout for $\alpha_2\delta$-1 ($\alpha_2\delta$-$1^{-/-}$; **Figure 1C**). Finally, $\alpha_2\delta$-2/-3 double knockout/mutant mice ($\alpha_2\delta$-$2^{du/du}$, $\alpha_2\delta$-$3^{-/-}$) were obtained by inter-crossing double heterozygous animals ($\alpha_2\delta$-$2^{du/+}$, $\alpha_2\delta$-$3^{+/-}$), or mice heterozygous for $\alpha_2\delta$-2 ($\alpha_2\delta$-$2^{du/+}$) and homozygous knockout for $\alpha_2\delta$-3 ($\alpha_2\delta$-$3^{-/-}$; **Figure 1D**). Most of the different breeding combinations did not yield the respective double knockout mice at the expected Mendelian ratios (see below). Hence, we observed

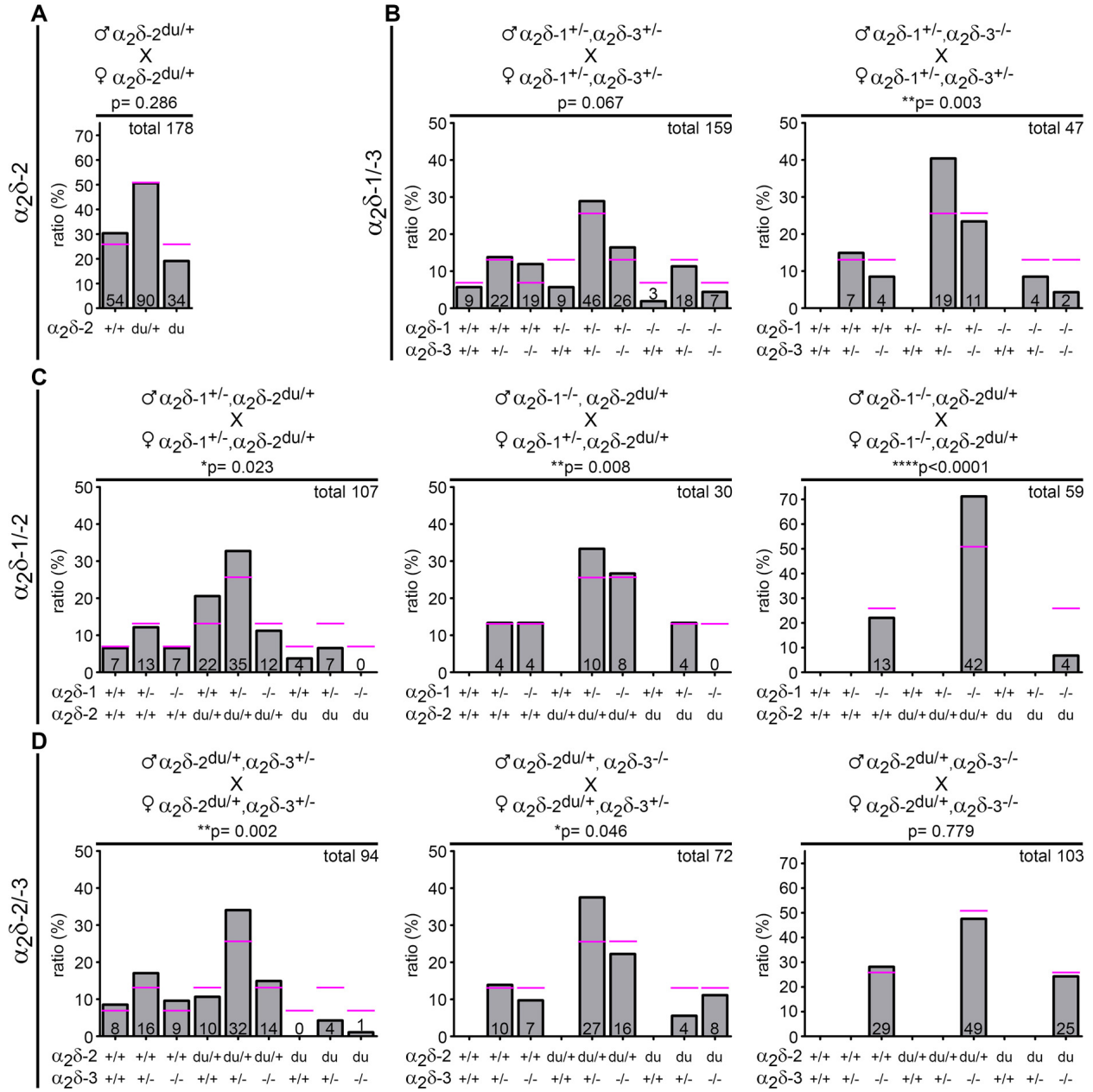

FIGURE 1 | Genotype distribution is altered in neonatal litters bred from distinct $\alpha_2\delta$ inter-crosses. Expected (magenta lines) and observed (bar graphs) genotypes of neonatal offspring (P0–1) obtained by crossbreeding different $\alpha_2\delta$ mutant or single knockout mice (parental genotypes are shown above respective graphs). Symbols indicate either wildtype (+) or mutated (–) $\alpha_2\delta$-1, $\alpha_2\delta$-2, or $\alpha_2\delta$-3 alleles. The absolute number of pups is displayed on the bars and the total amount of analyzed animals is depicted on the upper right side of each graph (confer **Table 1** for further information on the number of analyzed litters and mean litter size). While the observed genotype ratio in litters was close to expected values when crossbreeding heterozygous $\alpha_2\delta$-2 mutant mice **(A)** the frequency of distinct $\alpha_2\delta$ single knockout and double knockout mice was below expected ratios in $\alpha_2\delta$-1/-3 **(B)** $\alpha_2\delta$-1/-2 **(C)** and $\alpha_2\delta$-2/-3 **(D)** inter-crosses. *Statistics*: Chi-square test: **(A)** $\chi^2_{(2)} = 2.5$; **(B)** left: $\chi^2_{(8)} = 14.6$, right: $\chi^2_{(5)} = 18.1$; **(C)** left: $\chi^2_{(8)} = 17.8$, middle: $\chi^2_{(5)} = 15.6$, right: $\chi^2_{(2)} = 22.6$; **(D)** left: $\chi^2_{(8)} = 24.2$, middle: $\chi^2_{(5)} = 11.3$, right: $\chi^2_{(2)} = 0.5$. Exact *p*-values are given in the respective graphs. Asterisks in graphs indicate significance levels: $^*p < 0.05$, $^{**}p < 0.01$, $^{****}p < 0.0001$.

that individual double knockouts were best obtained using the following male and female genotype combinations: $\alpha_2\delta$-1/-3 double knockout mice by cross-breeding male $\alpha_2\delta$-$1^{+/-}$, $\alpha_2\delta$-$3^{+/-}$, or $\alpha_2\delta$-$3^{-/-}$ mice and female $\alpha_2\delta$-$1^{+/-}$, $\alpha_2\delta$-$3^{+/-}$, or $\alpha_2\delta$-$3^{-/-}$ mice (**Figure 1B**); $\alpha_2\delta$-1/-2 double knockout mice by cross-breeding male $\alpha_2\delta$-$1^{-/-}$, $\alpha_2\delta$-$2^{du/+}$, and female $\alpha_2\delta$-$1^{-/-}$, $\alpha_2\delta$-$2^{du/+}$ mice (**Figure 1C**); $\alpha_2\delta$-2/-3 double knockout mice by cross-breeding male $\alpha_2\delta$-$2^{du/+}$, $\alpha_2\delta$-$3^{-/-}$, and female $\alpha_2\delta$-$2^{du/+}$, $\alpha_2\delta$-$3^{+/-}$ mice (**Figure 1D**). For further analysis, double knockout mice obtained from these breeding combinations

were compared with wildtype, (double-) heterozygous, or single knockout littermates.

Mendelian Ratios are Altered in Neonatal Litters Bred From Different $\alpha_2\delta$ Inter-crosses

We first carried out breeding and offspring analysis in the ducky $\alpha_2\delta$-2 mouse line and the three double knockout mouse strains. When cross-breeding male and female mice heterozygous for $\alpha_2\delta$-2 ($\alpha_2\delta$-$2^{du/+}$ × $\alpha_2\delta$-$2^{du/+}$; **Figure 1A**) we observed that the detected genotypes in P0–1 litters were close to expected theoretical values for wildtype, heterozygous and ducky mice.

However, the genotypic distribution of neonatal litters in the double heterozygous breeding combinations did not conform to Mendel's law: the frequency of heterozygous pups was generally increased by 15–36% compared to expected percentages. In striking contrast, the prevalence of $\alpha_2\delta$ double knockout mice was ∼30% ($\alpha_2\delta$-1/-3; **Figure 1B**, left), 100% ($\alpha_2\delta$-1/-2; **Figure 1C**, left), and 80% ($\alpha_2\delta$-2/-3; **Figure 1D**, left) less than theoretically expected at birth, and even the number of single knockout pups was significantly reduced. The ratio of observed and predicted single knockout mice varied in the distinct $\alpha_2\delta$ cross-breedings: while the numbers of born $\alpha_2\delta$-2 mutant pups were reduced by 40% ($\alpha_2\delta$-1/-2; **Figure 1C**, left) and 100% ($\alpha_2\delta$-2/-3; **Figure 1D**, left), $\alpha_2\delta$-1 or $\alpha_2\delta$-3 single knockouts were close to or slightly above expected values in the respective mouse lines. In $\alpha_2\delta$-1/-3 inter-crosses (**Figure 1B**, left) the amount of born $\alpha_2\delta$-1 single knockout mice was 70% less than predicted, whereas 80% more $\alpha_2\delta$-3 single knockout mice were born.

Using male or female mice of different genotype combinations revealed further effects on genotype frequency in neonatal litters: cross-breeding male $\alpha_2\delta$-$1^{+/-}$, $\alpha_2\delta$-$3^{-/-}$, and female $\alpha_2\delta$-$1^{+/-}$, $\alpha_2\delta$-$3^{+/-}$ mice more strongly affected mendelian distribution compared with double heterozygous breedings, as the number of born single and double knockout pups was decreased by 32% and 68%, respectively (**Figure 1B**, right). Of note, the chance to obtain $\alpha_2\delta$-1/-2 double knockout pups was strikingly low in all $\alpha_2\delta$-1/-2 breeding combinations (**Figure 1C**, 73% or 100% less than expected). The observed genotypes were close to expected theoretical values by inter-crossing male and female $\alpha_2\delta$-$2^{du/+}$, $\alpha_2\delta$-$3^{-/-}$ mice (**Figure 1D**, right) and thus provided a relatively good chance to obtain $\alpha_2\delta$-2/-3 double knockout mice. Taken together, genotypes of parents were a critical factor for the birth/survival of single and double knockout offspring. This is best visualized by the total number of analyzed offspring and litters (**Table 1**): While data from heterozygous $\alpha_2\delta$-2 matings were collected within 2 years, double knockout mouse lines required a period of 4–5 years to collect enough data enabling statistical analysis. Taken together, our results suggest embryonic or neonatal lethality of distinct $\alpha_2\delta$ single and double knockout mice, therefore indicating that $\alpha_2\delta$ subunits are essential for survival.

Breeding Pairs of Distinct $\alpha_2\delta$-2/-3 Inter-crosses Display Skin Lesions Associated With Over-Grooming

Since genotypes of parents appeared to be a critical factor for the survival of single and double knockout offspring, we more thoroughly monitored breeding pairs. Besides the diabetic phenotype of male $\alpha_2\delta$-1 knockout animals (Mastrolia et al., 2017), no overt physiological or behavioral abnormalities have been observed in $\alpha_2\delta$-2, $\alpha_2\delta$-1/-3, and $\alpha_2\delta$-1/-2 mating combinations. In contrast, already $\alpha_2\delta$-2/-3 double heterozygous breeding pairs displayed signs of stress and anxiety-like behavior typically associated with neuropsychiatric disorders (Kalueff et al., 2016; Landmann et al., 2018a) comprising head trembling, increased grooming, and abnormal activity upon handling. Excessive grooming appeared enhanced in double heterozygous and even more in heterozygous/knockout matings, as we observed high incidences of skin lesions (**Table 2**, double heterozygous breeding: no overt lesions in six breeding cages; $\alpha_2\delta$-$2^{du/+}$, $\alpha_2\delta$-$3^{-/-}$ × $\alpha_2\delta$-$2^{du/+}$, $\alpha_2\delta$-$3^{+/-}$: lesions observed in 28% of 14 breeding cages). Of note, in $\alpha_2\delta$-$2^{du/+}$, $\alpha_2\delta$-$3^{-/-}$ × $\alpha_2\delta$-$2^{du/+}$, $\alpha_2\delta$-$3^{+/-}$ matings lesions were observed in 83% of 24 breeding cages which correlated with extraordinarily high infant mortality at P0–1, often resulting in the loss of complete litters. Thus, breedings were later switched to include BALB/c foster mothers (see "Materials and Methods" section). Similar incidences (loss of litters) have also been detected in $\alpha_2\delta$-1/-2 matings, although here no excessive grooming behavior was observed.

Lesions were usually first noticed within the first month after placing mating mice together and appeared as a patch of hairless skin at specific body regions including the head (neck, eyes, snout, and ears), back, belly, and genitals. Thorough monitoring of mice to ensure the timely use of humane endpoints revealed that the lesions quickly progressed into subcutaneous wounds

TABLE 1 | Mean litter sizes obtained from distinct $\alpha_2\delta$ mutant or knockout breeding combinations.

Breeding pair combination ♂ X ♀ (number of pairs)	Litter size (mean ± SD)	Total number of offspring	Total number of litters	Period of data collection (years)
$\alpha_2\delta$-$2^{du/+}$ X $\alpha_2\delta$-$2^{du/+}$ (11)	8.3 ± 2.1	178	21	2
$\alpha_2\delta$-$1^{+/-}$, $\alpha_2\delta$-$3^{+/-}$ X $\alpha_2\delta$-$1^{+/-}$, $\alpha_2\delta$-$3^{+/-}$ (8)	7.6 ± 2.7	159	21	5
$\alpha_2\delta$-$1^{+/-}$, $\alpha_2\delta$-$3^{-/-}$ X $\alpha_2\delta$-$1^{+/-}$, $\alpha_2\delta$-$3^{+/-}$ (2)	7.8 ± 2.5	47	6	2.5
$\alpha_2\delta$-$1^{+/-}$, $\alpha_2\delta$-$2^{du/+}$ X $\alpha_2\delta$-$1^{+/-}$, $\alpha_2\delta$-$2^{du/+}$ (6)	6.3 ± 3.3	107	17	2
$\alpha_2\delta$-$1^{-/-}$, $\alpha_2\delta$-$2^{du/+}$ X $\alpha_2\delta$-$1^{+/-}$, $\alpha_2\delta$-$2^{du/+}$ (3)	6.0 ± 2.1	30	5	4
$\alpha_2\delta$-$1^{-/-}$, $\alpha_2\delta$-$2^{du/+}$ X $\alpha_2\delta$-$1^{-/-}$, $\alpha_2\delta$-$2^{du/+}$ (9)	4.5 ± 1.7	59	13	4
$\alpha_2\delta$-$2^{du/+}$, $\alpha_2\delta$-$3^{+/-}$ X $\alpha_2\delta$-$2^{du/+}$, $\alpha_2\delta$-$3^{+/-}$ (4)	7.8 ± 2.7	94	12	2
$\alpha_2\delta$-$2^{du/+}$, $\alpha_2\delta$-$3^{-/-}$ X $\alpha_2\delta$-$2^{du/+}$, $\alpha_2\delta$-$3^{+/-}$ (7)	7.2 ± 2.5	72	10	4
$\alpha_2\delta$-$2^{du/+}$, $\alpha_2\delta$-$3^{-/-}$ X $\alpha_2\delta$-$2^{du/+}$, $\alpha_2\delta$-$3^{-/-}$ (10)	7.9 ± 1.0	103	13	4

TABLE 2 | $\alpha_2\delta$-2/-3 breeding pairs display abnormal grooming behavior and increased pup mortality.

Genotype female	Genotype male	Skin lesions in breeders		[a]Number of litters with infant mortality	Number of analyzed breeding pairs
$\alpha_2\delta$-$2^{du/+}$, $\alpha_2\delta$-$3^{+/-}$	$\alpha_2\delta$-$2^{du/+}$, $\alpha_2\delta$-$3^{+/-}$	♀ 0%	♂ 0%	6 of 24	6
$\alpha_2\delta$-$2^{du/+}$, $\alpha_2\delta$-$3^{+/-}$	$\alpha_2\delta$-$2^{du/+}$, $\alpha_2\delta$-$3^{-/-}$	♀ 0%	♂ 36%	3 of 8	11
$\alpha_2\delta$-$2^{du/+}$, $\alpha_2\delta$-$3^{-/-}$	$\alpha_2\delta$-$2^{du/+}$, $\alpha_2\delta$-$3^{+/-}$	♀ 0%	♂ 0%	4 of 24	3
$\alpha_2\delta$-$2^{du/+}$, $\alpha_2\delta$-$3^{-/-}$	$\alpha_2\delta$-$2^{du/+}$, $\alpha_2\delta$-$3^{-/-}$	♀ 67%	♂ 50%	23 of 31	24

[a]*Inclusion criteria: ≥25% of the pups from one litter found dead.*

encompassing larger parts. Because males and females were housed together during the entire breeding procedure we could not definitely determine whether lesions were caused by self-grooming, allogrooming, or could be the result of aggressive encounters. However, partners were not observed behaving aggressively against each other, and individuals were often seen engaged in scratching wounds themselves. Importantly, hardly any occurrences were observed in mice maintained in stock cages of same-sex and same-age littermates. Moreover, lesions were neither noticed in other mouse lines maintained in a C57BL/6N background ($\alpha_2\delta$-2 and $\alpha_2\delta$-3 single breedings) nor in the ones kept in a mixed 129J × C57BL/6N background ($\alpha_2\delta$-1/-3 and $\alpha_2\delta$-1/-2 double breedings). Thus, our findings rather exclude the possibility of background related symptoms or diseases and point towards abnormal behavior caused by the gradual decrease in the total amount of $\alpha_2\delta$-2 and particularly $\alpha_2\delta$-3.

General Descriptions of Phenotypes of $\alpha_2\delta$-2 Null (Ducky) Mice and $\alpha_2\delta$ Double Knockout Mice

We subsequently conducted a qualitative phenotypic evaluation looking for gross abnormalities in born ducky and double knockout offspring (see "Materials and Methods" section).

Similar to previously published reports, the $\alpha_2\delta$-2 mutant mice analyzed in this study displayed the ducky phenotype, described by an ataxic, wide-based gait (Snell, 1955) as well as symptoms typical for epileptic seizures including loss of balance, falling to the side, and behavioral immobility (Van Erum et al., 2019). However, while other studies stated that the majority of ducky mice hardly lived beyond 39 days (Meier, 1968; Barclay et al., 2001), we observed in several animals a highly extended life span (>12 months; Schoepf et al., 2019). The discrepancy in survival might be explained by the use of different background strains or the above-mentioned husbandry strategies including easily reachable food and water (see "Materials and Methods" section). Notably, constant monitoring revealed that adult mice exhibited to some extent normal activities such as climbing on the housing material and huddling behavior, all signs of general well-being.

Similar to ducky mice, $\alpha_2\delta$-1/-2 and $\alpha_2\delta$-2/-3 double knockout mice also showed abnormal behavioral phenotypes typically occurring during apparent epileptic episodes (see paragraph above). However, in contrast to ducky animals, $\alpha_2\delta$-1/-2 and $\alpha_2\delta$-2/-3 double knockout mice displayed a more severe disease progression peaking around weaning age, which often required the application of humane endpoints (see "Materials and Methods" section). Their generally affected condition was best evidenced by poor fur coat condition, low body weight (**Figure 2**), hypo-reactivity to handling, and highly reduced survival chance during the first postnatal weeks (Schoepf et al., 2019). We did therefore not pursue quantitative behavioral tests of sensory or motor abilities as these mice would have been unable to perform such tasks. Interestingly, while no motor phenotype has been so far detected in $\alpha_2\delta$-1 and $\alpha_2\delta$-3 single knockout animals, $\alpha_2\delta$-1/-3 double knockout mice showed locomotion difficulties comprising imbalance and abnormal posture while walking. However, gait appeared different compared to the previously described waddling gait of ducky mice, which was also evident in $\alpha_2\delta$-1/-2 and $\alpha_2\delta$-2/-3 knockout mice. When further examined, $\alpha_2\delta$-2 null mice displayed a frog-like position of the hind limbs as described in Meier (1968), whereas $\alpha_2\delta$-1/-3 double knockout animals exhibited a hopping gait lifting one of the hindlimbs. Notably, quantitative gait assessment using the CatWalk gait analysis system for fluorescent detection of footprint patterns already failed in $\alpha_2\delta$-1/-3 double knockout mice because of their highly reduced body weight (**Figure 2**).

Loss of Distinct $\alpha_2\delta$ Subunits Causes Impaired Development and Neurological Disease

To further characterize how the loss of distinct $\alpha_2\delta$ subunits affects postnatal development and neurological disease we next assessed body and brain weights of juvenile (3-4-week-old; $\alpha_2\delta$-2/-3 double knockout and ducky) or adult (8–13-week-old; $\alpha_2\delta$-1/-3 double knockout and ducky) male mice. Moreover, brain/body ratios were calculated to investigate whether an eventual decrement of brain size was associated with developmental impairment. Since delivery of $\alpha_2\delta$-1/-2 double knockout pups was rare (**Figure 1C**) they could not be included in this analysis. We observed that in all three analyzed mouse models juvenile mice showed a highly decreased bodyweight (ducky: 41%; $\alpha_2\delta$-1/-3: 61%; and $\alpha_2\delta$-2/-3: 68% reduction compared to control) together with a moderately reduced brain size (ducky: 10%; $\alpha_2\delta$-1/-3: 22%; and $\alpha_2\delta$-2/-3: 28% reduction to control) resulting in 1.5-fold (**Figure 2A**; ducky), 2-fold (**Figure 2B**; $\alpha_2\delta$-1/-3); or 2.2-fold (**Figures 2C,E**; $\alpha_2\delta$-2/-3), enhanced brain/body ratios compared to individual controls. Interestingly, differences in brain/body ratios were no longer apparent in adult $\alpha_2\delta$-1/-3 double knockout mice (**Figure 2B**). In contrast, adult ducky mice (**Figure 2A**; 2.4-fold) showed even higher brain/body ratios due to a relatively mild increase in body size during adolescence and unaltered brain weight (body: 61%; brain: 17% reduction to control). Moreover, comparing juvenile

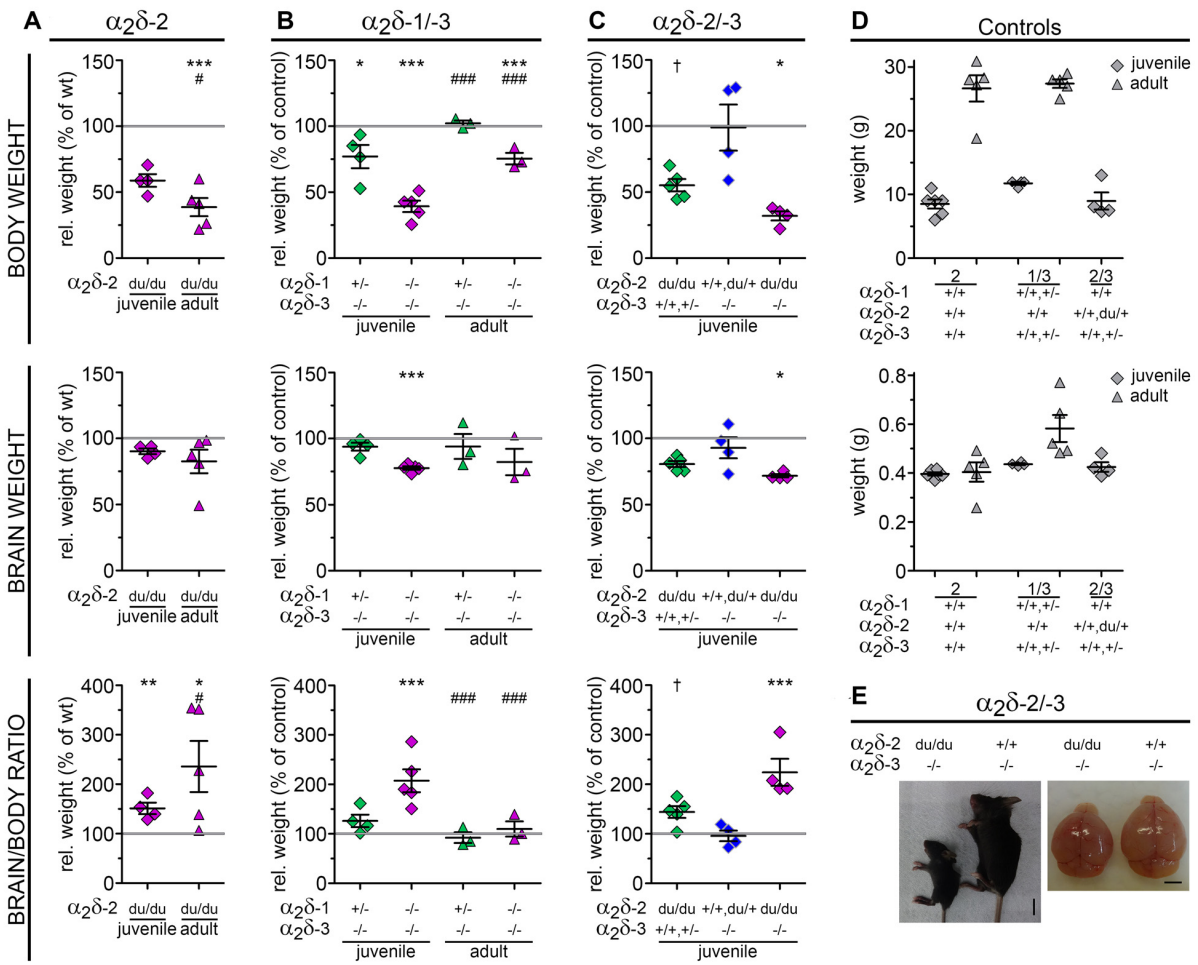

FIGURE 2 | Loss of distinct $\alpha_2\delta$ subunits causes impaired development. Relative body weight, brain weight and brain/body ratios calculated as percentage of controls (gray line and raw values in **D**) as a measure for proper development of $\alpha_2\delta$-2 mutant mouse ducky **(A)** and $\alpha_2\delta$-1/-3 **(B)** or $\alpha_2\delta$-2/-3 **(C)** double knockout mice. Juvenile (3-4-week-old) or adult mice (8–13-week-old) are depicted with squares or triangles, respectively. In all three mouse models juvenile mice showed a highly decreased body weight together with a moderately reduced brain size resulting in 1.5-fold (**A**, ducky), 2-fold (**B**, $\alpha_2\delta$-1/-3), or 2.2-fold (**C**, $\alpha_2\delta$-2/-3) higher brain/body ratios compared to controls. The magnitude of this effect varied with age: while brain/body ratios were normalized to control levels in adult $\alpha_2\delta$-1/-3 double knockout mice **(B)** a relatively mild increase in body weight during adulthood together with a moderately reduced brain size resulted in even more elevated brain/body ratios in ducky mice (**A**, 2.4-fold). Exemplary images of a $\alpha_2\delta$-2/-3 double knockout mouse (left) at P21, depicting the remarkably smaller body and brain size compared to its $\alpha_2\delta$-3 single knockout littermate **(E)**. Values for individual animals (dots) and means (line) ± SEM are shown. *N-numbers*: **(A)** wildtype controls: six (juvenile) and five (adult), ducky mutant: four (juvenile) and five (adult); **(B)** wildtype or heterozygous controls: four (juvenile) and five (adult), $\alpha_2\delta$-3 knockout: four (juvenile) and three (adult), $\alpha_2\delta$-1/-3 double knockout: five (juvenile) and three (adult); **(C)** wildtype or heterozygous controls: 4, $\alpha_2\delta$-2 knockout: 5, $\alpha_2\delta$-3 knockout: 4, $\alpha_2\delta$-2/-3 double knockout: 4. *Statistics*: two-way ANOVA with Holm–Sidak *posthoc* analysis: body weight: genotype: $F_{(1,16)} = 45.8$, $p < 0.001$, age: $F_{(1,16)} = 64$, $p < 0.001$, genotype × age: $F_{(1,16)} = 19.2$, $p < 0.001$; brain weight: genotype: $F_{(1,16)} = 3.9$, $p = 0.064$, age: $F_{(1,16)} = 0.1$, $p = 0.7$, genotype × age: $F_{(1,16)} = 0.3$, $p = 0.6$; Brain/body ratio: genotype: $F_{(1,16)} = 18.6$, $p < 0.001$, age: $F_{(1,16)} = 39.8$, $p < 0.001$, genotype × age: $F_{(1,16)} = 0.1$, $p = 0.8$; **(B)** two-way ANOVA with Holm–Sidak *posthoc* analysis: body weight: genotype: $F_{(2,18)} = 50.7$, $p < 0.001$, age: $F_{(2,18)} = 764.5$, $p < 0.001$, genotype × age: $F_{(2,18)} = 2.8$, $p = 0.09$; brain weight: genotype: $F_{(2,18)} = 5.9$, $p = 0.01$, age: $F_{(2,18)} = 28.2$, $p < 0.001$, genotype × age: $F_{(2,18)} = 0.1$, $p = 0.9$; Brain/body ratio: genotype: $F_{(2,18)} = 9.2$, $p = 0.002$, age: $F_{(2,18)} = 115.5$, $p < 0.001$, genotype × age: $F_{(2,18)} = 5.0$, $p = 0.02$; **(C)** one-way ANOVA with Holm–Sidak *posthoc* analysis: body weight: $F_{(3,11)} = 6.6$, $p = 0.008$, *post hoc*: $^{\dagger}p = 0.053$ between $\alpha_2\delta$-2 single knockout and control, $^{*}p < 0.05$ between $\alpha_2\delta$-2/-3 double knockout and $\alpha_2\delta$-3 single knockout/control; brain weight: $F_{(3,11)} = 5.8$, $p = 0.01$, *posthoc*: $^{\dagger}p = 0.07$ between $\alpha_2\delta$-2 single knockout and control, $^{*}p = 0.015$ between $\alpha_2\delta$-2/-3 double knockout and control; brain/body ratio: $F_{(3,11)} = 11.5$, $p = 0.001$, *posthoc*: $^{***}p = 0.001$ between $\alpha_2\delta$-2/-3 double knockout and control, $^{**}p = 0.002$ between $\alpha_2\delta$-2/-3 double knockout and $\alpha_2\delta$-3 single knockout, $^{*}p = 0.012$ between $\alpha_2\delta$-2/-3 double knockout and $\alpha_2\delta$-2 single knockout. Symbols in graphs indicate significance levels of factor genotype within (*), or factor age (#): $^{\dagger}p < 0.07$, $^{*/\#}p < 0.05$, $^{**}p < 0.01$, $^{***/\#\#\#}p < 0.001$.

$\alpha_2\delta$-2 and $\alpha_2\delta$-3 single knockout mice with $\alpha_2\delta$-2/-3 double knockout littermates further corroborated that loss of distinct $\alpha_2\delta$ subunits differentially affected brain and body size: while $\alpha_2\delta$-3 knockout mice had normal brain/body ratios compared to controls (**Figure 2C**, blue squares), brain/body ratios were strongly increased in $\alpha_2\delta$-2 null mice (**Figure 2C**, green squares, 1.4-fold) and even more dramatically in $\alpha_2\delta$-2/-3 double knockout mice (**Figure 2C**, magenta squares, 2.2-fold). Together,

these data are in accordance with the above-mentioned severe neurological phenotypes associated with the lack of $\alpha_2\delta$-2. These phenotypes were even stronger if $\alpha_2\delta$-3 or, most likely, $\alpha_2\delta$-1 were additionally missing in double knockout mice. Furthermore, our findings suggest that $\alpha_2\delta$-2 and $\alpha_2\delta$-3 differentially affect postnatal growth and brain development.

Volumes of Distinct Brain Regions Are Decreased in Ducky and Double Knockout Mice

Interestingly, we observed that the brain weight of ducky and double knockout mice was moderately to highly reduced compared to control littermates (**Figure 2**). Given the concomitant decrease in body weight, we reasoned that the decrement in brain size could be caused by a general developmental delay. If this applies, we assumed that distinct brain regions should be rather uniformly affected by the loss of $\alpha_2\delta$ subunits. However, taking the distinct phenotypes of the individual single and double knockout mice into account, $\alpha_2\delta$ subunits may also specifically influence the development of brain regions. In this scenario, the loss of $\alpha_2\delta$ subunits could lead to decreased volumes of discrete brain regions. Thus, we next examined overall brain architecture in juvenile ($\alpha_2\delta$-1/-2 and $\alpha_2\delta$-2/-3 double knockout) or adult ($\alpha_2\delta$-1/-3 double knockout) male mice. To our knowledge ducky mice of over 56-days of age have not been histologically examined thus far (Meier, 1968; Brodbeck et al., 2002) and were therefore included in our analysis.

To address potential $\alpha_2\delta$ knockout effects on brain structure, consecutive Nissl-stained sagittal cryosections from mutant brains obtained from one hemisphere were compared with control littermates. Moreover, volumes of distinct brain regions of interest, including the cerebellum, corpus callosum, hippocampus, neocortex, and whole hemisphere were calculated by applying the Cavalieri principle (see "Materials and Methods" section for selection criteria). While we found no overt anatomical abnormalities in cerebelli or hippocampi of all $\alpha_2\delta$ mutant and ducky mice (**Figure 3**), the volumetric analysis revealed size differences of specific brain regions (**Figure 4** and **Supplementary Table 2**): whole hemisphere volume of $\alpha_2\delta$-1/-3 double knockout mice was slightly reduced by 11% (**Figure 4B**), while brain size of ducky (**Figure 4A**), $\alpha_2\delta$-1/-2 (**Figure 4C**) and $\alpha_2\delta$-2/-3 (**Figure 4D**) double knockout mice was strongly decreased (25%, 27%, and 26%, respectively). Furthermore, the size of the cerebellum was markedly affected in $\alpha_2\delta$-2/-3 (40%) and $\alpha_2\delta$-1/-2 (37%) double knockout mice and to a lesser extent in ducky (29%) and $\alpha_2\delta$-1/-3 mice (16%). Interestingly, cortical volume was decreased in all three mouse strains lacking the $\alpha_2\delta$-2 isoform (ducky: 34%, $\alpha_2\delta$-1/-2: 21% and $\alpha_2\delta$-2/-3: 22%), while the corpus callosum was significantly reduced whenever $\alpha_2\delta$-3 was absent ($\alpha_2\delta$-1/-3: 23%, $\alpha_2\delta$-2/-3: 29%). Of note, albeit some alterations were not significantly different to controls, which might be linked to low n-numbers caused by inherently difficult breeding strategies and phenotypes, they were consistently detected in all mutant animals analyzed (**Supplementary Table 2**: cerebellum in $\alpha_2\delta$-1/-2; corpus callosum in ducky and $\alpha_2\delta$-1/-2; hippocampus in $\alpha_2\delta$-1/-3; neocortex in $\alpha_2\delta$-1/-2; whole hemisphere in ducky, $\alpha_2\delta$-1/-3 and $\alpha_2\delta$-1/-2). Taken together, our data display concurrent effects on specific brain regions caused by deletion of distinct $\alpha_2\delta$ subunits: sizes of cerebellum and cortex were highly reduced when $\alpha_2\delta$-2 was absent, and a lack of $\alpha_2\delta$-3 specifically elicited a volume decrease in the corpus callosum. Therefore, our findings argue that the reduction in brain size is not just caused by a general effect on overall development.

Adult Ducky Mice Display a Reduced Thickness of Cortical Layers and Increased Cell Densities

A potentially underlying cause for a reduction in the volume of distinct brain regions in $\alpha_2\delta$ mutant mice could be on the one hand loss of cells or on the other hand a paucity of neuropil, which includes neuronal and glial cell processes, dendritic spines, and synaptic contacts (Dudanova et al., 2007). The neocortex provides an intriguing brain region to further address these possibilities and thus shed light onto the role of $\alpha_2\delta$ subunits in the normal and diseased brain in several aspects: first, we found that the cortical volume was decreased in all three mouse models lacking the $\alpha_2\delta$-2 isoform (**Figure 4**, see ducky, $\alpha_2\delta$-1/-2 and $\alpha_2\delta$-2/-3), which has not been described in the original reports of young ducky mice (Meier, 1968). Second, abnormal structure and function of the cerebral cortex have been linked to neurodevelopmental and neurological disease, including autism spectrum disorders (Chen et al., 2015; Fenlon et al., 2015), motor dysfunction (Hong and Mah, 2015), and epilepsy (Toba and Hirotsune, 2012). Importantly, these phenotypes have been associated with aberrant $\alpha_2\delta$ expression both in mice and humans (reviewed in Geisler et al., 2015). Third, the cerebral cortex represents a six-layered structure that is generated during corticogenesis in a highly regulated manner: earlier born neurons reside in deeper layers, and later-born neurons migrate to superficial layers (Shao et al., 2017). Consequently, an effect of $\alpha_2\delta$ subunit mutations should also be examined during development.

Therefore, we next aimed to discern the relative contribution of cell densities to the cortical volume, which represents a reflection of spacing between cell somas (Chen et al., 2015). To this end, cortical cytoarchitecture of adult ducky and wild-type mice was analyzed measuring a battery of distinct parameters (**Figure 5**). Using sagittal cryosections counterstained with the nuclear marker Höchst (**Figure 5A**) we found that both anteroposterior length (**Figure 5B**) and thickness of the somatosensory cortex (**Figure 5C**) were significantly reduced by 10% compared to wildtype control littermates. These findings further validate the volume decrease observed on Nissl-stained cryosections (**Figure 4A**). Because total cortical volume was reduced by 34% in $\alpha_2\delta$-2 mutant mice (**Figure 4A**), these data likely suggest that cortical length is decreased to a similar extent along the rostrocaudal (**Figure 5B**), ventrodorsal (**Figure 5C**), and possibly also the mediolateral axis, therefore displaying a rather

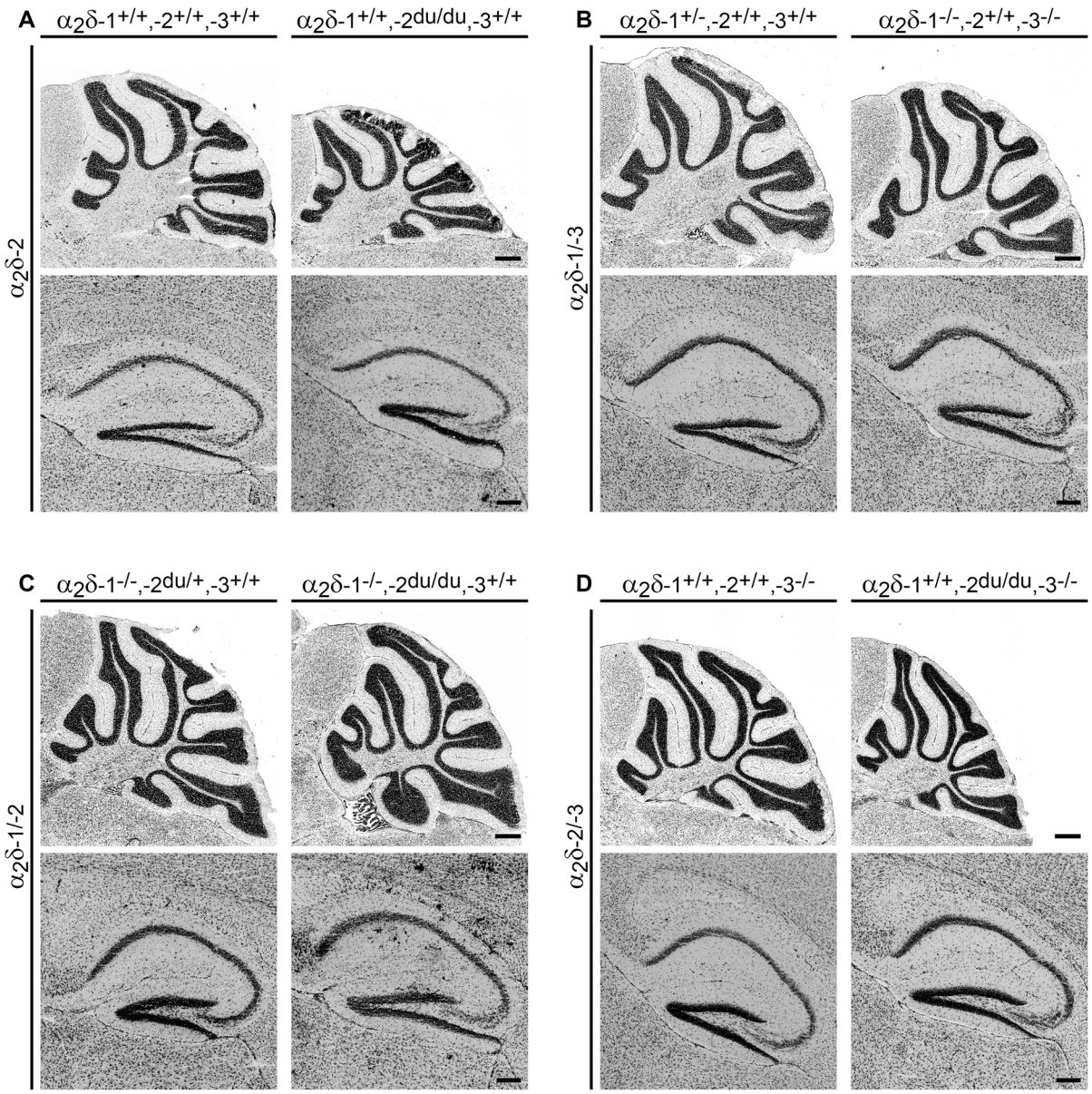

FIGURE 3 | General histologic examination of Nissl-stained brain sections does not reveal major morphological abnormalities. Representative micrographs of Nissl-stained sagittal cryosections obtained from adult (8–13-weeks-old; **A,B**) and juvenile (3–4-weeks-old; **C,D**) mouse brains. The cerebellum and hippocampus of ducky **(A)**, $\alpha_2\delta$-1/-3 **(B)**, $\alpha_2\delta$-1/-2 **(C)**, $\alpha_2\delta$-2/-3 **(D)** double knockout mice showed no overt anatomical defects compared to control mice. Scale bars, 400 μm (Cerebellum), and 200 μm (Hippocampus).

general effect on cortical expansion. Importantly, measuring nuclear densities along the entire ventrodorsal axis showed that the effect of reduced thickness was accompanied by a 2.5-fold increase in cell density (**Figure 5G**, number of all Höchst positive cells/mm^2 encompassing layer I to layer VI). Together, these results point towards a more compacted cortex in adult ducky mice compared to wild-type control littermates.

To evaluate whether the reduction in cortical thickness was linked to an altered layer composition we subsequently examined cortical lamination using well-established markers for upper-layer (Cux1: layer II–IV; **Figure 5D**) and deep-layer neurons (Ctip2: layer V; Tbr1: layer VI; **Figure 5E**; Shao et al., 2017). Triple immunofluorescence labeling of consecutive sagittal cryosections with Ctip2 (red channel) and either Cux1 or Tbr1 (green channel), as well as Höchst (blue channel), revealed that cortical lamination appeared preserved in adult ducky mice (**Figures 5D,E**, right panel). However, laminar thickness at the level of the somatosensory cortex was generally reduced in ducky mice, albeit the most severely

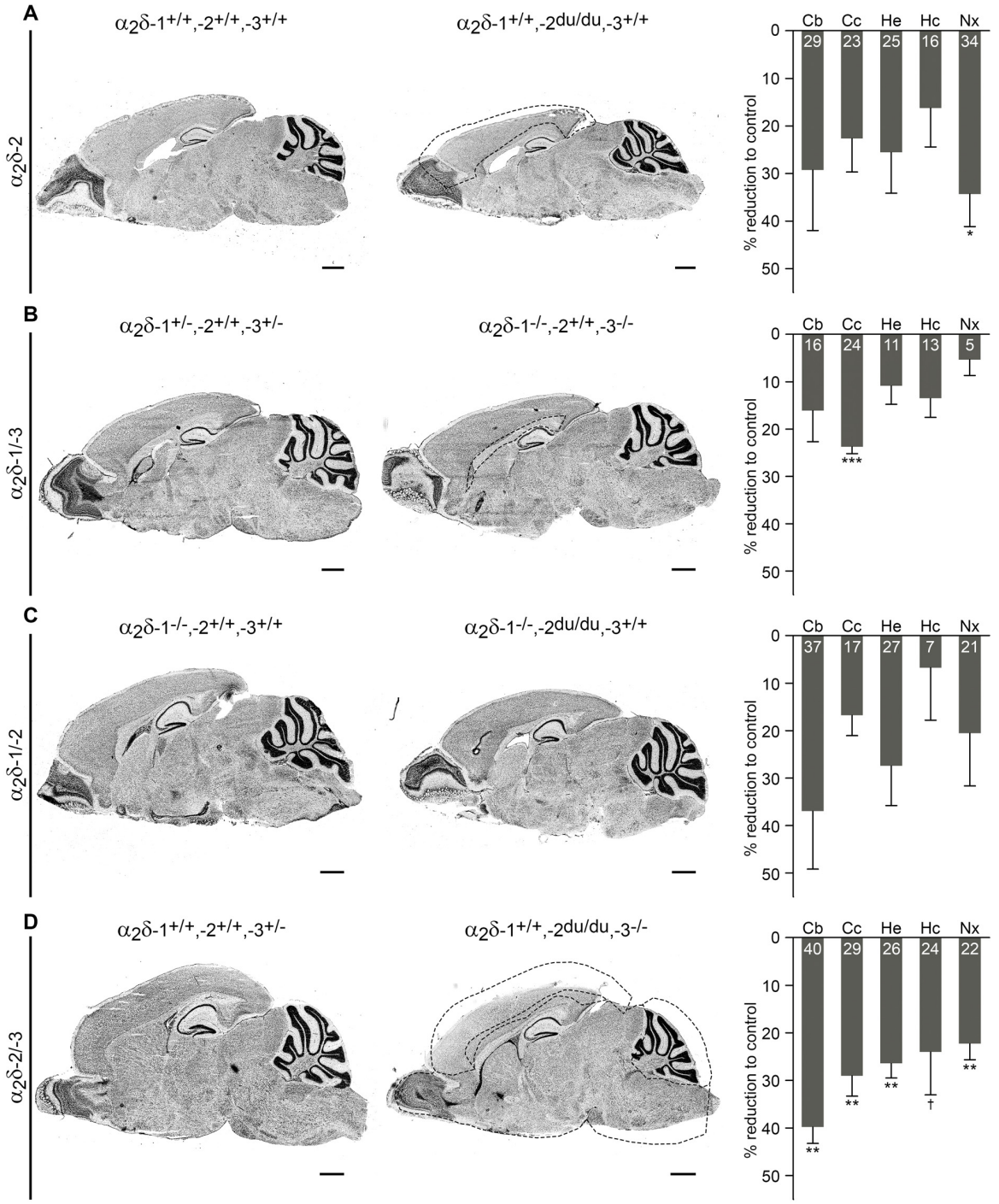

FIGURE 4 | Volumes of distinct brain regions are decreased in adult ducky and $\alpha_2\delta$ double knockout mice. Representative micrographs of Nissl-stained sagittal cryosections obtained from adult (8–13-weeks-old; **A,B**) and juvenile (3–4-week-old; **C,D**) mice. Consecutive slides were used for volume quantification of specific brain regions by applying the Cavalieri principle. Data from three mice per genotype were averaged and bar graphs depict means of respective knockout mice ± SEM, calculated as percentage reduction to corresponding controls (indicated with numbers in bars). Dashed lines in micrographs illustrate significantly decreased brain areas in knockout mice (right picture of each panel) compared to respective controls (left picture of each panel). **(A)** Ducky mice showed a generally reduced volume of all analyzed brain regions, with neocortical size being significantly decreased by 34%. **(B)** While the majority of analyzed structures were only slightly affected in $\alpha_2\delta$-1/-3 double knockout mice, a specific volume reduction of 24% was found in the corpus callosum. **(C)** Brain regions of $\alpha_2\delta$-1/-2 double knockout mice were not significantly different from control animals which already lacked $\alpha_2\delta$-1. However, additional knockout of $\alpha_2\delta$-2 caused an obvious trend towards reduced volumes of the cerebellum (37%), whole hemisphere (27%), and neocortex (21%). **(D)** $\alpha_2\delta$-2/-3 double knockout mice showed a drastic volume

(*Continued*)

FIGURE 4 | Continued
reduction of all analyzed brain regions ranging from 22 to 40%. The highly significant decrease of the cerebellum, whole hemisphere, and neocortex was similar to the one found in $\alpha_2\delta$-1/-2 double knockout mice. Furthermore, the size of the corpus callosum was significantly reduced by 29%. Confer **Supplementary Table 2** for raw data of individual mice and respective genotypes. *Abbreviations*: Cb, cerebellum, Cc, corpus callosum, He, whole hemisphere, Hc, hippocampus, Nx, neocortex. *Statistics*: unpaired *t*-test with Holm–Sidak correction for multiplicity (for *p*-values see **Supplementary Table 2**). Symbols in graphs indicate corrected significance levels compared to control: $^{\dagger}p < 0.06$; $^{*}p < 0.05$; $^{**}p < 0.01$; $^{***}p < 0.001$. Scale bars, 1 mm.

and consistently affected being layer V (23% reduction to control; **Figure 5F**). Because the proportion of marker positive cells relative to the number of Höchst$^+$ cells was not apparently altered (**Figure 5H** and **Supplementary Table 3**) our data imply that cortical thinning in adult ducky mice is primarily caused by decreased spacing, possibly reflecting a reduction of dendritic arborization, axonal contacts, and synapses.

Cortical Thinning and Compaction Manifests During Postnatal Development in Ducky Mice

To assess whether cortex size was already affected at earlier postnatal stages which would point towards a growth deficit, we next examined juvenile ducky mice and compared them to wildtype control littermates (3–4-week-old). Surprisingly, we found that the anteroposterior length was only slightly reduced by 6% (**Figures 6A,B**, $p = 0.06$) and cortical thickness was unaltered compared to wildtypes (**Figure 6C**, $p = 0.33$). Together, these findings suggest that, in contrast to adult ducky mice, total cortical expansion was still unaffected in juvenile mice. Since also total nuclear cell density was comparable to wildtype control (**Figure 6G**, number of all Höchst positive cells/mm^2 encompassing layer I to layer VI) our data further implicate that cortical thinning and compaction did not yet manifest in juvenile mice. Interestingly, however, immunofluorescence labeling of consecutive sagittal cryosections with layer-specific markers for upper-layer (Cux1: layer II–IV; **Figure 6D**) and deep-layer neurons (Ctip2: layer V; Tbr1: layer VI; **Figure 6E**) revealed differences in lamination: while layers I and II–IV showed a trend towards reduced thicknesses by 10%, layer VI displayed a concomitant increase of 25% (**Figure 6E**, right panel, and **Figure 6F**). Similar to adult ducky mice, we next assessed whether the increase in layer VI was linked to a relative increase in deep-layer neurons by calculating the fraction of marker positive cells relative to the number of Höchst$^+$ cells (**Figure 6H** and **Supplementary Table 3**). Since the proportion was not altered, our findings indicate that increased laminar thickness might be a result of augmented spacing in juvenile $\alpha_2\delta$-2 mutant mice.

Altogether, the above-described divergent observations in cortices of adult and juvenile ducky mice possibly reflect a reduction of spacing in adult mice which manifests after 3–4 weeks of age. Moreover, our results suggest that loss of neuronal $\alpha_2\delta$ subunits causes a paucity of neuropil, which includes neuronal and glial cell processes, spines, and synaptic contacts. Thus, the reduction of cortex volume cannot be solely explained by developmental retardation, further implicating the role of neuronal $\alpha_2\delta$ subunits in the stabilization of axonal and dendritic arborization.

DISCUSSION

This is the first study providing a general assessment of behavioral phenotypes and systemic analysis of different brain regions of three newly established $\alpha_2\delta$ double knockout mouse models ($\alpha_2\delta$-1/-3, $\alpha_2\delta$-1/-2, and $\alpha_2\delta$-2/-3) and adult $\alpha_2\delta$-2 mutant ducky mice. The findings described here provide evidence for general essential, but also individual roles of $\alpha_2\delta$ subunit isoforms in regulating survival, behavior, postnatal development, and the size of distinct brain regions. Importantly, we demonstrate for the first time that neurological disease phenotypes and the level of their severity critically depend on the type and quantity of $\alpha_2\delta$ isoforms.

Role of $\alpha_2\delta$ Isoforms in Premature Survival

Our offspring analysis on neonatal litters (P0–1) obtained by crossbreeding distinct $\alpha_2\delta$-1, $\alpha_2\delta$-2, and $\alpha_2\delta$-3 genotype combinations revealed that genotypic distribution did not conform to Mendel's law, thus suggesting embryonic or neonatal lethality of $\alpha_2\delta$-1/-3, $\alpha_2\delta$-1/-2, and $\alpha_2\delta$-2/-3 double knockout mice. Together with the fact that $\alpha_2\delta$ single knockout or mutant mice are born at expected Mendelian ratios in litters obtained from heterozygous breeding pairs, this finding may indicate a significant degree of $\alpha_2\delta$ subunit redundancy in premature survival and/or early development ($\alpha_2\delta$-1: Mastrolia et al., 2017; $\alpha_2\delta$-2: **Figure 1A**, present study; $\alpha_2\delta$-3: Neely et al., 2010; Landmann et al., 2018a,b). One intriguing observation presented here certainly is that not only the number of $\alpha_2\delta$ double knockout offspring but already the amount of single knockout pups was significantly reduced in double heterozygous breedings of all $\alpha_2\delta$ inter-crosses (**Figures 1B–D**, left graphs). This surprising discrepancy between single heterozygous and double heterozygous matings might suggest that even single knockouts display a decreased chance of survival if obtained together with a high number of heterozygous or wildtype siblings. Such premature mortality in offspring could result either from physiological and/or behavioral deficits in mutant parenting animals, pups themselves, or a combination of both.

In the first scenario, behaviorally affected female mice might display reduced parental care-taking abilities or even conduct infanticide (Kuroda and Tsuneoka, 2013), which is supported by the correlation of excessive grooming behavior with extraordinarily high infant mortality. Along these lines, a previous study found abnormal occurrences of infant mortality using $\alpha_2\delta$-3 knockout mice as breeders, likely associated with reduced maternal care-taking due to deficits in vocalization and hearing (Landmann et al., 2018a). While we did not detect any obvious occurrences in our $\alpha_2\delta$-3 single knockout mouse line, we specifically observed infant mortality in $\alpha_2\delta$-1/-2 and $\alpha_2\delta$-2/-3 matings, which often resulted in the loss of complete litters at P0–1. Therefore, we occasionally added BALB/c foster mothers to pregnant females, which helped to increase the

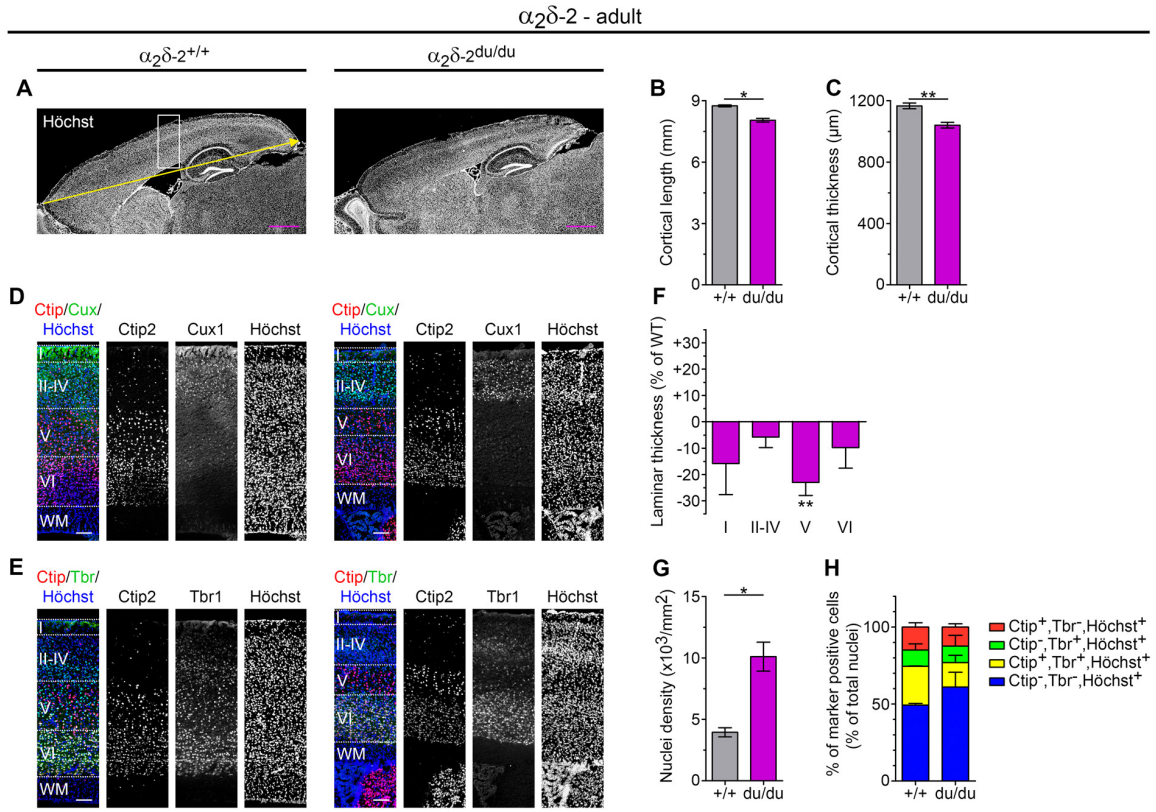

FIGURE 5 | Adult ducky mice display a reduced thickness of cortical layers and increased cell densities. **(A–C)** Representative micrographs of mid-sagittal cryosections obtained from adult (8–13-weeks-old) wildtype and $\alpha_2\delta$-2 mutant (ducky) mouse brains **(A)**. Slides were counterstained with the nuclear marker Höchst to analyze anterior-posterior length (yellow arrow and quantification in panel **(B)** and thickness **(C)** of the somatosensory cortex, which were both significantly decreased in ducky mice. Two **(B)** and three **(C)** mice per genotype were analyzed and bar graphs depict means of mice ± SEM. *Statistics*: unpaired *t*-test: **(B)** $t_{(2)}$:6.9, $p = 0.02$; **(C)** $t_{(4)}$:4.8, $p = 0.009$. Representative micrographs of triple immunofluorescence labelings of consecutive sagittal sections with layer-specific markers Ctip2 (red; layer V), Cux1 (green; layer II–IV) or Tbr1 (green; layer VI) and Höchst (blue) at the level of somatosensory cortex (see the boxed region in **A**), showing that cortical lamination is preserved in adult ducky mice **(D,E)**. Quantification of the laminar thickness **(F)**, total cell density **(G)**, and percentage of marker positive neurons of total cells **(H)**. The thickness of individual layers was reduced in ducky mice when compared to wild-type controls, the most affected being layer V (**F**, 23%). This effect was accompanied by a 2.5-fold increase in nuclear cell density **(G)** while the proportion of cells expressing individual markers remained unaffected **(H)**. Two mice per genotype were analyzed and bar graphs depict means of mice ± SEM. *Statistics*: **(F)** Two-way RM ANOVA with Holm–Sidak *posthoc* analysis: genotype: $F_{(1,6)} = 17.9$, $p = 0.05$, layer: $F_{(3,6)} = 150.5$, $p < 0.001$, genotype x layer: $F_{(3,6)} = 1.4$, $p = 0.34$, *posthoc*: $^{**}p < 0.001$ between ducky and wildtype within layer 5; **(G)** unpaired *t*-test: $t_{(2)}$:5.0, $p = 0.038$; **(H)** Two-way RM ANOVA with Holm–Sidak *posthoc* analysis: genotype: $F_{(1,6)} = 0.6$, $p = 0.5$, marker: $F_{(3,6)} = 26.3$, $p < 0.001$, genotype x marker: $F_{(3,6)} = 1.2$, $p = 0.39$. Symbols in graphs indicate significance levels: $^{*}p < 0.05$; $^{**}p < 0.01$. Scale bars, 1 mm (**A,B**) and 100 µm (**D,E**).

premature survival chance of $\alpha_2\delta$ mutant offspring. Alternatively, given that $\alpha_2\delta$-2 expression is also detected in the placenta (Klugbauer et al., 1999) and $\alpha_2\delta$-3 is discussed as a tumor suppressor for breast cancer (Palmieri et al., 2012), deficits in nutrient supply during pregnancy or lactation might be another conceivable cause for the observed premature mortality (Watkin et al., 2008). As our husbandry strategies were adapted to facilitate analysis of juvenile and adult mice future studies should focus on more detailed behavioral investigations of paternal care-taking abilities, including video analysis of feeding behavior with and without the use of foster mothers.

Alternatively, mutant progeny may also suffer from organ dysfunction or so far unidentified defects in embryonic or early postnatal development, which could affect nutrient supply or the pup's ability to compete with healthy siblings (Kuroda and Tsuneoka, 2013). This notion might be supported by $\alpha_2\delta$ isoform-specific effects we observed on premature survival (**Figures 1B–D**, left graphs): Mendelian ratios were exclusively reduced in $\alpha_2\delta$-2 mutant ducky mice obtained from $\alpha_2\delta$-1/-2 (**Figure 1C**) or $\alpha_2\delta$-2/-3 (**Figure 1D**) double heterozygous breedings, while $\alpha_2\delta$-1 and $\alpha_2\delta$-3 single knockouts were born at expected probabilities. Similarly, $\alpha_2\delta$-1 single knockout mice were detected at a significantly lower frequency than $\alpha_2\delta$-3 single knockouts obtained from $\alpha_2\delta$-1/-3 double heterozygous breedings (**Figure 1B**). These data implicate that $\alpha_2\delta$-1 and $\alpha_2\delta$-2 can partially compensate for the loss of $\alpha_2\delta$-3 in $\alpha_2\delta$-3 single knockout mice.

At present, our findings indicate a combination of the above-provided explanations for premature death. To ultimately determine the cause of infant mortality in $\alpha_2\delta$ single and

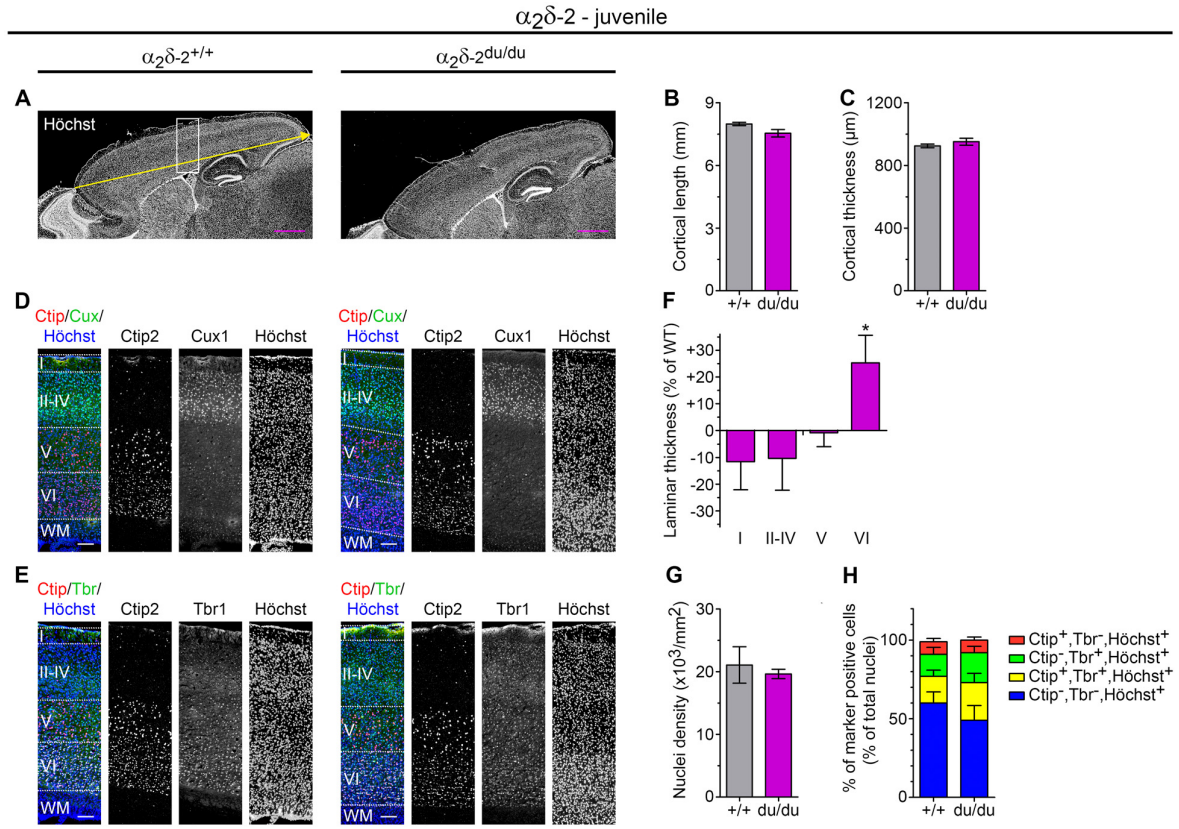

FIGURE 6 | Juvenile ducky mice display altered cortical cytoarchitecture. **(A–C)** Representative micrographs of mid-sagittal cryosections obtained from juvenile (3-weeks-old) wildtype and $\alpha_2\delta$-2 mutant (ducky) mouse brains **(A)**. Slides were counterstained with the nuclear marker Höchst to analyze anterior-posterior length (yellow arrow and quantification in panel **B**) and thickness **(C)** of the somatosensory cortex. Both cortex length and cortical thickness of ducky mice did not significantly differ compared to wildtypes. Four mice per genotype were analyzed and bar graphs depict means of mice ± SEM. *Statistics*: unpaired *t*-test: **(B)** $t_{(6)}$: 2.3, $p = 0.06$; **(C)** $t_{(6)}$: 1.1, $p = 0.33$. Representative micrographs of triple immunofluorescence labelings of consecutive sagittal sections with layer-specific markers Ctip2 (red; layer V), Cux1 (green; layer II–IV) or Tbr1 (green; layer VI) and Höchst (blue) at the level of somatosensory cortex (see the boxed region in **A**), indicating lamination is preserved in juvenile ducky mice **(D,E)**. However, further quantitative analysis of laminar thickness **(F)**, total cell density **(G)**, and percentage of marker positive neurons of total cells **(H)** revealed a significant increase of layer VI in juvenile ducky mice (**F**, 25%) without apparent effects on total cell density **(G)** or proportion of marker positive cells **(H)**. Four mice per genotype were analyzed and bar graphs depict means of mice ± SEM. *Statistics*: **(F)** two-way RM ANOVA with Holm–Sidak *posthoc* analysis: genotype: $F_{(1,18)} = 0.17$, $p = 0.7$, layer: $F_{(3,18)} = 124.7$, $p < 0.001$, genotype × layer: $F_{(3,18)} = 2.5$, $p = 0.095$, *posthoc*: $^*p < 0.05$ between ducky and wildtype within layer 6; **(G)** unpaired *t*-test: $t_{(6)}$: 5.0, $p = 0.65$; **(H)** two-way RM ANOVA with Holm–Sidak *post hoc* analysis: genotype: $F_{(1,18)} = 0.83$, $p = 0.4$, marker: $F_{(3,18)} = 21.6$, $p < 0.001$, genotype × marker: $F_{(3,18)} = 0.87$, $p = 0.48$. Symbols in graphs indicate significance levels: $^*p < 0.05$. Scale bars, 1 mm **(A,B)** and 100 µm **(D,E)**.

double knockout mice in $\alpha_2\delta$ inter-crosses, the challenge of future investigations will be to elucidate the still incompletely understood $\alpha_2\delta$ isoform expression levels in distinct tissues during development. Currently, comparative analysis of $\alpha_2\delta$ protein expression levels is prevented by the limited quality of available isoform-specific antibodies. For example, antibodies against $\alpha_2\delta$-1 are not suitable for detecting native proteins (Muller et al., 2010) and antibodies against $\alpha_2\delta$-3 do not allow protein detection at the cellular and sub-cellular level (Stephani et al., 2019).

Loss of $\alpha_2\delta$ Isoforms Differentially Affects Neurological Disease

We observed that $\alpha_2\delta$-2 mutant, $\alpha_2\delta$-1/-2, and $\alpha_2\delta$-2/-3 double knockout mice displayed the typical ducky phenotype described by an ataxic, wide-based gait and epileptic seizures. However, $\alpha_2\delta$-1/-2 and $\alpha_2\delta$-2/-3 double knockout mice showed a more severe disease progression than ducky individuals, which was best visualized by their highly reduced body weights (**Figure 2C**) and increased mortality during the first month after birth (Schoepf et al., 2019). In contrast, the $\alpha_2\delta$-1 and $\alpha_2\delta$-3 single knockout mouse strains used to generate $\alpha_2\delta$-1/-3 double knockout mice displayed relatively mild neurological phenotypes (Landmann et al., 2018a,b; Zhou et al., 2018). Moreover, no effects on survival ($\alpha_2\delta$-3), or less severely affected life expectancy ($\alpha_2\delta$-1) have been demonstrated so far, whereas $\alpha_2\delta$-1/-3 double knockout mice showed a decreased mean survival comparable to that of ducky mice (3 months; Schoepf et al., 2019). At a first glance, these data indicate redundant functions for $\alpha_2\delta$ isoforms in postnatal survival and development. This notion might be

supported by their partly overlapping and relatively ubiquitous distribution in distinct adult organs: $\alpha_2\delta$-1 and $\alpha_2\delta$-2 are expressed in the heart, skeletal muscle, and pancreas (Ellis et al., 1988; Klugbauer et al., 1999; Gao et al., 2000; Mastrolia et al., 2017), and $\alpha_2\delta$-1, $\alpha_2\delta$-2, and $\alpha_2\delta$-3 are detected in various regions of the brain (Cole et al., 2005; Schlick et al., 2010; Geisler et al., 2019). Therefore, simultaneous loss of two $\alpha_2\delta$ subunit isoforms might cause developmental defects or physiological dysfunction, which would be normally compensated by remaining isoforms in single knockout mice.

Alternatively, the reduced life spans of $\alpha_2\delta$-1/-3, $\alpha_2\delta$-1/-2, and $\alpha_2\delta$-2/-3 double knockout mice could be related to a compound effect which is triggered by the combination of two $\alpha_2\delta$ isoforms deleted. This idea might be underpinned by the partially tissue-specific expression patterns and distinct disease phenotypes of individual single knockout mice. For instance, deletion of $\alpha_2\delta$-1 impairs cortical excitatory synaptogenesis (Risher et al., 2018), cardiac function (Fuller-Bicer et al., 2009), and insulin release (Mastrolia et al., 2017) without apparently altering protein (Fuller-Bicer et al., 2009) or mRNA (Mastrolia et al., 2017) expression levels of other isoforms. These reports indicate that $\alpha_2\delta$-1 either exerts specific functions or that low amounts of the remaining isoforms likely do not suffice to compensate for the loss of $\alpha_2\delta$-1. Along those lines, the severe consequences of $\alpha_2\delta$-2 mutations in animal models (Barclay et al., 2001; Brill et al., 2004; Ivanov et al., 2004; Donato et al., 2006) are likely caused by its predominant expression in the cerebellum (Schlick et al., 2010). Notably, $\alpha_2\delta$-3 knockout mice display overexpression of Ca_V2 calcium channel subtypes in the brain, possibly resulting in enhanced neuronal excitability (Landmann et al., 2018b). Therefore, the increased postnatal lethality and severe neurological disease of $\alpha_2\delta$-1/-3, $\alpha_2\delta$-1/-2, and $\alpha_2\delta$-2/-3 double knockout animals might be related to a synthetic lethal effect, as suggested previously for the synaptic cell adhesion molecules neuroligins (Varoqueaux et al., 2006). Here, $\alpha_2\delta$ isoform-specific mutant phenotypes in distinct tissues possibly accumulate, leading to dysfunction of organs or pivotal brain networks.

Several principal observations argue for distinct disease mechanisms in the individual mouse models: first, ducky, $\alpha_2\delta$-1/-2, and $\alpha_2\delta$-2/-3 double knockout mice showed apparent epileptic episodes, while similar seizures during handling were never observed in $\alpha_2\delta$-1/-3 double knockout mice. Second, even though $\alpha_2\delta$-1/-3 double knockout mice displayed abnormal locomotion, gait appeared different compared to the typical waddling gait of ducky, $\alpha_2\delta$-1/-2, and $\alpha_2\delta$-2/-3 knockout mice. Third, breeding pairs of distinct $\alpha_2\delta$-2/-3 inter-crosses exhibited abnormal behavior including self-injurious repetitive grooming. Fourth, loss of $\alpha_2\delta$ isoforms differentially affected brain/body ratios in ducky, $\alpha_2\delta$-1/-3 and $\alpha_2\delta$-2/-3 double knockout mice (**Figure 2**): in all three analyzed mouse models juvenile mice showed a disproportionate body to brain growth, reflected as a highly decreased bodyweight together with a moderately reduced brain size. Whereas adult ducky mice displayed even higher brain/body ratios, this effect was normalized in $\alpha_2\delta$-1/-3 double knockout mice until adulthood. Fifth, although direct comparison of the distinct mouse models was precluded as mice were maintained in different genetic backgrounds (see "Materials and Methods" section), the volumetric analysis demonstrated concurrent effects on specific brain regions caused by deletion of distinct $\alpha_2\delta$ subunits (**Figure 4**): cerebellum and cortex were significantly reduced when $\alpha_2\delta$-2 was absent, and lack of $\alpha_2\delta$-3 specifically elicited a volume decrease in the corpus callosum. Of note, the fact that $\alpha_2\delta$-1/-3 and $\alpha_2\delta$-1/-2 double knockout mice, which were both maintained in a mixed 129J × C57BL/6N background, displayed distinct disease phenotypes argues against unspecific effects related to the use of different background strains. Thus, these data suggest that loss of $\alpha_2\delta$ isoforms differentially affects postnatal survival, development, and neurological disease.

Roles of $\alpha_2\delta$-2 in the Postnatal Brain and Implications for the Brain Motor Circuitry

Given the importance of $\alpha_2\delta$ subunits in synapse formation and wiring (Pirone et al., 2014; Fell et al., 2016; Risher et al., 2018; Geisler et al., 2019; Schoepf et al., 2019) a reduction of distinct brain regions could be either related to developmental impairment or neurodegenerative processes. Underdevelopment of selective regions of the CNS including the spinal cord, pons, and cerebellum was among the first documented features of young (<P26) $\alpha_2\delta$-2 mutant ducky mice (Meier, 1968; Brodbeck et al., 2002). Notably, besides decreased cerebellar volume, which is most likely associated with smaller and atrophic Purkinje cells (Meier, 1968; Brodbeck et al., 2002), we additionally observed that cortex size was significantly reduced in adult ducky mice. These data are insofar interesting as no overt cortical abnormalities have been described in the original reports of young ducky mice (Meier, 1968). Moreover, cortical malformations have been previously associated with aberrant $\alpha_2\delta$-1 signaling (Lau et al., 2017) and neurological disorders including epilepsy and autism (Chen et al., 2015; Fenlon et al., 2015; Hong and Mah, 2015). Because layer formation is largely complete by P7, and synapse formation and maturation stabilize until P21 in mice (Li et al., 2008; Farhy-Tselnicker and Allen, 2018), the cortex thus represents an intriguing model system to address possible neurodegenerative and neurodevelopmental processes in ducky mice.

Analyzing thickness, cell densities, and lamination in cortices of adult (8-week, **Figure 5**) and juvenile ducky mice (3-weeks, **Figure 6**) led us to draw several principal observations and conclusions: total cortex thickness and cell densities were not altered in juvenile ducky mice, thus corroborating previous studies detecting no obvious anatomical abnormalities in cortices of young mice (Meier, 1968). Importantly, however, adult ducky mice displayed a reduction in total thickness accompanied by a concomitant increase in cell densities. Moreover, cortical lamination was preserved both in juvenile and adult mice. Altogether, these data suggest a progressive decrease of cortical thickness, rather than atypical neuron migration or developmental retardation. Thus, we hypothesize that cortical thinning is likely associated with a reduction in spacing, which reflects the amount of neuronal and glial cell processes, spines, and synaptic contacts.

Notably, we found that the thickness of layer V was most severely and consistently reduced in somatosensory cortices of adult animals. What might be this finding's relevance to the neuropathological ducky phenotype? In general, layer V pyramidal cells receive excitatory and inhibitory inputs from cortical and thalamic neurons (Slater et al., 2019), while they project their axons to major subcortical motor systems including thalamic nuclei, striatum, pons, and spinal cord (Thomson and Lamy, 2007; Yu et al., 2008). A previous study showed that $\alpha_2\delta$-2 mRNA was specifically expressed within regions of the motor circuitry including the spinal cord, as well as GABAergic neurons of the cortex, brainstem, cerebellum, habenula, and nucleus reticularis of the thalamus (Cole et al., 2005), all of which are atrophic in young ducky mice (Meier, 1968). Together, these observations close the loop between the above-mentioned brain regions and the ducky phenotype: young ducky mice exhibit an ataxic gait (>P11) and spike-wave discharges (SWD) associated with aberrant thalamocortical oscillations (Meier, 1968; Barclay et al., 2001). We previously found that the presynaptic expression of $\alpha_2\delta$-2 modulates synaptic connectivity and the localization of inhibitory postsynaptic receptors (Geisler et al., 2019). Thus, it is tempting to speculate that reduced cortical thickness occurs secondary to aberrant connectivity of excitatory/inhibitory imbalance within the brain motor circuitry, ultimately causing destabilization and loss of synapses.

CACNA2D as Risk Genes for Autism Spectrum Disorders?

Large brain volumes which normalize until adulthood, as well as altered size of white matter structures, are mentioned as specific traits of autism patients (Vidal et al., 2006; Chen and Van Horn, 2017) and animal models with autistic-like phenotypes (Brodkin, 2007; Kane et al., 2012; Wang et al., 2016). Such disease characteristics are suggested to underlie developmental defects causing an excess number of neurons (Courchesne et al., 2011), increased number of synapses (Tang et al., 2014), and aberrant structural/functional connectivity (Wang et al., 2016). Previous studies showed that dysfunction in autistic-brain circuitry leads to abnormal behavior, comprising impaired reciprocal social interaction, communication deficits, and repetitive behaviors (Kane et al., 2012; Wang et al., 2016). Notably, we exclusively detected abnormal behavior comprising signs of stress, anxiety, and repetitive actions in $\alpha_2\delta$-2/-3 inter-crosses, whose severity was linked to a gradual decrease of the total amount of $\alpha_2\delta$-2 and particularly $\alpha_2\delta$-3 isoforms. The fact that all of the above-mentioned phenotypes demonstrated in the present study share similarities with other mutant mouse models displaying autistic-like characteristics (Peça et al., 2011; Kalueff et al., 2016; Wang et al., 2016), contributes to the accumulating evidence of CACNA2D3 as a potential risk gene for autism spectrum disorders (Iossifov et al., 2012; De Rubeis et al., 2014; Landmann et al., 2018a).

Future Perspectives

The neurological disease phenotypes described here are likely associated with different roles of $\alpha_2\delta$ isoforms associated with VGCC, NMDAR, and so-far unidentified interaction partners, which will inevitably influence each other. For instance, alterations in synapse differentiation will also affect VGCC expression and function, further influencing neuronal excitability and synaptic transmission (see discussion in Ablinger et al., 2020). Moreover, the partially severe phenotypes of existing single and double knockout mice further complicate the issue of addressing specific neuronal functions. In a nutshell, to study the roles of individual $\alpha_2\delta$ isoforms in the normal and diseased brain will require the development of conditional knockout animal models, which will further aid in assessing autism-like behavior in $\alpha_2\delta$ mutant mice.

DATA AVAILABILITY STATEMENT

The raw data supporting the conclusions of this article will be made available by the authors, without undue reservation.

ETHICS STATEMENT

The animal study was reviewed and approved by Austrian Federal Ministry of Education, Science and Research.

AUTHOR CONTRIBUTIONS

SG designed, performed, and analyzed experiments and wrote the manuscript. AB and CS participated in the experimental work and/or data analysis and/or planning/designing of experiments. CS, AS, and NS contributed analytic tools and/or planning of experiments. GO conceived the study, supervised the project, designed and analyzed experiments, and wrote the manuscript. All authors contributed to the article and approved the submitted version.

FUNDING

This work was supported by grants from the Austrian Science Fund (P24079, F4415, and DOC30-B30). This work was part of the Ph.D. thesis of SG and CS.

ACKNOWLEDGMENTS

We thank Hermann Dietrich, Anja Beierfuß, and their team for animal care; Jutta Engel for providing $\alpha_2\delta$-3 knockout mice; Bernhard Flucher for critical discussions; Georg Dechant for providing samples of Ctip2, Cux1, and Tbr1 antibodies.

SUPPLEMENTARY MATERIAL

The Supplementary Material for this article can be found online at: https://www.frontiersin.org/articles/10.3389/fnsyn.2021.634412/full#supplementary-material.

REFERENCES

Abdurakhmanova, S., Chary, K., Kettunen, M., Sierra, A., and Panula, P. (2017). Behavioral and stereological characterization of Hdc KO mice: relation to Tourette syndrome. *J. Comp. Neurol.* 525, 3476–3487. doi: 10.1002/cne.24279

Ablinger, C., Geisler, S. M., Stanika, R. I., Klein, C. T., and Obermair, G. J. (2020). Neuronal α2δ proteins and brain disorders. *Pflugers Arch.* 472, 845–863. doi: 10.1007/s00424-020-02420-2

Arikkath, J., and Campbell, K. P. (2003). Auxiliary subunits: essential components of the voltage-gated calcium channel complex. *Curr. Opin. Neurobiol.* 13, 298–307. doi: 10.1016/s0959-4388(03)00066-7

Arlotta, P., Molyneaux, B. J., Chen, J., Inoue, J., Kominami, R., and Macklis, J. D. (2005). Neuronal subtype-specific genes that control corticospinal motor neuron development *in vivo*. *Neuron* 45, 207–221. doi: 10.1016/j.neuron.2004.12.036

Barclay, J., Balaguero, N., Mione, M., Ackerman, S. L., Letts, V. A., Brodbeck, J., et al. (2001). Ducky mouse phenotype of epilepsy and ataxia is associated with mutations in the Cacna2d2 gene and decreased calcium channel current in cerebellar Purkinje cells. *J. Neurosci.* 21, 6095–6104. doi: 10.1523/JNEUROSCI.21-16-06095.2001

Betancourt, J., Katzman, S., and Chen, B. (2014). Nuclear factor one B regulates neural stem cell differentiation and axonal projection of corticofugal neurons. *J. Comp. Neurol.* 522, 6–35. doi: 10.1002/cne.23373

Bolivar, V. J., Walters, S. R., and Phoenix, J. L. (2007). Assessing autism-like behavior in mice: variations in social interactions among inbred strains. *Behav. Brain Res.* 176, 21–26. doi: 10.1016/j.bbr.2006.09.007

Brill, J., Klocke, R., Paul, D., Boison, D., Gouder, N., Klugbauer, N., et al. (2004). entla, a novel epileptic and ataxic Cacna2d2 mutant of the mouse. *J. Biol. Chem.* 279, 7322–7330. doi: 10.1074/jbc.M308778200

Brockhaus, J., Schreitmüller, M., Repetto, D., Klatt, O., Reissner, C., Elmslie, K., et al. (2018). α-Neurexins together with α2δ-1 auxiliary subunits regulate Ca^{2+} influx through Ca v 2.1 channels. *J. Neurosci.* 38, 8277–8294. doi: 10.1523/JNEUROSCI.0511-18.2018

Brodbeck, J., Davies, A., Courtney, J.-M., Meir, A., Balaguero, N., Canti, C., et al. (2002). The ducky mutation in Cacna2d2 results in altered Purkinje cell morphology and is associated with the expression of a truncated α 2 δ-2 protein with abnormal function. *J. Biol. Chem.* 277, 7684–7693. doi: 10.1074/jbc.M109404200

Brodkin, E. S. (2007). BALB/c mice: low sociability and other phenotypes that may be relevant to autism. *Behav. Brain Res.* 176, 53–65. doi: 10.1016/j.bbr.2006.06.025

Butler, K. M., Holt, P. J., Milla, S. S., da Silva, C., Alexander, J. J., and Escayg, A. (2018). Epileptic encephalopathy and cerebellar atrophy resulting from compound heterozygous CACNA2D2 variants. *Case Rep. Genet.* 2018:6308283. doi: 10.1155/2018/6308283

Calderon-Rivera, A., Andrade, A., Hernandez-Hernandez, O., Gonzalez-Ramirez, R., Sandoval, A., Rivera, M., et al. (2012). Identification of a disulfide bridge essential for structure and function of the voltage-gated Ca^{2+} channel α(2)δ-1 auxiliary subunit. *Cell Calcium* 51, 22–30. doi: 10.1016/j.ceca.2011.10.002

Catterall, W. A. (2000). Structure and regulation of voltage-gated Ca^{2+} channels. *Annu. Rev. Cell Dev. Biol.* 16, 521–555. doi: 10.1146/annurev.cellbio.16.1.521

Chang, M., Suzuki, N., and Kawai, H. D. (2018). Laminar specific gene expression reveals differences in postnatal laminar maturation in mouse auditory, visual and somatosensory cortex. *J. Comp. Neurol.* 526, 2257–2284. doi: 10.1002/cne.24481

Chen, Y., Huang, W.-C., Sejourne, J., Clipperton-Allen, A. E., and Page, D. T. (2015). Pten mutations alter brain growth trajectory and allocation of cell types through elevated -catenin signaling. *J. Neurosci.* 35, 10252–10267. doi: 10.1523/JNEUROSCI.5272-14.2015

Chen, J., Li, L., Chen, S.-R., Chen, H., Xie, J.-D., Sirrieh, R. E., et al. (2018). The α2δ-1-NMDA receptor complex is critically involved in neuropathic pain development and gabapentin therapeutic actions. *Cell Rep.* 22, 2307–2321. doi: 10.1016/j.celrep.2018.02.021

Chen, B., Schaevitz, L. R., and McConnell, S. K. (2005). Fezl regulates the differentiation and axon targeting of layer 5 subcortical projection neurons in cerebral cortex. *Proc. Natl. Acad. Sci. U S A* 102, 17184–17189. doi: 10.1073/pnas.0508732102

Chen, C., Van Horn, J. D., and GENDAAR Research Consortium. (2017). Developmental neurogenetics and multimodal neuroimaging of sex differences in autism. *Brain Imaging Behav.* 11, 38–61. doi: 10.1007/s11682-015-9504-3

Chioza, B. A., Aicardi, J., Aschauer, H., Brouwer, O., Callenbach, P., Covanis, A., et al. (2009). Genome wide high density SNP-based linkage analysis of childhood absence epilepsy identifies a susceptibility locus on chromosome 3p23–p14. *Epilepsy Res.* 87, 247–255. doi: 10.1016/j.eplepsyres.2009.09.010

Cole, R. L., Lechner, S. M., Williams, M. E., Prodanovich, P., Bleicher, L., Varney, M. A., et al. (2005). Differential distribution of voltage-gated calcium channel α-2 δ (α2δ) subunit mRNA-containing cells in the rat central nervous system and the dorsal root ganglia. *J. Comp. Neurol.* 491, 246–269. doi: 10.1002/cne.20693

Courchesne, E., Mouton, P. R., Calhoun, M. E., Semendeferi, K., Ahrens-Barbeau, C., Hallet, M. J., et al. (2011). Neuron number and size in prefrontal cortex of children with autism. *JAMA* 306, 2001–2010. doi: 10.1001/jama.2011.1638

De Jongh, K. S., Warner, C., and Catterall, W. A. (1990). Subunits of purified calcium channels α 2 and δ are encoded by the same gene. *J. Biol. Chem.* 265, 14738–14741. doi: 10.1016/S0021-9258(18)77174-3

De Rubeis, S., He, X., Goldberg, A. P., Poultney, C. S., Samocha, K., Ercument Cicek, A., et al. (2014). Synaptic, transcriptional and chromatin genes disrupted in autism. *Nature* 515, 209–215. doi: 10.1038/nature13772

Ding, M., Weng, C., Fan, S., Cao, Q., and Lu, Z. (2017). Purkinje cell degeneration and motor coordination deficits in a new mouse model of autosomal recessive spastic ataxia of charlevoix-saguenay. *Front. Mol. Neurosci.* 10:121. doi: 10.3389/fnmol.2017.00121

Dolphin, A. C. (2018). Voltage-gated calcium channel α2δ subunits: an assessment of proposed novel roles. *F1000Res.* 7:1830. doi: 10.12688/f1000research.16104.1

Donato, R., Page, K. M., Koch, D., Nieto-Rostro, M., Foucault, I., Davies, A., et al. (2006). The ducky(2J) mutation in Cacna2d2 results in reduced spontaneous Purkinje cell activity and altered gene expression. *J. Neurosci.* 26, 12576–12586. doi: 10.1523/JNEUROSCI.3080-06.2006

Dudanova, I., Tabuchi, K., Rohlmann, A., Südhof, T. C., and Missler, M. (2007). Deletion of α-neurexins does not cause a major impairment of axonal pathfinding or synapse formation. *J. Comp. Neurol.* 502, 261–274. doi: 10.1002/cne.21305

Edvardson, S., Oz, S., Abulhijaa, F. A., Taher, F. B., Shaag, A., Zenvirt, S., et al. (2013). Early infantile epileptic encephalopathy associated with a high voltage gated calcium channelopathy. *J. Med. Genet.* 50, 118–123. doi: 10.1136/jmedgenet-2012-101223

Ellis, S. B., Williams, M. E., Ways, N. R., Brenner, R., Sharp, A. H., Leung, A. T., et al. (1988). Sequence and expression of mRNAs encoding the α 1 and α 2 subunits of a DHP-sensitive calcium channel. *Science* 241, 1661–1664. doi: 10.1126/science.2458626

Eroglu, Ç., Allen, N. J., Susman, M. W., O'Rourke, N. A., Park, C. Y., Özkan, E., et al. (2009). Gabapentin receptor α2δ-1 is a neuronal thrombospondin receptor responsible for excitatory CNS synaptogenesis. *Cell* 139, 380–392. doi: 10.1016/j.cell.2009.09.025

Farhy-Tselnicker, I., and Allen, N. J. (2018). Astrocytes, neurons, synapses: a tripartite view on cortical circuit development. *Neural Dev.* 13:7. doi: 10.1186/s13064-018-0104-y

Favero, C. B., Henshaw, R. N., Grimsley-Myers, C. M., Shrestha, A., Beier, D. R., and Dwyer, N. D. (2013). Mutation of the BiP/GRP78 gene causes axon outgrowth and fasciculation defects in the thalamocortical connections of the mammalian forebrain. *J. Comp. Neurol.* 521, 677–696. doi: 10.1002/cne.23199

Felix, R., Gurnett, C. A., De Waard, M., and Campbell, K. P. (1997). Dissection of functional domains of the voltage-dependent Ca^{2+} channel α2δ subunit. *J. Neurosci.* 17, 6884–6891. doi: 10.1523/JNEUROSCI.17-18-06884.1997

Fell, B., Eckrich, S., Blum, K., Eckrich, T., Hecker, D., Obermair, G. J., et al. (2016). α2δ2 controls the function and trans-synaptic coupling of Cav1.3 channels in mouse inner hair cells and is essential for normal hearing. *J. Neurosci.* 36, 11024–11036. doi: 10.1523/JNEUROSCI.3468-14.2016

Fenlon, L. R., Liu, S., Gobius, I., Kurniawan, N. D., Murphy, S., Moldrich, R. X., et al. (2015). Formation of functional areas in the cerebral cortex is disrupted in a mouse model of autism spectrum disorder. *Neural Dev.* 10:10. doi: 10.1186/s13064-015-0033-y

Fuller-Bicer, G. A., Varadi, G., Koch, S. E., Ishii, M., Bodi, I., Kadeer, N., et al. (2009). Targeted disruption of the voltage-dependent calcium channel α 2 /δ-1-subunit. *Am. J. Physiol. Circ. Physiol.* 297, H117–H124. doi: 10.1152/ajpheart.00122.2009

Gao, B., Sekido, Y., Maximov, A., Saad, M., Forgacs, E., Latif, F., et al. (2000). Functional properties of a new voltage-dependent calcium channel α(2)δ auxiliary subunit gene (CACNA2D2). *J. Biol. Chem.* 275, 12237–12242. doi: 10.1074/jbc.275.16.12237

Gee, N. S., Brown, J. P., Dissanayake, V. U., Offord, J., Thurlow, R., and Woodruff, G. N. (1996). The novel anticonvulsant drug, gabapentin (Neurontin), binds to the α2δ subunit of a calcium channel. *J. Biol. Chem.* 271, 5768–5776. doi: 10.1074/jbc.271.10.5768

Geisler, S., Schopf, C. L., and Obermair, G. J. (2015). Emerging evidence for specific neuronal functions of auxiliary calcium channel α(2)δ subunits. *Gen. Physiol. Biophys.* 34, 105–118. doi: 10.4149/gpb_2014037

Geisler, S., Schöpf, C. L., Stanika, R., Kalb, M., Campiglio, M., Repetto, D., et al. (2019). Presynaptic α_2 δ-2 calcium channel subunits regulate postsynaptic $GABA_A$ -receptor abundance and axonal wiring. *J. Neurosci.* , 2218–2234. doi: 10.1016/j.neuron.2004.12.048

Glaser, J. R., and Glaser, E. M. (2000). Stereology, morphometry and mapping: the whole is greater than the sum of its parts. *J. Chem. Neuroanat.* 20, 115–126. doi: 10.1016/s0891-0618(00)00073-9

Gong, H. C., Hang, J., Kohler, W., Li, L., and Su, T. Z. (2001). Tissue-specific expression and gabapentin-binding properties of calcium channel α2δ subunit subtypes. *J. Membr. Biol.* 184, 35–43. doi: 10.1007/s00232-001-0072-7

Hevner, R. F. (2007). Layer-specific markers as probes for neuron type identity in human neocortex and malformations of cortical development. *J. Neuropathol. Exp. Neurol.* 66, 101–109. doi: 10.1097/nen.0b013e180301c06

Hobom, M., Dai, S., Marais, E., Lacinova, L., Hofmann, F., and Klugbauer, N. (2000). Neuronal distribution and functional characterization of the calcium channel α_2 δ-2 subunit. *Eur. J. Neurosci.* 12, 1217–1226. doi: 10.1046/j.1460-9568.2000.01009.x

Hong, S.-T., and Mah, W. (2015). A critical role of GIT1 in vertebrate and invertebrate brain development. *Exp. Neurobiol.* 24, 8–16. doi: 10.5607/en.2015.24.1.8

Huang, Z., Yu, Y., Shimoda, Y., Watanabe, K., and Liu, Y. (2012). Loss of neural recognition molecule NB-3 delays the normal projection and terminal branching of developing corticospinal tract axons in the mouse. *J. Comp. Neurol.* 520, 1227–1245. doi: 10.1002/cne.22772

Iossifov, I., Ronemus, M., Levy, D., Wang, Z., Hakker, I., Rosenbaum, J., et al. (2012). *De novo* gene disruptions in children on the autistic spectrum. *Neuron* 74, 285–299. doi: 10.1016/j.neuron.2012.04.009

Ivanov, S. V., Ward, J. M., Tessarollo, L., McAreavey, D., Sachdev, V., Fananapazir, L., et al. (2004). Cerebellar ataxia, seizures, premature death and cardiac abnormalities in mice with targeted disruption of the Cacna2d2 gene. *Am. J. Pathol.* 165, 1007–1018. doi: 10.1016/S0002-9440(10)63362-7

Jaitner, C., Reddy, C., Abentung, A., Whittle, N., Rieder, D., Delekate, A., et al. (2016). Satb2 determines miRNA expression and long-term memory in the adult central nervous system. *eLife* 5:e17361. doi: 10.7554/eLife.17361

Kalueff, A. V., Stewart, A. M., Song, C., Berridge, K. C., Graybiel, A. M., and Fentress, J. C. (2016). Neurobiology of rodent self-grooming and its value for translational neuroscience. *Nat. Rev. Neurosci.* 17, 45–59. doi: 10.1038/nrn.2015.8

Kane, M. J., Angoa-Peréz, M., Briggs, D. I., Sykes, C. E., Francescutti, D. M., Rosenberg, D. R., et al. (2012). Mice genetically depleted of brain serotonin display social impairments, communication deficits and repetitive behaviors: possible relevance to autism. *PLoS One* 7:e48975. doi: 10.1371/journal.pone.0048975

Kerov, V., Laird, J. G., Joiner, M.-L., Knecht, S., Soh, D., Hagen, J., et al. (2018). $\alpha_2\delta$-4 is required for the molecular and structural organization of rod and cone photoreceptor synapses. *J. Neurosci.* 38, 6145–6160. doi: 10.1523/JNEUROSCI.3818-16.2018

Klugbauer, N., Lacinová, L., Marais, E., Hobom, M., and Hofmann, F. (1999). Molecular diversity of the calcium channel α2δ subunit. *J. Neurosci.* 19, 684–691. doi: 10.1523/JNEUROSCI.19-02-00684.1999

Knoflach, D., Kerov, V., Sartori, S. B., Obermair, G. J., Schmuckermair, C., Liu, X., et al. (2013). Cav1.4 IT mouse as model for vision impairment in human congenital stationary night blindness type 2. *Channels* 7, 503–513. doi: 10.4161/chan.26368

Kroll, M. R., Viss, E. S., Lamb, J., Horstman, J., Powell, A., Van Wyk, A., et al. (2011). Asynchronous expression of the homeodomain protein CUX1 in Sertoli cells and spermatids during spermatogenesis in mice. *Biol. Reprod.* 84, 455–465. doi: 10.1095/biolreprod.110.084335

Kuroda, K. O., and Tsuneoka, Y. (2013). Assessing postpartum maternal care, alloparental behavior and infanticide in mice: with notes on chemosensory influences. *Methods Mol. Biol.* 1068, 331–347. doi: 10.1007/978-1-62703-619-1_25

Landmann, J., Richter, F., Classen, J., Richter, A., Penninger, J. M., and Bechmann, I. (2018a). Behavioral phenotyping of calcium channel (CACN) subunit $\alpha_2\delta$3 knockout mice: consequences of sensory cross-modal activation. *Behav. Brain Res.* 364, 393–402. doi: 10.1016/j.bbr.2017.12.032

Landmann, J., Richter, F., Oros-Peusquens, A.-M., Shah, N. J., Classen, J., Neely, G. G., et al. (2018b). Neuroanatomy of pain-deficiency and cross-modal activation in calcium channel subunit (CACN) $\alpha_2\delta$3 knockout mice. *Brain Struct. Funct.* 223, 111–130. doi: 10.1007/s00429-017-1473-4

Lau, L. A., Noubary, F., Wang, D., and Dulla, C. G. (2017). $\alpha_2\delta$-1 signaling drives cell death, synaptogenesis, circuit reorganization and gabapentin-mediated neuroprotection in a model of insult-induced cortical malformation. *eNeuro* 4:ENEURO.0316-17.2017. doi: 10.1523/ENEURO.0316-17.2017

Lee, S., Lee, E., Kim, R., Kim, J., Lee, S., Park, H., et al. (2018). Shank2 deletion in parvalbumin neurons leads to moderate hyperactivity, enhanced self-grooming and suppressed seizure susceptibility in mice. *Front. Mol. Neurosci.* 11:209. doi: 10.3389/fnmol.2018.00209

Li, H., Radford, J. C., Ragusa, M. J., Shea, K. L., McKercher, S. R., Zaremba, J. D., et al. (2008). Transcription factor MEF2C influences neural stem/progenitor cell differentiation and maturation *in vivo*. *Proc. Natl. Acad. Sci. U S A* 105, 9397–9402. doi: 10.1073/pnas.0802876105

Luong, M. X., van der Meijden, C. M., Xing, D., Hesselton, R., Monuki, E. S., Jones, S. N., et al. (2002). Genetic ablation of the CDP/Cux protein C terminus results in hair cycle defects and reduced male fertility. *Mol. Cell Biol.* 22, 1424–1437. doi: 10.1128/mcb.22.5.1424-1437.2002

Mairet-Coello, G., Tury, A., van Buskirk, E., Robinson, K., Genestine, M., and DiCicco-Bloom, E. (2012). p57 KIP2 regulates radial glia and intermediate precursor cell cycle dynamics and lower layer neurogenesis in developing cerebral cortex. *Development* 139, 475–487. doi: 10.1242/dev.067314

Mastrolia, V., Flucher, S. M., Obermair, G. J., Drach, M., Hofer, H., Renström, E., et al. (2017). Loss of $\alpha_2\delta$-1 calcium channel subunit function increases the susceptibility for diabetes. *Diabetes* 66, 897–907. doi: 10.2337/db16-0336

McKenna, W. L., Betancourt, J., Larkin, K. A., Abrams, B., Guo, C., Rubenstein, J. L. R., et al. (2011). Tbr1 and Fezf2 regulate alternate corticofugal neuronal identities during neocortical development. *J. Neurosci.* 31, 549–564. doi: 10.1523/JNEUROSCI.4131-10.2011

Meier, H. (1968). The neuropathology of ducky, a neurological mutation of the mouse. *Acta Neuropathol.* 11, 15–28. doi: 10.1007/BF00692792

Molyneaux, B. J., Arlotta, P., Menezes, J. R. L., and Macklis, J. D. (2007). Neuronal subtype specification in the cerebral cortex. *Nat. Rev. Neurosci.* 8, 427–437. doi: 10.1038/nrn2151

Moons, T., De Hert, M., Gellens, E., Gielen, L., Sweers, K., Jacqmaert, S., et al. (2016). Genetic evaluation of schizophrenia using the illumina humanexome chip. *PLoS One* 11:e0150464. doi: 10.1371/journal.pone.0150464

Muller, C. S., Haupt, A., Bildl, W., Schindler, J., Knaus, H.-G., Meissner, M., et al. (2010). Quantitative proteomics of the Cav2 channel nano-environments in the mammalian brain. *Proc. Natl. Acad. Sci. U S A* 107, 14950–14957. doi: 10.1073/pnas.1005940107

Nanou, E., and Catterall, W. A. (2018). Calcium channels, synaptic plasticity and neuropsychiatric disease. *Neuron* 98, 466–481. doi: 10.1016/j.neuron.2018.03.017

Neely, G. G., Hess, A., Costigan, M., Keene, A. C., Goulas, S., Langeslag, M., et al. (2010). A genome-wide *Drosophila* screen for heat nociception identifies α2δ3 as an evolutionarily conserved pain gene. *Cell* 143, 628–638. doi: 10.1016/j.cell.2010.09.047

Nieto, M., Monuki, E. S., Tang, H., Imitola, J., Haubst, N., Khoury, S. J., et al. (2004). Expression of Cux-1 and Cux-2 in the subventricular zone and upper layers II–IV of the cerebral cortex. *J. Comp. Neurol.* 479, 168–180. doi: 10.1002/cne.20322

Palmieri, C., Rudraraju, B., Monteverde, M., Lattanzio, L., Gojis, O., Brizio, R., et al. (2012). Methylation of the calcium channel regulatory subunit $\alpha_2\delta$-3 (CACNA2D3) predicts site-specific relapse in oestrogen receptor-positive primary breast carcinomas. *Br. J. Cancer* 107, 375–381. doi: 10.1038/bjc.2012.231

Patel, R., Bauer, C. S., Nieto-Rostro, M., Margas, W., Ferron, L., Chaggar, K., et al. (2013). α2δ-1 gene deletion affects somatosensory neuron function and delays mechanical hypersensitivity in response to peripheral nerve damage. *J. Neurosci.* 33, 16412–16426. doi: 10.1523/JNEUROSCI.1026-13.2013

Paxinos, G., and Franklin, K. B. J. (2012). *Paxinos and Franklin's the Mouse Brain in Stereotaxic Coordinates*, 4th edition. San Diego, CA: Academic Press.

Peça, J., Feliciano, C., Ting, J. T., Wang, W., Wells, M. F., Venkatraman, T. N., et al. (2011). Shank3 mutant mice display autistic-like behaviours and striatal dysfunction. *Nature* 472, 437–442. doi: 10.1038/nature09965

Pippucci, T., Parmeggiani, A., Palombo, F., Maresca, A., Angius, A., Crisponi, L., et al. (2013). A novel null homozygous mutation confirms CACNA2D2 as a gene mutated in epileptic encephalopathy. *PLoS One* 8:e82154. doi: 10.1371/journal.pone.0082154

Pirone, A., Kurt, S., Zuccotti, A., Ruttiger, L., Pilz, P., Brown, D. H., et al. (2014). $\alpha_2\delta$3 is essential for normal structure and function of auditory nerve synapses and is a novel candidate for auditory processing disorders. *J. Neurosci.* 34, 434–445. doi: 10.1523/JNEUROSCI.3085-13.2014

Purcell, S. M., Moran, J. L., Fromer, M., Ruderfer, D., Solovieff, N., Roussos, P., et al. (2014). A polygenic burden of rare disruptive mutations in schizophrenia. *Nature* 506, 185–190. doi: 10.1038/nature12975

Qin, N., Yagel, S., Momplaisir, M.-L., Codd, E. E., and D'Andrea, M. R. (2002). Molecular cloning and characterization of the human voltage-gated calcium channel α(2)δ-4 subunit. *Mol. Pharmacol.* 62, 485–496. doi: 10.1124/mol.62.3.485

Redwine, J. M., Kosofsky, B., Jacobs, R. E., Games, D., Reilly, J. F., Morrison, J. H., et al. (2003). Dentate gyrus volume is reduced before onset of plaque formation in PDAPP mice: a magnetic resonance microscopy and stereologic analysis. *Proc. Natl. Acad. Sci. U S A* 100, 1381–1386. doi: 10.1073/pnas.242746599

Risher, W. C., Kim, N., Koh, S., Choi, J.-E., Mitev, P., Spence, E. F., et al. (2018). Thrombospondin receptor $\alpha_2\delta$-1 promotes synaptogenesis and spinogenesis *via* postsynaptic Rac1. *J. Cell Biol.* 217, 3747–3765. doi: 10.1083/jcb.201802057

Sandoval, A., Oviedo, N., Andrade, A., and Felix, R. (2004). Glycosylation of asparagines 136 and 184 is necessary for the $\alpha_2\delta$ subunit-mediated regulation of voltage-gated Ca^{2+} channels. *FEBS Lett.* 576, 21–26. doi: 10.1016/j.febslet.2004.08.054

Schlick, B., Flucher, B. E., and Obermair, G. J. (2010). Voltage-activated calcium channel expression profiles in mouse brain and cultured hippocampal neurons. *Neuroscience* 167, 786–798. doi: 10.1016/j.neuroscience.2010.02.037

Schneider, C. A., Rasband, W. S., and Eliceiri, K. W. (2012). NIH image to ImageJ: 25 years of image analysis. *Nat. Methods* 9, 671–675. doi: 10.1038/nmeth.2089

Schoepf, C. L., Geisler, S., Stanika, R. I., Campiglio, M., Kaufmann, W. A., Nimmervoll, B., et al. (2019). Presynaptic α2δ subunits are key organizers of glutamatergic synapses. *bioRxiv* [Preprint]. doi: 10.1101/826016

Senawong, T., Peterson, V. J., Avram, D., Shepherd, D. M., Frye, R. A., Minucci, S., et al. (2003). Involvement of the histone deacetylase SIRT1 in chicken ovalbumin upstream promoter transcription factor (COUP-TF)-interacting protein 2-mediated transcriptional repression. *J. Biol. Chem.* 278, 43041–43050. doi: 10.1074/jbc.M307477200

Shao, Q., Herrlinger, S., Zhu, Y.-N., Yang, M., Goodfellow, F., Stice, S. L., et al. (2017). The African Zika virus MR-766 is more virulent and causes more severe brain damage than current Asian lineage and dengue virus. *Development* 144, 4114–4124. doi: 10.1242/dev.156752

Slater, B. J., Sons, S. K., Yudintsev, G., Lee, C. M., and Llano, D. A. (2019). Thalamocortical and intracortical inputs differentiate layer-specific mouse auditory corticocollicular neurons. *J. Neurosci.* 39, 256–270. doi: 10.1523/JNEUROSCI.3352-17.2018

Snell, G. D. (1955). Ducky, a new second chromosome mutation in the mouse. *J. Hered.* 46, 27–29. doi: 10.1093/oxfordjournals.jhered.a106505

Stephani, F., Scheuer, V., Eckrich, T., Blum, K., Wang, W., Obermair, G. J., et al. (2019). Deletion of the Ca^{2+} channel subunit $\alpha_2\delta$3 differentially affects Cav2.1 and Cav2.2 currents in cultured spiral ganglion neurons before and after the onset of hearing. *Front. Cell. Neurosci.* 13:278. doi: 10.3389/fncel.2019.00278

Tang, G., Gudsnuk, K., Kuo, S.-H., Cotrina, M. L., Rosoklija, G., Sosunov, A., et al. (2014). Loss of mTOR-dependent macroautophagy causes autistic-like synaptic pruning deficits. *Neuron* 83, 1131–1143. doi: 10.1016/j.neuron.2014.07.040

Tedeschi, A., Dupraz, S., Laskowski, C. J., Xue, J., Ulas, T., Beyer, M., et al. (2016). The calcium channel subunit α2δ 2 suppresses axon regeneration in the adult CNS. *Neuron* 92, 419–434. doi: 10.1016/j.neuron.2016.09.026

Thomson, A. M., and Lamy, C. (2007). Functional maps of neocortical local circuitry. *Front. Neurosci.* 1, 19–42. doi: 10.3389/neuro.01.1.1.002.2007

Toba, S., and Hirotsune, S. (2012). A unique role of dynein and nud family proteins in corticogenesis. *Neuropathology* 32, 432–439. doi: 10.1111/j.1440-1789.2012.01301.x

Tong, X.-J., López-Soto, E. J., Li, L., Liu, H., Nedelcu, D., Lipscombe, D., et al. (2017). Retrograde synaptic inhibition is mediated by α-neurexin binding to the $\alpha_2\delta$ subunits of N-type calcium channels. *Neuron* 95, 326.e5–340.e5. doi: 10.1016/j.neuron.2017.06.018

Truett, G. E., Heeger, P., Mynatt, R. L., Truett, A. A., Walker, J. A., and Warman, M. L. (2000). Preparation of PCR-quality mouse genomic DNA with hot sodium hydroxide and tris (HotSHOT). *Biotechniques* 29, 52–54. doi: 10.2144/00291bm09

Van Erum, J., Van Dam, D., and De Deyn, P. P. (2019). PTZ-induced seizures in mice require a revised Racine scale. *Epilepsy Behav.* 95, 51–55. doi: 10.1016/j.yebeh.2019.02.029

Varoqueaux, F., Aramuni, G., Rawson, R. L., Mohrmann, R., Missler, M., Gottmann, K., et al. (2006). Neuroligins determine synapse maturation and function. *Neuron* 51, 741–754. doi: 10.1016/j.neuron.2006.09.003

Vergult, S., Dheedene, A., Meurs, A., Faes, F., Isidor, B., Janssens, S., et al. (2015). Genomic aberrations of the CACNA2D1 gene in three patients with epilepsy and intellectual disability. *Eur. J. Hum. Genet.* 23, 628–632. doi: 10.1038/ejhg.2014.141

Vidal, C. N., Nicolson, R., DeVito, T. J., Hayashi, K. M., Geaga, J. A., Drost, D. J., et al. (2006). Mapping corpus callosum deficits in autism: an index of aberrant cortical connectivity. *Biol. Psychiatry* 60, 218–225. doi: 10.1016/j.biopsych.2005.11.011

Wang, X., Bey, A. L., Katz, B. M., Badea, A., Kim, N., David, L. K., et al. (2016). Altered mGluR5-Homer scaffolds and corticostriatal connectivity in a Shank3 complete knockout model of autism. *Nat. Commun.* 7:11459. doi: 10.1038/ncomms11459

Wang, Y., Fehlhaber, K. E., Sarria, I., Cao, Y., Ingram, N. T., Guerrero-Given, D., et al. (2017). The auxiliary calcium channel subunit $\alpha_2\delta$4 is required for axonal elaboration, synaptic transmission and wiring of rod photoreceptors. *Neuron* 93, 1359.e6–1374.e6. doi: 10.1016/j.neuron.2017.02.021

Watkin, H., Richert, M. M., Lewis, A., Terrell, K., McManaman, J. P., and Anderson, S. M. (2008). Lactation failure in Src knockout mice is due to impaired secretory activation. *BMC Dev. Biol.* 8:6. doi: 10.1186/1471-213X-8-6

Wycisk, K. A., Budde, B., Feil, S., Skosyrski, S., Buzzi, F., Neidhardt, J., et al. (2006). Structural and functional abnormalities of retinal ribbon synapses due to Cacna2d4 mutation. *Invest. Opthalmol. Vis. Sci.* 47, 3523–3530. doi: 10.1167/iovs.06-0271

Yu, J., Anderson, C. T., Kiritani, T., Sheets, P. L., Wokosin, D. L., Wood, L., et al. (2008). Local-circuit phenotypes of layer 5 neurons in motor-frontal cortex of YFP-H mice. *Front. Neural Circuits* 2:6. doi: 10.3389/neuro.04.006.2008

Zamponi, G. W., Striessnig, J., Koschak, A., and Dolphin, A. C. (2015). The physiology, pathology and pharmacology of voltage-gated calcium channels and their future therapeutic potential. *Pharmacol. Rev.* 67, 821–870. doi: 10.1124/pr.114.009654

Zhou, J.-J., Li, D.-P., Chen, S.-R., Luo, Y., and Pan, H.-L. (2018). The $\alpha_2\delta$-1-NMDA receptor coupling is essential for corticostriatal long-term potentiation and is involved in learning and memory. *J. Biol. Chem.* 293, 19354–19364. doi: 10.1074/jbc.RA118.003977

Conflict of Interest: The authors declare that the research was conducted in the absence of any commercial or financial relationships that could be construed as a potential conflict of interest.

Copyright © 2021 Geisler, Benedetti, Schöpf, Schwarzer, Stefanova, Schwartz and Obermair. This is an open-access article distributed under the terms of the Creative Commons Attribution License (CC BY). The use, distribution or reproduction in other forums is permitted, provided the original author(s) and the copyright owner(s) are credited and that the original publication in this journal is cited, in accordance with accepted academic practice. No use, distribution or reproduction is permitted which does not comply with these terms.

frontiers in Synaptic Neuroscience

MINI REVIEW
published: 26 February 2021
doi: 10.3389/fnsyn.2021.636103

Voltage-Gated Ca^{2+} Channels in Dopaminergic Substantia Nigra Neurons: Therapeutic Targets for Neuroprotection in Parkinson's Disease?

*Nadine J. Ortner**

Department of Pharmacology and Toxicology, Institute of Pharmacy, University of Innsbruck, Innsbruck, Austria

The loss of dopamine (DA)-producing neurons in the substantia nigra pars compacta (SN) underlies the core motor symptoms of the progressive movement disorder Parkinson's disease (PD). To date, no treatment to prevent or slow SN DA neurodegeneration exists; thus, the identification of the underlying factors contributing to the high vulnerability of these neurons represents the basis for the development of novel therapies. Disrupted Ca^{2+} homeostasis and mitochondrial dysfunction seem to be key players in the pathophysiology of PD. The autonomous pacemaker activity of SN DA neurons, in combination with low cytosolic Ca^{2+} buffering, leads to large somatodendritic fluctuations of intracellular Ca^{2+} levels that are linked to elevated mitochondrial oxidant stress. L-type voltage-gated Ca^{2+} channels (LTCCs) contribute to these Ca^{2+} oscillations in dendrites, and LTCC inhibition was beneficial in cellular and *in vivo* animal models of PD. However, in a recently completed phase 3 clinical trial, the dihydropyridine (DHP) LTCC inhibitor isradipine failed to slow disease progression in early PD patients, questioning the feasibility of DHPs for PD therapy. Novel evidence also suggests that R- and T-type Ca^{2+} channels (RTCCs and TTCCs, respectively) represent potential PD drug targets. This short review aims to (re)evaluate the therapeutic potential of LTCC, RTCC, and TTCC inhibition in light of novel preclinical and clinical data and the feasibility of available Ca^{2+} channel blockers to modify PD disease progression. I also summarize their cell-specific roles for SN DA neuron function and describe how their gating properties allow activity (and thus their contribution to stressful Ca^{2+} oscillations) during pacemaking.

Keywords: voltage-gated Ca^{2+} channels, Parkinson's disease, Ca^{2+} oscillations, Ca^{2+} channel blockers, L-type Ca^{2+} channels, R-type Ca^{2+} channels, T-type Ca^{2+} channels

OPEN ACCESS

Edited by:
Sigismund Huck,
Medical University of Vienna, Austria

Reviewed by:
Norbert Weiss,
Charles University, Czechia
Paolo Calabresi,
Catholic University of the Sacred Heart, Italy

***Correspondence:**
Nadine J. Ortner
nadine.ortner@uibk.ac.at

Received: *30 November 2020*
Accepted: *25 January 2021*
Published: *26 February 2021*

Citation:
Ortner NJ (2021) Voltage-Gated Ca^{2+} Channels in Dopaminergic Substantia Nigra Neurons: Therapeutic Targets for Neuroprotection in Parkinson's Disease? Front. Synaptic Neurosci. 13:636103. doi: 10.3389/fnsyn.2021.636103

INTRODUCTION

The primary motor symptoms of the neurodegenerative disorder Parkinson's disease (PD) are caused by a progressive loss of dopamine (DA)-producing neurons in the substantia nigra pars compacta (SN) and associated striatal DA depletion (Obeso et al., 2017). Although PD was first described in 1817 (Parkinson, 2002), to date only symptomatic treatments, but still no cure or disease-modifying therapy, exist (Schulz et al., 2016; Obeso et al., 2017). To develop an effective

treatment, it is essential to understand the contributing factors and the disease-underlying cellular mechanisms. Next to globally acting factors (e.g., toxins, aging, and genetic mutations), cell-autonomous ones have also been proposed and widely studied (Poewe et al., 2017; Surmeier et al., 2017b). Neighboring DA neurons in the ventral tegmental area (VTA) share many of the intrinsic properties but are spared in PD (Dauer and Przedborski, 2003). Both are autonomous pacemakers, but in vulnerable SN DA neurons, large oscillations of intracellular Ca^{2+} levels accompany pacemaking (Wilson and Callaway, 2000; Chan et al., 2007; Guzman et al., 2009, 2018; Hage and Khaliq, 2015). In contrast, no or much smaller Ca^{2+} transients were detected in VTA neurons (Guzman et al., 2010, 2018; Benkert et al., 2019) that rely on a different pacemaking mechanism with less contribution of Ca^{2+} currents (Khaliq and Bean, 2010; Philippart et al., 2016). Ca^{2+} influx is important to modulate neuronal excitability and to activate Ca^{2+}-dependent physiological processes, but the rhythmic Ca^{2+} load in SN DA neurons also triggers mitochondrial oxidative stress (Guzman et al., 2010, 2018; Surmeier et al., 2017a). Disrupted Ca^{2+} homeostasis and mitochondrial dysfunction are considered key players in PD pathophysiology (Schapira, 2008; Zaichick et al., 2017; Zampese and Surmeier, 2020), and many mutations causing inherited forms of PD affect proteins associated with mitochondrial homeostasis and stress responses (Park et al., 2018). Thus, reducing the activity-related Ca^{2+} load and associated mitochondrial stress in SN DA neurons represents a feasible strategy to increase their resistance to degenerative stressors. L-, R-, and T-type voltage-gated Ca^{2+} channels (LTCCs, RTCCs, and TTCCs, respectively) contribute to the stress-inducing cytosolic Ca^{2+} oscillations, and different approaches to decrease their activity produced promising protective effects in preclinical models of PD. However, a phase 3 clinical trial evaluating the efficacy of LTCC inhibition in early PD patients recently failed. This short review aims to give an overview of the (patho)physiological roles of Ca^{2+} channel activity in SN DA neurons and to (re)evaluate the therapeutic potential of Ca^{2+} channel inhibition (in light of novel preclinical and clinical evidence) and the availability of clinically applicable selective drugs.

VOLTAGE-GATED Ca^{2+} CHANNELS IN SN DA NEURONS

Plasmalemmal voltage-gated Ca^{2+} channels mediate controlled Ca^{2+} influx in response to membrane depolarization and contribute to important functions within the sensory, cardiac, endocrine, and nervous systems (Zamponi et al., 2015). Three main families (Cav1/Cav2/Cav3) and 10 individual isoforms are distinguished based on the biophysical and pharmacological properties of the pore-forming α1 subunit: Cav1.1–Cav1.4 (LTCCs), Cav2.1 (P/Q-type), Cav2.2 (N-type), Cav2.3 (RTCCs), and Cav3.1–3.3 (TTCCs) (Catterall, 2011; Zamponi et al., 2015). They are further classified into high-voltage (HVA; Cav1 and Cav2) and low-voltage activated (LVA; Cav3), and only HVA channels require the association with auxiliary β- and α2δ subunits for proper function (Dolphin, 2016; **Figure 1A**). This functional complexity (further fine-tuned by alternative splicing), their distinct tissue distribution, and subcellular localization enable them to differentially contribute to cellular processes (Dolphin, 2012, 2016; Zamponi et al., 2015).

Rodent SN DA neurons express all voltage-gated Ca^{2+} channel isoforms, except Cav1.1 and Cav1.4 (restricted to skeletal muscle and retina, respectively) (Cardozo and Bean, 1995; Chan et al., 2007; Sinnegger-Brauns et al., 2009; Dufour et al., 2014; Brichta et al., 2015; Shin, 2015; Philippart et al., 2016; Ortner et al., 2017; Guzman et al., 2018; Benkert et al., 2019; Verma and Ravindranath, 2019). The recording of individual current components in intact SN DA neurons is complicated, but in somatic nucleated outside-out patches from juvenile rat SN DA neurons, Ca^{2+} currents of all expressed isoforms were found, with a large LTCC contribution that was higher compared to VTA (Philippart et al., 2016). On the transcript level, RTCC Cav2.3 channels are most abundant in mouse SN DA neurons and levels increase with age (Benkert et al., 2019), while LTCCs (Cav1.2/Cav1.3) get downregulated in an age-dependent manner (Branch et al., 2014; Ortner et al., 2017; Benkert et al., 2019). Of the LVA TTCCs, Cav3.1, and Cav3.2 predominate in mouse SN DA neurons (Poetschke et al., 2015; Guzman et al., 2018; Benkert et al., 2019) and immunohistochemical stainings suggest a rise of somatodendritic TTCCs during development (Dufour et al., 2014) [also shown for Cav1.3, but antibody specificity was not demonstrated in brain (SN) tissue lacking Cav1.3]. SN DA neurons are constantly active and fire action potentials in a tonic single spike or transient high-frequency burst mode *in vivo*, resulting in axonal and somatodendritic DA release (Grace and Bunney, 1984a,b; Chiodo, 1988; Paladini and Roeper, 2014). Cav2 N- and P/Q-type channels drive fast presynaptic neurotransmission, but LTCCs, RTCCs, and TTCCs seem to also contribute to DA release from axonal and/or somatodendritic locations in rodent SN DA neurons (Bergquist and Nissbrandt, 2003; Chen et al., 2006; Brimblecombe et al., 2015; Yee et al., 2019). *In vitro*, even in complete synaptic isolation, SN DA neurons maintain an intrinsically generated regular pacemaker activity (0.5–4 Hz). Inhibition of Na^+ channels by tetrodotoxin abolished spike generation and revealed slow oscillatory membrane depolarizations ("SOPs," slow oscillatory potentials; Fujimura and Matsuda, 1989; Yee et al., 2019) that were absent in neighboring VTA neurons and abolished upon LTCC inhibition (Chan et al., 2007). However, LTCCs are not required for pacemaker generation but rather stabilize precision and robustness of pacemaking (Guzman et al., 2009, 2010; Poetschke et al., 2015; Ortner et al., 2017). Similarly, pharmacological inhibition of TTCCs decreased pacemaker precision (juvenile) and frequency (adult mice) (Wolfart and Roeper, 2002; Poetschke et al., 2015), while Cav2.3 knockout or its partial pharmacological inhibition reduced spike amplitude and afterhyperpolarization (AHP) (Benkert et al., 2019). Ca^{2+} influx through voltage-gated Ca^{2+} channels can drive depolarization, but its coupling to K^+ conductances [e.g., Ca^{2+}-sensitive small conductance K^+ (SK) or A-type K^+ channels] can also trigger the opposite—a functional coupling important for rhythmic activity (Wolfart and Roeper, 2002; Ji and Shepard, 2006; Duda et al., 2016). During *in vivo* high

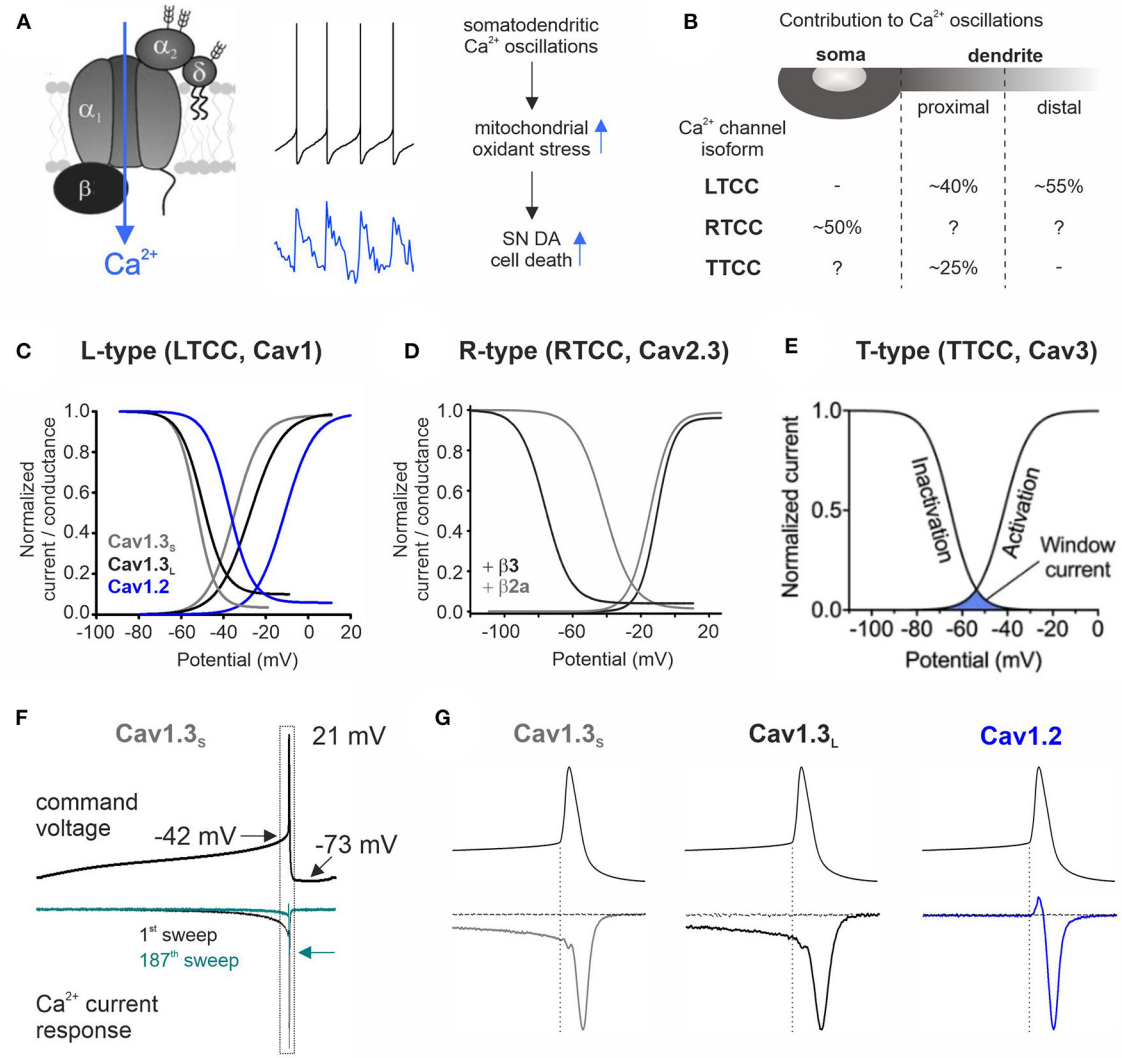

FIGURE 1 | Contribution to stressful somatodendritic Ca^{2+} oscillations, gating properties, and Ca^{2+} current responses of different Ca^{2+} channel isoforms during SN DA neuronal pacemaking. **(A)** Schematic of a plasmalemmal Ca^{2+} channel complex consisting of the pore-forming α1 subunit and auxiliary β and α2δ subunits [only HVA α1 subunits require auxiliary subunits for proper function (Dolphin, 2016)]. Membrane depolarization triggers channel opening and subsequent Ca^{2+} influx. The middle panel shows mouse SN DA neuron pacemaking (top) with the associated intracellular Ca^{2+} transients (bottom; blue) recorded at the cell soma (taken from Ortner et al., 2017). Somatodendritic Ca^{2+} oscillations have been linked to increased mitochondrial oxidative stress, implicated in the high vulnerability of SN DA neurons in PD (Guzman et al., 2010). **(B)** Contribution of different Ca^{2+} channel isoforms to intracellular Ca^{2+} oscillations in distinct cellular compartments (soma and proximal and distal dendrites) (Ortner et al., 2017; Guzman et al., 2018; Benkert et al., 2019). With a higher isradipine concentration [5 μM (Guzman et al., 2018) compared to 1 μM, 10 nM, or chronic *in vivo* isradipine application resulting in plasma levels of ~5 nM isradipine in the abovementioned refs], a complete inhibition of distal dendritic Ca^{2+} transients was observed (Guzman et al., 2009, 2010). Hyphen indicates no contribution found and question mark indicates not determined. **(C–E)** The voltage-conductance (activation) curve describes at which potential a certain Ca^{2+} channel isoform opens (activation threshold) and is in a Ca^{2+} conductive state. The voltage dependence of inactivation gives the proportion of inactivated (non-available) channels at a certain membrane potential. The overlap of these two curves defines the window current (see **E**) that represents the voltage range at which the respective Ca^{2+} channel is steadily active and can thus create a constant background influx of Ca^{2+}. **(C)** Cav1.2 or Cav1.3 α1 with β3 and α2δ1 (2 mM Ca^{2+}; modified from Ortner et al., 2017). Alternative splicing of the Cav1.3 C-terminus results in functionally distinct long ($Cav1.3_L$, black) and short splice variants (Cav1.3s, gray; Singh et al., 2008; Bock et al., 2011; Tan et al., 2011). **(D)** Cav2.3e α1 with β3 (black) or β2a (gray) and α2δ1 (2 mM Ca^{2+}). Association with membrane-bound β2a shifts the voltage dependence of inactivation of Cav2.3 channels ~35 mV toward more positive potentials (Olcese et al., 1994; Jones et al., 1998; Yasuda et al., 2004; Miranda-Laferte et al., 2012). **(E)** Voltage dependence of activation and inactivation of TTCCs with indicated window current (blue area; taken from Weiss and Zamponi, 2019a). **(F)** Representative Ca^{2+} current traces (I_{Ca}, lower panel) through $Cav1.3_S$ in response to a murine SN DA neuron action potential command voltage shown above (2 mM Ca^{2+}, tsA201 cells; modified from Ortner et al., 2017). Simulated pacemaking (2.5 Hz) resulted in a decrease of I_{Ca} to ~20% in steady state (cyan trace, arrow indicates decreased peak I_{Ca}) through all three investigated Cav1 subtypes (Cav1.2, $Cav1.3_S$, and $Cav1.3_L$). **(G)** Enlargement of the action potential spike region indicated in **(F)** (dotted rectangle). During the interspike interval (before the spike threshold indicated by the dotted vertical line), only Cav1.3 variants conducted Ca^{2+} while all LTCCs showed Ca^{2+} influx in response to the action potential spike. The horizontal current trace shows full LTCC inhibition at the end of the recording (3 μM isradipine).

DA states, Cav1.3 can sensitize the DA-D2 autoreceptor response resulting in activation of G protein-coupled GIRK2 K^+ channels and inhibition of spiking (Dragicevic et al., 2014). Moreover, voltage-gated Ca^{2+} channels can activate various cellular Ca^{2+}-dependent signaling processes, including gene expression as shown for LTCCs (Catterall, 2011; Ma et al., 2012).

VOLTAGE-GATED Ca^{2+} CHANNELS CONTRIBUTE TO STRESSFUL SOMATODENDRITIC Ca^{2+} OSCILLATIONS

The slow SN DA neuron pacemaker activity with its broad action potentials triggers large fluctuations of intracellular Ca^{2+} levels throughout the somatodendritic compartment (Chan et al., 2007; **Figure 1A**, middle panel). Dendritic Ca^{2+} transients occur despite spike inhibition or failure (Chan et al., 2007; Guzman et al., 2018), and their rising phase starts before the action potential threshold (Guzman et al., 2018). This points to a contribution of a Ca^{2+} conductance that is active at subthreshold potentials. Cav1.3 and TTCCs activate well before the spike threshold (as shown for Cav1.3 in tsA201 cells; Ortner et al., 2017; **Figure 1G**), and their specific gating properties create a "window current" permitting a constant background Ca^{2+} influx through a small fraction of non-inactivated channels (**Figures 1C,E**) in the average membrane potential range of SN DA neurons (**Figure 1F**). Pharmacological experiments in mouse brain slices found that LTCCs mediate Ca^{2+} transients in the dendrites (with a higher contribution in distal compartments) (Guzman et al., 2009, 2010, 2018) but not in the soma (Ortner et al., 2017), while TTCCs account for ∼25% of proximal dendritic transients (soma not tested) (Guzman et al., 2018; **Figure 1B**). LTCC dihydropyridine (DHP) inhibitors act on both LTCC isoforms (with higher potency for Cav1.2) (Koschak et al., 2001; Xu and Lipscombe, 2001) and thus cannot be used to discriminate Cav1.2- and Cav1.3-mediated effects. However, using a Cav1.3-specific shRNA-mediated knockdown approach (Guzman et al., 2018), Cav1.3 was identified as the major LTCC isoform underlying the Ca^{2+} oscillations. Similar effects were observed by knockdown and inhibition with DHPs, particularly before spike onset (Guzman et al., 2018) where Cav1.2 is not yet active (Ortner et al., 2017; **Figures 1C,G**). In the soma, HVA Cav2.3 channels mediate a large proportion of the Ca^{2+} oscillations [∼50% in Cav2.3$^{-/-}$ mice; ∼25% upon partial pharmacological inhibition by 100 nM SNX-482 (Benkert et al., 2019); dendrites not investigated; **Figure 1B**]. Cav1.2 and Cav2.3 start to activate at approximately−40 mV (**Figures 1C,D**) and conduct Ca^{2+} only in response to the strong depolarization of the action potential spike (shown for Cav1.2 in tsA201 cells; Ortner et al., 2017; **Figure 1G**). In contrast to Cav1.2, Cav2.3 channels typically inactivate at comparatively negative membrane potentials (black trace, steady-state inactivation curve in **Figure 1D**), which predicts almost complete channel inactivation during SN DA neuron pacemaking. Interaction with membrane-bound β2 splice variants (β2a and β2e) (Buraei and Yang, 2010) was shown to shift Cav2.3 voltage dependence of inactivation toward more positive potentials (Olcese et al., 1994; Jones et al., 1998; Yasuda et al., 2004; Miranda-Laferte et al., 2012, 2014) (gray trace, **Figure 1D**) and could thereby facilitate Cav2.3 steady-state availability during SN DA neuron activity. β2 accounts for ∼30% of β subunits in mouse SN DA neurons (Brichta et al., 2015; Shin, 2015); however, if and to which extent these β2 splice variants are expressed in SN DA neurons and regulate Cav2.3 RTCCs is not known.

Experiments in transgenic mice (mito-GFP mouse) that allow to monitor the oxidation state of mitochondria established a link between Ca^{2+} oscillations and elevated mitochondrial oxidative stress (Guzman et al., 2010, 2018; **Figure 1A**). Dendritic Ca^{2+} transients and associated mitochondrial oxidation increased with age (Guzman et al., 2018) and were almost absent in neighboring resistant VTA DA neurons (Guzman et al., 2010, 2018; Benkert et al., 2019). In addition, the already high basal oxidant stress level in SN DA neurons was further exacerbated in a genetic PD mouse model (DJ-1 knockout) (Guzman et al., 2010). Interestingly, factors contributing to vulnerability described in SN DA neurons, i.e., slow pacemaking, cytosolic Ca^{2+} oscillations, low intracellular Ca^{2+} buffering (Foehring et al., 2009), and elevated levels of mitochondrial oxidant stress, are also found in other vulnerable non-DA neurons (Surmeier et al., 2017b; Zampese and Surmeier, 2020).

Besides the metabolic challenging pacemaker activity, burst firing is also associated with high Ca^{2+} influx and intracellular Ca^{2+} levels (Hage and Khaliq, 2015; Philippart et al., 2016; Ortner et al., 2017), and membrane hyperpolarizations (e.g., during post-burst pauses) allow channels to recover from inactivation, in particular TTCCs. This mechanism underlies the large TTCC-mediated Ca^{2+} currents and the resulting afterdepolarizations that facilitate rebound spiking (Evans et al., 2017; Tracy et al., 2018). Interestingly, in PD, cells in the ventrolateral part of the SN are particularly prone to cell death and lateral SN DA neurons also show high *in vivo* bursting (Schiemann et al., 2012; Farassat et al., 2019). In line, knockout of K_{ATP} K^+ channels reduced *in vivo* burst firing and conferred protection in two PD mouse models (Liss et al., 2005; Schiemann et al., 2012).

NEUROPROTECTION BY LTCC INHIBITION: PRECLINICAL AND CLINICAL EVIDENCE

Over the last years, LTCCs (and particularly Cav1.3) were considered the main voltage-gated Ca^{2+} channel subtype underlying stressful Ca^{2+} oscillations and thus a major driver of SN DA neuronal cell death (Surmeier et al., 2017a; Guzman et al., 2018; Liss and Striessnig, 2019). Epidemiological studies found that the intake of brain-permeable DHP LTCC inhibitors (antihypertensives) reduced the risk to develop PD (Gudala et al., 2015; Lang et al., 2015; Mullapudi et al., 2016). DHPs have been extensively studied in preclinical PD models and showed promising protective effects in most (but not all) studies (**Table 1**; reviewed in Leandrou et al., 2019; Liss and Striessnig, 2019). The diverging outcomes of DHP treatment in toxin-based PD animal models have been recently discussed in great detail (Liss and Striessnig, 2019), but no definite explanation has been found.

Briefly, in eight out of 13 reports, DHPs significantly reduced mitochondrial-targeting toxin-induced SN DA cell death in mice, rats, and primates (**Table 1**), but the experimental design of all studies varied, complicating an overall conclusion. Differences included the used PD model (6-OHDA and MPTP), animals (species, strain, age, and sex), treatment regimen (DHP, treatment onset, route of administration, and dosing interval), readout (approach and methodology), and plasma concentrations (if even reported) (Liss and Striessnig, 2019). Thus, a standardized approach in future studies would help to better interpret and compare obtained results. In addition, one recent study (not included in Liss and Striessnig, 2019) tested the DHP felodipine in a genetic PD mouse model (expressing the A53T mutant α-synuclein) and found protective effects on SN DA neuron survival and motor deficits and autophagy-induced clearance of disease-associated proteins from brain (Siddiqi et al., 2019). Noteworthy, in contrast to other DHPs like isradipine (Uchida et al., 1997), felodipine accumulated in the brain with ∼2 to 5-fold higher brain levels compared to plasma (Siddiqi et al., 2019). Epidemiological and preclinical evidence, and the availability of safe and clinically approved LTCC DHP inhibitors, prompted the phase 3 STEADY-PD III clinical trial with the DHP isradipine as treatment in early PD patients (336 patients, randomized, double blind, and placebo controlled; Biglan et al., 2017), which however did not reach its primary endpoint (Parkinson Study Group STEADY-PD III Investigators, 2020). Several aspects may have contributed.

Protective DHP effects might require an earlier treatment onset, since at the time when first PD symptoms occur, pathologic mechanisms and neurodegeneration already started—which however would require reliable PD biomarkers (Poewe et al., 2017). In addition, the age-dependent decrease of LTCCs (Branch et al., 2014; Ortner et al., 2017) could limit the therapeutic window of DHPs in PD (especially in elderly patients), although disease state seems to affect LTCC expression [SN neurons from MPTP-treated mice (Verma and Ravindranath, 2019) and post-mortem brains of early-stage PD patients (Hurley et al., 2015) showed robust Cav1.3 levels, despite profound neuron loss]. When considering Cav1.3 as the primary target, the used maximal tolerable isradipine dose [10 mg/day; limited by Cav1.2-mediated peripheral side effects (Parkinson Study Group, 2013)] might be too low to sufficiently engage Cav1.3 LTCCs in SN DA neurons due to their low apparent drug sensitivity (Ortner et al., 2017). This especially applies to C-terminally short splice variants (Huang et al., 2013; Ortner et al., 2017) that are associated with higher Ca^{2+} influx (Singh et al., 2008; Bock et al., 2011; Tan et al., 2011; **Figure 1C**) and account for ∼50% of Cav1.3 transcript in mouse SN DA neurons (Ortner et al., 2017; Verma and Ravindranath, 2019) (higher compared to the cortex and striatum; Verma and Ravindranath, 2019). In this context, the use of an immediate-release isradipine formulation in the STEADY-PD III trial was unfavorable, since slow-onset continuous-release tablets [as used in the phase 2 trial (Parkinson Study Group, 2013), NCT00753636] result in higher average steady-state plasma levels (Liss and Striessnig, 2019). Thus, strategies to increase DHP brain concentrations (Yiu and Knaus, 1996; Ji et al., 2017) or DHPs that accumulate in the brain (e.g., nimodipine and felodipine; Kupsch et al., 1996; Siddiqi et al., 2019) could be an option. Noteworthy, microglia-specific Cav1.2 knockdown augmented MPTP-induced SN DA neurodegeneration and motor deficits in mice, associated with enhanced activation of "neuroinflammatory" M1 microglia (Wang et al., 2019). Thus, Cav1.2 inhibition might even be disadvantageous, which highlights the need for the development of reliable Cav1.3-selective inhibitory drugs. So far, only one putatively selective compound has been described (Cp8 in Kang et al., 2012 and cp-PYT in Cooper et al., 2020) but showed diverging results in follow-up studies from other laboratories (Huang et al., 2014; Ortner et al., 2014). Nevertheless, micromolar concentrations of cp-PYT could lower dendritic transients to a similar extent as isradipine and did not affect Ca^{2+} currents in Cav1.3 knockout mice (Cooper et al., 2020), suggesting Cav1.3-selective inhibition [lack of non-LTCC modulation was also shown in adrenal mouse chromaffin cells (Ortner et al., 2014)]. In the meantime, mice expressing DHP-insensitive Cav1.2 channels could be used to mimic selective pharmacological Cav1.3 inhibition *in vivo* (Sinnegger-Brauns et al., 2004). Lastly, another important aspect is a potential compensation by other Ca^{2+} channel isoforms during chronic isradipine treatment, as found in Cav1.3-deficient mice [upregulation of Cav3.1 TTCCs (Poetschke et al., 2015)]. However, this was not observed with systemic isradipine treatment for 7–10 days in mice [3 μg/g/day; ∼5 nM plasma isradipine (Guzman et al., 2018)], but longer exposure has not been tested.

RTCCs AND TTCCs EMERGE AS NOVEL PD DRUG TARGETS

Global Cav2.3 knockout fully prevented SN DA neuron degeneration in the gold-standard chronic low-dose MPTP/probenecid PD mouse model (**Table 1**) and profoundly reduced somatic Ca^{2+} oscillations (∼50%, dendrites not tested) (Benkert et al., 2019). Although a direct proof for knockout-induced lowering of high mitochondrial stress levels is missing, a similar inhibition of LTCC-mediated Ca^{2+} transients in proximal and distal dendrites (∼35–60%) was sufficient to lower mitochondrial oxidation (Guzman et al., 2010, 2018). The high Cav2.3 levels in vulnerable SN DA neurons (compared to VTA) and their increase with aging further strengthen a possible involvement of RTCCs in PD pathology. Unlike what is observed for Cav1.3 (Poetschke et al., 2015), loss of Cav2.3 did not trigger compensatory upregulation of other Ca^{2+} channels in SN DA neurons (Cav1.2, Cav1.3, and Cav3.1 were tested) (Benkert et al., 2019). In light of these promising findings, it is unfortunate that to date (like for Cav1.3) no selective RTCC inhibitors exist (Schneider et al., 2013). Note that the peptide toxin SNX-482 is selective for Cav2.3 channels only at low concentrations and also inhibits other channels at elevated concentrations ("Cav2.3-prevalent") (Newcomb et al., 1998; Bourinet et al., 2001; Schneider et al., 2013; Kimm and Bean, 2014). As mentioned above, association of Cav2.3 channels with membrane-bound β2 splice variants (β2a/β2e) may stabilize sustained Cav2.3 activity—a possible explanation for the large contribution of

TABLE 1 | Studies that directly tested neuroprotection by Ca^{2+} channel inhibition, knockdown, or knockout in cellular and animal PD models.

Model type	Drug/intervention	Experimental model	Outcome/result	References
LTCCs (Cav1)				
Cellular	Nifedipine	SH-SY5Ycells (α-synuclein treatment)	Reduction of α-synuclein-induced cell death and Ca^{2+} influx	Melachroinou et al., 2013
	Isradipine	Primary rat ventral midbrain neurons (DA treatment)	Reduction of DA-induced toxicity/cell death and clustering of α-synuclein	Lautenschlager et al., 2018
	Isradipine	Primary mouse midbrain SN DA neurons (MPP^+ treatment)	Attenuation of MPP^+-induced toxicity/cell death; mitochondrial oxidation; and intracellular Ca^{2+}, DA, and NO elevations	Lieberman et al., 2017
	Nimodipine		Attenuation of MPP^+-induced toxicity/cell death and intracellular Ca^{2+} and DA elevations	
	Global Cav1.3 knockout		Reduction of cytosolic DA levels compared to WT (untreated and MPP^+ treated)	
	Nimodipine	Primary mouse ventral midbrain SN DA neurons (L-DOPA treatment)	Reduction of L-DOPA-induced cell loss and cytosolic DA elevation	Mosharov et al., 2009
	Isradipine	PD patient-specific iPSC-derived DA neurons (rotenone treatment)	No rescue of rotenone-induced apoptosis (although a tendency toward a concentration-dependent reduction was observed)	Tabata et al., 2018
	Nifedipine		No rescue of rotenone-induced apoptosis	
Brain slice	Isradipine	Mouse brain slice (rotenone treatment)	Reduction of rotenone-induced SN DA neuron dendritic loss/fragmentation	Chan et al., 2007
	Global Cav1.3 knockout		Reduction of rotenone-induced SN DA neuron dendritic loss/fragmentation	
Animal	Isradipine	PD mouse model (MPTP treatment)	Reduction of MPTP-induced SN DA cell loss and rescue of motor deficits	
	Isradipine	PD mouse model (6-OHDA treatment)	Reduction of 6-OHDA-induced SN DA cell loss	
	Isradipine	PD mouse model (6-OHDA treatment)	Reduction of 6-OHDA-induced SN DA cell loss	Ilijic et al., 2011
	Isradipine	PD mouse model (MPTP treatment)	No rescue of SN DA neuron number or striatal DA content	Price, 2014*
	Isradipine	PD mouse model (MPTP treatment)	Reduction of MPTP-induced SN DA cell loss, striatal DA loss, and motor deficits	Wang et al., 2017
	Isradipine	PD mouse model (6-OHDA treatment)	No rescue of SN DA neuron number	Ortner et al., 2017
	Global Cav1.3 knockout		No rescue of SN DA neuron number	
	Nimodipine	PD mouse model (MPTP treatment)	Number of SN DA neurons not determined. No rescue of striatal DA content	Gerlach et al., 1993
	Nimodipine	PD mouse model (MPTP treatment)	Rescue of MPTP-induced SN DA cell loss. No rescue of striatal DA content	Kupsch et al., 1995
	Nimodipine	PD common marmosets model (MPTP treatment)	Rescue of MPTP-induced SN DA cell loss. No rescue of striatal DA content and motor deficits	Kupsch et al., 1996
	Nimodipine	PD rat model (6-OHDA treatment)	No rescue of 6-OHDA-induced SN DA cell loss, striatal DA content and motor deficits	Sautter et al., 1997
	Nimodipine	PD mouse model (MPTP treatment)	Reduction of MPTP-induced SN DA cell loss, striatal DA depletion and motor deficits	Singh et al., 2016
	Nifedipine	PD rat model (6-OHDA treatment)	Number of SN DA neurons not determined. Reduction of 6-OHDA-induced striatal DA depletion and motor deficits	Wang et al., 2012

(Continued)

TABLE 1 | Continued

Model type	Drug/intervention	Experimental model	Outcome/result	References
	Felodipine	Transgenic PD mouse model (SCNA mice expressing the PD-causing A53T mutant α-synuclein)	Reduction of transgene-induced SN DA cell loss, motor deficit and clearance of mutant α-synuclein in mouse brain (via induction of autophagy).	Siddiqi et al., 2019
RTCCs (Cav2.3)				
Animal	Global Cav2.3 knockout	PD mouse model (MPTP treatment)	Rescue of MPTP-induced SN DA cell loss	Benkert et al., 2019
TTCCs (Cav3)				
Cellular	ML218	PD patient-specific iPSC-derived DA neurons (rotenone treatment)	Reduction of rotenone-induced apoptosis and intracellular Ca^{2+} level elevation	Tabata et al., 2018
	Cav3.1 knockdown		Reduction of rotenone-induced apoptosis and intracellular Ca^{2+} level elevation	
	Cav3.2 knockdown			
	Cav3.3 knockdown			
Multiple Cav targets				
Cellular	Benidipine (L + N + T)	PD patient-specific iPSC-derived DA neurons (rotenone treatment)	Reduction of rotenone-induced apoptosis, intracellular Ca^{2+} level elevation, and impaired neurite outgrowth	Tabata et al., 2018

*Summary of studies that evaluated Ca^{2+} channel inhibition, knockdown, or knockout for neuroprotection in PD models. Drugs with multiple mechanisms of action in addition to inhibition of LTCCs, RTCCs, or TTCCs were not included (e.g., zonisamide, cinnarizine, and amiodarone; Tabata et al., 2018). Preclinical studies with LTCC inhibitors have been recently reviewed (Leandrou et al., 2019; Liss and Striessnig, 2019). *This study has not yet been published in a peer-reviewed journal (only abstract and poster with detailed experimental description). DA, dopamine; iPSC, inducible pluripotent stem cells; MPTP, 1-methyl-4phenyl-1,2,3,6-tetrahydropyridine; MPP^+, 1-methyl-4-phenyl-pyridine; NO, nitric oxide; SN, substantia nigra; VTA, ventral tegmental area; 6-OHDA, 6-hydroxydopamine.*

Cav2.3 channels to somatic Ca^{2+} oscillations (∼50%, Benkert et al., 2019). Interrupting this putative interaction in SN DA neurons might represent an alternative approach to lower Cav2.3-mediated Ca^{2+} load; however, if these β2 splice variants are indeed expressed in SN DA neurons and modulate Cav2.3 in these cells has not been studied yet. Since β subunits regulate other HVA channels as well, this targeting approach should ideally be Cav2.3-selective [as recently shown for the Cav2.2/β interaction, successfully reducing heterologously expressed and native Cav2.2 currents (Khanna et al., 2019)].

Evidence for a role of TTCCs in PD pathology comes from a study employing DA neurons derived from PD patient-specific iPSCs as *in vitro* PD model (Tabata et al., 2018). Compared to controls, PD patient-specific DA neurons showed pathological signs including reduced neurite length, enhanced oxidative stress, and elevated resting intracellular Ca^{2+} levels and apoptosis. Interestingly, levels of all three TTCC isoforms were also increased. Treatment with the mitochondrial toxin rotenone ("PD trigger") aggravated the observed effects on cell morphology and survival, which could be prevented by drugs targeting TTCCs as well as individual knockout of all TTCC isoforms. Two of the TTCC inhibitory compounds have complex mechanism of action besides inhibition of TTCCs, but one drug, ML218, specifically blocks TTCCs (Xiang et al., 2011). Interestingly, while LTCC inhibition (nifedipine and isradipine) had no effect, the DHP benidipine that acts on L-, N-, and T-type Ca^{2+} channels could prevent rotenone-induced apoptosis. Although promising, proof of SN DA neuroprotection in *in vivo* PD models is still missing. TTCC inhibition has been explored for the treatment of parkinsonism, but mainly based on their involvement in abnormal burst discharges within the thalamocortical circuitry and associated motor effects (Tai et al., 2011; Kopecky et al., 2014; Yang et al., 2014; Galvan et al., 2016). Zonisamide, an unselective TTCC inhibitor, ameliorated symptoms in PD patients (Murata, 2010), but due to its broad mechanism of action, it is difficult to assign observations to TTCC inhibition. Selective and clinically suitable TTCC inhibitors exist (analgesic/antiepileptic drugs) (Weiss and Zamponi, 2019a,b) and showed good tolerability and safety in phase 2 clinical trials (Richard et al., 2019, 2020), and one phase 2 trial plans to evaluate the selective blocker CX-8998 as treatment for PD-associated tremor (ClinicalTrials.gov #NCT03436953).

SUMMARY AND CONCLUSION

There is accumulating evidence that voltage-gated Ca^{2+} channels represent an attractive drug target for the therapy of PD. Their contribution to large somatodendritic Ca^{2+} oscillations, associated with increased mitochondrial oxidative stress, seems a likely mechanism by which their activity contributes to SN DA neuron degeneration. Pharmacological and genetic strategies to decrease the activity of LTCCs, RTCCs, and TTCCs showed promising neuroprotective effects in preclinical models of PD, but a phase 3 clinical trial found no slowing of disease progression in early PD patients upon treatment with the DHP LTCC inhibitor isradipine. Although DHPs are safe, brain permeable, and clinically available, their lack of selectivity for Cav1.3, the more likely LTCC target for neuroprotection, and adverse Cav1.2-mediated effects limit their potential for PD therapy. Selective

TTCC blockers exist, show good tolerability and safety, and could be repurposed for the therapy of PD; however, evidence for neuroprotection in *in vivo* PD models is still missing. In contrast, no selective inhibitors for Cav1.3 and Cav2.3 exist. The convincing preclinical data described in this review and the discovery of activity-enhancing mutations in neurological diseases (Ortner et al., 2020; Schneider et al., 2020; Weiss and Zamponi, 2020) highlight the urgent need for isoform-selective blockers that are suitable for clinical application. Further studies with available TTCC or multiple Ca^{2+} channel targeting blockers and, if once available, Cav1.3- and Cav2.3-selective inhibitors will help to uncover the full therapeutic potential of Ca^{2+} channel inhibition for neuroprotection in PD.

AUTHOR CONTRIBUTIONS

The author confirms being the sole contributor of this work and has approved it for publication.

FUNDING

This work was supported by the Erika-Cremer habilitation fellowship of the University of Innsbruck and the Austrian Science Fund (P27809).

ACKNOWLEDGMENTS

The author wants to thank all colleagues for helpful discussions.

REFERENCES

Benkert, J., Hess, S., Roy, S., Beccano-Kelly, D., Wiederspohn, N., Duda, J., et al. (2019). Cav2.3 channels contribute to dopaminergic neuron loss in a model of Parkinson's disease. *Nat. Commun.* 10:5094. doi: 10.1038/s41467-019-12834-x

Bergquist, F., and Nissbrandt, H. (2003). Influence of R-type (Cav2.3) and t-type (Cav3.1-3.3) antagonists on nigral somatodendritic dopamine release measured by microdialysis. *Neuroscience* 120, 757–764. doi: 10.1016/S0306-4522(03)00385-3

Biglan, K. M., Oakes, D., Lang, A. E., Hauser, R. A., Hodgeman, K., Greco, B., et al. (2017). A novel design of a phase III trial of isradipine in early Parkinson disease (STEADY-PD III). *Ann. Clin. Transl. Neurol.* 4, 360–368. doi: 10.1002/acn3.412

Bock, G., Gebhart, M., Scharinger, A., Jangsangthong, W., Busquet, P., Poggiani, C., et al. (2011). Functional properties of a newly identified C-terminal splice variant of Cav1.3 L-type Ca^{2+} channels. *J. Biol. Chem.* 286, 42736–42748. doi: 10.1074/jbc.M111.269951

Bourinet, E., Stotz, S. C., Spaetgens, R. L., Dayanithi, G., Lemos, J., Nargeot, J., et al. (2001). Interaction of SNX482 with domains III and IV inhibits activation gating of alpha(1E) (Ca(V)2.3) calcium channels. *Biophys. J.* 81, 79–88. doi: 10.1016/S0006-3495(01)75681-0

Branch, S. Y., Sharma, R., and Beckstead, M. J. (2014). Aging decreases L-type calcium channel currents and pacemaker firing fidelity in substantia nigra dopamine neurons. *J. Neurosci.* 34, 9310–9318. doi: 10.1523/JNEUROSCI.4228-13.2014

Brichta, L., Shin, W., Jackson-Lewis, V., Blesa, J., Yap, E. L., Walker, Z., et al. (2015). Identification of neurodegenerative factors using translatome-regulatory network analysis. *Nat. Neurosci.* 18, 1325–1333. doi: 10.1038/nn.4070

Brimblecombe, K. R., Gracie, C. J., Platt, N. J., and Cragg, S. J. (2015). Gating of dopamine transmission by calcium and axonal N-, Q-, T- and L-type voltage-gated calcium channels differs between striatal domains. *J. Physiol.* 593, 929–946. doi: 10.1113/jphysiol.2014.285890

Buraei, Z., and Yang, J. (2010). The ss subunit of voltage-gated Ca^{2+} channels. *Physiol. Rev.* 90, 1461–1506. doi: 10.1152/physrev.00057.2009

Cardozo, D. L., and Bean, B. P. (1995). Voltage-dependent calcium channels in rat midbrain dopamine neurons: modulation by dopamine and GABAB receptors. *J. Neurophysiol.* 74, 1137–1148. doi: 10.1152/jn.1995.74.3.1137

Catterall, W. A. (2011). Voltage-gated calcium channels. *Cold Spring Harb. Perspect. Biol.* 3:a003947. doi: 10.1101/cshperspect.a003947

Chan, C. S., Guzman, J. N., Ilijic, E., Mercer, J. N., Rick, C., Tkatch, T., et al. (2007). 'Rejuvenation' protects neurons in mouse models of Parkinson's disease. *Nature* 447, 1081–1086. doi: 10.1038/nature05865

Chen, A. P., Ohno, M., Giese, K. P., Kuhn, R., Chen, R. L., and Silva, A. J. (2006). Forebrain-specific knockout of B-raf kinase leads to deficits in hippocampal long-term potentiation, learning, and memory. *J. Neurosci. Res.* 83, 28–38. doi: 10.1002/jnr.20703

Chiodo, L. A. (1988). Dopamine-containing neurons in the mammalian central nervous system: electrophysiology and pharmacology. *Neurosci. Biobehav. Rev.* 12, 49–91. doi: 10.1016/S0149-7634(88)80073-3

Cooper, G., Kang, S., Perez-Rosello, T., Guzman, J. N., Galtieri, D., Xie, Z., et al. (2020). A single amino acid determines the selectivity and efficacy of selective negative allosteric modulators of CaV1.3 L-type calcium channels. *ACS Chem. Biol.* 15, 2539–2550. doi: 10.1021/acschembio.0c00577

Dauer, W., and Przedborski, S. (2003). Parkinson's disease: mechanisms and models. *Neuron* 39, 889–909. doi: 10.1016/S0896-6273(03)00568-3

Dolphin, A. C. (2012). Calcium channel auxiliary alpha2delta and beta subunits: trafficking and one step beyond. *Nat. Rev. Neurosci.* 13, 542–55. doi: 10.1038/nrn3311

Dolphin, A. C. (2016). Voltage-gated calcium channels and their auxiliary subunits: physiology and pathophysiology and pharmacology. *J. Physiol.* 94, 5369–5390. doi: 10.1113/JP272262

Dragicevic, E., Poetschke, C., Duda, J., Schlaudraff, F., Lammel, S., Schiemann, J., et al. (2014). Cav1.3 channels control D2-autoreceptor responses via NCS-1 in substantia nigra dopamine neurons. *Brain* 137, 2287–2302. doi: 10.1093/brain/awu131

Duda, J., Potschke, C., and Liss, B. (2016). Converging roles of ion channels, calcium, metabolic stress, and activity-pattern of substantia nigra dopaminergic neurons in health and Parkinson's disease. *J. Neurochem.* 139, 156-178. doi: 10.1111/jnc.13572

Dufour, M. A., Woodhouse, A., and Goaillard, J. M. (2014). Somatodendritic ion channel expression in substantia nigra pars compacta dopaminergic neurons across postnatal development. *J. Neurosci. Res.* 92, 981–999. doi: 10.1002/jnr.23382

Evans, R. C., Zhu, M., and Khaliq, Z. M. (2017). Dopamine inhibition differentially controls excitability of substantia nigra dopamine neuron subpopulations through T-type calcium channels. *J. Neurosci.* 37, 3704–3720. doi: 10.1523/JNEUROSCI.0117-17.2017

Farassat, N., Costa, K. M., Stojanovic, S., Albert, S., Kovacheva, L., Shin, J., et al. (2019). *In vivo* functional diversity of midbrain dopamine neurons within identified axonal projections. *Elife* 8:e48408. doi: 10.7554/eLife.48408

Foehring, R. C., Zhang, X. F., Lee, J. C., and Callaway, J. C. (2009). Endogenous calcium buffering capacity of substantia nigral dopamine neurons. *J. Neurophysiol.* 102, 2326–2333. doi: 10.1152/jn.00038.2009

Fujimura, K., and Matsuda, Y. (1989). Autogenous oscillatory potentials in neurons of the guinea pig substantia nigra pars compacta *in vitro*. *Neurosci. Lett.* 104, 53–57. doi: 10.1016/0304-3940(89)90328-5

Galvan, A., Devergnas, A., Pittard, D., Masilamoni, G., Vuong, J., Daniels, J. S., et al. (2016). Lack of antiparkinsonian effects of systemic injections of the specific T-type calcium channel blocker ML218 in MPTP-treated monkeys. *ACS Chem. Neurosci.* 7, 1543–1551. doi: 10.1021/acschemneuro.6b00186

Gerlach, M., Russ, H., Winker, J., Witzmann, K., Traber, J., Stasch, J. P., et al. (1993). Effects of nimodipine on the 1-methyl-4-phenyl-1,2,3,6-tetrahydropyridine-induced depletions in the biogenic amine levels in mice. *Arzneimittelforschung* 43, 413–415.

Grace, A. A., and Bunney, B. S. (1984a). The control of firing pattern in nigral dopamine neurons: burst firing. *J. Neurosci.* 4, 2877–2890. doi: 10.1523/JNEUROSCI.04-11-02877.1984

Grace, A. A., and Bunney, B. S. (1984b). The control of firing pattern in nigral dopamine neurons: single spike firing. *J. Neurosci.* 4, 2866–2876. doi: 10.1523/JNEUROSCI.04-11-02866.1984

Gudala, K., Kanukula, R., and Bansal, D. (2015). Reduced risk of Parkinson's disease in users of calcium channel blockers: a meta-analysis. *Int. J. Chronic Dis.* 2015:697404. doi: 10.1155/2015/697404

Guzman, J. N., Ilijic, E., Yang, B., Sanchez-Padilla, J., Wokosin, D., Galtieri, D., et al. (2018). Systemic isradipine treatment diminishes calcium-dependent mitochondrial oxidant stress. *J. Clin. Invest.* 128, 2266–2280. doi: 10.1172/JCI95898

Guzman, J. N., Sanchez-Padilla, J., Chan, C. S., and Surmeier, D. J. (2009). Robust pacemaking in substantia nigra dopaminergic neurons. *J. Neurosci.* 29, 11011–11019. doi: 10.1523/JNEUROSCI.2519-09.2009

Guzman, J. N., Sanchez-Padilla, J., Wokosin, D., Kondapalli, J., Ilijic, E., Schumacker, P. T., et al. (2010). Oxidant stress evoked by pacemaking in dopaminergic neurons is attenuated by DJ-1. *Nature* 468, 696–700. doi: 10.1038/nature09536

Hage, T. A., and Khaliq, Z. M. (2015). Tonic firing rate controls dendritic Ca^{2+} signaling and synaptic gain in substantia nigra dopamine neurons. *J. Neurosci.* 35, 5823–5836. doi: 10.1523/JNEUROSCI.3904-14.2015

Huang, H., Ng, C. Y., Yu, D., Zhai, J., Lam, Y., and Soong, T. W. (2014). Modest $Cav1.3_{42}$-selective inhibition by compound 8 is β-subunit dependent. *Nat. Commun.* 5:4481. doi: 10.1038/ncomms5481

Huang, H., Yu, D., and Soong, T. W. (2013). C-Terminal alternative splicing of CaV1.3 channels distinctively modulates their dihydropyridine sensitivity. *Mol. Pharmacol.* 84, 643–653. doi: 10.1124/mol.113.087155

Hurley, M. J., Gentleman, S. M., and Dexter, D. T. (2015). Calcium CaV1 channel subtype mRNA expression in Parkinson's disease examined by *in situ* hybridization. *J. Mol. Neurosci.* 55, 715–724. doi: 10.1007/s12031-014-0410-8

Ilijic, E., Guzman, J. N., and Surmeier, D. J. (2011). The L-type channel antagonist isradipine is neuroprotective in a mouse model of Parkinson's disease. *Neurobiol. Dis.* 43, 364–371. doi: 10.1016/j.nbd.2011.04.007

Ji, B., Wang, M., Gao, D., Xing, S., Li, L., Liu, L., et al. (2017). Combining nanoscale magnetic nimodipine liposomes with magnetic resonance image for Parkinson's disease targeting therapy. *Nanomedicine* 12, 237–253. doi: 10.2217/nnm-2016-0267

Ji, H., and Shepard, P. D. (2006). SK Ca^{2+}-activated K+ channel ligands alter the firing pattern of dopamine-containing neurons *in vivo*. *Neuroscience* 140, 623–633. doi: 10.1016/j.neuroscience.2006.02.020

Jones, L. P., Wei, S. K., and Yue, D. T. (1998). Mechanism of auxiliary subunit modulation of neuronal alpha1E calcium channels. *J. Gen. Physiol.* 112, 125–143. doi: 10.1085/jgp.112.2.125

Kang, S., Cooper, G., Dunne, S. F., Dusel, B., Luan, C. H., Surmeier, D. J., et al. (2012). Cav1.3-selective L-type calcium channel antagonists as potential new therapeutics for Parkinson's disease. *Nat. Commun.* 3:1146. doi: 10.1038/ncomms2149

Khaliq, Z. M., and Bean, B. P. (2010). Pacemaking in dopaminergic ventral tegmental area neurons: depolarizing drive from background and voltage-dependent sodium conductances. *J. Neurosci.* 30, 7401–7413. doi: 10.1523/JNEUROSCI.0143-10.2010

Khanna, R., Yu, J., Yang, X., Moutal, A., Chefdeville, A., Gokhale, V., et al. (2019). Targeting the CaVα-CaVβ interaction yields an antagonist of the N-type CaV2.2 channel with broad antinociceptive efficacy. *Pain* 160, 1644–1661. doi: 10.1097/j.pain.0000000000001524

Kimm, T., and Bean, B. P. (2014). Inhibition of A-type potassium current by the peptide toxin SNX-482. *J. Neurosci.* 34, 9182–9189. doi: 10.1523/JNEUROSCI.0339-14.2014

Kopecky, B. J., Liang, R., and Bao, J. (2014). T-type calcium channel blockers as neuroprotective agents. *Pflugers Arch.* 466, 757–765. doi: 10.1007/s00424-014-1454-x

Koschak, A., Reimer, D., Huber, I., Grabner, M., Glossmann, H., Engel, J., et al. (2001). alpha 1D (Cav1.3) subunits can form l-type Ca^{2+} channels activating at negative voltages. *J. Biol. Chem.* 276, 22100–22106. doi: 10.1074/jbc.M101469200

Kupsch, A., Gerlach, M., Pupeter, S. C., Sautter, J., Dirr, A., Arnold, G., et al. (1995). Pretreatment with nimodipine prevents MPTP-induced neurotoxicity at the nigral, but not at the striatal level in mice. *Neuroreport* 6, 621–625. doi: 10.1097/00001756-199503000-00009

Kupsch, A., Sautter, J., Schwarz, J., Riederer, P., Gerlach, M., and Oertel, W. H. (1996). 1-Methyl-4-phenyl-1,2,3,6-tetrahydropyridine-induced neurotoxicity in non-human primates is antagonized by pretreatment with nimodipine at the nigral, but not at the striatal level. *Brain Res.* 741, 185–196. doi: 10.1016/S0006-8993(96)00917-1

Lang, Y., Gong, D., and Fan, Y. (2015). Calcium channel blocker use and risk of Parkinson's disease: a meta-analysis. *Pharmacoepidemiol. Drug Saf.* 24, 559–566. doi: 10.1002/pds.3781

Lautenschlager, J., Stephens, A. D., Fusco, G., Strohl, F., Curry, N., Zacharopoulou, M., et al. (2018). C-terminal calcium binding of alpha-synuclein modulates synaptic vesicle interaction. *Nat. Commun.* 9:712. doi: 10.1038/s41467-018-03111-4

Leandrou, E., Emmanouilidou, E., and Vekrellis, K. (2019). Voltage-gated calcium channels and alpha-synuclein: implications in Parkinson's disease. *Front. Mol. Neurosci.* 12:237. doi: 10.3389/fnmol.2019.00237

Lieberman, O. J., Choi, S. J., Kanter, E., Saverchenko, A., Frier, M. D., Fiore, G. M., et al. (2017). α-Synuclein-dependent calcium entry underlies differential sensitivity of cultured SN and VTA dopaminergic neurons to a parkinsonian neurotoxin. *eNeuro* 4. doi: 10.1523/ENEURO.0167-17.2017

Liss, B., Haeckel, O., Wildmann, J., Miki, T., Seino, S., and Roeper, J. (2005). K-ATP channels promote the differential degeneration of dopaminergic midbrain neurons. *Nat. Neurosci.* 8, 1742–1751. doi: 10.1038/nn1570

Liss, B., and Striessnig, J. (2019). The potential of L-type calcium channels as a drug target for neuroprotective therapy in Parkinson's disease. *Annu. Rev. Pharmacol. Toxicol.* 59, 263–289. doi: 10.1146/annurev-pharmtox-010818-021214

Ma, H., Cohen, S., Li, B., and Tsien, R. W. (2012). Exploring the dominant role of Cav1 channels in signaling to the nucleus. *Biosci. Rep.* 33, 97–101. doi: 10.1042/BSR20120099

Melachroinou, K., Xilouri, M., Emmanouilidou, E., Masgrau, R., Papazafiri, P., Stefanis, L., et al. (2013). Deregulation of calcium homeostasis mediates secreted alpha-synuclein-induced neurotoxicity. *Neurobiol. Aging* 34, 2853–2865. doi: 10.1016/j.neurobiolaging.2013.06.006

Miranda-Laferte, E., Ewers, D., Guzman, R. E., Jordan, N., Schmidt, S., and Hidalgo, P. (2014). The N-terminal domain tethers the voltage-gated calcium channel beta2e-subunit to the plasma membrane via electrostatic and hydrophobic interactions. *J. Biol. Chem.* 289, 10387–10398. doi: 10.1074/jbc.M113.507244

Miranda-Laferte, E., Schmidt, S., Jara, A. C., Neely, A., and Hidalgo, P. (2012). A short polybasic segment between the two conserved domains of the beta2a-subunit modulates the rate of inactivation of R-type calcium channel. *J. Biol. Chem.* 287, 32588–32597. doi: 10.1074/jbc.M112.362509

Mosharov, E. V., Larsen, K. E., Kanter, E., Phillips, K. A., Wilson, K., Schmitz, Y., et al. (2009). Interplay between cytosolic dopamine, calcium, and alpha-synuclein causes selective death of substantia nigra neurons. *Neuron* 62, 218–229. doi: 10.1016/j.neuron.2009.01.033

Mullapudi, A., Gudala, K., Boya, C. S., and Bansal, D. (2016). Risk of Parkinson's disease in the users of antihypertensive agents: an evidence from the meta-analysis of observational studies. *J. Neurodegener. Dis.* 2016:5780809. doi: 10.1155/2016/5780809

Murata, M. (2010). Zonisamide: a new drug for Parkinson's disease. *Drugs Today* 46, 251–258. doi: 10.1358/dot.2010.46.4.1490077

Newcomb, R., Szoke, B., Palma, A., Wang, G., Chen, X., Hopkins, W., et al. (1998). Selective peptide antagonist of the class E calcium channel from the venom of the tarantula *Hysterocrates gigas*. *Biochemistry* 37, 15353–15362. doi: 10.1021/bi981255g

Obeso, J. A., Stamelou, M., Goetz, C. G., Poewe, W., Lang, A. E., Weintraub, D., et al. (2017). Past, present, and future of Parkinson's disease: a special essay on the 200th Anniversary of the Shaking Palsy. *Mov. Disord.* 32, 1264–1310. doi: 10.1002/mds.27115

Olcese, R., Qin, N., Schneider, T., Neely, A., Wei, X., Stefani, E., et al. (1994). The amino terminus of a calcium channel beta subunit sets rates of channel inactivation independently of the subunit's effect on activation. *Neuron* 13, 1433–1438. doi: 10.1016/0896-6273(94)90428-6

Ortner, N. J., Bock, G., Dougalis, A., Kharitonova, M., Duda, J., Hess, S., et al. (2017). Lower affinity of isradipine for L-type Ca^{2+} channels during substantia nigra dopamine neuron-like activity: implications

for neuroprotection in Parkinson's disease. *J. Neurosci.* 37, 6761–6777. doi: 10.1523/JNEUROSCI.2946-16.2017

Ortner, N. J., Bock, G., Vandael, D. H., Mauersberger, R., Draheim, H. J., Gust, R., et al. (2014). Pyrimidine-2,4,6-triones are a new class of voltage-gated L-type Ca^{2+} channel activators. *Nat. Commun.* 5:3897. doi: 10.1038/ncomms4897

Ortner, N. J., Kaserer, T., Copeland, J. N., and Striessnig, J. (2020). De novo CACNA1D Ca^{2+} channelopathies: clinical phenotypes and molecular mechanism. *Pflugers Arch.* 472, 755–773. doi: 10.1007/s00424-020-02418-w

Paladini, C. A., and Roeper, J. (2014). Generating bursts (and pauses) in the dopamine midbrain neurons. *Neuroscience* 282C, 109–121. doi: 10.1016/j.neuroscience.2014.07.032

Park, J. S., Davis, R. L., and Sue, C. M. (2018). Mitochondrial dysfunction in Parkinson's disease: new mechanistic insights and therapeutic perspectives. *Curr. Neurol. Neurosci. Rep.* 18:21. doi: 10.1007/s11910-018-0829-3

Parkinson Study Group (2013). Phase II safety, tolerability, and dose selection study of isradipine as a potential disease-modifying intervention in early Parkinson's disease (STEADY-PD). *Mov. Disord.* 28, 1823–1831. doi: 10.1002/mds.25639

Parkinson Study Group STEADY-PD III Investigators (2020). Isradipine versus placebo in early Parkinson disease: a randomized trial. *Ann. Intern. Med.* 172, 591-598. doi: 10.7326/M19-2534

Parkinson, J. (2002). An essay on the shaking palsy. *J. Neuropsychiatry Clin. Neurosci.* 14, 223–236; discussion: 222. doi: 10.1176/jnp.14.2.223

Philippart, F., Destreel, G., Merino-Sepulveda, P., Henny, P., Engel, D., and Seutin, V. (2016). Differential somatic Ca^{2+} channel profile in midbrain dopaminergic neurons. *J. Neurosci.* 36, 7234–7245. doi: 10.1523/JNEUROSCI.0459-16.2016

Poetschke, C., Dragicevic, E., Duda, J., Benkert, J., Dougalis, A., DeZio, R., et al. (2015). Compensatory T-type Ca^{2+} channel activity alters D2-autoreceptor responses of substantia nigra dopamine neurons from Cav1.3 L-type Ca^{2+} channel KO mice. *Sci. Rep.* 5:13688. doi: 10.1038/srep13688

Poewe, W., Seppi, K., Tanner, C. M., Halliday, G. M., Brundin, P., Volkmann, J., et al. (2017). Parkinson disease. *Nat. Rev. Dis. Primers* 3:17013. doi: 10.1038/nrdp.2017.13

Price, C. J. (2014). *Evaluation of Isradipine for Neuroprotection in the MPTP/p Mouse Model of Parkinson's Disease*. Washington, DC: Society for Neuroscience.

Richard, M., Kaufmann, P., Kornberger, R., and Dingemanse, J. (2019). First-in-man study of ACT-709478, a novel selective triple T-type calcium channel blocker. *Epilepsia* 60, 968–978. doi: 10.1111/epi.14732

Richard, M., Kaufmann, P., Ort, M., Kornberger, R., and Dingemanse, J. (2020). Multiple-ascending dose study in healthy subjects to assess the pharmacokinetics, tolerability, and CYP3A4 interaction potential of the T-type calcium channel blocker ACT-709478, a potential new antiepileptic drug. *CNS Drugs* 34, 311–323. doi: 10.1007/s40263-019-00697-1

Sautter, J., Kupsch, A., Earl, C. D., and Oertel, W. H. (1997). Degeneration of pre-labelled nigral neurons induced by intrastriatal 6-hydroxydopamine in the rat: behavioural and biochemical changes and pretreatment with the calcium-entry blocker nimodipine. *Exp. Brain Res.* 117, 111–119. doi: 10.1007/s002210050204

Schapira, A. H. (2008). Mitochondria in the aetiology and pathogenesis of Parkinson's disease. *Lancet Neurol.* 7, 97–109. doi: 10.1016/S1474-4422(07)70327-7

Schiemann, J., Schlaudraff, F., Klose, V., Bingmer, M., Seino, S., Magill, P. J., et al. (2012). K-ATP channels in dopamine substantia nigra neurons control bursting and novelty-induced exploration. *Nat. Neurosci.* 15, 1272–1280. doi: 10.1038/nn.3185

Schneider, T., Dibue, M., and Hescheler, J. (2013). How "pharmacoresistant" is Cav2.3, the major component of voltage-gated R-type Ca^{2+} channels? *Pharmaceuticals* 6, 759–776. doi: 10.3390/ph6060759

Schneider, T., Neumaier, F., Hescheler, J., and Alpdogan, S. (2020). Cav2.3 R-type calcium channels: from its discovery to pathogenic de novo CACNA1E variants: a historical perspective. *Pflugers Arch.* 472, 811–816. doi: 10.1007/s00424-020-02395-0

Schulz, J. B., Hausmann, L., and Hardy, J. (2016). 199 years of Parkinson disease - what have we learned and what is the path to the future? *J. Neurochem.* 139(Suppl. 1), 3–7. doi: 10.1111/jnc.13733

Shin, W. (2015). *RNASeq of DA neurons from SNpc and VTA*. Available online at: https://figshare.com/articles/dataset/RNASeq_of_DA_neurons_from_SNpc_and_VTA/926519

Siddiqi, F. H., Menzies, F. M., Lopez, A., Stamatakou, E., Karabiyik, C., Ureshino, R., et al. (2019). Felodipine induces autophagy in mouse brains with pharmacokinetics amenable to repurposing. *Nat. Commun.* 10:1817. doi: 10.1038/s41467-019-09494-2

Singh, A., Gebhart, M., Fritsch, R., Sinnegger-Brauns, M. J., Poggiani, C., Hoda, J. C., et al. (2008). Modulation of voltage- and Ca^{2+}-dependent gating of Cav1.3 L-type calcium channels by alternative splicing of a C-terminal regulatory domain. *J. Biol. Chem.* 283, 20733–20744. doi: 10.1074/jbc.M802254200

Singh, A., Verma, P., Balaji, G., Samantaray, S., and Mohanakumar, K. P. (2016). Nimodipine, an L-type calcium channel blocker attenuates mitochondrial dysfunctions to protect against 1-methyl-4-phenyl-1,2,3,6-tetrahydropyridine-induced parkinsonism in mice. *Neurochem. Int.* 99, 221–232. doi: 10.1016/j.neuint.2016.07.003

Sinnegger-Brauns, M. J., Hetzenauer, A., Huber, I. G., Renstrom, E., Wietzorrek, G., Berjukov, S., et al. (2004). Isoform-specific regulation of mood behavior and pancreatic beta cell and cardiovascular function by L-type Ca^{2+} channels. *J. Clin. Invest.* 113, 1430–1439. doi: 10.1172/JCI20208

Sinnegger-Brauns, M. J., Huber, I. G., Koschak, A., Wild, C., Obermair, G. J., Einzinger, U., et al. (2009). Expression and 1,4-dihydropyridine-binding properties of brain L-type calcium channel isoforms. *Mol. Pharmacol.* 75, 407–414. doi: 10.1124/mol.108.049981

Surmeier, D. J., Halliday, G. M., and Simuni, T. (2017a). Calcium, mitochondrial dysfunction and slowing the progression of Parkinson's disease. *Exp. Neurol.* 298(Pt B), 202–209.doi: 10.1016/j.expneurol.2017.08.001

Surmeier, D. J., Obeso, J. A., and Halliday, G. M. (2017b). Selective neuronal vulnerability in Parkinson disease. *Nat. Rev. Neurosci.* 18, 101–113. doi: 10.1038/nrn.2016.178

Tabata, Y., Imaizumi, Y., Sugawara, M., Andoh-Noda, T., Banno, S., Chai, M., et al. (2018). T-type calcium channels determine the vulnerability of dopaminergic neurons to mitochondrial stress in familial Parkinson disease. *Stem Cell Rep.* 11, 1171–1184. doi: 10.1016/j.stemcr.2018.09.006

Tai, C. H., Yang, Y. C., Pan, M. K., Huang, C. S., and Kuo, C. C. (2011). Modulation of subthalamic T-type Ca^{2+} channels remedies locomotor deficits in a rat model of Parkinson disease. *J. Clin. Invest.* 121, 3289–3305. doi: 10.1172/JCI46482

Tan, B. Z., Jiang, F., Tan, M. Y., Yu, D., Huang, H., Shen, Y., et al. (2011). Functional characterization of alternative splicing in the C terminus of L-type CaV1.3 channels. *J. Biol. Chem.* 286, 42725–42735. doi: 10.1074/jbc.M111.265207

Tracy, M. E., Tesic, V., Stamenic, T. T., Joksimovic, S. M., Busquet, N., Jevtovic-Todorovic, V., et al. (2018). CaV3.1 isoform of T-type calcium channels supports excitability of rat and mouse ventral tegmental area neurons. *Neuropharmacology* 135, 343–354. doi: 10.1016/j.neuropharm.2018.03.028

Uchida, S., Yamada, S., Nagai, K., Deguchi, Y., and Kimura, R. (1997). Brain pharmacokinetics and *in vivo* receptor binding of 1,4-dihydropyridine calcium channel antagonists. *Life Sci.* 61, 2083–2090. doi: 10.1016/S0024-3205(97)00881-3

Verma, A., and Ravindranath, V. (2019). CaV1.3 L-type calcium channels increase the vulnerability of substantia nigra dopaminergic neurons in MPTP mouse model of Parkinson's disease. *Front. Aging Neurosci.* 11:382. doi: 10.3389/fnagi.2019.00382

Wang, Q. M., Xu, Y. Y., Liu, S., and Ma, Z. G. (2017). Isradipine attenuates MPTP-induced dopamine neuron degeneration by inhibiting up-regulation of L-type calcium channels and iron accumulation in the substantia nigra of mice. *Oncotarget* 8, 47284-47295. doi: 10.18632/oncotarget.17618

Wang, R., Ma, Z., Wang, J., and Xie, J. (2012). L-type Cav1.2 calcium channel is involved in 6-hydroxydopamine-induced neurotoxicity in rats. *Neurotox. Res.* 21, 266–270. doi: 10.1007/s12640-011-9271-x

Wang, X., Saegusa, H., Huntula, S., and Tanabe, T. (2019). Blockade of microglial Cav1.2 Ca^{2+} channel exacerbates the symptoms in a Parkinson's disease model. *Sci. Rep.* 9:9138. doi: 10.1038/s41598-019-45681-3

Weiss, N., and Zamponi, G. W. (2019a). T-type calcium channels: from molecule to therapeutic opportunities. *Int. J. Biochem. Cell Biol.* 108, 34–39. doi: 10.1016/j.biocel.2019.01.008

Weiss, N., and Zamponi, G. W. (2019b). T-type channel druggability at a crossroads. *ACS Chem. Neurosci.* 10, 1124–1126. doi: 10.1021/acschemneuro.9b00031

Weiss, N., and Zamponi, G. W. (2020). Genetic T-type calcium channelopathies. *J. Med. Genet.* 57, 1–10. doi: 10.1136/jmedgenet-2019-106163

Wilson, C. J., and Callaway, J. C. (2000). Coupled oscillator model of the dopaminergic neuron of the substantia nigra. *J. Neurophysiol.* 83, 3084–3100. doi: 10.1152/jn.2000.83.5.3084

Wolfart, J., and Roeper, J. (2002). Selective coupling of T-type calcium channels to SK potassium channels prevents intrinsic bursting in dopaminergic midbrain neurons. *J. Neurosci.* 22, 3404–3413. doi: 10.1523/JNEUROSCI.22-09-03404.2002

Xiang, Z., Thompson, A. D., Brogan, J. T., Schulte, M. L., Melancon, B. J., Mi, D., et al. (2011). The discovery and characterization of ML218: a novel, centrally active T-type calcium channel inhibitor with robust effects in STN neurons and in a rodent model of Parkinson's disease. *ACS Chem. Neurosci.* 2, 730–742. doi: 10.1021/cn200090z

Xu, W., and Lipscombe, D. (2001). Neuronal Cav1.3α1 L-type channels activate at relatively hyperpolarized membrane potentials and are incompletely inhibited by dihydropyridines. *J. Neurosci.* 21, 5944–5951. doi: 10.1523/JNEUROSCI.21-16-05944.2001

Yang, Y. C., Tai, C. H., Pan, M. K., and Kuo, C. C. (2014). The T-type calcium channel as a new therapeutic target for Parkinson's disease. *Pflugers Arch.* 466, 747–755. doi: 10.1007/s00424-014-1466-6

Yasuda, T., Chen, L., Barr, W., McRory, J. E., Lewis, R. J., Adams, D. J., et al. (2004). Auxiliary subunit regulation of high-voltage activated calcium channels expressed in mammalian cells. *Eur. J. Neurosci.* 20, 1–13. doi: 10.1111/j.1460-9568.2004.03434.x

Yee, A. G., Forbes, B., Cheung, P. Y., Martini, A., Burrell, M. H., Freestone, P. S., et al. (2019). Action potential and calcium dependence of tonic somatodendritic dopamine release in the substantia nigra pars compacta. *J. Neurochem.* 148, 462–479. doi: 10.1111/jnc.14587

Yiu, S., and Knaus, E. E. (1996). Synthesis, biological evaluation, calcium channel antagonist activity, and anticonvulsant activity of felodipine coupled to a dihydropyridine-pyridinium salt redox chemical delivery system. *J. Med. Chem.* 39, 4576–4582. doi: 10.1021/jm960531r

Zaichick, S. V., McGrath, K. M., and Caraveo, G. (2017). The role of Ca^{2+} signaling in Parkinson's disease. *Dis. Model. Mech.* 10, 519–535. doi: 10.1242/dmm.028738

Zampese, E., and Surmeier, D. J. (2020). Calcium, bioenergetics, Parkinson's disease. *Cells* 9:2045. doi: 10.3390/cells9092045

Zamponi, G. W., Striessnig, J., Koschak, A., and Dolphin, A. C. (2015). The physiology, pathology, and pharmacology of voltage-gated calcium channels and their future therapeutic potential. *Pharmacol. Rev.* 67, 821–870. doi: 10.1124/pr.114.009654

Conflict of Interest: The author declares that the research was conducted in the absence of any commercial or financial relationships that could be construed as a potential conflict of interest.

Copyright © 2021 Ortner. This is an open-access article distributed under the terms of the Creative Commons Attribution License (CC BY). The use, distribution or reproduction in other forums is permitted, provided the original author(s) and the copyright owner(s) are credited and that the original publication in this journal is cited, in accordance with accepted academic practice. No use, distribution or reproduction is permitted which does not comply with these terms.

frontiers in Synaptic Neuroscience

ORIGINAL RESEARCH
published: 26 February 2021
doi: 10.3389/fnsyn.2021.635050

Multi-Electrode Array Analysis Identifies Complex Dopamine Responses and Glucose Sensing Properties of Substantia Nigra Neurons in Mouse Brain Slices

*Nadja Mannal[1], Katharina Kleiner[1], Michael Fauler[1], Antonios Dougalis[1], Christina Poetschke[1] and Birgit Liss[1,2]**

[1] Institute of Applied Physiology, University of Ulm, Ulm, Germany, [2] Linacre and New College, University of Oxford, Oxford, United Kingdom

Dopaminergic (DA) midbrain neurons within the substantia nigra (SN) display an autonomous pacemaker activity that is crucial for dopamine release and voluntary movement control. Their progressive degeneration is a hallmark of Parkinson's disease. Their metabolically demanding activity-mode affects Ca^{2+} homeostasis, elevates metabolic stress, and renders SN DA neurons particularly vulnerable to degenerative stressors. Accordingly, their activity is regulated by complex mechanisms, notably by dopamine itself, via inhibitory D2-autoreceptors and the neuroprotective neuronal Ca^{2+} sensor NCS-1. Analyzing regulation of SN DA neuron activity-pattern is complicated by their high vulnerability. We studied this activity and its control by dopamine, NCS-1, and glucose with extracellular multi-electrode array (MEA) recordings from midbrain slices of juvenile and adult mice. Our tailored MEA- and spike sorting-protocols allowed high throughput and long recording times. According to individual dopamine-responses, we identified two distinct SN cell-types, in similar frequency: dopamine-inhibited and dopamine-excited neurons. Dopamine-excited neurons were either silent in the absence of dopamine, or they displayed pacemaker-activities, similar to that of dopamine-inhibited neurons. Inhibition of pacemaker-activity by dopamine is typical for SN DA neurons, and it can undergo prominent desensitization. We show for adult mice, that the number of SN DA neurons with desensitized dopamine-inhibition was increased (~60–100%) by a knockout of NCS-1, or by prevention of NCS-1 binding to D2-autoreceptors, while time-course and degrees of desensitization were not altered. The number of neurons with desensitized D2-responses was also higher (~65%) at high glucose-levels (25 mM), compared to lower glucose (2.5 mM), while again desensitization-kinetics were unaltered. However, spontaneous firing-rates were significantly higher at high glucose-levels (~20%). Moreover, transient glucose-deprivation (1 mM) induced a fast and fully-reversible pacemaker frequency reduction. To directly address and quantify glucose-sensing properties of SN DA neurons, we continuously monitored their electrical activity, while altering extracellular glucose concentrations stepwise from 0.5 mM up to 25 mM.

OPEN ACCESS

Edited by:
Francesco Ferraguti, Innsbruck Medical University, Austria

Reviewed by:
Nicola B. Mercuri, University of Rome Tor Vergata, Italy
Valentina Carabelli, University of Turin, Italy

***Correspondence:**
Birgit Liss
birgit.liss@uni-ulm.de

Received: *29 November 2020*
Accepted: *08 January 2021*
Published: *26 February 2021*

Citation:
Mannal N, Kleiner K, Fauler M, Dougalis A, Poetschke C and Liss B (2021) Multi-Electrode Array Analysis Identifies Complex Dopamine Responses and Glucose Sensing Properties of Substantia Nigra Neurons in Mouse Brain Slices. Front. Synaptic Neurosci. 13:635050. doi: 10.3389/fnsyn.2021.635050

SN DA neurons were excited by glucose, with EC_{50} values ranging from 0.35 to 2.3 mM. In conclusion, we identified a novel, common subtype of dopamine-excited SN neurons, and a complex, joint regulation of dopamine-inhibited neurons by dopamine and glucose, within the range of physiological brain glucose-levels.

Keywords: glucose-excited GE-neurons, dopamine excited neurons, dopamine inhibited neurons, dopamine-autoreceptor, neuronal calcium sensor NCS-1, GIRK channel, dopamine receptor desensitization, glucose-responsive neurons

INTRODUCTION

Dopamine and dopamine-releasing (DA) neurons are important for a variety of brain functions and processes like movement control, habit-formation, conditioning, cognition, novelty-related behavior, motivation, reward prediction, and glucose homeostasis (Dodson et al., 2016; Koekkoek et al., 2017; Berke, 2018; Ter Horst et al., 2018; Collins and Saunders, 2020). DA midbrain neurons in the Substantia nigra (SN) are particularly important for voluntary movement control, and their progressive degeneration causes the main motor-symptoms of Parkinson's disease (PD), the 2nd most common neurodegenerative disease (Kordower et al., 2013; Obeso et al., 2017; Poewe et al., 2017; Hernandez et al., 2019). SN DA neurons are particularly vulnerable to degenerative stressors, while neighboring DA neurons in the ventral tegmental area (VTA) are less affected (Fu et al., 2016; Vogt Weisenhorn et al., 2016; Surmeier et al., 2017). The causes for this differential vulnerability of DA neurons and for their selective degeneration in PD are still unclear. However, a variety of intrinsic and extrinsic factors have been identified, pointing to converging mechanisms, in particular cell-specific electrical activity patterns, calcium homeostasis and elevated metabolic stress (Duda et al., 2016; Giguere et al., 2018; Gonzalez-Rodriguez et al., 2020; Lebowitz and Khoshbouei, 2020).

SN DA neurons display a high level of intrinsic metabolic stress already under control conditions. This is due to the size and complexity of their unmyelinated axonal arbors in their striatal target regions, which is an order of magnitude greater than that of less susceptible dopamine neurons (Bolam and Pissadaki, 2012; Giguere et al., 2019; Wong et al., 2019), as well as their particular mode of electrical activity. SN DA neurons display an autonomous pacemaker activity that is crucial for axonal and somatodendritic dopamine release (Rice and Patel, 2015; Sulzer et al., 2016; Liu and Kaeser, 2019). This activity causes additional metabolic stress, as it is associated, in SN but not in VTA DA neurons, with oscillatory elevated levels of free intracellular Ca^{2+}, due to the activation of voltage-gated Ca^{2+} channels (Cav) during action potentials (Zamponi et al., 2015; Philippart et al., 2016; Liss and Striessnig, 2019; Zampese and Surmeier, 2020). These activity-related Ca^{2+} dynamics stimulate electrical activity, ATP synthesis and dopamine release, and thus facilitate movement. But they also constitute an intrinsic metabolic burden that can trigger neurodegeneration. Consequently, the activity of SN DA neurons is tightly controlled by a variety of (still not fully understood) feed-back and feed-forward mechanisms (Dragicevic et al., 2015; Duda et al., 2016; Michel et al., 2016; Gantz et al., 2018).

Dopamine itself is modulating the activity of SN DA neurons in a negative feedback-loop by activation of inhibitory dopamine-autoreceptors of the D2-type (D2-AR) (Lacey et al., 1987; Beckstead et al., 2004; Ford, 2014). Somatodendritic D2-AR are best-known to activate G-protein coupled inwardly rectifying K^+ channels (GIRK2), and leading to hyperpolarized membrane potentials, but other signaling mechanisms are described (Cardozo and Bean, 1995; Evans et al., 2017; Philippart and Khaliq, 2018; Chen et al., 2020). Inhibitory dopamine responses can desensitize, meaning that neuronal activity is regained although dopamine is still present (Gainetdinov et al., 2004). D2-receptor desensitization is modulated by many (incompletely characterized) processes (Bonci and Hopf, 2005; Robinson et al., 2017a). In particular by Ca^{2+} dependent processes (Beckstead and Williams, 2007; Liu et al., 2008; Perra et al., 2011; Evans et al., 2017; Gantz et al., 2018), like the Ca^{2+} dependent binding of the neuronal Ca^{2+} sensor NCS-1 to D2-ARs, as demonstrated for SN DA neurons from juvenile mice (Kabbani et al., 2012; Dragicevic et al., 2014; Poetschke et al., 2015). NCS-1 is of special interest as it stimulates mitochondrial function and promotes neuronal survival (Catoni et al., 2019; Nakamura et al., 2019). In SN DA neurons, NCS-1 regulates the expression of genes involved in mitochondrial function, and NCS-1 loss increased their vulnerability in a PD mouse model (Benkert et al., 2019; Simons et al., 2019). In remaining human SN DA neurons from *post-mortem* PD brains, NCS-1 mRNA levels are elevated (Dragicevic et al., 2014), pointing to a neuroprotective role of NCS-1 in PD. Dopamine, D2-receptors, and NCS-1 are also important for regulation of glucose homeostasis, pancreatic

Abbreviations: ACSF, artificial cerebrospinal fluid; AMP, adenosine monophosphate; Arc, arcuate nucleus; Cav, voltage-gated calcium channel; CFTR, cystic fibrosis transmembrane conductance regulator; CV, coefficient of variation; D2-AR, autoreceptor of the D2 type; DA, dopamine; DMN, dorsomedial nuclei; DMV, dorsal motor nucleus of the vagus; DNIP, D2/NCS-1 interaction preventing peptide; EC50, half maximal effective concentration; GE, glucose excited; GFP, green fluorescent protein; GI, glucose inhibited; GIRK, G-protein coupled inwardly rectifying K^+; GK, glucokinase; GLUT, glucose transporter; HT, hypothalamus; ISI, interspike interval; K2P (TASK), two-pore domain potassium; K-ATP, ATP-sensitive K^+; KO, knockout; K_v, voltage-gated potassium channel; L-Dopa, Levodopa; LH, lateral hypothalamus; MEA, multi-electrode array; MUA, multi unit activity; NCS-1, neuronal Ca^{2+} sensor; PBM, parabrachial medial nucleus; PBS, phosphate buffered saline; PCA, principal component analysis; PD, Parkinson's disease; PN, post-natal; PVN, periventricular nucleus; SD, standard deviation; SE, standard error; SEM, standard error of the mean; SGLT, sodium glucose co-transporter; SN, substantia nigra; srDNIP, scrambled DNIP; SUA, single unit activity; T1R, sweet taste receptor; T2DM, diabetes mellitus type 2; TH, tyrosine hydroxylase; TRPC, transient receptor potential channel; VMH, ventromedial hypothalamus; VMN, ventromedial nucleus; VRAC, volume regulated anion channels; VTA, ventral tegmental area; WT, wildtype.

insulin secretion, and body weight (Gromada et al., 2005; Lopez Vicchi et al., 2016; Hassanabad and Fatehi, 2019; Ratai et al., 2019; Liu et al., 2020). SN DA neurons and pancreatic beta-cells (responsible for peripheral glucose sensing and insulin secretion) modulate each other's function and possess similar signaling mechanisms, like D2-receptors, K-ATP channels, and Cav mediated activity-modulation (Eberhard, 2013; Fiory et al., 2019; Farino et al., 2020; Liu et al., 2020). However, direct glucose sensing properties of SN DA neurons have not yet been reported. Glucose sensing neurons are best described in the hypothalamus, but also in other brain regions (Koekkoek et al., 2017; Alvarsson and Stanley, 2018). They alter their electrical activity with changes in extracellular glucose levels. Glucose-excited (GE) neurons increase their action potential frequency as glucose levels increase (similar to pancreatic beta cells), whereas glucose-inhibited (GI) neurons decrease their activity with rising glucose levels (Routh, 2010).

Here, we studied the modulation of SN DA neuron activity by dopamine, NCS-1, and glucose. As this analysis is complicated by the particularly high vulnerability of SN DA neurons toward metabolic stressors, we used optimized extracellular multi-electrode array (MEA) approaches to study neuronal activity in vital mouse brain slices. MEA recordings followed up by spike-sorting allowed us to analyze SN DA neurons without selection-bias and with much higher throughput compared to patch clamp techniques. Based on their dopamine-responses, we identified two types of SN neurons that were either dopamine-excited or dopamine-inhibited. Both SN populations were similar in size. The number of dopamine-inhibited SN DA neurons with desensitized responses was reduced by NCS-1 activity, and increased by elevated extracellular glucose, but the kinetics of inhibitory dopamine-responses were not altered. SN DA neurons displayed fast and reversible glucose-responsiveness in a dose-dependent manner, with higher electrical activity at elevated glucose levels, and within the physiological range of brain glucose levels. Thus, SN DA neurons display GE-neuron properties, similar as beta-cells.

MATERIALS AND METHODS

Animals

All mice were bred and housed in the facilities of the University of Ulm, according to the German Tierschutzgesetz and the directive 2010/63/EU. All animal procedures were approved by the Regierungspräsidium Tübingen (Reg. Nr. 0.147 and TV1043). Only male mice were analyzed. Wildtype mice are derived from C57BL/6J. NCS-1 KO mice (obtained by Olaf Pongs) were back-crossed at least 10 times into C57BL/6J (Ng et al., 2016), leading to a 99.9% analogy with C57BL/6J, and losing the 129/SvJ original background (Eisener-Dorman et al., 2009). Data from littermate NCS-1 +/+ were not significantly different from those of C57BL/6J and were pooled.

Patch Clamp Experiments

Coronal mouse brain slices were prepared (similar as detailed below for MEA experiments), and perforated patch clamp recordings were performed and analyzed, as previously described (Dragicevic et al., 2014; Poetschke et al., 2015).

Multi-Electrode Array (MEA) Experiments

Brain Slice Preparation

Juvenile and adult mice were deeply and terminally anesthetized with isoflurane, and decapitated. During slicing, for orientation, a tiny hole was punched into the left side of the brain using a blunted 21G cannula.

For juvenile mice (∼PN 13), after decapitation, the brain was quickly removed from the cranial cavity, cooled and cut into 250 μm coronal midbrain slices in ice cold artificial cerebrospinal fluid (ACSF) using a vibratome (Vibroslice^{TM} type: HA752, Campden Instruments, UK), and stainless steel blades (Campden Instruments Ltd.). ACSF contained (in mM): 125 NaCl, 2.5 KCL, 25 $NaHCO_3$, 1.25 NaH_2PO_4, 2 $MgCl_2$, 2 $CaCl_2$, and 25 glucose, bubbled with carbogen (95% CO_2/5% O_2) for pH adjustment (7.3) and oxygenation. Slices were allowed to recover for 30 min at room temperature in the same ACSF.

For adult mice, brain slice preparation was carried out utilizing a slightly altered version of the "slice it hot" protocol (Ankri et al., 2014). After brain removal, coronal midbrain slices (200 μm) were prepared using a vibratome (Leica VT1200S, amplitude 1.4 mm, speed 0.6 mm/s) with ceramic blades (Campden Instruments Ltd.) in ACSF at ∼36°C. This ACSF contained (in mM): 124 NaCl, 3 KCl, 26 $NaHC0_3$, 1.2 KH_2PO4, 1 $MgCl_2$, 1 $CaCl_2$, 10 glucose, bubbled with carbogen (95% CO_2/5% O_2) for pH adjustment (7.3) and oxygenation. Slices were allowed to recover for 1 h at 37°C in ACSF-recovery solution containing (in mM): 125 NaCl, 2.5 KCl, 25 $NaHCO_3$, 1.25 $NH2PO_4$, 1 $MgCl_2$, 1 $CaCl_2$, 25 mM glucose.

All chemicals were obtained from Sigma, if not stated otherwise.

MEA Recordings

The ACSF for MEA-recordings ("recording-ACSF") contained (in mM): 125 NaCl, 2.5 KCl, 25 $NaHCO_3$, 1.25 NH_2PO_4, 1 $MgCl_2$, 1 $CaCl_2$, with variable glucose concentrations (0.5–25 mM). We added 10 μM DNQX disodium salt (Tocris) and 10 μM Gabazine (Tocris) to block fast synaptic transmission. When glucose was below 25 mM, sucrose was added to get a total of 25 mM sugar in the solution to keep the osmolarity stable (300–315 mOsm/l). ACSF was bubbled with carbogen (95% CO_2/5% O_2) for pH adjustment (7.3) and oxygenation.

For MEA-recordings 3D-Biochips were used, manufactured by Qwane Biosciences SA (Switzerland). The electrode array layout of the MEA-chips was customized for covering the shape of the SN in coronal mouse brain sections. The MEA-chips contain 60 3D tip-shaped platinum electrodes, arranged in a 15 row × 4 column array. Interelectrode distance is 100 μm in rows and 90 μm in columns (measured from center to center). Each electrode is 30 μm in diameter, and the tip extends 25–40 μm from the base. The surface of the chips is covered by a 5 μm layer of SU-8 epoxy and has an electrical impedance of 500–800 kΩ. For optimized tissue to electrode contact, biochips were plasma cleaned every second week for 2 min under low vacuum (0.5 Torr, service of the Electron Microscopy Facility, University of

Ulm). MEA chips were stored at 4°C, and reused for 3–6 months depending on the intensity of usage.

MEA recordings were carried out using either a USB MEA1060-Up-BC System or a MEA2100-2x60 System (Multichannel Systems, Germany). For the MEA1060-System, slices were mounted onto the MEA-chip under a stereoscope (Leica M165C). For the 2100 MEA System, slices were directly mounted on the amplifier with help of a video table (MEA-VMTC-2, Multichannel Systems). Slices were kept in place by a self-made grid, consisting of nylon strings affixed to a semi-circle platinum wire (3 mm diameter of the wire, 1.3 g total weight). Careful and correct positioning of the slice on the chip and placing the grid without moving or harming the slice was crucial for successful experiments. Before and after placing the grid, images were taken to document the MEA chip positioning (**Figure 1**).

The recording chamber containing the MEA-chip was constantly perfused with the carbogenated recording-ACSF by a peristaltic pump (∼4 ml/min, Ismatec, Germany). The temperature control of the inlet cannula (TC02 with PH01, Multichannel Systems, Germany) was set to 35°C and the inbuilt amplifier heating plate to 40°C, resulting in a bath temperature of 31–33°C (checked by a hand-thermometer before each experiment). After transfer into the recording chamber, slices were allowed to equilibrate in recording-ACSF for 30 min.

Data were sampled at 20 kHz using the MC_Rack software (version 4, Multichannel Systems, Germany). Data was recorded using a low pass (3,000 Hz) and a high pass (200 Hz) butterworth 2nd order filter. The software allows simultaneous recordings and online analysis. The so-called spike analyzer tool was used to identify the electrodes displaying activity directly during recordings: This tool is an in-built spike sorter that detects spikes within the signals, recorded by each electrode. The threshold for spike detection is set automatically by the software and individually for each electrode depending on the signal to noise ratio. Detected spikes were continuously displayed in the spike analyzer display. Electrodes showing a reaction to DA application (i.e., change of event-rate, either elevated or reduced) were marked for further data analysis (see below).

The basic experimental design, carried out in recording-ACSF, was as follows (with 2.5 mM glucose if not stated otherwise): 10 min baseline recording of pacemaker-activities (for determining basal frequency and CV-ISI-values), followed by bath-application of 100 μM dopamine hydrochloride for 15 min, and a 20 min wash-out phase of dopamine. For DNIP (D2R/NCS-1 interaction prevention) experiments the DNIP peptide, or its scrambled (srDNIP) control, were synthesized by Genscript according to the published amino acid sequences (Saab et al., 2009; Kabbani et al., 2012). Peptides were dissolved in recording-ACSF, and bath-applied at a final concentration of 10 μM. DNIP-experiments were carried out as follows: after 10 min baseline recordings, slices were incubated for 30 min with recording-ACSF containing DNIP/srDNIP, followed by recording of 10 min baseline activity, 15 min dopamine application, and 20 min washout of dopamine (all in recording-ACSF with DNIP/srDNIP). For glucose sensing experiments, different glucose concentrations were bath-applied by switching recording-ACSFs with respective different glucose concentrations. Delay-time until dopamine/peptides/altered glucose reached the recording chamber was about 120 s. For NCS-1 experiments, results for adult mice (∼PN90) are shown, but SN DA neurons from juvenile mice displayed similar responses (data not shown; and see Dragicevic et al., 2014; Poetschke et al., 2015). For glucose sensing experiments, results for juvenile mice are shown (∼PN13) as they coped better with very low glucose concentrations, but SN DA neurons from adult mice displayed similar qualitative glucose responses.

Data Analysis

Spike Sorting

MEA-recording files were saved as mcd-files. Electrodes that recorded a response to dopamine (i.e., change of event-rate) were already marked during the recording, based on the online analysis options in the MC_Rack software. To minimize file sizes, recording files were re-recorded containing only the electrodes displaying a response to dopamine (either increased or decreased event-rate). The generated second mcd file was imported into Spike2 and converted to a smrx file.

Spike sorting of MEA recordings was carried out with Spike2 software (8.02e x64, Cambridge Electronic Design Ltd.). A threshold trigger was manually set by the experimenter, depending on the signal to noise ratio of the respective recording. The detected spikes displayed an amplitude of ∼25-50 μV with a background noise of 15-25 μV. Via principal component analysis (PCA), Spike2 generates so-called spike templates, by matching and grouping spikes according to their principal components. These principal components are distinct features of the spikes like shape, amplitude, and length. The algorithm tries to separate the spikes in a direction of the largest variance. Meaning that the principal components with the highest variation in-between are chosen to generate the final spike templates. Spikes were separated by the software choosing the first two or three principal components (Lewicki, 1998). Templates were then automatically plotted in a 3D coordinate system as clusters, where every spike is displayed as a single dot and the chosen principal components represent the three axes x, y, and z. This enables manual reassignment of spikes, if necessary. For further details see manual "Spike2 version 9 for Windows."

Identification of Single Unit Activity (SUA) With Spike2 Software

If spike sorting by automatic Spike2 analysis was successful, the activity will be split into separate single unit activities. This means, that each activity, recorded from the individual electrodes, can be assigned to a single neuron. Since this was not always the case, after the automatic principal component analysis by Spike2 software, manual cluster analysis optimization by the experimenter is often necessary, to sort out appropriate SUAs out of automatically classified multi unit activity (MUA).

For identification of a single unit activity (SUA), the sorted activity was manually checked in Spike2 for the following pre-selection criteria: (a) a lack of events occurring during the first 200 ms (short ISI range) shown in an interval histogram: the number of events before the first big peak of the interval

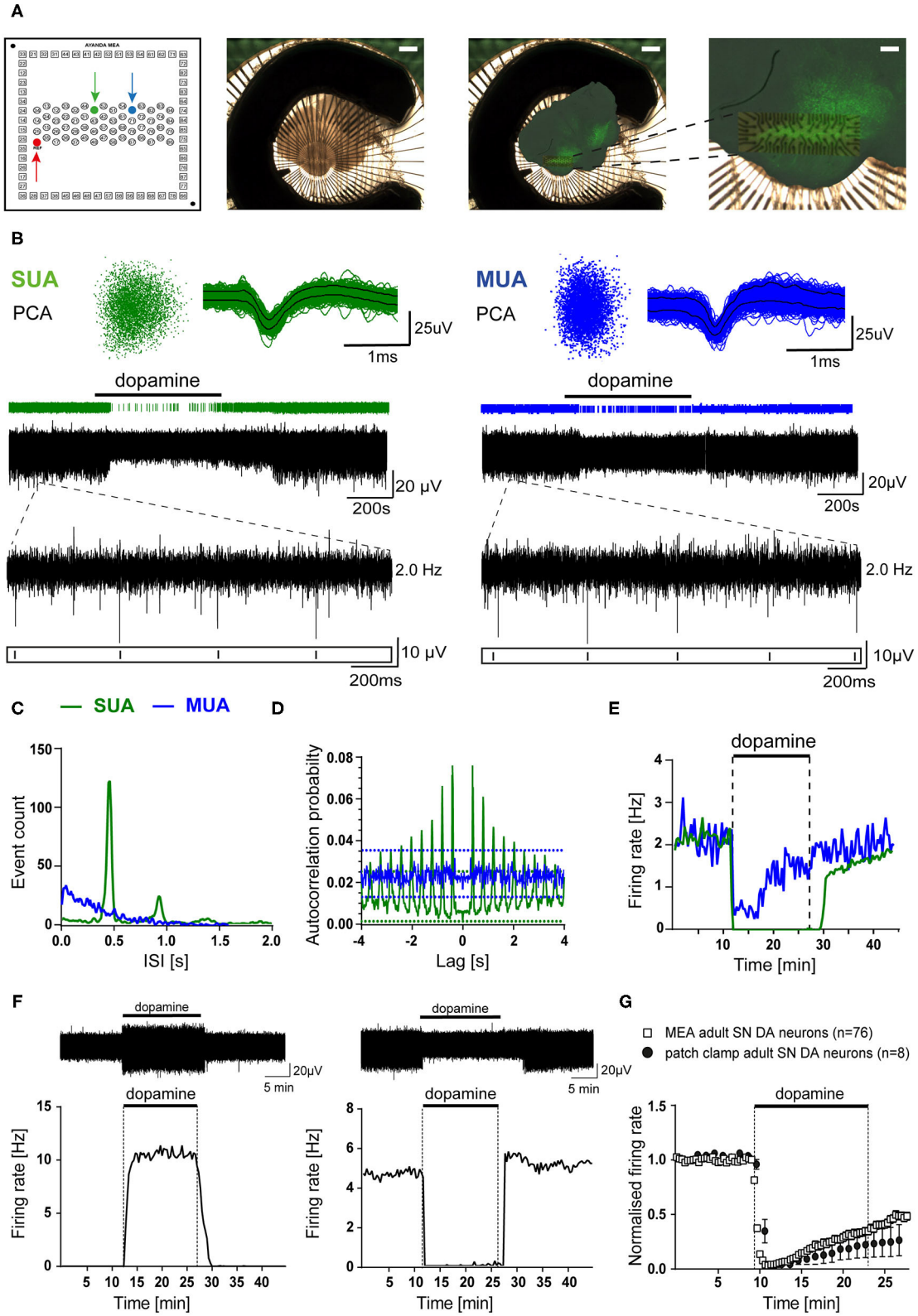

FIGURE 1 | MEA analysis identified dopamine-inhibited and dopamine-excited *Substantia nigra* neurons in mouse midbrain slices. Recordings were obtained from C57BL/6J mouse brain slices in ACSF containing 2.5 mM glucose **(A)** Left panel: schematic channel layout of the used 3D MEA chip, containing 60 platinum 3D-electrodes. The red arrow marks the reference-electrode. The electrodes marked by green and blue arrows correspond to the respective recordings shown

(Continued)

FIGURE 1 | in **(B–E)**. Middle panel: Image of a typical coronal midbrain slice, mounted on the 3D MEA biochip (scale bar: 1 mm). Right panels: Overlay of the image before recording with the respective image of the same slice, fixed and stained for tyrosine hydroxylase (TH), after MEA-recording. Magnification (far right) allows identification of the electrode array positioning within the SN (scale bars: 1 mm, and 250 μm, respectively). **(B)** Spike sorting analysis of MEA recordings from two individual electrodes (marked in **A**, left), with identified single unit activity (SUA, left) and multiunit activity (MUA, right) with inhibitory dopamine-responses (bath-application of 100 μM dopamine indicated by horizontal bars). Upper panel: 3D-spike templates after principal component analysis (PCA, left) and overlaid spike-waveforms (right). Lower panel: event-plots and original traces over time. Inserts display enlargements of 2 s, as indicated. **(C)** Histograms (event counts) of individual interspike-intervals (ISI, in 20 s bins) for the two electrodes from **(A,B)**. Note one clear peak and no activity below 200 ms, only in the SUA. **(D)** Autocorrelation probabilities, plotted against ISI (using a Boxcar filter smoothing routine of three bins in width). Note that only the SUA shows clear regular activity exceeding the 99% confidence interval. **(E)** Firing rates (in Hz) plotted over time (in 20 s bins) for both recordings. Note fully inhibited activity by dopamine, typical for SN DA neurons, only for the SUA. **(F)** Upper panels: Exemplary SUA MEA-recording traces. Lower panels: Firing rates plotted over time (in 20 s bins) of a dopamine-excited (left) and a dopamine-inhibited (right) SN neuron (bath application of 100 μM dopamine as indicated). **(G)** Comparison of mean normalized firing rates of dopamine-inhibited SN DA neurons from adult mice, recorded with MEA (white squares), or with perforated-patch clamp techniques (black circles). Shown are normalized mean frequencies, plotted over time (20 s bins for MEA, 1 min bins for patch clamp; MEA: $n = 76$, perforated patch: $n = 8$). Data are given as mean ± SEM. All data and statistics are detailed in **Supplementary Figures 1, 4A** and **Supplementary Tables 1, 2**.

histogram must not exceed 15% of this peak. (b) A clear and regular pacemaker activity, belonging to one unit, as judged by autocorrelation. The autocorrelation is defined as the correlation of the activity of a unit with a delayed copy of itself. (c) A lack of cross-correlation with other units recorded from the same electrode (for multi unit activity, only). (d) The appropriate typical shape of the waveform average of the unit. **Supplementary Figure 1** shows a typical example of a SUA, derived from a single SN DA neuron. Only units fulfilling these criteria were further analyzed. Clusters representing obvious multi unit activity, meaning that they very likely contain activities of more than one neuron, were excluded from further analysis. These criteria are used only for pre-selection of possible SUAs. Statistical analysis is carried out subsequently with Neuroexplorer, as the options offered by Spike2 are limited, but pre-selection is carried out to reduce the amount of data that has to be imported to Neuroexplorer later.

Verification of Single Unit Activity With Neuroexplorer Software, Exclusion of Multi Unit Activity (MUA), and of Duplicate Recordings

After Spike2 analysis, smrx files containing traces, including timepoints of each spike of potential SUAs, were imported into the Neuroexplorer software (vers. 4.032, Nex Technologies, USA) to further analyze spontaneous activities of all recorded units for all electrodes. For this, autocorrelation as well as cross-correlation probability histograms were generated and analyzed. As before, autocorrelation histograms correlate a unit with a delayed copy of itself, while cross-correlation analysis allows to identify if the same SUA is recorded by more than one electrode, as all units recorded on one slice are analyzed for correlation. For both, 10 min of baseline activities were analyzed using a Boxcar filter smoothing routine of 3 bins (30 ms) in width (Berretta et al., 2010). Auto-correlation probability had to exceed the 99% confidence interval to be identified as SUA and included into the dataset. All identified SUAs, recorded with the same MEA-chip were tested for synchrony via their cross-correlation probability plots. In case units display a peak cross-correlation probability exceeding the maximal 99% confidence interval, the electrode with the better sorted signal (better signal to noise ratio) was included, the other was excluded from the dataset, as this high correlation is typical if the same neuron had been recorded from two different electrodes (Berretta et al., 2010). However, we cannot exclude that this approach occasionally eliminates SUAs from different cells with highly synchronized firing-patterns.

Further Analysis of Verified SUA

For further analysis, the mean firing rate (in 20 s bins) of each verified SUA was exported into excel from Spike2. To define the basal firing rate, the mean firing rate of a stable 10 min control period at the beginning of each recording was calculated. For describing pacemaker-regularity, the mean interspike-interval (ISI = 1/frequency) and its standard deviation (SD) were determined for this 10 min control period, to calculate the coefficient of variation (CV) of the ISI:

$$CV\ [\%] = \frac{SD\ (ISI)}{mean\ (ISI)} * 100$$

Cells displaying a pacemaker frequency above 6 Hz or CV-ISI values higher than 30% were excluded from further analysis in all data-sets, as typical SN DA neurons in mouse brain slices in synaptic isolation display slower and very regular pacemaker activities in the range of ∼1–4 Hz with CV-ISI between about 5 and 15% (Wolfart and Roeper, 2002; Lammel et al., 2008; Poetschke et al., 2015). VTA DA neurons display a faster (still under 10 Hz) and a less regular pacemaker (Lammel et al., 2008; Khaliq and Bean, 2010; Morales and Margolis, 2017). Note that MEA-derived CV-ISI values can differ from those derived from patch clamp experiments, due to the automated spike-sorting process and missed spikes.

For analysis of relative firing-rates in dopamine, firing-rates in the last minute in dopamine (i.e., minute 15) were normalized to the mean firing rate during the 10 min control period. An inhibitory dopamine D2-AR response was classified as desensitized if the mean frequency in the last minute of dopamine was higher than 5% of the respective basal firing rate.

Cumulative glucose dose-response curves were fitted and EC_{50} values were determined by using the hill equation (in PRISM, equation type: log(agonist) vs. response-variable slope, according to Goutelle et al., 2008):

$$y = \text{bottom} + \frac{x^{\text{hillslope}} * (\text{top} - \text{bottom})}{x^{\text{hillslope}} + EC_{50}{}^{\text{hillslope}}}$$

With y = normalized firing rate, x = glucose concentration, hillslope = steepness of the curve, top = upper plateau of the curve, bottom = lower plateau of the curve. Top and bottom were set to 1 and zero, respectively. The hillslope was freely fitted. EC_{50} values are given as the mean of individual EC_{50}, derived from individual fits for each analyzed cell (mean of individual fits), as well as from the fit of the mean values (fit of means, population analysis).

Statistical Analysis

Data are given as mean ± standard error of mean (SEM) if not stated differently. Standard Error (SE) or Standard Deviation (SD) are given as indicated. The number of identified SUAs (i.e., individual cells) is given by n, number of mice is given by N. Data were probed for normal distribution by using the Shapiro-Wilk normality test. As some datasets were not normally distributed, for most comparisons, non-parametric tests were used for probing for significant differences. For statistical comparisons of basal firing rate, CV-ISI and relative activities at minute 15 in dopamine, a two-tailed, unpaired, non-parametric Mann-Whitney-test (for pair-wise comparisons) was used. Differences in the ratios of sensitized to desensitized D2-AR responses were assessed by chi-square test for pair-wise group comparisons. To evaluate differences in firing rates over time, two-way repeated-measures ANOVA (with Sidak's multiple comparison *post-hoc* test) was used. For comparison of mean firing rates and CV-ISI in different glucose concentrations, repeated-measures one-way ANOVA tests were used (Friedman test with Dunn's multiple comparison *post-hoc* test). For comparison of mean firing rates, CV-ISI and relative activities at minute 15 of DA between NCS-1 KO/WT and DNIP/srDNIP as well as DA-excited and -inhibited SN neurons unpaired Kruskal-Wallis tests with Dunn's multiple comparison were used. To detect differences in the change of firing-rate and the CV-ISI between decrease and increase of glucose concentration the Wilcoxon matched-pairs signed rank test was used. A single asterisk (*) denotes a $p < 0.05$, two (**), three (***), and four asterisks (****) denoting $p < 0.01$, 0.001, and 0.0001, respectively. All statistical analysis and data transformations were performed in Prism (GraphPad Software Inc., USA).

Immunohistochemistry and Anatomical Maps

To reconstruct the position of the electrodes, after MEA recording, slices were immunostained for tyrosine hydroxylase (TH), similar as previously described (Lammel et al., 2008; Benkert et al., 2019). Therefore, after recordings, the grid was removed carefully using a forceps, and slices were transferred, via a suction pipette, into a small glass containing recording ACSF. Slices were immediately fixed with 4% PFA (Thermofisher Scientific) in 1 × PBS (phosphate buffered saline, Thermofisher Scientific, tablets, dissolved according to instructions) for 1 h at room temperature. Slices were then transferred into a storing solution containing (in %): 0.05 sodium azide, and 99.95 PBS, and stored at 4°C. Slices were washed three times (10 min each) with PBS, and kept on a microplate shaker (300 rpm, VWR). Slices were then incubated in blocking solution containing (in %): 10 goatserum (Vector Labs), 0.2 BSA (Roth), 0.5 Triton X in PBS, for 2 h to prevent unspecific binding of the antibody. Afterwards, slices were washed one time (10 min) with PBS followed by an overnight incubation with the primary antibody (1: 1000, mouse anti-TH, Merck Millipore). Slices were then washed three times for 10 min with PBS, followed by incubation with the secondary antibody (1:1000, Alexa Fluor 488 goat anti-rabbit, Thermofisher Scientific) for 3 h at room temperature, under light protection, while shaking. The following steps were performed in darkness using tinfoil to cover the well plates: The slices were washed three times for 10 min with PBS. Afterwards, the slices were mounted on superfrost glass slides (VWR), dried for 10 min, and covered with Vectashield Antifade Mounting Medium (Vector Laboratories, United States), and stored in the dark at 4°C. Images were taken with an epifluorescent microscope (Leica DM6500 microscope with a Leica DFC7000 T camera), and documented with LAS-X software.

Graphical overlays of images taken before the recordings and of images after TH-staining were created using the GNU Image Manipulation Program (GIMP vers. 2.8.14). Neuroanatomical positioning in maps was based on a mouse brain atlas (Paxinos and Franklin, 2001).

Data Availability

All datasets presented in this study are available from the corresponding author upon request.

RESULTS

MEA Analysis Identifies Dopamine-Inhibited and Dopamine-Excited *Substantia nigra* Neurons in Mouse Midbrain Slices

To allow a comprehensive analysis of neuronal activity patterns, without compromising intracellular signaling and with high throughput, we established a suitable protocol for extracellular brain slice recordings using multi-electrode arrays (MEA). The utilized MEA-chip (custom-build by Qwane Biosciences SA) contained 60 3D tip-shaped platinum electrodes (30 μm tips), arranged in a 15 row × 4 column array (**Figure 1A**). Coronal midbrain slices were mounted on these chips, so that the electrodes were covering the SN region, and chip positioning was documented. For verification of correct positioning of the electrodes within the SN, after recordings, slices were PFA-fixed and stained for tyrosine hydroxylase (TH), a marker for DA neurons in the midbrain (**Figure 1A** right panels). Electrodes located outside of the TH-positive SN, according to picture-overlays, were excluded from further analysis.

Electrodes can record activity from more than one neuron (multi unit activity MUA), but only electrodes with identified single unit activity (SUA) were further analyzed. SUA and MUA were identified after spike-sorting and principal component analysis (PCA). **Figure 1B** shows examples of a typical SUA and MUA, derived from SN DA neurons. MUA were discriminated from SUA by a high number of events in the range before 200 ms (**Figure 1C**; >15% of big peak), an irregular pacemaker

activity, assessed by a higher variation of the inter-spike interval (ISI, **Figure 1D**), and an only partial inhibition by dopamine (100 μM, bath-applied for 15 min; **Figure 1E**). These criteria can be used for identifying SUA derived from SN DA neurons, as they display *in vitro* in synaptic isolation a slow, very regular pacemaker-activity (∼0.5-5 Hz, CV ISI: ∼5–10%), and a well-described full inhibition of pacemaker-activity in response to extracellular dopamine (Lacey et al., 1987; Mercuri et al., 1994; Beckstead et al., 2004; Lammel et al., 2008). SUA derived MEA recordings from SN DA neurons displayed a clear peak in the event count histogram, low number of events in the 1-200 ms range, an autocorrelation probability exceeding the 99% confidence interval (CI), and a full inhibition of spontaneous activity by dopamine (**Figures 1C–E**, **Supplementary Figure 1**). To identify and exclude recordings of the same neuron from more than one electrode, cross-correlation histograms were generated for all electrodes on one slice. For electrodes displaying a cross-correlation probability exceeding the 99% confidence interval, the one with lower signal was excluded (**Supplementary Figure 1C**). We excluded about 4 ± 1 electrodes as presumed MUA per recorded slice, and less than one in 10 slices based on the cross-correlation analysis. With this MEA recording and data analysis approach, we detected about 5 ± 1 SN neurons per brain-slice that showed a response to dopamine (∼5 lower activity, ∼3 higher activity, 33 experiments).

Electrodes that did not respond to dopamine with altered event-rates were not further analyzed, but we analyzed all electrodes that displayed responses to dopamine (higher or lower event-rate). Interestingly, we detected a large population of SUAs that were excited by dopamine (**Figure 1F**, **Supplementary Table 1**). We never saw these dopamine-excited neurons in our data-sets from perforated patch clamp or on-cell recordings, while pacemaker activity and responses of the dopamine-inhibited SN neurons, recorded with perforated patch clamp recordings, were not significantly different from those recorded with our MEA approach (**Figure 1G**, **Supplementary Figure 4A**, **Supplementary Table 2**) (Liss et al., 2005; Lammel et al., 2008; Dragicevic et al., 2015; Poetschke et al., 2015).

With MEA recordings, we robustly identified DA-excited SN cells in juvenile and adult mice, in a similar frequency as we detected DA-inhibited cells (**Figure 2**, **Supplementary Table 1**, juveniles: 44% of all dopamine-responsive cells; ∼3 cells/slice; $n = 30$ from 11 slices, $N = 7$ mice; adults: 42% of all dopamine-responsive cells; 3 cells/slice; $n = 42$ from 14 slices, $N = 7$ mice). In most recordings from juveniles (87%, $n = 26$ of 30), and in about 50% from adults ($n = 22$ of 42), these dopamine-excited SN cells showed no activity at all before dopamine application but got transiently excited by dopamine (juveniles: 3.39 ± 0.97 Hz, adults: 4.2 ± 2.6 Hz; mean ± SD). The subpopulation of adult dopamine-excited cells that did display pacemaker activity before dopamine-application (3.21 ± 2.99 Hz, mean ± SD) increased its frequency almost 3-fold during dopamine application to 8.8 ± 6.7 Hz (mean ± SD). Pacemaker frequencies in dopamine were significantly higher in neurons that displayed activity before dopamine-application compared to those without activity (about 50%). The baseline pacemaker-activity of dopamine-excited cells compared to that of dopamine-inhibited cells appeared a bit faster but was not significantly different. However, the pacemaker (before dopamine) was less precise in adults (CV-ISI inhibited: 9.70 ± 5.28%, excited: 16.07 ± 10.48%; $p = 0.0137$). We also mapped the anatomical location of dopamine-excited and dopamine-inhibited cells (**Figure 2**). However, we identified no specific localization of either of these cell-types.

For our further analysis, we focused on dopamine-inhibited SN neurons, as this response is well-described for SN DA neurons. In juveniles and adult, SN DA neurons with inhibitory dopamine-responses displayed prominent desensitization in <50% of analyzed neurons (**Figure 2**, **Supplementary Table 1**). Basal pacemaker-frequencies were ∼20% higher in SN DA neurons with desensitized D2-AR compared to those with sensitized responses. This difference was significant, when pooled datasets were analyzed (juveniles: sens: 1.54 ± 0.07 Hz, desens: 1.81 ± 0.09 Hz, $n = 75/141$, $p = 0.027$, pooled analysis of WT data from **Supplementary Tables 1, 3**; adult: sens: 1.64 ± 0.08 Hz, desens: 2.15 ± 0.11 Hz $n = 50/119$, $p = 0.0005$, pooled analysis of WT data from **Supplementary Tables 1, 5**). In SN DA neurons from juvenile mice, we have previously shown by perforated patch clamp experiments, that this desensitization depends on free intracellular Ca^{2+} and binding of NCS-1 to the D2-AR (Dragicevic et al., 2014; Poetschke et al., 2015). As SN DA neurons from adult mice are even more vulnerable than those of juveniles, we were not successful in addressing desensitization mechanisms with perforated patch clamp experiments.

The Neuronal Calcium Sensor NCS-1 Reduces the Number of SN DA Neurons With Desensitized Inhibitory Dopamine-Responses by Binding to D2-Receptors

We used our MEA-approach to address if the presence and the degree of desensitization of dopamine autoinhibition of SN DA neurons from adult mice also depended on NCS-1 binding to D2-AR. We analyzed adult NCS-1 KO mice and wildtype controls. In addition, we analyzed in adult wildtype the responses to a so-called DNIP peptide that prevents NCS-1 binding to D2-ARs, and scrambled DNIP for controls (**Figure 3**, **Supplementary Figures 2**, **4B**, **Supplementary Tables 3**, **4**). As before, in response to dopamine bath-application, we detected a full and reversible inhibition of pacemaker activity of SN DA neurons from adult wildtype mice, with desensitization of the response in about 65% (**Figure 3A**, **Supplementary Table 4**) of recorded neurons. The absence of NCS-1 or the prevention of its binding to the D2-AR in adult SN DA neurons increased the amount of desensitized dopamine-responses, as evident from plotting mean normalized frequencies over time, and from comparing relative activities at the last minute in dopamine (**Figures 3B,C**, **Supplementary Figures 2B,C**, **Supplementary Tables 3, 4**). As the MEA approach allowed us to analyze responses of a large number of neurons, we compared mean basal frequency between neurons with sensitized and desensitized dopamine-responses and analyzed the ratio of the responses (**Figures 3C,D**, **Supplementary Figures 2C,D**,

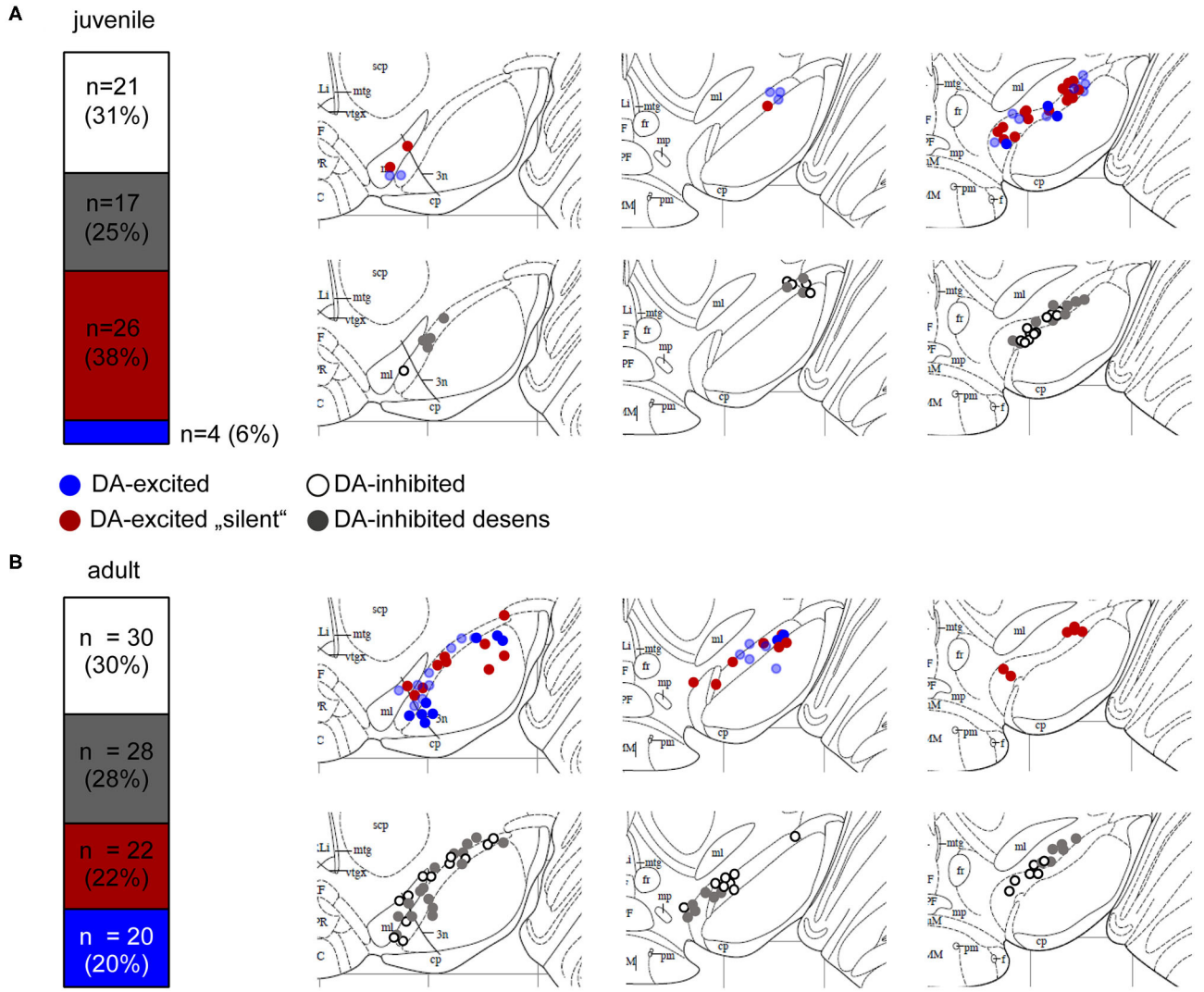

FIGURE 2 | Mouse SN neurons displayed four different types of dopamine responses. Relative frequencies of four identified different dopamine-responses, and anatomical locations of MEA-recorded neurons from juvenile **(A)** and adult **(B)** mice. Experiments, MEA recordings, and data analysis described in **Figure 1**. Data were derived from juvenile (∼PN13) and adult (∼13W) C57BL/6J mice, recorded in ACSF containing 2.5 mM glucose. Left panels: SN neurons were classified according to their dopamine responses in DA-excited (44%, juveniles, 42% adults) and DA-inhibited (56% juveniles, 58% adults) cells. DA-excited cells were subclassified in neurons with (blue) and without ("silent," red) spontaneous activity before DA-application. DA-inhibited cells were subdivided in neurons with ("desens," grey) and without (white) prominent desensitization of dopamine responses over time. Numbers of DA-excited neurons with activity before DA-application was significantly higher in adults ($p = 0.0025$). Right panels: Maps displaying the anatomical locations of the DA-excited (upper) and DA-inhibited (lower) neurons within the SN, on caudal (left), medial (middle), and rostral (right) coronal slices. Maps are derived form the Paxinos mouse brain atlas (reproduced with permission from Elsevier Ltd.), figures 56, 57, 60 (Bregma: −3.08, −3.16, −3.52), respectively (Paxinos and Franklin, 2001). All data and statistics are detailed in **Supplementary Table 1**.

Supplementary Tables 3, 4). This analysis revealed that a general knock out of NCS-1, as well as prevention of NCS-1 binding to D2-AR specifically in SN DA neurons, massively increased the number of SN DA neurons displaying desensitized D2-AR responses (about 60% in NCS-1 KO, and over 100% in DNIP). However, the time-course and degree of dopamine inhibition was neither altered by general NCS-1 knock out nor by the DNIP peptide. Hence the observed faster desensitization (**Figure 3B**, **Supplementary Figure 2B**) is only caused by higher numbers of SN DA neurons with desensitizing DA-responses and no change in the overall kinetic of the response. Moreover, these results indicate that SN DA neurons might switch between desensitized or sensitized dopamine responses, and that NCS-1 is stimulating sensitized responses.

Sensitized D2-autoreceptor responses by NCS-1 would reduce electrical activity, Ca^{2+} load and metabolic stress in SN DA neurons, while desensitized D2-AR responses would increase dopamine-release and thus facilitate movement—but also elevate Ca^{2+} load and metabolic stress levels. Hence, we hypothesized that general activity and the number of SN DA neurons

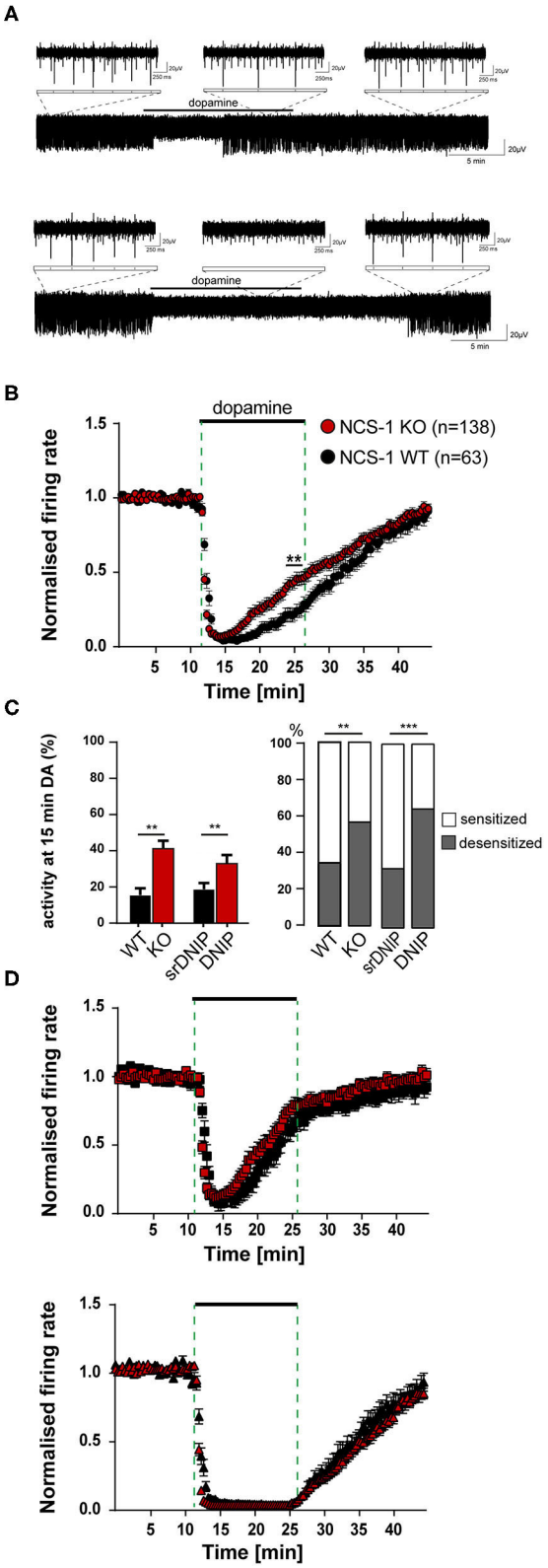

FIGURE 3 | Loss of NCS-1 function increases the number of SN DA neurons with desensitized inhibitory dopamine-responses. Experiments, MEA recordings, data analysis, and presentation similar as in **Figure 1**. Data were *(Continued)*

FIGURE 3 | derived from adult NCS-1 WT, NCS-1 KO, and C57BL/6J mice (for DNIP experiments; D2/NCS-1 interacting prevention peptide), recorded in ACSF containing 2.5 mM glucose. **(A)** Exemplary traces of a SN DA neuron with desensitized (upper) and with sensitized (lower) inhibitory dopamine responses (mediated by D2-autoreceptors, D2-AR). Bath application of 100 μM dopamine indicated by horizontal bars. Inserts display enlargements of 2 s during control period, DA application and wash-out phase. **(B)** Normalized mean firing rates plotted over time for all analyzed SN neurons from NCS-1 WT (black, $n = 63$) and NCS-1 KO (red, $n = 138$) mice. **(C)** Left panel: Mean relative firing frequencies in the last minute of dopamine. Right panel: Percentages of cells with desensitized dopamine-responses (grey), for SN DA neurons from NCS-1 WT and KO, and in the presence of 10 μM DNIP ($n = 64$), or 10 μM srDNIP ($n = 96$; scrambled DNIP, as control), as indicated. **(D)** Data from **(B)**, plotted separately for SN neurons with desensitized (upper, WT: $n = 22$, KO: $n = 77$) and with sensitized inhibitory dopamine responses (lower, WT: $n = 41$, KO: $n = 61$). Data are given as mean ± SEM. Significances/*p*-values according to unpaired Kruskal-Wallis test with Dunn's multiple comparison, Chi-square, and unpaired Mann-Whitney-test. All data and statistics are detailed in **Supplementary Figures 2**, **4B**, **Supplementary Tables 3, 4**.

with desensitized D2-AR responses could be higher at optimal metabolic conditions, and lower in metabolic stress situation. To test this, we analyzed pacemaker activity and dopamine-responses at different glucose concentrations.

Elevated Glucose Levels Increase the Number of SN DA Neurons With Desensitized Inhibitory Dopamine Responses and Their Pacemaker Firing-Rate

We performed similar experiments, as described before, but now comparing activity and the inhibitory dopamine response of SN DA neurons in 2.5 mM glucose with those in 25 mM glucose (**Figure 4**). In line with our hypothesis, the number of SN DA neurons with a desensitized D2-AR response was significantly higher in 25 mM glucose (∼50%, **Figures 4A,B**, **Supplementary Tables 5, 6**). Again, the mean time-course and degree of dopamine inhibition was not altered, neither in the group of neurons with sensitized nor desensitized responses (**Figure 4C**). Moreover, we observed that the mean pacemaker-frequency of SN DA neurons before dopamine application was significantly higher in 25 mM dopamine (∼20%; **Figure 4A**, **Supplementary Table 5**). Pacemaker precision (CV-ISI) was not different in 25 mM glucose.

These results suggested that SN DA neurons might display glucose sensing properties, similar as pancreatic beta-cells, with higher activity at higher glucose concentrations (termed GE-neurons; MacDonald et al., 2005).

Transient Glucose Deprivation Reversibly Reduces Pacemaker Activity of SN DA Neurons

To systematically address GE-properties of SN DA neurons, we carried out a set of MEA experiments, where we continuously recorded pacemaker activities of SN DA neurons while

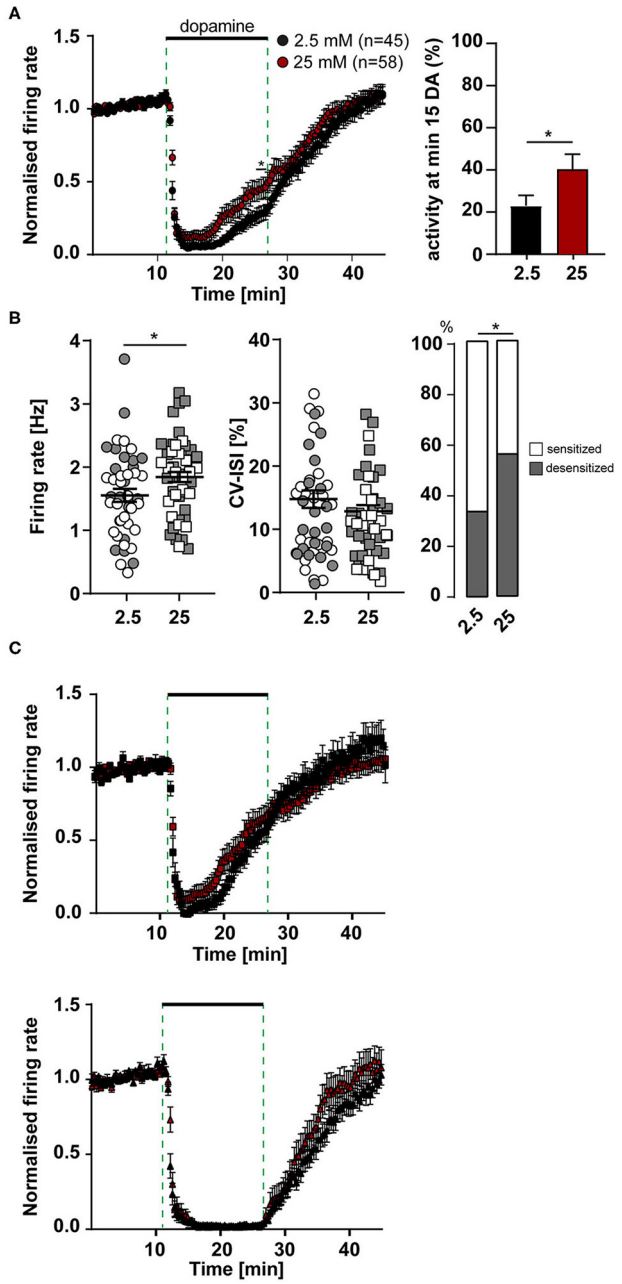

FIGURE 4 | More SN DA neurons with desensitized dopamine D2-AR responses, and with higher pacemaker frequencies in elevated glucose. MEA recordings, data analysis and presentation similar as in **Figures 1**, **3**. Data were derived from juvenile C57BL/6J mice, recorded in ACSF containing either 2.5 mM ($n = 45$) or 25 mM ($n = 58$) glucose. **(A)** Left panel: Normalized mean firing rates of all analyzed SN neurons, plotted over time. Right panel: activity at minute 15 in dopamine. **(B)** Left panels: Mean pacemaker frequencies and pacemaker precision (displayed as CV-ISI), during first 10 min of recordings. Right panel: Percentages of SN DA neurons with desensitized D2-AR responses (grey) in 2.5 and 25 mM glucose. **(C)** Data from **(A)**, plotted separately for SN neurons with desensitized (upper, 2.5 mM glucose: $n = 20$, 25 mM glucose: $n = 38$) and with sensitized inhibitory dopamine responses (lower, 2.5 mM: $n = 25$, 25 mM: $n = 20$). Data are given as mean ± SEM. Significances/*p*-values according to two-way ANOVA with Sidak's multiple comparison, Chi-square and unpaired Mann-Whitney-test. All data and statistics are detailed in **Supplementary Tables 5, 6**.

changing extracellular glucose levels, by switching recording-ACSF solutions. As glucose sensing neurons have been described in a wide range of glucose concentrations, with so-called high-GE neurons sensing glucose above 5 mM up to over 20 mM (Fioramonti et al., 2004; Routh, 2010; Alvarsson and Stanley, 2018), we chose 25 mM as an optimal glucose concentration, and switched to 1 mM to induce transient glucose deprivation and metabolic stress.

As illustrated in **Figure 5A**, after recording baseline pacemaker activity for 10 min in 25 mM glucose, we switched to 1 mM for 15 min (until frequencies were stable again) and back to 25 mM glucose for another 20 min, followed by application of dopamine (and wash-out), for identification of SN DA neurons. With this paradigm, spontaneous activity of SN DA neurons was reduced in all tested neurons by switch to 1 mM glucose, by about 25% (from a mean of 1.9 to 1.5 Hz), and pacemaking was less precise (∼40%; **Figures 5B,C**, **Supplementary Tables 7A,B**). Furthermore, we detected with about 75% a high amount of SN DA neurons with desensitized D2-AR responses (**Figure 5C**, **Supplementary Table 7**). We also analyzed the effect of transient glucose-deprivation separately for sensitized and desensitized neurons (**Supplementary Figures 3A**, **4C**, **Supplementary Table 7**). As before, firing rates were higher in SN DA neurons with desensitized D2-AR response (∼20%; **Supplementary Figures 3A**, **4C**, **Supplementary Table 7**).

SN DA Neurons Display Glucose Sensitivity Within the Physiological Range of Brain Glucose Levels

The transient glucose-deprivation experiments demonstrated for SN DA neurons glucose-sensing properties of the GE-type. To further quantify glucose sensitivity within the (patho-) physiological range of brain glucose levels, we carried out MEA experiments where glucose concentrations were stepwise elevated from 0.5 mM up to 25 mM to determine dose-response curves and EC_{50} values. Experimental design and a typical response of a SN DA neuron is given in **Figure 5D**. We also tried concentrations lower than 0.5 mM, however, SN DA neurons were not stable enough over the required long recording time (each recording took more than 2 h). To determine half maximal effective (EC_{50}) glucose-concentrations for individual SN DA, we fitted dose-response curves for each individual neuron, as well as the mean values at each concentration of all analyzed neurons (population analysis). Both approaches resulted in similar EC_{50} values, slightly below 1 mM glucose (mean ± SE: 0.87 ± 0.01 and 0.66 ± 0.1, $n = 13$ **Figure 5E**, **Supplementary Table 8**). As indicated by the high standard deviation (±1.04) and as evident in **Figure 5F**, the individual EC_{50} values varied substantially and were not homologous distributed ($p = 0.777$). Thus, we separated the analyzed cells into two groups (>1 mM, <1 mM) and fitted them separately. Indeed, the dose-response curves were better fitted by these two fits, than by one over-all fit and resulted in EC_{50} values of 2.23 mM ($n = 8$) and 0.35 mM ($n = 5$) glucose (**Figure 5G**, **Supplementary Table 8**), indicating the possibility of GE-neurons with different glucose sensitivities.

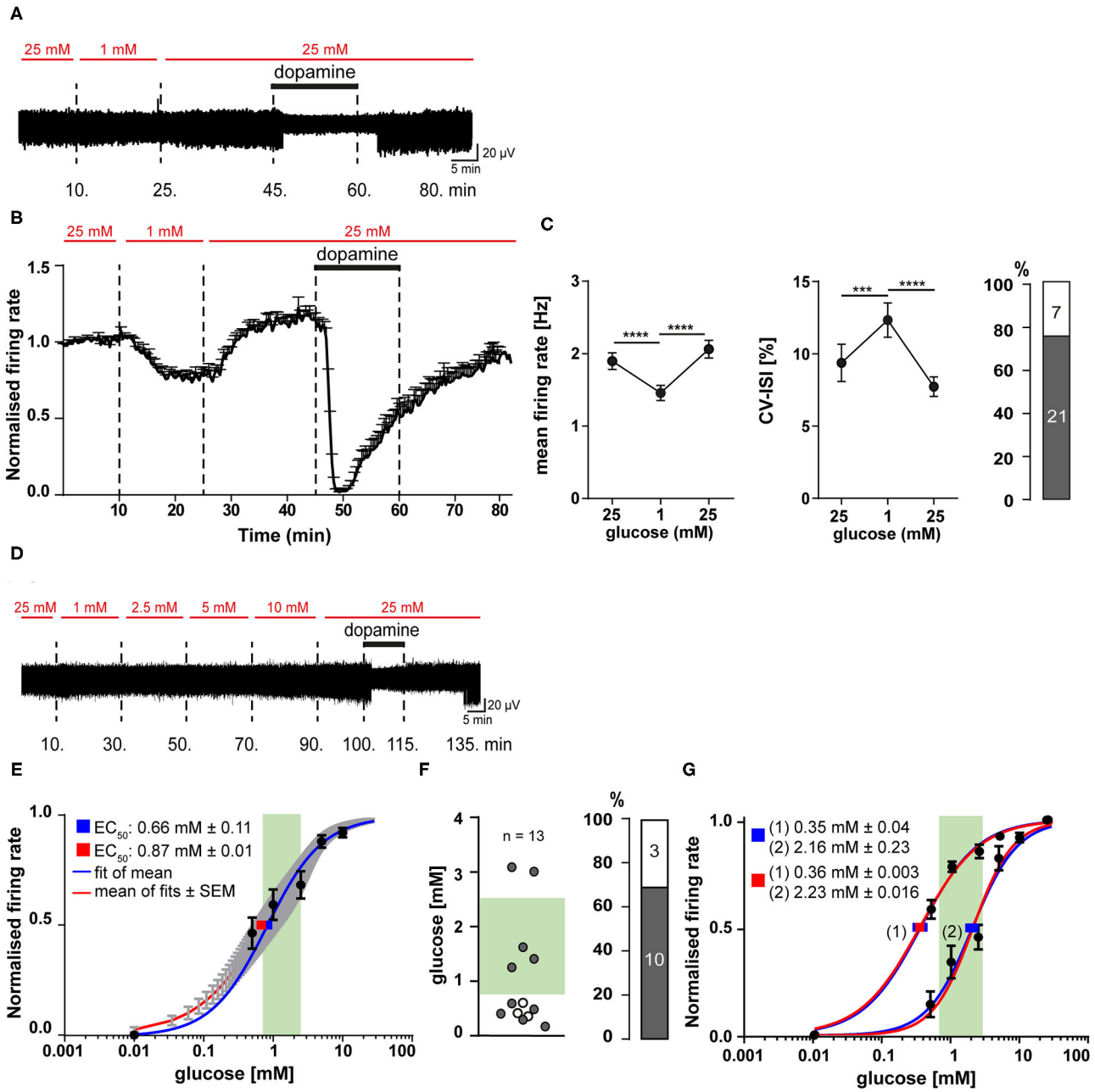

FIGURE 5 | SN DA neurons display fast and reversible glucose-sensitivity in the range of brain glucose levels. Experiments, MEA recordings, data analysis and presentation similar as in **Figures 1**, **3**. **(A)** Exemplary traces, recorded from a mouse SN DA neuron, while glucose was transiently reduced from 25 to 1 mM, as indicated by red horizontal bars. Bath application of 100 µM dopamine indicated by black horizontal bars. **(B)** Normalized mean firing rates of all analyzed SN DA neurons are plotted over time ($n = 28$). **(C)** Left/middle panel: Mean non-normalized firing rates (left) and pacemaker precision (given as CV-ISI, middle) during the first 10 min of the recording in 25 mM glucose, in 1 mM (last 10 min), and back in 25 mM glucose (last 10 min). Right panel: Number/percentage of SN DA neurons from **(B,C)** with desensitized D2-AR responses (grey). **(D)** Exemplary trace, recorded from a mouse SN DA neuron, while glucose concentrations were altered as indicated (0.5–25 mM). Bath application of different glucose concentrations (red) and of 100 µM dopamine (black) indicated by horizontal bars. **(E–G)** Dose-response curves and derived EC_{50} values for all analyzed SN DA neurons ($n = 13$). EC_{50} values were calculated according to the Hill-equation. Values are given as mean ± SE. The range of physiological brain glucose levels is indicated in green, [0.7–2.5 mM], according to Routh et al. (2014). **(E)** EC_{50} values were derived from fitting the mean relative firing rates of all cells at each concentration (blue), and by the mean fit of the fits for each individual neuron (red). Values are given as mean ± SE. **(F)** Left panel: Scatterplot of individual EC_{50} values, derived from individual fits for each cell (gray dots: cells with desensitized D2-AR responses; white dots: cells with sensitized responses). Right panel: Number/percentage of SN DA neurons from **(E)** with desensitized D2-AR responses (grey). **(G)** Separate dose-response curve fits; cells from **(E,F)** were subdivided into neurons with EC_{50} higher ($n = 5$) or lower ($n = 8$) than 1 mM glucose. Data are given as mean ± SEM. Significances/*p*-values according to paired Friedman test with Dunn's multiple comparison and Chi-square test. All data and statistics are detailed in **Supplementary Figures 3**, **4C,D**, **Supplementary Tables 7**, **8**.

We also determined EC_{50} values separately, for sensitized and desensitized neurons, leading to EC_{50} values of 0.35 ± 0.05 mM ($n = 3$) and 0.85 ± 0.17 mM ($n = 10$; mean $\pm$ SE **Supplementary Figure 3B**, **Supplementary Table 8**), respectively. All three SN DA neurons with sensitized DA-responses fell into the group of neurons <1 mM, and separate fittings indicated a trend for higher EC_{50} in the desensitized group that was however not significant (**Supplementary Figure 3B**, **Supplementary Table 8**).

These data demonstrated fast and reversible glucose-sensing in SN DA neurons, and they indicate two populations of SN DA neurons, according to their glucose-responsiveness: one with an EC_{50} in the euglycemic (0.7–2.5 mM) range of brain glucose-levels, another one in the hypoglycemic range (<0.7 mM) (Routh et al., 2014).

DISCUSSION

By using an optimized MEA recording and data analysis approach, we analyzed spontaneous pacemaker activities and dopamine-responses of SN neurons in mouse brain slices, along with their modulation by NCS-1 and glucose. Tyrosine-hydroxylase immunostainings of brain slices after recordings allowed to map localizations of individual recording-electrodes within the SN. This approach enabled us to analyze several hundreds of neurons, covering the full SN, without selection bias by the experimenter, and without disturbing the intracellular integrity. Thereby, we identified novel subtypes and physiological functions of SN neurons, in relation to their responses to dopamine, to loss of NCS-1 function, and to changes in extracellular glucose.

MEA Approaches for Analyzing SN Neurons in Brain Slice Preparations

The principal difference between MEA and patch clamp recordings is that either extracellular spikes or intracellular action potentials are recorded. The major advantage of the MEA approach is its relatively easy and fast execution, and the recording of multiple neurons in parallel, compared to perforated patch clamp or on-cell recordings (Spira and Hai, 2013). MEA allows a more unbiased analysis of all cellular populations in a region of interest, as choosing the cells to analyze by the experimenter is omitted. However, analysis of data from MEA recordings is more complicated compared to patch clamp recordings (Negri et al., 2020). This is due to the sheer size of data received from MEA recordings that needs to be further processed for automated spike detection and further downstream-analysis (Stevenson and Kording, 2011; Rey et al., 2015; Mahmud and Vassanelli, 2016, 2019). The file-size from our raw unprocessed MEA recordings was up to ∼16 GB, depending on the length of the recordings. A crucial issue is to extract those signals that reflect cell-derived single unit activities (SUAs), while avoiding analysis of the same cell recorded from more than one electrode. The fact that SN DA neurons display *in vitro*, even in full synaptic isolation, a regular low-frequency pacemaker activity (∼0.5–3 Hz with a maximal firing rate ∼10 Hz) and broad action potentials (>2 ms) (Wolfart and Roeper, 2002; Lammel et al., 2008; Khaliq and Bean, 2010; Poetschke et al., 2015) facilitates their identification. However, pacemaker-activity can be less regular, due to physiological variation (Marinelli and McCutcheon, 2014), and in particular in MEA recordings as spike detection can fail to recognize all spikes belonging to a single neuron. A disadvantage of MEA approaches is that it is not exactly clear from which cell a recording is derived, but only the placement/coordinates of the respective electrode that recorded its activity (Obien et al., 2019). Hence, the maps given here (**Figure 2**) reflect the location of the electrodes that recorded the respective SUAs with the responses, as indicated. We cannot rule out that our collectives of analyzed SN cells do also contain a fraction of VTA neurons and/or VTA-like calbindin-positive dorsal tier SN DA neurons, as their locations and their *in vitro* electrophysiological properties are partly overlapping (Margolis et al., 2006; Lammel et al., 2008; Khaliq and Bean, 2010; Krashia et al., 2017).

The number of neurons we recorded with our MEA approach are comparable to other MEA brain slice studies, e.g., in the hypothalamus (Hanna et al., 2019). Our general findings in respect to the dopamine-response are in line with other studies of SN neurons in horizontal brain slices from ∼1 month old rats (Geracitano et al., 2005; Berretta et al., 2010), and with a recent MEA study, where cultured DA neurons were analyzed, derived from dissected embryonal (E15) TH-GFP mouse brains, expressing the enhanced green fluorescent protein (GFP) under the tyrosine-hydroxylase promoter (Tomagra et al., 2019). In the latter study, micro-graphitic single crystal diamond Multi Electrode Arrays (μG-SCD-MEAs) were used, that allow, in addition to recording of electrical activity, amperometric analysis of dopamine release. We utilized 3D tip-shaped electrodes that entered the tissue and thus got closer to the neurons in the slice (Heuschkel et al., 2002).

Dopamine-Excited Cells in the SN

While with our MEA recordings we detected a large population of SN DA neurons that increased their electrical activity in response to dopamine, we never saw this type of response in our datasets of perforated patch clamp and on-cell recordings. However, pacemaker activities and dopamine-responses of the dopamine-inhibited SN neurons, recorded with perforated patch clamp recordings were not significantly different from those recorded with our MEA approach (**Figure 1G**, **Supplementary Table 2**), and (Liss et al., 2005; Lammel et al., 2008; Dragicevic et al., 2014; Poetschke et al., 2015). To our knowledge, dopamine-excited neurons have also not been reported in other brain slice patch clamp studies. Possible explanation might be e.g., a preferential selection by the experimenter or differential accessibility of subpopulations of SN DA neurons with patch clamp approaches, or methodological impacts of either approach.

DA-excited neurons were also described in a similar brain slice MEA study, analyzing rat SN DA neurons in horizontal brain slices in response to 30 μM dopamine, applied for 1–2 min (Berretta et al., 2010), and in the MEA study analyzing cultured, embryonal, TH-GFP mice derived neurons (Tomagra et al., 2019). In the latter, L-DOPA (20 μM), the precursor of

dopamine, was given, and it also either excited or inhibited DA neurons. Further, they found TH-GFP positive neurons that were excited by dopamine with MEA as well as with patch clamp whole-cell recordings (personal communication, Valentina Carabelli). However, in another MEA brain slice study of TH-GFP mice (PN17–PN30), almost all SN neurons in horizontal slices were inhibited by dopamine (30 μM for 2-3 min), dopamine-excited cells were not reported (Krashia et al., 2017). The proportion of dopamine (or L-DOPA)—inhibited and—excited SN neurons was about 50:50% in our study, 81:2% (remaining 17% were insensitive) and 80:17% (remaining 3% were insensitive) in the other MEA slice, and MEA DA culture study, respectively (Berretta et al., 2010; Tomagra et al., 2019). Discrepancies in the detection of dopamine-excited SN cells are likely caused by different ages and/or types of analyzed neurons, or technical differences.

What is the anatomical and neurochemical nature of the dopamine excited SN cells? By mapping the electrodes that recorded DA-excited cells, we found no specific anatomical localization. With our approach, we could neither identify the projections of DA-excited cells, nor whether they were dopaminergic or non-dopaminergic—or even neurons. However, the L-DOPA/dopamine excited SN cells in Tomagra et al. (2019) displayed a positive fluorescence TH-GFP signal, indicating these cells were indeed dopaminergic neurons—or at least tyrosine-hydroxylase positive cells. Together with the high number of dopamine-excited SN cells detected, we conclude that they are dopaminergic, and a subpopulation of SN DA neurons exists that is excited by dopamine. The mechanism for the dopamine-mediated stimulation of presumed SN DA neurons is unclear. Several ways are possible. It could be mediated directly, via stimulatory D1-type dopamine receptors [a small population of D1/D5 expressing SN DA neurons is described (Liss and Roeper, 2004; Hetzel, 2008; Jang et al., 2011)]. Or D2-AR could stimulate depolarizing low threshold T-Type Cav channels, as described for calbindin-negative ventral tier SN DA neurons (Evans et al., 2017). Also, depolarization by the electrogenic dopamine-transporter (DAT, co-importing netto one positive charge with each dopamine molecule), in the absence or full desensitization of inhibitory D2-AR, offers a possible mechanism (Sonders et al., 1997; Ingram et al., 2002; Carvelli et al., 2004). Or stimulation could be mediated more indirectly, e.g. by D2-receptor inhibition of inhibitory interneurons that control the activity of DA neurons, as described for VTA DA neurons (Nestler, 2005; Morales and Margolis, 2017; Bouarab et al., 2019). Identity, mechanisms, and functions of DA-excited neurons will be addressed in future studies.

Two Types of Dopamine Inhibited SN DA Neurons: Loss of NCS-1 Function and Elevated Glucose Promote Desensitized D2-AR Response

We identified SN DA neurons with either sustained or desensitized dopamine inhibition of spontaneous activity. As MEA allowed us to record much more neurons, compared to our previous patch clamp studies, n-numbers were high enough to allow separate analysis of neurons with sensitized and desensitized D2-AR responses as two populations. This analysis revealed that time course and degree of desensitization were surprisingly very similar in all analyzed neurons with desensitized responses, in all conditions. Hence, SN DA neurons do not display a spectrum of autoreceptor responses with different degrees of desensitization, as previously assumed (Dragicevic et al., 2014; Poetschke et al., 2015), but only two states of D2-AR responses: sensitized or desensitized. The dopamine-responses when NCS-1 function was lost and when extracellular glucose was elevated support this binary view, as again, the kinetics of individual desensitization was not altered, but only the number of SN DA neurons with desensitized dopamine responses. We propose that SN DA neurons switch between these two distinct states, rather than gradually change desensitization of D2-AR responses.

Accordingly, we conclude that the previously reported less pronounced desensitization of dopamine responses—in adult vs. juvenile mice, in cocaine vs. saline treated mice, in Cav1.3 KO vs. wildtype mice (Dragicevic et al., 2014; Poetschke et al., 2015; Robinson et al., 2017b)—identified by analysis of SN DA neurons as one population, is reflecting a reduction of the number of SN DA neurons with desensitized responses, not a change in desensitization-kinetics, similar as reported here for loss of NCS-1 function and elevated glucose. An alternative explanation could be that due to NCS-1 function or at lower glucose levels SN DA neurons with desensitized D2-AR responses die, or were no longer recorded by MEA, and thus we detect more neurons with sustained dopamine responses. However, our very long and metabolically stressful glucose experiments for dose-response curves that ended with dopamine-application and still showing ∼75% desensitized responses, argue against this.

We have not yet addressed the mechanism of the proposed switch from desensitized to sensitized D2-AR responses. Mechanisms of D2-receptor desensitization have been identified mainly in heterologous systems. Best described is receptor-phosphorylation and subsequent beta-arrestin mediated internalization (Beaulieu et al., 2015; Chen et al., 2020). However, for D2-ARs, an internalization-independent, Ca^{2+} involving desensitization mechanism is described (Gantz et al., 2015; Robinson et al., 2017a). Our data would support the latter mechanism. The electrogenic DAT (importing 2 Na^+ and 1 Cl^- ion with each dopamine molecule), could also be involved in mediating desensitization of inhibitory dopamine responses in SN DA neurons, possibly in interplay with D2-receptors and other conductances, as already described (Sonders et al., 1997; Ingram et al., 2002; Carvelli et al., 2004; Aversa et al., 2018).

What is the physiological function of altered somatodendritic D2-AR responses? The physiological function of somatodendritic local dopamine-release in general is still unclear. However, it creates activity-related increases in extracellular dopamine in the SN that inhibit autoactivity and the activity of neighboring neurons, and could contribute to synchronization (Joshua et al., 2009; van der Velden et al., 2020). D2-AR function reduces SN DA neuron activity, and thus also excitotoxicity related processes (Rice and Patel, 2015; Duda et al., 2016). A lower number of SN DA neurons with desensitized D2-AR response would prolong

these effects of dopamine, and thus reduce the overall-activity of SN DA neurons and related metabolic stress. Accordingly, SN DA neurons from NCS-1 KO mice with less sensitized SN DA responses should be more vulnerable to degenerative stressors—and this is indeed the case in a PD model (Benkert et al., 2019; Simons et al., 2019).

In this context, it is noteworthy that in general, the number of SN DA neurons with desensitized inhibitory dopamine responses appeared to be decreased when the brain slices were not in optimal condition, e.g., due to suboptimal slice-preparation, mounting, or perfusion. D2-AR responses of SN DA neurons from adult mice were particularly sensitive to these kinds of stressors.

SN DA Neurons Are Glucose Sensors (GE-Neurons)

SN DA neurons are particularly vulnerable to metabolic stressors (Dragicevic et al., 2015), express insulin receptors, and are regulated by insulin (Figlewicz et al., 2003; Fiory et al., 2019), but physiological glucose sensing had not yet been reported. We show here for the first time that most SN DA neurons (75%) display glucose sensing properties, with higher pacemaker-activities at higher glucose levels (as defined for glucose-excited GE-neurons), independently from their D2-AR responses. GE-neurons are typically found in the hypothalamic and brainstem nuclei (Fioramonti et al., 2017; Guemes and Georgiou, 2018; Lopez-Gambero et al., 2019). We demonstrated here in individual SN DA neurons a fast and reversible decrease of activity with lower glucose, and an increase in response to higher glucose, with EC_{50} values in the (patho-) physiological range of brain glucose levels. Individual dose-response curves indicate that SN DA neurons might display different glucose sensitivities, with one population displaying EC_{50} values in the euglycemic range (EC_{50}: ∼2.0 mM) and another one within hypoglycaemic (EC_{50}: ∼0.35 mM) brain glucose levels. These values correspond well with those described for GE neurons in the lateral hypothalamus, with an EC_{50} of ∼0.8 mM glucose (Burdakov et al., 2005) and in the nucleus arcuatus, with ∼2 mM (Wang et al., 2004).

What is the physiological function of glucose sensing in SN DA neurons? Brain glucose-levels are lower compared to blood glucose levels (∼2 mM and 7–8 mM, respectively; Routh et al., 2014; Fioramonti et al., 2017). Glucose is the primary fuel for the brain, and its levels remain relatively constant, even when plasma levels are fluctuating (Dunn-Meynell et al., 2009; Hwang et al., 2019). However, brain glucose levels can reach locally much higher levels, and corresponding so-called high-GE-neurons are described, sensing glucose above 5 mM, up to 10, or even over 20 mM (Routh, 2010; Fioramonti et al., 2017; Alvarsson and Stanley, 2018), reflected by our chosen glucose concentrations (ranging from 0.5 to 25 mM).

Reduced activity at lower glucose levels will reduce the activity of the Na^+/K^+ ATPase, and thus ATP consumption and metabolic stress in metabolic demand. Similar as it has been described for SN DA neurons in horizontal brain slices from juvenile rats, where glucose levels were drastically reduced from 10 mM down to zero mM (Marinelli et al., 2000, 2001). But what could be long term consequences? A number of studies indicate that activity of SN DA neurons is not only crucial for dopamine release and related functions, but also for their maintenance and survival, in line with the classical "use it or lose it" principle of neuronal loss (reviewed e.g., in Swaab et al., 2002; Duda et al., 2016; Michel et al., 2016). Thus, while reduced activity of SN DA neurons at low glucose levels likely has acute beneficial effects, in the long run it could contribute to degeneration and PD, similar as shown for K-ATP channel activity (Liss et al., 2005; Schiemann et al., 2012; Duda et al., 2016).

The molecular mechanisms of glucose sensing in SN DA neurons is currently unclear. However, for GE- and GI-neurons in other brain regions mechanisms have been identified, involving plasmalemma glucose transporters for glucose uptake (GLUT1-14, SGLT1-6), hexokinases/glucokinase (GK) for intracellular glucose phosphorylation, and a variety of downstream ion channels and receptors (reviewed e.g., in Routh et al., 2014; Fioramonti et al., 2017; Lopez-Gambero et al., 2019; Stanley et al., 2019; Hirschberg et al., 2020). GE-neuron glucose sensing is best described in neurons of the ventromedial hypothalamus (VMH), and it is similar to the mechanism in pancreatic beta cells, involving GK, GLUT2, KATP, and Cav channels (Pozo and Claret, 2018; Rorsman and Ashcroft, 2018), all of them expressed in SN DA neurons. Other proteins involved in GE-neuron glucose sensing are metabolically sensitive chloride channels, purinergic receptors, sweet taste receptors (T1R2/3) and transient receptor potential channels (TRPC3, TRPM). For GI-neuron glucose sensing mechanisms, in particular the Na^+/K^+ ATPase, as well as AMP Kinase, nNOS/nitric oxide, CFTR chloride channels, glutamate receptors, or two-pore-domain potassium channels (K2P, TASK) have been described (Marinelli et al., 2000, 2001) Kv7 potassium channels and volume regulated anion channels (VRAC) have also been linked to glucose sensing (Stuhlmann et al., 2018; Di Fulvio and Aguilar-Bryan, 2019; Manville and Abbott, 2020).

Future studies will address the molecular mechanisms of glucose sensing in SN DA neurons. Our first experiments indicate a complex mechanism that is not simply explained by activation of K-ATP channels or A-type K^+ channels, as described for pathophysiological reduction of SN DA activity in response to PD stressors (Liss et al., 1999, 2005; Subramaniam et al., 2014; Dragicevic et al., 2015; Subramaniam and Roeper, 2017). Dissecting these mechanism is particularly relevant in view of the high vulnerability of SN DA neurons in PD, and the emerging link between pancreatic beta cells and SN DA neurons, as well as between type II diabetes (T2DM) and PD (Eberhard, 2013; Hassan et al., 2020; Sportelli et al., 2020). T2DM, with elevated blood glucose levels and increasing insulin resistance, seemingly increases the risk for developing PD later in life, and both diseases share similar pathomechanisms (Camargo Maluf et al., 2019; Cheong et al., 2020). Understanding physiological and pathophysiological glucose sensing of SN DA neurons, also in context of T2DM, will lead to a better understanding of the high vulnerability of these neurons to degeneration in PD. It could help identifying early changes in SN DA neurons, before they degenerate, and thus help identifying

PD patients before motor systems manifest and most SN DA neurons are already lost—a prerequisite for neuroprotective PD therapies.

DATA AVAILABILITY STATEMENT

The original contributions presented in the study are included in the article/**Supplementary Material**, further inquiries can be directed to the corresponding author/s.

ETHICS STATEMENT

The animal study was reviewed and approved by the Regierungspräsidium, Referat 35, Konrad Adenauer Strasse 20, 72072 Tübingen.

AUTHOR CONTRIBUTIONS

NM and KK performed MEA experiments and data analysis. CP carried out perforated patch clamp experiments. NM and KK performed immunohistology. MF and AD carried out initial MEA pilot-experiments. BL designed the study and data analysis. BL and NM wrote the manuscript. All authors revised the manuscript.

FUNDING

This work was supported by the German DFG (LI-1745/1), the Austrian Science Fund FWF (F44-12), and the Alfried Krupp foundation (all to BL), NM was supported by the International Graduate School in Molecular Medicine at Ulm University.

ACKNOWLEDGMENTS

We would like to thank Olaf Pongs for providing the NCS-1 KO mice, Sonja Müller for excellent technical support, and Nicola Berretta, Dennis Kätzel, and Valentina Carabelli for helpful methodological advice and critical discussion.

SUPPLEMENTARY MATERIAL

The Supplementary Material for this article can be found online at: https://www.frontiersin.org/articles/10.3389/fnsyn.2021.635050/full#supplementary-material

REFERENCES

Alvarsson, A., and Stanley, S. A. (2018). Remote control of glucose-sensing neurons to analyze glucose metabolism. *Am. J. Physiol. Endocrinol. Metab.* 315, E327–E339. doi: 10.1152/ajpendo.00469.2017

Ankri, L., Yarom, Y., and Uusisaari, M. Y. (2014). Slice it hot: acute adult brain slicing in physiological temperature. *J. Vis. Exp.* 92, e52068. doi: 10.3791/52068

Aversa, D., Martini, A., Guatteo, E., Pisani, A., Mercuri, N. B., and Berretta, N. (2018). Reversal of dopamine-mediated firing inhibition through activation of the dopamine transporter in substantia nigra pars compacta neurons. *Br. J. Pharmacol.* 175, 3534–3547. doi: 10.1111/bph.14422

Beaulieu, J. M., Espinoza, S., and Gainetdinov, R. R. (2015). Dopamine receptors - IUPHAR review 13. *Br. J. Pharmacol.* 172, 1–23. doi: 10.1111/bph.12906

Beckstead, M. J., Grandy, D. K., Wickman, K., and Williams, J. T. (2004). Vesicular dopamine release elicits an inhibitory postsynaptic current in midbrain dopamine neurons. *Neuron* 42, 939–946. doi: 10.1016/j.neuron.2004.05.019

Beckstead, M. J., and Williams, J. T. (2007). Long-term depression of a dopamine IPSC. *J. Neurosci.* 27, 2074–2080. doi: 10.1523/JNEUROSCI.3251-06.2007

Benkert, J., Hess, S., Roy, S., Beccano-Kelly, D., Wiederspohn, N., Duda, J., et al. (2019). Cav2.3 channels contribute to dopaminergic neuron loss in a model of Parkinson's disease. *Nat. Commun.* 10:5094. doi: 10.1038/s41467-019-12834-x

Berke, J. D. (2018). What does dopamine mean? *Nat. Neurosci.* 21, 787–793. doi: 10.1038/s41593-018-0152-y

Berretta, N., Bernardi, G., and Mercuri, N. B. (2010). Firing properties and functional connectivity of substantia nigra pars compacta neurones recorded with a multi-electrode array *in vitro*. *J. Physiol.* 588, 1719–1735. doi: 10.1113/jphysiol.2010.189415

Bolam, J. P., and Pissadaki, E. K. (2012). Living on the edge with too many mouths to feed: why dopamine neurons die. *Mov. Disord.* 27, 1478–1483. doi: 10.1002/mds.25135

Bonci, A., and Hopf, F. W. (2005). The dopamine D2 receptor: new surprises from an old friend. *Neuron* 47, 335–338. doi: 10.1016/j.neuron.2005.07.015

Bouarab, C., Thompson, B., and Polter, A. M. (2019). VTA GABA neurons at the interface of stress and reward. *Front. Neural Circuits* 13:78. doi: 10.3389/fncir.2019.00078

Burdakov, D., Gerasimenko, O., and Verkhratsky, A. (2005). Physiological changes in glucose differentially modulate the excitability of hypothalamic melanin-concentrating hormone and orexin neurons *in situ*. *J. Neurosci.* 25, 2429–2433. doi: 10.1523/JNEUROSCI.4925-04.2005

Camargo Maluf, F., Feder, D., and Alves de Siqueira Carvalho, A. (2019). Analysis of the relationship between type II diabetes mellitus and Parkinson's disease: a systematic review. *Parkinson's Dis.* 2019:4951379. doi: 10.1155/2019/4951379

Cardozo, D. L., and Bean, B. P. (1995). Voltage-dependent calcium channels in rat midbrain dopamine neurons: modulation by dopamine and GABAB receptors. *J. Neurophysiol.* 74, 1137–1148. doi: 10.1152/jn.1995.74.3.1137

Carvelli, L., McDonald, P. W., Blakely, R. D., and DeFelice, L. J. (2004). Dopamine transporters depolarize neurons by a channel mechanism. *Proc. Natl. Acad. Sci. U.S.A.* 101, 16046–16051. doi: 10.1073/pnas.0403299101

Catoni, C., Cali, T., and Brini, M. (2019). Calcium, dopamine and neuronal calcium sensor 1: their contribution to Parkinson's disease. *Front. Mol. Neurosci.* 12:55. doi: 10.3389/fnmol.2019.00055

Chen, R., Ferris, M. J., and Wang, S. (2020). Dopamine D2 autoreceptor interactome: targeting the receptor complex as a strategy for treatment of substance use disorder. *Pharmacol. Ther.* 213:107583. doi: 10.1016/j.pharmthera.2020.107583

Cheong, J. L. Y., de Pablo-Fernandez, E., Foltynie, T., and Noyce, A. J. (2020). The Association between type 2 diabetes mellitus and Parkinson's disease. *J. Parkinson's Dis.* 10, 775–789. doi: 10.3233/JPD-191900

Collins, A. L., and Saunders, B. T. (2020). Heterogeneity in striatal dopamine circuits: form and function in dynamic reward seeking. *J. Neurosci. Res.* 98, 1046–1069. doi: 10.1002/jnr.24587

Di Fulvio, M., and Aguilar-Bryan, L. (2019). Chloride transporters and channels in beta-cell physiology: revisiting a 40-year-old model. *Biochem. Soc. Trans.* 47, 1843–1855. doi: 10.1042/BST20190513

Dodson, P. D., Dreyer, J. K., Jennings, K. A., Syed, E. C., Wade-Martins, R., Cragg, S. J., et al. (2016). Representation of spontaneous movement by dopaminergic neurons is cell-type selective and disrupted in parkinsonism. *Proc. Natl. Acad. Sci. U.S.A.* 113, E2180–2188. doi: 10.1073/pnas.1515941113

Dragicevic, E., Poetschke, C., Duda, J., Schlaudraff, F., Lammel, S., Schiemann, J., et al. (2014). Cav1.3 channels control D2-autoreceptor responses via NCS-1 in substantia nigra dopamine neurons. *Brain* 137, 287–302. doi: 10.1093/brain/awu131

Dragicevic, E., Schiemann, J., and Liss, B. (2015). Dopamine midbrain neurons in health and Parkinson's disease: emerging roles of voltage-gated calcium channels and ATP-sensitive potassium channels. *Neuroscience* 284C, 798–814. doi: 10.1016/j.neuroscience.2014.10.037

Duda, J., Potschke, C., and Liss, B. (2016). Converging roles of ion channels, calcium, metabolic stress, and activity pattern of Substantia nigra dopaminergic neurons in health and Parkinson's disease. *J. Neurochem.* 139(Suppl. 1), 156–178. doi: 10.1111/jnc.13572

Dunn-Meynell, A. A., Sanders, N. M., Compton, D., Becker, T. C., Eiki, J., Zhang, B. B., et al. (2009). Relationship among brain and blood glucose levels and spontaneous and glucoprivic feeding. *J. Neurosci.* 29, 7015–7022. doi: 10.1523/JNEUROSCI.0334-09.2009

Eberhard, D. (2013). Neuron and beta-cell evolution: learning about neurons is learning about beta-cells. *Bioessays* 35:584. doi: 10.1002/bies.201300035

Eisener-Dorman, A. F., Lawrence, D. A., and Bolivar, V. J. (2009). Cautionary insights on knockout mouse studies: the gene or not the gene? *Brain Behav. Immun.* 23, 318–324. doi: 10.1016/j.bbi.2008.09.001

Evans, R. C., Zhu, M., and Khaliq, Z. M. (2017). Dopamine inhibition differentially controls excitability of substantia nigra dopamine neuron subpopulations through T-type calcium channels. *J. Neurosci.* 37, 3704–3720. doi: 10.1523/JNEUROSCI.0117-17.2017

Farino, Z. J., Morgenstern, T. J., Maffei, A., Quick, M., De Solis, A. J., Wiriyasermkul, P., et al. (2020). New roles for dopamine D2 and D3 receptors in pancreatic beta cell insulin secretion. *Mol. Psychiatry* 25, 2070–2085. doi: 10.1038/s41380-018-0344-6

Figlewicz, D. P., Evans, S. B., Murphy, J., Hoen, M., and Baskin, D. G. (2003). Expression of receptors for insulin and leptin in the ventral tegmental area/substantia nigra (VTA/SN) of the rat. *Brain Res.* 964, 107–115. doi: 10.1016/S0006-8993(02)04087-8

Fioramonti, X., Chretien, C., Leloup, C., and Penicaud, L. (2017). Recent advances in the cellular and molecular mechanisms of hypothalamic neuronal glucose detection. *Front. Physiol.* 8:875. doi: 10.3389/fphys.2017.00875

Fioramonti, X., Lorsignol, A., Taupignon, A., and Penicaud, L. (2004). A new ATP-sensitive K+ channel-independent mechanism is involved in glucose-excited neurons of mouse arcuate nucleus. *Diabetes* 53, 2767–2775. doi: 10.2337/diabetes.53.11.2767

Fiory, F., Perruolo, G., Cimmino, I., Cabaro, S., Pignalosa, F. C., Miele, C., et al. (2019). The relevance of insulin action in the dopaminergic system. *Front. Neurosci.* 13:868. doi: 10.3389/fnins.2019.00868

Ford, C. P. (2014). The role of D2-autoreceptors in regulating dopamine neuron activity and transmission. *Neuroscience* 282, 13–22. doi: 10.1016/j.neuroscience.2014.01.025

Fu, Y., Paxinos, G., Watson, C., and Halliday, G. M. (2016). The substantia nigra and ventral tegmental dopaminergic neurons from development to degeneration. *J. Chem. Neuroanat.* 76, 98–107. doi: 10.1016/j.jchemneu.2016.02.001

Gainetdinov, R. R., Premont, R. T., Bohn, L. M., Lefkowitz, R. J., and Caron, M. G. (2004). Desensitization of G protein-coupled receptors and neuronal functions. *Annu. Rev. Neurosci.* 27, 107–144. doi: 10.1146/annurev.neuro.27.070203.144206

Gantz, S. C., Ford, C. P., Morikawa, H., and Williams, J. T. (2018). The evolving understanding of dopamine neurons in the substantia nigra and ventral tegmental area. *Annu. Rev. Physiol.* 80, 219–241. doi: 10.1146/annurev-physiol-021317-121615

Gantz, S. C., Robinson, B. G., Buck, D. C., Bunzow, J. R., Neve, R. L., Williams, J. T., et al. (2015). Distinct regulation of dopamine D2S and D2L autoreceptor signaling by calcium. *Elife* 4:e09358. doi: 10.7554/eLife.09358

Geracitano, R., Tozzi, A., Berretta, N., Florenzano, F., Guatteo, E., Viscomi, M. T., et al. (2005). Protective role of hydrogen peroxide in oxygen-deprived dopaminergic neurones of the rat substantia nigra. *J. Physiol.* 568, 97–110. doi: 10.1113/jphysiol.2005.092510

Giguere, N., Burke Nanni, S., and Trudeau, L. E. (2018). On cell loss and selective vulnerability of neuronal populations in Parkinson's disease. *Front. Neurol.* 9:455. doi: 10.3389/fneur.2018.00455

Giguere, N., Delignat-Lavaud, B., Herborg, F., Voisin, A., Li, Y., Jacquemet, V., et al. (2019). Increased vulnerability of nigral dopamine neurons after expansion of their axonal arborization size through D2 dopamine receptor conditional knockout. *PLoS Genet.* 15:e1008352. doi: 10.1371/journal.pgen.1008352

Gonzalez-Rodriguez, P., Zampese, E., and Surmeier, D. J. (2020). Selective neuronal vulnerability in Parkinson's disease. *Prog. Brain Res.* 252, 61–89. doi: 10.1016/bs.pbr.2020.02.005

Goutelle, S., Maurin, M., Rougier, F., Barbaut, X., Bourguignon, L., Ducher, M., et al. (2008). The Hill equation: a review of its capabilities in pharmacological modelling. *Fundament. Clin. Pharmacol.* 22, 633–648. doi: 10.1111/j.1472-8206.2008.00633.x

Gromada, J., Bark, C., Smidt, K., Efanov, A. M., Janson, J., Mandic, S. A., et al. (2005). Neuronal calcium sensor-1 potentiates glucose-dependent exocytosis in pancreatic beta cells through activation of phosphatidylinositol 4-kinase beta. *Proc. Natl. Acad. Sci. U.S.A.* 102, 10303–10308. doi: 10.1073/pnas.0504487102

Guemes, A., and Georgiou, P. (2018). Review of the role of the nervous system in glucose homoeostasis and future perspectives towards the management of diabetes. *Bioelectr. Med.* 4:9. doi: 10.1186/s42234-018-0009-4

Hanna, L. K. T. J., Beall, C., and Ellacott, K. L. J. (2019). Changes in neuronal activity across the mouse ventromedial nucleus of the hypothalamus in response to low glucose: evaluation using an extracellular multi-electrode array approach. *Neuroendocrinology* 32:e12824. doi: 10.1111/jne.12824

Hassan, A., Sharma Kandel, R., Mishra, R., Gautam, J., Alaref, A., and Jahan, N. (2020). Diabetes mellitus and Parkinson's disease: shared pathophysiological links and possible therapeutic implications. *Cureus* 12:e9853. doi: 10.7759/cureus.9853

Hassanabad, M. F., and Fatehi, M. (2019). Current views on dopaminergic drugs affecting glucose homeostasis. *Curr. Diabetes Rev.* 15, 93–99. doi: 10.2174/1573399814666180424123912

Hernandez, L. F., Obeso, I., Costa, R. M., Redgrave, P., and Obeso, J. A. (2019). Dopaminergic vulnerability in Parkinson disease: the cost of humans' habitual performance. *Trends Neurosci.* 42, 375–383. doi: 10.1016/j.tins.2019.03.007

Hetzel, A. (2008). *Elektrophysiologische und Molekularbiologische Charakterisierung der Dopamin-Autorezeptorantwort Individueller Dopaminerger Mittelhirnneurone der Maus (Mus musculus L.) unter Kontrollbedingungen und nach Einmaliger in-vivo-Injektion von Kokain*. vol. Dr. rer. nat. Marburg: Marburg University.

Heuschkel, M. O., Fejtl, M., Raggenbass, M., Bertrand, D., and Renaud, P. (2002). A three-dimensional multi-electrode array for multi-site stimulation and recording in acute brain slices. *J. Neurosci. Methods* 114, 135–148. doi: 10.1016/S0165-0270(01)00514-3

Hirschberg, P. R., Sarkar, P., Teegala, S. B., and Routh, V. H. (2020). Ventromedial hypothalamus glucose-inhibited neurones: a role in glucose and energy homeostasis? *J. Neuroendocrinol.* 32:e12773. doi: 10.1111/jne.12773

Hwang, J. J., Jiang, L., Sanchez Rangel, E., Fan, X., Ding, Y., Lam, W., et al. (2019). Glycemic variability and brain glucose levels in type 1 diabetes. *Diabetes* 68, 163–171. doi: 10.2337/db18-0722

Ingram, S. L., Prasad, B. M., and Amara, S. G. (2002). Dopamine transporter-mediated conductances increase excitability of midbrain dopamine neurons. *Nat. Neurosci.* 5, 971–978. doi: 10.1038/nn920

Jang, J. Y., Jang, M., Kim, S. H., Um, K. B., Kang, Y. K., Kim, H. J., et al. (2011). Regulation of dopaminergic neuron firing by heterogeneous dopamine autoreceptors in the substantia nigra pars compacta. *J. Neurochem.* 116, 966–974. doi: 10.1111/j.1471-4159.2010.07107.x

Joshua, M., Adler, A., Prut, Y., Vaadia, E., Wickens, J. R., and Bergman, H. (2009). Synchronization of midbrain dopaminergic neurons is enhanced by rewarding events. *Neuron* 62, 695–704. doi: 10.1016/j.neuron.2009.04.026

Kabbani, N., Woll, M. P., Nordman, J. C., and Levenson, R. (2012). Dopamine receptor interacting proteins: targeting neuronal calcium sensor-1/D2 dopamine receptor interaction for antipsychotic drug development. *Curr. Drug Targets* 13, 72–79. doi: 10.2174/138945012798868515

Khaliq, Z. M., and Bean, B. P. (2010). Pacemaking in dopaminergic ventral tegmental area neurons: depolarizing drive from background and voltage-dependent sodium conductances. *J. Neurosci.* 30, 7401–7413. doi: 10.1523/JNEUROSCI.0143-10.2010

Koekkoek, L. L., Mul, J. D., and la Fleur, S. E. (2017). Glucose-sensing in the reward system. *Front. Neurosci.* 11:716. doi: 10.3389/fnins.2017.00716

Kordower, J. H., Olanow, C. W., Dodiya, H. B., Chu, Y. P., Beach, T. G., Adler, C. H., et al. (2013). Disease duration and the integrity of the nigrostriatal system in Parkinson's disease. *Brain* 136, 2419–2431. doi: 10.1093/brain/awt192

Krashia, P., Martini, A., Nobili, A., Aversa, D., D'Amelio, M., Berretta, N., et al. (2017). On the properties of identified dopaminergic neurons in the mouse substantia nigra and ventral tegmental area. *Eur. J. Neurosci.* 45, 92–105. doi: 10.1111/ejn.13364

Lacey, M. G., Mercuri, N. B., and North, R. A. (1987). Dopamine acts on D2 receptors to increase potassium conductance in neurones of the rat substantia nigra zona compacta. *J. Physiol.* 392, 397–416. doi: 10.1113/jphysiol.1987.sp016787

Lammel, S., Hetzel, A., Hackel, O., Jones, I., Liss, B., and Roeper, J. (2008). Unique properties of mesoprefrontal neurons within a dual mesocorticolimbic dopamine system. *Neuron* 57, 760–773. doi: 10.1016/j.neuron.2008.01.022

Lebowitz, J. J., and Khoshbouei, H. (2020). Heterogeneity of dopamine release sites in health and degeneration. *Neurobiol. Dis.* 134:104633. doi: 10.1016/j.nbd.2019.104633

Lewicki, M. S. (1998). A review of methods for spike sorting: the detection and classification of neural action potentials. *Network* 9, R53–R78. doi: 10.1088/0954-898X_9_4_001

Liss, B., Bruns, R., and Roeper, J. (1999). Alternative sulfonylurea receptor expression defines metabolic sensitivity of K-ATP channels in dopaminergic midbrain neurons. *EMBO J.* 18, 833–846. doi: 10.1093/emboj/18.4.833

Liss, B., Haeckel, O., Wildmann, J., Miki, T., Seino, S., and Roeper, J. (2005). K-ATP channels promote the differential degeneration of dopaminergic midbrain neurons. *Nat. Neurosci.* 8, 1742–1751. doi: 10.1038/nn1570

Liss, B., and Roeper, J. (2004). Correlating function and gene expression of individual basal ganglia neurons. *Trends Neurosci.* 27, 475–481. doi: 10.1016/j.tins.2004.06.007

Liss, B., and Striessnig, J. (2019). The potential of L-type calcium channels as a drug target for neuroprotective therapy in Parkinson's disease. *Annu. Rev. Pharmacol. Toxicol.* 59, 263–289. doi: 10.1146/annurev-pharmtox-010818-021214

Liu, C., and Kaeser, P. S. (2019). Mechanisms and regulation of dopamine release. *Curr. Opin. Neurobiol.* 57, 46–53. doi: 10.1016/j.conb.2019.01.001

Liu, M., Ren, L., Zhong, X., Ding, Y., Liu, T., Liu, Z., et al. (2020). D2-like receptors mediate dopamine-inhibited insulin secretion via ion channels in rat pancreatic beta-cells. *Front. Endocrinol.* 11:152. doi: 10.3389/fendo.2020.00152

Liu, Y., Buck, D. C., and Neve, K. A. (2008). Novel interaction of the dopamine D2 receptor and the Ca2+ binding protein S100B: role in D2 receptor function. *Mol. Pharmacol.* 74, 371–378. doi: 10.1124/mol.108.044925

Lopez Vicchi, F., Luque, G. M., Brie, B., Nogueira, J. P., Garcia Tornadu, I., and Becu-Villalobos, D. (2016). Dopaminergic drugs in type 2 diabetes and glucose homeostasis. *Pharmacol. Res.* 109, 74–80. doi: 10.1016/j.phrs.2015.12.029

Lopez-Gambero, A. J., Martinez, F., Salazar, K., Cifuentes, M., and Nualart, F. (2019). Brain Glucose-sensing mechanism and energy homeostasis. *Mol. Neurobiol.* 56, 769–796. doi: 10.1007/s12035-018-1099-4

MacDonald, P. E., Joseph, J. W., and Rorsman, P. (2005). Glucose-sensing mechanisms in pancreatic beta-cells. *Philos. Trans. R. Soc. Lond. B Biol. Sci.* 360, 2211–2225. doi: 10.1098/rstb.2005.1762

Mahmud, M., and Vassanelli, S. (2016). Processing and analysis of multichannel extracellular neuronal signals: state-of-the-art and challenges. *Front. Neurosci.* 10:248. doi: 10.3389/fnins.2016.00248

Mahmud, M., and Vassanelli, S. (2019). Open-source tools for processing and analysis of *in vitro* extracellular neuronal signals. *Adv. Neurobiol.* 22, 233–250. doi: 10.1007/978-3-030-11135-9_10

Manville, R. W., and Abbott, G. W. (2020). Potassium channels act as chemosensors for solute transporters. *Commun. Biol.*. 3:90. doi: 10.1038/s42003-020-0820-9

Margolis, E. B., Lock, H., Hjelmstad, G. O., and Fields, H. L. (2006). The ventral tegmental area revisited: is there an electrophysiological marker for dopaminergic neurons? *J. Physiol.* 577, 907–924. doi: 10.1113/jphysiol.2006.117069

Marinelli, M., and McCutcheon, J. E. (2014). Heterogeneity of dopamine neuron activity across traits and states. *Neuroscience* 282, 176–197. doi: 10.1016/j.neuroscience.2014.07.034

Marinelli, S., Bernardi, G., Giacomini, P., and Mercuri, N. B. (2000). Pharmacological identification of the K(+) currents mediating the hypoglycemic hyperpolarization of rat midbrain dopaminergic neurones. *Neuropharmacology* 39, 1021–1028. doi: 10.1016/S0028-3908(99)00186-0

Marinelli, S., Federici, M., Giacomini, P., Bernardi, G., and Mercuri, N. B. (2001). Hypoglycemia enhances ionotropic but reduces metabotropic glutamate responses in substantia nigra dopaminergic neurons. *J. Neurophysiol.* 85, 1159–1166. doi: 10.1152/jn.2001.85.3.1159

Mercuri, N. B., Bonci, A., Calabresi, P., Stratta, F., Stefani, A., and Bernardi, G. (1994). Effects of dihydropyridine calcium antagonists on rat midbrain dopaminergic neurones. *Br. J. Pharmacol.* 113, 831–838. doi: 10.1111/j.1476-5381.1994.tb17068.x

Michel, P. P., Hirsch, E. C., and Hunot, S. (2016). Understanding dopaminergic cell death pathways in Parkinson disease. *Neuron* 90, 675–691. doi: 10.1016/j.neuron.2016.03.038

Morales, M., and Margolis, E. B. (2017). Ventral tegmental area: cellular heterogeneity, connectivity and behaviour. *Nat. Rev. Neurosci.* 18, 73–85. doi: 10.1038/nrn.2016.165

Nakamura, T. Y., Nakao, S., and Wakabayashi, S. (2019). Emerging roles of neuronal Ca(2+) sensor-1 in cardiac and neuronal tissues: a mini review. *Front. Mol. Neurosci.* 12:56. doi: 10.3389/fnmol.2019.00056

Negri, J., Menon, V., and Young-Pearse, T. L. (2020). Assessment of spontaneous neuronal activity *in vitro* using multi-well multi-electrode arrays: implications for assay development. *eNeuro* 7:ENEURO.0080-0019.2019. doi: 10.1523/ENEURO.0080-19.2019

Nestler, E. J. (2005). Is there a common molecular pathway for addiction? *Nat. Neurosci.* 8, 1445–1449. doi: 10.1038/nn1578

Ng, E., Varaschin, R. K., Su, P., Browne, C. J., Hermainski, J., Le Foll, B., et al. (2016). Neuronal calcium sensor-1 deletion in the mouse decreases motivation and dopamine release in the nucleus accumbens. *Behav. Brain Res.* 301, 213–225. doi: 10.1016/j.bbr.2015.12.037

Obeso, J. A., Stamelou, M., Goetz, C. G., Poewe, W., Lang, A. E., Weintraub, D., et al. (2017). Past, present, and future of Parkinson's disease: a special essay on the 200th anniversary of the shaking palsy. *Mov. Disord.* 32, 1264–1310. doi: 10.1002/mds.27115

Obien, M. E. J., Hierlemann, A., and Frey, U. (2019). Accurate signal-source localization in brain slices by means of high-density microelectrode arrays. *Sci. Rep.* 9:788. doi: 10.1038/s41598-018-36895-y

Paxinos, G., and Franklin, K. B. J. (2001). *The Mouse Brain in Stereotaxic Coordinates*. San Diego, CA; London: Academic.

Perra, S., Clements, M. A., Bernier, B. E., and Morikawa, H. (2011). *In vivo* ethanol experience increases D(2) autoinhibition in the ventral tegmental area. *Neuropsychopharmacology* 36, 993–1002. doi: 10.1038/npp.2010.237

Philippart, F., Destreel, G., Merino-Sepulveda, P., Henny, P., Engel, D., and Seutin, V. (2016). Differential somatic Ca2+ channel profile in midbrain dopaminergic neurons. *J. Neurosci.* 36, 7234–7245. doi: 10.1523/JNEUROSCI.0459-16.2016

Philippart, F., and Khaliq, Z. M. (2018). Gi/o protein-coupled receptors in dopamine neurons inhibit the sodium leak channel NALCN. *Elife* 7:e40984. doi: 10.7554/eLife.40984.021

Poetschke, C., Dragicevic, E., Duda, J., Benkert, J., Dougalis, A., DeZio, R., et al. (2015). Compensatory T-type Ca2+ channel activity alters D2-autoreceptor responses of Substantia nigra dopamine neurons from Cav1.3 L-type Ca2+ channel KO mice. *Sci. Rep.* 5:13688. doi: 10.1038/srep13688

Poewe, W., Seppi, K., Tanner, C. M., Halliday, G. M., Brundin, P., Volkmann, J., et al. (2017). Parkinson disease. *Nat. Rev. Dis. Primers* 3:17013. doi: 10.1038/nrdp.2017.13

Pozo, M., and Claret, M. (2018). Hypothalamic control of systemic glucose homeostasis: the pancreas connection. *Trends Endocrinol. Metab.* 29, 581–594. doi: 10.1016/j.tem.2018.05.001

Ratai, O., Hermainski, J., Ravichandran, K., and Pongs, O. (2019). NCS-1 deficiency is associated with obesity and diabetes type 2 in mice. *Front. Mol. Neurosci.* 12:78. doi: 10.3389/fnmol.2019.00078

Rey, H. G., Pedreira, C., and Quian Quiroga, R. (2015). Past, present and future of spike sorting techniques. *Brain Res. Bull.* 119, 106–117. doi: 10.1016/j.brainresbull.2015.04.007

Rice, M. E., and Patel, J. C. (2015). Somatodendritic dopamine release: recent mechanistic insights. *Philos. Trans. R. Soc. Lond. B Biol. Sci.* 370:20140185. doi: 10.1098/rstb.2014.0185

Robinson, B. G., Bunzow, J. R., Grimm, J. B., Lavis, L. D., Dudman, J. T., Brown, J., et al. (2017a). Desensitized D2 autoreceptors are resistant to trafficking. *Sci. Rep.* 7:4379. doi: 10.1038/s41598-017-04728-z

Robinson, B. G., Condon, A. F., Radl, D., Borrelli, E., Williams, J. T., and Neve, K. A. (2017b). Cocaine-induced adaptation of dopamine D2S, but not D2L autoreceptors. *Elife* 6:e31924. doi: 10.7554/eLife.31924

Rorsman, P., and Ashcroft, F. M. (2018). Pancreatic beta-cell electrical activity and insulin secretion: of mice and men. *Physiol. Rev.* 98, 117–214. doi: 10.1152/physrev.00008.2017

Routh, V. H. (2010). Glucose sensing neurons in the ventromedial hypothalamus. *Sensors* 10, 9002–9025. doi: 10.3390/s101009002

Routh, V. H., Hao, L., Santiago, A. M., Sheng, Z., and Zhou, C. (2014). Hypothalamic glucose sensing: making ends meet. *Front. Syst. Neurosci.* 8:236. doi: 10.3389/fnsys.2014.00236

Saab, B. J., Georgiou, J., Nath, A., Lee, F. J., Wang, M., Michalon, A., et al. (2009). NCS-1 in the dentate gyrus promotes exploration, synaptic plasticity, and rapid acquisition of spatial memory. *Neuron* 63, 643–656. doi: 10.1016/j.neuron.2009.08.014

Schiemann, J., Schlaudraff, F., Klose, V., Bingmer, M., Seino, S., Magill, P. J., et al. (2012). K-ATP channels in dopamine substantia nigra neurons control bursting and novelty-induced exploration. *Nat. Neurosci.* 15, 1272–1280. doi: 10.1038/nn.3185

Simons, C., Benkert, J., Deuter, N., Poetschke, C., Pongs, O., Schneider, T., et al. (2019). NCS-1 Deficiency affects mRNA levels of genes involved in regulation of ATP synthesis and mitochondrial stress in highly vulnerable substantia nigra dopaminergic neurons. *Front. Mol. Neurosci.* 12:252. doi: 10.3389/fnmol.2019.00252

Sonders, M. S., Zhu, S. J., Zahniser, N. R., Kavanaugh, M. P., and Amara, S. G. (1997). Multiple ionic conductances of the human dopamine transporter: the actions of dopamine and psychostimulants. *J. Neurosci.* 17, 960–974. doi: 10.1523/JNEUROSCI.17-03-00960.1997

Spira, M. E., and Hai, A. (2013). Multi-electrode array technologies for neuroscience and cardiology. *Nat. Nanotechnol.* 8, 83–94. doi: 10.1038/nnano.2012.265

Sportelli, C., Urso, D., Jenner, P., and Chaudhuri, K. R. (2020). Metformin as a potential neuroprotective agent in prodromal Parkinson's disease-viewpoint. *Front. Neurol.* 11:556. doi: 10.3389/fneur.2020.00556

Stanley, S., Moheet, A., and Seaquist, E. R. (2019). Central mechanisms of glucose sensing and counterregulation in defense of hypoglycemia. *Endocr. Rev.* 40, 768–788. doi: 10.1210/er.2018-00226

Stevenson, I. H., and Kording, K. P. (2011). How advances in neural recording affect data analysis. *Nat. Neurosci.* 14, 139–142. doi: 10.1038/nn.2731

Stuhlmann, T., Planells-Cases, R., and Jentsch, T. J. (2018). LRRC8/VRAC anion channels enhance beta-cell glucose sensing and insulin secretion. *Nat. Commun.* 9:1974. doi: 10.1038/s41467-018-04353-y

Subramaniam, M., Althof, D., Gispert, S., Schwenk, J., Auburger, G., Kulik, A., et al. (2014). Mutant alpha-synuclein enhances firing frequencies in dopamine substantia nigra neurons by oxidative impairment of A-type potassium channels. *J. Neurosci.* 34, 13586–13599. doi: 10.1523/JNEUROSCI.5069-13.2014

Subramaniam, M., and Roeper, J. (2017). "Subtypes of midbrain dopamine neurons," in *Handbook of Basal Ganglia Structure and Function*, Vol. 24, eds H. Steiner and K. Y. Tseng (London: Elsevier), 317–334.

Sulzer, D., Cragg, S. J., and Rice, M. E. (2016). Striatal dopamine neurotransmission: regulation of release and uptake. *Basal Ganglia* 6, 123–148. doi: 10.1016/j.baga.2016.02.001

Surmeier, D. J., Obeso, J. A., and Halliday, G. M. (2017). Selective neuronal vulnerability in Parkinson disease. *Nat. Rev. Neurosci.* 18, 101–113. doi: 10.1038/nrn.2016.178

Swaab, D. F., Dubelaar, E. J., Hofman, M. A., Scherder, E. J., van Someren, E. J., and Verwer, R. W. (2002). Brain aging and Alzheimer's disease; use it or lose it. *Prog. Brain Res.* 138, 343–373. doi: 10.1016/S0079-6123(02)38086-5

Ter Horst, K. W., Lammers, N. M., Trinko, R., Opland, D. M., Figee, M., Ackermans, M. T., et al. (2018). Striatal dopamine regulates systemic glucose metabolism in humans and mice. *Sci. Transl. Med.* 10:eaar3752. doi: 10.1126/scitranslmed.aar3752

Tomagra, G., Picollo, F., Battiato, A., Picconi, B., De Marchis, S., Pasquarelli, A., et al. (2019). Quantal release of dopamine and action potential firing detected in midbrain neurons by multifunctional diamond-based microarrays. *Front. Neurosci.* 13:288. doi: 10.3389/fnins.2019.00288

van der Velden, L., Vinck, M. A., and Wadman, W. J. (2020). Resonance in the mouse ventral tegmental area dopaminergic network induced by regular and poisson distributed optogenetic stimulation *in-vitro*. *Front. Comput. Neurosci.* 14:11. doi: 10.3389/fncom.2020.00011

Vogt Weisenhorn, D. M., Giesert, F., and Wurst, W. (2016). Diversity matters - heterogeneity of dopaminergic neurons in the ventral mesencephalon and its relation to Parkinson's Disease. *J. Neurochem.* 139(Suppl. 1), 8–26. doi: 10.1111/jnc.13670

Wang, R., Liu, X., Hentges, S. T., Dunn-Meynell, A. A., Levin, B. E., Wang, W., et al. (2004). The regulation of glucose-excited neurons in the hypothalamic arcuate nucleus by glucose and feeding-relevant peptides. *Diabetes* 53, 1959–1965. doi: 10.2337/diabetes.53.8.1959

Wolfart, J., and Roeper, J. (2002). Selective coupling of T-type calcium channels to SK potassium channels prevents intrinsic bursting in dopaminergic midbrain neurons. *J. Neurosci.* 22, 3404–3413. doi: 10.1523/JNEUROSCI.22-09-03404.2002

Wong, Y. C., Luk, K., Purtell, K., Burke Nanni, S., Stoessl, A. J., Trudeau, L. E., et al. (2019). Neuronal vulnerability in Parkinson disease: should the focus be on axons and synaptic terminals? *Mov. Disord.* 34, 1406–1422. doi: 10.1002/mds.27823

Zampese, E., and Surmeier, D. J. (2020). Calcium, bioenergetics, and Parkinson's disease. *Cells* 9:2045. doi: 10.3390/cells9092045

Zamponi, G. W., Striessnig, J., Koschak, A., and Dolphin, A. C. (2015). The physiology, pathology, and pharmacology of voltage-gated calcium channels and their future therapeutic potential. *Pharmacol. Rev.* 67, 821–870. doi: 10.1124/pr.114.009654

Conflict of Interest: The authors declare that the research was conducted in the absence of any commercial or financial relationships that could be construed as a potential conflict of interest.

Copyright © 2021 Mannal, Kleiner, Fauler, Dougalis, Poetschke and Liss. This is an open-access article distributed under the terms of the Creative Commons Attribution License (CC BY). The use, distribution or reproduction in other forums is permitted, provided the original author(s) and the copyright owner(s) are credited and that the original publication in this journal is cited, in accordance with accepted academic practice. No use, distribution or reproduction is permitted which does not comply with these terms.

frontiers in Synaptic Neuroscience

MINI REVIEW
published: 01 March 2021
doi: 10.3389/fnsyn.2021.635879

Dopamine in Fear Extinction

*Ximena I. Salinas-Hernández and Sevil Duvarci**

Institute of Neurophysiology, Neuroscience Center, Goethe University, Frankfurt, Germany

The ability to extinguish fear memories when threats are no longer present is critical for adaptive behavior. Fear extinction represents a new learning process that eventually leads to the formation of extinction memories. Understanding the neural basis of fear extinction has considerable clinical significance as deficits in extinction learning are the hallmark of human anxiety disorders. In recent years, the dopamine (DA) system has emerged as one of the key regulators of fear extinction. In this review article, we highlight recent advances that have demonstrated the crucial role DA plays in mediating different phases of fear extinction. Emerging concepts and outstanding questions for future research are also discussed.

Keywords: dopamine, fear extinction, amygdala, medial prefrontal cortex, nucleus accumbens

INTRODUCTION

Learning to associate stimuli and situations with danger or safety is critical for survival and adaptive behavior. In the laboratory, these forms of learning are typically studied using Pavlovian fear conditioning and extinction. Fear conditioning is an example of associative learning in which an initially neutral stimulus such as a tone (conditioned stimulus, CS) comes to elicit fear responses after being paired in time with an aversive outcome such as a foot shock (unconditioned stimulus, US). Once the CS-US association is learned, subsequently repeated presentations of the CS in the absence of the aversive US result in a gradual decrease in conditioned fear responses, a process known as fear extinction. In the last decades, fear extinction has attracted much interest in part because deficits in extinction learning are thought to underlie human anxiety disorders, such as post-traumatic stress disorder (PTSD) and phobias (Graham and Milad, 2011; Pitman et al., 2012; Craske et al., 2017), and thus, understanding the neural basis of fear extinction has high clinical significance. Decades of research has revealed that a distributed network of brain structures including mainly the amygdala and the medial prefrontal cortex (mPFC) mediates the acquisition and consolidation of fear extinction memories (Pape and Pare, 2010; Sotres-Bayon and Quirk, 2010; Maren et al., 2013; Duvarci and Pare, 2014; Tovote et al., 2015).

In recent years, the dopamine (DA) system has also emerged as an important mediator of fear extinction. DA is a neurotransmitter critically involved in a wide range of functions including reward learning, motivation, motor control, and cognitive functioning. DA neurons that are mainly located in the ventral tegmental area (VTA) and substantia nigra (SN) in the midbrain. DA receptors are metabotropic receptors that can be classified into two main types with the DA D1-type receptors (Gs-coupled) comprised of D1 and D5 and the DA D2-type receptors (Gi-coupled) comprised of D2, D3, and D4 subtypes (Missale et al., 1998). Systemic administration of DA precursor L-DOPA or D1-type receptor agonists before

OPEN ACCESS

Edited by:
Francesco Ferraguti, Innsbruck Medical University, Austria

Reviewed by:
Nicolas Singewald, University of Innsbruck, Austria
Ingrid Ehrlich, University of Stuttgart, Germany

****Correspondence:***
Sevil Duvarci
duvarci@med.uni-frankfurt.de

Received: *30 November 2020*
Accepted: *09 February 2021*
Published: *01 March 2021*

Citation:
Salinas-Hernández XI and Duvarci S (2021) Dopamine in Fear Extinction. Front. Synaptic Neurosci. 13:635879. doi: 10.3389/fnsyn.2021.635879

or right after extinction enhances acquisition and retention of fear extinction, respectively (Haaker et al., 2013; Abraham et al., 2016; Whittle et al., 2016), indicating the involvement of DA during both acquisition and consolidation of extinction memories. In particular, DA neurons located in the VTA, through their projections to the structures involved in fear extinction such as the amygdala and mPFC, are implicated in fear extinction. In this review, we highlight recent findings that have revealed the role DA plays in mediating different phases of fear extinction. We focus the discussion on the extinction of cued fear conditioning in rodents where recent progress has been made. We begin by discussing how fear extinction learning is initiated and driven by the activity of VTA DA neurons. We also discuss the emerging concept that fear extinction may be an appetitive learning process mediated by the brain's reward circuitry. We next focus on how DA regulates the acquisition and expression of fear extinction in the amygdala. We consider the possible targets in the amygdala microcircuitry that DA can act on to mediate fear extinction. Finally, we discuss the role of DA in the mPFC in mediating the consolidation of extinction memories.

A DOPAMINE PREDICTION ERROR SIGNAL INITIATES FEAR EXTINCTION LEARNING

Considerable evidence indicates that fear extinction represents new learning rather than forgetting or erasure of the original fear memory (Bouton et al., 2006; Myers and Davis, 2007). During extinction, the animal learns the new association between the presence of the CS and an unexpected safe outcome (i.e., the absence of the expected aversive US). Classical theories of associative learning postulate that learning is initiated by prediction errors (PE) that signal the discrepancy between expected and actual outcomes (Rescorla and Wagner, 1972) and new learning happens when outcomes do not match predictions. In fear extinction, the unexpected omission of the US induces a PE signal that leads to an update in the prediction associated with the CS so that it comes to be recognized as signaling safety. This in turn leads to a decay of conditioned fear responses.

Because not receiving an expected aversive US may be experienced as a rewarding event, the prediction error caused by the US omission during extinction (extinction prediction error, EPE) could be conceptualized as an appetitive or reward-like prediction error. Thus, fear extinction may be mediated by the reward learning system (Abraham et al., 2014; Josselyn and Frankland, 2018; Kalisch et al., 2019). It is well established that midbrain DA neurons encode reward prediction error (RPE) signals to drive reward learning (Schultz, 2006). Consistently, recent studies demonstrate that a subset of DA neurons, located in the VTA, is activated by the omission of the aversive US during fear extinction, and this increased DA neuron firing is indeed necessary to initiate fear extinction learning (Luo et al., 2018; Salinas-Hernández et al., 2018). Importantly, the timing of this DA signal fulfills the requirements of a prediction error: (i) it is specific to the time of the US omission; and (ii) it is observed during the early, but not late, trials of extinction learning indicating that it occurs specifically when the US omission is unexpected (Salinas-Hernández et al., 2018). Interestingly, a more recent study has further shown that although DA neurons located in both the medial and the lateral VTA, but not the SN, are activated by the omission of the US, particularly the medial VTA DA neurons encode an EPE signal to drive fear extinction. On the other hand, DA neurons that are found in the lateral VTA signal salience but not EPE (Cai et al., 2020). Together, these studies demonstrate that a PE signal encoded by a subset of DA neurons in the medial VTA is crucial to initiate and drive fear extinction learning (**Figure 1A**). If the PE encoded during fear extinction is an RPE signal, it is expected that the same DA neurons and DAergic circuits mediate these two signals. In support of this hypothesis, a recent study in fruit flies has shown that fear extinction is driven by the same distinct population of DA neurons that also mediates reward, but not fear, learning (Felsenberg et al., 2018). Whether in mammals the same DA neurons encode extinction and reward PE signals and whether these two distinct signals share similar properties are important questions for future research.

How and through which neural circuits this DA signal initiates extinction learning and ultimately leads to the plasticity underlying formation of extinction memories is currently unknown. The first step in addressing these questions is identifying the projection target of DA neurons that encode the EPE signal. Since DA neurons projecting to the nucleus accumbens (NAc), the main DA output region in the rodent ventral striatum, form the canonical reward circuitry (Wise, 2002), NAc constitutes a good candidate to fulfill this role (**Figure 1A**). Supporting this, an increase in DA release during fear extinction has been observed in the NAc (Badrinarayan et al., 2012) and the pharmacological blockade of DA receptors in the NAc impairs fear extinction learning (Holtzman-Assif et al., 2010). Furthermore, fear extinction learning in humans is accompanied by a prediction error-like activation in the ventral striatum (Raczka et al., 2011). However, in contrast with these findings, inhibition of DA terminals in NAc at the time of the US omission surprisingly does not affect extinction learning, although it does impair consolidation of extinction memory (Luo et al., 2018). Notably, single-unit recordings demonstrate that a small subpopulation of DA neurons mediate the EPE signal (Salinas-Hernández et al., 2018). It is therefore possible that this subpopulation of DA neurons projects to a specific and restricted subregion of NAc that was not targeted by Luo et al. (2018). In addition to NAc, other possible candidates include DA neurons projecting to the amygdala and/or mPFC. However, at odds with these possibilities, inhibition of DA terminals in the amygdala or mPFC during EPE signaling does not impair extinction learning (Luo et al., 2018). How a DA PE signal initiates extinction learning and leads to the acquisition and consolidation of extinction memories within the fear extinction circuitry is one of the key questions towards understanding the neural basis of fear extinction. Future research determining the exact projection target of EPE encoding

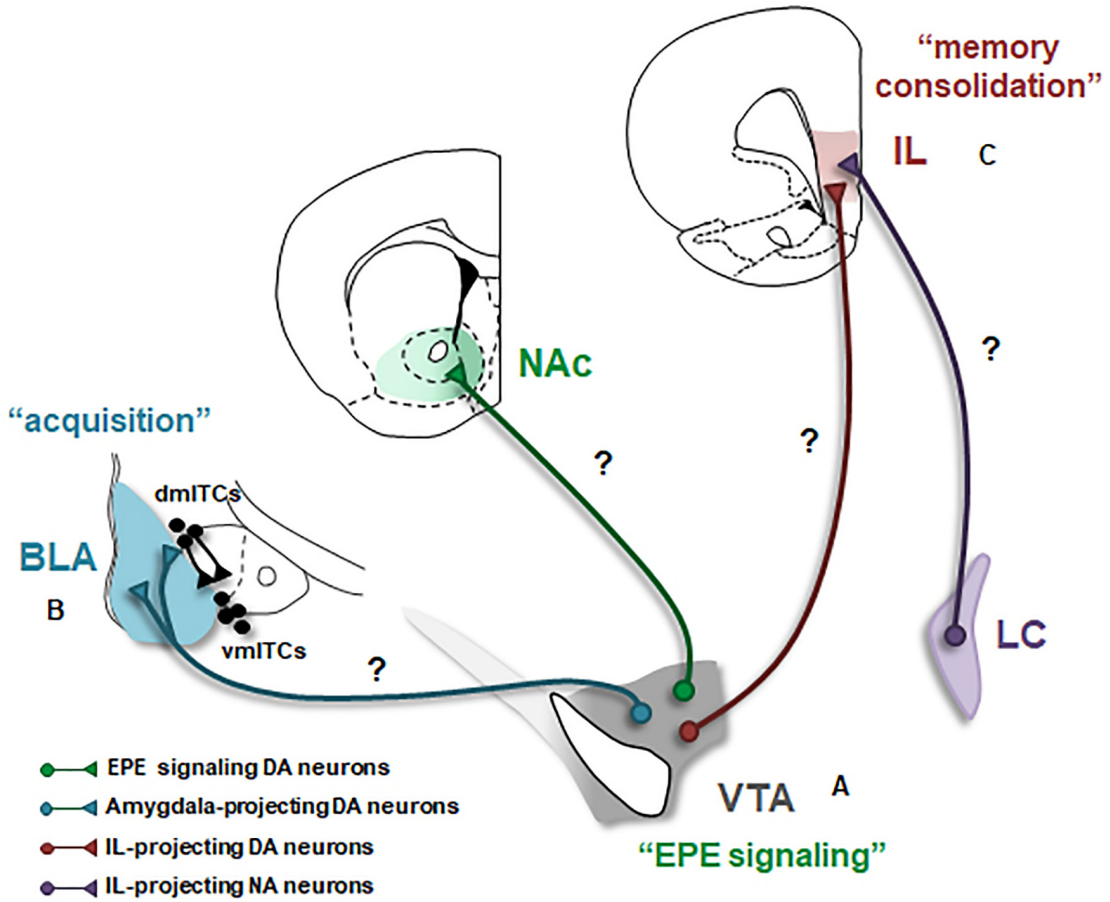

FIGURE 1 | Dopaminergic modulation of the neural circuitry underlying fear extinction. Schematic of the three major projections of the ventral tegmental area (VTA) dopamine (DA) neurons likely involved in fear extinction are shown. BLA, basolateral amygdala; EPE, extinction prediction error; IL, infralimbic cortex; ITCs, intercalated cell masses (dm: dorsomedial, vm: ventromedial); LC, locus coeruleus; NA, noradrenalin; NAc, nucleus accumbens. Question marks (?) indicate possible DAergic projections mediating fear extinction. The involvement of these projections in extinction remains to be tested. **(A)** A subset of VTA DA neurons encodes an EPE signal that is necessary to initiate fear extinction learning. The projection target of EPE encoding DA neurons is currently unknown. NAc constitutes an ideal candidate however the exact subregion of NAc receiving the EPE signal remains to be determined. **(B)** Activation of DA receptors in the BLA mediates the acquisition of fear extinction memories. However, the source of DA input to the amygdala during extinction has not directly been demonstrated. Whether VTA DA projections to the BLA and also likely to dmITCs, are involved in fear extinction is an important outstanding question. **(C)** DA is crucial for the consolidation of extinction memories in the IL. The source of DA input to IL during fear extinction has remained elusive, however, IL receives its main DA input from the VTA and IL-projecting VTA DA neurons are thus plausible candidates. However, recent studies suggest that this DA projection is pro-aversive; and thus, DA released from other sources, such as NA neurons located in the LC might be more likely to mediate fear extinction.

DA neurons will be an important step in addressing this question (**Figure 1A**).

DOPAMINE IN THE AMYGDALA MEDIATES THE ACQUISITION OF FEAR EXTINCTION MEMORIES

The amygdala is a key structure underlying the acquisition and expression of fear extinction memories. Specifically, two subregions within the amygdala microcircuitry, the basolateral amygdala (BLA) and the intercalated cell masses (ITCs) are critically involved in fear extinction (Herry et al., 2010; Duvarci and Pare, 2014). Much evidence indicates that the BLA, consisting of the lateral and basal nuclei, is particularly required for the acquisition of extinction memories (Herry et al., 2008; Amano et al., 2011; Sierra-Mercado et al., 2011). A subpopulation of BLA neurons termed "extinction neurons" increases their firing to the CS during fear extinction, specifically late in the extinction session right before the animals show a decrease in conditioned fear responses (Herry et al., 2008; Amano et al., 2011). Furthermore, considerable evidence implicates GABAergic inhibition in the BLA during fear extinction. Both strengthening and also weakening of GABAergic transmission has been shown in the BLA during extinction (Marsicano et al., 2002; Chhatwal et al., 2005; Heldt and Ressler, 2007; Sangha et al., 2009; Kasugai et al., 2019), suggesting that particular

subtypes of GABAergic interneurons are likely differentially recruited during extinction (Duvarci and Pare, 2014; Krabbe et al., 2018). However, the involvement of different subtypes of BLA interneurons in extinction has remained elusive. Importantly, GABAergic neurons are critical targets of DA in the amygdala and DAergic signaling has been demonstrated to suppress feedforward inhibition onto principal BLA neurons and facilitate synaptic plasticity in the BLA through activation of both D1 and D2 receptors (Bissière et al., 2003; Marowsky et al., 2005). For more detailed information on how DA regulates activity in the amygdala circuitry, the reader is referred to prior reviews (Abraham et al., 2014; Lee et al., 2017). Pharmacological studies show that blockade of both D1 and D2 receptors in the BLA impairs fear extinction. Notably, DA receptor antagonism in the BLA selectively affects the acquisition, but not consolidation, of fear extinction memories (Hikind and Maroun, 2008; Shi et al., 2017). Whether DA exerts its effects on fear extinction in the BLA through regulation of GABAergic interneurons is a critical question for further research. Furthermore, it will also be important to determine whether and how DA controls the activity of different subtypes of GABAergic interneurons in the BLA during extinction.

While pharmacological studies indicate the important role DA plays in the BLA during fear extinction, exactly how DA modulates extinction-related neuronal activity is not well understood. Research investigating reward learning in the BLA may provide some clues. Indeed, recent studies demonstrate that a genetically distinct and projection-defined subpopulation of BLA neurons mediates reward learning (Namburi et al., 2015; Kim et al., 2016). Intriguingly, supporting the hypothesis that fear extinction is an appetitive learning process, "reward neurons" overlap with "extinction neurons" in the BLA and these two types of neurons are functionally interchangeable (Zhang et al., 2020), suggesting that reward learning and fear extinction are indeed mediated by the same population of neurons in the BLA. Thus, studies investigating the role of DA in BLA during reward learning can provide valuable insights. In keeping with this, a recent study showed that VTA DA terminals in the BLA are activated during reward learning. Specifically, these terminals are activated by rewards and also reward-predicting CSs (Lutas et al., 2019). Whether VTA DA neurons projecting to BLA are also activated by CSs following fear extinction and whether DA input is critical for the CS responsiveness of "extinction neurons" will be key questions to address for future studies (**Figure 1B**).

As mentioned earlier, the second component of the amygdala microcircuitry crucial for fear extinction is the intercalated cell masses (ITCs), which are a network of interconnected GABAergic cell groups located in the external and intermediate capsules surrounding the BLA. Notably, the ITCs located within the intermediate capsule are comprised of the dorsomedial (dmITCs) and ventromedial (vmITCs) clusters where dmITCs exert a unidirectional inhibitory control over vmITCs (Paré et al., 2003; Ehrlich et al., 2009). Mounting evidence indicates that particularly the vmITCs, located between the BLA and the centromedial nucleus of the amygdala (CeM) are necessary for acquisition and expression of fear extinction memories (Jüngling et al., 2008; Likhtik et al., 2008; Amano et al., 2010; Busti et al., 2011). CeM constitutes the main output station of the amygdala necessary for fear expression (Ciocchi et al., 2010); and hence, vmITCs are indeed in an ideal position to suppress the expression of fear responses during fear extinction. They receive excitatory input from BLA and send inhibitory projections to CeM, and thus mediate feedforward inhibition of CeM (Paré et al., 2003; Mańko et al., 2011; Gregoriou et al., 2019). Anatomical studies show that D1 receptors are abundantly expressed in the ITCs (Jacobsen et al., 2006), suggesting an important role for DA in regulating the activity of these neurons. D1 receptors are typically Gs-coupled receptors and when activated they are expected to function in an excitatory fashion (Missale et al., 1998). Interestingly, D1 receptor signaling is unusual in ITCs, that is, DA through activation of D1 receptors hyperpolarizes ITCs and thus inhibits these neurons (Marowsky et al., 2005; Mańko et al., 2011). Furthermore, a recent study shows that the ITCs within the vmITC cluster are likely connected (Gregoriou et al., 2019; but also see Mańko et al., 2011) and activation of D1 receptors inhibits these local connections suggesting a general reduction in the output of the vmITCs (Gregoriou et al., 2019). Together, these studies indicate that dopamine inhibits the activity of ITCs and hence reduces the output of these neurons. Dopamine is therefore anticipated to reduce vmITC mediated feedforward inhibition of CeM. Because vmITCs are expected to be excited during extinction, whether DA plays a role in regulating the activity of vmITCs to mediate fear extinction is questionable. One plausible scenario is that DA might regulate the activity of vmITCs indirectly by inhibiting dmITCs and thereby disinhibiting vmITCs during extinction. According to this scenario, DA neurons are expected to differentially innervate and modulate these two distinct clusters of ITCs (**Figure 1B**). It will therefore be important for future studies to investigate whether and how DA input regulates the activity in distinct ITC clusters during fear extinction.

DOPAMINE IN THE MEDIAL PREFRONTAL CORTEX MEDIATES CONSOLIDATION OF FEAR EXTINCTION MEMORIES

The mPFC, in particular the infra-limbic (IL) subregion of mPFC, is crucial for the consolidation of fear extinction memories (Sotres-Bayon and Quirk, 2010). Since dopaminergic signaling enhances signal-to-noise ratios and modulates synaptic plasticity in the mPFC (Seamans and Yang, 2004; Weele et al., 2019), DA is expected to play a vital role in the formation of extinction memories. Consistent with this, DA levels increase in the mPFC during fear extinction and remain elevated following extinction learning (Hugues et al., 2007). Conversely, selective ablation of mPFC-projecting catecholaminergic neurons has been found to impair retention of extinction (Morrow et al., 1999; Fernandez Espejo, 2003). Supporting these earlier findings, pharmacological studies have further revealed the role of prefrontal DA receptors in fear extinction. Administration of a D4 receptor antagonist in the IL following extinction impairs

extinction retention the next day (Pfeiffer and Fendt, 2006). In addition, studies investigating the role of D1 and D2 receptors have found that inhibition of both D1 and D2 receptors in the IL during extinction learning impairs retention of extinction while acquisition remains intact (Hikind and Maroun, 2008; Mueller et al., 2010). Together, these findings suggest that activation of both D1- and D2-type receptors are required for consolidation, but not acquisition, of fear extinction memories in the IL.

Long-lasting plastic changes in the activity of IL neurons underlie extinction memories (Sotres-Bayon and Quirk, 2010). However, how different DA receptors contribute to the extinction-related changes in IL neurons is not yet well understood. Studies combining pharmacological manipulations with electrophysiology can provide some clues. Notably, IL neurons exhibit increased firing to the CS during retention of extinction (Milad and Quirk, 2002) and administration of a D2 receptor antagonist in the IL has been shown to attenuate these extinction-related CS responses (Mueller et al., 2010). Furthermore, consolidation of extinction memories requires NMDA receptor-dependent burst firing of IL neurons shortly after extinction learning, that is, during the period when memory consolidation takes place (Burgos-Robles et al., 2007). Since activation of D1 receptors enhances neuronal excitability in the mPFC (Seamans and Yang, 2004), activation of these receptors may play a role in the increased burst firing of IL neurons Investigating the effect of D1 receptor antagonists on the extinction-related activity of IL neurons may define the exact role these receptors play during fear extinction. In the mPFC, D1- and D2-type receptors are expressed in both glutamatergic and GABAergic neurons (Vincent et al., 1993; Gaspar et al., 1995; Benes and Berretta, 2001). An important question is therefore how DA modulates activity in the IL microcircuitry to mediate consolidation of extinction memories. Future studies combining DA receptor pharmacology with cell-type-specific recordings of IL neuronal activity during extinction will be essential to address this question.

In line with findings in rodents, a recent study in humans shows that fMRI activity patterns observed in the vmPFC (the human analog of the IL) during extinction learning are reactivated shortly after extinction during memory consolidation and the number of these reactivations predicts extinction memory strength when tested the next day. Importantly, systemic administration of L-DOPA enhances vmPFC reactivations in parallel to improving extinction memory (Gerlicher et al., 2018) suggesting a critical role of DA in this process. Whether the vmPFC activity pattern reactivations in humans are related to burst firing of IL neurons observed in rodents during the consolidation of extinction memories and whether DA receptor activation in the IL/vmPFC mediates these extinction-related neuronal activity patterns in rodents and humans are open questions for further research.

While the studies summarized above highlight the crucial role DA plays in extinction memories, the source of DA release in the mPFC during fear extinction has not yet been identified. Anatomical studies demonstrate that the mPFC-projecting DA neurons are mainly located in the VTA (Lammel et al., 2008; Beier et al., 2015). Yet, the activity patterns of mPFC-projecting VTA DA neurons during consolidation and retrieval of extinction memories have remained elusive (**Figure 1C**). Interestingly, recent studies show that mPFC-projecting DA neurons are involved in encoding aversive events (Lammel et al., 2011, 2012; Vander Weele et al., 2018) and optogenetic activation of VTA DA terminals in the mPFC biases behavior toward aversion (Vander Weele et al., 2018). Further supporting the aversive nature of this DA input, optogenetic inhibition of VTA DA terminals in the IL enhances, rather than impairs, fear extinction (Luo et al., 2018). Together, these studies suggest that VTA DA input to mPFC is pro-aversive and therefore is unlikely to play a role in fear extinction. This raises the question of whether fear extinction is mediated by another source of DA input to mPFC. Supporting this idea, recent studies show that noradrenaline (NA) neurons located in the locus coeruleus (LC), in addition to NA, also co-release DA in the mPFC (Devoto et al., 2020). Furthermore, memory consolidation in the hippocampus is regulated by DA released from the LC, but not VTA, neurons (Kempadoo et al., 2016; Takeuchi et al., 2016). Therefore, the source of DA release in mPFC during fear extinction could be LC NA neurons (**Figure 1C**). Consistent with this possibility, LC projections to mPFC are indeed critical for the consolidation of extinction memories (Uematsu et al., 2017). Identifying the source of DA release in IL during fear extinction is an important outstanding question for further research.

CONCLUDING REMARKS

Considerable progress has been made towards understanding the role DA plays in fear extinction. The studies reviewed above provide insights into how DA mediates different phases of extinction through its actions in the distinct components of the neural circuitry underlying fear extinction. The main conclusions and outstanding questions permitted from these studies are summarized in **Figure 1**. Overall, these findings highlight DA as a key regulator of fear extinction. An important implication of these findings is that enhancing DA signaling during extinction-based exposure therapy can be utilized as a therapeutic strategy in the treatment of anxiety disorders in humans. In line with this, systemic application of L-DOPA following fear extinction enhances extinction memories in humans (Haaker et al., 2013; Gerlicher et al., 2018); however, this enhancement depends on successful extinction learning (Gerlicher et al., 2019) indicating a boundary condition for facilitating the consolidation of extinction memories. Notably, in a genetic mouse strain with deficient extinction, systemic L-DOPA administration before extinction enhances extinction learning and memory (Whittle et al., 2016). Whether pre-extinction administration of L-DOPA can facilitate extinction learning in humans with deficient fear extinction and resistance to exposure therapy will be essential to investigate. Nevertheless, it is important to emphasize that DA is also a crucial mediator of fear learning and memory as well as aversive processing (Abraham et al., 2014; Lee et al., 2017; Likhtik and Johansen, 2019; Weele et al., 2019; Verharen et al., 2020), and hence systemic administration of pharmacological agents that enhance DA signaling globally in the brain can influence aversive processing and the strength of fear memories, as well. Caution

is therefore required when systemically enhancing DA signaling. The development of more specific therapeutic approaches in the treatment of anxiety disorders would benefit from a deeper circuit-level understanding of how DA regulates different phases of fear extinction in distinct brain circuits.

AUTHOR CONTRIBUTIONS

XS-H and SD wrote the manuscript. All authors contributed to the article and approved the submitted version.

REFERENCES

Abraham, A. D., Neve, K. A., and Lattal, K. M. (2014). Dopamine and extinction: a convergence of theory with fear and reward circuitry. *Neurobiol. Learn. Mem.* 108, 65–77. doi: 10.1016/j.nlm.2013.11.007

Abraham, A. D., Neve, K. A., and Lattal, K. M. (2016). Activation of D1/5 dopamine receptors: a common mechanism for enhancing extinction of fear and reward-seeking behaviors. *Neuropsychopharmacology* 41, 2072–2081. doi: 10.1038/npp.2016.5

Amano, T., Duvarci, S., Popa, D., and Paré, D. (2011). The fear circuit revisited: contributions of the basal amygdala nuclei to conditioned fear. *J. Neurosci.* 31, 15481–15489. doi: 10.1523/JNEUROSCI.3410-11.2011

Amano, T., Unal, C. T., and Paré, D. (2010). Synaptic correlates of fear extinction in the amygdala. *Nat. Neurosci.* 13, 489–494. doi: 10.1038/nn.2499.

Badrinarayan, A., Wescott, S. A., Vander Weele, C. M., Saunders, B. T., Couturier, B. E., Maren, S., et al. (2012). Aversive stimuli differentially modulate real-time dopamine transmission dynamics within the nucleus accumbens core and shell. *J. Neurosci.* 32, 15779–15790. doi: 10.1523/JNEUROSCI.3557-12.2012

Beier, K. T., Steinberg, E. E., DeLoach, K. E., Xie, S., Miyamichi, K., Schwarz, L., et al. (2015). Circuit architecture of VTA dopamine neurons revealed by systemic input-output mapping. *Cell* 162, 622–634. doi: 10.1016/j.cell.2015.07.015

Benes, F. M., and Berretta, S. (2001). GABAergic interneurons: implications for understanding schizophrenia and bipolar disorder. *Neuropsychopharmacology* 25, 1–27. doi: 10.1016/S0893-133X(01)00225-1

Bissière, S., Humeau, Y., and Lüthi, A. (2003). Dopamine gates LTP induction in lateral amygdala by suppressing feedforward inhibition. *Nat. Neurosci.* 6, 587–592. doi: 10.1038/nn1058

Bouton, M. E., Westbrook, R. F., Corcoran, K. A., and Maren, S. (2006). Contextual and temporal modulation of extinction: behavioral and biological mechanisms. *Biol. Psychiatry* 60, 352–360. doi: 10.1016/j.biopsych.2005.12.015

Burgos-Robles, A., Vidal-Gonzalez, I., Santini, E., and Quirk, G. J. (2007). Consolidation of fear extinction requires NMDA receptor-dependent bursting in the ventromedial prefrontal cortex. *Neuron* 53, 871–880. doi: 10.1016/j.neuron.2007.02.021

Busti, D., Geracitano, R., Whittle, N., Dalezios, Y., Manko, M., Kaufmann, W., et al. (2011). Different fear states engage distinct networks within the intercalated cell clusters of the amygdala. *J. Neurosci.* 31, 5131–5144. doi: 10.1523/JNEUROSCI.6100-10.2011

Cai, L. X., Pizano, K., Gundersen, G. W., Hayes, C. L., Fleming, W. T., Holt, S., et al. (2020). Distinct signals in the medial and lateral VTA dopamine neurons modulate fear extinction at different times. *eLife* 9:e54936. doi: 10.7554/eLife.54936

Chhatwal, J. P., Myers, K. M., Ressler, K. J., and Davis, M. (2005). Regulation of gephyrin and GABAA receptor binding within the amygdala after fear acquisition and extinction. *J. Neurosci.* 25, 502–506. doi: 10.1523/JNEUROSCI.3301-04.2005

Ciocchi, S., Herry, C., Grenier, F., Wolff, S. B., Letzkus, J. J., Vlachos, I., et al. (2010). Encoding of conditioned fear in central amygdala inhibitory circuits. *Nature* 468, 277–282. doi: 10.1038/nature09559

FUNDING

This work was supported by the Deutsche Forschung sgemeinschaft [DFG SFB1193 Grants INST247/852-1 and INST 247/858-1 (subprojects B01 and C02) to SD].

ACKNOWLEDGMENTS

We would like to thank Torfi Sigurdsson for helpful discussions and comments on the manuscript.

Craske, M. G., Stein, M. B., Eley, T. C., Milad, M. R., Holmes, A., Rapee, R. M., et al. (2017). Anxiety disorders. *Nat. Rev. Dis. Primers* 3:17024. doi: 10.1038/nrdp.2017.24

Devoto, P., Sagheddu, C., Santoni, M., Flore, G., Saba, P., Pistis, M., et al. (2020). Noradrenergic source of dopamine assessed by microdialysis in the medial prefrontal cortex. *Front. Pharmacol.* 11:588160. doi: 10.3389/fphar.2020.588160

Duvarci, S., and Pare, D. (2014). Amygdala microcircuits controlling learned fear. *Neuron* 82, 966–980. doi: 10.1016/j.neuron.2014.04.042

Ehrlich, I., Humeau, Y., Grenier, F., Ciocchi, S., Herry, C., and Lüthi, A. (2009). Amygdala inhibitory circuits and the control of fear memory. *Neuron* 62, 757–771. doi: 10.1016/j.neuron.2009.05.026

Felsenberg, J., Jacob, P. F., Walker, T., Barnstedt, O., Edmondson-Stait, A. J., Pleijzier, M. W., et al. (2018). Integration of parallel opposing memories underlies memory extinction. *Cell* 175, 709.e15–722.e15. doi: 10.1016/j.cell.2018.08.021

Fernandez Espejo, E. (2003). Prefrontocortical dopamine loss in rats delays long-term extinction of contextual conditioned fear and reduces social interaction without affecting short-term social interaction memory. *Neuropsychopharmacology* 28, 490–498. doi: 10.1038/sj.npp.1300066

Gaspar, P., Bloch, B., and Le Moine, C. (1995). D1 and D2 receptor gene expression in the rat frontal cortex: cellular localization in different classes of efferent neurons. *Eur. J. Neurosci.* 7, 1050–1063. doi: 10.1111/j.1460-9568.1995.tb01092.x

Gerlicher, A. M. V., Tüscher, O., and Kalisch, R. (2018). Dopamine-dependent prefrontal reactivations explain long-term benefit of fear extinction. *Nat. Commun.* 9:4294. doi: 10.1038/s41467-018-06785-y

Gerlicher, A. M. V., Tüscher, O., and Kalisch, R. (2019). L-DOPA improves extinction memory retrieval after successful fear extinction. *Psychopharmacology* 36, 3401–3412. doi: 10.1007/s00213-019-05301-4

Graham, B. M., and Milad, M. R. (2011). The study of fear extinction: implications for anxiety disorders. *Am. J. Psychiatry* 168, 1255–1265. doi: 10.1176/appi.ajp.2011.11040557

Gregoriou, G. C., Kissiwaa, S. A., Patel, S. D., and Bagley, E. E. (2019). Dopamine and opioids inhibit synaptic outputs of the main island of the intercalated neurons of the amygdala. *Eur. J. Neurosci.* 50, 2065–2074. doi: 10.1111/ejn.14107

Haaker, J., Gaburro, S., Sah, A., Gartmann, N., Lonsdorf, T. B., Meier, K., et al. (2013). Single dose of L-dopa makes extinction memories context-independent and prevents the return of fear. *Proc. Natl. Acad. Sci. U S A* 110, E2428–E2436. doi: 10.1073/pnas.1303061110

Heldt, S. A., and Ressler, K. J. (2007). Training-induced changes in the expression of GABAA-associated genes in the amygdala after the acquisition and extinction of pavlovian fear. *Eur. J. Neurosci.* 26, 3631–3644. doi: 10.1111/j.1460-9568.2007.05970.x

Herry, C., Ciocchi, S., Senn, V., Demmou, L., Müller, C., and Lüthi, A. (2008). Switching on and off fear by distinct neuronal circuits. *Nature* 454, 600–606. doi: 10.1038/nature07166

Herry, C., Ferraguti, F., Singewald, N., Letzkus, J. J., Ehrlich, I., and Lüthi, A. (2010). Neuronal circuits of fear extinction. *Eur. J. Neurosci.* 31, 599–612. doi: 10.1111/j.1460-9568.2010.07101.x

Hikind, N., and Maroun, M. (2008). Microinfusion of the D1 receptor antagonist, SCH23390 into the IL but not the BLA impairs consolidation of extinction of

auditory fear conditioning. *Neurobiol. Learn. Mem.* 90, 217–222. doi: 10.1016/j.nlm.2008.03.003

Holtzman-Assif, O., Laurent, V., and Westbrook, R. F. (2010). Blockade of dopamine activity in the nucleus accumbens impairs learning extinction of conditioned fear. *Learn. Mem.* 17, 71–75. doi: 10.1101/lm.1668310

Hugues, S., Garcia, R., and Léna, I. (2007). Time course of extracellular catecholamine and glutamate levels in the rat medial prefrontal cortex during and after extinction of conditioned fear. *Synapse* 61, 933–937. doi: 10.1002/syn.20448

Jacobsen, K. X., Höistad, M., Staines, W. A., and Fuxe, K. (2006). The distribution of dopamine D1 receptor and mu-opioid receptor 1 receptor immunoreactivities in the amygdala and interstitial nucleus of the posterior limb of the anterior commissure: relationships to tyrosine hydroxylase and opioid peptide terminal systems. *Neuroscience* 141, 2007–2018. doi: 10.1016/j.neuroscience.2006.05.054

Josselyn, S. A., and Frankland, P. W. (2018). Fear extinction requires reward. *Cell* 175, 639–640. doi: 10.1016/j.cell.2018.09.036

Jüngling, K., Seidenbecher, T., Sosulina, L., Lesting, J., Sangha, S., Clark, S. D., et al. (2008). Neuropeptide S-mediated control of fear expression and extinction: role of intercalated GABAergic neurons in the amygdala. *Neuron* 59, 298–310. doi: 10.1016/j.neuron.2008.07.002

Kalisch, R., Gerlicher, A. M. V., and Duvarci, S. (2019). A dopaminergic basis for fear extinction. *Trends Cogn. Sci.* 23, 274–277. doi: 10.1016/j.tics.2019.01.013

Kasugai, Y., Vogel, E., Hörtnagl, H., Schönherr, S., Paradiso, E., Hauschild, M., et al. (2019). Structural and functional remodeling of amygdala gabaergic synapses in associative fear learning. *Neuron* 104, 781.e4–794.e4. doi: 10.1016/j.neuron.2019.08.013

Kempadoo, K. A., Mosharov, E. V., Choi, S. J., Sulzer, D., and Kandel, E. R. (2016). Dopamine release from the locus coerulous to the dorsal hippocampus promotes spatial learning and memory. *Proc. Natl. Acad. Sci. U S A* 113, 14835–14840. doi: 10.1073/pnas.1616515114

Kim, J., Pignatelli, M., Xu, S., Itohara, S., and Tonegawa, S. (2016). Antagonistic positive and negative neurons of the basolateral amygdala. *Nat. Neurosci.* 19, 1636–1646. doi: 10.1038/nn.4414

Krabbe, S., Gründemann, J., and Lüthi, A. (2018). Amygdala inhibitory circuits regulate associative fear conditioning. *Biol. Psychiatry* 83, 800–809. doi: 10.1016/j.biopsych.2017.10.006

Lammel, S., Hetzel, A., Häckel, O., Jones, I., Liss, B., and Roeper, J. (2008). Unique properties of mesoprefrontal neurons within a dual mesocorticolimbic dopamine system. *Neuron* 57, 760–773. doi: 10.1016/j.neuron.2008.01.022

Lammel, S., Ion, D. I., Roeper, J., and Malenka, R. C. (2011). Projection-specific modulation of dopamine neuron synapses by aversive and rewarding stimuli. *Neuron* 70, 855–862. doi: 10.1016/j.neuron.2011.03.025

Lammel, S., Lim, B. K., Ran, C., Huang, K. W., Betley, M. J., Tye, K. M., et al. (2012). Input-specific control of reward and aversion in the ventral tegmental area. *Nature* 491, 212–217. doi: 10.1038/nature11527

Lee, J. H., Lee, S., and Kim, J.-H. (2017). Amygdala circuits for fear memory: a key role for dopamine regulation. *Neuroscientist* 23, 542–553. doi: 10.1177/1073858416679936

Likhtik, E., and Johansen, J. P. (2019). Neuromodulation in circuits of aversive emotional learning. *Nat. Neurosci.* 22, 1586–1597. doi: 10.1038/s41593-019-0503-3

Likhtik, E., Popa, D., Apergis-Schoute, J., Fidacaro, G. A., and Paré, D. (2008). Amygdala intercalated neurons are required for expression of fear extinction. *Nature* 454, 642–645. doi: 10.1038/nature07167

Luo, R., Uematsu, A., Weitemier, A., Aquili, L., Koivumaa, J., McHugh, T. J., et al. (2018). A dopaminergic switch for fear to safety transitions. *Nat. Commun.* 9:2483. doi: 10.1038/s41467-018-04784-7

Lutas, A., Kucukdereli, H., Alturkistani, O., Carty, C., Sugden, A. U., Fernando, K., et al. (2019). State-specific gating of salient cues by midbrain dopaminergic input to basal amygdala. *Nat. Neurosci.* 22, 1820–1833. doi: 10.1038/s41593-019-0506-0

Mańko, M., Geracitano, R., and Capogna, M. (2011). Functional connectivity of the main intercalated nucleus of the amygdala. *J. Physiol.* 15, 1911–1925. doi: 10.1113/jphysiol.2010.201475

Maren, S., Phan, K. L., and Liberzon, I. (2013). The contextual brain: implications for fear conditioning, extinction and psychopathology. *Nat. Rev. Neurosci.* 14, 417–428. doi: 10.1038/nrn3492

Marowsky, A., Yanagawa, Y., Obata, K., and Vogt, K. E. (2005). A specialized subclass of interneurons mediates dopaminergic facilitation of amygdala function. *Neuron* 48, 1025–1037. doi: 10.1016/j.neuron.2005.10.029

Marsicano, G., Wotjak, C. T., Azad, S. C., Bisogno, T., Rammes, G., Cascio, M. G., et al. (2002). The endogenous cannabinoid system controls extinction of aversive memories. *Nature* 418, 530–534. doi: 10.1038/nature00839

Milad, M. R., and Quirk, G. J. (2002). Neurons in medial prefrontal cortex signal memory for fear extinction. *Nature* 420, 70–74. doi: 10.1038/nature01138

Missale, C., Nash, S. R., Robinson, S. W., Jaber, M., and Caron, M. G. (1998). Dopamine receptors: from structure to function. *Physiol. Rev.* 78, 189–225. doi: 10.1152/physrev.1998.78.1.189

Morrow, B. A., Elsworth, J. D., Rasmusson, A. M., and Roth, R. H. (1999). The role of mesoprefrontal dopamine neurons in the acquisition and expression of conditioned fear in the rat. *Neuroscience* 92, 553–564. doi: 10.1016/s0306-4522(99)00014-7

Mueller, D., Bravo-Rivera, C., and Quirk, G. J. (2010). Infralimbic D2 receptors are necessary for fear extinction and extinction-related tone responses. *Biol. Psychiatry* 68, 1055–1060. doi: 10.1016/j.biopsych.2010.08.014

Myers, K. M., and Davis, M. (2007). Mechanisms of fear extinction. *Mol. Psychiatry* 12, 120–150. doi: 10.1038/sj.mp.4001939

Namburi, P., Beyeler, A., Yorozu, S., Calhoon, G. G., Halbert, S. A., Wichmann, R., et al. (2015). A circuit mechanism for differentiating positive and negative associations. *Nature* 520, 675–678. doi: 10.1038/nature14366

Pape, H.-C., and Pare, D. (2010). Plastic synaptic networks of the amygdala for the acquisition, expression and extinction of conditioned fear. *Physiol. Rev.* 90, 419–463. doi: 10.1152/physrev.00037.2009

Paré, D., Royer, S., Smith, Y., and Lang, E. J. (2003). Contextual inhibitory gating of impulse traffic in the intra-amygdaloid network. *Ann. N. Y. Acad. Sci.* 985, 78–91. doi: 10.1111/j.1749-6632.2003.tb07073.x

Pfeiffer, U. J., and Fendt, M. (2006). Prefrontal dopamine D4 receptors are involved in encoding fear extinction. *Neuroreport* 17, 847–850. doi: 10.1097/01.wnr.0000220142.29413.6f

Pitman, R. K., Rasmusson, A. M., Koenen, K. C., Shin, L. M., Orr, S. P., Gilbertson, M. W., et al. (2012). Biological studies of post-traumatic stress disorder. *Nat. Rev. Neurosci.* 13, 769–787. doi: 10.1038/nrn3339

Raczka, K. A., Mechias, M.-L., Gartmann, N., Reif, A., Deckert, J., Pessiglione, M., et al. (2011). Empirical support for an involvement of the mesostriatal dopamine system in human fear extinction. *Transl. Psychiatry* 1:e12. doi: 10.1038/tp.2011.10

Rescorla, R. A., and Wagner, A. R. (1972). "A theory of pavlovian conditioning: variations in the effectiveness of reinforcement and nonreinforcement," in *Classical Conditioning II: Current Research and Theory*, eds A. H. Black and W. F. Prokasy (New York, NY: Appleton Century Crofts), 64–99.

Salinas-Hernández, X. I., Vogel, P., Betz, S., Kalisch, R., Sigurdsson, T., and Duvarci, S. (2018). Dopamine neurons drive fear extinction learning by signaling the omission of expected aversive outcomes. *eLife* 7:e38818. doi: 10.7554/eLife.38818

Sangha, S., Narayanan, R. T., Bergado-Acosta, J. R., Stork, O., Seidenbecher, T., and Pape, H. C. (2009). Deficiency of the 65 kDa isoform of glutamic acid decarboxylase impairs extinction of cued but not contextual fear memory. *J. Neurosci.* 29, 15713–15720. doi: 10.1523/JNEUROSCI.2620-09.2009

Schultz, W. (2006). Dopamine reward prediction-error signaling: a two component response. *Nat. Rev. Neurosci.* 17, 183–195. doi: 10.1038/nrn.2015.26

Seamans, J. K., and Yang, C. R. (2004). The principal features and mechanisms of dopamine modulation in the prefrontal cortex. *Prog. Neurobiol.* 74, 1–58. doi: 10.1016/j.pneurobio.2004.05.006

Shi, Y.-W., Fan, B.-F., Xue, L., Wen, J.-L., and Zhao, H. (2017). Regulation of fear extinction in the basolateral amygdala by dopamine D2 receptors accompanied by altered GluR1, GluR1-Ser845 and NR2B levels. *Front. Behav. Neurosci.* 11:116. doi: 10.3389/fnbeh.2017.00116

Sierra-Mercado, D., Padilla-Coreano, N., and Quirk, G. J. (2011). Dissociable roles of prelimbic and infralimbic cortices, ventral hippocampus and basolateral amygdala in the expression and extinction of conditioned

fear. *Neuropsychopharmacology* 36, 529–538. doi: 10.1038/npp.2010.184

Sotres-Bayon, F., and Quirk, G. J. (2010). Prefrontal control of fear: more than just extinction. *Curr. Opin. Neurobiol.* 20, 231–235. doi: 10.1016/j.conb.2010.02.005

Takeuchi, T., Duszkiewicz, A. J., Sonneborn, A., Spooner, P. A., Yamasaki, M., Watanabe, M., et al. (2016). Locus coeruleus and dopaminergic consolidation of everyday memory. *Nature* 537, 357–362. doi: 10.1038/nature19325

Tovote, P., Fadok, J. P., and Lüthi, A. (2015). Neuronal circuits for fear and anxiety. *Nat. Rev. Neurosci.* 16, 317–331. doi: 10.1038/nrn3945

Uematsu, A., Tan, B. Z., Ycu, E. A., Cuevas, J. S., Koivumaa, J., Junyent, F., et al. (2017). Modular organization of the brainstem noradrenalin system coordinates opposing learning states. *Nat. Neurosci.* 20, 1602–1611. doi: 10.1038/nn.4642

Vander Weele, C. M., Siciliano, C. A., Matthews, G. A., Namburi, P., Izadmehr, E. M., Espinel, I. C., et al. (2018). Dopamine enhances signal-to-noise ratioin cortical-brainstem encoding of aversive stimuli. *Nature* 563, 397–401. doi: 10.1038/s41586-018-0682-1

Verharen, J. P. H., Zhu, Y., and Lammel, S. (2020). Aversion hot spots in the dopamine system. *Curr. Opin. Neurobiol.* 64, 46–52. doi: 10.1016/j.conb.2020.02.002

Vincent, S. L., Khan, Y., and Benes, F. M. (1993). Cellular distribution of dopamine D1 and D2 receptors in rat medial prefrontal cortex. *J. Neurosci.* 13, 2551–2564. doi: 10.1523/JNEUROSCI.13-06-02551.1993

Weele, C. M. V., Siciliano, C. A., and Tye, K. M. (2019). Dopamine tunes prefrontal outputs to orchestrate aversive processing. *Brain Res.* 1713, 16–31. doi: 10.1016/j.brainres.2018.11.044

Whittle, N., Maurer, V., Murphy, C., Rainer, J., Bindreither, D., Hauschild, M., et al. (2016). Enhancing dopaminergic signaling and histone acetylation promotes long-term rescue of deficient fear extinction. *Transl. Psychiatry* 6:e974. doi: 10.1038/tp.2016.231

Wise, R. A. (2002). Brain reward circuitry: insights from unsensed incentives. *Neuron* 36, 229–240. doi: 10.1016/s0896-6273(02)00965-0

Zhang, X., Kim, J., and Tonegawa, S. (2020). Amygdala reward neurons form and store fear extinction memory. *Neuron* 105, 1077.e7–1093.e7. doi: 10.1016/j.neuron.2019.12.025

Conflict of Interest: The authors declare that the research was conducted in the absence of any commercial or financial relationships that could be construed as a potential conflict of interest.

Copyright © 2021 Salinas-Hernández and Duvarci. This is an open-access article distributed under the terms of the Creative Commons Attribution License (CC BY). The use, distribution or reproduction in other forums is permitted, provided the original author(s) and the copyright owner(s) are credited and that the original publication in this journal is cited, in accordance with accepted academic practice. No use, distribution or reproduction is permitted which does not comply with these terms.

frontiers in Synaptic Neuroscience

REVIEW
published: 03 March 2021
doi: 10.3389/fnsyn.2021.634760

Voltage-Gated Ca^{2+}-Channel α1-Subunit *de novo* Missense Mutations: Gain or Loss of Function – Implications for Potential Therapies

*Jörg Striessnig**

Department of Pharmacology and Toxicology, Institute of Pharmacy, Center for Molecular Biosciences Innsbruck, University of Innsbruck, Innsbruck, Austria

This review summarizes our current knowledge of human disease-relevant genetic variants within the family of voltage gated Ca^{2+} channels. Ca^{2+} channelopathies cover a wide spectrum of diseases including epilepsies, autism spectrum disorders, intellectual disabilities, developmental delay, cerebellar ataxias and degeneration, severe cardiac arrhythmias, sudden cardiac death, eye disease and endocrine disorders such as congential hyperinsulinism and hyperaldosteronism. A special focus will be on the rapidly increasing number of *de novo* missense mutations identified in the pore-forming α1-subunits with next generation sequencing studies of well-defined patient cohorts. In contrast to likely gene disrupting mutations these can not only cause a channel loss-of-function but can also induce typical functional changes permitting enhanced channel activity and Ca^{2+} signaling. Such gain-of-function mutations could represent therapeutic targets for mutation-specific therapy of Ca^{2+}-channelopathies with existing or novel Ca^{2+}-channel inhibitors. Moreover, many pathogenic mutations affect positive charges in the voltage sensors with the potential to form gating-pore currents through voltage sensors. If confirmed in functional studies, specific blockers of gating-pore currents could also be of therapeutic interest.

Keywords: calcium-channels, channelopathies, mutations, neurodevelopmental disorders, gating pore currents

OPEN ACCESS

Edited by:
Filippo Tempia,
University of Turin, Italy

Reviewed by:
Norbert Weiss,
Charles University, Czechia
Dimitri M. Kullmann,
University College London,
United Kingdom

***Correspondence:**
Jörg Striessnig
joerg.striessnig@uibk.ac.at

Received: *28 November 2020*
Accepted: *02 February 2021*
Published: *03 March 2021*

Citation:
Striessnig J (2021) Voltage-Gated Ca^{2+}-Channel α1-Subunit de novo Missense Mutations: Gain or Loss of Function – Implications for Potential Therapies. Front. Synaptic Neurosci. 13:634760. doi: 10.3389/fnsyn.2021.634760

INTRODUCTION

Decreasing cost for next-generation sequencing (NGS) has allowed to diagnose pathogenic mutations in an increasing number of patients affected by genetic diseases. Genome-wide association studies mainly identify disease-associated common genetic variants, which explain only a very small proportion of overall phenotypic variance. In contrast, trio-based whole-exome or whole-genome sequencing genetic studies in well-phenotyped patient cohorts can detect rare, recurrent damaging variants of large effect size that can account for most phenotypic variance and can be considered causative (Sullivan and Geschwind, 2019). Such variants explain a wide variety of symptoms, especially in early-onset sporadic pediatric genetic disorders (Consortium et al., 2013; Allen et al., 2017; Satterstrom et al., 2020). This informs not only diagnosis and genetic counseling, but can also refine a patients' prognosis, initiate surveillance for other symptoms in multisystem disorders and guide therapeutic decision-making (Helbig et al., 2016; Weber et al., 2017; Noebels, 2019). In addition, the identification of multiple risk genes within defined signaling networks provides valuable novel insight into dysregulated molecular pathways underlying a pathology.

Disorders that have strongly benefited from NGS – based genetic diagnostics are neuropsychiatric and neurodevelopmental disorders, including epilepsies, in particular childhood epilepsies, autism spectrum disorders (ASD), and intellectual disability (ID) with a large collective contribution of rare, large-effect pathogenic variants (Allen et al., 2017; Howard and Baraban, 2017; Weber et al., 2017; Myers et al., 2020; Satterstrom et al., 2020). Rare large-effect variants in the same gene may not be specific for one of these disorders (e.g., ASD, Myers et al., 2020) and other sources of genetic variation, such as polygenic risk from common variants or genetic mosaicism, as well as environmental factors can affect phenotypic expression. Whereas the significance of a novel *de novo* mutation identified only in a single individual is difficult to interpret, the identification of a *recurrent* pathogenic variant strongly supports a large genetic contribution to the phenotype in an individual within this disease spectrum. In some cases, this can even guide therapies either with new drugs or by repurposing drugs already licensed for other indications. Although often experimental in nature and mainly symptomatic, such individualized therapies can enhance the quality of life for affected individuals and their caregivers. For example, everolimus has been repurposed for the treatment of Tuberosclerosis TSC1 and TSC2 (Krueger et al., 2016; Samueli et al., 2016), and 5-hydroxytryptophan is used to treat patients with DOPA-responsive dystonia (DRD, OMIM #128230) caused by Sepiapterin Reductase Deficiency (Bainbridge et al., 2011). Among patients with epilepsy referred to diagnostic whole exome sequencing the diagnostic yield of characterized disease genes is > 30% (Helbig et al., 2016; Symonds and McTague, 2020) and genetic diagnosis has significant impact on patient management, such as choosing or avoiding certain antiepileptic medications (Symonds and McTague, 2020).

Some rare disease phenotypes are associated with only a single or a few defective genes (like TSC or DRD). More common, pathophysiologically more complex, and clinically often overlapping phenotypes such as ASD, childhood epilepsies, ID or cardiac arrhythmias are associated with a larger number of risk genes (e.g., over 100 in ASD and more than 650 in ID; Kochinke et al., 2016; Satterstrom et al., 2020). However, most of them account only for a very small fraction of affected individuals. This increases the probability that a new sporadic variant of unknown pathogenicity is found in one of these genes. In the case of *de novo* mutations (DNMs, newly formed during gamete development or very early in embryonic development, not inherited from the parents), bioinformatics pipelines can help to separate likely disease - causing from other variants. This involves eliminating variants exceeding a defined allele frequency in likely unaffected control populations as, for example, available in the gnomAD database (Karczewski et al., 2020). Validated DNMs can then be classified according to the predicted impact of the genetic variation on gene and protein function. A protein loss of function (pLOF) can reliably be predicted from *de novo* deleterious, likely gene-disrupting mutations, such as nonsense, stop gain, splice site or frameshift variants. In contrast, *missense* DNMs change the amino acid composition of a protein but usually do not prevent its complete translation. Therefore, their functional consequences are more difficult to predict: they can be functionally silent, induce a decrease (**loss-of-function, LOF**) or an increase (**gain-of-function, GOF**) of protein function. On average each offspring harbors at least one *de novo* protein – coding missense variant (Gratten et al., 2013; Krumm et al., 2015). Therefore, in diseases with many risk genes (see above) the probability of observing a new missense DNM in one of them by chance is high but its pathogenicity remains often unclear, even if present in a known high risk gene. Therefore, standards and guidelines for the interpretation of sequence variants have been developed by the American College of Medical Genetics (ACMG, Richards et al., 2015) to classify variants according to their predicted pathogenicity ("pathogenic", "likely pathogenic", "uncertain significance", "likely benign", and "benign"). Ideally, functional assays are available to test for GOF or LOF changes, which can support classification as is the case for voltage-gated Ca^{2+}-channel (Cavs, see section "Functional Analysis of Protein-Coding Missense Variants").

This review summarizes our current knowledge of disease-relevant genetic variants within the family of voltage gated Ca^{2+}-channels. A special focus will be on missense DNMs in their pore-forming α1-subunits, which are increasingly reported in NGS studies and can help to explain sporadic cases of Ca^{2+}-channel-associated pathologies. These include epilepsies, ASD, ID, developmental delay, cerebellar ataxias, severe cardiac arrhythmias, sudden cardiac death and endocrine disorders such as congential hyperinsulinism and hyperaldosteronism. Since potential personalized therapeutic approaches depend on whether a missense DNM induces a loss- or gain of channel function, we will discuss the complex question of how altered gating of these ion channels can translate into such functional changes.

First, this review provides a brief overview about the ten members of the Cav-channel family and highlights the most common macroscopic gating changes induced by single amino acid substitutions. Finally, the spectrum of variants known to cause Ca^{2+}-channelopathies is described. Since the protein structures of the pore-forming Ca^{2+}-channel α1-subunits are highly conserved (Wu et al., 2016; Zhao et al., 2019a,b; Catterall et al., 2020), we will also discuss if the location and functional effects in one of the Cav family members can help to predict pathogenicity of a novel variant in another Cav. This could refine predictions based on the ACMG guidelines and thus help in genetic counseling.

THE VOLTAGE-GATED CA^{2+}-CHANNEL FAMILY

Excellent reviews have recently been published on this topic (Zamponi et al., 2015; Catterall et al., 2020; Dolphin and Lee, 2020; Ablinger et al., 2020) and valuable detailed information on the physiology, tissue distribution and pharmacology of these channels can be found in the NC-IUPHAR Guide to Pharmacology[1] (Alexander et al., 2019).

[1] www.guidetopharmacology.org

Cavs are found in all electrically excitable cells. Voltage-dependent Ca^{2+} influx through Cavs serves a dual function in cell signaling. It generates intracellular Ca^{2+} signals controlling Ca^{2+}-dependent cellular processes. In addition, Ca^{2+} ion inward current also drives membrane depolarization and thus directly contributes to a cell's electrical activity (Zamponi et al., 2015). Consequently, Cavs are essential for key physiological functions, such as learning and memory, neurotransmitter and hormone release, muscle contraction, cardiac pacemaking and sensory functions, including hearing and visual function (Zamponi et al., 2015; Nanou and Catterall, 2018; Pangrsic et al., 2018). Ten types of Cavs are formed by different pore-forming α1-subunits (**Figure 1**), each encoded by a separate gene (Zamponi et al., 2015; Alexander et al., 2019) (**Table 1**). Differences in their biophysical properties, tissue expression, subcellular targeting, association with other interacting proteins in signalosomes and in their modulation by other signaling pathways generates the functional diversity required for the many physiological functions they support (Zamponi et al., 2015; Nanou and Catterall, 2018; Liu et al., 2020). Extensive alternative splicing and association with various modulatory accessory subunits (β1-β4, α2δ1-α2δ4), posttranslational modifications and RNA-editing (Huang et al., 2012; Zamponi et al., 2015; Li et al., 2017; Loh et al., 2020) further fine-tunes their biophysical and pharmacological properties (Buraei and Yang, 2010; Zamponi et al., 2015; Ablinger et al., 2020). This requirement for tight functional control explains why even minor changes in the activity of these channels induced by genetic variants can cause human disease.

Based on sequence homology between their pore-forming α1-subunits (**Figure 1**) as well as their functional and pharmacological properties, three Cav families are distinguished: Cav1, Cav2 and Cav3 (**Table 1**; Alexander et al., 2019).

Cav1.1-Cav1.4 α1- subunits form the family of **L-type** Ca^{2+}-channels (Cav1). They have unique sensitivity to low nanomolar concentrations of dihydropyridine (DHP) Ca^{2+}-channel blockers (Alexander et al., 2019; **Table 1**). Cav1.2 and Cav1.3 are expressed, often together, in most electrically excitable cells (Zamponi et al., 2015). In contrast, Cav1.1 and Cav1.4 expression and function is largely restricted to skeletal muscle (Cav1.1) and the retina (Cav1.4). Cav1.2 controls cardiac inotropy and arterial vascular tone (Zamponi et al., 2015). It is the main therapeutic target for Ca^{2+}-channel blockers (such as amlodipine, felodipine), which are approved since decades for the treatment of angina and hypertension (Striessnig and Ortner, 2020). Cav1.3 activates at more negative voltages than Cav1.2 (Koschak et al., 2001; Zamponi et al., 2015). Therefore it serves as a pacemaker channel in the sinoatrial and AV-node (Marger et al., 2014) and is essential for cochlear inner hair cell function and hearing (Zamponi et al., 2015). Cav1.2 and Cav1.3 are both present in central neurons, predominantly postsynaptically at dendritic spines. Both channels control the short- and long-term regulation of neuronal activity in several brain circuits, and contribute to different types of learning, memory and emotional behaviors (Zamponi et al., 2015; Kabir et al., 2017; Nanou and Catterall, 2018).

Members of the Cav2 family (Cav2.1-Cav2.3, giving rise to **P/Q-, N- and R-type** voltage-gated Ca^{2+} currents) are also located at pre-synaptic active zones and support fast neurotransmitter release in neurons. Together with L-type channels they also trigger hormone release in endocrine cells (Zamponi et al., 2015).

Low-voltage activated Cav3 channels (Cav3.1-Cav3.3) comprise the family of **T-type** Ca^{2+}-channels. They activate and inactivate at more negative membrane potentials than Cav1 (including Cav1.3) and Cav2 (Perez-Reyes and Lory, 2006; Zamponi et al., 2015). This negative operation range allows them to be active at subthreshold voltages, and provides them with a prominent role for integration and control of neuronal firing patterns (Kim et al., 2001; Zamponi et al., 2015).

Recently, the cryo-EM structures of the pore-forming α1-subunits of two members of the Cav family have been solved in complex with selective channel blockers: Cav1.1 (Wu et al., 2016; Zhao et al., 2019b; Gao and Yan, 2020) and the evolutionary more distantly related Cav3.1 (Zhao et al., 2019a) channel. Together with previous work on related channels (Catterall et al., 2020), these structures provide exciting new information about the molecular details involved in voltage-sensing, channel gating (**Figures 1C,D**, based on the cryo-EM structure of Cav1.1; Wu et al., 2016) and ion permeation as well as isoform-specific functional and pharmacological differences. As will be discussed below, these common structural features can be instrumental for predicting functional consequences of disease-causing mutations across different α1-subunits.

GAIN- AND LOSS- OF CA^{2+} -CHANNEL FUNCTION INDUCED BY MISSENSE MUTATIONS

For proper function and subcellular targeting Cav1 and Cav2 channels require association with one of four different β- and one of four different α2δ-subunits (**Figure 1A**; Buraei and Yang, 2010; Zamponi et al., 2015; Ablinger et al., 2020). Therefore, genetic variants in any of these accessory subunits can indirectly affect channel function. Signaling changes resulting from genetic variation in these subunits are mechanistically more complex to interpret, because any of the four different β- and of the four different α2δ isoforms may associate with the different Cav1 and Cav2 α1- subunits in a given cell (such as a neuron). Moreover, these subunits also appear to serve functions independent of Cavs (Hofmann et al., 2015; Dolphin, 2018; Striessnig, 2018). This review therefore exclusively focuses on channelopathies resulting from genetic variants in the pore forming α1-subunit genes. These can be directly related to the known physiological functions of a particular channel type and thus provide more specific hints for molecular disease mechanisms.

Functional Analysis of Protein-Coding Missense Variants

As mentioned above, the functional consequences of protein-coding missense DNMs (including in-frame deletions/insertions) are more difficult to predict and different amino acid

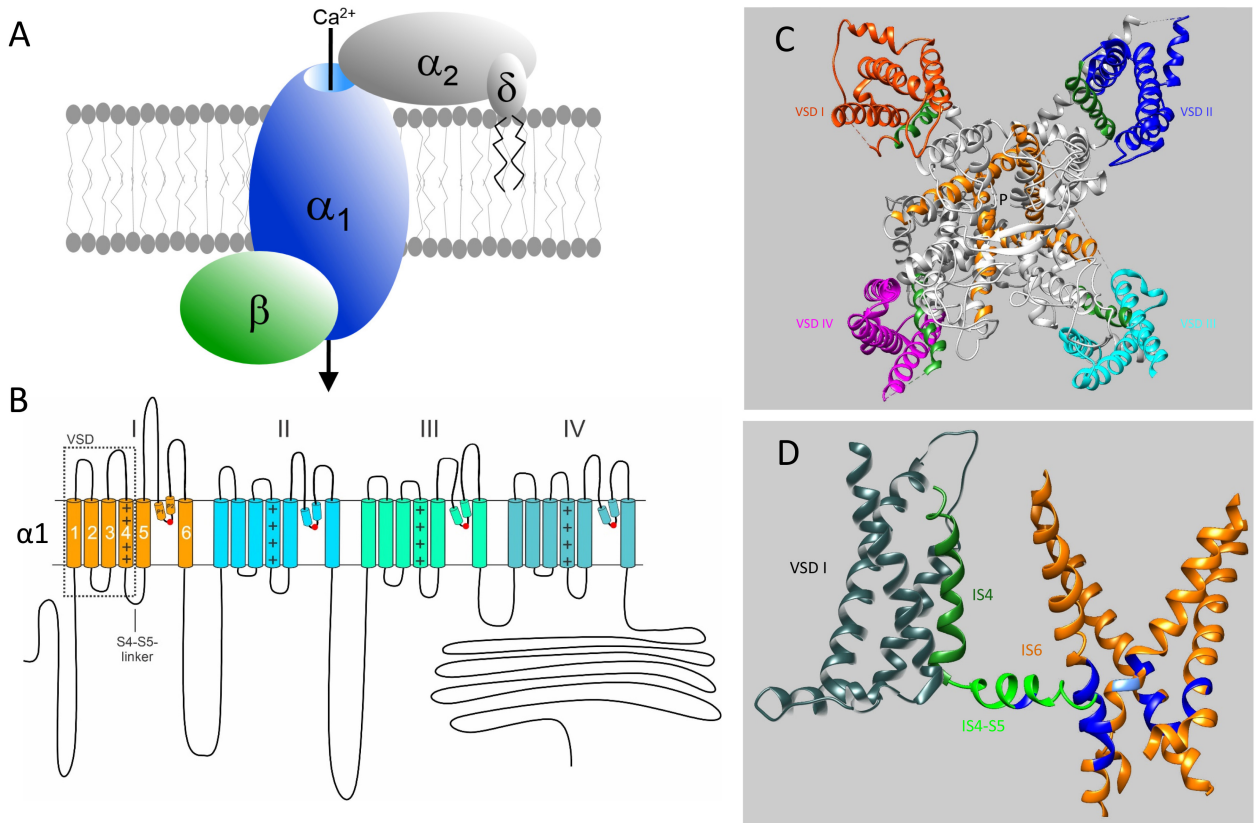

FIGURE 1 | Subunit structure of voltage-gated Ca^{2+} channels and their mutation-sensitive regions. **(A)** The pore-forming α1-subunit determines most of the biophysical properties of voltage-gated Ca^{2+} channels and also carries the binding domains for subtype-selective drugs and toxins. β-and α2δ-subunits associate with α1-subunits of Cav1 and Cav2 channels but not with Cav3 T-type channels. They support channel trafficking to the membrane, fine-tune gating properties but appear to have also channel-independent functions. Here we only discuss pathogenic mutations in α1-subunit genes. **(B)** Transmembrane folding topology of α1-subunits. Four homologous domains (I-IV) each form a voltage sensing domain (VSD, S1-S4; dotted box). The S6 helices together with the connecting S5-S6 linkers of each domain contribute to the formation of a single central Ca^{2+}-selective pore. The S4-S5 linkers in each domain transmit the voltage-dependent conformational changes of the S4-helix movements to the cytoplasmic side of the pore by interactions with adjacent S4-S5 – linkers (Hofer et al., 2020) and S6 helices (Wu et al., 2016; Catterall et al., 2020). Mutations neutralizing the voltage-sensing positive charges in each voltage sensor can open an additional ion conducting pathway (termed ω-pore) through the voltage –sensing domain, which can conduct pathogenic gating pore currents (see **Figure 5** and text for details). P1 and P2 are helices contributing to the formation of the external part of the pore. They coordinate the formation of the Ca^{2+}-selectivity filter formed by four negatively charged amino acid residues indicated by the red circles. **(C)** Cryo-electron microscopy structure of the Cav1.1 calcium channel complex purified from rabbit skeletal muscle (PDB 5GJV). Only a top view of the pore-forming α1-subunit is shown to illustrate the position of the four voltage-sensing domains (VSD I – IV, highlighted in different colors). The voltage-sensing positively charged S4 helices of the VSD domains are shown in green (positive charges are not indicated). The central pore-forming region including the intracellular activation gate are formed by the S6 helices indicated in orange. P indicates the ion conducting pathway. The structure is in a presumably inactivated state with S4 voltage-sensors "up" and the activation gate closed (Wu et al., 2016). **(D)** Most of the missense mutations (in particular GOF mutations) causing Ca^{2+} -channelopathies occur in regions important for voltage-dependent channel gating. These functional modules consists of S4 (green) and the cytoplasmic S4-S5 linkers (light green), which are tightly coupled through multiple interactions (not illustrated) to the activation gate formed by the four S6 helices (orange). For clarity the VSD (gray), S4 and S4-S5 linker are only shown for domain I together with all 4 S6 helices (orange). Positions where pathogenic mutations occur in all Cavs (**Figures 3**, **4**) are indicated in blue. In IS4-S5 this represents the position of the FHM1 mutation S218L (*CACNA1A*) and the CSNB2 mutation S229P (*CACNA1F*), which both cause GOF (type 2 gating; see text for details). The position of the Timothy Syndrome mutation G402R/S (*CACNA1C*) is indicated in light blue. Note that pathogenic GOF mutations at the same position also occur in Cav1.3, Cav1.4, and Cav2.3 (**Figure 3**). The schemes in **(C,D)** were generated using UCSF Chimera 1.13.1 (Pettersen et al., 2004). The position of mutations in the Cav1.1 α1-subunit is shown based on the sequence alignments in **Figures 3**, **4** and does not account for potential differences in the folding structure of the different α1-subunits.

substitutions at the same position may even cause opposite functional effects (Hofer et al., 2020). While missense DNMs may also induce a LOF by generating functionally silent channels (e.g., by an in-frame glycine insertion in Cav1.3 α1; Baig et al., 2011), they can have more complex effects by affecting channel gating or ion conductance. In this case, it is difficult to predict if a given gating change enhances or reduces channel activity in the context of a cell's characteristic firing pattern. It is very important that we keep this in mind when referring to a "GOF" phenotype. It only implies that functional changes induced by a mutation can *permit* enhanced channel activity and Ca^{2+} influx *under certain circumstances*, such as during a given electrical firing pattern of a cell. As outlined below, it does not necessarily exclude that the same

TABLE 1 | Voltage-gated Ca^{2+} channels: classification and human genetic diseases.

Family	α 1-Subunit Gene	α 1-Subunit	Channelopathies (OMIM)
Cav1 (L-type)	*CACNA1S*	Cav1.1	• Hypokalemic Periodic Paralysis Type 1 (# 170400, AD, DN) • Normokalemic Periodic Paralysis (#170600, AD) • Malignant Hypothermia Susceptibility 5 (#601887, AD)
	CACNA1C	Cav1.2	• Timothy Syndrome (#601005, AD) • Long QT Syndrome 8 (LQT8) (#618447, AD) • Brugada Syndrome 3 (#611875)
	CACNA1D	Cav1.3	• Sinoatrial Node Dysfunction and Deafness Syndrome (#614896, AR)[• Primary aldosteronism, seizures, and neurologic abnormalities (#615474, DN) • Autism spectrum disorder (with or without more severe manifestations including intellectual disability, neurological abnormalities, primary aldosteronism and/or congenital hyperinsulinism (not listed in OMIM, DN) • Aldosterone producing adenomas (APAs, somatic, DN)
	CACNA1F	Cav1.4	• Congenital Stationary Night Blindness Type 2 (#300071, XL) • X-linked Cone-Rod Dystrophy 3 (#300476, XL) • Aland Island Eye Disease (#300600, XL)
Cav2	*CACNA1A*	Cav2.1 (P/Q-type)	• Familial and Sporadic Hemiplegic Migraine Type 1 with or without progressive cerebellar ataxia (#141500, AD, DN) • Episodic Ataxia Type 2 (#108500, AD) • Spinocerebellar Ataxia Type 6 (#183086, AD)* • Early Infantile Epileptic Encephalopathy 42 (#617106, AD) • Congenital Ataxia*
	CACNA1B	Cav2.2	• Neurodevelopmental disorder with seizures and non-epileptic hyperkinetic movements (#618497, AR)
	CACNA1E	Cav2.3	• Early Infantile Epileptic Encephalopathy 69 (#618285, AD)
Cav3 (T-type)	*CACNA1G*	Cav3.1	• Spinocerebellar Ataxia Type 42 (#616795, AD) • Spinocerebellar Ataxia Type 42 early-onset, with neurodevelopmental deficits (Childhood-Onset Cerebellar Atrophy; #618087, AD)
	CACNA1H	Cav3.2	• Familial Hyperaldosteronism type IV (#617027, AD) • Aldosterone producing adenomas (APAs, somatic, DN)
	CACNA1I	Cav3.3	• Neurodevelopmental disorder with epilepsy and intellectual disability (not yet listed in OMIM)

*Human diseases caused by inherited and de novo missense Ca^{2+} channel α1-subunit variants. Only diseases are listed in which the high pathogenic potential of mutations is either evident from their high penetrance in families or from functional studies of recurrent mutations in de novo variants. *, phenotypic and genotypic overlap with other channelopathies of this gene. AD, inheritance: autosomal dominant; AR, autosomal recessive; XL, X-linked; DN, de novo. For most familial disorders with autosomal dominant inheritance pathogenic de novo mutations have also been described.*

"GOF" variant can also *reduce* channel activity in a different functional context.

Analysis of mutation-induced functional changes in cells expressing Cavs is complicated by the fact that tissues cannot be routinely obtained from patients (skeletal muscle biopsies are an exception). Moreover, individual Cavs are difficult to study in native tissues, because often currents of many different Cav types contribute to the total Ca^{2+} current in a cell. This requires isolation of the current component of interest, which is possible for some (e.g., Cav2.1-mediated P/Q-type currents in cerebellar Purkinje cells, Cav1.2-mediated L-type currents in cardiomyocytes; see below) but very difficult for others (e.g., Cav1.3-mediated L-type currents, Cav2.3-mediated R-type currents; Forti and Pietrobon, 1993; Sinnegger-Brauns et al., 2004). Moreover, currents recorded in native cells expressing heterozygous variants are "contaminated" by wildtype currents, making subtle changes of mutant current components more difficult to detect than in a heterologous system (Miki et al., 2008).

These restrictions require expression of missense variants in mammalian heterologous systems, such as HEK-293 or baby hamster kidney cells, and quantification of functional changes in patch-clamp experiments. In general, it appears that macroscopic gating changes observed in heterologous expression systems reproduce the changes observed in native cells reasonably well. This is evident from animal models harboring specific human mutations (Drum et al., 2014; Rose et al., 2014; Calorio et al., 2019) or from human cells differentiated from patient-derived induced pluripotent stem cells (iPSCs; e.g., neuron-like or cardiomyocyte-like cells; Yazawa et al., 2011; Krey et al., 2013; Song et al., 2017; Estes et al., 2019; Chavali et al., 2019). In contrast, it is less clear how well changes of current density and of channel protein expression observed in heterologous overexpression systems reflect changes of current density in native tissues (Chavali et al., 2019). Obviously, many other regulatory factors absent in heterologous expression systems, in particular cell-type specific protein-protein interactions, affect channel protein stability and its plasma membrane-targeting in their native environment.

Special attention should also be paid to missense mutations located in alternatively spliced exons, which may restrict the mutation only to channels expressing this exon. Conversely, a single missense mutation may even promote the expression of the exon in which it is located. This has recently been

shown in iPSC-derived neural progenitor cells and neurons (Panagiotakos et al., 2019) generated from patients with Timothy syndrome (see below). The GOF mutation G406R in exon 8a of *CACNA1C* (Cav1.2α1; see section on *CACNA1C* below) inhibits the developmental splicing switch to exon 8 – containing Cav1.2 channels, which do not harbor the mutation. This favors extended use of the mutant, exon 8a-containing channel permitting enhanced mutant channel activity during brain development. This is likely due to the position of the mutation in the splice acceptor site of exon 8a (Panagiotakos et al., 2019).

Channel Loss of Function Mutations

Like for other proteins (see above), genetic variants can cause disease (or increase disease risk) by disrupting channel function. This can be predicted for likely gene-disrupting mutations expected to prevent the synthesis of functional α1-subunit proteins (pLOF). If no protein is made from the defective allele, heterozygous LOF mutations may cause disease resulting from *haploinsufficiency*. However, if a defective (e.g., truncated) protein is still synthesized it may even exert a *dominant negative* effect on the wildtype channel produced from the unaffected allele. This requires a mechanism enabling functional coupling between (wildtype and mutant) α1-subunits. In addition, the mutant RNA must escape nonsense-mediated RNA decay (Holbrook et al., 2004). In the case of Cavs such dominant negative effects appear likely: substantial expression of mRNA transcripts from mutated alleles of both frameshift and nonsense mutations (in the case of Cav2.1) has been reported in humans (Sintas et al., 2017; Balck et al., 2018). Moreover, binding of misfolded mutants to wildtype α1-subunits occurs *in vitro* thereby promoting channel degradation (Mezghrani et al., 2008; Page et al., 2010). It is therefore possible that some heterozygous LOF mutations will reduce channel activity even below 50%, a consideration especially important for understanding the pathology of Cav2.1 channelopathies (see below). However, it should be kept in mind that the *in vitro* studies were carried out with cDNA constructs in heterologous overexpression systems with yet unclear relevance for the *in vivo* situation, and the detection of transcripts of the mutant alleles is still very indirect evidence.

Common Macroscopic Gating Changes Induced by Protein-Coding Missense Mutations

Missense-mutations can affect the macroscopic gating properties of Cavs in a complex manner, evident as changes of the voltage-dependence of current activation and inactivation. These alterations are very similar across different Cavs. For further discussion **Figure 2** illustrates the most frequently observed gating changes in a simplified manner as type 1 – 4, although overlaps exist between them (Pinggera et al., 2018; Ortner and Striessnig, 2020). A gating change unambiguously interpretable as a phenotype permitting enhanced channel function (GOF) is illustrated in panel A ("type 1"). Its hallmark is an almost complete failure of a large fraction of current to inactivate during depolarization. This is often quantified in whole-cell patch-clamp experiments during square pulse depolarizations (ΔV) from a negative holding potential (hp) to the maximum of the voltage of maximal inward current (V_{max}, **Figure 3A**, right panel). This failure to inactivate can even prevent meaningful measurements of steady-state inactivation. At the same time, the half-maximal activation voltage ($V_{0,5,act}$) can be either unchanged or shifted to more negative voltages (blue curves, **Figure 2A**, left panel). Note that the time course of inactivation is controlled by Ca^{2+}-dependent as well as voltage-dependent inactivation. The latter occurs in the absence of Ca^{2+} and with Ba^{2+} as charge carrier (for reviews see Ben-Johny et al., 2015; Hardie and Lee, 2016). For L-type channels the differential effects on Ca^{2+}- and voltage-dependent inactivation have been quantified for some mutations, showing that this pronounced slowing of inactivation is mainly due to reduced voltage-dependent inactivation (Splawski et al., 2004; Pinggera et al., 2018). Why can we be confident that this type of macroscopic gating change in HEK-293 cells can also translate to enhanced cellular Ca^{2+} signaling *in vivo*? As mentioned below, a type 1 gating change has been reported for Cav1.2 channels in LQT8 and explains the prolongation of the cardiac action potential driven by the failure of the channel to inactivate (Yazawa et al., 2011; Drum et al., 2014; Estes et al., 2019). Moreover, in Cav1.3 channels type 1 gating is associated with ASD (G407R, Pinggera et al., 2015) and a more severe neurodevelopmental syndrome (G403D, Scholl et al., 2013; **Figure 3A**) which cannot be explained by a Cav1.3 channel LOF (Ortner and Striessnig, 2020). In addition, the GOF phenotype is supported by somatic mutations in Cav1.3 (G403R,G403D) in aldosterone-producing adenomas (APAs), in which enhanced Ca^{2+} entry is known to drive excess Ca^{2+}-dependent aldosterone production (Boulkroun et al., 2020). When expressed in HEK-293 cells, some type 1 mutations result in smaller current amplitudes but, due to slow inactivation, mutant currents exceed the amplitude of wildtype currents upon prolonged depolarization (**Figure 2A**, right panel, dashed line; Pinggera et al., 2018). Accordingly, expression of such a type 1 Cav1.3 channel mutant (G407R) in cultured GLT muscle cells enhanced intracellular transients (Pinggera et al., 2015).

Figure 2B illustrates another typical pathological pattern, termed "type 2" for further discussion. Its characteristic feature is a shift of the activation voltage range to more negative voltages. The steady-state inactivation voltage range is either unchanged (e.g., Cav1.3-V401L, Cav2.1-S218L; Tottene et al., 2005; Pinggera et al., 2017) or is shifted to more negative potentials (e.g., Cav1.3-S652L, Cav3.1-A961T, Cav3.2-M1549V; Scholl et al., 2015; Chemin et al., 2018; Hofer et al., 2020) (**Figures 3**, **4**). As a consequence, the voltage-range at which channels can conduct a steady-state Ca^{2+} inward current (the so-called "window current", i.e., the voltage range at which the steady-state activation and inactivation curves overlap) is also shifted to more negative voltages (see legend to **Figure 3B**). The time course of Ca^{2+}-current inactivation may be accelerated (e.g., Cav1.3-S652L, Cav2.1-V714A; Kraus et al., 1998; Hofer et al., 2020) or slowed (Cav1.3 –V401L, Cav2.1-S218L, Cav3.1-A961T, Cav3.2-M1549V;

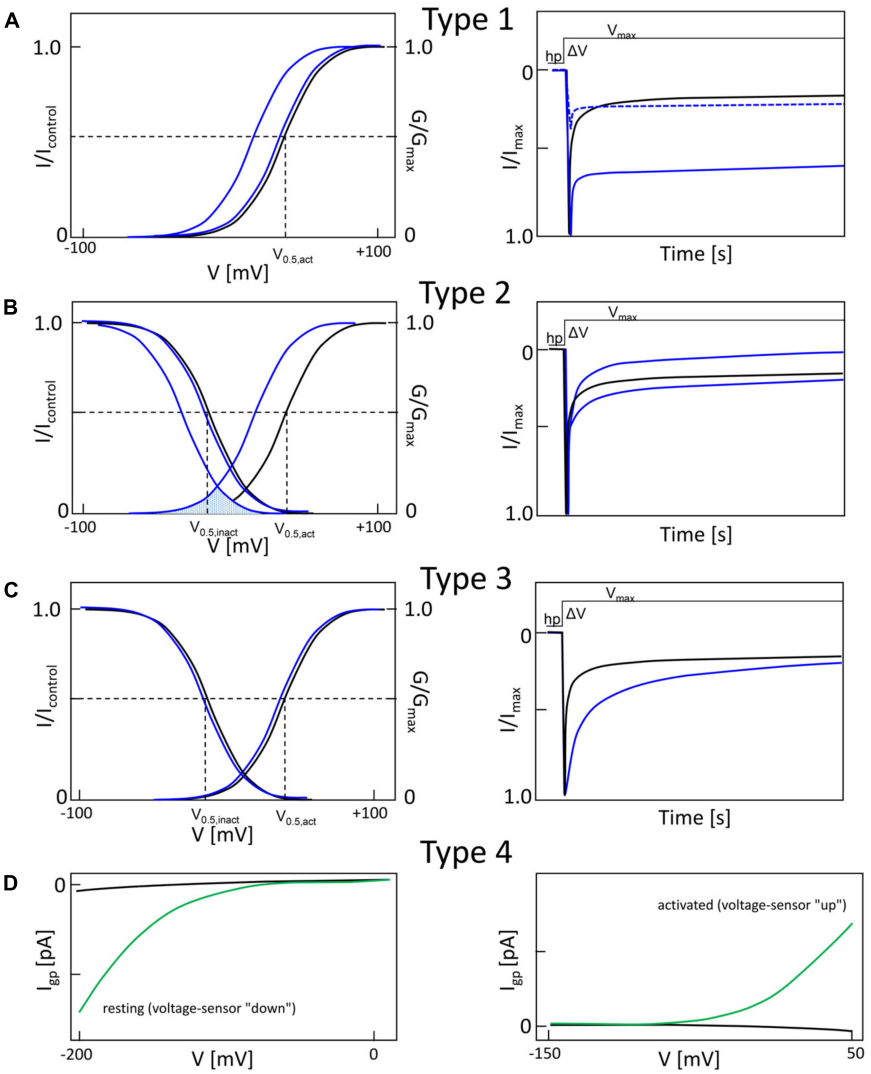

FIGURE 2 | Typical gain-of-function macroscopic gating changes described for inherited or *de novo* missense mutations in voltage-gated Ca^{2+} channel α1-subunits. To facilitate discussion the most frequently observed gating changes are classified into types 1-4. For details see text. Mutant current properties are indicated in blue **(A–C)** or green curves **(D)**, wildtype current in black. **(A)** Type 1 is characterized by the appearance of a large fraction of a non-inactivating current component (as e.g., during long depolarizations from a negative holding potential to the potential of maximal inward current; right panel). Changes in the voltage-dependence of activation gating (left) may or may not be present (blue curves, left). Note that even if maximal inward current is reduced by a mutation, current amplitude may exceed wildtype current later during depolarization due to the slowly inactivating current component (right, dotted curve). **(B)** The main feature of type 2 changes is a strong shift of the voltage-dependence of activation to more negative voltages independent of smaller effects on current inactivation during depolarizations. The voltage-dependence of inactivation may or may not be shifted to more negative voltages (left). The voltage range in which steady-state inward current ("window current") may be observed (i.e., the overlap of voltage-dependence of activation and inactivation curves) is indicated for mutant current (shaded) **(C)**. Some mutations do not affect the voltage-dependence of gating (left) but cause a slowing of inactivation (weaker than in type 1). **(D)** As described in **Figure 5**, gating pore currents are enabled by mutations of an S4 gating charge (green lines). The position of the mutation relative to the hydrophobic constriction site (HCS, **Figure 5**) determines if the pore is open during the hyperpolarized "down"-state of the S4 helix at negative voltages (left) or during the depolarized "up"-state at positive voltages (right). In the "down" state, at potentials near the K^+-equilibrium potential, inward gating-pore currents would be primarily carried by Na^+. In the "up" state, at potentials positive to the activation threshold of the channel, potassium outward gating-pore current predominates. However, upon fast repolarization of the action potential to negative potentials Na^+ inward gating-pore current may predominate until the voltage sensor moves back to the "down" position" (especially relevant in "slowly inactivated" Na^+-channels," for details see ref. Sokolov et al., 2008). G/G_{max}, normalized conductance (steady-state activation); I/I_{max}, normalized inward current (steady-state inactivation). $V_{0.5,act}$, $V_{0.5,inact}$, half maximal voltages of activation and inactivation; hp, holding potential; ΔV, depolarization from a negative holding potential to the voltage of maximal inward current (V_{max}).

Tottene et al., 2005; Scholl et al., 2015; Pinggera et al., 2017; Chemin et al., 2018). A slowing of current deactivation upon repolarization can also occur but is not illustrated here (Cav1.3-S652L, Cav1.3-A749G, Limpitikul et al., 2016; Hofer et al., 2020) (**Figures 3**, **4**). In L-type channels, this type of gating change appears to be associated with reduced

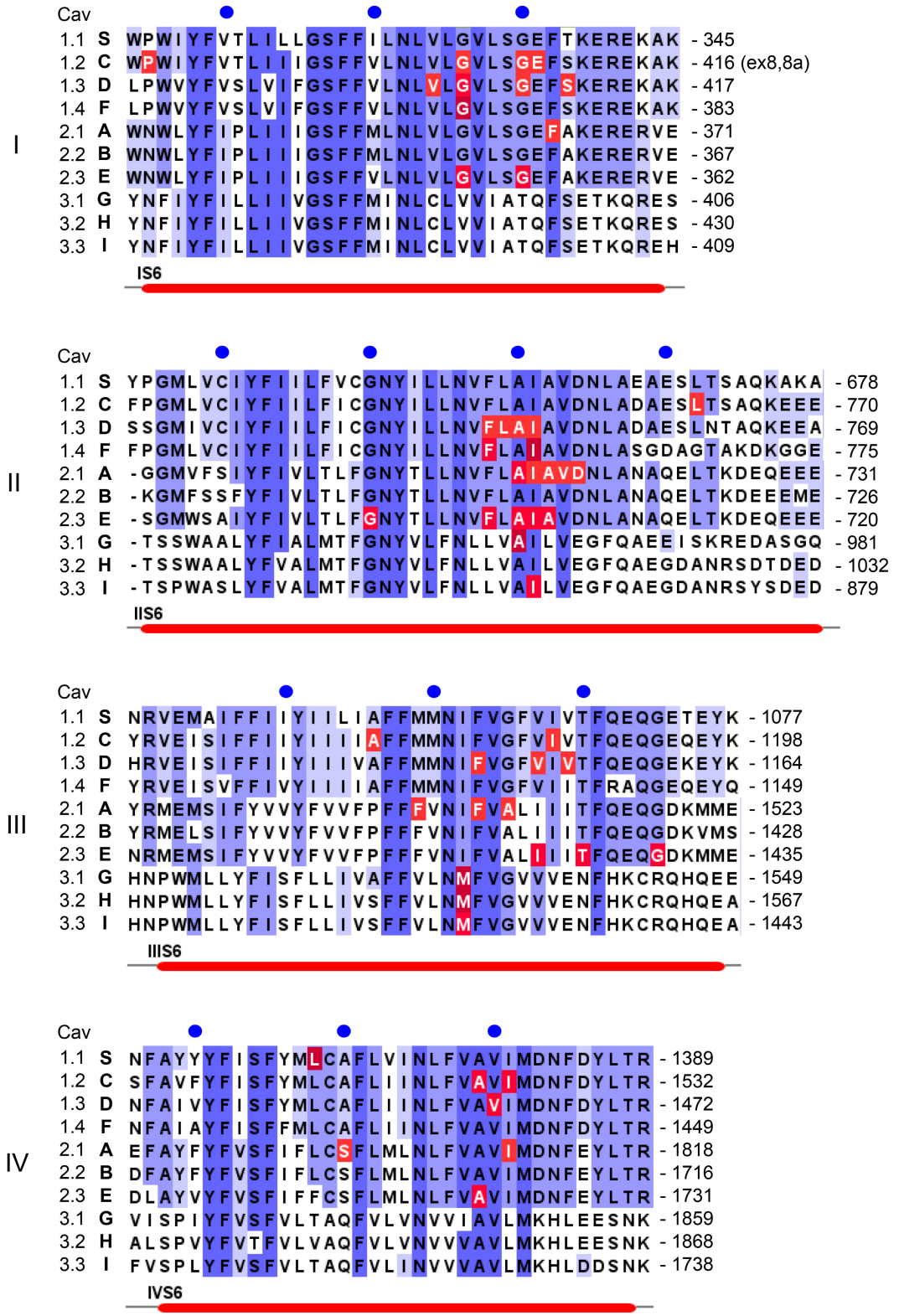

FIGURE 3 | Position of pathogenic mutations within S6 helices of the ten different Ca^{2+} channel α1-subunits. Sequence alignment and labeling is as described in legend to **Figure 4**.

Ca^{2+}-dependent inactivation (as shown for Cav1.3 mutations V401L, S652L, A749G; Limpitikul et al., 2016; Pinggera et al., 2017; Hofer et al., 2020). While the negative shift of activation voltage is compatible with a GOF, more negative steady-state inactivation and the faster current inactivation time course can can lead to reduced channel activity. This LOF will be mainly relevant in cells, which, on average, rest at a membrane potential positive enough to allow more channels to inactivate along the more negative steady-state inactivation voltage-dependence. In addition, the faster inactivation time course would mainly be relevant if the cell's firing pattern involves prolonged depolarized states. Therefore, it appears that more negative activation and window current are sufficient to induce GOF disease phenotypes, like in Cav2.1 for Familial hemiplegic Migraine Type I (FHM1; e.g., V714L, T501M, Hans et al., 1999; Carreño et al., 2013), in Cav1.3 for severe neurodevelopmental disorders (e.g., S652L, A749G, Ortner and Striessnig, 2020), in Cav1.2 for Timothy Syndrome (e.g., I1166T, Boczek et al., 2015) and in other Cavs (see below).

Type 3 changes refer to slowing of the inactivation time course alone as a GOF feature without detectable changes in the voltage-dependence of gating (**Figure 2C**) and has also been found for some pathogenic mutations (e.g., Cav1.3-P1336R, Azizan et al., 2013).

In addition to macroscopic gating changes, protein-coding missense variants can also alter ion permeation through the channels by affecting unitary conductance or ion selectivity. Especially mutations close to the channels' selectivity filter can alter single channel conductance, open probability and the voltage-dependence of single channel gating. The selectivity filter is formed by four conserved negatively charged residues (red dots in **Figure 1B**) held in place by two supporting pore helices (P1, P2 in **Figure 1B**, Wu et al., 2016; Catterall et al., 2020) in the S5-S6 linker of each domain. This has been studied for the Cav2.1 FHM1 variant T666M (2 residues N-terminal of the selectivity filter glutamate; Hans et al., 1999; Tottene et al., 2002). Mutations in the activation gate formed by the cytoplasmic ends of the S6 helices also affect ion selectivity and single channel conductance (e.g., Cav2.1-V714L, Cav1.4-I756T in IIS6; **Figure 3**; Hans et al., 1999; Tottene et al., 2002; Williams et al., 2020). A dramatic effect on ion selectivity has recently been reported for *CACNA1F* mutation I756T (**Figure 3**), which depends on C-terminal splicing and the associated β-subunit isoform (Williams et al., 2020).

Pathogenic variants directly hitting the negative charges forming the Ca^{2+} selectivity filter are rare but have been reported for Cav1.2 (E1135K) associated with LQT8 and Cav2.1 associated with a Spinocerebellar Ataxia Type 6 (SCA6) phenotype (not illustrated; see below). This can create a channel population permeable for monovalent cations with Na^+-mediated inward currents and K^+-mediated outward currents. It can explain the prolongation of the cardiac action potential in cardiomyocyte-like cells derived from human induced pluripotent stem cells expressing the E1135K LQT8 variant (Ye et al., 2019).

Pathogenic Gating Pore Currents

In addition to altering the ion flow through the canonical central pore, missense mutations can even generate a new ion-conducting pathway theoretically within each of the four VSDs (**Figure 1C**; Cannon, 2017; Groome et al., 2017; Jiang et al., 2018; Männikkö et al., 2018; Jiang D. et al., 2019). Whereas the pore-lining S6 helices of all four homologous α1-subunit domains together form the single, central Ca^{2+}-selective pore (orange helices in **Figures 1C,D**), the voltage-sensing apparatus consists of four separate but cooperatively gating VSDs (Pantazis et al., 2014; Catterall et al., 2020). Each of the VSDs exists as a four-helix bundle (S1-S4 helices; Catterall et al., 2020). The S4 helix contains at least 4 positively charged arginine or lysine residues (gating charges, **Figure 5**; arrows in **Figure 4**) spaced at three (or four) residue intervals. These charges sense changes in transmembrane voltage and depolarization drives them outward across the transmembrane electric field (**Figure 5**; Catterall et al., 2020). The intracellularly connected S4-S5 linkers (illustrated for domain I in **Figure 1D**) open the pore by transmitting the S4 movements to the so-called "activation gate", the narrow part of the pore formed by the S6 helices on their cytoplasmic ends (**Figures 1C,D**; Wu et al., 2016; Catterall et al., 2020). While moving through the membrane, the S4 positive charges are stabilized by ion pairs formed with negative countercharges from neighboring helices (NC in **Figure 5**) in- and outside of a hydrophobic constriction site (HCS in **Figure 5**) whereby ion pair partners are exchanged dynamically during this "sliding helix movement" (**Figure 5**; Wu et al., 2016; Catterall et al., 2020). The HCS helps to shield the structure from the extracellular hydrophilic milieu and prevents transmembrane flux of water and ions through the VSD. Positive charges are stabilized around the HCS and thereby also prevent ion flux (**Figure 5**). However, if one of these positive charges is mutated and replaced by a smaller or hydrophilic amino acid this seal can open, allowing water molecules to enter. The resulting pore can be large enough to conduct either measurable Na^+ and K^+ currents or proton currents if a positive gating charge is replaced by a protonable histidine (**Figure 5**). When open, this artificial pore ("gating-pore" or "ω-pore") can conduct outward or inward current depending on the driving forces imposed by transmembrane voltage. Depending on the position of a mutation within the S4 helix a "gating pore current" can develop in the resting state when the outermost gating charges are affected. As illustrated in **Figure 5**, these residues are close to the HCS when the S4 helix is "down" and, when mutated, allow formation of a water wire through which ions can pass. In contrast, inner gating charges are close to the HCS when the S4 helix is "up." Their neutralization can support gating pore current when S4 is "up," which is the case during the open and inactivated state until repolarization forces S4 helices again into their "down" state (Sokolov et al., 2008; Cannon, 2017; Groome et al., 2017; Jiang et al., 2018; Männikkö et al., 2018; Jiang D. et al., 2019). Notably, also variants outside the S4 helix can induce gating pore currents by inducing conformational rearrangements within the VSD (Fuster et al., 2017; Monteleone et al., 2017; Flucher, 2020; see section on *CACNA1S* below).

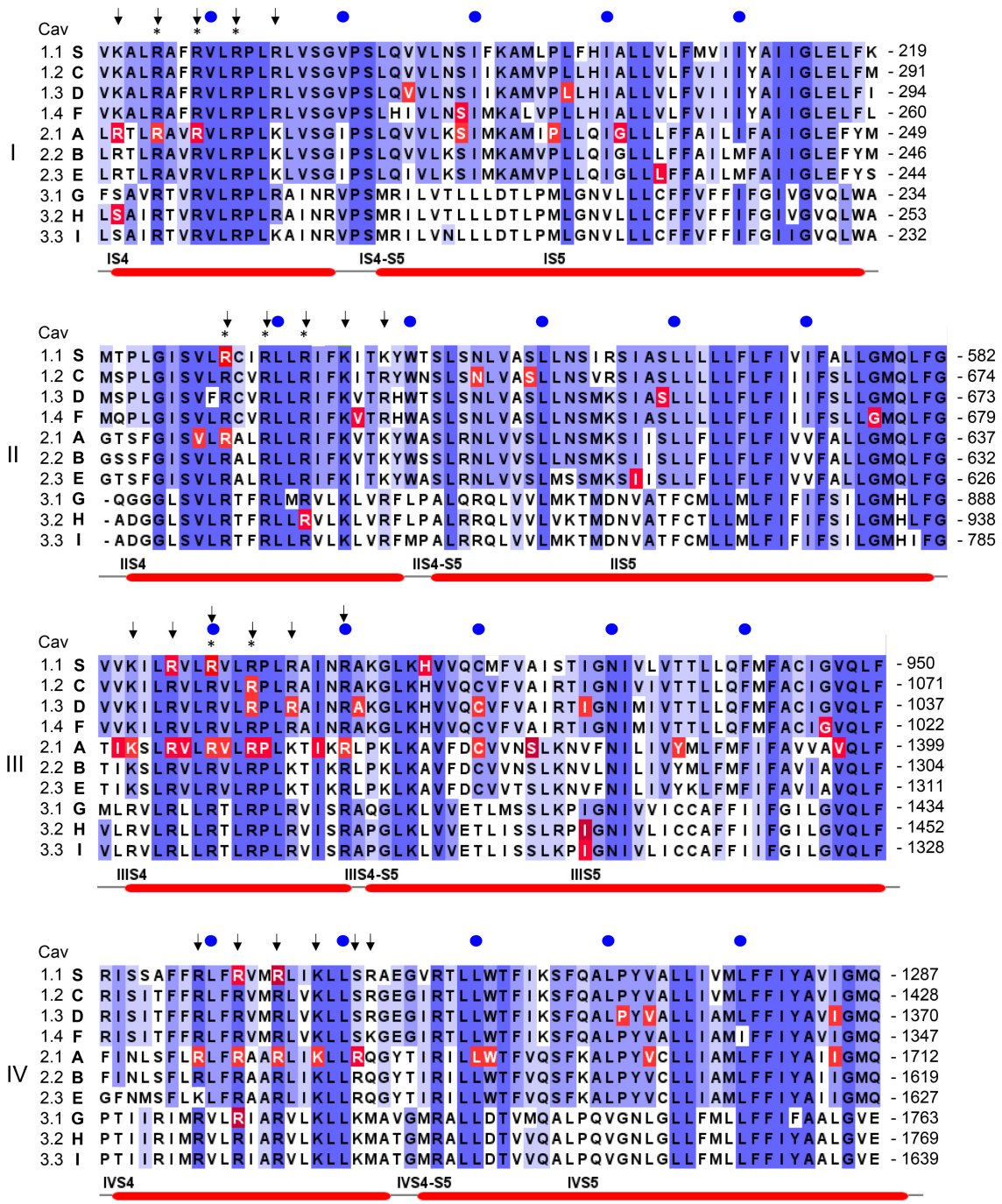

FIGURE 4 | Position of pathogenic mutations within S4, the S4-S5 linkers and S5 helices of the ten different Ca^{2+} channel α1-subunits. The sequence alignment for the human α1-subunits was generated using Clustal omega and Jalview software (www.jalview.org; Waterhouse et al., 2009). Conserved residues are highlighted in blue. The accession numbers are identical to the alignment in Wu et al. (2016): *CACNA1S* (S, Cav1.1): Q13698; *CACNA1C* [C, Cav1.2; contains exon 8a (Splawski et al., 2005)]: Q13936; *CACNA1D* (D, Cav1.3): Q01668; *CACNA1F* (F, hCav1.4): O60840; *CACNA1A* (A, Cav2.1): O00555; *CACNA1B* (B, Cav2.2): Q00975; *CACNA1E* (E, hCav2.3): Q15878; *CACNA1G* (G, hCav3.1): O43497; *CACNA1H* (H, hCav3.2): O95180; *CACNA1I* (I, hCav3.3: Q9P0 × 4. All amino acid positions in the text are numbered according to the above Uniprot accession numbers and may differ in the original publications or other databases. Arrows indicate the position of positively charged residues (gating charges) in S4 helices, asterisks indicate the presence of pathogenic gating pore mutations in human Nav1.4 (*SCNA4*) or Nav1.5 (*SCNA5*) Na^{+}-channels. Numbers on the right indicate the amino acid position of the last residue in each line, blue circles are 10 residues apart. Red lines on the bottom denote secondary structural elements of the rabbit Cav1.1 channel (Wu et al., 2016) with labels placed at the start of a feature. Residues affected by a mutation are highlighted in red. Note that not all highlighted mutations are discussed in the text. For information on mutations in all Ca^{2+} channels refer to the Uniprot-database and to reviews cited in the text.

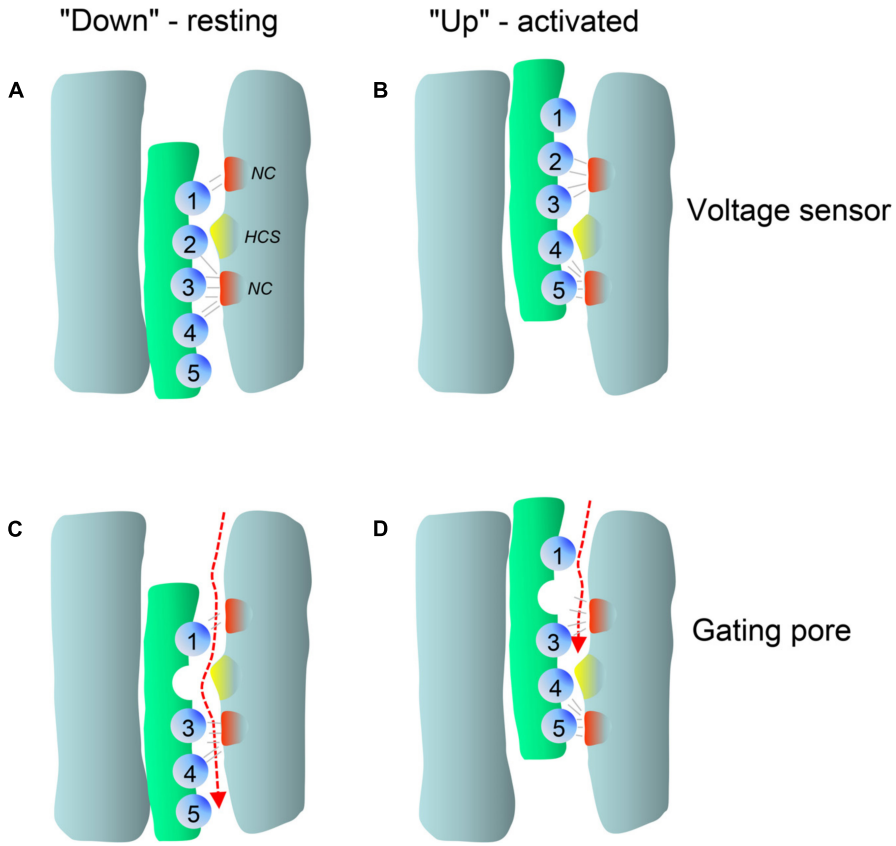

FIGURE 5 | Membrane potential dependent conformations of the voltage-sensor allow pathogenic gating pore current. Simplified scheme illustrating the membrane potential dependent conformations of a single voltage-sensor and the effects of a mutation in gating charge R2. Membrane-spanning S4 helices are shown in green, positively charged residues (mostly arginines spaced at three residue intervals) as blue spheres. Clusters of extracellular and intracellular negative counter-charges (NC) forming ion pair interactions with the gating charges are shown in red. The hydrophobic constriction site is indicated in yellow (HCS). **(A)** In the resting state, the positively charged S4 helix is pulled inside by the negative resting potential (**A**, S4 "down"). **(B)** Upon depolarization, the S4 segment moves outward according to a sliding-helix model (Catterall et al., 2020; **B**, S4 "up"), and transports positive gating charges through the HCS. Inside and outside the HCS the arginine side chains are stabilized by forming ion pairs with negative charges within the VSD (gray lines). Upon S4 movement the ion pair partners are exchanged and the large arginine side chains seal the VSD and prevent formation of a water filled space through which ions can flow (Catterall et al., 2020). Replacement of a positive gating charge by a smaller or hydrophilic residue can disrupt this seal as exemplified here for a neutralizing mutation in R2 **(C)**. This position of the mutation permits an inward gating-pore current during the hyperpolarized "down"-state of the S4 helix at negative voltages but not during the depolarized "up"-state at positive voltages **(D)**. In contrast, mutations of one of the inner gating charges would permit gating pore current to flow in the activated but not the resting position of S4 (for X-ray structures of mutant voltage-gated Na^{+}-channels see Jiang et al., 2018; Jiang D. et al., 2019).

In addition to pathogenic gating pore current, S4 mutations can also impair voltage-sensor movement thus affecting channel gating and Ca^{2+} inward current through the canonical central pore (Jurkat-Rott et al., 2012). However, in the case of Periodic Paralysis mutations in Cav1.1 Ca^{2+}- (*CACNA1S*) and Nav1.4 Na^{+}- channels (*SCN4A*) only the gating-pore currents are disease-relevant (see section on *CACNA1S* below). The function and structure of VSDs is highly conserved among voltage-gated ion channels, including Cavs, Na^{+}- (Navs) and K^{+}-channels. Therefore, S4 mutations in Cav1.1 or in Nav1.4 VSDs can both cause Periodic Paralysis in humans (Cannon, 2017; Groome et al., 2017; Jiang et al., 2018). Notably, this has important implications also for the discussion of the functional consequences of variants found in other Ca^{2+}-channelopathies, since VSD mutations in the same conserved position of different Cavs may cause similar gating-pore currents and perhaps even similar phenotypes. Indeed, when discussing a number of gating charge mutations for the individual channels below, we need to consider the possibility that gating pore currents may explain the pathogenic phenotype better than alterations of macroscopic Ca^{2+} currents (e.g., Cav1.3 – R990H, Cav3.1 – R1715H, Cav3.2 R890H; **Figure 4**). As a take home message, for gating charge missense variants the possibility of a gating pore current leading to abnormal channel function should always also be considered as a pathogenic mechanism independent of the mutation's effect on the macroscopic Ca^{2+} current.

Other Mechanisms

Especially for variants outside the classical regions responsible for ion permeation, gating and voltage-sensing other molecular pathogenic mechanisms have to be considered. This includes sites for protein interactions with one of the channel's accessory

subunits or with other proteins. Several examples exist: the (expected) LOF phenotype of the Episodic Ataxia *CACNA1A* variant L437F may be explained by reduced affinity for β-subunits (which are essential for channel function, Buraei and Yang, 2010), because this mutation occurs within the α1-subunit's cytoplasmic I-II linker where β-subunits bind (Van Petegem et al., 2004). In LQT8 families Cav1.2 channel variants were found to cluster within four-residues (857-860, a PRPR-motif, not illustrated) in the cytosolic II–III loop region and enhance channel activity through a so far unknown mechanism. Recently, crystal structures and homology modeling provided compelling evidence that this region binds SH3-domain-containing proteins (e.g., STAC) and LQT8 variants are expected to weaken this interaction (Mellor et al., 2019). Another example is the slow inactivation of the Cav1.2-G406R type 1 mutation, which appears to be mediated by cyclin-dependent kinase 5 (CDK-5; Song et al., 2017).

These examples highlight another weakness of heterologous expression systems in which mutations affecting protein-protein interactions are less likely to be detected.

CA^{2+}-CHANNELOPATHIES

How do these GOF or LOF mechanisms translate into different clinical syndromes? As mentioned above, we only focus on disorders in which rare single missense variants explain high disease risk. We will not discuss variants weakly contributing to polygenic disease risk.

Cav1.1 (*CACNA1S*)

Cav1.1 is the only relevant Cav species expressed in adult skeletal muscle. Due to the slow activation kinetics of the adult splice variant and its positive activation voltage-range (Tuluc and Flucher, 2011) Ca^{2+} entry through the channel does not directly contribute to fast excitation-contraction coupling in skeletal muscle (Zamponi et al., 2015). Instead, fast conformational changes of its VSDs open the ryanodine receptor and induce fast SR Ca^{2+} release through the cytoplasmic linker connecting domains II and III (**Figure 1**) and the associated essential EC-coupling protein STAC3 (for review see Flucher and Campiglio, 2019).

Heterozygous LOF mutations in the Cav1.1 α1-subunit appear clinically silent, unless variants on the second allele reduce function further. This is the case in recessively inherited *CACNA1S*-associated **Congenital Myopathy** (Schartner et al., 2017; Flucher, 2020), a disorder characterized by marked neonatal hypotonia, generalized weakness with pronounced axial involvement, variable symptoms such as respiratory and swallowing issues, delayed motor development and peculiar histological features in muscle biopsies (Schartner et al., 2017). Interestingly, *heterozygous*, dominantly inherited protein-coding missense mutations were also identified in 3 unrelated families located in functionally sensitive regions of the channel (with P742Q and P742S in the II-III linker; not illustrated) expected to weaken channel coupling to the ryanodine receptor (Schartner et al., 2017). Like with recessive mutations, Western blots of patient muscle biopsies showed that the dominant missense variants also induced a strong decrease in overall Cav1.1 protein expression below a level expected from haploinsuffiency. This suggests a dominant-negative effect on wildtype protein expression (Schartner et al., 2017). It is therefore tempting to speculate that, as described for *CACNA1A* LOF variants (see section on *CACNA1A* below; Mezghrani et al., 2008), this may result from the interaction of wildtype with mutant Cav1.1 α1-subunits and the formation of complexes susceptible to early protein degradation.

As mentioned above, *CACNA1S* variants causing **Hypokalemic** (HypoPP1, familial autosomal dominant inheritance or sporadic *de novo*) and **Normokalemic Periodic Paralysis** (NormoPP, **Table 1**) are the most relevant also for our understanding of the potential functional effects of gating charge mutations in other Cav isoforms. HypoPP1 mutations affect arginines of S4 voltage sensors in domains II–IV and produce an anomalous gating pore leak current (the positions of the mutations are highlighted in red in **Figure 4**). Like gating pore currents in Nav1.4, these currents, and not changes in the function of the central pore, cause attacks of weakness in HypoPP1 (Cannon, 2017; Flucher, 2020). Seven of the 9 known variants affect arginines. Exceptions are V876E in IIIS3, which also produces gating pore currents (Fuster et al., 2017; Monteleone et al., 2017) and H916Q in the IIIS4-S5 linker (Flucher, 2020; **Figure 4**). In addition to *CACNA1S* arginine mutations (Flucher, 2020), gating pore currents have so far only been investigated and confirmed experimentally for Cav1.3-R990H, which therefore is expected to induce a GOF phenotype (see section on *CACNA1D* below) despite a LOF gating change (Monteleone et al., 2017). It is therefore possible that S4 gating charge variants in other Cav isoforms also generate disease-relevant gating pore currents. **Figure 4** illustrates that outside of Cav1.1 α1, disease-associated mutations were reported in a total of at least 17 S4 gating charges in 5 different Cav isoforms (Cav1.2, Cav1.3, Cav2.1, Cav3.1, Cav3.2). Many of them are located in the same homologous positions as Cav1.1 HypoPP1 mutations or pathogenic Nav1.4 (HypoPP2) or Nav1.5 (arrhythmias and dilatated cardiomyopathy) mutations (indicated by asterisks in **Figure 4**; Groome et al., 2017; Jiang D. et al., 2019; Kubota et al., 2020).

For missense variants causing other skeletal muscle disorders (**Malignant Hyperthermia Susceptibility**) the disease-inducing mechanism is less well understood. Malignant Hyperthermia Susceptibility mutations sensitize RyR1 Ca^{2+} release to activation by caffeine and volatile anesthetics but their location in different regions of the channel currently provides no clue about the molecular mechanism (see reference Flucher, 2020 for details).

Cav1.2 (*CACNA1C*)

Cav1.2 GOF mutations can cause both a syndromic (Timothy syndrome, TS) and non-syndromic form of long-QT syndrome (LQT8). In contrast, LOF mutations shorten the cardiac action potential and are associated with Brugada syndrome and short-QT syndrome (LQTS; Antzelevitch and Yan, 2015; Priori et al., 2015; Antzelevitch et al., 2017). Excellent articles have reviewed this topic recently (Antzelevitch et al., 2017;

Marcantoni et al., 2020). Like in other Cavs, GOF mutations are located preferentially in the functionally most sensitive regions of the gating apparatus, the S4 helices, the coupling machinery of the S4-S5 linker and the activation gate formed by the S6 helices (**Figure 1D**). Examples for regions affected by mutations in different Cavs are indicated in blue in **Figure 1D**.

Timothy syndrome is a rare systemic disorder originally described as the *heart-hand syndrome* (Reichenbach et al., 1992). This refers to the typical diagnostic findings of LQTS, often leading to fatal arrhythmias at young age, and unilateral or bilateral cutaneous syndactyly of fingers or toes. In surviving individuals other characteristic clinical features were described compatible with a multi-organ disease. In most cases facial anomalies (including depressed nasal bridge, low-set ears, thin vermilion of the upper lip), congenital heart defects and developmental delay (language, motor, and generalized cognitive impairment) are present. Autism, seizures, and intellectual disability as well as hypoglycemia were also reported (Splawski et al., 2004). These symptoms are in accordance with the known role of Cav1.2 for cardiac function, neuronal development and plasticity (Krey et al., 2013; Zamponi et al., 2015), craniofacial development (Ramachandran et al., 2013), and insulin secretion (Sinnegger-Brauns et al., 2004; Zamponi et al., 2015).

Classical TS is caused by GOF mutations in Cav1.2. Originally, only mutations in alternatively spliced exons 8a (G406R, **TS1**) and 8 (G406R, G402S, **TS2**) had been described (Splawski et al., 2004; Splawski et al., 2005) (**Figure 3**; exon 8a sequence). All of them cause GOF by a pronounced reduction of (voltage-dependent) channel inactivation (type 1, **Figure 2A**). This can explain a sustained depolarizing Ca^{2+} influx with broadening of the action potential and QT-prolongation. A more severe LQT phenotype (QTc > 620 ms) has been reported in TS2. This was explained by the higher abundance of exon 8 in heart and brain. Interestingly, the first two TS2 patients had no syndactyly, one of the diagnostic features of the syndrome, but were affected by facial dysmorphism and developmental delay. The phenotype in the patient with the G402S mutation was milder. It was attributed to somatic mosaicism with the mutation being much less abundant in oral mucosa than in blood DNA (Splawski et al., 2005). This was an important observation because it shows that the severity of the phenotype is also determined by mutation load. Mosaicism is also evident from severely affected TS1 and TS2 cases who inherited the mutation from a parent with germline mosaicism. The parent had either no symptoms (Splawski et al., 2004), or, upon full medical work-up, revealed diagnostic features, such as syndactyly with and without LQT8 (Etheridge et al., 2011; Dufendach et al., 2013; Fröhler et al., 2014; Baurand et al., 2017). Therefore mosaicism has to be considered in the interpretation of phenotype-genotype relationships (Lim et al., 2017; Myers et al., 2018; Cao et al., 2019) not only of *CACNA1C*-associated disorders but also of other Ca^{2+}-channelopathies (e.g., *CACNA1A*, Cao et al., 2019; see below).

In addition to the classical TS mutations, four mutations outside exon 8 and 8a were reported. A GOF phenotype has either been proven in functional experiments or can be assumed based on their locations in S6 or the S4-S5 linkers. The affected individuals presented as atypical TS with LQT8 but some other clinical features of TS missing, such as syndactyly (S643F, type 1; **Figure 4**; Ozawa et al., 2018), or facial dysmorphisms (E407A, adjacent to G406R, **Figure 3**; Colson et al., 2019). In other cases, an even broader phenotypic spectrum was reported, including osteopenia, cerebral and cerebellar atrophy, intractable irritability (I1186T, type 2; **Figure 3**; Boczek et al., 2015) or intractable seizures and stroke (A1521G, type 2, **Figure 3**; Gillis et al., 2012).

Two additional variants deserve attention because their clinical phenotypes are even more distinct, R1024G and E1135K: R1024G (**Figure 4**) was reported in a 5-year-old girl with profound developmental and speech delay, TS-like craniofacial dysmorphism and syndactyly but *without* LQTS upon repeated ECG measurements (Kosaki et al., 2018). Pulmonary hypertension was also diagnosed. Although no functional studies have been performed, the position of this variant is intriguing. It neutralizes one of the positive gating charges in voltage sensor IIIS4. It corresponds to the R990G and R990H mutations in Cav1.3 (**Figure 4**; somatic mutations in APAs, see section on *CACNA1D* below). In Cav1.3 R990H destabilizes the VSD and can conduct a depolarizing gating pore current at negative membrane potentials (Monteleone et al., 2017). VSD mutations R1135H and R1135C in Nav1.4, which cause HypoPP2 (see above, position indicated by asterisk in **Figure 4C**) also occur in the equivalent positions. One possible scenario therefore is that R1024G also induces a gating pore current in Cav1.2. Assuming that it destabilizes the VSD in a similar manner as R990H in Cav1.3 it could contribute depolarizing current at more negative potentials. In arterial smooth muscle cells increased arterial muscular tone could explain pulmonary hypertension, whereas in neurons enhanced subthreshold neuronal depolarization could drive abnormal neuronal firing underlying the severe neurodevelopmental phenotype. However, upon activation of the Cav1.2 voltage-sensors (S4 "up" in open and inactivated channels) during the plateau of the cardiac AP, this gating pore current is expected to turn off and may thus not affect AP duration and QT-interval.

E1135K (not illustrated) was found in a 14-year-old male proband with idiopathic QT prolongation, autism spectrum disorder and unexplained hyperglycemia (Ye et al., 2019). This mutation reverses one of the four essential negative charges of the channel's selectivity filter. Functional expression in tsA-201 cells confirmed the expected conversion of a Ca^{2+}-selective channel into a *non-selective* cation channel with marked increase in both peak and persistent inward Na^+- and outward K^+-currents (Ye et al., 2019). Its expression in human iPSC-derived cardiomyocytes prolonged the cardiac AP. By favoring membrane depolarization, it can therefore be considered a GOF variant in the heart and likely also in neurons, which could affect neuronal excitability and underlie the autism phenotype. The mutation may also account for the "unexplained" hyperglycemia reported in this patient due to reduced insulin secretion. An increased membrane depolarization of the pancreatic β-cell could result in an increased basal intracellular Ca^{2+} level and reduced glucose-induced insulin secretion as observed upon genetic deletion of the K_{ATP} K^+-channel subunits (Miki et al., 1998). Alternatively, while mediating a non-selective pore current, the mutated channels are not expected to conduct

Ca^{2+}. This could impair Ca^{2+}-dependent processes depending on Cav1.2, including insulin secretion (Zamponi et al., 2015; Mastrolia et al., 2017).

In addition to TS, GOF Cav1.2 mutations can also cause **a non-syndromic form of LQT8**. LQT8 can be regarded as part of a *CACNA1C* disease spectrum because with some variants the clinical phenotype can be either LQT8 alone (G402S, Mellor et al., 2019), LQT with syndactyly but without other TS-typical features (G402S, I1186T; Fröhler et al., 2014; Wemhöner et al., 2015) or Timothy syndrome. Somatic mosaicism and/or genetic background can explain these variable phenotypes. Many of the LQT8-associated variants were confirmed to induce GOF (Hennessey et al., 2014; Fukuyama et al., 2014b; Boczek et al., 2015; Wemhöner et al., 2015; Landstrom et al., 2016; Chavali et al., 2019; Estes et al., 2019) with slowing of the inactivation time course and increased late currents. Introduction of LQT8 mutations into human iPSC-derived cardiomyocytes confirmed the broadening of the action potential in the heterozygous state (Estes et al., 2019; Chavali et al., 2019). It is possible that mutations shifting the voltage-dependence of activation and inactivation to more negative voltages favor more severe extracardiac manifestations (in particular the nervous system; Marcantoni et al., 2020). However, some variants may predominantly affect the function of cardiac channels. This has recently been shown for a cluster of variants (affecting residues P857, R858, R860; not illustrated) located within the long cytoplasmic II-III – linker without obvious role in channel gating and conductance. However, this proline-rich region serves as a binding site for SH3-domain containing proteins, such as STAC proteins, known to affect the expression and function of L-type channels (Mellor et al., 2019; Flucher and Campiglio, 2019). For a complete list of LQT8 mutations see recent reviews (Giudicessi and Ackerman, 2016; Zhang et al., 2018; Marcantoni et al., 2020).

LOF *CACNA1C* variants are associated with so-called J-wave syndromes (named after the typical electrocardiographic "J-wave"), consisting of the **Brugada syndrome** and **short-QT** syndromes (Priori et al., 2015; Antzelevitch and Yan, 2015; Antzelevitch et al., 2017). Variants leading to altered Cav1.2 activity in the heart were also reported in β- (*CACNB2* gene) and α2δ1 (*CACNA2D1*) subunits (Antzelevitch et al., 2007; Burashnikov et al., 2010). LOF *CACNA1C* variants are protein-coding variants predominantly located in the cytoplasmic regions of the channel and it is less clear how they induce the observed reduction in Ca^{2+} current when heterologously expressed. Synonymous variants in splice sites inducing nonsense-mediated RNA-decay have also been described (Fukuyama et al., 2014a). Interestingly, unlike with pathogenic *CACNA1F* and *CACNA1A* LOF mutations (see below), *no protein-truncating variants* have been reported so far. This could indicate that these phenotypes are not simply due to haploinsufficiency.

Cav1.3 (*CACNA1D*)

Current evidence from knockout mouse models and human genetics indicate that heterozygous Cav1.3 LOF is unlikely to cause a disease phenotype. About 20 heterozygous LOF genotypes[2] are listed for mostly healthy control individuals in the gnomAD database. Only homozygous Cav1.3-deficiency causes sinoatrial node dysfunction and deafness in mice (Platzer et al., 2000; Zamponi et al., 2015). The same phenotype (**Sinoatrial Node Dysfunction and Deafness**, **Table 1**) is observed in humans with a homozygous LOF mutations in exon 8 (also referred to as exon 8b; Baig et al., 2011), which is the predominant splice variant in brain, sinoatrial node and the cochlea (Baig et al., 2011; Zamponi et al., 2015; Liaqat et al., 2019).

In contrast, heterozygous *de novo* GOF missense mutations cause human disease by affecting multiple Cav1.3-dependent physiological functions. Since we have recently reviewed the disease spectrum associated with *CACNA1D* GOF variants (Ortner and Striessnig, 2020), this is only briefly summarized here.

In most affected individuals germline missense DNMs lead to a **severe neurodevelopmental disorder** with ID, developmental delay, seizures, auto-aggressive behaviors, delayed or no speech development, muscle hypotonia and autism spectrum disorder (V401L, S652L, A749T; **Figure 3**). In even more severe cases congenital hyperinsulinemic hypoglycemia and/or congenital aldosteronism (Ortner and Striessnig, 2020) can be present at birth (V259A, G403D, I750M, L271H; **Figures 3**, **4**). A syndrome, **Primary Aldosteronism with Seizures and Neurological Abnormalities (PASNA)** is part of this disease spectrum. Less severe cases were diagnosed with ASD with (A749G) and without (G407R) mild intellectual impairment (**Figure 3**). So far, for these Cav1.3 – linked disorders type 1 and 2 GOF gating changes were reported for nine mutations in 12 individuals (Ortner and Striessnig, 2020) but unpublished cases with pathogenic mutations exist and are currently being characterized. For a detailed list of mutations and associated phenotypes see Ortner and Striessnig (2020). Like most other GOF mutations, they are located in the activation gate (cytoplasmic region of S6 helices) as well as in the S5-S6 linkers, see above and **Figures 1D**, **3**, **4**). Interestingly, the positions of G403R and G403D (exon 8) and G407R (exon 8a) are identical to the Timothy syndrome mutations G402 and G406 (see above) in *CACNA1C* and also cause very similar gating defects (type 1; Scholl et al., 2013; Pinggera et al., 2018). When present as *somatic* mutations in **APAs**, these variants induce excessive Ca^{2+}-dependent aldosterone production resulting in drug-resistant hypertension (Azizan et al., 2013; Scholl et al., 2013). Some of these mutations affect the same amino acid or are even identical to the ones identified germline. Importantly, some of the germline mutations exhibit *increased* sensitivity to DHP LTCC blockers (Hofer et al., 2020). Future clinical research should therefore test the potential of these drugs to improve symptoms in severely affected individuals. Preliminary evidence suggests that muscle hypotonia may respond to treatment with DHPs (De Mingo Alemany et al., 2020).

[2]Predicted from truncating mutations within the transmembrane portion of the channel protein (gnomAD Ver2.1.1).

Cav1.4 (*CACNA1F*)

Cav1.4 L-type calcium channels are essential for tonic glutamate release from retinal photoreceptors (as is Cav1.3 in cochlear inner hair cells; Zamponi et al., 2015; Pangrsic et al., 2018). Their α1-subunit gene (*CACNA1F*) was originally discovered as the target of LOF mutations causing **X-linked Congenital Stationary Night Blindness Type 2 (CSNB2)**, a non-progressive vision disorder with characteristic clinical findings (Zamponi et al., 2015). Since then a large number of *CACNA1F* LOF mutations, most of them protein-truncating variants, have been reported to be associated with CSNB2 as well as other eye disorders, including **Åland Island Eye Disease, Cone-Rod Dystrophy, X-linked retinal disorder**, and **Night Blindness-Associated Transient Tonic Downgaze**, which share a variety of clinical symptoms (Hope et al., 2005; Stockner and Koschak, 2013) (**Table 1**). As expected for an X-linked disorder females are rarely affected. The absence of the channel protein or the absence of functioning channels leads to abnormal cellular organization of synapses within the retina and defective neurotransmission between photoreceptors and second-order neurons (Zamponi et al., 2015).

Interestingly, a number of missense variants have also been identified. While some of them decrease channel function or expression (Hoda et al., 2006; Stockner and Koschak, 2013), others show the typical gating changes compatible with a gain of channel function. For example, G369D in domain I and F753C and I756T in the activation gate of domain II (**Figure 3**) cause a dramatic type 2 gating change and slow inactivation as expected from their locations (Hemara-Wahanui et al., 2005; Hoda et al., 2005; Peloquin et al., 2007). One plausible explanation of how these gating changes can actually decrease Cav1.4 channel activity is that the pronounced negative shift of voltage-dependent activation gating moves the channel out of its optimal operating range within the voltage window during light exposure (about − 55 mV) and darkness (up to −36 mV). During illumination a larger fraction of mutated Cav1.4 channels may already be activated thus limiting the maximal gain during depolarization in the dark (Stockner and Koschak, 2013). This is another example demonstrating that a given "GOF" gating change can either increase or decrease channel signaling depending on the context of a cell's electrical activity pattern (see above).

Cav2.1 (*CACNA1A*)

Cav2.1 channels are widely expressed in the central (including thalamocortical, cortical, cerebellar neurons) and peripheral nervous system. Together with Cav2.2 channels they are tightly coupled to fast neurotransmitter release at presynaptic terminals, including motoneurons (Zamponi et al., 2015). Homozygous knockout mice develop rapidly progressive neurological symptoms with ataxia and dystonia and die a few weeks after birth (Jun et al., 1999; Fletcher et al., 2001). Therefore, homozygous LOF of Cav2.1 is also expected to be incompatible with life in humans. Accordingly, no homozygous *CACNA1A* pLOF variants are reported in the gnomAD database.

CACNA1A mutations cause several dominantly inherited or sporadic neurologic disorders with a wide spectrum of neurological symptoms (Spacey, 2015): hemiplegic migraine with aura (including severe forms with cerebral edema and coma), cerebellar signs (including episodic, permanent, early or late onset progressive ataxia, cerebellar atrophy, nystagmus, vertigo, dysarthria), seizures, and developmental delay. Although symptoms often overlap, the three main neurological *CACNA1A* disorders reveal some genotype-phenotype correlation. **Episodic ataxia type 2 (EA-2)** typically starts in childhood or early adolescence and is characterized by paroxysmal attacks of ataxia and other cerebellar signs and can be associated with other symptoms including hemiplegia and headache (Spacey, 2015). Attacks may last from minutes to days. The majority of EA-2-associated mutations are pLOF mutations or missense mutations, which typically reduce current amplitudes and/or lead to LOF gating changes. When expressed as trunctated proteins *in vitro* some of them also exert a dominant negative effect on wildtype channels (see above). Excellent reviews summarizing the position of pLOF and missense LOF variants associated with EA-2 have been published recently (Eising and van den Maagdenberg, 2017; Tyagi et al., 2020).

In contrast, GOF mutations cause **Familial (FHM-1) or Sporadic (SHM-1) Hemiplegic Migraine Type 1**, a form of migraine with aura, which, in addition to other aura symptoms, is characterized by the presence of motor weakness, i.e. hemiparesis (Jen, 2015).

FHM-1-associated mutations mostly exhibit GOF gating changes with enhanced channel activity at more negative voltages (Tottene et al., 2002; Pietrobon and Striessnig, 2003). They are mainly located at the positions within voltage-sensors (e.g., R192Q, R195K, V581L/M, R583Q, K1343Q, R1352Q, R1667W, K1670R), the S4-S5 linkers (e.g., S2181L, C1369Y, L1682P, W1683R) and the cytoplasmic S6 activation gates (e.g., F363S, V714A, D715E, F1506S, I1810L; **Figures 3**, **4**) where other GOF channelopathy mutations are typically located (Eising and van den Maagdenberg, 2017; Tyagi et al., 2020). Moreover, some variants associated with FHM-1 also neutralize S4 gating charges, including positions in which also Cav1.1 and Nav1.4 gating-pores were reported (e.g., R195K, R583Q, K1343Q, R1352Q; asterisks in **Figure 4**; note that R195K in Cav2.1 and R219K in Nav1.4 are both charge-retaining substitutions; Ducros et al., 2001; Kubota et al., 2020) and may therefore affect neuronal excitability also through gating pore currents (Jurkat-Rott et al., 2012). This hypothesis should be tested experimentally and by molecular modeling like for other Cavs (Monteleone et al., 2017; Flucher, 2020).

As a monogenic form of migraine, FHM-1 offered important insight into the pathophysiology of migraine with aura (Pietrobon and Striessnig, 2003; Goadsby et al., 2017; Brennan and Pietrobon, 2018). Human *CACNA1A* GOF mutations (R192Q, S218L; **Figure 4**), when introduced in mice, promote cortical spreading depression, a self-propagating wave of neuronal and glial depolarization that spreads slowly across the cerebral cortex and underlies the aura symptoms in humans

(Pietrobon and Striessnig, 2003; Brennan and Pietrobon, 2018). Moreover, enhanced excitatory, but not inhibitory synaptic transmission and alterations of cortical excitatory-inhibitory balance can explain the altered sensory and pain processing in FHM1 (Tottene et al., 2019) and likely also in more common forms of migraine.

Unlike EA-2, **Spinocerebellar Ataxia Type 6 (SCA-6)** is characterized by adult onset, slowly progressive rather than episodic cerebellar ataxia, dysarthria, and nystagmus with a mean age of onset between 43 and 52 years (Du and Gomez, 2018; Casey and Gomez, 2019). Genetic diagnosis of SCA-6 requires documentation of an expanded polyglutamine repeat within the C-terminus of the Cav2.1 α1-subunit. There is strong experimental evidence that, unlike the other Ca^{2+}-channelopathies described here, SCA6 is not caused by a dysfunction of the Cav2.1 channel itself, but instead by a separate protein, the transcription factor α1ACT. This protein is also encoded by the *CACNA1A* gene due to the presence of an internal ribosomal entry site (IRES) within its mRNA (for a detailed review see Du and Gomez, 2018). α1ACT is important for normal perinatal cerebellar developmental and motor function (Du and Gomez, 2018). Wildtype α1ACT, but not α1ACT-containing SCA6 poly-glutamine expansions (α1ACTSCA6), can rescue neurological deficits when transgenically expressed in Cav2.1 knockout mice (Du and Gomez, 2018). α1ACTSCA6 is also toxic to cultured cells and when expressed transgenically in Purkinje cells (Du and Gomez, 2018).

Substantial phenotypic overlap is observed for these three *CACNA1A* disorders, complicating the interpretation of this genotype-phenotype relationship. For example, a large fraction of FHM-1 families with GOF variants report cerebellar signs ranging from nystagmus to progressive, usually late-onset mild ataxia (Ducros et al., 2001; Jen, 1993). EA-2 individuals (i.e., with LOF variants) may also eventually develop interictal symptoms and cerebellar signs such as truncal ataxia and nystagmus. Such late-onset progressive ataxia makes the clinical phenotype similar to SCA-6 (Di Cristofori et al., 2012). In some families progressive ataxia due to missense variants and without expanded polyglutamine repeat was the major clinical feature, with some family members also diagnosed with EA-2 (Yue et al., 1997; Jen et al., 2004; Romaniello et al., 2010).

Congential ataxia, with presentation before the age of 2 years, is mostly associated with GOF variants, many of them also found in FHM-1 patients. Examples are S218L, D715E, I1810L, V1396M (**Figures 3**, **4**) and T666M (close to selectivity filter in domain II, not illustrated). For an excellent detailed recent review on congential ataxia see reference Izquierdo-Serra et al. (2020).

Interestingly, a slowly progressing non-episodic spinocerebellar ataxia without migraine symptoms differing from SCA-6 and EA-2 has been associated with the mutation E668K. This mutation reverses the negative charge of the selectivity filter glutamate in domain II, similar to *CACNA1C* mutation E1135K (domain III, not illustrated) mentioned above. Non-selective ion currents and loss of Ca^{2+}-conductance through this mutant may therefore contribute to the observed atypical phenotype.

CACNA1A mutations have also been associated with severe neurodevelopmental syndromes including early-onset epilepsy (**Early Infantile Epileptic Encephalopathy 42)** and other neurocognitive (intellectual impairment, learning disabilities) and neurological symptoms, such as ataxia, nystagmus, hypotonia (Damaj et al., 2015; Epi4K Consortium, 2016; Epperson et al., 2018; Jiang X. et al., 2019). It appears that both *CACNA1A* haploinsufficiency (like in EA-2; Damaj et al., 2015; Jiang X. et al., 2019) and FHM1-like GOF gating changes (A711T, A713T, Ser218L, **Figure 3**; Epi4K Consortium, 2016; Epperson et al., 2018; Jiang X. et al., 2019) can cause this phenotype. Recent studies indicate that neuropsychiatric and developmental symptoms are common in patients with episodic *CACNA1A* disorders and should be considered in the differential diagnosis of otherwise unexplained developmental delay (Indelicato et al., 2019; Humbertclaude et al., 2020).

Taken together, *in vitro* gating changes indicating increased activity of Cav2.1 at more negative voltages is mostly associated with FHM1/SHM1 and congenital ataxias, whereas channel LOF causes EA-2. However, both GOF and LOF mutations are associated with progressive ataxia and epilepsy. At present, there is no clear explanation for this observation. One hint could come from the finding that Purkinje cell-specific *Cacna1a* knockout is sufficient to cause cerebellar ataxia in mice (Mark et al., 2011; Todorov et al., 2012). This strongly suggests that reduced Cav2.1 activity is responsible for this phenotype. It is therefore possible that, as outlined above, certain gating changes can cause both, GOF (e.g., by shifting activation voltage to more negative potentials) and LOF (e.g., by shifting inactivation voltage also to more negative potentials and/or by reducing maximal channel open probability at more positive voltages) (Tottene et al., 2002). This could lead to a scenario where GOF changes predominate at e.g., cortical synaptic terminals and LOF changes at Purkinje cell bodies. At presynaptic active zones the higher open probability at threshold voltages due to type 2 gating changes could facilitate nanodomain Ca^{2+} influx and glutamate release and underlie the enhanced neuronal excitability predisposing to migraine attacks (Tottene et al., 2002). At the same time, global cellular Cav2.1 current density during action potentials at cell bodies and dendrites of cerebellar neurons may be reduced (LOF), the latter predisposing to ataxia and cerebellar neurodegeneration.

Another open question is how missense mutations inducing only a partial LOF cause EA-2. In a knock-in mouse model the EA-2-associated missense mutation F1403C (F1406C in Rose et al., 2014) reduced Cav2.1 current density in Purkinje cells of homozygous knock-in mice by about 70%, as predicted from expression in HEK-293 cells. However, this mutation failed to induce a motor phenotype as observed in other recessive *Cacna1a* mouse mutant lines with mutations resulting in similar biophysical alterations (Rose et al., 2014).

Cav2.2 (*CACNA1B*)

Like Cav2.1-mediated P/Q-type currents, Cav2.2-mediated N-type Ca^{2+} currents also play an essential role for

presynaptic neurotransmitter release. However, in contrast to Cav2.1, homozygous knockout mice show only minor abnormalities. This includes reduced pain hypersensitivity in models of inflammatory and neuropathic pain, hyperactivity, increased aggression and altered blood pressure control (Kim et al., 2009; Zamponi et al., 2015). This suggests that homozygous LOF may also not cause severe disease in humans. However, this is in contrast to recent reports, describing bi-allelic LOF variants in an autosomal recessive, complex and progressive neurologic disorder with severe neurodevelopmental delay and developmental regression, drug-resistant epileptic encephalopathy, postnatal microcephaly, hypotonia, and a non-epileptic hyperkinetic movement disorder (**Neurodevelopmental disorder with seizures and non-epileptic hyperkinetic movements**, **NEDNEH**; Gorman et al., 2019). This was confirmed in three unrelated families with different protein-truncating mutations. A possible association between a form of autosomal dominant myoclonic dystonia and the *CACNA1B* variant R1389H has also been postulated (Groen et al., 2014). However, its pathogenic potential is questionable, because it is a common variant (1:500) observed at comparable frequencies in affected and in neurologically healthy individuals (Mencacci et al., 2015). Similarly, the significance of two variants associated with adult-onset isolated focal dystonia is unclear (Cocos et al., 2020).

Taken together, current evidence suggests that heterozygous Cav2.2 LOF does not confer high risk for disease but that homozygous LOF due to protein truncating mutations can cause a severe neurodevelopmental disorder in humans.

Interestingly, unlike for other Cavs, so far no GOF variants have been reported for Cav2.2. However, rare genetic variants located within the gating-sensitive regions of Cav2.2 (**Figure 1D**) are reported in apparently healthy control individuals in the gnomAD database at high allele numbers. Some of these variants are even located in the identical homologous positions causing typical and disease-associated GOF gating changes in other Cavs. Variant V351E (2 residues upstream of the Timothy syndrome mutations in *CACNA1C*) is located in exactly the same position as mutation V401L (**Figure 3**), which causes a pronounced type 2 gating change in Cav1.3 and is associated with a severe neurodevelopmental phenotype (Ortner and Striessnig, 2020). Variants S215A and S215L affect the same serine residue in the IS4-S5 linker causing GOF changes in Cav2.1 (S218L) and Cav1.4 (S229P; highlighted in blue in **Figure 1D**) (Tottene et al., 2005; Hoda et al., 2005). Also, variants V1408I and N1409S in IIIS6 are surrounded by GOF variants in Cav1.2, Cav1.3, Cav2.1, Cav3.1 and Cav3.2 (**Figure 3**). Possible explanations are that these variants are either functionally silent or induce a LOF phenotype, which, as mentioned above, is not expected to cause disease in the heterozygous state. Alternatively, these variants may induce robust GOF changes that are not compatible with life and cause intrauterine death. Functional analysis of these variants in heterologous expression systems could answer this interesting question.

Cav2.3 (*CACNA1E*)

Helbig and colleagues recently described *de novo CACNA1E* missense variants causing Cav2.3 GOF in 30 individuals with **Developmental and Epileptic Encephalopathies** (Helbig et al., 2018). Most affected individuals presented with pharmacoresistant seizures beginning in the first year of life, profound developmental impairment, hyperkinetic movement disorders, severe axial hypotonia and some had spastic quadriplegia. Most were non-verbal and non-ambulatory. Developmental regression occurred in 9/30 individuals often in association with seizure onset. Two recurrent variants G352R and A702T accounted for half of the cohort and with a severe phenotype. Out of the 14 variants four were functionally tested and showed type 2 gating behavior with slight slowing of inactivation. They are located within the typical regions involved in channel gating (**Figures 1D**, **3**).

The same study also reported 3 individuals with variants introducing premature termination codons predicted to result in haploinsufficiency. These individuals had a milder phenotype, achieved independent ambulation at 15–18 months and acquired single words. Two of them had epilepsy (Helbig et al., 2018). One of them inherited the mutation from the apparently healthy father. Due to the small number of cases and the fact that a few heterozygous pLOF variants are also reported in gnomAD ("non-neuro" subset), the disease-causing potential of these variants is at present less clear.

T-Type Ca^{2+} Channels

Based on the expression pattern of T-type channels and their special functional properties (low-voltage activated and inactivated, window current at negative voltages, recruitment upon hyperpolarization enabling low-threshold spike/rebound bursting observed in seen in many types of neurons) together with the known anti-epileptic properties of T-type channel blockers makes these channels major suspects for genetic causes of epilepsy. Cav3.1 and Cav3.2 knockout protects mice from epilepsies (Weiss and Zamponi, 2019; Lory et al., 2020). However, so far the association of most genetic variants in *CACNA1G* and *CACNA1H* and their functional mechanism of action in terms of GOF or LOF for idiopathic genetic epilepsies is less well understood (Weiss and Zamponi, 2019; Lory et al., 2020) and mutations in Cav3.1 or Cav3.2 causing high risk for epilepsy have not been described. However, changes in their activity (as shown for Cav3.1 in mice, Calhoun et al., 2016) may serve as genetic modifiers of other genetic risk factors for idiopathic genetic epilepsies. These are generally considered to have complex inheritance patterns with combinations of common with rare genetic risk variants required to cause disease. Some *CACNA1G* variants may therefore also interact with other genes, rather than being pathogenic *per se* (Weiss and Zamponi, 2019).

Excellent reviews summarizing all Cav3 channelopathies (except for *CACNA1I*, see below) have recently been published (Weiss and Zamponi, 2019; Lory et al., 2020).

Cav3.1 (*CACNA1G*)

De novo mutations A961T and M1531T were recently found in **Childhood-Onset Cerebellar Atrophy (ChCA; Spinocerebellar Ataxia Type 42 (SCA42) early-onset with neurodevelopmental deficits)** patients in unrelated pedigrees (Chemin et al., 2018; Barresi et al., 2020). ChCA is an early-onset neurodevelopmental disorder, with cerebellar atrophy, severe motor and cognitive impairments, and variable features including epilepsy and facial dysmorphisms. The mutations are located in "classical sites" of the S6 activation gates in domains II and III (**Figure 2**) and cause typical type 2 gating changes (Chemin et al., 2018).

In contrast, **autosomal-dominant SCA42** is characterized by a slowly progressive ataxia with an onset mainly in young adulthood. Another *CACNA1G* mutation, R1715H, has been identified in SCA42 families by different groups (Coutelier et al., 2015; Morino et al., 2015; Hashiguchi et al., 2019). When expressed in HEK-293 cells (Coutelier et al., 2015; Morino et al., 2015) it caused a positive shift of the activation and steady-state inactivation voltage with a shift of the window current to more positive voltages. A mouse animal model of SCA42 harboring this mutation confirmed these gating changes in Purkinje cells and recapitulated the phenotype (adult onset, gait instability) and pathology (Purkinje cells degeneration) of the disease (Hashiguchi et al., 2019). In contrast to R1715H knockin in mice, heterozygous and homozygous knockout of Cav3.1 in mice does not cause progressive ataxia and cerebellar atrophy indicating that the observed gating change is not a simple LOF. Again, an alternative explanation could be that this mutation affects a gating charge in the VSD of domain IV (**Figure 4**). While this can explain the reduced voltage-sensing of the mutant channels, it could also generate an additional gating pore current resulting in a depolarizing drive. This is also supported by the finding that R1664Q located in the homologous position in *CACNA1A* also causes an early-onset and progressive form of ataxia not characterized by the typical episodic features of EA-2 (Tonelli et al., 2006; Luo et al., 2017). Moreover, this residue corresponds to R1239 in *CACNA1S* in which R1239H- and R1239G- induced gating pore currents cause HypoPP1 (see above, 91). If the *CACNA1G* R1715H variant induces gating pore-currents it should be classified as a "GOF" variant.

Another variant, M1574K, was found in three SCA42 patients from a Chinese family but it has not been functionally characterized yet. It is located within the III-IV-linker (not illustrated) of the channel, outside the classical regions causing gating defects (Li et al., 2018). It is located within a short alternatively spliced region (exon 25 splice variant, Latour et al., 2004) and may therefore not affect all Cav3.1 channel species in the cerebellum. However, alternative splicing in this region has been found to affect Cav3.1 recovery from inactivation (Latour et al., 2004). In the structurally highly related Cav3.2 channels alternative splicing in this position (exon 25) is required for permitting the functional effects of the adjacent R1584P mutation found in the GAERS (Genetic Absence Epilepsy Rats from Strasbourg) rat model of idiopathic generalized epilepsies (Powell et al., 2009). This GOF mutation in combination with exon 25 promotes recovery from channel inactivation and enhances channel expression by disrupting the interaction of the III-IV-linker with calnexin (Proft et al., 2017). Since calnexin also reduces the expression of Cav3.1 channels (Proft et al., 2017), it is possible that the introduction of a positive charge in the M1574K variant also affects channel function and/or expression. However, this hypothesis needs to be tested in functional and biochemical studies.

Cav3.2 (*CACNA1H*)

Like Cav1.3, Cav3.2 is important for mediating depolarization-induced aldosterone production. As a consequence, inherited (**Familial Hyperaldosteronism Type 4**) and *de novo* germline GOF missense mutations S196L, M1549I, M1549V (**Figures 3**, **4**), P2083L (not illustrated) (Scholl et al., 2015; Daniil et al., 2016) and R890H (**Figure 4**, Wulczyn et al., 2019) cause hyperaldosteronism. Neurodevelopmental symptoms (such as mild ID, social skills alterations and learning) were also reported in carriers of the M1549 variants (Daniil et al., 2016). Two somatic variants were found in **APAs** (I1430T, V1951E; Daniil et al., 2016; Nanba et al., 2020). From the five mutations reported so far, three show typical type 2 (M1549I/V) or type-3 (S196L) gating changes. I1430T corresponds to the position of the *CACNA1D* APA mutations I1015S and I1015V (IIIS5) (Ortner and Striessnig, 2020).

Unlike other mutations, R890H caused a pronounced LOF phenotype when expressed in HEK-293 cells (Wulczyn et al., 2019), a puzzling finding considering the Ca^{2+}-dependence of aldosterone secretion and the other disease-causing GOF mutations in *CACNA1D* and *CACNA1H*. However, a GOF in this mutation may again be due to the induction of gating-pore currents. This is strongly supported by the observation that pathogenic gating charge mutations in the homologous positions of Nav1.4 (e.g., R675Q; Sokolov et al., 2007) and of Nav1.5 channels (R814W, Moreau et al., 2015; asterisks in **Figure 4**) also conduct gating pore currents.

CACNA1H variants V1951E and P2093L are located in the cytoplasmic C-terminus and it is less clear how they affect channel function.

Cav3.3 (*CACNA1I*)

Although *CACNA1I* variants seem to contribute to the polygenic risk of neuropsychiatric disorders (including autism and schizophrenia, Lory et al., 2020; Ghoshal et al., 2020), rare missense mutations causing a monogenic disorder have only been published very recently (Ghaleb et al., 2021). The *de novo* missense variant (I860N, IIS6, **Figure 3**) was found in a girl with a **severe neurodevelopmental disorder** with epilepsy, muscle hypotonia, hyperexcitability, severe global developmental delay, no cognitive development and progressive brain atrophy. It induces typical type 2 GOF gating properties with significantly left-shifted voltage-dependence of activation and inactivation, increased window currents, slowed activation, inactivation, and deactivation of Cav3.3 currents. Another mutation in the same position, I860M, induced less severe biophysical changes and was

present in a mother and her two children with intellectual disability but no epilepsy. Two other missense mutations, I1306T (*de novo*, IIIS5, **Figure 4**) in a 21-month-old female and M1425I (likely *de novo*, IIIS6, **Figure 2**) in an 8-year old male patient were also associated with seizures, severe developmental delay, hypotonia, severe speech impairment, and cortical visual impairment. Again, all these variants affect residues in homologous positions for which cause GOF channelopathies also in other Cavs (**Figures 3**, **4**).

Inspection of the activation gate formed by IIS6 nicely demonstrates the accumulation of pathogenic GOF mutations within this structurally and functionally highly conserved region. Together with similar aggregations of mutations in other conserved regions of the gating apparatus (**Figure 1D**), functionally validated pathogenic mutations in one Cav should - in combination with other ACMG critera - help to predict the level of pathogenicity of newly diagnosed variants in another Cav.

IMPLICATIONS FOR THERAPY

The appraisal of functional changes introduced by missense mutations in terms of gain- or loss-of Ca^{2+}-channel function may guide the development of potential new therapies for Ca^{2+}-channelopathies.

In particular, in case of pathogenic GOF mutations, specific inhibitors of the channel isoform affected by the mutation are obvious therapeutic candidates. An intriguing example was the discovery of heterozygous activating mutations in the genes encoding ATP-sensitive K^+-channel subunits (KCNJ11, ABCC8; De Franco et al., 2020). By keeping pancreatic β-cells hyperpolarized they prevent insulin release and cause permanent neonatal diabetes and in about 20% of patients also neurodevelopmental delay (Gloyn et al., 2004; De Franco et al., 2020). In most patients switching from insulin injections to high oral doses of sulfonylureas, known well-tolerated blockers of these channels, increases quality of life, glycemic control and ameliorates some of the neurological disabilities (Ashcroft et al., 2017).

Unfortunately, not all channelopathies respond to such gene-specific pharmacotherapy. Long QT-syndromes, including LQT3 (Nav1.5 sodium channels, Arbelo et al., 2016) and LQT8 (see above), are such examples. Although LQT8 is caused by GOF mutations in Cav1.2 LTCCs, case reports of patients treated with the LTCC blockers verapamil or diltiazem for prevention of ventricular fibrillation episodes (Jacobs et al., 2006; Shah et al., 2012; Liu et al., 2016) showed mixed effects. Verapamil may not be the best choice for these patients because it is also a potent blocker of HERG K^+-channels, favoring QT-prolongation (this explains why verapamil usually does not affect the QT-interval because it also blocks L-type channels; Zhang et al., 1999). DHP L-type channel blockers would be another option but due to their state-dependent action (with preferential inhibition of arterial smooth muscle channels and blood pressure lowering) they are only weak blockers of cardiac L-type channels (Zamponi et al., 2015). Moreover, pathogenic mutations may decrease the apparent sensitivity for DHP, as shown for nisoldipine-inhibition of the TS1 mutation G406R (3-fold increase in IC_{50}; Splawski et al., 2004). Therefore, as suggested also for GOF Na^+-channel mutations causing LQT3-syndrome (Arbelo et al., 2016), mutation-specific management may be necessary. This requires extensive characterization of the biophysical and biochemical properties of mutations (ideally in human iPSC-derived cells) to identify patient populations most likely to respond to a given channel blocker in prospective clinical trials. In contrast to the type-1 TS1 mutation G406R, the type-2 Cav1.3 mutation S652L *increases* the sensitivity to the DHP isradipine about 3-fold (Hofer et al., 2020). Therefore, carriers of this mutation should be the most likely candidates for clinical (off-label) testing. The recent observation that nifedipine may improve some neurological symptoms in a patient with a pathogenic Cav1.3 GOF mutation provides some hope for a therapeutic benefit of this strategy (De Mingo Alemany et al., 2020). Evidence for a mutation-specific therapeutic benefit also comes from the observation that some patients with an epileptic encephalopathy due to *CACNA1E* GOF mutations, who were resistant to multiple anti-epileptic drugs, reported significant improvement in seizure control with topiramate. This antiepileptic can inhibit Cav2.3 currents at therapeutically relevant concentrations (Kuzmiski et al., 2005).

Mutation-specific strategies would require new drugs that are capable of reversing some or all of the gating changes of Ca^{2+}-channel GOF mutations. As a proof-of-concept it has already been shown that the tert-butyl dihydroquinone (BHQ) can modulate Cav2.1 channels in a manner that oppose altered channel gating of the FHM-1 mutation S218L (type 2, **Figures 1D**, **4**; Inagaki et al., 2014). BHQ inhibited voltage-dependent activation thereby also reducing the enhanced current amplitudes in the mutant channel at negative voltages. At the Drosophila neuromuscular junctions expressing the S218L channel, BHQ largely restored the abnormally elevated evoked postsynaptic potentials and the impaired synaptic plasticity to the wildtype phenotypes.

Another relevant aspect to be considered for GOF mutations is the fact that increased channel activity may not only affect the electrical properties directly by enhancing depolarizing current but may also affect downstream Ca^{2+}-dependent signals that could be accessible to therapeutic intervention. Enhanced Ca^{2+}-channel signaling may activate Ca^{2+}-dependent K^+-channels, which are closely coupled to different types of Ca^{2+}-channels in different cells (Berkefeld et al., 2006; Marcantoni et al., 2010). Another example exists for the TS1 mutation G406R. Roscovitine, a CDK kinase inhibitor, enhances the inactivation of LTCCs and partially reverses the abnormal, slow inactivation of G406R channels (Paşca et al., 2011; Yazawa et al., 2011 for references). It rescues the phenotypes in iPSC-derived cardiomyocytes (prolonged action potential duration) and neurons (aberrant activity-dependent gene-expression) from

TS patients (Yazawa et al., 2011; Paşca et al., 2011; Song et al., 2017). In iPSC-derived cardiomyocytes this was explained by enhanced Ca^{2+}-dependent activation of the ERK/EGR1 pathway by G406R, which drives overexpression of CDK5. CDK5 inhibition by roscovitine, dominant-negative CDK5 constructs or shRNAs alleviated the TS1 phenotype (Song et al., 2017), and may therefore guide a novel therapeutic approach.

Mutation-specific approaches could also target gating-pore currents. If, as speculated in this review, gating-pore currents contribute to pathology not only in Cav1.1 channelopathies (HypoPP, NormoPP) but also in other Cav channelopathies, then gating-pore blockers would be another attractive approach. Both toxins (e.g., spider toxin Hm-3 from *Heriaeus melloteei*, Männikkö et al., 2018) as well as guanidinium-derivatives (Sokolov et al., 2010) have already been shown to block gating-pore currents through Nav1.4 channel mutants causing periodic paralysis. Together with high-resolution crystal structures of channel mutants (Jiang et al., 2018), molecular dynamics simulations and pharmacophore modeling these studies provided valuable molecular templates for the further development of hit compounds specifically targeting gating-pores.

AUTHOR CONTRIBUTIONS

The author confirms being the sole contributor of this work and has approved it for publication.

FUNDING

The author's work is supported by the Austrian Science Fund (FWF P27809, CavX/Doc-30-B30), the European Community (DP-ARDRE/H2020 Marie Skłodowska-Curie Actions COFUND 847681), and the University of Innsbruck.

ACKNOWLEDGMENTS

The author thanks Nadine J. Ortner, Petronel Tuluc, and Bernhard E. Flucher for stimulating discussions and continuous support and Sylvia Boesch for neurological counseling. **Figures 1C,D** were generated with UCSF Chimera, developed by the Resource for Biocomputing, Visualization, and Informatics at the University of California, San Francisco, with support from NIH P41-GM103311. This work is devoted to Wilhelm Strießnig (1917–2020).

REFERENCES

Ablinger, C., Geisler, S. M., Stanika, R. I., Klein, C. T., and Obermair, G. J. (2020). Neuronal alpha2delta proteins and brain disorders. *Pflugers. Arch.* 472, 845–863. doi: 10.1007/s00424-020-02420-2

Alexander, S. P. H., Mathie, A., Peters, J. A., Veale, E. L., Striessnig, J., Kelly, E., et al. (2019). The concise guide to pharmacology 2019/20: ion channels. *Br. J. Pharmacol.* 176(Suppl. 1), S142–S228. doi: 10.1111/bph.14749

Allen, A. S., Bellows, S. T., Berkovic, S. F., Bridgers, J., Burgess, R., Cavalleri, G., et al. (2017). Ultra-rare genetic variation in common epilepsies: a case-control sequencing study. *Lancet Neurol.* 16, 135–143. doi: 10.1016/S1474-4422(16)30359-3

Antzelevitch, C., Pollevick, G. D., Cordeiro, J. M., Casis, O., Sanguinetti, M. C., Aizawa, Y., et al. (2007). Loss-of-function mutations in the cardiac calcium channel underlie a new clinical entity characterized by ST-segment elevation, short QT intervals, and sudden cardiac death. *Circulation* 115, 442–449. doi: 10.1161/CIRCULATIONAHA.106.668392

Antzelevitch, C., and Yan, G.-X. (2015). J-wave syndromes: brugada and early repolarization syndromes. *Heart Rhythm* 12, 1852–1866. doi: 10.1016/j.hrthm.2015.04.014

Antzelevitch, C., Yan, G.-X., Ackerman, M. J., Borggrefe, M., Corrado, D., Guo, J., et al. (2017). J-Wave syndromes expert consensus conference report: emerging concepts and gaps in knowledge. *Europace* 19, 665–694. doi: 10.1093/europace/euw235

Arbelo, E., Sarquella-Brugada, G., and Brugada, J. (2016). Gene-specific therapy for congenital long QT syndrome. *J. Am. Coll. Cardiol.* 67, 1059–1061. doi: 10.1016/j.jacc.2015.12.030

Ashcroft, F. M., Puljung, M. C., and Vedovato, N. (2017). Neonatal diabetes and the KATP channel: from mutation to therapy. *Trends Endocrinol. Metab.* 28, 377–387. doi: 10.1016/j.tem.2017.02.003

Azizan, E. A. B., Poulsen, H., Tuluc, P., Zhou, J., Clausen, M. V., Lieb, A., et al. (2013). Somatic mutations in ATP1A1 and CACNA1D underlie a common subtype of adrenal hypertension. *Nat. Genet.* 45, 1055–1060. doi: 10.1038/ng.2716

Baig, S. M., Koschak, A., Lieb, A., Gebhart, M., Dafinger, C., et al. (2011). Loss of Ca(v)1.3 (CACNA1D) function in a human channelopathy with bradycardia and congenital deafness. *Nat. Neurosci.* 14, 77–84. doi: 10.1038/nn.2694

Bainbridge, M. N., Wiszniewski, W., Murdock, D. R., Friedman, J., Gonzaga-Jauregui, C., Newsham, I., et al. (2011). Whole-genome sequencing for optimized patient management. *Sci. Transl. Med.* 3:87re3. doi: 10.1126/scitranslmed.3002243

Balck, A., Tunc, S., Schmitz, J., Hollstein, R., Kaiser, F. J., and Brüggemann, N. (2018). A novel frameshift CACNA1A mutation causing episodic ataxia type 2. *Cerebellum* 17, 504–506. doi: 10.1007/s12311-018-0931-8

Barresi, S., Dentici, M. L., Manzoni, F., Bellacchio, E., Agolini, E., Pizzi, S., et al. (2020). Infantile-onset syndromic cerebellar ataxia and CACNA1G mutations. *Pediatr. Neurol.* 104, 40–45. doi: 10.1016/j.pediatrneurol.2019.09.005

Baurand, A., Falcon-Eicher, S., Laurent, G., Villain, E., Bonnet, C., Thauvin-Robinet, C., et al. (2017). Incomplete Timothy syndrome secondary to a mosaic mutation of the CACNA1C gene diagnosed using next-generation sequencing. *Am. J. Med. Genet. A* 173, 531–536. doi: 10.1002/ajmg.a.38045

Ben-Johny, M., Dick, I. E., Sang, L., Limpitikul, W. B., Kang, P. W., Niu, J., et al. (2015). Towards a unified theory of calmodulin regulation (Calmodulation) of voltage-gated calcium and sodium channels. *Curr. Mol. Pharmacol.* 8, 188–205. doi: 10.2174/1874467208666150507110359

Berkefeld, H., Sailer, C. A., Bildl, W., Rohde, V., Thumfart, J.-O., Eble, S., et al. (2006). BKCa-Cav channel complexes mediate rapid and localized Ca2+-activated K+ signaling. *Science* 314, 615–620. doi: 10.1126/science.1132915

Boczek, N. J., Miller, E. M., Ye, D., Nesterenko, V. V., Tester, D. J., Antzelevitch, C., et al. (2015). Novel timothy syndrome mutation leading to increase in CACNA1C window current. *Heart Rhythm* 12, 211–219. doi: 10.1016/j.hrthm.2014.09.051

Boulkroun, S., Fernandes-Rosa, F. L., and Zennaro, M. C. (2020). Old and new genes in primary aldosteronism. *Best Pract. Res. Clin. Endocrinol. Metab.* 34:101375. doi: 10.1016/j.beem.2020.101375

Brennan, K. C., and Pietrobon, D. (2018). A systems neuroscience approach to migraine. *Neuron* 97, 1004–1021. doi: 10.1016/j.neuron.2018.01.029

Buraei, Z., and Yang, J. (2010). The ß subunit of voltage-gated Ca2+ channels. *Physiol. Rev.* 90, 1461–1506. doi: 10.1152/physrev.00057.2009

Burashnikov, E., Pfeiffer, R., Barajas-Martinez, H., Delpón, E., Hu, D., Desai, M., et al. (2010). Mutations in the cardiac L-type calcium channel associated with inherited J-wave syndromes and sudden cardiac death. *Heart Rhythm* 7, 1872–1882. doi: 10.1016/j.hrthm.2010.08.026

Calhoun, J. D., Hawkins, N. A., Zachwieja, N. J., and Kearney, J. A. (2016). Cacna1g is a genetic modifier of epilepsy caused by mutation of voltage-gated sodium channel Scn2a. *Epilepsia* 57, e103–e107. doi: 10.1111/epi.13390

Calorio, C., Gavello, D., Guarina, L., Salio, C., Sassoè-Pognetto, M., Riganti, C., et al. (2019). Impaired chromaffin cell excitability and exocytosis in autistic Timothy syndrome TS2-neo mouse rescued by L-type calcium channel blockers. *J. Physiol.* 597, 1705–1733. doi: 10.1113/JP277487

Cannon, S. C. (2017). An atypical CaV1.1 mutation reveals a common mechanism for hypokalemic periodic paralysis. *J. Gen. Physiol.* 149, 1061–1064. doi: 10.1085/jgp.201711923

Cao, Y., Tokita, M. J., Chen, E. S., Ghosh, R., Chen, T., Feng, Y., et al. (2019). A clinical survey of mosaic single nucleotide variants in disease-causing genes detected by exome sequencing. *Genome Med.* 11:48. doi: 10.1186/s13073-019-0658-2

Carreño, O., Corominas, R., Serra, S. A., Sintas, C., Fernández-Castillo, N., Vila-Pueyo, M., et al. (2013). Screening of CACNA1A and ATP1A2 genes in hemiplegic migraine: clinical, genetic, and functional studies. *Mol. Genet. Genomic Med.* 1, 206–222. doi: 10.1002/mgg3.24

Casey, H. L., and Gomez, C. M. (2019). "Spinocerebellar Ataxia Type 6," in *GeneReviews® [Internet]*, eds M. P. Adam, H. H. Ardinger, R. A. Pagon, S. E. Wallace, L. J. Bean, K. Stephens (Seattle, WA: University of Washington).

Catterall, W. A., Lenaeus, M. J., and Gamal El-Din, T. M. (2020). Structure and pharmacology of voltage-gated sodium and calcium channels. *Annu. Rev. Pharmacol. Toxicol.* 60, 133–154. doi: 10.1146/annurev-pharmtox-010818-021757

Chavali, N. V., Kryshtal, D. O., Parikh, S. S., Wang, L., Glazer, A. M., Blackwell, D. J., et al. (2019). Patient-independent human induced pluripotent stem cell model: a new tool for rapid determination of genetic variant pathogenicity in long QT syndrome. *Heart Rhythm* 16, 1686–1695. doi: 10.1016/j.hrthm.2019.04.031

Chemin, J., Siquier-Pernet, K., Nicouleau, M., Barcia, G., Ahmad, A., Medina-Cano, D., et al. (2018). De novo mutation screening in childhood-onset cerebellar atrophy identifies gain-of-function mutations in the CACNA1G calcium channel gene. *Brain* 141, 1998–2013. doi: 10.1093/brain/awy145

Cocos, R., Raicu, F., Bajenaru, O. L., Olaru, I., Dumitrescu, L., and Popescu, B. O. (2020). CACNA1B gene variants in adult-onset isolated focal dystonia. *Neurol. Sci.* doi: 10.1007/s10072-020-04778-8 [Epub ahead of print].

Colson, C., Mittre, H., Busson, A., Leenhardt, A., Denjoy, I., Fressard, V., et al. (2019). Unusual clinical description of adult with Timothy syndrome, carrier of a new heterozygote mutation of CACNA1C. *Eur. J. Med. Genet.* 62:103648. doi: 10.1016/j.ejmg.2019.04.005

Consortium, E. K., Project, E. P. G., Allen, A. S., Berkovic, S. F., Cossette, P., Delanty, N., et al. (2013). De novo mutations in epileptic encephalopathies. *Nature* 501, 217–221. doi: 10.1038/nature12439

Coutelier, M., Blesneac, I., Monteil, A., Monin, M.-L., Ando, K., Mundwiller, E., et al. (2015). A recurrent mutation in CACNA1G Alters Cav3.1 T-type calcium-channel conduction and causes autosomal-dominant cerebellar Ataxia. *Am. J. Hum. Genet.* 97, 726–737. doi: 10.1016/j.ajhg.2015.09.007

Damaj, L., Lupien-Meilleur, A., Lortie, A., Riou, É, Ospina, L. H., Gagnon, L., et al. (2015). CACNA1A haploinsufficiency causes cognitive impairment, autism and epileptic encephalopathy with mild cerebellar symptoms. *Eur. J. Hum. Genet.* 23, 1505–1512. doi: 10.1038/ejhg.2015.21

Daniil, G., Fernandes-Rosa, F. L., Chemin, J., Blesneac, I., Beltrand, J., Polak, M., et al. (2016). CACNA1H mutations are associated with different forms of primary aldosteronism. *EBioMedicine* 13, 225–236. doi: 10.1016/j.ebiom.2016.10.002

De Franco, E., Saint-Martin, C., Brusgaard, K., Knight Johnson, A. E., Aguilar-Bryan, L., Bowman, P., et al. (2020). Update of variants identified in the pancreatic β-cell KATP channel genes KCNJ11 and ABCC8 in individuals with congenital hyperinsulinism and diabetes. *Hum. Mutat.* 41, 884–905. doi: 10.1002/humu.23995

De Mingo Alemany, M. C., Mifsud Grau, L., Moreno Macián, F., Ferrer Lorente, B., and León Cariñena, S. (2020). A de novo CACNA1D missense mutation in a patient with congenital hyperinsulinism, primary hyperaldosteronism and hypotonia. *Channels* 14, 175–180. doi: 10.1080/19336950.2020.1761171

Di Cristofori, A., Fusi, L., Gomitoni, A., Grampa, G., and Bersano, A. (2012). R583Q CACNA1A variant in SHM1 and ataxia: case report and literature update. *J. Headache Pain* 13, 419–423. doi: 10.1007/s10194-012-0444-7

Dolphin, A. C. (2018). Voltage-gated calcium channel alpha 2delta subunits: an assessment of proposed novel roles. *F1000Res.* 7:F1000 Faculty Rev-1830. doi: 10.12688/f1000research.16104.1

Dolphin, A. C., and Lee, A. (2020). Presynaptic calcium channels: specialized control of synaptic neurotransmitter release. *Nat. Rev. Neurosci.* 21, 213–229. doi: 10.1038/s41583-020-0278-2

Drum, B. M. L., Dixon, R. E., Yuan, C., Cheng, E. P., and Santana, L. F. (2014). Cellular mechanisms of ventricular arrhythmias in a mouse model of Timothy syndrome (long QT syndrome 8). *J. Mol. Cell Cardiol.* 66, 63–71. doi: 10.1016/j.yjmcc.2013.10.021

Du, X., and Gomez, C. M. (2018). "Spinocerebellar ataxia type 6: molecular mechanisms and calcium channel genetics," in *Polyglutamine Disorders*, eds C. Nóbrega and L. Pereira de Almeida (Cham: Springer).

Ducros, A., Denier, C., Joutel, A., Cecillon, M., Lescoat, C., Vahedi, K., et al. (2001). The clinical spectrum of familial hemiplegic migraine associated with mutations in a neuronal calcium channel. *N. Engl. J. Med.* 345, 17–24. doi: 10.1056/nejm200107053450103

Dufendach, K. A., Giudicessi, J. R., Boczek, N. J., and Ackerman, M. J. (2013). Maternal mosaicism confounds the neonatal diagnosis of type 1 Timothy syndrome. *Pediatrics* 131, e1991–e1995. doi: 10.1542/peds.2012-2941

Eising, E., and van den Maagdenberg, A. M. J. M. (2017). "Hemiplegic migraine and channel disorders," in *Reference Module in Neuroscience and Biobehavioral Psychology*, (Amsterdam: Elsevier). doi: 10.1016/B978-0-12-809324-5.01969-6

Epi4K Consortium. (2016). *De novo* mutations in SLC1A2 and CACNA1A are important causes of epileptic encephalopathies. *Am. J. Hum. Genet.* 99, 287–298. doi: 10.1016/j.ajhg.2016.06.003

Epperson, M. V., Haws, M. E., Standridge, S. M., and Gilbert, D. L. (2018). An atypical Rett syndrome phenotype due to a novel missense mutation in CACNA1A. *J. Child Neurol.* 33, 286–289. doi: 10.1177/0883073818754987

Estes, S. I., Ye, D., Zhou, W., Dotzler, S. M., Tester, D. J., Bos, J. M., et al. (2019). Characterization of the CACNA1C-R518C missense mutation in the pathobiology of long-QT syndrome using human induced pluripotent stem cell cardiomyocytes shows action potential prolongation and L-type calcium channel perturbation. *Circ. Genom. Precis. Med.* 12:e002534. doi: 10.1161/CIRCGEN.119.002534

Etheridge, S. P., Bowles, N. E., Arrington, C. B., Pilcher, T., Rope, A., Wilde, A. A. M., et al. (2011). Somatic mosaicism contributes to phenotypic variation in Timothy syndrome. *Am. J. Med. Genet. A* 155A, 2578–2583. doi: 10.1002/ajmg.a.34223

Fletcher, C. F., Tottene, A., Lennon, V. A., Wilson, S. M., Dubel, S. J., Paylor, R., et al. (2001). Dystonia and cerebellar atrophy in Cacna1a null mice lacking P/Q calcium channel activity. *FASEB J.* 15, 1288–1290. doi: 10.1096/fj.00-0562fje

Flucher, B. E. (2020). Skeletal muscle CaV1.1 channelopathies. *Pflügers Arch.* 472, 739–754. doi: 10.1007/s00424-020-02368-3

Flucher, B. E., and Campiglio, M. (2019). STAC proteins: the missing link in skeletal muscle EC coupling and new regulators of calcium channel function. *Biochim. Biophys. Acta Mol. Cell Res.* 1866, 1101–1110. doi: 10.1016/j.bbamcr.2018.12.004

Forti, L., and Pietrobon, D. (1993). Functional diversity of L-type calcium channels in rat cerebellar neurons. *Neuron* 10, 437–450. doi: 10.1016/0896-6273(93)90332-l

Fröhler, S., Kieslich, M., Langnick, C., Feldkamp, M., Opgen-Rhein, B., Berger, F., et al. (2014). Exome sequencing helped the fine diagnosis of two siblings afflicted with atypical Timothy syndrome (TS2). *BMC Med. Genet.* 15:48. doi: 10.1186/1471-2350-15-48

Fukuyama, M., Ohno, S., Wang, Q., Shirayama, T., Itoh, H., and Horie, M. (2014a). Nonsense-mediated mRNA decay due to a CACNA1C splicing mutation in a patient with Brugada syndrome. *Heart Rhythm* 11, 629–634. doi: 10.1016/j.hrthm.2013.12.011

Fukuyama, M., Wang, Q., Kato, K., Ohno, S., Ding, W.-G., Toyoda, F., et al. (2014b). Long QT syndrome type 8: novel CACNA1C mutations causing QT prolongation and variant phenotypes. *Europace* 16, 1828–1837. doi: 10.1093/europace/euu063

Fuster, C., Perrot, J., Berthier, C., Jacquemond, V., Charnet, P., and Allard, B. (2017). Na leak with gating pore properties in hypokalemic periodic paralysis V876E mutant muscle Ca channel. *J. Gen. Physiol.* 149, 1139–1148. doi: 10.1085/jgp.201711834

Gao, S., and Yan, N. (2020). Structural basis of the modulation of the voltage-gated calcium ion channel Cav 1.1 by dihydropyridine compounds. *Angew. Chem. Int. Ed. Engl.* doi: 10.1002/anie.202011793 [Epub ahead of print].

Ghaleb, Y. E., Schneeberger, P. E., Fernández-Quintero, M. L., Geisler, S. M., Pelizzari, S., Polstra, A. M., et al. (2021). CACNA1I gain-of-function mutations differentially affect channel gating and cause neurodevelopmental disorders. *Brain.* (in press).

Ghoshal, A., Uygun, D. S., Yang, L., McNally, J. M., Lopez-Huerta, V. G., Arias-Garcia, M. A., et al. (2020). Effects of a patient-derived de novo coding alteration of CACNA1I in mice connect a schizophrenia risk gene with sleep spindle deficits. *Transl. Psychiatry* 10:29. doi: 10.1038/s41398-020-0685-1

Gillis, J., Burashnikov, E., Antzelevitch, C., Blaser, S., Gross, G., Turner, L., et al. (2012). Long QT, syndactyly, joint contractures, stroke and novel CACNA1C mutation: expanding the spectrum of Timothy syndrome. *Am. J. Med. Genet. A* 158A, 182–187. doi: 10.1002/ajmg.a.34355

Giudicessi, J. R., and Ackerman, M. J. (2016). Calcium revisited: new insights into the molecular basis of long-QT syndrome. *Circ. Arrhythm. Electrophysiol.* 9:e002480. doi: 10.1161/CIRCEP.116.002480

Gloyn, A. L., Pearson, E. R., Antcliff, J. F., Proks, P., Bruining, G. J., Slingerland, A. S., et al. (2004). Activating mutations in the gene encoding the ATP-sensitive potassium-channel subunit Kir6.2 and permanent neonatal diabetes. *N. Engl. J. Med.* 350, 1838–1849. doi: 10.1056/NEJMoa032922

Goadsby, P. J., Holland, P. R., Martins-Oliveira, M., Hoffmann, J., Schankin, C., and Akerman, S. (2017). Pathophysiology of migraine: a disorder of sensory processing. *Physiol. Rev.* 97, 553–622. doi: 10.1152/physrev.00034.2015

Gorman, K. M., Meyer, E., Grozeva, D., Spinelli, E., McTague, A., et al. (2019). Bi-allelic Loss-of-function CACNA1B mutations in progressive epilepsy-dyskinesia. *Am. J. Hum. Genet.* 104, 948–956. doi: 10.1016/j.ajhg.2019.03.005

Gratten, J., Visscher, P. M., Mowry, B. J., and Wray, N. R. (2013). Interpreting the role of de novo protein-coding mutations in neuropsychiatric disease. *Nat. Genet.* 45, 234–238. doi: 10.1038/ng.2555

Groen, J. L., Andrade, A., Ritz, K., Jalalzadeh, H., Haagmans, M., Bradley, T. E. J., et al. (2014). CACNA1B mutation is linked to unique myoclonus-dystonia syndrome. *Hum. Mol. Genet.* 24, 987–993. doi: 10.1093/hmg/ddu513

Groome, J. R., Moreau, A., and Delemotte, L. (2017). "Gating pore currents in sodium channels," in *Voltage-gated Sodium Channels: Structure, Function and Channelopathies*, ed. M. Chahine (Cham: Springer).

Hans, M., Luvisetto, S., Williams, M. E., Spagnolo, M., Urrutia, A., Tottene, A., et al. (1999). Functional consequences of mutations in the human alpha1A calcium channel subunit linked to familial hemiplegic migraine. *J. Neurosci.* 19, 1610–1619. doi: 10.1523/jneurosci.19-05-01610.1999

Hardie, J., and Lee, A. (2016). Decalmodulation of Cav1 channels by CaBPs. *Channels* 10, 33–37. doi: 10.1080/19336950.2015.1051273

Hashiguchi, S., Doi, H., Kunii, M., Nakamura, Y., Shimuta, M., Suzuki, E., et al. (2019). Ataxic phenotype with altered CaV3.1 channel property in a mouse model for spinocerebellar ataxia 42. *Neurobiol. Dis.* 130:104516. doi: 10.1016/j.nbd.2019.104516

Helbig, K. L., Farwell Hagman, K. D., Shinde, D. N., Mroske, C., Powis, Z., Li, S., et al. (2016). Diagnostic exome sequencing provides a molecular diagnosis for a significant proportion of patients with epilepsy. *Genet. Med.* 18, 898–905. doi: 10.1038/gim.2015.186

Helbig, K. L., Lauerer, R. J., Bahr, J. C., Souza, I. A., Myers, C. T., Uysal, B., et al. (2018). *De novo* pathogenic variants in CACNA1E cause developmental and epileptic encephalopathy with contractures, macrocephaly, and dyskinesias. *Am. J. Hum. Genet.* 103, 666–678. doi: 10.1016/j.ajhg.2018.09.006

Hemara-Wahanui, A., Berjukow, S., Hope, C. I., Dearden, P. K., Wu, S. B., Wilson-Wheeler, J., et al. (2005). A CACNA1F mutation identified in an X-linked retinal disorder shifts the voltage dependence of Cav1.4 channel activation. *Proc. Natl. Acad. Sci. U.S.A.* 102, 7553–7558. doi: 10.1073/pnas.0501907102

Hennessey, J. A., Boczek, N. J., Jiang, Y.-H., Miller, J. D., Patrick, W., Pfeiffer, R., et al. (2014). A CACNA1C variant associated with reduced voltage-dependent inactivation, increased CaV1.2 channel window current, and arrhythmogenesis. *PLoS One* 9:e106982. doi: 10.1371/journal.pone.0106982

Hoda, J. C., Zaghetto, F., Koschak, A., and Striessnig, J. (2005). Congenital stationary night blindness type 2 mutations S229P, G369D, L1068P, and W1440X alter channel gating or functional expression of Cav1.4 L-type calcium channels. *J. Neurosci.* 25, 252–259. doi: 10.1523/jneurosci.3054-04.2005

Hoda, J. C., Zaghetto, F., Singh, A., Koschak, A., and Striessnig, J. (2006). Effects of congenital stationary night blindness type 2 mutations R508Q and L1364H on Cav1.4 L-type calcium channel function and expression. *J. Neurochem.* 96, 1648–1658. doi: 10.1111/j.1471-4159.2006.03678.x

Hofer, N. T., Tuluc, P., Ortner, N. J., Nikonishyna, Y. V., Fernándes-Quintero, M. L., Liedl, K. R., et al. (2020). Biophysical classification of a CACNA1D de novo mutation as a high-risk mutation for a severe neurodevelopmental disorder. *Mol. Autism* 11:4. doi: 10.1186/s13229-019-0310-4

Hofmann, F., Belkacemi, A., and Flockerzi, V. (2015). Emerging alternative functions for the auxiliary subunits of the voltage-gated calcium channels. *Curr. Mol. Pharmacol.* 8, 162–168. doi: 10.2174/1874467208666150507110202

Holbrook, J. A., Neu-Yilik, G., Hentze, M. W., and Kulozik, A. E. (2004). Nonsense-mediated decay approaches the clinic. *Nat. Genet.* 36, 801–808. doi: 10.1038/ng1403

Hope, C. I., Sharp, D. M., Hemara-Wahanui, A., Sissingh, J. I., Lundon, P., Mitchell, E. A., et al. (2005). Clinical manifestations of a unique X-linked retinal disorder in a large New Zealand family with a novel mutation in CACNA1F, the gene responsible for CSNB2. *Clin. Exp. Ophthalmol.* 33, 129–136. doi: 10.1111/j.1442-9071.2005.00987.x

Howard, M. A., and Baraban, S. C. (2017). Catastrophic epilepsies of childhood. *Annu. Rev. Neurosci.* 40, 149–166. doi: 10.1146/annurev-neuro-072116-031250

Huang, H., Tan, B. Z., Shen, Y., Tao, J., Jiang, F., Sung, Y. Y., et al. (2012). RNA editing of the IQ domain in Cav1.3 channels modulates their Ca2+-dependent inactivation. *Neuron* 73, 304–316. doi: 10.1016/j.neuron.2011.11.022

Humbertclaude, V., Riant, F., Krams, B., Zimmermann, V., Nagot, N., Annequin, D., et al. (2020). Cognitive impairment in children with CACNA1A mutations. *Dev. Med. Child Neurol.* 62, 330–337. doi: 10.1111/dmcn.14261

Inagaki, A., Frank, C. A., Usachev, Y. M., Benveniste, M., and Lee, A. (2014). Pharmacological correction of gating defects in the voltage-gated Cav2.1 Ca^2 channel due to a familial hemiplegic migraine mutation. *Neuron* 81, 91–102. doi: 10.1016/j.neuron.2013.10.056

Indelicato, E., Nachbauer, W., Karner, E., Eigentler, A., Wagner, M., Unterberger, I., et al. (2019). The neuropsychiatric phenotype in CACNA1A mutations: a retrospective single center study and review of the literature. *Eur. J. Neurol.* 26:66-e7. doi: 10.1111/ene.13765

Izquierdo-Serra, M., Fernández-Fernández, J. M., and Serrano, M. (2020). Rare CACNA1A mutations leading to congenital ataxia. *Pflugers Arch.* 472, 791–809. doi: 10.1007/s00424-020-02396-z

Jacobs, A., Knight, B. P., McDonald, K. T., and Burke, M. C. (2006). Verapamil decreases ventricular tachyarrhythmias in a patient with Timothy syndrome (LQT8). *Heart Rhythm* 3, 967–970. doi: 10.1016/j.hrthm.2006.04.024

Jen, J., Kim, G. W., and Baloh, R. W. (2004). Clinical spectrum of episodic ataxia type 2. *Neurology* 62, 17–22. doi: 10.1212/01.wnl.0000101675.61074.50

Jen, J. C. (1993). "Familial Hemiplegic Migraine," in *GeneReviews [Internet]*, eds M. P. Adam, H. H. Ardinger, R. A. Pagon, S. E. Wallace, L. J. Bean, K. Stephens, et al. (Seattle, WA: University of Washington).

Jen, J. C. (2015). "Familial Hemiplegic Migraine," in *GeneReviews® [Internet]*, eds M. P. Adam, H. H. Ardinger, R. A. Pagon, S. E. Wallace, L. J. Bean, K. Stephens (Seattle, WA: University of Washington).

Jiang, D., Gamal El-Din, T. M., Ing, C., Lu, P., Pomes, R., Zheng, N., et al. (2018). Structural basis for gating pore current in periodic paralysis. *Nature* 557, 590–594. doi: 10.1038/s41586-018-0120-4

Jiang, D., Shi, H., Tonggu, L., Gamal El-Din, T. M., Lenaeus, M. J., Zhao, Y., et al. (2019). Structure of the cardiac sodium channel. *Cell* 180, 122–134.e10. doi: 10.1016/j.cell.2019.11.041

Jiang, X., Raju, P. K., D'Avanzo, N., Lachance, M., Pepin, J., Dubeau, F., et al. (2019). Both gain-of-function and loss-of-function de novo CACNA1A mutations cause severe developmental epileptic encephalopathies in the spectrum of Lennox-Gastaut syndrome. *Epilepsia* 60, 1881–1894. doi: 10.1111/epi.16316

Jun, K., Piedras-Renteria, E. S., Smith, S. M., Wheeler, D. B., Lee, S. B., Lee, T. G., et al. (1999). Ablation of P/Q-type Calcium channel currents, altered synaptic transmission, and progressive ataxia in mice lacking the alpha1A- subunit. *Proc. Natl. Acad. Sci. U.S.A.* 96, 15245–15250. doi: 10.1073/pnas.96.26.15245

Jurkat-Rott, K., Groome, J., and Lehmann-Horn, F. (2012). Pathophysiological role of omega pore current in channelopathies. *Front. Pharmacol.* 3:112. doi: 10.3389/fphar.2012.00112

Kabir, Z. D., Martinez-Rivera, A., and Rajadhyaksha, A. M. (2017). From gene to behavior: L-type calcium channel mechanisms underlying neuropsychiatric symptoms. *Neurotherapeutics* 14, 588–613. doi: 10.1007/s13311-017-0532-0

Karczewski, K. J., Francioli, L. C., Tiao, G., Cummings, B. B., Alföldi, J., Wang, Q., et al. (2020). The mutational constraint spectrum quantified from variation in 141,456 humans. *Nature* 581, 434–443. doi: 10.1038/s41586-020-2308-7

Kim, C., Jeon, D., Kim, Y.-H., Lee, C. J., Kim, H., and Shin, H.-S. (2009). Deletion of N-type Ca(2+) channel Ca(v)2.2 results in hyperaggressive behaviors in mice. *J. Biol. Chem.* 284, 2738–2745. doi: 10.1074/jbc.M807179200

Kim, D., Song, I., Keum, S., Lee, T., Jeong, M. J., Kim, S. S., et al. (2001). Lack of the burst firing of thalamocortical relay neurons and resistance to absence seizures in mice lacking alpha1G T-type Calcium channels. *Neuron* 31, 35–45. doi: 10.1016/s0896-6273(01)00343-9

Kochinke, K., Zweier, C., Nijhof, B., Fenckova, M., Cizek, P., Honti, F., et al. (2016). Systematic phenomics analysis deconvolutes genes mutated in intellectual disability into biologically coherent modules. *Am. J. Hum. Genet.* 98, 149–164. doi: 10.1016/j.ajhg.2015.11.024

Kosaki, R., Ono, H., Terashima, H., and Kosaki, K. (2018). Timothy syndrome-like condition with syndactyly but without prolongation of the QT interval. *Am. J. Med. Genet. A* 176, 1657–1661. doi: 10.1002/ajmg.a.38833

Koschak, A., Reimer, D., Huber, I., Grabner, M., Glossmann, H., Engel, J., et al. (2001). α1D (Cav1.3) subunits can form L-type calcium channels activating at negative voltages. *J. Biol. Chem.* 276, 22100–22106. doi: 10.1074/jbc.m101469200

Kraus, R. L., Sinnegger, M. J., Glossmann, H., Hering, S., and Striessnig, J. (1998). Familial hemiplegic migraine mutations change alpha1A Ca2+ channel kinetics. *J. Biol. Chem.* 273, 5586–5590. doi: 10.1074/jbc.273.10.5586

Krey, J. F., Pasca, S. P., Shcheglovitov, A., Yazawa, M., Schwemberger, R., Rasmusson, R., et al. (2013). Timothy syndrome is associated with activity-dependent dendritic retraction in rodent and human neurons. *Nat. Neurosci.* 16, 201–209. doi: 10.1038/nn.3307

Krueger, D. A., Wilfong, A. A., Mays, M., Talley, C. M., Agricola, K., Tudor, C., et al. (2016). Long-term treatment of epilepsy with everolimus in tuberous sclerosis. *Neurology* 87, 2408–2415. doi: 10.1212/WNL.0000000000003400

Krumm, N., Turner, T. N., Baker, C., Vives, L., Mohajeri, K., Witherspoon, K., et al. (2015). Excess of rare, inherited truncating mutations in autism. *Nat. Genet.* 47, 582–588. doi: 10.1038/ng.3303

Kubota, T., Wu, F., Vicart, S., Nakaza, M., Sternberg, D., Watanabe, D., et al. (2020). Hypokalaemic periodic paralysis with a charge-retaining substitution in the voltage sensor. *Brain Commun.* 2:fcaa103. doi: 10.1093/braincomms/fcaa103

Kuzmiski, J. B., Barr, W., Zamponi, G. W., and MacVicar, B. A. (2005). Topiramate inhibits the initiation of plateau potentials in CA1 neurons by depressing R-type calcium channels. *Epilepsia* 46, 481–489. doi: 10.1111/j.0013-9580.2005.35304.x

Landstrom, A. P., Boczek, N. J., Ye, D., Miyake, C. Y., De la Uz, C. M., Allen, H. D., et al. (2016). Novel long QT syndrome-associated missense mutation, L762F, in CACNA1C-encoded L-type calcium channel imparts a slower inactivation tau and increased sustained and window current. *Int. J. Cardiol.* 220, 290–298. doi: 10.1016/j.ijcard.2016.06.081

Latour, I., Louw, D. F., Beedle, A. M., Hamid, J., Sutherland, G. R., and Zamponi, G. W. (2004). Expression of T-type calcium channel splice variants in human glioma. *Glia* 48, 112–119. doi: 10.1002/glia.20063

Li, G., Wang, J., Liao, P., Bartels, P., Zhang, H., Yu, D., et al. (2017). Exclusion of alternative exon 33 of CaV1.2 calcium channels in heart is proarrhythmogenic. *Proc. Natl. Acad. Sci. U.S.A.* 114, E4288–E4295. doi: 10.1073/pnas.1617205114

Li, X., Zhou, C., Cui, L., Zhu, L., Du, H., Liu, J., et al. (2018). A case of a novel CACNA1G mutation from a Chinese family with SCA42: a case report and literature review. *Medicine* 97:e12148. doi: 10.1097/MD.0000000000012148

Liaqat, K., Schrauwen, I., Raza, S. I., Lee, K., Hussain, S., Chakchouk, I., et al. (2019). Identification of CACNA1D variants associated with sinoatrial node dysfunction and deafness in additional Pakistani families reveals a clinical significance. *J. Hum. Genet.* 64, 153–160. doi: 10.1038/s10038-018-0542-8

Lim, E. T., Uddin, M., De Rubeis, S., Chan, Y., Kamumbu, A. S., Zhang, X., et al. (2017). Rates, distribution and implications of postzygotic mosaic mutations in autism spectrum disorder. *Nat. Neurosci.* 20, 1217–1224. doi: 10.1038/nn.4598

Limpitikul, W. B., Dick, I. E., Ben-Johny, M., and Yue, D. T. (2016). An autism-associated mutation in CaV1.3 channels has opposing effects on voltage- and Ca(2+)-dependent regulation. *Sci. Rep.* 6:27235. doi: 10.1038/srep27235

Liu, G., Papa, A., Katchman, A. N., Zakharov, S. I., Roybal, D., Hennessey, J. A., et al. (2020). Mechanism of adrenergic CaV1.2 stimulation revealed by proximity proteomics. *Nature* 577, 695–700. doi: 10.1038/s41586-020-1947-z

Liu, Y., Xue, Y., Wu, S., Duan, J., Lin, L., Wang, L., et al. (2016). Effect of verapamil in the treatment of type 2 long QT syndrome is not a dose-dependent pattern: a study from bedside to bench, and back. *Eur. Heart J. Suppl.* 18(Suppl. A), A37–A46. doi: 10.1093/eurheartj/suw006

Loh, K. W. Z., Liang, M. C., Soong, T. W., and Hu, Z. (2020). Regulation of cardiovascular calcium channel activity by post-translational modifications or interacting proteins. *Pflugers Arch.* 472, 653–667. doi: 10.1007/s00424-020-02398-x

Lory, P., Nicole, S., and Monteil, A. (2020). Neuronal Cav3 channelopathies: recent progress and perspectives. *Pflügers Arch.* 472, 831–844. doi: 10.1007/s00424-020-02429-7

Luo, X., Rosenfeld, J. A., Yamamoto, S., Harel, T., Zuo, Z., Hall, M., et al. (2017). Clinically severe CACNA1A alleles affect synaptic function and neurodegeneration differentially. *PLoS Genet.* 13:e1006905. doi: 10.1371/journal.pgen.1006905

Männikkö, R., Shenkarev, Z. O., Thor, M. G., Berkut, A. A., Myshkin, M. Y., Paramonov, A. S., et al. (2018). Spider toxin inhibits gating pore currents underlying periodic paralysis. *Proc. Natl. Acad. Sci. U.S.A.* 115, 4495–4500. doi: 10.1073/pnas.1720185115

Marcantoni, A., Calorio, C., Hidisoglu, E., Chiantia, G., and Carbone, E. (2020). Cav1.2 channelopathies causing autism: new hallmarks on Timothy syndrome. *Pflugers Arch.* 472, 775–789. doi: 10.1007/s00424-020-02430-0

Marcantoni, A., Vandael, D. H., Mahapatra, S., Carabelli, V., Sinnegger-Brauns, M. J., Striessnig, J., et al. (2010). Loss of Cav1.3 channels reveals the critical role of L-type and BK channel coupling in pacemaking mouse adrenal chromaffin cells. *J. Neurosci.* 30, 491–504. doi: 10.1523/JNEUROSCI.4961-09.2010

Marger, L., Mesirca, P., Alig, J., Torrente, A., Dübel, S., Engeland, B., et al. (2014). Functional roles of Ca v 1.3, Ca v 3.1 and HCN channels in automaticity of mouse atrioventricular cells. *Channels* 5, 251–261. doi: 10.4161/chan.5.3.15266

Mark, M. D., Maejima, T., Kuckelsberg, D., Yoo, J. W., Hyde, R. A., Shah, V., et al. (2011). Delayed postnatal loss of P/Q-type calcium channels recapitulates the absence epilepsy, dyskinesia, and ataxia phenotypes of genomic Cacna1a mutations. *J. Neurosci.* 31, 4311–4326. doi: 10.1523/JNEUROSCI.5342-10.2011

Mastrolia, V., Flucher, S. M., Obermair, G. J., Drach, M., Hofer, H., Renstrom, E., et al. (2017). Loss of alpha2delta-1 calcium channel subunit function increases the susceptibility for diabetes. *Diabetes* 66, 897–907. doi: 10.2337/db16-0336

Mellor, G. J., Panwar, P., Lee, A. K., Steinberg, C., Hathaway, J. A., Bartels, K., et al. (2019). Type 8 long QT syndrome: pathogenic variants in CACNA1C-encoded Cav1.2 cluster in STAC protein binding site. *Europace* 21, 1725–1732. doi: 10.1093/europace/euz215

Mencacci, N. E., R'bibo, L., Bandres-Ciga, S., Carecchio, M., Zorzi, G., Nardocci, N., et al. (2015). The CACNA1B R1389H variant is not associated with myoclonus-dystonia in a large European multicentric cohort. *Hum. Mol. Genet.* 24, 5326–5329. doi: 10.1093/hmg/ddv255

Mezghrani, A., Monteil, A., Watschinger, K., Sinnegger-Brauns, M. J., Barrère, C., Bourinet, E., et al. (2008). A destructive interaction mechanism accounts for dominant-negative effects of misfolded mutants of voltage-gated calcium channels. *J. Neurosci.* 28, 4501–4511. doi: 10.1523/JNEUROSCI.2844-07.2008

Miki, T., Nagashima, K., Tashiro, F., Kotake, K., Yoshitomi, H., Tamamoto, A., et al. (1998). Defective insulin secretion and enhanced insulin action in KATP channel-deficient mice. *Proc. Natl. Acad. Sci. U.S.A.* 95, 10402–10406. doi: 10.1073/pnas.95.18.10402

Miki, T., Zwingman, T. A., Wakamori, M., Lutz, C. M., Cook, S. A., Hosford, D. A., et al. (2008). Two novel alleles of tottering with distinct Ca(v)2.1 calcium channel neuropathologies. *Neuroscience* 155, 31–44. doi: 10.1016/j.neuroscience.2008.05.028

Monteleone, S., Lieb, A., Pinggera, A., Negro, G., Fuchs, J. E., Hofer, F., et al. (2017). Mechanisms responsible for omega-pore currents in Cav calcium channel voltage-sensing domains. *Biophys. J.* 113, 1485–1495. doi: 10.1016/j.bpj.2017.08.010

Moreau, A., Gosselin-Badaroudine, P., Boutjdir, M., and Chahine, M. (2015). Mutations in the voltage sensors of domains I and II of Nav1.5 that are associated with arrhythmias and dilated cardiomyopathy generate gating pore currents. *Front. Pharmacol.* 6:301. doi: 10.3389/fphar.2015.00301

Morino, H., Matsuda, Y., Muguruma, K., Miyamoto, R., Ohsawa, R., Ohtake, T., et al. (2015). A mutation in the low voltage-gated calcium channel CACNA1G alters the physiological properties of the channel, causing spinocerebellar ataxia. *Mol. Brain* 8:89. doi: 10.1186/s13041-015-0180-4

Myers, C. T., Hollingsworth, G., Muir, A. M., Schneider, A. L., Thuesmunn, Z., Knupp, A., et al. (2018). Parental mosaicism in "*De novo*" epileptic encephalopathies. *N. Engl. J. Med.* 378, 1646–1648. doi: 10.1056/nejmc1714579

Myers, S. M., Challman, T. D., Bernier, R., Bourgeron, T., Chung, W. K., Constantino, J. N., et al. (2020). Insufficient evidence for "Autism-Specific" genes. *Am. J. Hum. Genet.* 106, 587–595. doi: 10.1016/j.ajhg.2020.04.004

Nanba, K., Blinder, A. R., Rege, J., Hattangady, N. G., Else, T., Liu, C.-J., et al. (2020). Somatic CACNA1H mutation as a cause of aldosterone-producing adenoma. *Hypertension* 75, 645–649. doi: 10.1161/HYPERTENSIONAHA.119.14349

Nanou, E., and Catterall, W. A. (2018). Calcium channels, synaptic plasticity, and neuropsychiatric disease. *Neuron* 98, 466–481. doi: 10.1016/j.neuron.2018.03.017

Noebels, J. L. (2019). Predicting the impact of sodium channel mutations in human brain disease. *Epilepsia* 60(Suppl. 3), S8–S16. doi: 10.1111/epi.14724

Ortner, N. J., and Striessnig, J. (2020). *De novo* CACNA1D Ca2+ channelopathies: clinical phenotypes and molecular mechanism. *Pflügers Arch.* 472, 755–773. doi: 10.1007/s00424-020-02418-w

Ozawa, J., Ohno, S., Saito, H., Saitoh, A., Matsuura, H., and Horie, M. (2018). A novel CACNA1C mutation identified in a patient with Timothy syndrome without syndactyly exerts both marked loss- and gain-of-function effects. *HeartRhythm Case Rep.* 4, 273–277. doi: 10.1016/j.hrcr.2018.03.003

Page, K. M., Heblich, F., Margas, W., Pratt, W. S., Nieto-Rostro, M., Chaggar, K., et al. (2010). N terminus is key to the dominant negative suppression of Ca(V)2 calcium channels: implications for episodic ataxia type 2. *J. Biol. Chem.* 285, 835–844. doi: 10.1074/jbc.M109.065045

Panagiotakos, G., Haveles, C., Arjun, A., Petrova, R., Rana, A., Portmann, T., et al. (2019). Aberrant calcium channel splicing drives defects in cortical differentiation in Timothy syndrome. *eLife* 8:e51037. doi: 10.7554/eLife.51037

Pangrsic, T., Singer, J. H., and Koschak, A. (2018). Voltage-gated calcium channels: key players in sensory coding in the retina and the inner ear. *Physiol. Rev.* 98, 2063–2096. doi: 10.1152/physrev.00030.2017

Pantazis, A., Savalli, N., Sigg, D., Neely, A., and Olcese, R. (2014). Functional heterogeneity of the four voltage sensors of a human L-type calcium channel. *Proc. Natl. Acad. Sci. U.S.A.* 111, 18381–18386. doi: 10.1073/pnas.1411127112

Paşca, S. P., Portmann, T., Voineagu, I., Yazawa, M., Shcheglovitov, A., Paşca, A. M., et al. (2011). Using iPSC-derived neurons to uncover cellular phenotypes associated with Timothy syndrome. *Nat. Med.* 17, 1657–1662. doi: 10.1038/nm.2576

Peloquin, J. B., Rehak, R., Doering, C. J., and McRory, J. E. (2007). Functional analysis of congenital stationary night blindness type-2 CACNA1F mutations F742C, G1007R, and R1049W. *Neuroscience* 150, 335–345. doi: 10.1016/j.neuroscience.2007.09.021

Perez-Reyes, E., and Lory, P. (2006). Molecular biology of T-type calcium channels. *CNS Neurol. Disord. Drug Targets* 5, 605–609. doi: 10.2174/187152706779025508

Pettersen, E. F., Goddard, T. D., Huang, C. C., Couch, G. S., Greenblatt, D. M., Meng, E. C., et al. (2004). UCSF Chimera–a visualization system for exploratory research and analysis. *J. Comput. Chem.* 25, 1605–1612. doi: 10.1002/jcc.20084

Pietrobon, D., and Striessnig, J. (2003). Neurobiology of migraine. *Nat. Rev. Neurosci.* 4, 386–398.

Pinggera, A., Lieb, A., Benedetti, B., Lampert, M., Monteleone, S., Liedl, K. R., et al. (2015). CACNA1D de novo mutations in autism spectrum disorders activate Cav1.3 L-type calcium channels. *Biol. Psychiatry* 77, 816–822. doi: 10.1016/j.biopsych.2014.11.020

Pinggera, A., Mackenroth, L., Rump, A., Schallner, J., Beleggia, F., Wollnik, B., et al. (2017). New gain-of-function mutation shows CACNA1D as recurrently mutated gene in autism spectrum disorders and epilepsy. *Hum. Mol. Genet.* 26, 2923–2932. doi: 10.1093/hmg/ddx175

Pinggera, A., Negro, G., Tuluc, P., Brown, M. J., Lieb, A., and Striessnig, J. (2018). Gating defects of disease-causing de novo mutations in Cav1.3 Ca(2+) channels. *Channels* 12, 388–402. doi: 10.1080/19336950.2018.1546518

Platzer, J., Engel, J., Schrott-Fischer, A., Stephan, K., Bova, S., Chen, H., et al. (2000). Congenital deafness and sinoatrial node dysfunction in mice lacking class D L-type Ca2+ channels. *Cell* 102, 89–97. doi: 10.1016/s0092-8674(00)00013-1

Powell, K. L., Cain, S. M., Ng, C., Sirdesai, S., David, L. S., Kyi, M., et al. (2009). A Cav3.2 T-type calcium channel point mutation has splice-variant-specific effects on function and segregates with seizure expression in a polygenic rat model of absence epilepsy. *J. Neurosci.* 29, 371–380. doi: 10.1523/JNEUROSCI.5295-08.2009

Priori, S. G., Blomström-Lundqvist, C., Mazzanti, A., Blom, N., Borggrefe, M., Camm, J., et al. (2015). 2015 ESC Guidelines for the management of patients with ventricular arrhythmias and the prevention of sudden cardiac death: the Task Force for the Management of Patients with Ventricular Arrhythmias and the Prevention of Sudden Cardiac Death of the European Society of Cardiology (ESC)Endorsed by: association for European Paediatric and Congenital Cardiology (AEPC). *Eur. Heart J.* 36, 2793–2867. doi: 10.1093/eurheartj/ehv316

Proft, J., Rzhepetskyy, Y., Lazniewska, J., Zhang, F.-X., Cain, S. M., Snutch, T. P., et al. (2017). The Cacna1h mutation in the GAERS model of absence epilepsy enhances T-type Ca2+ currents by altering calnexin-dependent trafficking of Cav3.2 channels. *Sci. Rep.* 7:11513. doi: 10.1038/s41598-017-11591-5

Ramachandran, K. V., Hennessey, J. A., Barnett, A. S., Yin, X., Stadt, H. A., Foster, E., et al. (2013). Calcium influx through L-type CaV1.2 Ca2+ channels regulates mandibular development. *J. Clin. Invest.* 123, 1638–1646. doi: 10.1172/jci66903

Reichenbach, H., Meister, E. M., and Theile, H. (1992). [The heart-hand syndrome. A new variant of disorders of heart conduction and syndactylia including osseous changes in hands and feet]. *Kinderarztl. Prax.* 60, 54–56.

Richards, S., Aziz, N., Bale, S., Bick, D., Das, S., Gastier-Foster, J., et al. (2015). Standards and guidelines for the interpretation of sequence variants: a joint consensus recommendation of the American College of Medical Genetics and Genomics and the Association for Molecular Pathology. *Genet. Med.* 17, 405–424. doi: 10.1038/gim.2015.30

Romaniello, R., Zucca, C., Tonelli, A., Bonato, S., Baschirotto, C., Zanotta, N., et al. (2010). A wide spectrum of clinical, neurophysiological and neuroradiological abnormalities in a family with a novel CACNA1A mutation. *J. Neurol. Neurosurg. Psychiatry* 81, 840–843. doi: 10.1136/jnnp.2008.163402

Rose, S. J., Kriener, L. H., Heinzer, A. K., Fan, X., Raike, R. S., van den Maagdenberg, A. M. J. M., et al. (2014). The first knockin mouse model of episodic ataxia type 2. *Exp. Neurol.* 261, 553–562. doi: 10.1016/j.expneurol.2014.08.001

Samueli, S., Abraham, K., Dressler, A., Gröppel, G., Mühlebner-Fahrngruber, A., Scholl, T., et al. (2016). Efficacy and safety of Everolimus in children with TSC - associated epilepsy – Pilot data from an open single-center prospective study. *Orphanet J. Rare Dis.* 11:145. doi: 10.1186/s13023-016-0530-z

Satterstrom, F. K., Kosmicki, J. A., Wang, J., Breen, M. S., De Rubeis, S., An, J.-Y., et al. (2020). Large-scale exome sequencing study implicates both developmental and functional changes in the neurobiology of autism. *Cell* 180, 568–584. doi: 10.1016/j.cell.2019.12.036

Schartner, V., Romero, N. B., Donkervoort, S., Treves, S., Munot, P., Pierson, T. M., et al. (2017). Dihydropyridine receptor (DHPR, CACNA1S) congenital myopathy. *Acta Neuropathol.* 133, 517–533. doi: 10.1007/s00401-016-1656-8

Scholl, U. I., Goh, G., Stolting, G., de Oliveira, R. C., Choi, M., Overton, J. D., et al. (2013). Somatic and germline CACNA1D calcium channel mutations in aldosterone-producing adenomas and primary aldosteronism. *Nat. Genet.* 45, 1050–1054. doi: 10.1038/ng.2695

Scholl, U. I., Stölting, G., Nelson-Williams, C., Vichot, A. A., Choi, M., Loring, E., et al. (2015). Recurrent gain of function mutation in calcium channel CACNA1H causes early-onset hypertension with primary aldosteronism. *eLife* 4:e06315. doi: 10.7554/eLife.06315

Shah, D. P., Baez-Escudero, J. L., Weisberg, I. L., Beshai, J. F., and Burke, M. C. (2012). Ranolazine safely decreases ventricular and atrial fibrillation in Timothy syndrome (LQT8). *Pacing Clin. Electrophysiol.* 35, e62–e64. doi: 10.1111/j.1540-8159.2010.02913.x

Sinnegger-Brauns, M. J., Hetzenauer, A., Huber, I. G., Renstrom, E., Wietzorrek, G., Berjukov, S., et al. (2004). Isoform-specific regulation of mood behavior and pancreatic beta cell and cardiovascular function by L-type Calcium channels. *J. Clin. Invest.* 113, 1430–1439. doi: 10.1172/jci20208

Sintas, C., Carreño, O., Fernàndez-Castillo, N., Corominas, R., Vila-Pueyo, M., Toma, C., et al. (2017). Mutation spectrum in the CACNA1A gene in 49 patients with episodic ataxia. *Sci. Rep.* 7:2514. doi: 10.1038/s41598-017-02554-x

Sokolov, S., Scheuer, T., and Catterall, W. A. (2007). Gating pore current in an inherited ion channelopathy. *Nature* 446, 76–78. doi: 10.1038/nature05598

Sokolov, S., Scheuer, T., and Catterall, W. A. (2008). Depolarization-activated gating pore current conducted by mutant sodium channels in potassium-sensitive normokalemic periodic paralysis. *Proc. Natl. Acad. Sci. U.S.A.* 105, 19980–19985. doi: 10.1073/pnas.0810562105

Sokolov, S., Scheuer, T., and Catterall, W. A. (2010). Ion permeation and block of the gating pore in the voltage sensor of NaV1.4 channels with hypokalemic periodic paralysis mutations. *J. Gen. Physiol.* 136, 225–236. doi: 10.1085/jgp.201010414

Song, L., Park, S.-H. E., Isseroff, Y., Morikawa, K., and Yazawa, M. (2017). Inhibition of CDK5 alleviates the cardiac phenotypes in timothy syndrome. *Stem Cell Rep.* 9, 50–57. doi: 10.1016/j.stemcr.2017.05.028

Spacey, S. (2015). "Episodic ataxia type 2," in *GeneReviews§[Internet]*, eds M. P. Adam, H. H. Ardinger, R. A. Pagon, et al. (Seattle, WA; University of Washington).

Splawski, I., Timothy, K. W., Decher, N., Kumar, P., Sachse, F. B., Beggs, A. H., et al. (2005). Severe arrhythmia disorder caused by cardiac L-type calcium channel mutations. *Proc. Natl. Acad. Sci. U.S.A.* 102, 8089–8096; discussion 8086-8088. doi: 10.1073/pnas.0502506102

Splawski, I., Timothy, K. W., Sharpe, L. M., Decher, N., Kumar, P., Bloise, R., et al. (2004). Cav 1.2 calcium channel dysfunction causes a multisystem disorder including arrhythmia and autism. *Cell* 119, 19–31. doi: 10.1016/j.cell.2004.09.011

Stockner, T., and Koschak, A. (2013). What can naturally occurring mutations tell us about Ca(v)1.x channel function? *Biochim. Biophys. Acta* 1828, 1598–1607. doi: 10.1016/j.bbamem.2012.11.026

Striessnig, J. (2018). Getting a handle on CaV2.2 (N-type) voltage-gated Ca(2+) channels. *Proc. Natl. Acad. Sci. U.S.A.* 115, 12848–12850. doi: 10.1073/pnas.1818608115

Striessnig, J., and Ortner, N. J. (2020). "Ca2+ channel blockers," in *Encyclopedia of Molecular Pharmacology*, eds S. Offermanns and W. Rosenthal (Cham: Springer).

Sullivan, P. F., and Geschwind, D. H. (2019). Defining the genetic, genomic, cellular, and diagnostic architectures of psychiatric disorders. *Cell* 177, 162–183. doi: 10.1016/j.cell.2019.01.015

Symonds, J. D., and McTague, A. (2020). Epilepsy and developmental disorders: next generation sequencing in the clinic. *Eur. J. Paediatr. Neurol.* 24, 15–23. doi: 10.1016/j.ejpn.2019.12.008

Todorov, B., Kros, L., Shyti, R., Plak, P., Haasdijk, E. D., Raike, R. S., et al. (2012). Purkinje cell-specific ablation of Cav2.1 channels is sufficient to cause cerebellar ataxia in mice. *Cerebellum* 11, 246–258. doi: 10.1007/s12311-011-0302-1

Tonelli, A., D'Angelo, M. G., Salati, R., Villa, L., Germinasi, C., Frattini, T., et al. (2006). Early onset, non fluctuating spinocerebellar ataxia and a novel missense mutation in CACNA1A gene. *J. Neurol. Sci.* 241, 13–17. doi: 10.1016/j.jns.2005.10.007

Tottene, A., Favero, M., and Pietrobon, D. (2019). Enhanced Thalamocortical Synaptic Transmission and Dysregulation of the Excitatory-Inhibitory Balance at the Thalamocortical Feedforward Inhibitory Microcircuit in a Genetic Mouse Model of Migraine. *J. Neurosci.* 39, 9841–9851. doi: 10.1523/JNEUROSCI.1840-19.2019

Tottene, A., Fellin, T., Pagnutti, S., Luvisetto, S., Striessnig, J., Fletcher, C., et al. (2002). Familial hemiplegic migraine mutations increase calcium influx through single human Cav2.1 channels and decrease maximal Cav2.1 current density in neurons. *Proc. Natl. Acad. Sci. U.S.A.* 99, 13284–13289. doi: 10.1073/pnas.192242399

Tottene, A., Pivotto, F., Fellin, T., Cesetti, T., van den Maagdenberg, A. M., and Pietrobon, D. (2005). Specific kinetic alterations of human CaV2.1 calcium channels produced by mutation S218L causing familial hemiplegic migraine and delayed cerebral edema and coma after minor head trauma. *J. Biol. Chem.* 280, 17678–17686. doi: 10.1074/jbc.m501110200

Tuluc, P., and Flucher, B. E. (2011). Divergent biophysical properties, gating mechanisms, and possible functions of the two skeletal muscle Ca(V)1.1 calcium channel splice variants. *J Muscle Res. Cell Motil.* 32, 249–256. doi: 10.1007/s10974-011-9270-9

Tyagi, S., Ribera, A. B., and Bannister, R. A. (2020). Zebrafish as a Model System for the Study of Severe CaV2.1 (α1A) Channelopathies. *Front. Mol. Neurosci.* 12:329. doi: 10.3389/fnmol.2019.00329

Van Petegem, F., Clark, K. A., Chatelain, F. C., and Minor, D. L. Jr. (2004). Structure of a complex between a voltage-gated calcium channel beta-subunit and an alpha-subunit domain. *Nature* 429, 671–675.

Waterhouse, A. M., Procter, J. B., Martin, D. M., Clamp, M., and Barton, G. J. (2009). Jalview Version 2–a multiple sequence alignment editor and analysis workbench. *Bioinformatics* 25, 1189–1191. doi: 10.1093/bioinformatics/btp033

Weber, Y. G., Biskup, S., Helbig, K. L., Von Spiczak, S., and Lerche, H. (2017). The role of genetic testing in epilepsy diagnosis and management. *Expert Rev. Mol. Diagn.* 17, 739–750. doi: 10.1080/14737159.2017.1335598

Weiss, N., and Zamponi, G. W. (2019). Genetic T-type calcium channelopathies. *J. Med. Genet.* 57, 1–10. doi: 10.1136/jmedgenet-2019-106163

Wemhöner, K., Friedrich, C., Stallmeyer, B., Coffey, A. J., Grace, A., Zumhagen, S., et al. (2015). Gain-of-function mutations in the calcium channel CACNA1C (Cav1.2) cause non-syndromic long-QT but not Timothy syndrome. *J. Mol. Cell. Cardiol.* 80, 186–195. doi: 10.1016/j.yjmcc.2015.01.002

Williams, B., Lopez, J. A., Maddox, J. W., and Lee, A. (2020). Functional impact of a congenital stationary night blindness type 2 mutation depends on subunit composition of Cav1.4 Ca(2+) channels. *J. Biol. Chem.* 295, 17215–17226. doi: 10.1074/jbc.RA120.014138

Wu, J., Yan, Z., Li, Z., Qian, X., Lu, S., Dong, M., et al. (2016). Structure of the voltage-gated calcium channel Cav1.1 at 3.6Å resolution. *Nature* 537, 191–196. doi: 10.1038/nature19321

Wulczyn, K., Perez-Reyes, E., Nussbaum, R. L., and Park, M. (2019). Primary aldosteronism associated with a germline variant in CACNA1H. *BMJ Case Rep.* 12:e229031. doi: 10.1136/bcr-2018-229031

Yazawa, M., Hsueh, B., Jia, X., Pasca, A. M., Bernstein, J. A., Hallmayer, J., et al. (2011). Using induced pluripotent stem cells to investigate cardiac phenotypes in Timothy syndrome. *Nature* 471, 230–234. doi: 10.1038/nature09855

Ye, D., Tester, D. J., Zhou, W., Papagiannis, J., and Ackerman, M. J. (2019). A pore-localizing CACNA1C-E1115K missense mutation, identified in a patient with idiopathic QT prolongation, bradycardia, and autism spectrum disorder, converts the L-type calcium channel into a hybrid nonselective monovalent cation channel. *Heart Rhythm* 16, 270–278. doi: 10.1016/j.hrthm.2018.08.030

Yue, Q., Jen, J. C., Nelson, S. F., and Baloh, R. W. (1997). Progressive ataxia due to a missense mutation in a calcium-channel gene. *Am. J. Hum. Genet.* 61, 1078–1087. doi: 10.1086/301613

Zamponi, G. W., Striessnig, J., Koschak, A., and Dolphin, A. C. (2015). The physiology, pathology, and pharmacology of voltage-gated calcium channels and their future therapeutic potential. *Pharmacol. Rev.* 67, 821–870. doi: 10.1124/pr.114.009654

Zhang, Q., Chen, J., Qin, Y., Wang, J., and Zhou, L. (2018). Mutations in voltage-gated L-type calcium channel: implications in cardiac arrhythmia. *Channels* 12, 201–218. doi: 10.1080/19336950.2018.1499368

Zhang, S., Zhou, Z., Gong, Q., Makielski, J. C., and January, C. T. (1999). Mechanism of block and identification of the verapamil binding domain to HERG potassium channels. *Circ. Res.* 84, 989–998. doi: 10.1161/01.RES.84.9.989

Zhao, Y., Huang, G., Wu, Q., Wu, K., Li, R., Lei, J., et al. (2019a). Cryo-EM structures of apo and antagonist-bound human Cav3.1. *Nature* 576, 492–497. doi: 10.1038/s41586-019-1801-3

Zhao, Y., Huang, G., Wu, J., Wu, Q., Gao, S., Yan, Z., et al. (2019b). Molecular basis for ligand modulation of a mammalian voltage-Gated Ca^{2+} Channel. *Cell* 177, 1495–1506.e12. doi: 10.1016/j.cell.2019.04.043

Conflict of Interest: The author declares that the research was conducted in the absence of any commercial or financial relationships that could be construed as a potential conflict of interest.

Copyright © 2021 Striessnig. This is an open-access article distributed under the terms of the Creative Commons Attribution License (CC BY). The use, distribution or reproduction in other forums is permitted, provided the original author(s) and the copyright owner(s) are credited and that the original publication in this journal is cited, in accordance with accepted academic practice. No use, distribution or reproduction is permitted which does not comply with these terms.

frontiers in Synaptic Neuroscience

ORIGINAL RESEARCH
published: 26 May 2021
doi: 10.3389/fnsyn.2021.635726

NPY Released From GABA Neurons of the Dentate Gyrus Specially Reduces Contextual Fear Without Affecting Cued or Trace Fear

Lucas B. Comeras†, Noa Hörmer†, Pradeepa Mohan Bethuraj and Ramon O. Tasan†*

Department of Pharmacology, Medical University Innsbruck, Innsbruck, Austria

Disproportionate, maladapted, and generalized fear are essential hallmarks of posttraumatic stress disorder (PTSD), which develops upon severe trauma in a subset of exposed individuals. Among the brain areas that are processing fear memories, the hippocampal formation exerts a central role linking emotional-affective with cognitive aspects. In the hippocampus, neuronal excitability is constrained by multiple GABAergic interneurons with highly specialized functions and an extensive repertoire of co-released neuromodulators. Neuropeptide Y (NPY) is one of these co-transmitters that significantly affects hippocampal signaling, with ample evidence supporting its fundamental role in emotional, cognitive, and metabolic circuitries. Here we investigated the role of NPY in relation to GABA, both released from the same interneurons of the dorsal dentate gyrus (DG), in different aspects of fear conditioning. We demonstrated that activation of dentate GABA neurons specifically during fear recall reduced cue-related as well as trace-related freezing behavior, whereas inhibition of the same neurons had no significant effects. Interestingly, concomitant overexpression of NPY in these neurons did not further modify fear recall, neither under baseline conditions nor upon chemogenetic stimulation. However, potentially increased co-release of NPY substantially reduced contextual fear, promoted extinction learning, and long-term suppression of fear in a foreground context–conditioning paradigm. Importantly, NPY in the dorsal DG was not only expressed in somatostatin neurons, but also in parvalbumin-positive basket cells and axoaxonic cells, indicating intense feedback and feedforward modulation of hippocampal signaling and precise curtailing of neuronal engrams. Thus, these findings suggest that co-release of NPY from specific interneuron populations of the dorsal DG modifies dedicated aspects of hippocampal processing by sharpening the activation of neural engrams and the consecutive fear response. Since inappropriate and generalized fear is the major impediment in the treatment of PTSD patients, the dentate NPY system may be a suitable access point to ameliorate PTSD symptoms and improve the inherent disease course.

Keywords: neuropeptide Y, NPY, fear, fear extinction, hippocampus, dentate gyrus

OPEN ACCESS

Edited by:
Sigismund Huck,
Medical University of Vienna, Austria

Reviewed by:
Syed Ahsan Raza,
Otto von Guericke University Magdeburg, Germany
Charles Jason Frazier,
University of Florida, United States

****Correspondence:***
Ramon O. Tasan
ramon.tasan@i-med.ac.at

†These authors have contributed equally to this work

Received: *30 November 2020*
Accepted: *20 April 2021*
Published: *26 May 2021*

Citation:
Comeras LB, Hörmer N, Mohan Bethuraj P and Tasan RO (2021) NPY Released From GABA Neurons of the Dentate Gyrus Specially Reduces Contextual Fear Without Affecting Cued or Trace Fear. Front. Synaptic Neurosci. 13:635726. doi: 10.3389/fnsyn.2021.635726

INTRODUCTION

Neuropeptide Y (NPY) is a 36 amino acid peptide neurotransmitter (Tatemoto et al., 1982) and extensively expressed in the peripheral and central nervous systems (Gehlert et al., 1987; Morris, 1989). By acting on at least five different Gi/o-coupled receptors, it modulates multiple physiological processes, such as energy homeostasis and emotional-affective behaviors (Hokfelt et al., 2007; Gilpin, 2012; Loh et al., 2015; Reichmann and Holzer, 2016; Schmeltzer et al., 2016; Tasan et al., 2016). Endogenous NPY has been suggested as a resilience factor associated with post-traumatic stress disorder (PTSD); however, the underlying mechanisms are still unclear (Kautz et al., 2017).

A hallmark of PTSD is dysregulated fear, which often appears as fear generalization and the inability to suppress and extinguish established fear memories. Individual aspects of PTSD can be modeled by Pavlovian fear conditioning, a simple form of associative learning, in which an initially neutral stimulus (CS, conditioned stimulus) or a specific context is repetitively paired with an aversive signal, for instance, an electric foot shock (US, unconditioned stimulus; LeDoux, 2000). Multiple brain areas, including the amygdala, hippocampus and, cortical structures, are controlling fear learning and consecutive adaptive behaviors (Ehrlich et al., 2009; Pape and Pare, 2010; Bowers et al., 2012; Tasan et al., 2016; Comeras et al., 2019). The hippocampal formation, for instance, is processing and integrating particular contextual contents about place and time into other fear-relevant brain circuitries (Maren and Fanselow, 1995; Cox et al., 2013; Hubner et al., 2014; McDonald and Mott, 2017). These phenomena can be investigated by cued, contextual and trace fear conditioning.

Synaptic transmission in the hippocampus is generally organized in an excitatory tri-synaptic pathway (Amaral and Witter, 1989) with a multitude of highly specialized inhibitory interneurons generating appropriate fine-tuning by the release of GABA and several neuromodulators. NPY is one of these neuromodulators and in the hippocampus, it can activate postsynaptic Y1 and presynaptic Y2 receptors (Stanic et al., 2011). NPY is usually co-released with GABA from various types of interneurons, while Y1 and Y2Rs are both expressed predominantly on glutamatergic projection neurons (Kopp et al., 2002; Stanic et al., 2006, 2011), such as CA pyramidal neurons and dentate granule cells. Ample evidence emphasizes strong fear-reducing properties of exogenously applied NPY in various rodent models (Flood et al., 1987, 1989; Gutman et al., 2008; Fendt et al., 2009; Tasan et al., 2016). In particular, Y1Rs seem to suppress fear learning in multiple brain areas, including the amygdala and hippocampus (Gutman et al., 2008; Lach and De Lima, 2013). On the other hand, activation of Y2Rs also inhibits acquisition and promotes extinction of fear memories (Verma et al., 2012), predominantly in the extended amygdala and hippocampus (Verma et al., 2015, 2018a,b; Tasan et al., 2016; Hormer et al., 2018). For example, local re-expression of hippocampal Y2Rs in Y2KO mice resulted in specific suppression of fear, by reducing fear recall and promoting fear extinction (Hormer et al., 2018).

Thus, while several pharmacological and genetic studies indicate a role of exogenous NPY in the modulation of fear memories, a direct investigation of the specific contribution of endogenous NPY specifically co-released from GABAergic interneurons would be of particular interest.

Here, we focused on the contribution of local inhibitory neurons to hippocampus-dependent fear processing and investigated the specific role of the co-released neuromodulator NPY. We activated and inhibited dorsal DG GABA neurons during cued and trace fear recall. Furthermore, concomitant overexpression of NPY in activated GABA neurons was used to identify the specific role of co-released NPY in various aspects of fear conditioning, including cued, trace, and contextual fear. To narrow down the underlying neuronal subpopulations, we analyzed the co-localization of NPY with specific neurochemical markers in different sub-regions of the dorsal and ventral hippocampus. Our data suggest that the co-release of NPY from hippocampal GABA neurons modulates highly selective aspects of hippocampal fear conditioning and extinction learning.

MATERIALS AND METHODS

Animals

Adult male VGAT-cre (B6.FVB-Tg(Slc32a1-cre)2.1Hzo/FrkJ, The Jackson Laboratory, USA) mice, NPY-GFP (B6.FVB-Tg(Npy-hrGFP)1Lowl/J, The Jackson Laboratory, USA) mice and wild type mice (WT, C57BL/6NCrl, Charles River Laboratories, Sulzfeld, Germany) were bred in the Department of Pharmacology at the Medical University Innsbruck, Austria. Following weaning they were group-housed in groups of three to five animals per cage under standard laboratory conditions (12 h light/dark cycle, lights on at 07:00). Both transgenic mouse lines were backcrossed with C57BL/6NCrl (Charles River Laboratories, Sulzfeld, Germany) for at least 10 generations.

All procedures involving animals and animal care were conducted in accordance with international laws and policies (Directive 2010/63/EU of the European Parliament and of the council of 22 September 2010 on the protection of animals used for scientific purposes; Guide for the Care and Use of Laboratory Animals, U.S. National Research Council, 2011, and ARRIVE (Animal Research: Reporting *in vivo* Experiments) guidelines) and were approved by the Austrian Ministry of Science. All effort was taken to minimize the number of animals used and their suffering.

Viral Vectors

Plasmids for recombinant adeno-associated viral (rAAV) vectors, rAAV6-hSyn-DIO-hM3D(Gq)-mCherry (Addgene 44361, B. Roth) and rAAV6-hSyn-DIO-hM4D(Gi)-mCherry (Addgene 44362, B. Roth), were kindly provided by B. Roth, obtained from Addgene (USA) and packaged in our laboratory as described in detail previously (Tasan et al., 2010; Verma et al., 2015). A codon-optimized plasmid containing the coding sequence of mouse preproNPY (NCBI Reference Sequence: NM_023456.3) was ordered from GeneScript (USA) and cloned into the open-reading frame of Addgene plasmid 26968 (rAAV6-EF1a-DIO-preproNPY). In order to promote the

proper processing of transgene preproNPY into functional NPY, we did not include an additional reporter gene into the final construct. All vectors were diluted to obtain final titers of 10^{12} gp/ml.

Stereotaxic Microinjections

Mice were anesthetized (150 mg/kg ketamine ip, Ketasol, Animedica) and received analgesia (1.5 mg/kg Meloxicam s.c., Movalis®, Boehringer Ingelheim, Germany) prior to mounting in a stereotaxic frame (David Kopf Instruments, USA). During the procedure, anesthesia was maintained by 1–3% sevoflurane (Sevorane, AbbVie) inhalation. Mice were bilaterally injected with 0.5 μl of rAAV into the dorsal DG (coordinates relative to bregma in mm: dorsoventral −2.0, rostrocaudal −2.0, mediolateral ±1.5) by micropumps (Nexus 3000, Science Products GmbH, Germany) at a flow rate of 0.1 μl/min. The injection site was verified by immunohistochemistry for RFP/mCherry requiring that >90% of labeled neuronal cell bodies must reside within the dorsal DG, excluding, in particular, the ventral DG and other parts of the hippocampal formation, such as CA1 to CA3 areas.

Fear Conditioning

Several groups of VGAT-cre mice were compared in behavioral experiments. For manipulating DG GABA neurons, rAAV6-hSyn-DIO-hM3D(Gq)-mCherry and rAAV6-hSyn-DIO-hM4D(Gi)-mCherry vectors were locally injected into the dorsal DG to activate or inhibit DG GABA neurons, respectively by intraperitoneal (ip) injection of clozapine-N-oxide (CNO, ip, 1 mg/kg, Carbosynth, UK) 30 min before behavioral testing (Gq and Gi groups). Pilot studies revealed that a dose of 1 mg/kg of CNO was sufficient to activate and inhibit hM3D (Gq) and hM4D (Gi)-expressing neurons, respectively. As controls, both groups, Gq and Gi, were injected ip with 0.9% NaCl before testing (saline group). To investigate the role of concomitantly released NPY, a group of mice was injected with a combination of rAAV6-hSyn-DIO-hM3D (Gq)-mCherry and rAAV6-EF1a-DIO-preproNPY (Gq + NPY group) into the dorsal DG and compared to Gq littermates (Gq group), both injected ip with CNO before the respective behavioral test.

For behavioral testing, mice were single-housed in cages covered by filter tops with food and water available *ad libitum* and transferred to the experimental rooms 3 days before behavioral testing. Fear conditioning experiments were performed as described previously (Verma et al., 2012; Hormer et al., 2018).

In brief, trace fear acquisition was performed in context A, consisting of a fear conditioning arena made of a transparent acrylic chamber with a metal grid floor (Ugo Basile, Italy). Illumination was 80 lux and the chambers were cleaned with 70% ethanol. On acquisition day, after a 120 s habitation period, 5 CS (white noise, 20 s, 70 db) each followed by a 5 s trace period and a US (0.5 mA foot-shock for 2 s) were provided with a random inter-trial interval of 40–60 s. For testing of contextual fear, mice were placed in context A for 25 min on day 2. On the third day, to test for CS-induced and trace-induced fear expression the mice received 25 CS separated by 20 s pauses in context B, consisting of an arena with black and white striped walls, white floor, 10 lux illumination and an odor of 1% acetic acid. The first 5 CS were used for testing fear recall and the next 20 CS as cued fear extinction. The 5 s period immediately following each CS was used for analysis of trace fear.

Contextual foreground conditioning was performed in context A. Following a habituation period of 120 s, mice were fear conditioned to the context by delivery of 5 US (unconditioned stimulus, 0.5 mA foot-shock for 2 s) with a random inter-trial interval of 40–60 s. Freezing behavior was determined in the 20 s preceding each US (PreUS). After this procedure, mice remained in the test apparatus for an additional 120 s and were then returned to their home cage. On the next day, fear test and fear extinction were performed by exposing the mice to the same context A for 25 min. The first 5 min were considered as fear recall and the next 20 min as fear extinction. Finally, recall of context extinction was tested on the next day by putting the mice into the same context for 5 min. For re-conditioning experiments, mice were exposed to two additional context fear extinction sessions (each 25 min) on days 4 and 5, followed by 1 week of resting in their home cage. Re-conditioning and CNO injection before CS/trace fear recall was performed similar to trace fear conditioning described above but in a different context. Freezing behavior was recorded and quantified by a pixel based analysis software and expressed as percentage freezing per CS, trace or min for cued, trace, and context fear, respectively (AnyMaze, Stoelting, USA). The parameters of the analysis software were validated by manual measurements of time spent freezing, defined as the absence of all movements except those necessary for breathing.

Feeding Drinking and Activity

Food intake, water intake, and home-cage activity were recorded continuously using an automated home cage phenotyping system (PhenoMaster, TSE, Bad Homburg, Germany). Mice had access *ad libitum* to food and water and they were kept under standard laboratory conditions (12 h light/dark cycle, lights on at 07:00).

Immunohistochemistry

Immunohistochemistry was performed as described earlier (Tasan et al., 2010, 2011; Wood et al., 2016). Mice were injected ip with thiopental (150 mg/kg, ip, Sandoz, Austria) for deep anesthesia. Transaortal perfusion with phosphate buffered saline (PBS) at room temperature for 3 min followed by 4% paraformaldehyde (PFA) at 4°C for 10 min was performed by a peristaltic pump at a flow rate of 9 ml/min (Ismatec, IPC, Cole-Parmer GmbH). Subsequently, brains were removed and postfixed in 4% PFA for 90 min at 4°C, cryoprotected for 48 h in 20% sucrose at 4°C and then snap-frozen in isopentane (2-methylbutane, Merck KGaA, Germany) for 3 min at −60°C. Brains were transferred to pre-cooled open tubes and stored at −70°C until further use.

For immunohistochemistry, coronal 40 μm sections were cut on a cryostat from rostral to caudal and collected in Tris-buffered saline (TBS) + 0.1% sodium azide. Sections from the hippocampus were incubated for 30 min in TBS-triton (0.4%) and 90 min in 10% normal horse serum. Subsequently,

sections were incubated overnight with the first primary antibody (**Table 1**) diluted in 10% serum containing 0.1% sodium azide. After washing with TBS-buffer 3 × 5 min, the secondary antibody was added to the sections for 150 min. Then, sections were incubated in the dark for 8 min in TSA-TAMRA (in-house, 1:2,000) staining solution. For dual labeling immunohistochemistry, sections were incubated in 100 mM sodium azide for 45 min. Subsequently, they were rinsed with TBS-buffer 3 × 5 min and incubated with the corresponding second primary antibody (diluted in 10% serum containing 0.1% sodium azide) overnight (**Table 1**). On the next day, after washing with TBS-buffer 3 × 5 min, TSA biotin was added to the sections for 6 min, followed by rinsing 3 × 5 min in TBS buffer and then incubated for 100 min in a solution of streptavidin dylight 649 (Vector Laboratories, Inc., USA) in TBS buffer. Fluorescently stained sections were mounted on slides using gelatine and cover-slipped with glycerol-DABCO anti-fading mounting medium.

Imaging and Counting

Images were taken using a fluorescent microscope (Zeiss Axio Imager M1, Germany) equipped with a halogen light source, respective filter sets, a Hamamatsu monochrome camera (Hamamatsu ORCA ER C4742-80-12AG, Japan), and Improvision Openlab software (PerkinElmer, USA). For each mouse, numbers of immuno-positive neurons per sub-region were obtained bilaterally from coronal sections comprising the dorsal (bregma −1.70 to −2.30 mm) and ventral hippocampus (bregma −2.92 to −3.16 mm; Paxinos and Franklin, 2004). In order to assess the overexpression of NPY in the DG, mean gray values of the DG were obtained using ImageJ FIJI (ImageJ, USA) from inverted photomicrographs of NPY immunohistochemistry of the dorsal hippocampus. Mean gray values were calculated using a circular area placed in the center of each DG. The mean gray value of the background (area of the slide without positive signal) was calculated for each slide and subtracted from the mean gray value of the DG. Relative optical density (ROD) was calculated using the formula: ROD = log (255/mean gray value).

Statistical Analysis

Data are shown as means ± SEM and were analyzed for normal distribution and equal variances using GraphPad Prism software (Prism 8, GraphPad Software Inc.). Measurements of treatment, time, and interaction were analyzed by repeated two-way ANOVA, followed by Tukey's *post hoc* test. Comparisons of the two groups were done by unpaired or paired Student's *t*-tests or Fisher's exact test for proportions.

RESULTS

Activation of GABAergic Neurons of the Dentate Gyrus Reduces Trace Fear Recall

To investigate the role of hippocampal GABA neurons in fear processing we injected male VGAT-cre mice with an activatory (rAAV-hSyn-DIO-hM3DGq) or inhibitory (rAAV-hSyn-DIO-hM4DGi) DREADD vector (**Figure 1A**) into the dorsal DG. A detailed analysis of the injection site revealed that transgene expression was confined to the dorsal DG, but absent from its ventral parts (**Supplementary Figure 1A**). Two weeks after rAAV injection, hippocampus-dependent fear processing was tested by trace fear conditioning, a paradigm that relies on dorsal hippocampal signaling (Misane et al., 2005; Esclassan et al., 2009). Trace fear conditioning was optimized in pilot studies for C57Bl6N/Crl mice. Using a 5 s trace interval provided optimal conditions for differential freezing behavior. Thus, the highest freezing levels were detected during the trace period compared to medium and lowest freezing behavior during CS and inter-trial intervals, respectively (**Supplementary Figure 2B**). Following fear acquisition and contextual testing, hippocampal interneurons were activated or inhibited by peripheral injection of CNO or saline in controls 30 min before fear recall (**Figure 1B**).

In the absence of CNO injection, Gi, Gq, and saline control groups displayed equal fear acquisition (**Figure 1C**) and context fear expression (**Figure 1D**). However, on day 3, when CNO or saline was injected 30 min before fear testing, CS-induced and trace-induced freezing was reduced in Gq mice, as demonstrated by repeated two-way ANOVA (**Figure 1E**, $F_{(2,28)}$ = 7.998, P = 0.0018 for treatment). This difference was mainly attributed to a reduction in CS-induced freezing of the Gq mice injected with CNO compared to Gi and saline groups (**Figure 1E** saline vs. Gq: 23.5, 95%—CI

TABLE 1 | Primary and secondary antibodies.

	Species	Code	Source	Dilution
Primary antibodies				
c-Fos	Rabbit	226003	Synaptic systems	1:10,000
GABA	Rabbit	A2052	Sigma	1:2,000
NPY	Rabbit	In-house	Bellmann et al. (1991)	1:10,000
Parvalbumin	Rabbit	PV 25	Swant	1:20,000
RFP	Rabbit	600-401-379	Rockland	1:10,000
Somatostatin	Rabbit	In-house	Sperk and Widmann, 1985	1:20,000
Secondary antibodies				
Anti-Rabbit-HRP	Goat	P0448	Dako	1:250
Anti-Rabbit-HRP	Donkey	A16023	Invitrogen	1:500
HRP-subtrate				
Streptavidin 649			Vector Laboratories	1:100
TSA TAMRA			Thermo Fisher	1:2,000
TSA Biotin			Thermo Fisher	1:100

(4.93, 42.07), P = 0.0109; Gi vs. Gq: 31.4, 95%—CI (8.92, 53.89), P = 0.0049), indicating reduced fear expression upon activation of DG GABA neurons. Furthermore, during fear testing, Gq mice injected with CNO also exhibited lower freezing during the initial five traces when compared to saline-injected controls and to the CNO injected Gi group (**Figure 1F**; $F_{(2,28)}$ = 14.04, P = 0.0001 for treatment). Interestingly, the contingency of CS and trace was not influenced by treatment in any of the groups as demonstrated by the consistently increased freezing levels to the trace when compared to the preceding CS-period (**Figure 1G**; Gq: $t_{(14)}$ = 2.573, P = 0.0232, Gi: $t_{(6)}$ = 4.766, P = 0.0050, saline: $t_{(11)}$ = 4.964, P = 0.0006). Together these data suggest that the activation of GABA neurons in the dorsal DG reduces CS-related and trace-related fear while keeping the identification of salient predictive stimuli unaffected. Analyses of the injected brain areas with dual immunohistochemistry revealed RFP expression in somatostatin (SST)- and parvalbumin (PV)-expressing interneurons of the dorsal DG (**Supplementary Figures 1B,C**).

Overexpression of NPY in GABAergic Neurons of the Dorsal Dentate Gyrus Does Not Affect Trace Fear Recall

Under physiological conditions, NPY in the hippocampus is almost exclusively expressed and released from specific populations of GABAergic interneurons. Consequently, to explore the role of NPY in hippocampus-dependent fear processing, we injected a combination of rAAV-hSyn-DIO-hM3DGq and rAAV-EF1a-DIO-NPY into the dorsal DG of VGAT-cre mice (**Figure 2A**). This approach resulted in an overexpression of NPY specifically in DG GABA neurons (**Figure 2B**; $t_{(8)}$ = 8.324, P = 0.0000085) and provided the opportunity to induce locally restricted NPY release together with GABA by peripheral injection of CNO.

No significant changes in freezing time were observed during fear acquisition (**Figure 2C**) and context fear testing (**Figure 2D**) under baseline conditions, suggesting that the isolated overexpression of NPY in DG GABA neurons does not modify fear learning. Similarly, when CNO was injected before cued CS-induced and trace-induced fear tests, Gq + NPY mice displayed equal freezing to the CS (**Figure 2E**) and trace (**Figure 2F**) as Gq mice. Importantly, the contingency of CS and trace was maintained in both groups (**Figure 2G**; Gq: $t_{(14)}$ = 2.573, P = 0.0232, Gq + NPY: $t_{(11)}$ = 2.903, P = 0.0158). These data indicate that NPY released from hippocampal GABA neurons does not interfere with CS-related nor trace-related fear recall. Analyses of the injected brain areas with dual immunohistochemistry revealed NPY expression in almost all PV- and SST-expressing interneurons of the dorsal DG (**Figures 2H,I**).

Overexpression of NPY in GABAergic Neurons of the Dorsal Dentate Gyrus Reduces Context Fear Recall

To investigate whether NPY released from DG GABA neurons has a role in specific forms of Pavlovian fear conditioning, such as foreground contextual fear, we subjected Gq and Gq + NPY injected mice to pure context fear conditioning (**Figure 3A**). Overexpression of NPY did not alter fear acquisition (**Figure 3B**) in the absence of CNO. However, 24 h after acquisition, context fear recall was performed in the presence of CNO (**Figures 3A–C**), followed by extinction learning (**Figures 3A–D**). Compared to Gq mice, Gq + NPY injected mice showed lower levels of freezing in contextual fear recall on day 2, performed 30 min after injection of CNO (**Figure 3C**; $t_{(7)}$ = 2.896, P = 0.0231). Similarly, Gq + NPY injected mice also showed an accelerated extinction learning in the presence of CNO-mediated activation of DG GABA neurons (**Figure 3D**, $F_{(1,7)}$ = 10.88, P = 0.0131 for treatment). Extinction recall was performed on day 3 without CNO injection (**Figure 3E**). Importantly, contextual freezing was also reduced during extinction recall in Gq + NPY mice compared to Gq alone (**Figure 3E**; $t_{(7)}$ = 2.604, P = 0.0352). These data indicate that NPY reduces the expression and promotes extinction especially of foreground context fear when released from GABAergic interneurons of the dorsal DG. To substantiate these findings, we subjected the same mice to an extensive context extinction protocol and re-conditioned them in the same trace fear paradigm as described above. Importantly, there was no change in CS or trace fear recall upon injection of CNO (**Supplementary Figures 3A–C**), confirming the previous findings (**Figures 2E–G**) and strengthening the selectivity of NPY for foreground contextual fear (**Figures 3C–E**). Interestingly, context fear and trace fear expression were not correlated in these mice (**Supplementary Figure 3C**).

Overexpression of NPY Did Not Change Food Intake, Water Intake or Activity

Ample evidence supports an important role of NPY in the modulation of food intake and metabolic processes, in particular when released from neurons of the arcuate hypothalamic nucleus. In order to identify if also hippocampal NPY plays a role in metabolic processes, we measured food intake, water intake and home-cage activity in Gq and Gq + NPY mice, both in the absence and presence of ip CNO injections. Food and water intake and general home-cage activity was neither changed by DG NPY overexpression (**Figures 4A–E**) nor during concomitant activation of DG GABA neurons by ip CNO injection (**Figures 4B–F**). These data exclude the involvement of unspecific alterations in motor activity and confirms that NPY in the dorsal DG does not affect metabolically induced behaviors.

Distribution of NPY Neurons in the Different Hippocampal Subregions

In order to specify the underlying neuronal subpopulations that may be responsible for NPY-mediated reduction of contextual fear, we performed immunohistochemical analyses in NPY-GFP mice. In the hippocampus, NPY was almost exclusively expressed in GABA-expressing neurons (**Figures 5A–E**; **Table 2**). According to their projection targets, gene expression profile, and electrophysiological properties, inhibitory interneurons in the hippocampus

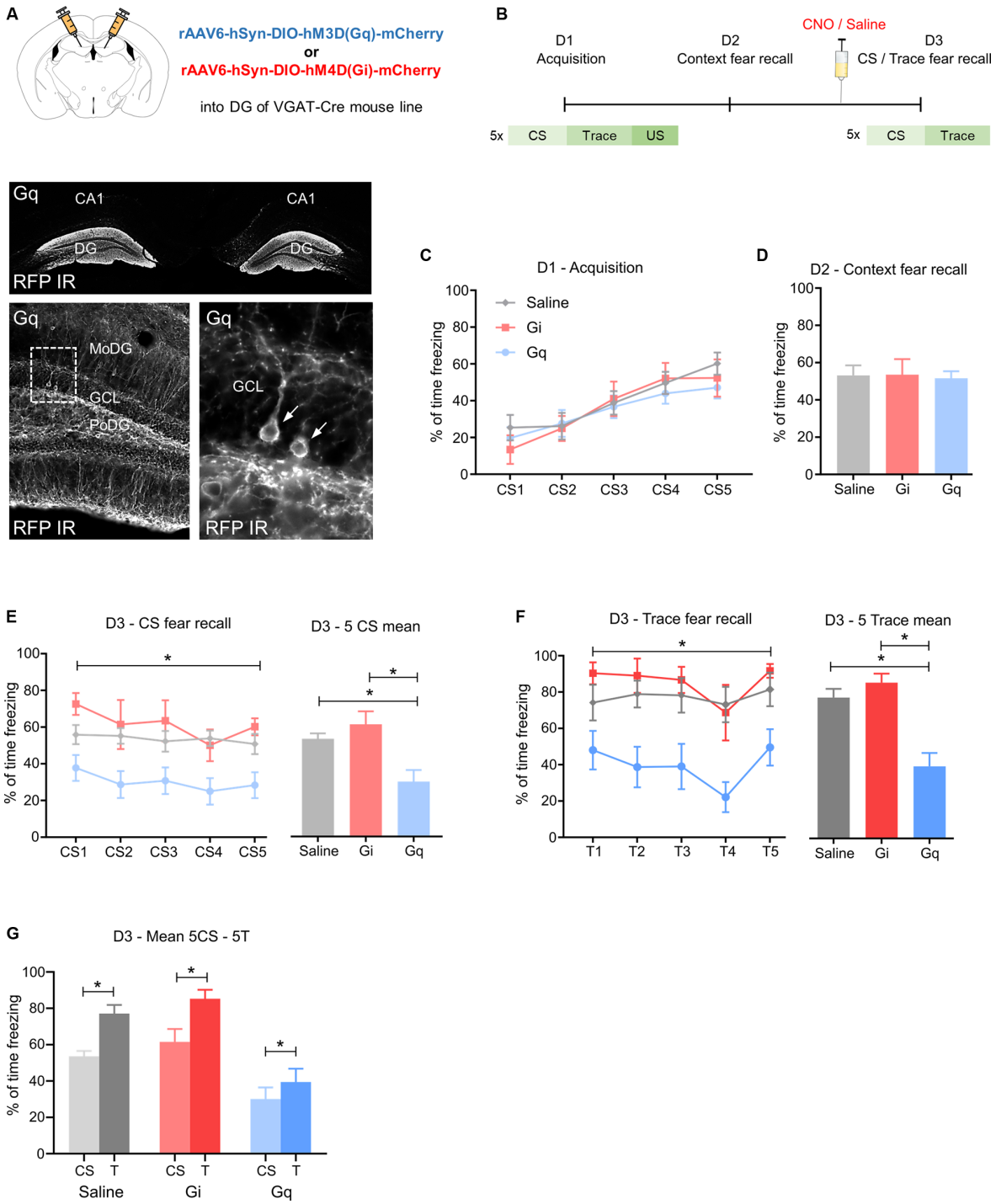

FIGURE 1 | Activation of GABA neurons in the dorsal dentate gyrus reduces fear expression. **(A)** Upper image: schematic illustration of the injection site of rAAV-hSyn-DIO-hM3DGq-mCherry (Gq) or rAAV-hSyn-DIO-hM4DGi-mCherry (Gi) in the dorsal dentate gyrus (DG) of VGAT-cre mice. Lower image: immunohistochemical distribution of mCherry in the dorsal DG (arrows point towards individual immuno-positive GABA neurons). **(B)** Schematic fear conditioning protocol. On day 1 (D1), five pairings of a CS (20 s) followed by a 5 s trace and a 0.5 mA footshock were delivered with a variable inter-trial interval of 40–60 s. On day 2 (D2), mice were placed into the acquisition context for 25 min. On day 3 (D3), mice were injected with 1 mg/kg clozapine-N-oxide (CNO) 30 min before fear recall testing, consisting of 5CS presentations in a different context. **(C)** Equal fear acquisition for all groups, **(D)** no change in contextual fear, **(E)** during testing of CS-induced fear recall, Gq group showed a lower percentage of freezing than Gi and saline during 5 CS as demonstrated by two-way ANOVA for repeated measurements and Tukey's *post hoc* test. **(F)** A similar reduction of the percentage of freezing was seen during the trace period. **(G)** Saline, Gq, and Gi injected mice showed a higher percentage of freezing during the trace period compared to the CS, suggesting intact stimulus contingency. Data are presented as means ± SEM, $^*P < 0.05$. Saline: $n = 11$, Gi: $n = 6$, Gq: $n = 14$. Abbreviation: CS, conditioned stimulus.

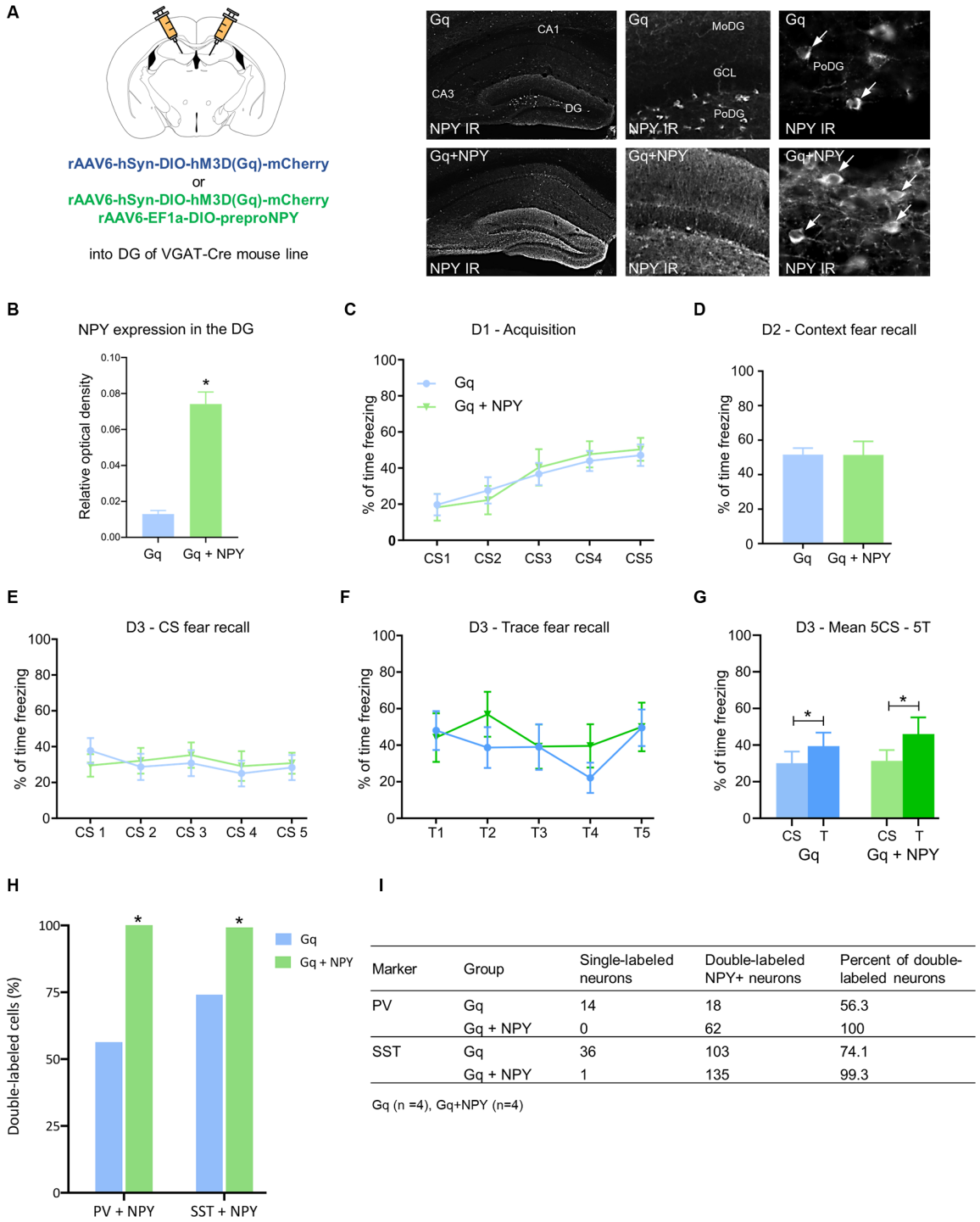

Marker	Group	Single-labeled neurons	Double-labeled NPY+ neurons	Percent of double-labeled neurons
PV	Gq	14	18	56.3
	Gq + NPY	0	62	100
SST	Gq	36	103	74.1
	Gq + NPY	1	135	99.3

Gq (n =4), Gq+NPY (n=4)

FIGURE 2 | Overexpression of neuropeptide Y (NPY) in dentate gyrus GABA neurons does not further reduce CS-related and trace-related fear expression upon chemogenetic activation. **(A)** Photomicrographs of NPY immunohistochemistry in coronal mouse brain sections and quantification of relative optical density (ROD) demonstrate higher expression of NPY in the dorsal hippocampus of mice injected with rAAV-hSyn-DIO-hM3DGq-mCherry/rAAV-EF1a-DIO-NPY (Gq + NPY) than those injected with rAAV-hSyn-DIO-hM3DGq-mCherry (Gq) alone. **(B)** Increased expression of NPY-IR in the dorsal DG of a Gq + NPY injected mice compared to Gq injected controls. **(C)** No change in percentage of freezing during fear acquisition on day 1 (D1) and **(D)** equal freezing during contextual fear testing on day 2 (D2). **(E)** Similarly, there was no difference in freezing time during the CS and **(F)** trace period on day 3 (D3) following injection of CNO to activate dentate GABA neurons. **(G)** Both, Gq and Gq + NPY injected mice showed higher freezing during trace than during CS-period. **(H)** Quantification of dual-immunofluorescence demonstrating increased expression of NPY-IR in parvalbumin (PV) and somatostatin (SST) neurons of the dorsal DG of Gq + NPY mice compared to Gq-injected controls. **(I)** Tabular results for individual groups of DG interneurons in Gq + NPY and Gq mice. Data are presented as means ± SEM, $^*P < 0.05$. Gq: $n = 14$, Gq + NPY: $n = 11$.

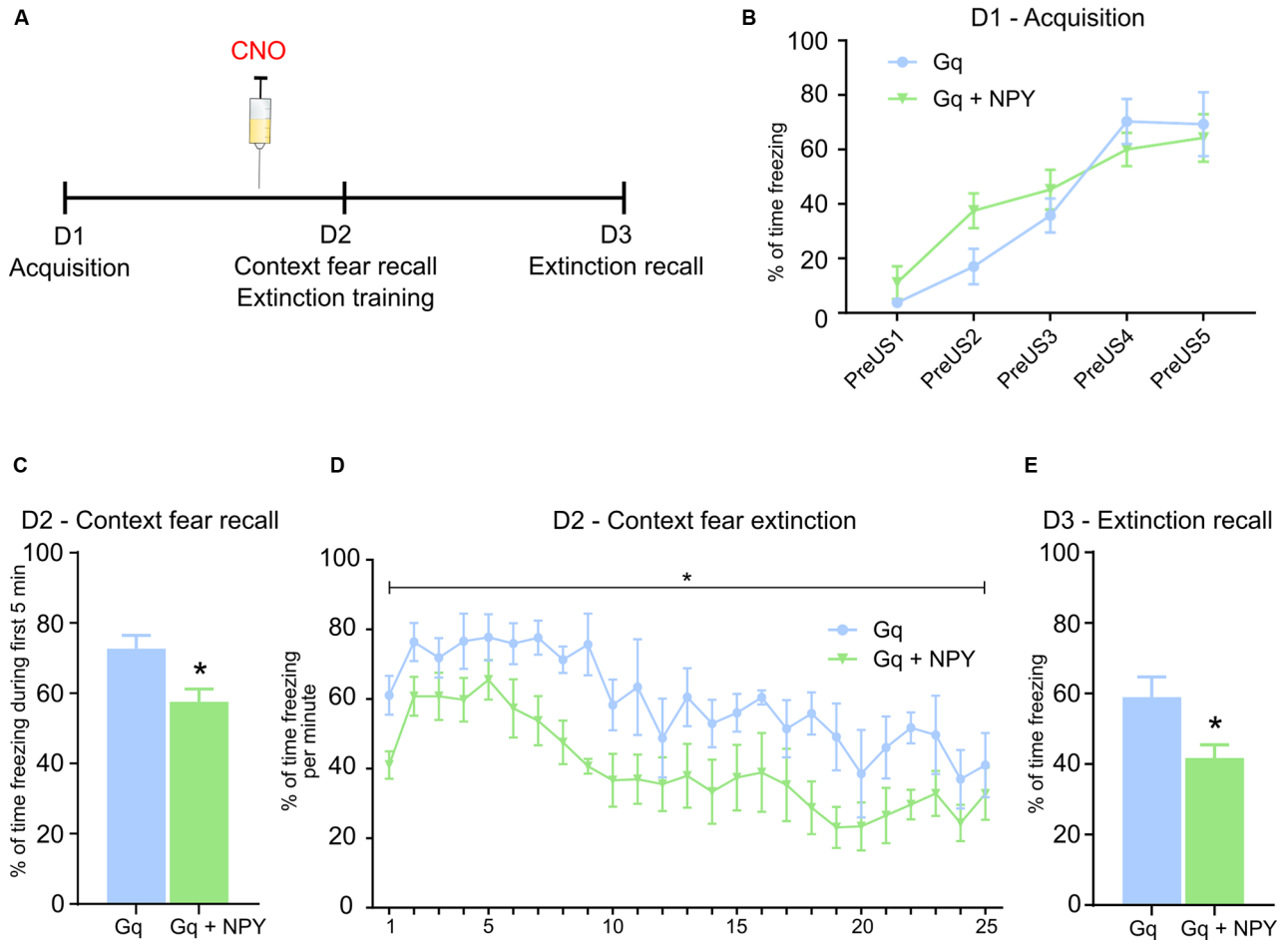

FIGURE 3 | NPY over-expression in GABAergic neurons of the dorsal dentate gyrus reduces context fear expression upon activation. **(A)** Foreground context fear protocol: On day 1 (D1), during fear acquisition mice received 5 US separated by a variable time interval. On day 2 (D2), mice were injected 30 min before the test with CNO (ip, 1 mg/kg). Fear testing and extinction training: On day 3 (D3), mice were placed again into the same context for 5 min to test for extinction recall in the absence of CNO injection. **(B)** No change in percentage of freezing measured during the 20 s period before each US (PreUS1–5) between Gq and Gq + NPY injected mice. **(C)** During testing of contextual fear recall following peripheral injection of CNO, Gq + NPY mice exhibited a lower percentage of freezing compared to Gq mice. **(D)** Similarly, Gq + NPY mice displayed a lower percentage of freezing during context fear extinction upon peripheral injection of CNO. **(E)** On D3, in the absence of peripheral CNO injection, Gq + NPY mice showed a lower percentage of freezing during 5 min of context fear recall. Data are presented as means ± SEM, $^*P < 0.05$. Gq: $n = 4$, Gq + NPY: $n = 5$. Abbreviation: US, unconditioned stimulus.

are highly specialized and diverse. Here, we showed that NPY was expressed mainly by SST neurons. In the dorsal hippocampus, the percentage of NPY and SST co-expressing neurons was 8.1, 22.5, and 20.6% for the CA1, CA3 and DG, respectively (**Figures 6A,B,D**; **Table 3**). In the ventral hippocampus, the percentage of NPY and SST dual-labeled neurons was 52.4, 71.4 and 93.5% in the CA1, CA3, and DG, respectively (**Figures 6A,C,E**; **Table 1**). Interestingly, we found that NPY also co-localized with PV expressing interneurons, in particular in the dorsal hippocampus. There, 9.5, 15.6, and 14.9% expressed NPY and PV (**Figures 7A,B,D**; **Table 4**), while in the ventral hippocampus the co-localization was only 2.0, 3.7, and 2.2% for CA1, CA3, and DG, respectively (**Figures 7A,C,E**; **Table 4**). In order to confirm the co-localization of NPY and PV in the dorsal DG, we performed dual immunohistochemistry in C57Bl6/NCrl wild type mice. Similar to the results in NPY-GFP mice, we found that 15.7% of NPY neurons in the dorsal DG co-express PV (**Supplementary Figure 3**).

DISCUSSION

While the NPY system has demonstrated considerable potential in modulating emotional-affective processes (Kask et al., 2002; Bowers et al., 2012; Holzer et al., 2012; Verma et al., 2012; Comeras et al., 2019), the contribution of NPY neurons in the dorsal hippocampus was still unclear.

Here, we show that activation of inhibitory neurons in the dorsal DG suppresses cued and trace fear recall, while inhibition of DG GABA neurons had no detectable effect. Interestingly, concomitantly released NPY did not contribute to cued or trace fear expression, but rather

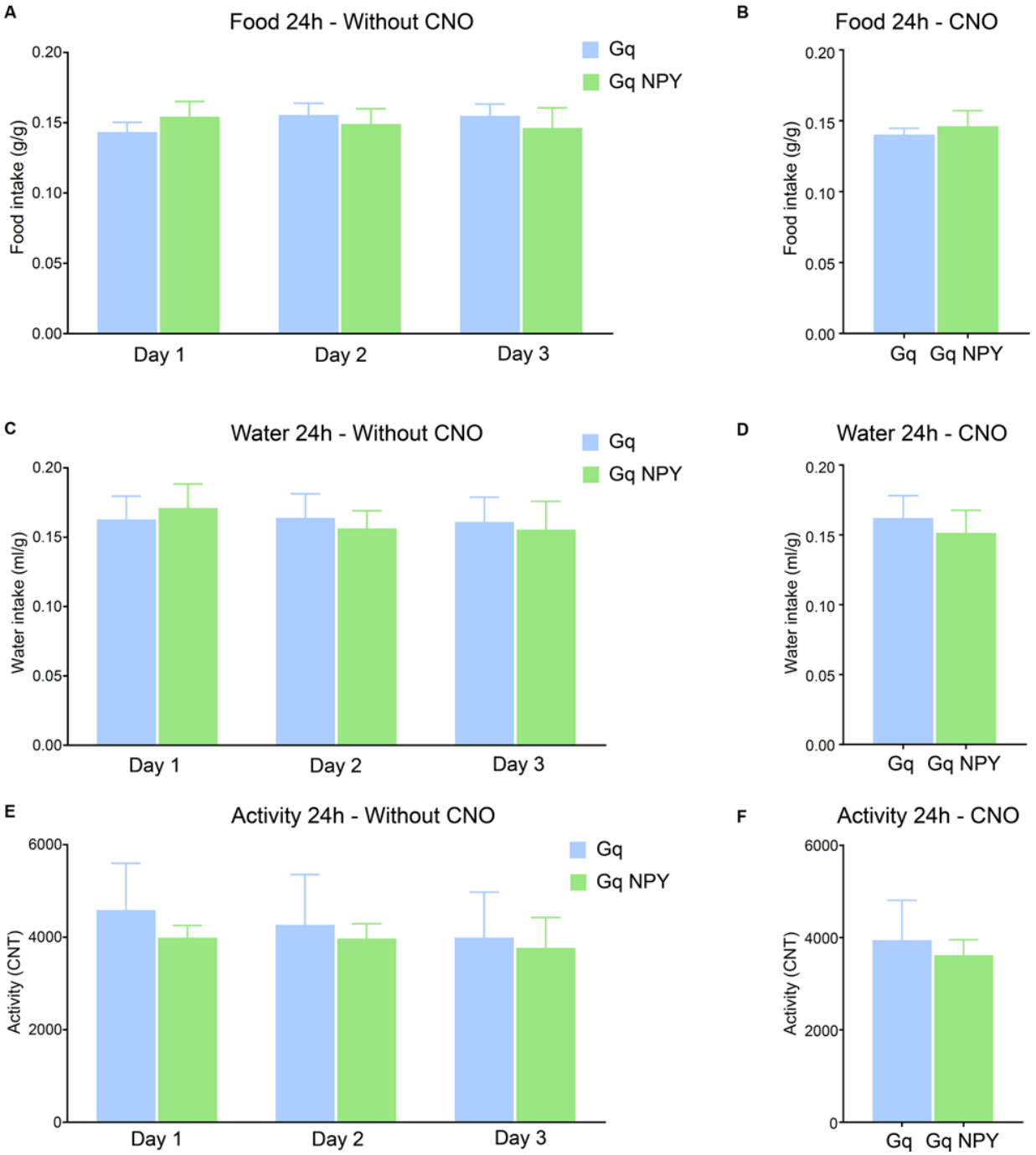

FIGURE 4 | Activation of GABAergic neurons in the dorsal dentate gyrus with or without overexpression of NPY does not alter food intake, water intake, or home cage activity. **(A)** No difference in cumulative 24 h food intake per body weight (g/g) across three consecutive light/dark cycles. **(B)** No change in cumulative 24 h food intake per body weight after ip injection of CNO. **(C)** No difference in cumulative 24 h water intake per body weight (ml/g) on three consecutive days. **(D)** No change in cumulative 24 h water intake per body weight after ip CNO injection. **(E)** There was also no difference in cumulative 24 h home cage activity under baseline conditions or **(F)** after peripheral CNO injection. Gq: $n = 4$, Gq + NPY: $n = 4$.

suppressed the contextual component in a foreground-conditioning paradigm and promoted extinction learning. This finding clearly disentangles effects exerted by the principal neurotransmitter GABA from those of NPY released simultaneously by the same interneuron population in the dorsal DG.

Pavlovian fear conditioning is a form of associative learning that replicates essential aspects of PTSD in animal models

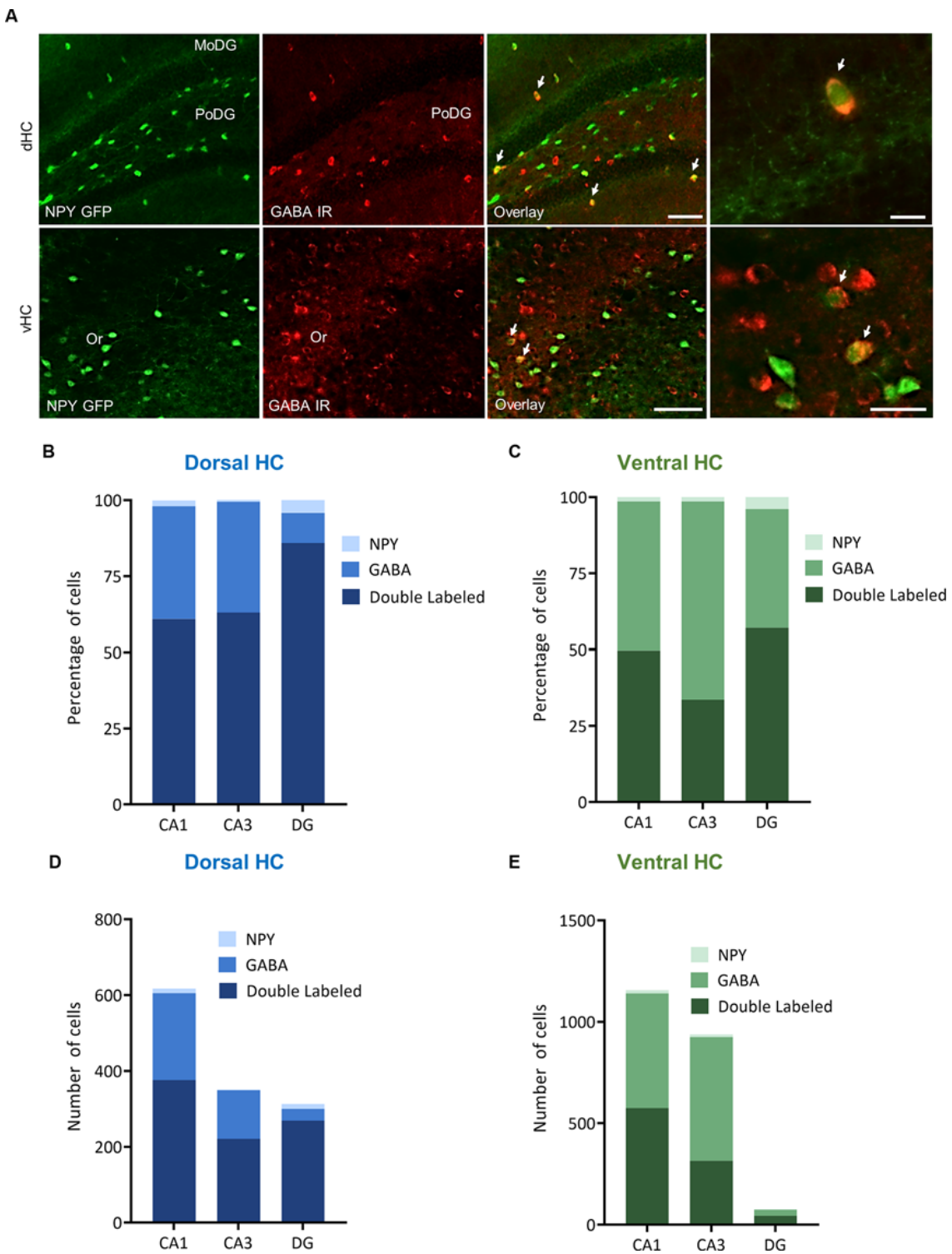

FIGURE 5 | Distribution and quantification of co-expression of GABA with NPY in the dorsal (dHC) and ventral (vHC) mouse hippocampus. **(A)** Dual immunohistochemistry for GABA and NPY-GFP auto-fluorescence in the dorsal (dHC) and ventral hippocampus (vHC) of NPY-GFP mice. Cells in green indicate NPY-GFP + neurons and cells in red indicate GABA expressing neurons. **(B)** Histograms showing the percentage of NPY-GFP neurons in CA1, CA3, and DG of the dorsal hippocampus that are co-labeling with GABA. **(C)** Histograms showing the percentage of NPY-GFP neurons in CA1, CA3, and DG of the ventral hippocampus that are co-labeling with GABA. Note that NPY neurons are exclusively GABAergic. **(D)** Number of NPY-GFP and GABA neurons in CA1, CA3, and DG of the dorsal and **(E)** ventral hippocampus. Scale bars: lower magnification 200 μm (third column), higher magnification 50 μm (last column). Abbreviations: MoDG, molecular layer of the dentate gyrus; PoDG, hilus/polymorph layer of the dentate gyrus; Or, stratum oriens.

TABLE 2 | Co-localization of NPY-GFP and GABA in the hippocampus.

Region	Subdivision	Single-labeled NPY-GFP+ neurons	Single-labeled GABA+ neurons	Double-labeled neurons	Percent of single-labeled NPY-GFP+ neurons	Percent of single-labeled GABA+ neurons	Percent of double-labeled neurons
Dorsal HC	CA1	12	229	376	1.9	37.1	60.9
	CA3	2	128	221	0.6	36.5	63.0
	DG	13	31	269	4.2	9.9	85.9
Ventral HC	CA1	16	565	575	1.4	48.9	49.7
	CA3	13	610	315	1.4	65.0	33.6
	DG	3	30	44	3.9	39.0	57.1

NPY-GABA: n = 3.

(Bowers and Ressler, 2015). Although simple in nature, it has the capacity to investigate the contribution of individual brain areas by various modifications of the original paradigm (Misane et al., 2005; Esclassan et al., 2009; Herry et al., 2010; Daldrup et al., 2015). For instance, the strength of the pairing between the initially neutral CS and the aversive US can be influenced by subtle changes of the separating time interval. Co-termination of CS/US strongly depends on amygdala processing, while increasing the time interval, the so-called "trace", will eventually involve several other brain areas, such as the hippocampus as well as several cortical areas. Trace fear may further trigger complex learning events, including safety learning and correct timing (Raybuck and Lattal, 2014). While the ventral hippocampus provides general guidance for emotional-affective regulation, including anxiety and fear-related responses, the dorsal hippocampus seems to play a more selective role in trace fear processing (Raybuck and Lattal, 2014). Importantly, we optimized trace fear conditioning for our mouse strains ultimately deciding for a 5 s trace interval. This was a crucial step in order to avoid alternative learning processes, such as explicit un-pairing and safety learning. Thus, we tested the influence of inhibitory neurons of the dorsal DG in trace fear retrieval. We demonstrated that the activation of DG GABA neurons reduced fear expression to the cue and trace, while inhibition of the same neurons did not have an obvious effect. Accordingly, the increasing inhibitory tone may interrupt the recall of the CS-trace-US association, while increasing excitatory drive during trace fear recall would not further enhance memory-dependent freezing behavior. Such a concept could support the conventional hypothesis suggesting that the preservation of neuronal activity bridges the trace period. However, recently this view has been challenged by two studies stating that temporal coding and sequential activity are not underlying trace fear learning. Zhang et al. (2019) reported that in fact specific neuronal ensembles in the CA1 of the dorsal hippocampus were activated during fear retrieval by the CS presentation and by the stimulus-free trace period likewise. In a similar approach, it was proposed that both, CS and trace, were encoded by a sparse subset of hippocampal pyramidal neurons forming a specific engram (Ahmed et al., 2020). Thus, in our study, the activation of DG GABA neurons during fear retrieval may have inhibited the reactivation of a specific fear engram equally encoding for CS-related and trace-related memories. If on the other hand, activation of DG GABA neurons interrupted the temporal bridging of CS and trace, one would expect to see a specific reduction of trace-related freezing but not CS-induced freezing. We, however, found that freezing behavior to the CS and trace was fairly correlated across all treatment groups albeit at different expression levels, supporting a general reduction of specific fear engram cell activation (**Figure 1G**). There may be several reasons why inhibition of DG GABA neurons did not enhance fear recall. Most likely, a ceiling effect of freezing masked the detection of significantly increased freezing levels. Conversely, if dedicated neuronal ensembles control the expression of CS/trace fear, then inhibition of DG GABA neurons would not further enhance the reactivation of a specific engram. In other words, if a CS/trace assigned engram is completely recalled, inhibiting local GABA neurons cannot further promote it, but would rather result in unspecific events, such as fear generalization. Future studies using different US intensities and training schemes, such as differential fear conditioning paradigms with predictive and non-predictive cues may shed more light upon this issue (Verma et al., 2012).

Interestingly, over-expression of NPY with or without consecutive chemogenetic activation of DG GABA neurons did not further modify CS-related and trace-related freezing behavior during fear recall. These data indicate that freezing behavior induced by discrete stimuli, such as CS and trace, is strongly dependent on acute inhibition/excitation balance by GABA and glutamate release, but less on the effects of a modulating neuropeptide transmitter that acts on much longer time scales. Limitations of the current experiment are the very low freezing levels upon chemogenetic activation of DG interneurons, which may have resulted in a floor effect that precluded the detection of further freezing suppression caused by concomitantly released NPY.

Contextual information provides a dedicated aspect of episodic memories, specifying their temporal and spatial representation. In fear conditioning paradigms, the context may consist of a set of features defining the external conditions under which the pairing of a specific CS with a related US was performed. Under these conditions, the context provides a "background" representation and induces, on its own, only weak fear expression during consecutive testing. On the other hand, in "foreground" contextual conditioning the context representation serves as the only predictor and may thus induce full fear memory retrieval. We found that NPY potentially co-released

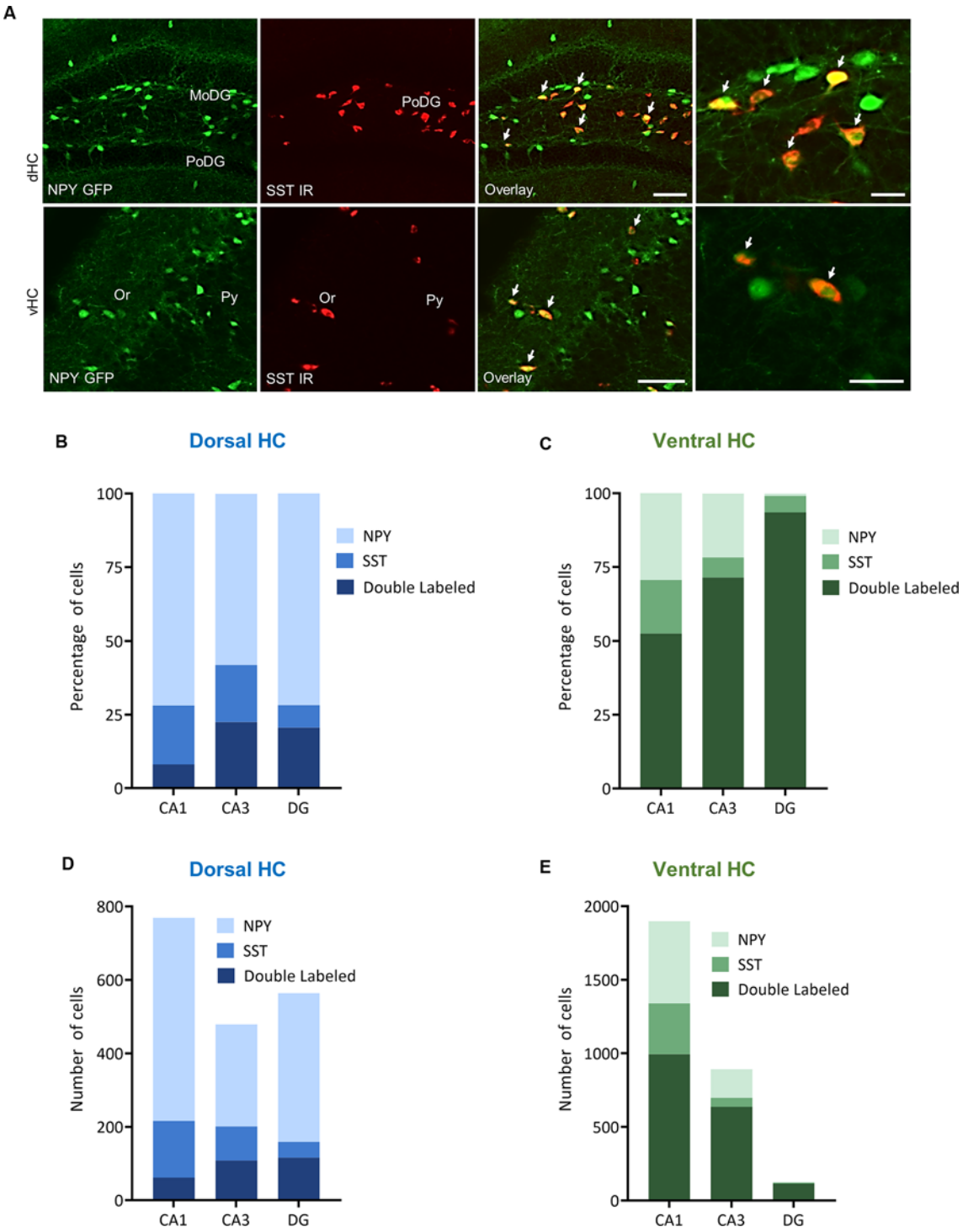

FIGURE 6 | Distribution and quantification of co-expression of somatostatin (SST) with NPY in the dorsal (dHC) and ventral (vHC) mouse hippocampus. **(A)** Dual immunohistochemistry for SST and NPY-GFP auto-fluorescence in the dorsal (dHC) and ventral hippocampus (vHC) of NPY-GFP mice. Cells in green indicate NPY-GFP + neurons and cells in red indicate SST expressing neurons. **(B)** Histograms showing the percentage of NPY-GFP neurons in CA1, CA3, and DG of the dorsal hippocampus that are co-labeling with SST. **(C)** Histograms showing the percentage of NPY-GFP neurons in CA1, CA3, and DG of the ventral hippocampus that are co-labeling with SST. In the ventral hippocampus a very high proportion of NPY neurons co-express SST. **(D)** Number of NPY-GFP and SST neurons in CA1, CA3, and DG of the dorsal and **(E)** ventral hippocampus. Scale bars: lower magnification 200 μm (third column), higher magnification 50 μm (last column). Abbreviations: MoDG, molecular layer of the dentate gyrus; PoDG, hilus/polymorph layer of the dentate gyrus; SGZ, subgranular zone; Or, stratum oriens; Py, stratum pyramidale.

TABLE 3 | Co-localization of NPY-GFP and SST in the hippocampus.

Region	Subdivision	Single-labeled NPY-GFP+ neurons	Single-labeled SST+ neurons	Double-labeled neurons	Percent of single-labeled NPY-GFP+ neurons	Percent of single-labeled SST+ neurons	Percent of double-labeled neurons
Dorsal HC	CA1	553	154	62	71.9	20.0	8.1
	CA3	278	93	108	58.0	19.4	22.5
	DG	405	43	116	71.8	7.6	20.6
Ventral HC	CA1	558	346	994	29.4	18.2	52.4
	CA3	194	61	637	21.7	6.8	71.4
	DG	1	7	116	0.8	5.6	93.5

NPY-SST: n = 4.

(Noe et al., 2008; Verma et al., 2015) from activated DG GABA neurons significantly reduced the recall of contextually relevant fear in a "foreground" context fear paradigm. In addition, in the same paradigm extinction of context fear was facilitated, resulting also in a reduced freezing time when tested for extinction recall 24 h later and in the absence of CNO injection. Since no additional saline control was present in these experiments, we do not know whether activation of DG GABA neurons alone is sufficient to reduce contextual fear expression. However, the data suggest that simultaneously released NPY may interfere specifically with the contextual representation of hippocampal fear engrams, while it is not involved in the processing of CS-related or trace-related hippocampal processing. This makes sense when considering context as a complex episodic memory that needs time to be appropriately recollected, as demonstrated by the bell-shaped curve of a typical context fear retrieval session. Thus, slowly developing modulatory activity of neuropeptide transmitters may especially affect this kind of cerebral processing. In contrast, simple and more specific cues, such as a tone and the adjacent trace period, are less susceptible to neuromodulators, but rather depend on the balance of the fast-acting neurotransmitters GABA and glutamate. Therefore, increasing GABAergic tone upon fear recall may affect cued, trace and context fear likewise, while possible co-release of NPY would address specifically the contextual components. While we did not specifically address the question of how NPY overexpression alone would have affected individual aspects of fear processing, it is important to note that overexpression of NPY alone did not modify fear expression during acquisition or background context testing (**Figures 2C,D**, **3C**). Considering the disease course and inherent properties of PTSD, with fear generalization increasing over time and extending towards various triggers and circumstances, interference with the hippocampal NPY system seems to be a promising treatment strategy.

Several classes of interneurons are populating different regions of the hippocampal DG. These inhibitory neurons are orchestrating the activity of dentate granule cells by restricting their activation and assigning dedicated neuronal ensembles to specific contextual representations. In particular, hilar perforant path-associated (HIPP) cells receive inputs from dentate granule cells and perforant path terminals, while targeting granule cell dendrites in the outer molecular layer. These neurons provide powerful feedback inhibition and curtail the size of the hippocampal fear engram. Importantly, in addition to GABA, they release SST and NPY as modulatory neurotransmitters. Recently, it has been suggested that NPY HIPP cells in the DG especially modulate "background" context fear expression by inhibiting DG granule cells (Raza et al., 2017). Y1 receptors seem to be predominantly involved in this phenomenon. Indeed, we showed that in the dorsal DG more than 70% of SST neurons also express NPY.

However, we also demonstrated that NPY is expressed by several other DG interneuron populations, including PV basket cells. DG PV basket cells are activated by granule cells and provide powerful lateral inhibition (Espinoza et al., 2018). This effect limits the size of the resulting fear engram and enables the simultaneous storage and differentiation of multiple highly similar representations, a phenomenon called pattern separation. Activation of PV cells during fear memory recall may increase the specificity of the memory by providing efficient lateral inhibition and protection from the propagation of PTSD-related phenomena, such as fear generalization. We showed that in the dorsal DG, 64% of the PV neurons also contain NPY. The dentate PV cell population consists of basket cells and axo-axonic cells. Thus, co-expressed NPY may reach postsynaptic Y1 Rs on granule cell dendrites as well as pre-synaptic Y2 Rs on granule cells axons, *via* neuropeptide-specific volume transmission. A general inhibition of dentate granule cells may reduce fear expression and at the same time, result in a downscaling of synaptic activity affecting in particular weakly activated granule cells. This in turn could sharpen the overall contrast of the respective neuronal engrams and reduce fear generalization while promoting fear extinction learning.

In order to shed more light on the role of NPY in hippocampus-dependent fear learning, we activated or inhibited DG GABA neurons in VGAT-cre mice, including SST and PV neurons, which were mostly NPY positive. By addressing both neuronal subpopulations, our approach may have inhibited granule cells on various neuronal specializations and targeted dendritic Y1 and axonal Y2R likewise. It is also interesting to note that mere overexpression of NPY in dentate interneurons did not alter fear expression in a conditioning protocol in which context was used in the background. Under the selected conditions, NPY release may have been too weak, or the respective receptors could have been already saturated, precluding a detectable effect of increased NPY levels. However, when we excited these neurons in the presence of NPY, a reduction was seen in conventional context conditioning during fear recall and extinction. Initially, this may contradict the results reported earlier (Raza et al., 2017),

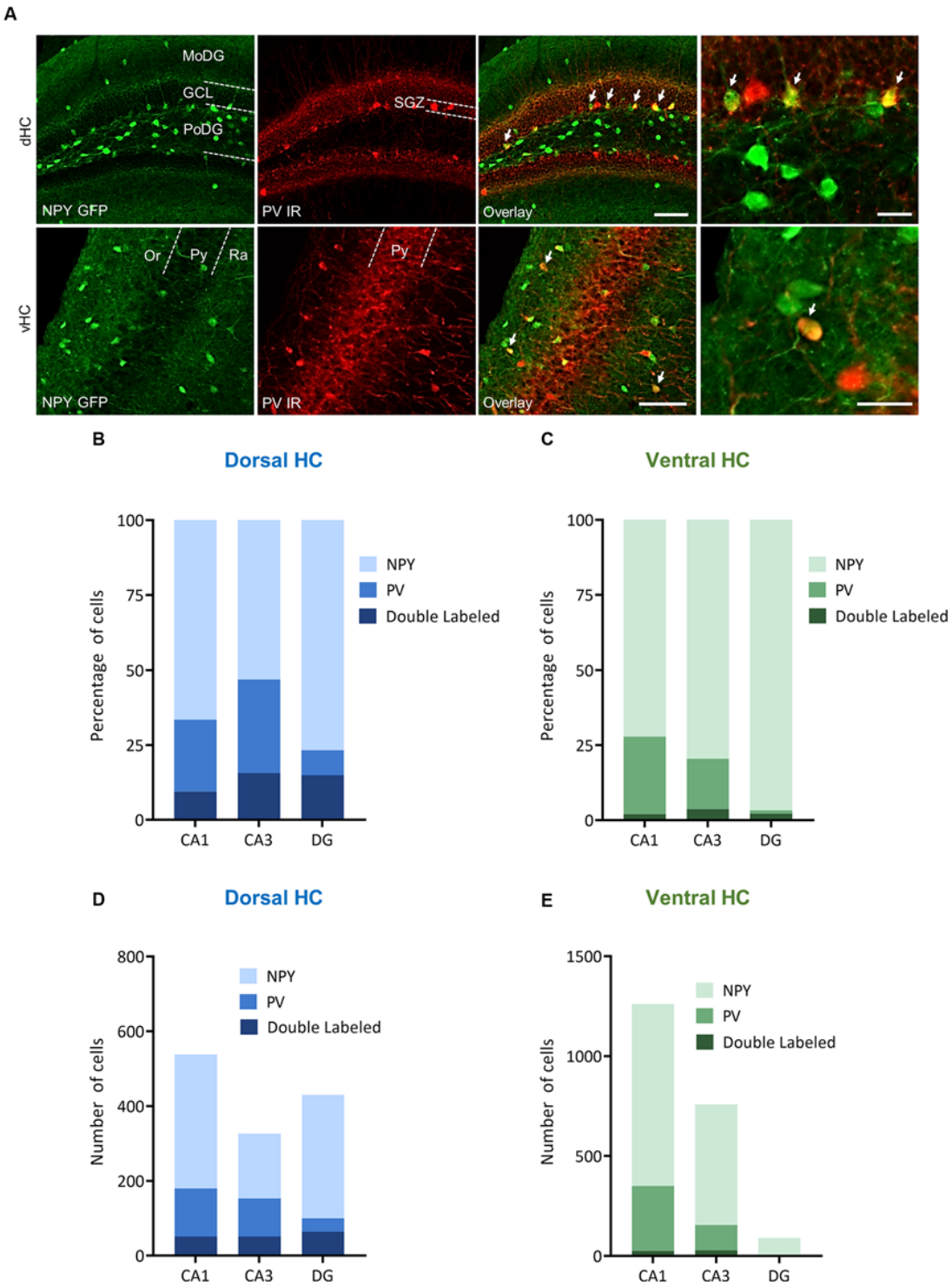

FIGURE 7 | Distribution and quantification of co-expression of parvalbumin (PV) with NPY in the dorsal (dHC) and ventral (vHC) mouse hippocampus. **(A)** Immunohistochemical labeling for PV and NPY-GFP auto-fluorescence depicting dual-labeled neurons (upper panel: dorsal dentate gyrus, lower panel: ventral hippocampus CA1, arrows depict dual-labeled neurons) of NPY-GFP mice. Cells in green indicate NPY-GFP + neurons and cells in red indicate PV expressing neurons. **(B)** Histograms showing the percentage of NPY-GFP neurons in CA1, CA3, and DG of the dorsal hippocampus that are co-labeling with PV. **(C)** Histograms showing the percentage of NPY-GFP neurons in CA1, CA3, and DG of the ventral hippocampus that are co-labeling with PV. In the ventral hippocampus the amount of NPY and PV dual labeling is very low. **(D)** Number of NPY-GFP and PV neurons in CA1, CA3, and DG of the dorsal and **(E)** ventral hippocampus. Scale bars: lower magnification 200 μm (third column), higher magnification 50 μm (last column). Abbreviations: MoDG, Molecular layer of the dentate gyrus; GCL, granule cell layer; PoDG, hilus/polymorph layer of the dentate gyrus; SGZ, subgranular zone; Or, stratum oriens; Py, stratum pyramidale; and Ra, stratum radiatum.

TABLE 4 | Co-localization of NPY-GFP and PV in the hippocampus.

Region	Subdivision	Single-labeled NPY-GFP+ neurons	Single-labeled PV+ neurons	Double-labeled neurons	Percent of single-labeled NPY-GFP+ neurons	Percent of single-labeled PV+ neurons	Percent of double-labeled neurons
Dorsal HC	CA1	358	129	51	66.5	24.0	9.5
	CA3	173	102	51	53.1	31.3	15.6
	DG	330	36	64	76.7	8.4	14.9
Ventral HC	CA1	910	326	25	72.2	25.9	2.0
	CA3	603	127	28	79.6	16.8	3.7
	DG	87	1	2	96.7	1.1	2.2

NPY-PV: n = 3.

however, several methodological subtleties could explain these differences. Further studies are needed to elucidate the role of NPY and in particular of the individual Y receptors in the different variations of Pavlovian fear conditioning.

Taken together, we demonstrated that NPY is expressed by different populations of GABA neurons within the mouse DG, including not only SST but also PV basket cells or axo-axonic cells. Furthermore, we showed that activation of DG GABA neurons reduced CS and trace fear recall. Importantly, concomitantly released NPY did not interfere with DG-dependent modulation of cued or trace fear, but significantly reduced contextual foreground fear, while promoting extinction learning. Thus, co-release of neuropeptide transmitters may affect specific emotional-affective and cognitive aspects of a fear memory and could provide a promising therapeutic add-on for the treatment of PTSD.

DATA AVAILABILITY STATEMENT

The original contributions presented in the study are included in the article/**Supplementary Material**, further inquiries can be directed to the corresponding author.

ETHICS STATEMENT

The animal study was reviewed and approved by the Austrian Ministry of Science.

AUTHOR CONTRIBUTIONS

The manuscript was prepared by LC, NH, PM, and RT. LC and NH performed the viral injections and the behavioral testing. PM made the histological analysis. RT designed and supervised the experiments.

FUNDING

The authors declare that this work was funded by the Austrian Science Fund (P 25851).

ACKNOWLEDGMENTS

We thank Anneliese Bukovac for technical assistance.

SUPPLEMENTARY MATERIAL

The Supplementary Material for this article can be found online at: https://www.frontiersin.org/articles/10.3389/fnsyn.2021.635726/full#supplementary-material.

SUPPLEMENTARY FIGURE 1 | Variation of trace length in trace fear conditioning in male C57Bl6/NCrl mice. **(A)** A 20 s trace length between conditioned stimulus (CS) and unconditioned stimulus presentation resulted in an equal percentage of freezing during CS, trace (T), and inter-trial interval (P). **(B)** In contrast, a 5 s trace interval after CS produced an increased percentage of freezing during the trace compared to medium freezing levels upon CS presentation and lowest freezing levels during the inter-trial interval. **(C)** Analysis of a 20 s trace in 5 s bins revealed increased percentage of freezing only during the first 5 s after the CS, but not in the following time intervals. Data are presented as means ± SEM and were analyzed by one-way ANOVA for repeated measurements, $^*P < 0.05$, $n = 12$.

SUPPLEMENTARY FIGURE 2 | Analysis of the injection sites and affected neuronal subpopulations throughout the hippocampal formation. **(A)** Immunohistochemically labeling of RFP in the hippocampus of an rAAV-hSyn-DIO-hM3DGq-mCherry injected VGAT-Cre mouse. Note that neuronal expression is confined to the dorsal DG, however, a lower number of fibers was also present in other hippocampal subregions, probability representing a restricted number of axonal projections. **(B)** Immunohistochemically labeled neurons for parvalbumin (PV, red) and RFP (green) in the granule cell layer of the dorsal DG (arrows illustrate dual-labeled neurons). **(C)** Immunohistochemically labeled neurons for somatostatin (SST, red) and RFP (green; arrows illustrate dual-labeled neurons). LV: lateral ventricle DG: dentate gyrus, CA1, 2 and 3: cornu ammonis 1, 2, and 3, respectively. Scale bars: **(A)**: 200 μm, **(B,C)**: 50 μm.

SUPPLEMENTARY FIGURE 3 | Specific reduction in context fear but not in cued or trace fear following over-expression of NPY in VGAT neurons of the dorsal dentate gyrus (DG). **(A)** rAAV-hSyn-DIO-hM3DGq-mCherry/rAAV-EF1a-DIO-NPY (Gq + NPY) injected mice freeze less than those injected with rAAV-hSyn-DIO-hM3DGq-mCherry (Gq) alone during context fear test. **(B)** There was no difference in freezing time during cued and trace fear test between Gq + NPY and Gq alone injected mice after reconditioning. **(C)** There was no correlation between the freezing levels to CS and context fear. Both Gq + NPY and Gq alone mice were injected 30 min before the test with CNO (ip, 1 mg/kg). Data are presented as means ± SEM, $^*P < 0.05$, Gq: $n = 4$, Gq + NPY: $n = 5$.

SUPPLEMENTARY FIGURE 4 | Immunohistochemical distribution and quantification of co-expression of parvalbumin (PV) with NPY in the dorsal dentate gyrus (DG). **(A)** Immunohistochemical labeling for NPY (green) and PV (red) depicting dual-labeled neurons (upper panel: individual immunoreactivities in the dorsal dentate gyrus, lower panel: dual-labeling and higher magnification) in male C57Bl6/NCrl mice. **(B)** Histogram depicting the percentage of NPY, PV, and dual-labeled neurons in the dorsal DG. **(C)** Tabular results of respective quantifications. Scale bars: lower magnification 200 μm, higher magnification 50 μm. Abbreviations: MoDG, molecular layer of the dentate gyrus; GCL, granule cell layer; PoDG, hilus/polymorph layer of the dentate gyrus; SGZ, subgranular zone.

REFERENCES

Ahmed, M. S., Priestley, J. B., Castro, A., Stefanini, F., Solis Canales, A. S., Balough, E. M., et al. (2020). Hippocampal network reorganization underlies the formation of a temporal association memory. *Neuron* 107, e6.283–e6.291. doi: 10.1016/j.neuron.2020.04.013

Amaral, D. G., and Witter, M. P. (1989). The three-dimensional organization of the hippocampal formation: a review of anatomical data. *Neuroscience* 31, 571–591. doi: 10.1016/0306-4522(89)90424-7

Bellmann, R., Widmann, R., Olenik, C., Meyer, D. K., Maas, D., Marksteiner, J., et al. (1991). Enhanced rate of expression and biosynthesis of neuropeptide Y after kainic acid-induced seizures. *J. Neurochem.* 56, 525–530. doi: 10.1111/j.1471-4159.1991.tb08181.x

Bowers, M. E., Choi, D. C., and Ressler, K. J. (2012). Neuropeptide regulation of fear and anxiety: implications of cholecystokinin, endogenous opioids and neuropeptide Y. *Physiol. Behav.* 107, 699–710. doi: 10.1016/j.physbeh.2012.03.004

Bowers, M. E., and Ressler, K. J. (2015). An overview of translationally informed treatments for posttraumatic stress disorder: animal models of pavlovian fear conditioning to human clinical trials. *Biol. Psychiatry* 78, E15–27. doi: 10.1016/j.biopsych.2015.06.008

Comeras, L. B., Herzog, H., and Tasan, R. O. (2019). Neuropeptides at the crossroad of fear and hunger: a special focus on neuropeptide Y. *Ann. N Y Acad. Sci.* 1455, 59–80. doi: 10.1111/nyas.14179

Cox, D., Czerniawski, J., Ree, F., and Otto, T. (2013). Time course of dorsal and ventral hippocampal involvement in the expression of trace fear conditioning. *Neurobiol. Learn Mem.* 106, 316–323. doi: 10.1016/j.nlm.2013.05.009

Daldrup, T., Remmes, J., Lesting, J., Gaburro, S., Fendt, M., Meuth, P., et al. (2015). Expression of freezing and fear-potentiated startle during sustained fear in mice. *Genes Brain Behav.* 14, 281–291. doi: 10.1111/gbb.12211

Ehrlich, I., Humeau, Y., Grenier, F., Ciocchi, S., Herry, C., Luthi, A., et al. (2009). Amygdala inhibitory circuits and the control of fear memory. *Neuron* 62, 757–771. doi: 10.1016/j.neuron.2009.05.026

Esclassan, F., Coutureau, E., Di Scala, G., and Marchand, A. R. (2009). Differential contribution of dorsal and ventral hippocampus to trace and delay fear conditioning. *Hippocampus* 19, 33–44. doi: 10.1002/hipo.20473

Espinoza, C., Guzman, S. J., Zhang, X., and Jonas, P. (2018). Parvalbumin(+) interneurons obey unique connectivity rules and establish a powerful lateral-inhibition microcircuit in dentate gyrus. *Nat. Commun.* 9:4605. doi: 10.1038/s41467-018-06899-3

Fendt, M., Burki, H., Imobersteg, S., Lingenhohl, K., McAllister, K. H., Orain, D., et al. (2009). Fear-reducing effects of intra-amygdala neuropeptide Y infusion in animal models of conditioned fear: an NPY Y1 receptor independent effect. *Psychopharmacology* 206, 291–301. doi: 10.1007/s00213-009-1610-8

Flood, J. F., Baker, M. L., Hernandez, E. N., and Morley, J. E. (1989). Modulation of memory processing by neuropeptide Y varies with brain injection site. *Brain Res.* 503, 73–82. doi: 10.1016/0006-8993(89)91706-x

Flood, J. F., Hernandez, E. N., and Morley, J. E. (1987). Modulation of memory processing by neuropeptide Y. *Brain Res.* 421, 280–290. doi: 10.1016/0006-8993(87)91297-2

Gehlert, D. R., Chronwall, B. M., Schafer, M. P., and O'Donohue, T. L. (1987). Localization of neuropeptide Y messenger ribonucleic acid in rat and mouse brain by *in situ* hybridization. *Synapse* 1, 25–31. doi: 10.1002/syn.890010106

Gilpin, N. W. (2012). Neuropeptide Y (NPY) in the extended amygdala is recruited during the transition to alcohol dependence. *Neuropeptides* 46, 253–259. doi: 10.1016/j.npep.2012.08.001

Gutman, A. R., Yang, Y., Ressler, K. J., and Davis, M. (2008). The role of neuropeptide Y in the expression and extinction of fear-potentiated startle. *J. Neurosci.* 28, 12682–12690. doi: 10.1523/JNEUROSCI.2305-08.2008

Herry, C., Ferraguti, F., Singewald, N., Letzkus, J. J., Ehrlich, I., Luthi, A., et al. (2010). Neuronal circuits of fear extinction. *Eur. J. Neurosci.* 31, 599–612. doi: 10.1111/j.1460-9568.2010.07101.x

Hokfelt, T., Brumovsky, P., Shi, T., Pedrazzini, T., and Villar, M. (2007). NPY and pain as seen from the histochemical side. *Peptides* 28, 365–372. doi: 10.1016/j.peptides.2006.07.024

Holzer, P., Reichmann, F., and Farzi, A. (2012). Neuropeptide Y, peptide YY and pancreatic polypeptide in the gut-brain axis. *Neuropeptides* 46, 261–274. doi: 10.1016/j.npep.2012.08.005

Hormer, B. A., Verma, D., Gasser, E., Wieselthaler-Holzl, A., Herzog, H., Tasan, R. O., et al. (2018). Hippocampal NPY Y2 receptors modulate memory depending on emotional valence and time. *Neuropharmacology* 143, 20–28. doi: 10.1016/j.neuropharm.2018.09.018

Hubner, C., Bosch, D., Gall, A., Luthi, A., and Ehrlich, I. (2014). *Ex vivo* dissection of optogenetically activated mPFC and hippocampal inputs to neurons in the basolateral amygdala: implications for fear and emotional memory. *Front. Behav. Neurosci.* 8:64. doi: 10.3389/fnbeh.2014.00064

Kask, A., Harro, J., von Horsten, S., Redrobe, J. P., Dumont, Y., Quirion, R., et al. (2002). The neurocircuitry and receptor subtypes mediating anxiolytic-like effects of neuropeptide Y. *Neurosci. Biobehav. Rev.* 26, 259–283. doi: 10.1016/s0149-7634(01)00066-5

Kautz, M., Charney, D. S., and Murrough, J. W. (2017). Neuropeptide Y, resilience and PTSD therapeutics. *Neurosci. Lett.* 649, 164–169. doi: 10.1016/j.neulet.2016.11.061

Kopp, J., Xu, Z. Q., Zhang, X., Pedrazzini, T., Herzog, H., Kresse, A., et al. (2002). Expression of the neuropeptide Y Y1 receptor in the CNS of rat and of wild-type and Y1 receptor knock-out mice. focus on immunohistochemical localization. *Neuroscience* 111, 443–532. doi: 10.1016/s0306-4522(01)00463-8

Lach, G., and De Lima, T. C. (2013). Role of NPY Y1 receptor on acquisition, consolidation and extinction on contextual fear conditioning: dissociation between anxiety, locomotion and non-emotional memory behavior. *Neurobiol. Learn Mem.* 103, 26–33. doi: 10.1016/j.nlm.2013.04.005

LeDoux, J. E. (2000). Emotion circuits in the brain. *Annu. Rev. Neurosci.* 23, 155–184. doi: 10.1146/annurev.neuro.23.1.155

Loh, K., Herzog, H., and Shi, Y. C. (2015). Regulation of energy homeostasis by the NPY system. *Trends Endocrinol. Metab.* 26, 125–135. doi: 10.1016/j.tem.2015.01.003

Maren, S., and Fanselow, M. S. (1995). Synaptic plasticity in the basolateral amygdala induced by hippocampal formation stimulation *in vivo*. *J. Neurosci.* 15, 7548–7564. doi: 10.1523/JNEUROSCI.15-11-07548.1995

McDonald, A. J., and Mott, D. D. (2017). Functional neuroanatomy of amygdalohippocampal interconnections and their role in learning and memory. *J. Neurosci.* 95, 797–820. doi: 10.1002/jnr.23709

Misane, I., Tovote, P., Meyer, M., Spiess, J., Ogren, S. O., Stiedl, O., et al. (2005). Time-dependent involvement of the dorsal hippocampus in trace fear conditioning in mice. *Hippocampus* 15, 418–426. doi: 10.1002/hipo.20067

Morris, B. J. (1989). Neuronal localisation of neuropeptide Y gene expression in rat brain. *J. Comp. Neurol.* 290, 358–368. doi: 10.1002/cne.902900305

Noe, F., Pool, A. H., Nissinen, J., Gobbi, M., Bland, R., Rizzi, M., et al. (2008). Neuropeptide Y gene therapy decreases chronic spontaneous seizures in a rat model of temporal lobe epilepsy. *Brain* 131, 1506–1515. doi: 10.1093/brain/awn079

Pape, H. C., and Pare, D. (2010). Plastic synaptic networks of the amygdala for the acquisition, expression and extinction of conditioned fear. *Physiol. Rev.* 90, 419–463. doi: 10.1152/physrev.00037.2009

Paxinos, G., and Franklin, K. B. J. (2004). *The Mouse Brain in Stereotaxic Coordinates*, Compact 2nd edition. Boston, FL: Elsevier Academic Press, Amsterdam.

Raybuck, J. D., and Lattal, K. M. (2014). Bridging the interval: theory and neurobiology of trace conditioning. *Behav. Processes* 101, 103–111. doi: 10.1016/j.beproc.2013.08.016

Raza, S. A., Albrecht, A., Caliskan, G., Muller, B., Demiray, Y. E., Ludewig, S., et al. (2017). HIPP neurons in the dentate gyrus mediate the cholinergic modulation of background context memory salience. *Nat. Commun.* 8:189. doi: 10.1038/s41467-017-00205-3

Reichmann, F., and Holzer, P. (2016). Neuropeptide Y: a stressful review. *Neuropeptides* 55, 99–109. doi: 10.1016/j.npep.2015.09.008

Schmeltzer, S. N., Herman, J. P., and Sah, R. (2016). Neuropeptide Y (NPY) and posttraumatic stress disorder (PTSD): a translational update. *Exp. Neurol.* 284, 196–210. doi: 10.1016/j.expneurol.2016.06.020

Sperk, G., and Widmann, R. (1985). Somatostatin precursor in the rat striatum: changes after local injection of kainic acid. *J. Neurochem.* 45, 1441–1447. doi: 10.1111/j.1471-4159.1985.tb07211.x

Stanic, D., Brumovsky, P., Fetissov, S., Shuster, S., Herzog, H., Hokfelt, T., et al. (2006). Characterization of neuropeptide Y2 receptor protein expression in the mouse brain: I. Distribution in cell bodies and nerve terminals. *J. Comp. Neurol.* 499, 357–390. doi: 10.1002/cne.21046

Stanic, D., Mulder, J., Watanabe, M., and Hokfelt, T. (2011). Characterization of NPY Y2 receptor protein expression in the mouse brain. II. Coexistence with NPY, the Y1 receptor and other neurotransmitter-related molecules. *J. Comp. Neurol.* 519, 1219–1257. doi: 10.1002/cne.22608

Tasan, R. O., Bukovac, A., Peterschmitt, Y. N., Sartori, S. B., Landgraf, R., Singewald, N., et al. (2011). Altered GABA transmission in a mouse model of increased trait anxiety. *Neuroscience* 183, 71–80. doi: 10.1016/j.neuroscience.2011.03.051

Tasan, R. O., Nguyen, N. K., Weger, S., Sartori, S. B., Singewald, N., Heilbronn, R., et al. (2010). The central and basolateral amygdala are critical sites of neuropeptide Y/Y2 receptor-mediated regulation of anxiety and depression. *J. Neurosci.* 30, 6282–6290. doi: 10.1523/JNEUROSCI.0430-10.2010

Tasan, R. O., Verma, D., Wood, J., Lach, G., Hormer, B., De Lima, T. C., et al. (2016). The role of Neuropeptide Y in fear conditioning and extinction. *Neuropeptides* 55, 111–126. doi: 10.1016/j.npep.2015.09.007

Tatemoto, K., Carlquist, M., and Mutt, V. (1982). Neuropeptide Y—a novel brain peptide with structural similarities to peptide YY and pancreatic polypeptide. *Nature* 296, 659–660. doi: 10.1038/296659a0

Verma, D., Jamil, S., Tasan, R. O., Lange, M. D., and Pape, H. C. (2018a). Single stimulation of Y2 receptors in BNSTav facilitates extinction and dampens reinstatement of fear. *Psychopharmacology* 236, 281–291. doi: 10.1007/s00213-018-5080-8

Verma, D., Tasan, R., Sperk, G., and Pape, H. C. (2018b). Neuropeptide Y2 receptors in anteroventral BNST control remote fear memory depending on extinction training. *Neurobiol. Learn Mem.* 149, 144–153. doi: 10.1016/j.nlm.2018.01.011

Verma, D., Tasan, R. O., Herzog, H., and Sperk, G. (2012). NPY controls fear conditioning and fear extinction by combined action on Y(1) and Y(2) receptors. *Br. J. Pharmacol.* 166, 1461–1473. doi: 10.1111/j.1476-5381.2012.01872.x

Verma, D., Wood, J., Lach, G., Mietzsch, M., Weger, S., Heilbronn, R., et al. (2015). NPY Y2 receptors in the central amygdala reduce cued but not contextual fear. *Neuropharmacology* 99, 665–674. doi: 10.1016/j.neuropharm.2015.08.038

Wood, J., Verma, D., Lach, G., Bonaventure, P., Herzog, H., Sperk, G., et al. (2016). Structure and function of the amygdaloid NPY system: NPY Y2 receptors regulate excitatory and inhibitory synaptic transmission in the centromedial amygdala. *Brain Struct. Funct.* 221, 3373–3391. doi: 10.1007/s00429-015-1107-7

Zhang, L., Chen, X., Sindreu, C., Lu, S., Storm, D. R., Zweifel, L. S., et al. (2019). Dynamics of a hippocampal neuronal ensemble encoding trace fear memory revealed by *in vivo* Ca^{2+} imaging. *PLoS One* 14:e0219152. doi: 10.1371/journal.pone.0219152

Conflict of Interest: The authors declare that the research was conducted in the absence of any commercial or financial relationships that could be construed as a potential conflict of interest.

Copyright © 2021 Comeras, Hörmer, Mohan Bethuraj and Tasan. This is an open-access article distributed under the terms of the Creative Commons Attribution License (CC BY). The use, distribution or reproduction in other forums is permitted, provided the original author(s) and the copyright owner(s) are credited and that the original publication in this journal is cited, in accordance with accepted academic practice. No use, distribution or reproduction is permitted which does not comply with these terms.

frontiers in Synaptic Neuroscience

ORIGINAL RESEARCH
published: 06 July 2021
doi: 10.3389/fnsyn.2021.634558

Fear Memory Retrieval Is Associated With a Reduction in AMPA Receptor Density at Thalamic to Amygdala Intercalated Cell Synapses

Anna Seewald[1], Sabine Schönherr[1], Heide Hörtnagl[1], Ingrid Ehrlich[2,3], Claudia Schmuckermair[1] and Francesco Ferraguti[1]**

[1] Department of Pharmacology, Medical University of Innsbruck, Innsbruck, Austria, [2] Center for Integrative Neuroscience, Hertie Institute for Clinical Brain Research, University of Tübingen, Tübingen, Germany, [3] Department of Neurobiology, Institute of Biomaterials and Biomolecular Systems, University of Stuttgart, Stuttgart, Germany

OPEN ACCESS

Edited by:
Joachim H. R. Lübke,
Helmholtz-Verband Deutscher Forschungszentren (HZ), Germany

Reviewed by:
Ronald Sebastian Petralia,
National Institute on Deafness and Other Communication Disorders (NIDCD), United States
Eric Hanse,
University of Gothenburg, Sweden
Yugo Fukazawa,
University of Fukui, Japan

***Correspondence:**
Claudia Schmuckermair
claudia.schmuckermair@i-med.ac.at
Francesco Ferraguti
francesco.ferraguti@i-med.ac.at

Received: 28 November 2020
Accepted: 14 June 2021
Published: 06 July 2021

Citation:
Seewald A, Schönherr S, Hörtnagl H, Ehrlich I, Schmuckermair C and Ferraguti F (2021) Fear Memory Retrieval Is Associated With a Reduction in AMPA Receptor Density at Thalamic to Amygdala Intercalated Cell Synapses.
Front. Synaptic Neurosci. 13:634558.
doi: 10.3389/fnsyn.2021.634558

The amygdala plays a crucial role in attaching emotional significance to environmental cues. Its intercalated cell masses (ITC) are tight clusters of GABAergic neurons, which are distributed around the basolateral amygdala complex. Distinct ITC clusters are involved in the acquisition and extinction of conditioned fear responses. Previously, we have shown that fear memory retrieval reduces the AMPA/NMDA ratio at thalamic afferents to ITC neurons within the dorsal medio-paracapsular cluster. Here, we investigate the molecular mechanisms underlying the fear-mediated reduction in the AMPA/NMDA ratio at these synapses and, in particular, whether specific changes in the synaptic density of AMPA receptors underlie the observed change. To this aim, we used a detergent-digested freeze-fracture replica immunolabeling technique (FRIL) approach that enables to visualize the spatial distribution of intrasynaptic AMPA receptors at high resolution. AMPA receptors were detected using an antibody raised against an epitope common to all AMPA subunits. To visualize thalamic inputs, we virally transduced the posterior thalamic complex with Channelrhodopsin 2-YFP, which is anterogradely transported along axons. Using face-matched replica, we confirmed that the postsynaptic elements were ITC neurons due to their prominent expression of μ-opioid receptors. With this approach, we show that, following auditory fear conditioning in mice, the formation and retrieval of fear memory is linked to a significant reduction in the density of AMPA receptors, particularly at spine synapses formed by inputs of the posterior intralaminar thalamic and medial geniculate nuclei onto identified ITC neurons. Our study is one of the few that has directly linked the regulation of AMPA receptor trafficking to memory processes in identified neuronal networks, by showing that fear-memory induced reduction in AMPA/NMDA ratio at thalamic-ITC synapses is associated with a reduced postsynaptic AMPA receptor density.

Keywords: fear conditioning, memory, freeze-fracture, plasticity, medial geniculate nucleus, glutamate receptor

INTRODUCTION

Associative learning is an adaptive process that allows an individual to predict events and requires long-lasting modifications in the strength of synaptic connections, generally known as synaptic plasticity (Martin et al., 2000; Malenka and Bear, 2004; Kessels and Malinow, 2009; Poo et al., 2016).

Pavlovian fear (threat) conditioning is one of the most prominently studied forms of associative learning (LeDoux, 2000; Maren, 2001), in which a neutral sensory stimulus (conditioned stimulus or CS) is repeatedly paired with an aversive stimulus (unconditioned stimulus or US; most commonly an electric shock), which leads to the formation of a strong CS-US association. In conditioned subjects, the presentation of the CS alone can trigger a fear response, that in rodents is commonly measured as freezing (LeDoux, 2000; Maren, 2001).

Somatosensory inputs arising from the neocortex and thalamus and carrying information about the CS and US converge in the lateral nucleus of the amygdala (LA) where persistent changes in synaptic transmission are linked to the encoding of the CS-US association and the storage of fear memories (Rogan et al., 1997; Pape and Paré, 2010). LA neurons then transfer the association *via* the basal and basomedial nuclei to the medial division of the central nucleus (CeA) to generate fear outputs (Maren and Quirk, 2004). This simple model has been recently challenged since other amygdaloid structures besides the LA, e.g., the lateral part of the CeA (CeL) and the intercalated cell masses of the amygdala (ITCs), were also shown to receive direct sensory information and undergo fear-related synaptic and cellular plasticity (Ciocchi et al., 2010; Haubensak et al., 2010; Li et al., 2013; Herry and Johansen, 2014; Asede et al., 2015; Barsy et al., 2020).

ITCs are a specialized group of tightly clustered GABAergic medium spiny neurons characterized by high μ-opioid receptor expression levels, exceeding those observed in the CeA and LA (Likhtik et al., 2008; Busti et al., 2011; Blaesse et al., 2015). The ITCs consist of several dispersed clusters located around the basolateral complex of the amygdala (BLA) (Millhouse, 1986; Busti et al., 2011). Two main ITC clusters are situated along the intermediate capsule, a dorsal medio-paracapsular (mpITC) and a larger ventrally located (vmITC) cluster (Millhouse, 1986; Kaoru et al., 2010; Busti et al., 2011; Hagihara et al., 2021). The vmITC is critically involved in the formation and/or recall of fear extinction memory (Likhtik et al., 2008; Amano et al., 2010; Hagihara et al., 2021). In contrast, the mpITC was found to be active during the expression of fear (Busti et al., 2011; Huang et al., 2014; Kwon et al., 2015; Hagihara et al., 2021). The vmITC has been proposed to be directly inhibited by the mpITC leading to disinhibition of the CeM and facilitation of fear responses (Royer et al., 2000; Busti et al., 2011). The engagement of different ITCs in distinct fear states may in part depend on their afferents, allowing a dual function to either facilitate or suppress conditioned fear responses (Busti et al., 2011; Duvarci and Paré, 2014).

We and others have recently demonstrated that efferents from the posterior intralaminar nuclei of the thalamus (PIN) and the medial subdivision of the medial geniculate nucleus (MGm), that convey pain- and auditory US- and CS-related information, innervate not only the LA but also the mpITC, whereas the vmITC is spared by this innervation (Asede et al., 2015; Strobel et al., 2015). The formation of both short- and long-term fear memory requires the potentiation of glutamatergic PIN/MGm to LA synapses (McKernan and Shinnick-Gallagher, 1997; Kim and Cho, 2017). We extended this by reporting a lasting decrease in pre- and post-synaptic strength upon fear memory retrieval at PIN/MGm to mpITC synapses (Asede et al., 2015).

Several studies have shown that the potentiation of LA synapses underlying fear memory formation involves a number of cellular and molecular mechanisms. These include modifications in transmitter release and gating properties of ionotropic glutamate receptors, such as α-amino-3-hydroxy-5-methyl-4-isoxazolepropionic acid (AMPA) and *N*-methyl-D-aspartate (NMDA) receptors (Huang and Kandel, 1998; Humeau et al., 2003; Rodrigues et al., 2004; Pape and Paré, 2010), but also an increase in the number of postsynaptic AMPA receptors (Rumpel et al., 2005; Yeh et al., 2006; Humeau et al., 2007; Migues et al., 2010). In particular, a sustained and long-lasting increase in AMPA to NMDA receptor EPSC amplitude ratio (A/N ratio) at thalamic to LA inputs was observed following auditory fear conditioning in mice (Clem and Huganir, 2010). The same behavioral paradigm, on the other hand, produced a significant decrease in A/N ratio at PIN/MGm to mpITC synapses upon fear memory retrieval (Asede et al., 2015).

Here, we hypothesize that the fear memory-associated reduction in the A/N ratio observed at PIN/MGm to mpITC synapses results from a change in the postsynaptic density of AMPA receptors. To investigate this at the level of single synapses, we took advantage of the Freeze-fracture replica immunolabeling technique (FRIL), which offers a two-dimensional planar view of synapses and thus allows the quantification of integral membrane proteins.

Abbreviations: AMPA, α-amino-3-hydroxy-5-methyl-4-isoxazolepropionic acid; A/N ratio, AMPA to NMDA receptor EPSC amplitude ratio; AAV-ChR2-YFP, AAV2/9-h.Syn-hChR2(H134R)-eYFP; BLA, basolateral complex of the amygdala; CS, conditioned stimulus; CeA, central nucleus of the amygdala; CeL, lateral part of the CeA; FM, fear memory; IMPs, intramembrane particles; ITCs, intercalated cell masses of the amygdala; LA, lateral nucleus of the amygdala; MGm, medial subdivision of the medial geniculate nucleus; mpITC, dorsal medio-paracapsular cluster; NMDA, *N*-methyl-D-aspartate; NND, nearest neighbor distance; PB, phosphate-buffer; PIN, posterior intralaminar nuclei of the thalamus; PPR, paired pulse ratio; PSD, postsynaptic membrane specialization; TBS, Tris-buffered saline; US, unconditioned stimulus; vmITC, ventral medial cluster.

MATERIALS AND METHODS

Animals

All procedures involving animals were performed according to methods approved by the Austrian Animal Experimentation Ethics Board (license: BMWF-66.011/004/wf/v/3b/2015 and BMWFW-66.011/0021-WF/V/3b/2016) and in compliance with the European convention for the protection of vertebrate animals used for experimental and other scientific purposes (ETS number 123). Every effort was taken to minimize animal suffering and the number of animals used. For this study, adult, 8–12 week

old, male C57BL/6J mice (obtained at 7 weeks of age from Charles Rivers, Sulzfeld, Germany) were used. Mice were kept on a 12 h light/12 h dark cycle (lights off at 19:00). Mice had *ad libitum* access to standard chow and water and were housed in pairs of two.

Viral Injections

For axonal tracing, the adenoviral vector AAV2/9-h.Syn-hChR2(H134R)-eYFP (AAV-ChR2-YFP) (Penn Vector Core, Philadelphia, PA, United States) was injected into the PIN/MGm at a concentration of 1.0×10^{12} gc/ml.

Surgery

Stereotactic injection of the viral vector was carried out according to previously published procedures with minor modifications (Bosch et al., 2016; Schönherr et al., 2016). Eight week old mice were anaesthetized with an intraperitoneal (i.p.) injection of Ketasol/Xylazine (80/5 mg/kg). Anesthesia was maintained with 2% Sevofluran (SEVOrane, Abbvie) delivered *via* a face mask specifically designed for mice. For analgesia, 2 mg/kg Meloxicam (Metacam, Boehringer Ingelheim, Germany) were injected subcutaneously at the beginning of the surgery. Anesthetized mice were fixed in a stereotactic frame (DAVID KOPF Instruments, Tujunga, CA, United States) and injected bilaterally in the PIN/MGm at the following coordinates from bregma (in mm): posterior −2.70, lateral ± 1.60, ventral −3.60. Injections were performed with NEUROS Syringes (32G, 0.5 µl, HAMILTON, Reno, NV, United States), delivering a volume of 0.25 µl at an injection rate of 0.05 µl/min. Behavioral tests started 3 weeks after vector injection.

Fear Conditioning

Fear conditioning and memory recall were performed on two consecutive days in 17 cm × 17 cm × 25 cm chambers (Ugo Basile, Comerio, Italy) with distinct floors (metal grid for footshock delivery vs. flat surface), wall patterns (transparent acrylic plastic vs. black and white stripes), lightning (100 lux white light vs. infrared light) and scents (70% EtOH vs. 1% acetic acid, also used as cleaning compound between subjects). For fear conditioning, mice were placed in the conditioning chamber for a total time of 10 min. Following a 120 s baseline period, mice were presented five times with a 30 s 80 dB white noise (WN) conditioned stimulus [CS, pseudorandom inter-stimulus interval (ISI) = 48–80 s] co-terminating with a 1s 0.7 mA footshock. The control group (CS only) underwent the same protocol, but footshock delivery was omitted. Fear memory retrieval was performed 24 h after fear conditioning and lasted 10 min. Following a 120 s baseline period, mice were presented four times with the CS (30 s, 80 dB, WN, pseudorandom ISI = 56–120 s). Freezing was measured as an index of fear by an automated procedure with the ANY-maze software (Stoelting Europe, Dublin, Ireland), using a freezing minimum duration threshold of 1 s, and manually cross-checked by a trained person.

Histology

Thirty min after fear memory retrieval, animals were deeply anesthetized with thiopental sodium (150 mg/kg, i.p.) and transcardially perfused with a fixative [1% paraformaldehyde + 15% picric acid in 0.1 M phosphate-buffer (PB), pH 7.2–7.4]. Brains were immediately removed from the skull and placed in ice-cold 0.1 M PB. Coronal slices were cut with a vibratome (Leica VT1000S; Leica Microsystems, Vienna, Austria) at a thickness of 140 µm and collected in six well-dishes filled with 0.1 M PB. Sections containing the mpITC were then trimmed out under a stereomicroscope using an ophthalmic scalpel. Sections were cryoprotected with 30% glycerol in 0.1 M PB overnight at 6°C. Prior to the trimming, one slice/mouse containing the mpITC was mounted on an uncoated glass slide in 0.1 M PB, covered with a coverslip and the ChR2-YFP endogenous fluorescence was analyzed under an epifluorescence AxioImager M1 microscope (Carl Zeiss, Jena, Germany) to evaluate the pattern of distribution of ChR2-YFP-containing fibers. Digital images were taken using the Openlab software (Version 5.5.0, RRID:SCR_012158) through an Orca-ER CCD camera (Hamamatsu, Hamamatsu City, Japan). These slices were then demounted and the mpITC trimmed out as described above. Slices of the midbrain containing the injection site were similarly analyzed. Moreover, some slices were subsequently washed in Tris-buffered saline (TBS), incubated with a rabbit polyclonal anti-GFP primary antibody (Molecular Probes, Leiden, Netherlands, cat. no. A11122) diluted 1:1.000 in a solution containing 2% normal goat serum (NGS), 0.2% Triton X-100 in TBS (TBS-T) for 72 h at 6°C with constant shaking. Slices were then washed in TBS (three times for 10 min) and incubated overnight (6°C) with a donkey Alexa 488-conjugated anti-rabbit secondary antibody (1:1.000, Invitrogen, ThermoFisher Scientific, Waltham, MA, cat. no. A32790) in TBS-T and 2% NGS. To visualize general brain morphology, slices were counterstained with a DAPI solution (2 µg/ml, Sigma, cat. no. D-9564) for 4 min. Slices were then extensively washed in TBS, mounted onto gelatin-coated slides, and coverslipped with Vectashield (Vector Laboratory, Burlingame, CA, United States).

Freeze-Fracture Replica Immunolabeling

The FRIL technique was originally introduced by Fujimoto (1995) and further developed by Shigemoto and coworkers (Tanaka et al., 2005). This study was carried out according to the procedures described in Schönherr et al. (2016). Briefly, trimmed sections were sandwiched between two copper carriers and frozen with a high-pressure freezing machine (HPM010; Bal-Tec, Balzers, Liechtenstein) followed by storage in liquid nitrogen. Carriers containing frozen sections were fractured and replicated using a freeze fracture machine (BAF060; Bal-Tec, Balzers, Liechtenstein). During this procedure, the plasma membrane breaks along the central hydrophobic core and, as a consequence, is split into two halves. The inner leaflet represents the protoplasmic halve of the membrane (P-face), whereas the outer leaflet faces the exoplasmic space (E-face). After fracturing, both faces were replicated through the deposition of platinum/carbon layers. At first, a carbon coat was applied at a speed of 0.1–0.2 nm/s to a thickness of 5 nm followed by a unidirectional platinum shadowing at a speed of 0.06–0.1 nm/s and to a thickness of 2 nm, with the platinum gun positioned at a 60° angle. Finally, a further 15 nm carbon layer

was deposited at a speed of 0.3–0.5 nm/s. After thawing, the tissue attached to replicas was solubilized with shaking at 80°C overnight in the following solubilization buffer: 20% sucrose, 2.5% sodium dodecyl sulfate in 15 mM Tris buffer (TB), pH 8.3. Replicas were then transferred to a porcelain plate filled with fresh solubilization buffer and washed in TBS with 2.5% bovine serum albumin (BSA) for 5 min, followed by three washes, 10 min each, in 0.1% BSA-TBS. Non-specific binding sites were blocked by incubating the replicas in a blocking solution consisting of 5% BSA-TBS for 1 h. Primary antibodies were diluted in 2% BSA-TBS and then applied to the replicas. For each replicated specimen, one replica was incubated with the following primary antibodies: anti-pan-AMPA receptor (GluA1-4) diluted 1:200 (Frontier Institute, Hokkaido, Japan) and anti-green fluorescent protein (GFP) diluted 1:300 (Molecular Probes) that also detects YFP. The other corresponding replica was labeled with an antibody against μ-opioid receptors (dilution 1:500; ImmunoStar, Hudson, WI, United States). All incubations were performed in a 30 μl drop in a humid chamber at 15°C for 72 h. After the incubation in primary antibodies, replicas were washed in 0.1% BSA-TBS three times for 15 min and then transferred to a 2% BSA-TBS 30 μl drop, to which gold-conjugated secondary antibodies were added at a dilution of 1:30. To prevent confounds, AMPA receptors were visualized with antibodies conjugated to gold particles with a size of 5 nm, whereas ChR2-YFP with gold particles of 15 nm in diameter. Secondary antibodies against μ-opioid receptors were conjugated to 10 nm gold particles. **Table 1** lists sources and concentrations of all primary and secondary antibodies used for FRIL experiments. Replicas were then mounted on pioloform-coated mesh (100-line parallel bars) copper grids and analyzed using a transmission electron microscope (Philips CM120) at 80 kV. Digital images were recorded with a Morada CCD camera (Olympus Soft Imaging Solutions GmbH, Münster, Germany) and the imaging software program iTEM (Olympus Soft Imaging Systems).

Measurement of Immunogold Particle Density

Synaptic density of AMPA receptors was calculated from electron micrographs of synapses taken at a magnification of 53 k. The postsynaptic membrane specialization (PSD) of glutamatergic synapses can be observed in replicas as a cluster of intramembrane particles (IMPs) on the E-face of the plasma membrane (Sandri et al., 1972; Masugi-Tokita and Shigemoto, 2007), and is often accompanied by the P-face of its presynaptic plasma membrane (Tarusawa et al., 2009). The synaptic area was delineated manually by following the perimeter of IMP clusters on the E-face using ImageJ Software (1.37 v, Java 1.6.0_65, Wayne Rasband, National Institutes of Health, United States). Postsynaptic specializations directly adjacent to the labeled plasma membrane of thalamic terminals were identified as targets of thalamic inputs. Receptor density was obtained by counting the number of gold particles within the synaptic area and is given as number of gold particles per μm^2. The analyzed extrasynaptic area was the area of the plasma membrane adjacent to the IMP cluster and present within the 53 k digital images of the synapses. The pan-AMPA antibody was directed against extracellular epitopes and could thus be observed on the E-face of the plasma membrane, whereas GFP-labeling was detectable on the P-face of the plasma membrane. Non-specific labeling by the pan-AMPA antibody was determined on the P-face of surrounding structures and was subtracted from synaptic and extrasynaptic labeling densities.

As the mpITC is relatively small and did not fill the entire section, we took advantage of the fact that ITC neurons express high amounts of μ-opioid receptors in order to identify their postsynaptic processes. Therefore, every postsynaptic profile containing a synapse formed by a labeled thalamic terminal was confirmed to belong to a mpITC neuron by providing evidence of μ-opioid receptor labeling on the other membrane half (density > 7 gold particles/μm^2).

Gold Particle Analysis for Nanoscale Distribution of Synaptic AMPA Receptors

Spatial coordinates of the immunogold particles were extracted from electron micrographs and their arrangement was analyzed using the open source Python-based pipeline GoldExt (Szoboszlay et al., 2017). The nearest neighbor distance (NND) between gold particles within synapses was used to detect potential deviations from random distributions (50 random values calculated per synapse). For these analyses, only 80% of the sampled synapses were used, which, however, included all fully exposed synapses.

Data Analysis

Data are presented as mean ± standard error of the mean (SEM). Comparison of multiple groups was done using one-way analysis of variance (ANOVA) followed by the Bonferroni

TABLE 1 | List of primary and secondary antibodies used for FRIL.

Primary antibodies	Target molecule	Species	Dilution	Source	Catalog no.
Anti-GFP	Green fluorescent protein	Rabbit	1:300	Molecular probes	A11122
Anti-pan-AMPA	AMPA receptor (GluR1-4)	G. pig	1:200	Frontier Science	Pan-AMPA-GP-Af580-1
Anti-μ-opioid	μ-opioid receptor	Rabbit	1:500	Immunostar	24216
Secondary antibodies	Conjugated gold particle	Species	Dilution	Source	Batch no.
Anti-rabbit	10 nm	Donkey	1:30	Aurion	DAR-21211/2
Anti-rabbit	15 nm	Goat	1:30	BB International	7190
Anti-G. pig	5 nm	Goat	1:30	BB International	1175

post hoc test. Two-way ANOVA was used to analyse the effect of time and groups in the behavioral experiments. Cumulative distributions and correlations between synaptic area and number of gold particles were examined by the Kolmogorov–Smirnov and Pearson's correlation coefficient tests. The Wilcoxon matched-pairs signed rank test was used to compare experimental with random NND distributions. Data were considered significant when $p < 0.05$. All statistical analyses were performed using the Prism 9 software (GraphPad, La Jolla, CA, United States).

RESULTS

We stereotactically injected eight-week-old male mice ($n = 15$) with AAV-ChR2-YFP into the PIN/MGm (**Figures 1A–D**) and then randomly subdivided them into three groups ($n = 5$ each). Three weeks after the injection, one group was fear conditioned by subjecting the mice to five pairings of a neutral auditory CS co-terminating with a footshock (US), whereas a second group was exposed only to the CS in the conditioning chamber (**Figure 2A**). Animals in the third group (naïve) were always maintained in their home cage and did not undergo any behavioral manipulation (besides regular handling). Fear conditioned mice (FM group), but not the control group (CS-only), showed a progressive increase (2-way ANOVA, $p < 0.001$) in freezing (**Figure 2B**), demonstrating successful acquisition of a conditioned fear response. Subsequent to the behavioral testing, mice were returned to their home cages. Twenty-four hours later, they were re-exposed to four CS in a different context. Fear memory retrieval was clearly observed in previously fear conditioned mice, whereas mice in the CS-only group showed baseline freezing (**Figure 2B**). Thirty min after the end of the fear memory retrieval protocol, mice were perfused with fixative and brains processed for FRIL.

Analysis of ChR2-YFP-transduced neurons revealed labeled somata in the MGm and PIN, including the posterior thalamic nuclear group (PoT), posterior intralaminar nucleus (PIL), and peripeduncular nucleus (PP). ChR2-YFP-positive thalamic projections showed dense innervation of the LA, the amygdalostriatal transition area (AStr) and the mpITC cluster (**Figures 3A,B**), a pattern fully consistent with previous tracing studies (Turner and Herkenham, 1991; Linke et al., 2000; Asede et al., 2015; Bienvenu et al., 2015). At the electron microscope, intense gold immunolabeling for ChR2-YFP was observed on the P-face of thalamic axons (**Figures 3C,D**). AMPA receptors were detected using an antibody that recognizes all four subunits (GluA1-4). Spines and dendrites of ITC neurons were identified by their labeling for μ-opioid receptors on the corresponding replica P-face (**Figure 3D**), as these neurons express high-levels of these receptors (Likhtik et al., 2008; Busti et al., 2011; Blaesse et al., 2015; Schönherr et al., 2016). Synapses made by ChR2-YFP labeled axon terminals were sampled from replicas obtained from four animals per group (naïve = 123, CS-only = 188, FM = 200 synapses). However, for only about 58% of them (naïve = 98, CS-only = 109, FM = 88) the other halve of the plasma membrane could be identified in the corresponding replica labeled for μ-opioid receptors. This

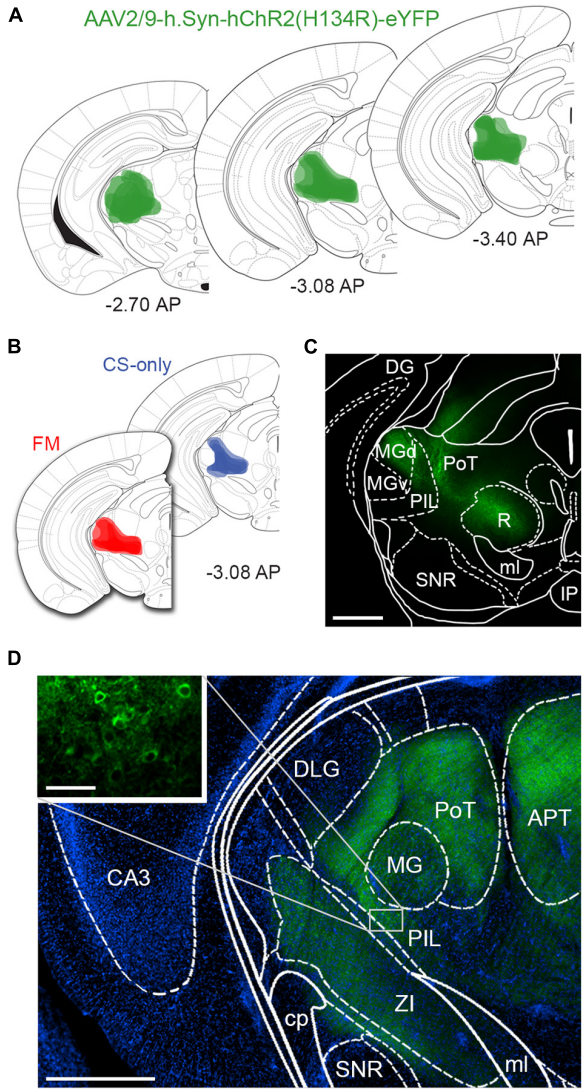

FIGURE 1 | Intrathalamic injection sites of AAV-ChR2-YFP. **(A)** Schematic drawing of AAV-ChR2-YFP injection sites, where labeled neuronal cell bodies could be identified, at different rostro-caudal levels confirming that the microinjections were correctly placed into the PIN/MGm. Color intensity reflects the frequency of overlapping injection sites ($n = 5$ animals/group). Bregma levels are indicated in panels **(A,B)**. **(B)** Schematic drawings of AAV-ChR2-YFP injection sites in CS-only (blue) and fear conditioned mice (red). The two groups were largely similar in terms of injection sites, excluding a bias due to location differences in the microinjections. **(C)** Micrograph taken from a 140 μm thick coronal section of the midbrain showing ChR2-YFP endogenous fluorescence, overlaid with the brain atlas. Scale bar: 500 μm. **(D)** Immunodetection of ChR2-YFP transduced neurons and fibers (green); DAPI staining (blue) was used to reveal the macrostructure of the brain slice overlaid with the brain atlas. The inset shows somata of neurons in the PIL transduced with ChR2-YFP. The fluorescence signal in several brain areas close to the injection site, such as the APT and R, results from axonal fibers. Scale bar: 500 μm; inset: 50 μm. APT, anterior pretectal nucleus; CA3, field CA3 of hippocampus; cp, cerebral peduncle; DG, dentate gyrus; DLG, dorsal lateral geniculate nucleus; IP, interpeduncular nucleus; MG, medial geniculate nucleus; MGd, medial geniculate nucleus dorsal part; MGv, medial geniculate nucleus ventral part; ml, medial lemniscus; PAG, periaqueductal gray; PIL, posterior intralaminar thalamic nucleus; PoT, posterior thalamic nuclear group; R, red nucleus; SNR, Substantia Nigra pars reticulata; ZI, zona incerta.

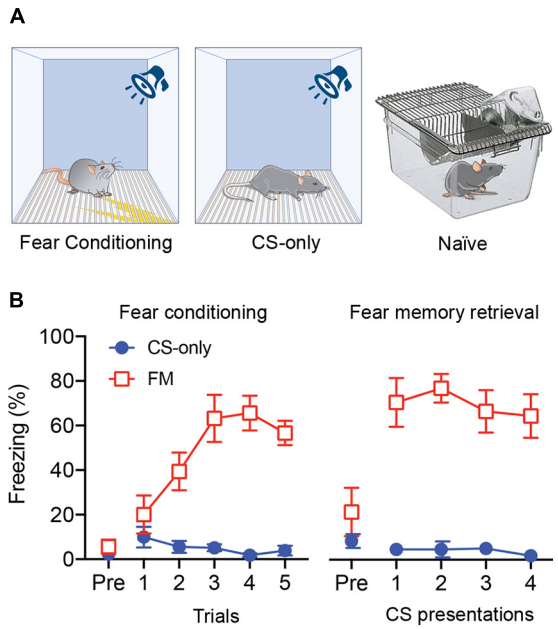

FIGURE 2 | Auditory fear conditioning and fear memory retrieval. **(A)** Schematic diagram of the experimental groups. **(B)** Left: Average freezing responses of mice exposed to fear conditioning (FM) or only to the CS (CS-only) ($n = 5$ in each group) for each of the five CS-US pairing trials. Fear conditioned mice (FM) showed a progressive increase in freezing (2-way ANOVA, $p < 0.0001$) that was significantly higher compared to CS-only animals ($p < 0.001$). Right: When re-exposed, 24 h later, to the same CS for four times in a different context, fear conditioned mice (FM) showed higher freezing level compared to the pre-CS (Pre) period ($p < 0.0001$) and compared to CS-only mice ($p < 0.001$).

was mostly due to the fact that the region was placed over a mesh grid. The density of AMPA receptors was analyzed in both fully and partially exposed synapses (**Figures 4A–I**) by an experimenter blind to the behavioral treatment and limited to the confirmed ITC synapses. Data were pooled as they did not differ amongst animals within each group [One-way ANOVA; naïve: $F(3,94) = 1.23$, $p = 0.30$; CS-only: $F(3,105) = 0.80$, $p = 0.49$; FM: $F(3,84) = 1.21$, $p = 0.31$]. Upon fear memory retrieval, conditioned mice (FM group) showed a significant reduction in AMPA receptor density (529 ± 23.8 gold particles/μm^2) when compared to both CS-only [743 ± 22.9 gold particles/μm^2; One-way ANOVA, $F(2, 292) = 22.00$, $p < 0.001$, Bonferroni's multiple comparisons test, $p < 0.0001$] and naïve (622 ± 21.8 gold particles/μm^2; Bonferroni's multiple comparisons test, $p = 0.02$) animals (**Figure 5A**). Thalamic to mpITC synapses in CS-only animals showed a higher AMPA receptor density than naïve mice (Bonferroni's multiple comparisons test, $p = 0.0005$). Cumulative frequency distributions consistently revealed a significant shift to the left of the synaptic AMPA receptor density in FM vs. CS-only (Kolmogorov–Smirnov test, $p < 0.0001$) and naïve (Kolmogorov–Smirnov test, $p = 0.004$) animals, and a significant shift to the right (Kolmogorov–Smirnov test, $p = 0.003$) in synapses from the CS-only vs. naïve animals (**Figure 5B**). Given that AMPA receptors can shuttle between extrasynaptic and synaptic sites, we wanted to address if density changes were limited to PSDs, or also occurred in the proximity of synapses. By analyzing the AMPA receptor density in the extrasynaptic area proximal to the investigated synapses (up to ∼1 μm from the synapse outer border), we found that density differed significantly among groups [One-way ANOVA, $F(2, 227) = 14.28$, $p < 0.0001$]. The density of AMPA receptors was higher in the CS-only group (22.2 ± 2.06; Bonferroni's multiple comparisons test, CS-only vs. both naïve and FM $p < 0.0001$), but similar in naïve (11.7 ± 1.21) and FM (11.3 ± 1.32) mice (Bonferroni's multiple comparisons test, naïve vs. FM: $p = 0.99$; **Figure 5C**). A similar overall extrasynaptic area was analyzed for each group (Naïve: 43.56 μm^2; CS-only: 31.13 μm^2; FM: 33.59 μm^2). Of note, the density of AMPA receptors in thalamo-mpITC synapses was approximately 60 times higher than in the adjacent extrasynaptic area (**Figures 5A,C**).

Analysis of the correlation between the number of gold immunoparticles for AMPA receptors and the sampled area of individual synapses was found to be positively correlated in all three groups (**Figure 6A**), consistent with previous studies (Tanaka et al., 2005; Tarusawa et al., 2009; Fukazawa and Shigemoto, 2012; Xie et al., 2019). When the correlation coefficients were compared, after transforming the r values into z scores, no significant differences were found between the CS-only and the naïve (z test statistic: 1.38, $p = 0.084$) or FM (z test statistic: 0.538, $p = 0.295$) groups. On the other hand, the comparison of the correlations between FM and naïve animals significantly differed from each other (z test statistic: 1.829, $p = 0.034$). These data further support plasticity in the synaptic AMPA receptor content associated with fear memory retrieval. Next, we analyzed the intrasynaptic spatial arrangement of AMPA receptors using the open source software GoldExt (Szoboszlay et al., 2017). We measured the mean NND for each synapse and examined whether the population distribution differed from random arrangements. Since there was no difference in the calculated NND between fully and partially exposed synapses (Mann–Whitney test, naïve: synapses on dendrites $p = 0.20$, synapses on spines: $p = 0.89$; CS-only: synapses on dendrites $p = 0.17$, synapses on spines: $p = 0.65$; FM: synapses on dendrites $p = 0.86$, synapses on spines: $p = 0.58$), data were pooled. The distribution across the NND populations obtained from naïve, CS-only and FM mice significantly differed from random distributions (Wilcoxon matched-pairs signed rank test, $p < 0.001$ for all three groups; **Figure 6B**). Furthermore, the mean NND was similar [One-way ANOVA, $F(2, 236) = 2.39$, $p = 0.09$] among the three experimental groups (naïve: 0.024 ± 0.001, CS-only: 0.023 ± 0.001; FM: 0.026 ± 0.001 μm; **Figure 6C**). These findings suggest that synaptic AMPA receptors do not change their homogeneous, though clustered, intrasynaptic nano-arrangement as a consequence of sensory stimulation and/or fear memory retrieval.

Finally, as we found that thalamic afferents provide inputs onto both dendritic shafts (**Figures 4A,D,G**) and spines (**Figures 4B,E,H**), we wanted to understand if experience-induced changes (**Figure 5A**) could be more prominent, or differentially observed in one of these two synapse types. Therefore, we analyzed whether spine and shaft synapses differed

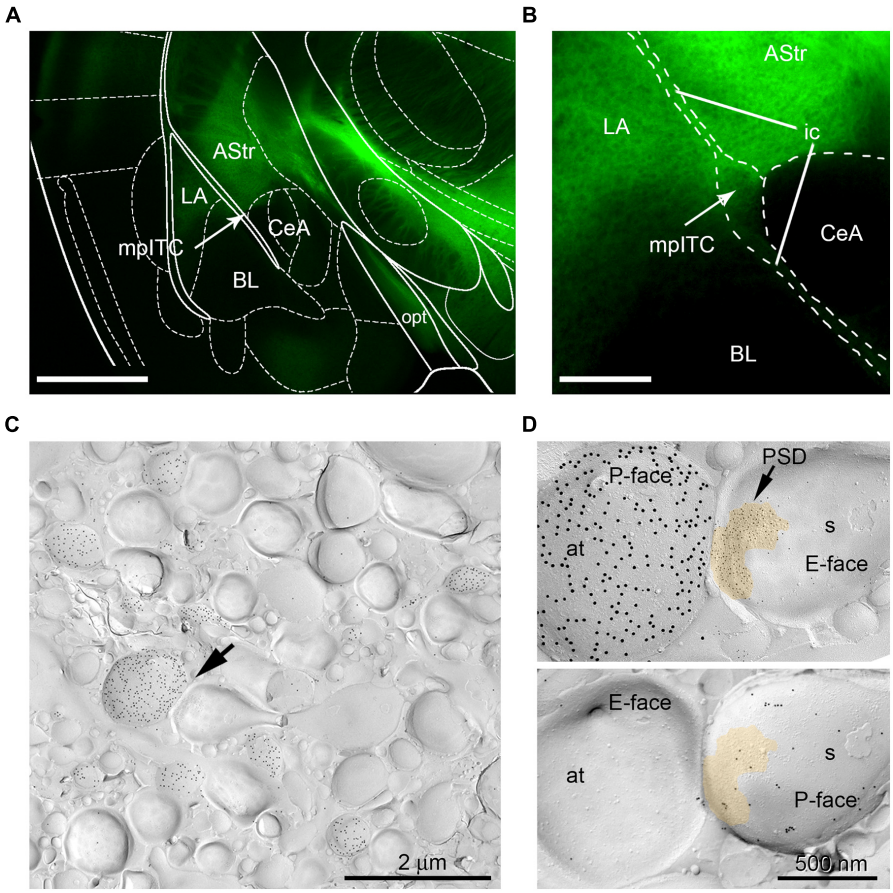

FIGURE 3 | mpITC innervation by thalamic afferents from the PIN/MGm. **(A)** Fluorescence image of PIN/MGm efferent projections (green) innervating the amygdala. The LA, mpITC (indicated by the arrow) and AStr receive strong ChR2-YFP labeled inputs. Little to no fibers were observed in the BL and lateral CeA. Scale bar: 1 mm. **(B)** Higher magnification image of the PIN/MGm innervation of the mpITC. Scale bar: 250 µm. **(C)** Electron-micrograph of a mpITC replica from a CS-only animal. Labeling for ChR2-YFP (15 nm gold particles) on the P-face of axons originating from the PIN/MGm. Note the relatively high density of labeled axons. An axon terminal, indicated by the arrow, forms an asymmetric synapse with a spine. **(D)** Top: Higher magnification of the synapse marked (arrow) in panel **(C)**. The postsynaptic membrane specialization on the E-face shows a characteristic cluster of IMPs labeled with 5 nm gold particles revealing AMPA receptors. A pseudocolor is used to outline the postsynaptic specialization. The P-face of the axon terminal expresses a high density of ChR2-YFP (15 nm gold particles). Bottom: Corresponding P-face of the same spine labeled for µ-opioid receptors (10 nm gold particles). at, axon terminal; AStr, amygdalostriatal transition area; BL, basolateral nucleus of the amygdala; CeA, central nucleus of the amygdala; ic, internal capsule; LA, lateral nucleus of the amygdala; mpITC, dorsal medioparacapsular intercalated cluster; opt, optic tract; s, spine.

in AMPA receptor density. In all three behavioral groups synapses on spines had a higher density of AMPA receptors [naïve: 673 ± 31.7 (n = 44); CS-only: 810 ± 25.0 (n = 70); FM: 566 ± 29.1 (n = 58) gold particles/µm^2] compared to those on dendrites [naïve: 579 ± 29.1 (n = 54); CS-only: 622 ± 39.4 (n = 39); FM: 458 ± 38.1 (n = 30) gold particles/µm^2], although only in CS-only and FM mice it reached statistical significance (Mann–Whitney test 2 tailed; naïve: p = 0.082; CS-only: p < 0.0001; FM: p = 0.046). For spine synapses, the FM group showed a marked reduction in AMPA receptor density [One-way ANOVA, $F(2, 169)$ = 21.08, p < 0.0001] when compared to both CS-only (Bonferroni's multiple comparisons test, p < 0.0001) and naïve (p = 0.038) animals (**Figure 6D**). In contrast, synapses on dendrites in FM mice showed a lower density of AMPA receptors [One-way ANOVA, $F(2, 120)$ = 4.75, p < 0.010] only when compared to the CS-only (Bonferroni's multiple comparisons test, synapses on spines: p = 0.001] but not the naïve (p = 0.058) group (**Figure 6E**). Remarkably, AMPA receptor density increased in synapses made by thalamic inputs in CS-only compared to naïve mice only for spine (Bonferroni's multiple comparisons test, p = 0.003) but not for shaft synapses (Bonferroni's multiple comparisons test p = 0.99). Taken together these data suggest that experience-dependent changes in AMPA receptor density in FM and CS-only groups are more prominently observed in dendritic spine than shaft synapses onto mpITCs.

DISCUSSION

We show here that following auditory fear conditioning in mice, the formation and retrieval of fear memory is linked to a significant reduction in the density of AMPA receptors

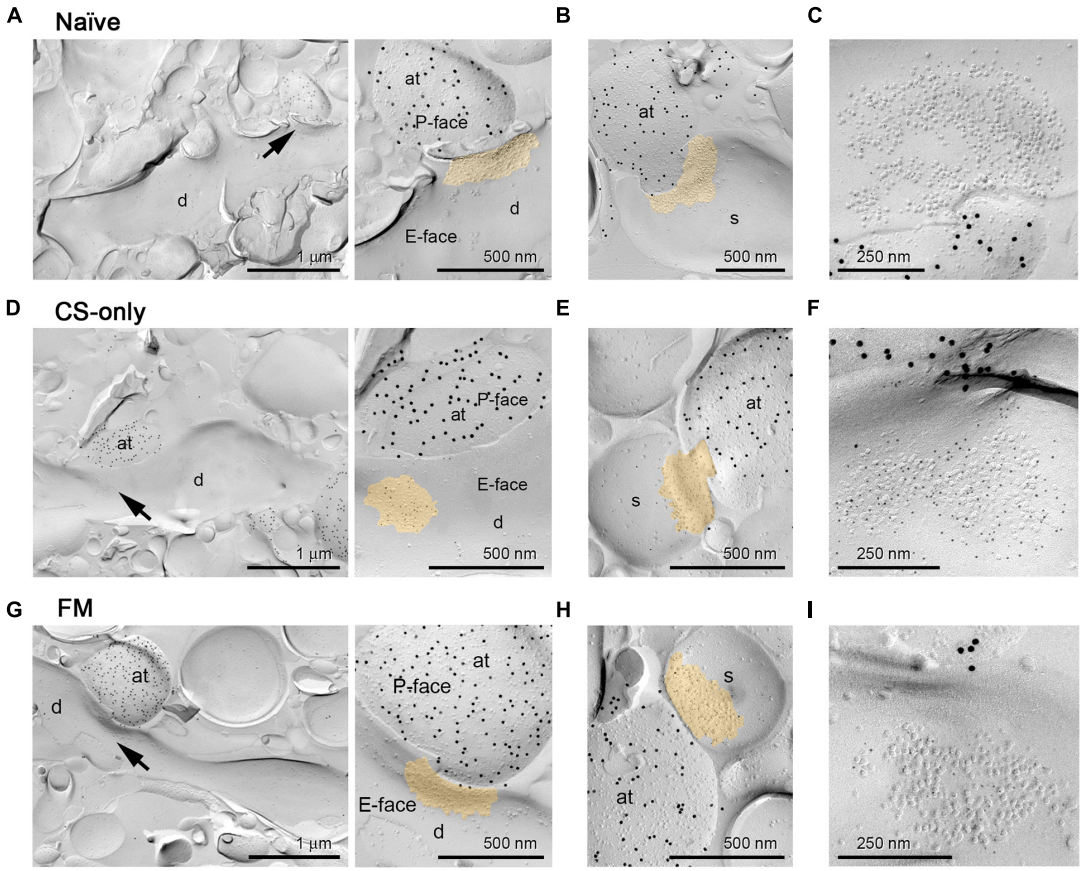

FIGURE 4 | AMPA receptor immunogold labeling at PIN/MGm to mpITC synapses. Representative electron micrographs of PIN/MGm-mpITC shaft and spine synapses in all behavioral groups. **(A–C)** Naïve animals. **(A)** A ChR2-YFP expressing axon terminal (labeled with 15 nm gold particles on the P-face) forms a synaptic contact (arrow) with a spiny mpITC dendrite. An enlarged view of the pre- and post-synaptic membranes is shown on the right. **(B)** A ChR2-YFP expressing axon terminal (labeled with 15 nm gold particles) forms a synaptic contact with a dendritic spine of a mpITC neuron. **(C)** High magnification micrograph of an IMP cluster (postsynaptic specialization) on the E-face labeled for pan-AMPA receptors (5 nm gold particles). **(D–F)** CS-only animals. **(D)** A ChR2-YFP expressing axon terminal (labeled with 15 nm gold particles) forms a synaptic contact (arrow) with a spiny mpITC dendrite. An enlarged view of the pre- and post-synaptic membranes is shown on the right. **(E)** A ChR2-YFP expressing axon terminal (labeled with 15 nm gold particles) forms a synaptic contact with a dendritic spine of a mpITC neuron. **(F)** High magnification micrograph of an IMP cluster labeled for pan-AMPA receptors (5 nm gold particles). **(G–I)** FM animals. **(G)** A ChR2-YFP expressing axon terminal (labeled with 15 nm gold particles) forms a synaptic contact (arrow) with a spiny mpITC dendrite. An enlarged view of the pre- and post-synaptic membranes is shown on the right. **(H)** A ChR2-YFP expressing axon terminal (labeled with 15 nm gold particles) forms a synaptic contact with a dendritic spine of a mpITC neuron. **(I)** High magnification micrograph of an IMP cluster labeled for pan-AMPA receptors (5 nm gold particles). A pseudocolor is used to outline the postsynaptic specialization in A, B, D, E, G and H. Abbreviations: at, axon terminal; d, dendrite, s, dendritic spine.

in synapses made by PIN/MGm inputs onto identified mpITC neurons. Our findings suggest that the decrease in A/N ratio observed at the same synapses upon fear memory retrieval (Asede et al., 2015) results from an altered trafficking of AMPA receptors, and in particular their removal from the PSD of spine synapses. While many mechanisms can influence the A/N ratio, the addition and removal of AMPA receptors from synapses is one of the fundamental processes controlling synaptic efficacy during experience-dependent plasticity (Choquet and Triller, 2013; Huganir and Nicoll, 2013; Henley and Wilkinson, 2016; Choquet, 2018; Diering and Huganir, 2018). In addition, we have previously reported that fear memory retrieval is associated with an increase in paired pulse ratio (PPR) of the AMPA-EPSC at PIN/MGm-mpITC synapses (Asede et al., 2015). Despite changes in PPR have been typically viewed as a hallmark of presynaptic modulation of transmitter release, it has been suggested that postsynaptic AMPA receptor mobility could also influence PPR (Frischknecht et al., 2009; Choquet, 2018).

In the last decade, the development of the FRIL technique has considerably improved the ability to analyses the intrasynaptic distribution of signaling molecules (Masugi-Tokita and Shigemoto, 2007). One of the greatest advantages of this approach relies on its high detection sensitivity, for instance in comparison with the post-embedding immunogold technique. Indeed, a tight correlation between the number of immunogold particles detecting synaptic AMPA receptors and functional channels was observed in immature rat cerebellar Purkinje cell synapses (Tanaka et al., 2005). Although in our study we did not attempt to quantify the number of functionally active AMPA channels at PIN/MGm to mpITC synapses, we assume that it

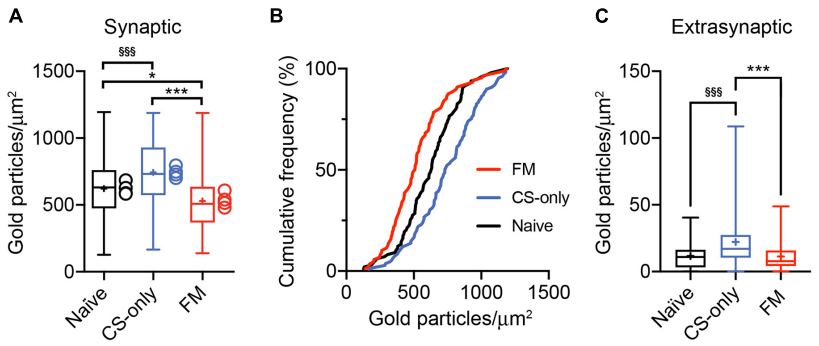

FIGURE 5 | Reduction in AMPA receptor density at PIN/MGm to mpITC synapses upon fear memory retrieval. **(A)** Synapses from FM mice show a significant decrease in synaptic AMPA receptor density when compared to both CS-only ($p < 0.0001$, One-way ANOVA followed by the Bonferroni's multiple comparison test) and naïve ($p = 0.02$) animals. Synapses (Naïve $n = 98$, CS-only $n = 109$, FM $n = 88$) were collected from 4 mice/group. CS-only animals showed a higher AMPA receptor density compared to naïve mice ($p = 0.0005$, Bonferroni's multiple comparison test). Boxplots show the median (line inside the box), mean (+), 25th–75th percentiles (box edges) and minimum and maximum values (whiskers). The mean values for each mouse are shown as circles beside the box plots. **(B)** Significant left shift of the cumulative frequency distribution of synaptic AMPA receptor density in FM compared to the CS-only ($p < 0.0001$, Kolmogorov–Smirnov test) and naïve ($p = 0.004$) group. The cumulative frequency distribution of the AMPA receptor density is also significantly shifted to the right ($p = 0.003$) in CS-only compared to naïve synapses. **(C)** The density of extrasynaptic AMPA receptors is significantly higher in CS-only ($p < 0.0001$, One-way ANOVA followed by the Bonferroni's multiple comparison test) compared to both naïve and FM animals. Boxplots show the median (line inside the box), mean (+), 25th–75th percentiles (box edges) and minimum and maximum values (whiskers). **(A,C)** Significantly higher than FM $^{*}p < 0.05$, $^{***}p < 0.001$; Significantly higher than Naïve §§§ $p < 0.001$.

is highly correlated with the number of detected gold particles. AMPA receptor labeling at these synapses showed a tight positive correlation with the sampled synaptic area corroborating the view that this is a common feature of many excitatory synaptic connections in the central nervous system (Fukazawa and Shigemoto, 2012). The selective identification of PIN/MGm axon terminals in replicas was enabled by a novel approach that takes advantage of the anterograde transport of tagged opsins, such as ChR2-YFP, and their detection at defined presynaptic sites, since they are integral membrane proteins (Schönherr et al., 2016).

So far, two types of AMPA receptor intrasynaptic distributions have been described (reviewed in Fukazawa and Shigemoto, 2012): (1) a highly variable mosaic-type distribution, such as in corticogeniculate (Tarusawa et al., 2009) and CA3-CA1 synapses (Matsubara et al., 1996; Nusser et al., 1998), and (2) a homogeneous distribution with high density, such as in reticulogeniculate synapses (Tarusawa et al., 2009). The synapses made by PIN/MGm inputs onto mpITC neurons showed, despite a fairly wide density range (from 127 to 1,195 particles/μm^2), a dense and relatively uniform pattern of distribution of AMPA receptors. However, the mean NND was significantly shorter than expected from random arrangements. PIN/MGm to mpITC synapses, therefore, appear to possess most of the features typical of the second type. This homogeneous AMPA receptor distribution might serve to ensure high transmission fidelity, as observed for several GABAergic interneurons. For example, synapses made with interneurons distributed throughout multiple layers of the hippocampus have a higher and less variable density of AMPA receptors compared to synapses made with spines of pyramidal neurons (Nusser et al., 1998). Likewise, a very dense and homogeneous AMPA receptor labeling was described for synapses made by parallel fibers with interneurons of the cerebellar cortex, unlike those made with Purkinje cell spines (Masugi-Tokita et al., 2007). Interestingly, it has been suggested that synaptic connections with high and homogeneous intrasynaptic distribution of AMPA receptors have different plastic properties than mosaic-type synapses, e.g., they could undergo more pronounced structural modifications of the postsynaptic density (Fukazawa and Shigemoto, 2012). Therefore, our observed reduction in AMPA receptor density linked to fear memory retrieval may also result, at least in part, from a synaptic enlargement. Because the full exposure of the postsynaptic specialization was relatively rare under our experimental conditions, fear-mediated changes in the synaptic area could not be analyzed. Future studies will have to address whether mpITC synapses made by PIN/MGm inputs undergo structural plasticity.

AMPA receptors are homo- and/or hetero-tetramers made from four subunits (GluA1-4). Synaptic AMPA receptors are predominantly combinations of GluA1 and GluA2 (Lu et al., 2009). Memory consolidation in the BLA is commonly associated with increased GluA1 and GluA2 subunit expression (Yeh et al., 2006; Ferrara et al., 2017). However, at thalamo-amygdala synapses alterations in GluA3 subunit expression have been reported (Radley et al., 2007). To circumvent confounds caused by different subunit compositions, we used a pan-AMPA antibody recognizing all four subunits. Hence, our data allow conclusions only about global changes of synaptic AMPA receptor density, but not specific alterations in subunit composition.

Our work revealed that synapses made by PIN/MGm inputs onto mpITC neurons have a significantly higher density of AMPA receptors when they are made with dendritic spines than shafts. This finding is consistent with a previous study showing that latero-capsular division neurons in the CeA have higher AMPA receptor density in spine compared to shaft synapses (Dong et al., 2010). Spine synapses are the most common type of excitatory

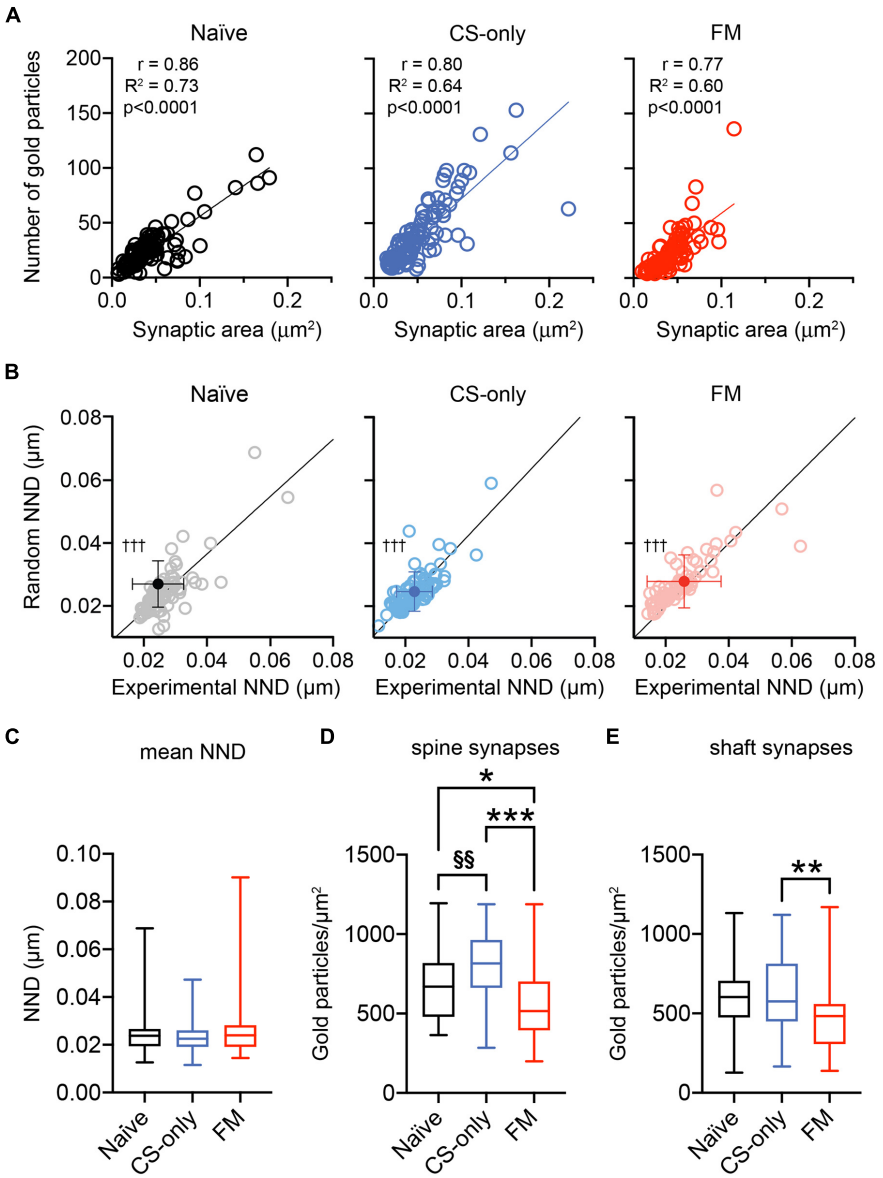

FIGURE 6 | Nano-scale distribution of AMPA receptors and density at dendritic spine and shaft PIN/MGm-mpITC synapses. **(A)** PIN/MGm-mpITC synapses in all three experimental groups (FM, CS-only, and Naïve) show a highly significant positive correlation (Pearson's correlation) between the number of gold particles detecting AMPA receptors and the synaptic area. The regression line is shown as a solid line passing through the origin. **(B)** Comparison of the experimentally determined mean nearest neighbor distance (NND) of intrasynaptic gold particles with random distributions ($n = 50$ for each PSD) reveals a significant difference from random distributions in all experimental groups ($^{†††}p < 0.001$). **(C)** Boxplot summary of the NND obtained experimentally from PSDs of naïve ($n = 80$), CS-only ($n = 89$) and FM ($n = 70$) mice ($n = 4$ mice/group). Boxplots show the median (line inside the box), 25th–75th percentiles (box edges) and minimum and maximum values (whiskers). **(D–E)** Fear memory retrieval causes a marked decrease in AMPA receptor density in dendritic spine synapses when compared to both CS-only ($p < 0.0001$, One-way ANOVA followed by the Bonferroni's multiple comparison test) and naïve ($p = 0.038$) animals. In FM mice, synapses made by PIN/MGm inputs onto dendrites had a lower density of AMPA receptors only in comparison to the CS-only (Bonferroni's multiple comparisons test, $p = 0.001$) but not the naïve ($p = 0.058$) group. CS-only animals showed a higher AMPA receptor density than naïve mice, but only in spine (Bonferroni's multiple comparisons test, $p = 0.003$) synapses. Synapses were collected from 4 animals/group. Boxplots show the median (line inside the box), 25th–75th percentiles (box edges) and minimum and maximum values (whiskers). Significantly higher than FM $^{*}p < 0.05$, $^{**}p < 0.01$, $^{***}p < 0.001$; Significantly higher than Naïve $^{§§}p < 0.01$.

synapses in both cortical and striatal-like structures and a large body of evidence demonstrated that they undergo structural and functional changes associated with synaptic plasticity (Sala and Segal, 2014; Segal, 2017). Conversely, little is known about shaft synapses. Dong et al. (2010) suggested that the difference in AMPA receptor density between spine and shaft synapses in the CeA was most likely related to different presynaptic inputs. This may be unlikely for mpITC neurons. Indeed, several studies reported that axons arising from the PIN/MGm form

synapses with both spines and dendrites in the LA (Radley et al., 2007; Smith et al., 2019). We cannot, however, exclude that different neuronal populations within the PIN/MGm give rise to inputs preferentially targeting dendritic spines vs. shafts of mpITC neurons. Spine and shaft synapses may also vary in their molecular composition, which in turn could affect their plasticity and ability to cluster AMPA receptors (Mi et al., 2002; Bissen et al., 2019). Notably, we report that the decrease in AMPA receptor density following fear memory retrieval was more prominently observed at spine synapses. This new finding is consistent with the notion of a considerable ability of spine synapses to undergo plasticity. Alternatively, it could also be hypothesized that changes at spine synapses last longer than at shaft synapses, perhaps due to their tortuous geometry that slows down receptor diffusion, and consequently, the recovery from internalization (Ashby et al., 2006; Newpher and Ehlers, 2008). Surprisingly, we also observed a significant increase in the density of AMPA receptors in spine, but not shaft, synapses upon sensory stimulation in CS-only animals in comparison to naïve mice. This was paralleled also by an increased density in the extrasynaptic area. Indeed, mpITC neurons respond to a variety of auditory stimuli (Collins and Paré, 1999), which could lead to sensory-driven synaptic strengthening by recruitment of synaptic AMPA receptors. Previous studies have shown that exocytosis of intracellular vesicles harboring AMPA receptors occurs near the postsynaptic membrane (Ehlers, 2013; Wu et al., 2017). Therefore, a recruitment of synaptic AMPA receptors is consistent with a concurrent increase of these receptors in extrasynaptic areas neighboring postsynaptic specializations.

A remarkable feature of synapses made by PIN-MGm inputs is their divergent forms of plasticity depending on the postsynaptic targets, e.g., LA and mpITC neurons (Clem and Huganir, 2010; Asede et al., 2015). Although we do not know whether LA and mpITC neurons are contacted by axons of the same PIN-MGm neurons or independently by distinct neuronal populations, the first postulation appears to be the most parsimonious one. A factor that may influence this postsynaptic cell-dependent form of plasticity is the very different firing rate of these two classes of target neurons. While LA pyramidal neurons have a very low spontaneous firing rate (Paré and Gaudreau, 1996), ITC cells fire at higher rates in all behavioral states. The high spontaneous firing rates of mpITCs suggest that they provide a tonic inhibition onto their downstream targets, such as the vmITC, to promote fear expression (Collins and Paré, 1999; Royer et al., 2000; Busti et al., 2011). An additional intriguing feature of mpITC neurons is the long-term inverse heterosynaptic modification reported to occur after a particular input has undergone activity-dependent enhancement, which may be needed to the stabilization of total synaptic weights (Royer and Paré, 2003). A decrease in sensory input strength may, in turn, help to facilitate plasticity at inputs from activated LA neurons onto mpITC cells (Huang et al., 2014) and consequently fear learning. Therefore, an opposing plasticity at mpITC and LA synapses could serve to coordinate state-dependent changes of activity in these parallel fear circuits.

In conclusion, our study is one of the few that have attempted to link the regulation of AMPA receptor trafficking to memory processes in identified neuronal networks. In particular, we show that fear-memory induced reduction in A/N ratio at thalamic-mpITC synapses is associated with a reduced postsynaptic AMPA receptor density. However, we still do not know precisely how this is mediated, or how stable these synaptic changes are. Future investigations are needed to unravel other potential contributions to the fear-mediated plasticity of mpITC synapses, such as changes in AMPA receptor subunit configuration and/or NMDA receptor expression.

DATA AVAILABILITY STATEMENT

The raw data supporting the conclusions of this article will be made available by the authors, without undue reservation.

ETHICS STATEMENT

The animal study was reviewed and approved by the Austrian Animal Experimentation Ethics Board.

AUTHOR CONTRIBUTIONS

AS, IE, CS, and FF conceived and designed the project. AS, SS, HH, CS, and FF were involved with experimental and analytical aspects of the manuscript. AS, CS, and FF wrote the manuscript. All authors commented on the manuscript.

FUNDING

We would like to acknowledge financial support from the Austrian Science Fund (FWF) grant I-2215 to FF and from the German Research Foundation (DFG) EH 197/3-1 to IE.

ACKNOWLEDGMENTS

The authors would like to thank Y. Kasugai for helping with the trimming and freezing of FRIL samples.

REFERENCES

Amano, T., Unal, C. T., and Paré, D. (2010). Synaptic correlates of fear extinction in the amygdala. *Nat. Neurosci.* 13, 489–494. doi: 10.1038/nn.2499

Asede, D., Bosch, D., Lüthi, A., Ferraguti, F., and Ehrlich, I. (2015). Sensory inputs to intercalated cells provide fear-learning modulated inhibition to the basolateral amygdala. *Neuron* 86, 541–554. doi: 10.1016/j.neuron.2015.03.008

Ashby, M. C., Maier, S. R., Nishimune, A., and Henley, J. M. (2006). Lateral diffusion drives constitutive exchange of AMPA receptors at dendritic spines and is regulated by spine morphology. *J. Neurosci.* 26, 7046–7055. doi: 10.1523/JNEUROSCI.1235-06.2006

Barsy, B., Kocsis, K., Magyar, A., Babiczky, A., Szabo, M., Veres, J. M., et al. (2020). Associative and plastic thalamic signaling to the lateral amygdala controls fear behavior. *Nat. Neurosci.* 23, 625–637. doi: 10.1038/s41593-020-0620-z

Bienvenu, T. C., Busti, D., Micklem, B. R., Mansouri, M., Magill, P. J., Ferraguti, F., et al. (2015). Large intercalated neurons of amygdala relay noxious sensory information. *J. Neurosci.* 35, 2044–2057. doi: 10.1523/JNEUROSCI.1323-14.2015

Bissen, D., Foss, F., and Acker-Palmer, A. (2019). AMPA receptors and their minions: auxiliary proteins in AMPA receptor trafficking. *Cell. Mol. Life Sci.* 76, 2133–2169. doi: 10.1007/s00018-019-03068-7

Blaesse, P., Goedecke, L., Bazelot, M., Capogna, M., Pape, H. C., and Jüngling, K. (2015). μ-opioid receptor-mediated inhibition of intercalated neurons and effect on synaptic transmission to the central amygdala. *J. Neurosci.* 35, 7317–7325. doi: 10.1523/JNEUROSCI.0204-15.2015

Bosch, D., Asede, D., and Ehrlich, I. (2016). Ex Vivo Optogenetic Dissection of Fear Circuits in Brain Slices. *J. Vis. Exp.* 2016:e53628. doi: 10.3791/53628

Busti, D., Geracitano, R., Whittle, N., Dalezios, Y., Mañko, M., Kaufmann, W., et al. (2011). Different fear states engage distinct networks within the intercalated cell clusters of the amygdala. *J. Neurosci.* 31, 5131–5144. doi: 10.1523/JNEUROSCI.6100-10.2011

Choquet, D. (2018). Linking nanoscale dynamics of AMPA receptor organization to plasticity of excitatory synapses and learning. *J. Neurosci.* 38, 9318–9329. doi: 10.1523/JNEUROSCI.2119-18.2018

Choquet, D., and Triller, A. (2013). The dynamic synapse. *Neuron* 80, 691–703. doi: 10.1016/j.neuron.2013.10.013

Ciocchi, S., Herry, C., Grenier, F., Wolff, S. B., Letzkus, J. J., Vlachos, I., et al. (2010). Encoding of conditioned fear in central amygdala inhibitory circuits. *Nature* 468, 277–282. doi: 10.1038/nature09559

Clem, R. L., and Huganir, R. L. (2010). Calcium-permeable AMPA receptor dynamics mediate fear memory erasure. *Science* 330, 1108–1112. doi: 10.1126/science.1195298

Collins, D. R., and Paré, D. (1999). Spontaneous and evoked activity of intercalated amygdala neurons. *Eur. J Neurosci.* 11, 3441–3448. doi: 10.1046/j.1460-9568.1999.00763.x

Diering, G. H., and Huganir, R. L. (2018). The AMPA Receptor Code of Synaptic Plasticity. *Neuron* 100, 314–329. doi: 10.1016/j.neuron.2018.10.018

Dong, Y.-L., Fukazawa, Y., Wang, W., Kamasawa, N., and Shigemoto, R. (2010). Differential postsynaptic compartments in the laterocapsular division of the central nucleus of amygdala for afferents from the parabrachial nucleus and the basolateral nucleus in the rat. *J. Comp. Neurol.* 518, 4771–4791. doi: 10.1002/cne.22487

Duvarci, S., and Paré, D. (2014). Amygdala microcircuits controlling learned fear. *Neuron* 82, 966–980. doi: 10.1016/j.neuron.2014.04.042

Ehlers, M. D. (2013). Dendritic trafficking for neuronal growth and plasticity. *Biochem. Soc. Trans.* 41, 1365–1382. doi: 10.1042/bst20130081

Ferrara, N. C., Cullen, P. K., Pullins, S. P., Rotondo, E. K., and Helmstetter, F. J. (2017). Input from the medial geniculate nucleus modulates amygdala encoding of fear memory discrimination. *Learn. Mem.* 24, 414–421. doi: 10.1101/lm.044131.116

Frischknecht, R., Heine, M., Perrais, D., Seidenbecher, C. I., Choquet, D., and Gundelfinger, E. D. (2009). The brain extracellular matrix limits lateral diffusion of AMPA receptors and modulates short-term synaptic plasticity. *Nat. Neurosci.* 12, 897–904. doi: 10.1038/nn.2338

Fujimoto, K. (1995). Freeze-fracture replica electron microscopy combined with SDS digestion for cytochemical labeling of integral membrane proteins. Application to the immunogold labeling of intercellular junctional complexes. *J. Cell. Sci.* 108, 3443–3449. doi: 10.1242/jcs.108.11.3443

Fukazawa, Y., and Shigemoto, R. (2012). Intra-synapse-type and inter-synapse-type relationships between synaptic size and AMPAR expression. *Curr. Opin. Neurobiol.* 22, 446–452. doi: 10.1016/j.conb.2012.01.006

Hagihara, K. M., Bukalo, O., Zeller, M., Aksoy-Aksel, A., Karalis, N., Limoges, A., et al. (2021). Intercalated amygdala clusters orchestrate a switch in fear state. *Nature* 594, 403–407. doi: 10.1038/s41586-021-03593-1 Online ahead of print,

Haubensak, W., Kunwar, P. S., Cai, H., Ciocchi, S., Wall, N. R., Ponnusamy, R., et al. (2010). Genetic dissection of an amygdala microcircuit that gates conditioned fear. *Nature* 468, 270–276. doi: 10.1038/nature09553

Henley, J. M., and Wilkinson, K. A. (2016). Synaptic AMPA receptor composition in development, plasticity and disease. *Nat. Rev. Neurosci.* 17, 337–350. doi: 10.1038/nrn.2016.37

Herry, C., and Johansen, J. P. (2014). Encoding of fear learning and memory in distributed neuronal circuits. *Nat. Neurosci.* 17, 1644–1654. doi: 10.1038/nn.3869

Huang, C.-C., Chen, C.-C., Liang, Y.-C., and Hsu, K.-S. (2014). Long-term potentiation at excitatory synaptic inputs to the intercalated cell masses of the amygdala. *Int. J. Neuropsychopharmacol.* 17, 1233–1242. doi: 10.1017/S1461145714000133

Huang, Y. Y., and Kandel, E. R. (1998). Postsynaptic induction and PKA-dependent expression of LTP in the lateral amygdala. *Neuron* 21, 169–178. doi: 10.1016/s0896-6273(00)80524-3

Huganir, R. L., and Nicoll, R. A. (2013). AMPARs and synaptic plasticity: the last 25 years. *Neuron* 80, 704–717. doi: 10.1016/j.neuron.2013.10.025

Humeau, Y., Reisel, D., Johnson, A. W., Borchardt, T., Jensen, V., Gebhardt, C., et al. (2007). A pathway-specific function for different AMPA receptor subunits in amygdala long-term potentiation and fear conditioning. *J. Neurosci.* 27, 10947–10956. doi: 10.1523/JNEUROSCI.2603-07.2007

Humeau, Y., Shaban, H., Bissiére, S., and Lüthi, A. (2003). Presynaptic induction of heterosynaptic associative plasticity in the mammalian brain. *Nature* 426, 841–845. doi: 10.1038/nature02194

Kaoru, T., Liu, F. C., Ishida, M., Oishi, T., Hayashi, M., Kitagawa, M., et al. (2010). Molecular characterization of the intercalated cell masses of the amygdala: implications for the relationship with the striatum. *Neuroscience* 166, 220–230. doi: 10.1016/j.neuroscience.2009.12.004

Kessels, H. W., and Malinow, R. (2009). Synaptic AMPA receptor plasticity and behavior. *Neuron* 61, 340–350. doi: 10.1016/j.neuron.2009.01.015

Kim, W. B., and Cho, J. H. (2017). Encoding of discriminative fear memory by input-specific LTP in the amygdala. *Neuron* 95, 1129–1146. doi: 10.1016/j.neuron.2017.08.004

Kwon, O. B., Lee, J. H., Kim, H. J., Lee, S., Lee, S., Jeong, M. J., et al. (2015). Dopamine Regulation of Amygdala Inhibitory Circuits for Expression of Learned Fear. *Neuron* 88, 378–389. doi: 10.1016/j.neuron.2015.09.001

LeDoux, J. E. (2000). Emotion circuits in the brain. *Annu. Rev. Neurosci.* 23, 155–184. doi: 10.1146/annurev.neuro.23.1.155

Li, H., Penzo, M. A., Taniguchi, H., Kopec, C. D., Huang, Z. J., and Li, B. (2013). Experience-dependent modification of a central amygdala fear circuit. *Nat. Neurosci.* 16, 332–339. doi: 10.1038/nn.3322

Likhtik, E., Popa, D., Apergis-Schoute, J., Fidacaro, G. A., and Paré, D. (2008). Amygdala intercalated neurons are required for expression of fear extinction. *Nature* 454, 642–645. doi: 10.1038/nature07167

Linke, R., Braune, G., and Schwegler, H. (2000). Differential projection of the posterior paralaminar thalamic nuclei to the amygdaloid complex in the rat. *Exp. Brain Res.* 134, 520–532. doi: 10.1007/s002210000475

Lu, W., Shi, Y., Jackson, A. C., Bjorgan, K., During, M. J., Sprengel, R., et al. (2009). Subunit composition of synaptic AMPA receptors revealed by a single-cell genetic approach. *Neuron* 62, 254–268. doi: 10.1016/j.neuron.2009.02.027

Malenka, R. C., and Bear, M. F. (2004). LTP and LTD: an embarrassment of riches. *Neuron* 44, 5–21. doi: 10.1016/j.neuron.2004.09.012

Maren, S. (2001). Neurobiology of Pavlovian fear conditioning. *Annu. Rev. Neurosci.* 24, 897–931. doi: 10.1146/annurev.neuro.24.1.897

Maren, S., and Quirk, G. J. (2004). Neuronal signalling of fear memory. *Nat. Rev. Neurosci.* 5, 844–852. doi: 10.1038/nrn1535

Martin, S. J., Grimwood, P. D., and Morris, R. G. (2000). Synaptic plasticity and memory: an evaluation of the hypothesis. *Annu. Rev. Neurosci.* 23, 649–711. doi: 10.1146/annurev.neuro.23.1.649

Masugi-Tokita, M., and Shigemoto, R. (2007). High-resolution quantitative visualisation of glutamate and GABA receptors at central synapses. *Curr. Opin. Neurobiol.* 17, 387–393. doi: 10.1016/j.conb.2007.04.012

Masugi-Tokita, M., Tarusawa, E., Watanabe, M., Molnár, E., Fujimoto, K., and Shigemoto, R. (2007). Number and density of AMPA receptors in individual synapses in the rat cerebellum as revealed by SDS-digested freeze-fracture replica labeling. *J. Neurosci.* 27, 2135–2144. doi: 10.1523/JNEUROSCI.2861-06.2007

Matsubara, A., Laake, J. H., Davanger, S., Usami, S., and Ottersen, O. P. (1996). Organization of AMPA receptor subunits at a glutamate synapse: a quantitative immunogold analysis of hair cell synapses in the rat organ of Corti. *J. Neurosci.* 16, 4457–4467. doi: 10.1523/JNEUROSCI.16-14-04457.1996

McKernan, M. G., and Shinnick-Gallagher, P. (1997). Fear conditioning induces a lasting potentiation of synaptic currents in vitro. *Nature* 390, 607–611. doi: 10.1038/37605

Mi, R., Tang, X., Sutter, R., Xu, D., Worley, P., and O'Brien, R. J. (2002). Differing mechanisms for glutamate receptor aggregation on dendritic spines and shafts in cultured hippocampal neurons. *J. Neurosci.* 22, 7606–7616. doi: 10.1523/JNEUROSCI.22-17-07606.2002

Migues, P. V., Hardt, O., Wu, D. C., Gamache, K., Sactor, T. C., Wang, Y. T., et al. (2010). PKMζ maintains memories by regulating GluR2-dependent AMPA receptor trafficking. *Nat. Neurosci.* 13, 630–634. doi: 10.1038/nn.2531

Millhouse, O. E. (1986). The intercalated cells of the amygdala. *J. Comp. Neurol.* 247, 246–271. doi: 10.1002/cne.902470209

Newpher, T. M., and Ehlers, M. D. (2008). Glutamate receptor dynamics in dendritic microdomains. *Neuron* 58, 472–497. doi: 10.1016/j.neuron.2008.04.030

Nusser, Z., Lujan, R., Laube, G., Roberts, J. D., Molnar, E., and Somogyi, P. (1998). Cell type and pathway dependence of synaptic AMPA receptor number and variability in the hippocampus. *Neuron* 21, 545–559. doi: 10.1016/s0896-6273(00)80565-6

Pape, H. C., and Paré, D. (2010). Plastic synaptic networks of the amygdala for the acquisition, expression, and extinction of conditioned fear. *Physiol. Rev.* 90, 419–463. doi: 10.1152/physrev.00037.2009

Paré, D., and Gaudreau, H. (1996). Projection cells and interneurons of the lateral and basolateral amygdala: distinct firing patterns and differential relation to theta and delta rhythms in conscious cats. *J. Neurosci.* 16, 3334–3350. doi: 10.1523/JNEUROSCI.16-10-03334.1996

Poo, M. M., Pignatelli, M., Ryan, T. J., Tonegawa, S., Bonhoeffer, T., Martin, K. C., et al. (2016). What is memory? The present state of the engram. *BMC Biol.* 14:40. doi: 10.1186/s12915-016-0261-6

Radley, J. J., Farb, C. R., He, Y., Janssen, W. G., Rodrigues, S. M., Johnson, L. R., et al. (2007). Distribution of NMDA and AMPA receptor subunits at thalamo-amygdaloid dendritic spines. *Brain Res.* 1134, 87–94. doi: 10.1016/j.brainres.2006.11.045

Rodrigues, S. M., Farb, C. R., Bauer, E. P., LeDoux, J. E., and Schafe, G. E. (2004). Pavlovian fear conditioning regulates Thr286 autophosphorylation of Ca2+/calmodulin-dependent protein kinase II at lateral amygdala synapses. *J. Neurosci.* 24, 3281–3288. doi: 10.1523/JNEUROSCI.5303-03.2004

Rogan, M. T., Stäubli, U. V., and LeDoux, J. E. (1997). Fear conditioning induces associative long-term potentiation in the amygdala. *Nature* 390, 604–607. doi: 10.1038/37601

Royer, S., Martina, M., and Paré, D. (2000). Polarized synaptic interactions between intercalated neurons of the amygdala. *J .Neurophysiol.* 83, 3509–3518. doi: 10.1152/jn.2000.83.6.3509

Royer, S., and Paré, D. (2003). Conservation of total synaptic weight through balanced synaptic depression and potentiation. *Nature* 422, 518–522. doi: 10.1038/nature01530

Rumpel, S., LeDoux, J. E., Zador, A., and Malinow, R. (2005). Postsynaptic receptor trafficking underlying a form of associative learning. *Science* 308, 83–88. doi: 10.1126/science.1103944

Sala, C., and Segal, M. (2014). Dendritic spines: the locus of structural and functional plasticity. *Physiol. Rev.* 94, 141–188. doi: 10.1152/physrev.00012.2013

Sandri, C., Akert, H., Livingston, R. B., and Moor, H. (1972). Particle aggregations at specialized sites in freeze-etched postsynaptic membranes. *Brain Res.* 41, 1–16. doi: 10.1016/0006-8993(72)90612-9

Schönherr, S., Seewald, A., Kasugai, Y., Bosch, D., Ehrlich, I., and Ferraguti, F. (2016). Combined Optogenetic and Freeze-fracture Replica Immunolabeling to Examine Input-specific Arrangement of Glutamate Receptors in the Mouse Amygdala. *J. Vis. Exp.* 2016:53853. doi: 10.3791/53853

Segal, M. (2017). Dendritic spines: morphological building blocks of memory. *Neurobiol. Learn. Mem.* 138, 3–9. doi: 10.1016/j.nlm.2016.06.007

Smith, P. H., Ulrich, D. J., and Manning, K. A. (2019). Evaluation of medial division of the medial geniculate (MGM) and posterior intralaminar nucleus (PIN) inputs to the rat auditory cortex, amygdala, and striatum. *J. Comp. Neurol.* 527, 1478–1494. doi: 10.1002/cne.24644

Strobel, C., Marek, R., Gooch, H. M., Sullivan, R. K., and Sah, P. (2015). Prefrontal and auditory input to intercalated neurons of the amygdala. *Cell. Rep.* 10, 1435–1442. doi: 10.1016/j.celrep.2015.02.008

Szoboszlay, M., Kirizs, T., and Nusser, Z. (2017). Objective quantification of nanoscale protein distributions. *Sci Rep.* 7:15240. doi: 10.1038/s41598-017-15695-w

Tanaka, J., Matsuzaki, M., Tarusawa, E., Momiyama, A., Molnar, E., Kasai, H., et al. (2005). Number and density of AMPA receptors in single synapses in immature cerebellum. *J. Neurosci.* 25, 799–807. doi: 10.1523/JNEUROSCI.4256-04.2005

Tarusawa, E., Matsui, K., Budisantoso, T., Molnár, E., Watanabe, M., Matsui, M., et al. (2009). Input-specific intrasynaptic arrangements of ionotropic glutamate receptors and their impact on postsynaptic responses. *J. Neurosci.* 29, 12896–12908. doi: 10.1523/JNEUROSCI.6160-08.2009

Turner, B. H., and Herkenham, M. (1991). Thalamoamygdaloid projections in the rat: a test of the amygdala's role in sensory processing. *J. Comp. Neurol.* 313, 295–325. doi: 10.1002/cne.903130208

Wu, D., Bacaj, T., Morishita, W., Goswami, D., Arendt, K. L., Xu, W., et al. (2017). Postsynaptic synaptotagmins mediate AMPA receptor exocytosis during LTP. *Nature* 544, 316–321. doi: 10.1038/nature21720

Xie, M. J., Ishikawa, Y., Yagi, H., Iguchi, T., Oka, Y., Kuroda, K., et al. (2019). PIP3-Phldb2 is crucial for LTP regulating synaptic NMDA and AMPA receptor density and PSD95 turnover. *Sci. Rep.* 9:4305. doi: 10.1038/s41598-019-40838-6

Yeh, S., Mao, S., Lin, H., and Gean, P. (2006). Synaptic expression of glutamate receptor after encoding of fear memory in the rat amygdala. *Mol. Pharmacol.* 69, 299–308. doi: 10.1124/mol.105.017194

Conflict of Interest: The authors declare that the research was conducted in the absence of any commercial or financial relationships that could be construed as a potential conflict of interest.

Copyright © 2021 Seewald, Schönherr, Hörtnagl, Ehrlich, Schmuckermair and Ferraguti. This is an open-access article distributed under the terms of the Creative Commons Attribution License (CC BY). The use, distribution or reproduction in other forums is permitted, provided the original author(s) and the copyright owner(s) are credited and that the original publication in this journal is cited, in accordance with accepted academic practice. No use, distribution or reproduction is permitted which does not comply with these terms.

Advantages of publishing in Frontiers

OPEN ACCESS
Articles are free to read for greatest visibility and readership

FAST PUBLICATION
Around 90 days from submission to decision

HIGH QUALITY PEER-REVIEW
Rigorous, collaborative, and constructive peer-review

TRANSPARENT PEER-REVIEW
Editors and reviewers acknowledged by name on published articles

Frontiers
Avenue du Tribunal-Fédéral 34
1005 Lausanne | Switzerland

Visit us: www.frontiersin.org
Contact us: frontiersin.org/about/contact

REPRODUCIBILITY OF RESEARCH
Support open data and methods to enhance research reproducibility

DIGITAL PUBLISHING
Articles designed for optimal readership across devices

FOLLOW US
@frontiersin

IMPACT METRICS
Advanced article metrics track visibility across digital media

EXTENSIVE PROMOTION
Marketing and promotion of impactful research

LOOP RESEARCH NETWORK
Our network increases your article's readership